КИЇВСЬКИЙ НАЦІОНАЛЬНИЙ УНІВЕРСИТЕТ
імені ТАРАСА ШЕВЧЕНКА

НАЦІОНАЛЬНА АКАДЕМІЯ НАУК УКРАЇНИ
ІНСТИТУТ ТЕОРЕТИЧНОЇ ФІЗИКИ імені М.М. БОГОЛЮБОВА

Горкавенко Володимир Миколайович

УДК 530.145; 539.12

Дисертація

Пошук проявів частинок та топологічних струноподібних об'єктів за межами Стандартної моделі

01.04.02 – теоретична фізика

Подається на здобуття наукового ступеня
доктора фізико-математичних наук

Дисертація містить результати власних досліджень. Використання ідей, результатів і текстів інших авторів мають посилання на відповідне джерело.

_____ В. М. Горкавенко

Київ – 2023

АНОТАЦІЯ

Горкавенко В.М. Пошук проявів частинок та топологічних струноподібних об'єктів за межами Стандартної моделі.

Дисертація на здобуття наукового ступеня доктора фізико-математичних наук за спеціальністю 01.04.02 "теоретична фізика" (10 – Природничі науки). – Київський національний університет імені Тараса Шевченка, Інститут теоретичної фізики ім. М.М. Боголюбова НАН України, Київ, 2023.

Дисертацію присвячено дослідженню фізики за межами Стандартної моделі фізики елементарних частинок (СМ) на різних енергетичних масштабах. На масштабі енергій, доступних на сучасних прискорювачах, розглядалися різні аспекти можливих експериментальних проявів частинок фізики за межами Стандартної моделі, а саме: скалярного, нейтринного та із взаємодією типу Черна-Саймонса розширень СМ. Також розглядалися можливі прояви топологічних об'єктів у вигляді космічних струн з "магнітним" полем калібрувальної групи $U_X(1)$, що могли утворитися внаслідок фазових переходів у ранньому Всесвіті на масштабі енергій, що значно перевищує можливості сучасних прискорювачів. А саме, розглядалися квантові ефекти у вакуумі полів скалярної та ферміонної матерії в присутності космічної "магнітної" струни, що моделювалася непроникливою для полів матерії трубкою скінченого радіуса з "магнітним" полем. Використана модель дозволила розглянути квантові ефекти у вакуумі полів матерії в найбільш загальному випадку незалежно від конкретної природи утворення космічної струни.

У першому розділі дисертації розглянуто скалярне, ферміонне та із взаємодією типу Черна-Саймонса розширення СМ. Розглядаються деякі загальні питання розширень СМ та канали народження та розпаду частинок за межами Стандартної моделі з масою порядку декількох ГеВ.

У підрозділі 1.1 зроблено повний і самоузгоджений опис всіх каналів народження та розпаду масивних скалярів з масою в декілька ГеВ в скалярному розширенні СМ. Знайдено та досліджено домінуючі канали народження та розпаду масивних скалярів для умов експериментів DUNE (Fermilab), SHiP (SPS CERN) та експериментів на LHC. У підрозділі 1.2 отримано ефективний лагранжіан взаємодії масивного векторного бозону (в розширенні СМ зі взаємодією типу Черна-Саймонса) з кварками різних ароматів. Показано, що ефективна взаємодія векторного бозону з кварками різних ароматів не вимагає застосування процедури перенормування. Послідовно розглянуто всі канали народження масивного векторного бозону з розпадів B та K мезонів. У підрозділі 1.3 отримано оригінальні розв'язки та виражено елементи юкавівської матриці в нейтринному розширенні СМ з параметрами масової матриці активних нейтрино. У підрозділі 1.4 зроблена оцінка похибки в розрахунках області чутливості експерименту SHiP, пов'язаної з використанням для опису народження правокіральних масивних нейтрино в тричастинкових розпадах мезонів спрощених матричних елементів, що використовуються в програмі моделювання процесів зіткнення частинок при високих енергіях PYTHIA, в порівнянні з використанням коректних матричних елементів. Запроновано вибір спрощених матричних елементів середовища PYTHIA, що дають найменше відхилення від коректних розрахунків.

У другому розділі розглядаються ефекти поляризації вакууму скалярного поля матерії у вигляді індукування вакуумної енергії за наявності топологічного дефекту, а саме космічної "магнітної" струни, що моделюється непроникливою для полів матерії трубкою скінченого радіуса з "магнітним" полем. Вважається, що поля матерії є зарядженими відносно калібрувальної групи $U_X(1)$.

У підрозділі 2.1 розглядається індукування вакуумної енергії скаляр-

ного поля матерії за наявності граничної умови типу Діріхле на поверхні трубки скінченого радіусу. У підрозділі 2.2 розглядається індукування вакуумної енергії скалярного поля матерії за наявності граничної умови типу Неймана на поверхні трубки скінченого радіусу. Показано, що поляризація вакууму за наявності граничної умови типу Неймана суттєво перевищує її значення за наявності граничної умови типу Діріхле. Показано, що поляризація вакууму буде суттєвою у випадку, коли маса квантованого поля матерії є значно меншою за масу хіггсівського поля, що призвело до спонтанного порушення симетрії і виникнення топологічного дефекту у вигляді "магнітної" космічної струни. У підрозділі 2.3 розглядається індукування вакуумної енергії скалярного поля матерії за різних значень сталої зв'язку скалярного поля з кривизною простору-часу для випадку граничної умови на поверхні трубки типу Діріхле. Показано, що в цьому випадку повна індукована енергія вакууму не залежить від сталої зв'язку скалярного поля з кривизною простору-часу. У підрозділі 2.4 розглядається індукування вакуумної енергії скалярного поля матерії за різних значень сталої зв'язку скалярного поля з кривизною простору-часу для випадку граничної умови на поверхні трубки типу Діріхле у просторі-часі довільної розмірності.

У третьому розділі розглядаються ефекти поляризації вакууму скалярного та ферміонного полів матерії у вигляді індукування у вакуумі магнітного потоку за наявності топологічного дефекту, а саме космічної "магнітної" струни, що моделюється непроникливою для полів матерії трубкою скінченого радіуса з "магнітним" полем. Вважається, що поля матерії є зарядженими відносно калібрувальної групи $U_X(1)$ та мають електричні заряди.

У підрозділі 3.1 розглядається індукування магнітного потоку у вакуумі скалярного поля матерії за наявності граничної умови типу Діріхле на поверхні трубки скінченого радіусу. У підрозділі 3.2 розглядається індуку-

вання магнітного потоку у вакуумі скалярного поля матерії за наявності граничної умови типу Неймана на поверхні трубки скінченого радіусу. У підрозділі 3.3 розглядається індукування магнітного потоку у вакуумі скалярного поля матерії за наявності граничної умови типу Робена на поверхні трубки скінченого радіусу в просторі-часі довільної розмірності. Досліджується ефект індукування магнітного потоку у вакуумі скалярного поля матерії за всіх можливих значень параметра граничної умови типу Робена. Показано суттєво різну поведінку індукованого магнітного потоку за додатніх та від'ємних значень параметра граничної умови типу Робена. У підрозділі 3.4 розглядається загальний вигляд граничної умови на поверхні трубки для випадку ферміонного поля матерії з умови самоспряженого розширення діраковського гамільтоніану у просторі-часі розмірності 2+1. Розглядається індукування магнітного потоку у вакуумі ферміонного поля матерії за наявності "магнітної" трубки скінченого радіусу за різних значень параметра самоспряженого розширення. Показано, що лише при деяких значеннях параметра самоспряженого розширення індукований магнітний потік буде скінченним. Показано, що для знаходження фізичних значень параметра самоспряженого розширення необхідно додатково накладати вимогу спадання величини квантових ефектів при збільшенні товщини магнітної трубки.

Ключові слова: фізика за межами Стандартної моделі, рідкісні мезонні розпади, скалярне розширення Стандартної моделі, важкі нейтральні лептони, розширення калібрувального сектора Стандартної моделі, теорія Черна-Саймонса, топологічні дефекти, космічні струни, поляризація вакууму, ефект Казимира, ефект Ааронова-Бома.

ABSTRACT

Gorkavenko V.M. The search for manifestations of particles and topological string-like objects beyond the Standard Model.

Thesis for the degree of Doctor of Physical and Mathematical Sciences by speciality 01.04.02 – theoretical physics (104 — physics and astronomy). — Taras Shevchenko National University of Kyiv, Bogolyubov Institute for Theoretical Physics of the NAS of Ukraine, Kyiv, 2023.

This thesis is dedicated to exploring physics beyond the Standard Model of particle physics (SM) at different energy scales. It examines various aspects of potential experimental manifestations of particles beyond the Standard Model of the scalar, neutrino, and Chern-Simons extensions of the SM at energy scales available for modern accelerators. Possible manifestations of topological objects in the form of cosmic strings with "magnetic" field of gauge group $U_X(1)$, which could have formed due to phase transitions in the early Universe at energy scales significantly exceeding the capabilities of modern accelerators, were also considered. Specifically, quantum effects in the vacuum state of scalar and fermion fields in the presence of a cosmic "magnetic" string, modeled as an impermeable for the fields of matter tube of finite radius with "magnetic" field were considered. The employed model allows for a comprehensive examination of quantum effects in the vacuum of the matter fields in the most general case, irrespective of the specific nature of cosmic string formation.

The first section explores SM extensions involving scalar, fermion, and Chern-Simons portals. It addresses general issues concerning these SM extensions and investigates the production and decay channels of beyond the Standard Model particles with mass of the GeV scale.

In subsection 1.1, a complete and self-consistent account of all the production and decay channels of massive scalars at the GeV mass scale of the scalar

SM extension is presented. Dominant production and decay channels of massive scalars have been identified and studied for experiment conditions at DUNE (Fermilab), SHiP (SPS CERN), and LHC experiments. In subsection 1.2, an effective Lagrangian for the interaction of a massive vector boson (of the SM extension with Chern-Simons-like interactions) with quarks of different flavors has been derived. It has been shown that the effective interaction of the vector boson with quarks of different flavors does not require a renormalization procedure. All the production channels of a massive vector boson in decays of B and K mesons were systematically considered. Subsection 1.3 shows the derivation of an original solution and expresses Yukawa elements of the neutrino SM extension via the parameters of active neutrinos' mass matrix. In subsection 1.4, an estimation of the error in the computations of the SHiP experiment sensitivity region, caused by the usage of simplified matrix elements for describing the production of right-handed massive neutrinos in three-particle decays of mesons in PYTHIA (simulation program for particle collisions at high energies), has been made. The choice of simplified matrix elements in the PYTHIA environment that minimizes deviations from exact calculations has been proposed.

The second section delves into the effects of vacuum polarization of a scalar matter field in the form of induction of vacuum energy in the presence of a topological defect, namely a cosmic "magnetic" string, modeled as a finite radius impenetrable tube for matter field with a "magnetic" field inside. It is considered that matter fields are charged with respect to the $U_X(1)$ gauge group.

Subsection 2.1 examines the induction of a scalar field vacuum energy in the presence of a tube of finite radius with Dirichlet boundary condition at the edge of the tube. In subsection 2.2, the induction of vacuum energy of a scalar field of matter under a Neumann boundary condition at the edge of the tube is studied. It is demonstrated that the vacuum polarization effect in

the case of a Neumann boundary condition significantly surpasses the vacuum polarization effect under a Dirichlet boundary condition. It is also shown that vacuum polarization will be substantial when the mass of the quantized field of matter is considerably smaller than the mass of the Higgs field that leads to spontaneous symmetry breaking and the emergence of a topological defect in the form of a "magnetic" cosmic string. Subsection 2.3 addresses the induction of vacuum energy of a scalar field of matter for various values of the scalar field's coupling to space-time curvature, under a Dirichlet boundary condition at the edge of the tube. It is demonstrated that in this case, the total induced vacuum energy does not depend on the scalar field's coupling to space-time curvature. In subsection 2.4, the induction of vacuum energy of a scalar field of matter is studied for different values of the scalar field's coupling to space-time curvature, under a Dirichlet boundary condition on the tube's surface in a space-time of arbitrary dimension.

In the third section, the effects of vacuum polarization of scalar and fermion matter fields in the form of induction of vacuum magnetic flux in the presence of a topological defect, specifically a cosmic "magnetic" string, modeled as a finite radius impenetrable tube for matter field with a "magnetic" field inside, are investigated. It is considered that matter fields are charged with respect to the gauge group $U_X(1)$ and also possess electric charges.

Subsection 3.1 examines the induction of a vacuum magnetic flux for a scalar field of matter in the presence of a Dirichlet boundary condition at the edge of the tube. In subsection 3.2, the induction of a vacuum magnetic flux for a scalar field of matter under the presence of a Neumann boundary condition at the edge of the tube is studied. Subsection 3.3 addresses the induction of vacuum magnetic flux for a scalar field of matter under the presence of a Robin boundary condition at the edge of the tube in the space-time of arbitrary dimension. The effect of inducing vacuum magnetic flux for a scalar field of matter is

explored for all possible values of the Robin boundary condition parameter. The substantially different behavior of the induced magnetic flux for positive and negative values of the Robin boundary condition parameter is demonstrated. In subsection 3.4, the general form of the boundary condition on the tube's edge is considered for the case of fermion matter fields from the condition of self-adjoint extension of the Dirac Hamiltonian in 2+1 dimensional space-time. The induction of vacuum magnetic flux for a fermion field of matter in the presence of a "magnetic" tube of finite radius is examined for different values of the self-adjoint extension parameter. It is shown that only for certain values of the self-adjoint extension parameter, the induced magnetic flux will be finite. Additionally, it is demonstrated that to determine the physical values of the self-adjoint extension parameter, an additional requirement of the decrement of quantum effects with an increase in the thickness of the magnetic tube needs to be imposed.

Key words: Beyond Standard Model, rare decays of mesons, scalar extension of Standard Model, heavy neutral leptons, extensions of gauge sector, Chern–Simons theories, topological defects, cosmic string, vacuum polarization, Casimir effect, Aharonov–Bohm effect.

СПИСОК НАУКОВИХ ПРАЦЬ, В ЯКИХ ОПУБЛІКОВАНО ОСНОВНІ НАУКОВІ РЕЗУЛЬТАТИ ДИСЕРТАЦІЇ

[1a] **V.M. Gorkavenko**, Yu.A. Sitenko, O.B. Stepanov, Polarization of the vacuum of a quantized scalar field by an impenetrable magnetic vortex of finite thickness, *J. Phys. A: Math. Theor.* **43**(17), 175401 (12 pages) (2010).

[2a] **V.M. Gorkavenko**, S.I. Vilchynskiy, Some constraints on the Yukawa parameters in the neutrino modification of the Standard Model (νMSM) and CP-violation, *Eur. Phys. J. C* **70**(4), 1091-1098 (2010).

[3a] **V.M. Gorkavenko**, Yu.A Sitenko, O.B. Stepanov, Vacuum energy induced by an impenetrable flux tube of finite radius, *Intern. J. Mod. Phys. A* **26**(22), 3889-3899 (2011).

[4a] **V.M. Gorkavenko**, Yu.A. Sitenko, O.B. Stepanov, Casimir energy and force induced by an impenetrable flux tube of finite radius, *Intern. J. Mod. Phys. A* **28**(31), 1350161 (17 pages) (2013).

[5a] **V.M. Gorkavenko**, I.V. Ivanchenko, Yu.A. Sitenko, Induced vacuum current and magnetic field in the background of a vortex, *Intern. J. Mod. Phys. A* **31**(06), 1650017 (11 pages) (2016).

[6a] Yu.A. Sitenko, **V.M. Gorkavenko**, Induced vacuum magnetic flux in quantum spinor matter in the background of a topological defect in two-dimensional space, *Phys. Rev. D* **100**(8), 085011 (36 pages) (2019).

[7a] I. Boiarska, K. Bondarenko, A. Boyarsky, **V. Gorkavenko**, M. Ovchynnikov, A. Sokolenko, Phenomenology of GeV-scale scalar portal, *J. High Energ. Phys.* **2019**(11), 1-45 (2019).

[8a] **V.M. Gorkavenko**, Y.R. Borysenkova, M.S. Tsarenkova, Production of GeV-scale heavy neutral leptons in three-body decays. Comparison with the PYTHIA approach, *J. Phys. G: Nucl. Part. Phys.* **48**(10), 105001 (25 pages) (2021).

[9a] Yu. Borysenkova, P. Kashko, M. Tsarenkova, K. Bondarenko, **V. Gorkavenko**, Production of Chern-Simons bosons in decays of mesons, *J. Phys. G: Nucl. Part. Phys.* **49**(8), 085003 (29 pages) (2022).

[10a] Yu.A. Sitenko, **V.M. Gorkavenko**, M.S. Tsarenkova, Magnetic flux in the vacuum of quantum bosonic matter in the cosmic string background, *Phys. Rev. D* **106**(10), 105010 (20 pages) (2022).

[11a] **V.M. Gorkavenko**, T.V. Gorkavenko, Yu.A. Sitenko, M.S. Tsarenkova, Induced vacuum current and magnetic flux in quantum scalar matter in the background of a vortex defect with the Neumann boundary condition, *Ukr. J. Phys.* **67**(1), 3-10 (2022).

[12a] **V.M. Gorkavenko**, T.V. Gorkavenko, Yu.A. Sitenko, M.S. Tsarenkova, Induced vacuum energy density of quantum charged scalar matter in the background of an impenetrable magnetic tube with the Neumann boundary condition, *Ukr. J. Phys.* **67**(10), 715-721 (2022).

ТЕЗИ ДОПОВІДЕЙ НА НАУКОВИХ КОНФЕРЕНЦІЯХ

1. **В.М. Горкавенко**, Ю.О. Сітенко, О. Б. Степанов, Густина вакуумної енергії, індукована непроникним магнітним вихором скінченого поперечного розміру. Міжнародна конференція молодих вчених та аспірантів "ІЕФ, 2011". 24-27 травня, 2011, Інститут Електронної Фізики НАН України, Ужгород (Україна). Науковий вісник Ужгородського університету, серія Фізика, випуск **30**, с. 234-239 (2011).

2. S.I. Vilchinskii, **V.M. Gorkavenko**, I.V Rudenok, The influence of the non-zero value of θ_{13} mixing angle on the parameters of the neutrino modification of the Standard Model (νMSM). III Young Scientists Conference Modern Problems of Theoretical Physics. December 21-23, 2011, Bogolyubov Institute for Theoretical Physics of the NAS of Ukraine, Kyiv (Ukraine). Book of abstracts, 13 (2011).

3. **V.M. Gorkavenko**, Yu.A. Sitenko, O.B.Stepanov, Casimir force induced by impenetrable flux tube of finite radius. III Young Scientists Conference Modern Problems of Theoretical Physics. December 21-23, 2011, Bogolyubov Institute for Theoretical Physics of the NAS of Ukraine, Kyiv (Ukraine). Book of abstracts, 55 (2011).

4. I. Ivanchenko, **V.M. Gorkavenko**, Yu. A. Sitenko, Induced vacuum current and magnetic field in the background of a cosmic string modeled by impenetrable magnetic-flux-carrying tube. 20-th Open Young Scientists' Conference on Astronomy and Space Physics. April 22-27, 2013, Kyiv (Ukraine). Abstracts.– K.: ТОВ "Компанія BAITE", 30 (2013).

5. Yu.A. Sitenko, **V.M. Gorkavenko**, Self-adjointness, confinement and the Casimir effect. International Conference on p-Adic Mathematical Physics and its Applications. September 7-12, 2015, Belgrade (Serbia). Conference proceedings: Facta Universitatis, Series Physics, Chemistry and Technology **14**(3), 319-335 (2016).

6. **V. Gorkavenko**, K. Bondarenko, O. Seleznov, S. Vilchynskiy, Search for light Higgs-like particles in proton collisions with a target at the SHiP experiment. 3-rd Walter THIRRING International School "Fundamentals of Astroparticle and Quantum Physics". September 17-23, 2017, Bogolyubov Institute for Theoretical Physics of the NAS of Ukraine,

Kyiv (Ukraine). List of invited speakers
http://quark.itp.tuwien.ac.at/∼diefaust/2017/

7. **V. Gorkavenko**, Search for light Higgs-like particles in proton collisions with a target at the SHiP experiment. The International Conference "CERN-Ukraine Cooperation: Current State and Prospects". May 15-17, 2018, Institute for Scintillation Materials NAS of Ukraine, Kharkiv (Ukraine). Conference Programme
https://kipt.kharkov.ua/conferences/itp/2018/Programme_CERN-Ukraine.pdf

8. **V.M. Gorkavenko**, Search for Hidden Particles in Intensity Frontier Experiment SHiP. New trends in high-energy physics, 21-th International conference organized by the Bogolyubov Institute for Theoretical Physics, National Academy of Sciences of Ukraine. May 12–18, 2019, Odessa (Ukraine). Proceeding of the conference, 147-152
https://indico.bitp.kiev.ua/event/1/attachments/3/163/Book_conf.pdf

9. **V.M. Gorkavenko** and Yu.A. Sitenko, Polarization of the vacuum of quantized spinor field by a topological defect in two-dimensional space. XI Bolyai-Gauss-Lobachevsky Conference: Non-Euclidean, Non-Commutative Geometry and Quantum Physics. May 19-24, 2019, Bogolyubov Institute for Theoretical Physics, Kyiv (Ukraine). Book of Abstracts, 14 (2019).

10. **V. Gorkavenko**, P. Kashko, K. Bondarenko, Chern-Simons portal. X Young Scientists Conference Modern Problems of Theoretical Physics. December 23-24, 2019, Bogolyubov Institute for Theoretical Physics of the NAS of Ukraine, Kyiv (Ukraine). Book of abstracts, 55 (2019).

11. Y. Borysenkova, K. Bondarenko, **V. Gorkavenko**, A. Svetlichnyi, M. Tsarenkova, Production of HNL in 3-body decays of mesons. Comparison with PYTHIA approach. XI Young Scientists Conference Modern Problems of Theoretical Physics. December 21-23, 2020, Bogolyubov Institute for Theoretical Physics of the NAS of Ukraine, Kyiv (Ukraine). Book of abstracts, 7-9 (2021).

12. M. Tsarenkova, K. Bondarenko, Y. Borysenkova, **V. Gorkavenko**, P. Kashko, Phenomenology of GeV-scale Chern-Simons boson. XI Young Scientists Conference Modern Problems of Theoretical Physics. December 21-23, 2020, Bogolyubov Institute for Theoretical Physics of the NAS of Ukraine, Kyiv (Ukraine). Book of abstracts, 10-13 (2021).

ЗМІСТ

ВСТУП **17**

РОЗДІЛ 1 Пошук проявів частинок нової фізики **43**

1.1. Феноменологія скалярного порталу на масштабі в декілька ГеВ 43

1.2. Народження бозонів Черна-Саймонса в розпадах мезонів 89

1.3. Обмеження на юкавівські параметри в нейтринній модифікації СМ 119

1.4. Народження масивних нейтрино з правою кіральністю у 3-частинкових розпадах мезонів 127

РОЗДІЛ 2 Поляризація енергії у вакуумі топологічним струноподібним об'єктом **152**

2.1. Індукування енергії у вакуумі скалярного поля матерії у випадку граничної умови типу Діріхле 152

2.2. Індукування енергії у вакуумі скалярного поля матерії у випадку граничної умови Неймана 165

2.3. Поляризація вакууму скалярного поля матерії з урахуванням сталої зв'язку скалярного поля з кривизною простору-часу . 172

2.4. Поляризація вакууму скалярного поля матерії в просторі-часі довільної розмірності 183

РОЗДІЛ 3 Індукування магнітного потоку топологічним дефектом **200**

3.1. Індукування у вакуумі скалярного поля.
Гранична умова типу Діріхле 200
3.2. Індукування у вакуумі скалярного поля.
Гранична умова типу Неймана 212
3.3. Індукування у вакуумі скалярного поля.
Гранична умова типу Робена 220
3.4. Індукування у вакуумі спінорного поля.
Загальний вигляд граничної умови 240

ВИСНОВКИ **276**

СПИСОК ВИКОРИСТАНИХ ДЖЕРЕЛ **282**

ПОДЯКИ **293**

ДОДАТОК А **294**

ВСТУП

Обґрунтування та актуальність теми досліджень. Стандартна модель фізики елементарних частинок (СМ) [1–3] — це теоретична модель, яка з високою точністю описує процеси електромагнітної, слабкої та сильної взаємодії за участю елементарних частинок. Вона є самоузгодженою до великого енергетичного масштабу (можливо, до масштабу Планка) і перевірена в численних експериментах на прискорювачах до енергії ~ 15 ТеВ. Однак СМ не може пояснити деякі явища, такі як масивність нейтрино (див., наприклад, [4–6]), темну матерію (для оглядів див., наприклад, [7–9]), баріонну асиметрію Всесвіту (див., наприклад, [11–13]) тощо. Тому СМ вважається неповною теорією і потребує розширення. Існує багато можливостей, як саме це зробити. Фізика в розширеннях Стандартної моделі називається фізикою за межами Стандартної моделі, або новою фізикою (див., наприклад, [14–17]).

Багато з наведених проблем СМ можна пояснити розширенням СМ за допомогою введення нових частинок та нових взаємодій. Значення мас частинок за межами СМ можуть лежати в дуже широкому діапазоні значень. Наприклад, малі маси нейтрино, темну матерію та баріонну асиметрію Всесвіту можна пояснити введенням нових частинок як з масами меншими за 1 еВ, так і з масами аж до масштабів теорії великого об'єднання, див. [5,18]. З іншого боку, можна припустити, що нових частинок в "прихованому" секторі СМ може бути досить багато і не всі з них мають відношення до вирішення наведених вище проблем СМ.

Той факт, що ми не спостерігаємо частинок нової фізики в експериментах на прискорювачах, має два можливі пояснення. Або ці частинки занадто масивні, щоб їх можна було утворити на сучасних прискорювачах, таких як Великий адронний колайдер, або вони дуже слабо взаємодіють з частинками СМ. Якщо частинки нової фізики досить важкі, тоді для їх пошуку необхідно будувати більш потужні, дорожчі прискорювачі та проводити високоенергетичні експерименти (energy frontier experiments), див. [19, 20]. Але випадок легких, дуже слабко взаємодіючих частинок нової фізики є також дуже актуальним для експериментального пошуку проявів частинок нової фізики прямо зараз, на вже існуючих прискорювачах. Щоб знайти їх, нам потрібні експерименти з високою світністю, тобто з великою кількістю подій (intensity frontier experiments) [21, 22]. За останні декілька років було запропоновано кілька таких експериментів: MATHUSLA [23], FACET [24], FASER [25, 26], SHiP [27, 28], NA62 [29–31], DUNE [32, 33] тощо.

Важливою характеристикою таких експериментів є область чутливості, яка визначає діапазон значень маси та сталої зв'язку частинки нової фізики, при яких вона може буде зареєстрована в даному експерименті. Розрахунок області чутливості є складною математичною задачею. Для того, щоб область чутливості можна було теоретично розрахувати необхідно знати домінуючі канали народження та розпадів частинок нової фізики в умовах конкретного експерименту.

Приклади явного вигляду області чутливості для різних експериментів та існуючих обмежень на параметри моделі наведені на Рис. 1, 2.

Зараз немає відповіді на запитання якими саме мають бути частинки нової фізики: це можуть бути скалярні, псевдоскалярні, векторні, ферміонні частинки. Жодному з існуючих варіантів не можна надати переваги, тому пошуки частинок нової фізики потрібно проводити перебираючи всі можливі варіанти (див. оглядові роботи [23, 27]). При цьому в якості лагран-

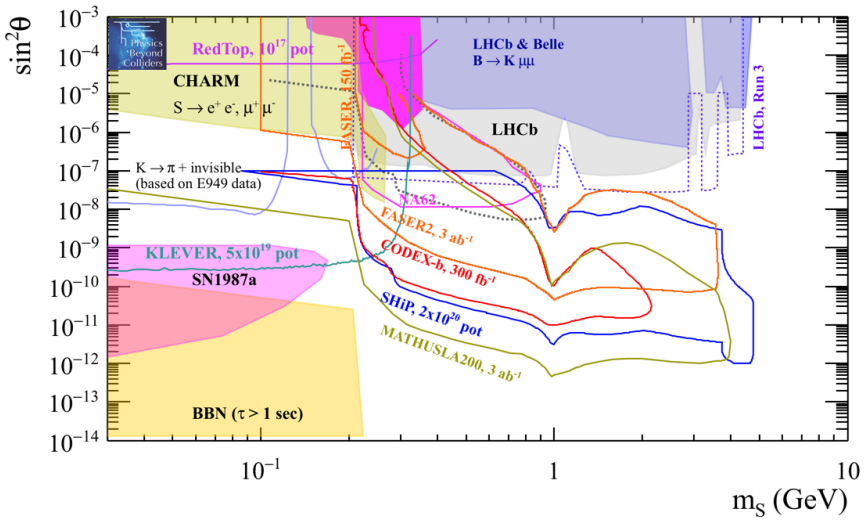

Рис. 1: Області чутливості різних експериментів до пошуку нової скалярної частинки, випадок $\alpha_2 = 0$. Зафарбовані області – виключені області параметрів скалярів. Незафорбавоні контури – області чутливості майбутніх експериментів. Рис. взято з [21].

жіанів взаємодії частинок нової фізики з частинками СМ зручно брати найбільш загальні калібрувально-інваріантні та, по можливості, перенормовні вирази. Такі лагранжіани взаємодії отримали назви порталів, див., наприклад, [27]. Вони можуть являти собою перенормовні взаємодії, а можуть представляти і ефективні неперенормовні взаємодії. В останньому випадку портали являють собою оператори розмірностей вищих за 4, що подавлені масштабом Λ^{-n}, де Λ – розмірний параметр, що визначає певний енергетичний масштаб прихованого сектора СМ, наприклад маси іншої "прихованої" частинки переносника взаємодії (за аналогією з фізичним змістом сталої Фермі G_F в ефективній теорії Фермі).

Виділяють три портали перенормованої взаємодії для частинок нової фізики. Вони всі є операторами розмірності ГеВ^4 (розмірність добутків всіх польових функцій), але відрізняються розмірністю складових СМ:

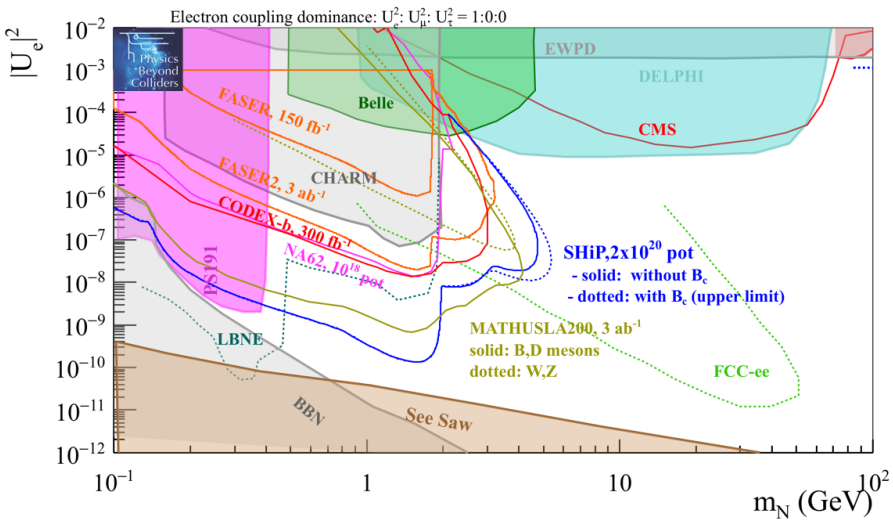

Рис. 2: Обмеження на параметри правокірального нейтрино в електронно-домінантній моделі згори вниз, відповідно. Зафарбовані області відповідають вже виключеним параметрам правокірального нейтрино. Наведені контури області чутливості для майбутніх експериментів. Рис. взято з [43].

- Скалярний портал (див., наприклад, [34–37]): розмірність складових СМ ГеВ^2; до СМ додається нове скалярне масивне поле S; лагранжіан взаємодії має вигляд $\mathcal{L}_{int} = (\alpha_1 S + \alpha_2 S^2)(H^\dagger H)$;

- Векторний портал (див., наприклад, [38–40]), розмірність складових СМ ГеВ^2; до СМ додається нове векторне масивне поле A'; лагранжіан взаємодії має вигляд $\mathcal{L}_{int} = \epsilon F'_{\mu\nu} F_Y^{\mu\nu}$;

- Нейтринний портал (див., наприклад, [41–44]), розмірність складових СМ ГеВ$^{2.5}$; до СМ додаються одне чи декілька нових ферміонних масивних полів нейтрино з правою кіральністю N_I; лагранжіан взаємодії має вигляд $\mathcal{L}_{int} = y_{\alpha I}(\bar{L}_\alpha \cdot \tilde{H}) N_I$.

Відзначимо, що в рамках нейтринної модифікації СМ в роботах [41, 42] було запропоновано доповнити СМ трьома масивними правокіральними нейтрино (модель нейтринного мінімального розширення СМ, νMSM). При

цьому до лагранжіана СМ додається 18 нових параметрів, які можна підібрати таким чином, щоб одночасно вирішити декілька проблем СМ: найлегше правокіральне нейтрино (з масою порядку 10 кеВ) в цій моделі є кандидатом на роль частинки темної матерії, два інших важких правокіральних нейтрино з майже однаковими масами забезпечують появу баріонної асиметрії у Всесвіті, модель також може пояснити існуючі дані по масам активних нейтрино та параметри спостережуваних нейтринних осциляцій.

Виділяють також дві ефективні неперенормовні взаємодії, що складаються з операторів вищих розмірностей: псевдоскалярний портал та портал зі взаємодією Черна-Саймонса.

У псевдоскалярному порталі (див., наприклад, [45–48]) до СМ додається нове псевдоскалярне поле (поле аксіонів або або аксіоноподібних частинок) a, що взаємодіє з калібрувальними полями та ферміонами СМ як $\mathcal{L}_{int} = \frac{g_i}{\Lambda} a\, F^i_{\mu\nu}\tilde{F}^{i,\mu\nu} + \frac{h_i}{\Lambda}\partial_\mu a \bar{f}\gamma^\mu\gamma^5 f$. Оператор взаємодії має розмірність ГеВ^5. Зазначимо, що цей портал цікавий тим, що легкі аксіони (з масами порядку 10^{-6} еВ) утворюються в багатьох розширеннях СМ і є чудовими кандидатами на роль частинок темної матерії [18]. Важливо також відзначити, що спостереження за ефектом гравітаційного лінзування галактик вказує, що модель темної матерії з надзвичайно легких аксіоноподібних частинок краще узгоджується з даними спостережень, ніж модель з важкими частинками темної матерії [49].

Інтерес до порталу зі взаємодією типу Черна-Саймонса викликаний тим фактом, що дана взаємодія випливає з явища скорочення квантових аномалій. Це є надзвичайно теоретично привабливим, оскільки в такому підході внесок важких ферміонів (недоступних для прямого пошуку на прискорювачах) у скасування аномалії залишається неподавленим при низьких енергіях [50, 51] і може себе проявити в експериментах. Якщо розглядати нетривіальне скорочення квантових аномалій в рамках калібрувальних

полів СМ, то це призводить до появи дуже малих параметрів теорії типу маси фотона чи мікрозарядів нових частинок, див. наприклад, [52]. На ці параметри існують досить сильні експериментальні обмеження.

Щоб уникнути дуже малих параметрів, вводиться нова калібрувальна група $U_X(1)$ відносно якої заряджені важкі ферміони, а ферміони СМ з нею не взаємодіють. В цьому випадку важкі ферміони можуть виступати в ролі посередників та призвести до появи спостережуваної взаємодії частинок СМ з новими легкими векторними частинками групи $U_X(1)$ з "прихованого" сектора СМ. Детальне пояснення походження такої взаємодії наведено в [53]. Виявилося, що калібрувально інваріантний лагранжіан відносно перетворень групи $U_Y(1) \times SU_W(2)$ в цьому випадку матиме мінімальну розмірність ГеВ^6:

$$\mathcal{L}_1 = \frac{C_Y}{\Lambda_Y^2} \cdot X_\mu (\mathfrak{D}_\nu H)^\dagger H B_{\lambda\rho} \cdot \epsilon^{\mu\nu\lambda\rho} + h.c.,$$
$$\mathcal{L}_2 = \frac{C_{SU(2)}}{\Lambda_{SU(2)}^2} \cdot X_\mu (\mathfrak{D}_\nu H)^\dagger F_{\lambda\rho} H \cdot \epsilon^{\mu\nu\lambda\rho} + h.c.$$

Цікавим є те, після спонтанного порушення електрослабкої симетрії зазначені взаємодії перетворюються на можливо перенормовні взаємодії (є операторами розмірності ГеВ^4) бозона Черна-Саймонса з векторними полями СМ, див. [53]:

$$\mathcal{L}_{CS} = c_z \epsilon^{\mu\nu\lambda\rho} X_\mu Z_\nu \partial_\lambda Z_\rho + c_\gamma \epsilon^{\mu\nu\lambda\rho} X_\mu Z_\nu \partial_\lambda A_\rho + \left\{ c_w \epsilon^{\mu\nu\lambda\rho} X_\mu W_\nu^- \partial_\lambda W_\rho^+ + h.c. \right\}.$$

Таким чином отримано лагранжіан зі взаємодією нового калібрувального бозону X_μ зі струмом, схожим на струм Черна-Саймонса, калібрувальних бозонів СМ. Це є цікавим і з тієї позиції, що струми Черна-Саймонса мають топологічне походження [54].

Взаємодії типу Черна-Саймонса з'являються в різних теоретичних моделях, включаючи додаткові виміри та теорію струн, див. [55–60]. Якщо нова векторна частинка (бозон Черна-Саймонса) буде експериментально

виявленою, це однозначно вкаже на наявність нової фізики на високих енергетичних масштабах. Важливо відзначити, що бозон Черна-Саймонса був включений в програму пошуку експерименту SHiP [27], розглядається можливість його пошуку на Великому адронному колайдері [61].

Напрямок пошуку проявів частинок нової фізики на прискорювачах з великою світністю чи на прискорювачах з великою енергією, звичайно, є дуже перспективним та обнадійливим для пошуку важких або дуже слабко взаємодіючих нових частинок. Але треба усвідомлювати, що експерименти на прискорювачах мають обмеження по енергії. Однак високоенергетичні процеси (при енергіях, недосяжних для сучасних прискорювачів) могли активно відбуватися у ранньому Всесвіті. Більш того, сліди або релікти цих процесів можуть спостерігатися і в наш час, даючи інформацію про події в далекому минулому.

Згідно зі Стандартною космологічною моделлю, після Великого Вибуху Всесвіт розширювався та охолоджувався. В процесі свого охолодження Всесвіт проходив через ряд фазових переходів [62,63]. Передбачується, що у ранньому Всесвіті могли відбутися такі фазові переходи: фазовий перехід, що відділяє електромагнітну взаємодію від слабкої (відбувся через 10^{-10} с після Великого Вибуху при температурі близько $T_{EW} \sim 100$ ГеВ); фазовий перехід деконфайнмент-конфайнмент (перехід від кварк-глюонної плазми до адронів відбувся через 10^{-5} с після Великого Вибуху при температурі нижчій за 200 МеВ). Згідно з теорією Великого об'єднання взаємодій є теоретичні передбачення існування фазового переходу, що відділяє електрослабку та сильну взаємодії (очікується, що він мав відбутися через 10^{-35} с після Великого Вибуху при температурі $T_{GUT} \sim 10^{16}$ ГеВ). Не виключено, що у ранньому Всесвіті могли відбутися і інші фазові переходи при температурах $T_{EW} < T < T_{GUT}$.

Якщо певний фазовий перехід незалежно відбувався в різних ділянках

простору-часу, то на границі цих ділянок могли утворитися топологічні об'єкти різних типів: доменні стінки, струни, монополі та похідні від них об'єкти (доменні стінки з'єднані струнами, монополі з'єднані струнами). Одновимірні топологічні дефекти отримали назву космічних струн. Топологічні космічні струни не можуть мати вільних кінців і можуть бути двох типів: у вигляді нестабільних петель (розпадаються за рахунок втрати енергії внаслідок випромінення гравітаційних хвиль) та стабільних, майже прямих ліній, що простягаються до горизонту. Якщо космічні струни утворилися в результаті спонтанного порушення симетрії деякої групи $U_X(1)$, то вони можуть містити в собі аналог магнітного поля, що відповідає калібрувальному полю даної групи [64–68]. Зазначимо, що інтерес до дослідження та пошуку космічних струн пов'язаний ще й з тим, що вони можуть утворюватися в різних розширеннях СМ в тому числі в теорії суперструн, див. [69–72].

Всередині космічної струни польова конфігурація фази з непорушеною симетрією має енергію та характеризується масою на одиницю довжини струни $\mu \sim \eta^2$, де η – енергетичний масштаб порушення симетрії, що визначається перебудовою ефективного потенціалу з появою ненульового вакуумного середнього поля в новому мінімумі потенціалу (аналог поля Гіґса $\eta \sim m_H$, m_H – маса поля Гіґса), що є відповідальним за порушення відповідної симетрії. Зокрема, для космічних струн, що утворилися на масштабі теорії Великого об'єднання маса одиниці довжини космічної струни становить 10^{22} г/см, а поперечний радіус $r_0 \sim 10^{-30}$ см (визначається умовою $m_H r_0 \sim 1$).

В астрофізиці космічні струни можуть проявити себе по впливу на анізотропію реліктового випромінення [73], можуть виступати в ролі гравітаційних лінз [74], джерела гравітаційних хвиль [75–77].

Модельно незалежні дані спостережень анізотропії реліктового випромі-

нення накладають обмеження на безрозмірний параметр $G\mu < 1.07 \cdot 10^{-5}$. Існують більш жорсткі обмеження, що враховують існування сітки струн у Всесвіті, і становлять $G\mu < 1.1 \cdot 10^{-7}$ [78]. Параметр $G\mu \sim (m_H/M_{Pl})^2$, де m_H – маса поля Гіґса, яке відповідальне за спонтанне порушення відповідної симетрії. Отже, існуючі обмеження з даних спостережень закривають лише космічні струни, що могли утворитися на дуже великих масштабах енергій, трохи менших за масштаб теорії Великого об'єднання.

Однак, ще не всі макроефекти, обумовлені космічними струнами, є достатньо дослідженими. Зокрема, ще не достатньо теоретично досліджені явища, пов'язані з впливом космічної струни на вакуум полів матерії. Зокрема, ефект має полягати у поляризації вакууму (зміні густини енергії вакууму), індукуванню вакуумних струмів, магнітного поля та інших квантових чисел. Це є важливим з таких міркувань.

Найпростіша модель, в якій виникають космічні струни з калібрувальним полем, це абелева калібрувально інваріантна модель Гіґса відносно групи $U_X(1)$, в якій відбулося спонтанне порушення симетрії [64]. Якщо в такій моделі, в результаті фазового переходу, утвориться лінійний топологічний дефкт, то ззовні нього поле Гіґса матиме ненульове вакуумне середнє. Всередині ж топологічного дефекту поле Гіґса знаходитиметься у фазі з непорушеною симетрією і калібрувальне поле групи $U_X(1)$ буде безмасовим. Для стану з найменшою енергією відповідні аналоги електричного та магнітного полів групи $U_X(1)$ ззовні топологічного дефекту дорівнюватимуть нулю, але статичний векторний потенціал можна обрати у вигляді "чистого" калібрування $\mathbf{A} = \boldsymbol{\nabla}\chi$. Зміна фази польової функції при обході навколо струни дорівнюватиме

$$\Delta\alpha = 2\pi n = e_H \oint \mathbf{A}\, d\mathbf{r} = e_H \oint \boldsymbol{\nabla}\chi\, d\mathbf{r} = e_H \chi|_{\varphi=0}^{\varphi=2\pi} = e_H \Phi, \quad n \in \mathbb{Z}$$

тобто функція χ не є однозначною, що є можливим лише в неоднозв'язному

просторі, тобто в просторі, де не всі криві можуть бути неперервним чином стиснуті в точку за рахунок наявності топологічного дефекту. Тобто польові розв'язки в просторі з космічною струною будуть характеризуватися приналежністю до першої гомотопічної групи.

Як видно з останньої формули, всередині космічної струни буде існувати "магнітне" поле (створюється калібрувальним полем групи $U_X(1)$), потік якого всередині струни є квантованим $\Phi = 2\pi n/e_H$, де e_H – стала зв'язку кванта поля Гіґсівського конденсату з калібрувальним полем групи $U_X(1)$.

Розглянемо тепер квантовані поля матерії на фоні космічної струни, частинки яких взаємодіють з калібрувальним полем групи $U_X(1)$ зі сталою зв'язку e_{matter}. Виявиться, що польові розв'язки будуть визначатися параметром $e_{matter}\Phi/(2\pi) = ne_{matter}/e_H$, що може приймати нецілі значення. Квантові ефекти, які будуть далі описані, призводять до виникнення вакуумного струму полів матерії навколо космічної струни. Якщо припустити, що поля матерії заряджені також відносно електромагнітної групи $U_{EM}(1)$, то відповідний струм електрично заряджених частинок створюватиме навколо космічної струни магнітне поле, прояви якого можна шукати з даних спостережень. Можуть спостерігатися і інші ефекти поляризації вакууму навколо космічної струни. Дослідження цих ефектів може пролити світло на фізику раннього Всесвіту та фізику за межами СМ.

Необхідно відзначити, що у фізиці конденсованого стану аналогом космічних струн з калібрувальним полем можуть виступати вихори Абрикосова в надпровідниках другого роду [79]. В цьому випадку $U_X(1)$ це група електромагнітного поля, $e_H = 2e$ – заряд куперівських пар, $e_{matter} = e$, де e – заряд електрона.

Історично, задачу поляризації вакууму навколо космічної струни з калібрувальним полем спершу розв'язували в наближенні струни нульової товщини і для випадку скалярного поля матерії. Були отримані вирази для

індукованої густини вакуумної енергії, вакуумного струму та індукованого магнітного потоку [80–85]. В цьому випадку на розв'язки польових функцій скалярного поля матерії накладалася умова регулярності на поверхні струни (польові функції занулялися). Накладанням граничної умови фактично забезпечувалася умова непроникнення матерії в область "магнітного" поля струни, а вакуумні ефекти, які при цьому виникали можна пов'язати з ефектом Казимира [86, 87]. З іншого боку, в даній задачі розв'язки польових функцій матерії залежали від потенціалу калібрувального поля ззовні струни, хоча "магнітне" поле містилося лише в серцевині струни. Це є проявом ефекту Ааронова-Бома [88]. В результаті вплив "магнітної" струни на поля матерії ззовні струни отримав назву ефекту Казимира-Ааронова-Бома [81]. Недоліками моделі сингулярної "магнітної" струни були нескінченні значення індукованих величин поблизу струни: густина індукованої енергії вела себе як $\sim r^{-(d+1)}$, а поведінка індукованого струму навколо струни $\sim r^{-d}$, де r – відстань від струни в поперечному напрямку, d – кількість просторових вимірів. Зазначимо, що при віддаленні струни квантові ефекти експоненційно спадали e^{-mr} (m – маса кванта поля матерії), а ефект залежав лише від дробової частини "магнітного" потоку космічної струни $F = e_{matter}\Phi/(2\pi) - [[e_{matter}\Phi/(2\pi)]]$ та зникав при цілих значеннях "магнітного" потоку.

Для задачі впливу сингулярної "магнітної" струни на вакуум спінорного поля матерії виявилося, що на поверхні вихору не можна накласти умову регулярності. Справа в тому, що ферміонні функції багатокомпонентні (4 компоненти для випадку 3+1 простору-часу, 2 компоненти для 2+1 простору-часу) і для деяких окремих (особливих) мод одні компоненти можуть задовільняти умові регулярності, а інші ні. Вперше цю проблему було вирішено в роботах [89,90]. Було зазначено, що проблема нерегулярності розв'язку спінорних функцій пов'язана з тим, що парціальні діраковські

гамільтоніани для особливих мод не є самоспряженим. Справді, нехай h є оператором, що діє на регулярні функції $\psi^0(r)$, тоді спряжений до нього оператор h^+ визначається з умови

$$\int_0^\infty r\,dr[h^+\psi(r)]^+\psi^0(r) = \int_0^\infty r\,dr[\psi(r)]^+[h\psi^0(r)],$$

де функція $\psi(r)$ не обов'язково має бути регулярною.

Оператор h стане самоспряженим, якщо розширити набір функцій на які діє оператор h, так щоб він та оператор, спряжений до нього, діяли на спільний набір функцій. Це можна зробити для випадку сингулярного "магнітного" вихору користуючись теорією самоспряженого розширення операторів фон Неймана (див. [91, 92]), що визначає всі можливі значення константи в лінійній комбінації двох розв'язків для особливої моди та фіксованому "магнітному" потоці за допомогою одного параметра Θ ($0 \leq \Theta < 2\pi$). Цей параметр отримав назву параметра самоспряженого розширення. Для випадку сингулярної "магнітної" струни всі значення параметра Θ є теоретично дозволеними.

В роботі [93] було вперше отримано вираз для густини індукованої вакуумної енергії та індукованого струму для спінорного вакууму в присутності сингулярної "магнітної" струни для часткового значення параметра самоспряженого розширення Θ. Для довільного значення параметра Θ ці величини були пораховані в роботах [94, 95]. Було показано, що індуковані квантові ефекти також залежать лише від дробової частини "магнітного" потоку F та мали степеневу розбіжність поблизу струни. Зазначимо також, що у випадку, коли рух частинок зафіксований в площині перпендикулярній до космічної струни (компонента імпульсу $p_z = 0$), то тривимірну задачу можна звести до двовимірної, що суттєво спрощує розрахунки. В роботі [96] було показано яким чином можна записати розв'язок у $3+1$ вимірному просторі-часі знаючи розв'язок у $2+1$ вимірному просторі-часі.

Підсумовуючи, зазначимо, що велика перевага наближення нульового радіуса "магнітної" струни полягає в достатньо простих розв'язках для польових функцій, що дозволяє явно виконати всі розрахунки та отримати результати в аналітичному вигляді. Проблемою ж наближення нульового радіуса струни є степенева розбіжність індукованих величин поблизу "магнітної" струни $\sim r^{-\alpha}$.

Очевидно, що для позбавлення розбіжності викликаних нульовою товщиною "магнітної" струни слід розглядати фізичну постановку задачу та враховувати скінченне значення товщини струни. Це було зроблено аналітично для окремих конфігурацій розподілу "магнітного" поля всередині струни [97–99]. В роботі [100] був запропонований метод чисельного розрахунку для задачі космічної струни скінченного радіуса з довільним розподілом "магнітного" поля всередині струни. Цей метод дозволив отримати індуковану вакуумну енергію спінорного чи бозонного полів за наявності космічної струни скінченного радіуса з "магнітним" полем різноманітної конфігурації [101–106]. В наведених роботах вважалося, що поле матерії проникає в область, де знаходиться "магнітне" поле струни. Виявилося, що квантові ефекти в області з "магнітним" полем струни залежать від повного "магнітного" потоку струни, а квантові явища ззовні області "магнітного" поля струни залежать лише від дробової частини "магнітного" потоку струни [107–109]. Тому квантові ефекти, що мають враховувати область з "магнітним" полем та без нього (наприклад, повна індукована енергія вакууму) в такій постановці задачі виявилася залежними від значення повного "магнітного" потоку струни.

Основну увагу в дисертаційній роботі присвячено дослідженню фізики за межами Стандартної моделі фізики елементарних частинок. Дослідження проводилися на масштабі енергій доступних на сучасних прискорювачах, а саме розглядалися різні аспекти можливих експериментальних про-

явів частинок нової фізики, а саме скалярного, нейтринного та із взаємодією типу Черна-Саймонса порталів фізики за межами СМ. Розглядалися можливі топологічні прояви фізики за межами СМ з масштабом енергій, що значно перевищує можливості сучасних прискорювачів. А саме, розглядалися квантові ефекти у вакуумі полів скалярної та ферміонної матерії в присутності космічної струни з "магнітним" полем калібрувальної групи $U_X(1)$, що могла утворитися внаслідок фазових переходів у ранньому Всесвіті. Космічна струна моделювалася непроникливою для полів матерії трубкою скінченого радіуса з "магнітним" полем, що дозволило розглянути квантові ефекти у вакуумі полів матерії в самому загальному випадку незалежно від конкретної природи утворення космічної струни припускаючи, що поля матерії заряджені відносно калібрувальної групи $U_X(1)$.

Актуальність роботи обумовлена розробкою багаточисельних експериментів на прискорювачах (SHiP, FASER, FACET, MATHUSLA, DUNE тощо), що почнуть свою роботу в найближче десятиліття з метою пошуку проявів легких частинок нової фізики, а також зростаючі можливості астрофізичних спостережень, зокрема в напрямку анізотропії реліктового випромінення та спостереження гравітаційних хвиль. Проведені в дисертаційній роботі дослідження мають і фундаментальне значення, розкриваючи теоретико-польовий прояв ефектів Ааронова-Бома та ефекту Казимира.

Зв'язок роботи з науковими програмами і темами. Робота виконана у рамках досліджень, що проводяться на кафедрі квантової теорії поля та космомікрофізики фізичного факультету Київського національного університету імені Тараса Шевченка: тема №16БФ051-05 "Дослідження фундаментальних проблем фізики ядра, елементарних частинок та космомікрофізики"; тема №19БФ051-06 "Топологічні властивості кіральної матерії та бозе-айнштайнівських конденсатів у магнітному полі"; тема

№22БФ051-06 "Фундаментальні закони фізики в космології раннього Всесвіту". Робота також виконувалася в рамках проекту ДФФД №Ф54.1/019 "Ефекти неевклідової геометрії і топології в мікро- та макросистемах у зовнішніх полях" та гранту Швейцарського національного наукового фонду SCOPE IZ 7370-152581. Згідно з договором між Київським національним університетом та Європейської організації з ядерних досліджень (ЦЕРН), Горкавенко В.М. є членом міжнародної колаборації SHiP (Search for hidden particles), що займається пошуком частинок нової фізики.

Мета дослідження: розгляд можливих експериментальних проявів частинок нової фізики в експериментах на прискорювачах та проявів лінійних топологічних дефектів у вигляді космічних струн з "магнітним" полем калібрувальної групи $U_X(1)$, що виникли внаслідок фазових переходів у ранньому Всесвіті.

Завдання дослідження:

1. В скалярному розширенні СМ знайти та дослідити домінуючі канали народження та розпаду нових скалярів з масою в декілька ГеВ для експериментів DUNE (Fermilab), SHiP (SPS CERN) та експериментів на LHC.

2. У нейтринному розширенні СМ трьома масивними правокіральними нейтрино дослідити зв'язок юкавівської матриці, що визначає взаємодію правокіральних нейтрино з параметрами активних нейтрино.

3. У нейтринному розширенні СМ дослідити коректність використання матричних елементів в середовищі PYTHIA для опису народження правокіральних нейтрино в тричастинкових розпадах мезонів в умовах експерименту SHiP.

4. В розширенні СМ зі взаємодією типу Черна-Саймонса побудувати ефе-

ктивний лагранжіан взаємодії нових калібрувальних векторних бозонів з кварками різних ароматів та дослідити народження зазначених бозонів в мезонних розпадах.

5. Дослідити індуковану густину енергії та повну індуковану енергію у вакуумі квантованого масивного скалярного поля зарядженого відносно поля калібрувальної групи $U_X(1)$ в присутності космічної струни з "магнітним" полем калібрувальної групи $U_X(1)$, що моделюється непроникливою для полів матерії трубкою скінченного радіуса з "магнітним" полем у просторі довільної розмірності за наявності сталої зв'язку скалярного поля з кривизною простору-часу.

6. Дослідити індукований магнітний потік у вакуумі квантованого масивного скалярного поля зарядженого відносно поля калібрувальної групи $U_X(1)$ та електромагнітного поля в присутності космічної струни з "магнітним" полем калібрувальної групи $U_X(1)$, що моделюється непроникливою для полів матерії трубкою скінченного радіуса з "магнітним" полем у конічному просторі довільної розмірності в загальному випадку граничної умови типу Робена. Дослідити залежність індукованого магнітного потоку в цьому випадку від значень параметра граничної умови.

7. Дослідити індукований магнітний потік у вакуумі квантованого масивного ферміонного поля зарядженого відносно поля калібрувальної групи $U_X(1)$ та електромагнітного поля в присутності космічної струни з "магнітним" полем калібрувальної групи $U_X(1)$, що моделюється непроникливою для полів матерії трубкою скінченного радіуса з "магнітним" полем у конічному просторі-часі розмірності 2+1.

8. Записати загальний вигляд граничної умови на ферміонне поле матерії на поверхні трубки скінченого радіусу виходячи з умови самоспря-

женого розширення оператора дираковського гамільтоніана. Накласти фізичні обмеження на можливі значення параметра самоспряженого розширення виходячи з умови скінченності значень індукованого магнітного потоку.

Об'єктом дослідження є скалярні, ферміонні та векторні масивні частинки за межами Стандартної моделі фізики елементарних частинок; вакуум бозе та фермі полів матерії за наявності лінійного топологічного дефекту у вигляді "магнітної" космічної струни.

Предметом дослідження є канали народження та розпаду нових скалярів з масою в декілька ГеВ (в скалярному розширенні СМ) для експериментів DUNE, SHiP та експериментів на LHC; народження масивних правокіральних нейтрино (в нейтринному розширенні СМ) в тричастинкових розпадах мезонів в умовах експерименту SHiP; зв'язок юкавівської матриці, що визначає взаємодію правокіральних нейтрино нейтринного розширення СМ з параметрами активних нейтрино; народження масивних векторних бозонів в розпадах мезонів в розширенні СМ зі взаємодією типу Черна-Саймонса; індукування енергії у вакуумі скалярного поля в присутності топологічного дефекту у вигляді "магнітної" космічної струни; індукування магнітного потоку у вакуумі квантованого масивного зарядженого скалярного та ферміонного полів в присутності топологічного дефекту у вигляді "магнітної" космічної струни.

Методи дослідження полягають у застосуванні апарату вторинного квантування, методів регуляризації і перенормування в квантовій теорії поля, формалізму діаграмної техніки Фейнмана, а також чисельних методів для розрахунку на комп'ютері функцій розподілу народжених частинок, розрахунку значень інтегралів та суми рядів.

Наукова новизна одержаних результатів. Наукова новизна результатів, наведених в дисертаційній роботі, міститься в дослідженнях пошуку проявів частинок нової фізики скалярного, нейтринного та векторного розширень СМ, а також дослідженнях квантових ефектів, що індукуються у вакуумі скалярного та ферміонного полів матерії топологічним дефектом у вигляді космічної струни з "магнітним" полем калібрувальної групи $U_X(1)$, що моделюється непроникливою для полів матерії трубкою скінченного радіуса з "магнітним" полем. Дана модель дозволила розглянути квантові ефекти у вакуумі полів матерії в самому загальному випадку незалежно від конкретної природи утворення космічної струни припускаючи, що поля матерії заряджені відносно калібрувальної групи $U_X(1)$.

Основними науковими результатами, що виносяться на захист, є такі:

- Зроблено повний і самоузгоджений опис всіх каналів розпаду масивних скалярів з масою в декілька ГеВ в скалярному розширенні СМ.
- Послідовно розглянуто всі канали народження масивного скаляру з розпадів K та B мезонів, включаючи народження скалярів у розпадах B мезонів у різні збуджені стани каонів.
- Проаналізовано прямі канали народження масивного скаляру в протон-нуклонних зіткненнях в залежності від енергії частинок, що зіштовхуються.
- Знайдено домінуючі канали народження та розпаду масивних скалярів для умов експериментів DUNE, SHiP та експериментів на LHC.
- Послідовно розглянуто всі канали народження масивного векторного бозону (в розширенні СМ зі взаємодією типу Черна-Саймонса) з розпадів K та B мезонів, включаючи народження векторних бозонів у розпадах B мезонів у різні збуджені стани каонів.

- Отримано оригінальні розв'язки та виражено елементи юкавівської матриці в нейтринному розширенні СМ з параметрами масової матриці активних нейтрино.

- Проаналізовано коректність використання матричних елементів середовища PYTHIA для опису народження правокіральних масивних нейтрино в тричастинкових розпадах мезонів в умовах експерименту SHiP. Запропоновано вибір спрощених матричних елементів середовища PYTHIA, що дають найменше відхилення від коректних розрахунків.

- Отримано аналітичні вирази у вигляді інтегралів від рядів з нескінченними межами для поляризації вакууму квантованого масивного зарядженого скалярного поля матерії в присутності "магнітної" космічної струни в просторі-часі довільної розмірності. За допомогою чисельних методів побудовано графічні залежності індукованої густини енергії у вакуумі скалярного поля матерії за різних значень сталої зв'язку скалярного поля з кривизною простору-часу для випадку граничної умови на поверхні трубки типу Діріхле.

- Отримано чисельні значення повної індукованої енергії у вакуумі квантованого масивного зарядженого скалярного поля в просторі-часі довільної розмірності в присутності "магнітної" космічної струни в просторі-часі довільної розмірності. Показано, що у випадку граничної умови на поверхні трубки типу Діріхле повна індукована енергія не залежить від сталої зв'язку скалярного поля з кривизною простору-часу.

- Показано, що ефект поляризації вакууму квантованого зарядженого скалярного поля матерії в присутності "магнітної" космічної струни у

випадку граничної умови на поверхні трубки типу Неймана є суттєво більшим в порівнянні з випадком граничної умови на поверхні трубки типу Діріхле.

- Показано, що поляризація вакууму буде суттєвою у випадку, коли маса квантованого поля матерії є значно меншою за масу Гіґсівського поля, що призвело до спонтанного порушення симетрії і виникнення топологічного ефекту у вигляді "магнітної" космічної струни. Іншими словами, "магнітна" космічна струна, що була сформована на масштабах теорії Великого об'єднання буде поляризувати вакуум сучасних полів матерії, але не зможе впливати на вакуум полів з масою порядку масштабу теорії Великого об'єднання.

- Отримано аналітичні вирази у вигляді інтегралів від рядів з нескінченними межами для індукованого магнітного потоку у вакуумі квантованого масивного зарядженого скалярного поля в присутності "магнітної" космічної струни у конічному просторі довільної розмірності в загальному випадку граничної умови типу Робена. Для генерації в системі магнітного поля кванти поля матерії повинні також мати електричні заряди.

- За допомогою чисельних методів досліджено поведінку індукованого магнітного потоку у вакуумі квантованого масивного зарядженого скалярного поля в присутності "магнітної" космічної струни від значень параметра граничної умови типу Робена на всьому проміжку можливих значень цього параметра $-\pi/2 \leq \theta < \pi/2$.

- Показано, що за недодатних значень параметра $-\pi/2 \leq \theta \leq 0$ індукований магнітний потік у вакуумі квантованого масивного зарядженого скалярного поля в присутності "магнітної" космічної струни є

найбільшим для випадку $\theta = -\pi/2$ (гранична умова типу Неймана), а найменшим він є для випадку $\theta = 0$ (гранична умова типу Діріхле).

- Показано, що за додатніх значень параметра $0 < \theta < \pi/2$ існують розв'язки, що відповідають зв'язаним станам. Індукований магнітний потік у вакуумі квантованого масивного зарядженого скалярного поля в присутності "магнітної" космічної струни має складну поведінку з особливими точками яких тим більше, чим ближче значення параметра θ до нуля. Індукований магнітний потік може бути більшим та не занулятися при значно більших товщинах космічної струни в порівнянні з потоком, що індукується за граничної умови типу Робена з недодатним значенням параметра θ.

- Отримано загальний вигляд граничної умови на ферміонне поле матерії на поверхні трубки скінченого радіусу виходячи з умови самоспряженого розширення оператора діраковського гамільтоніана в присутності "магнітної" космічної струни у конічному просторі-часі розмірності 2+1.

- Отримано аналітичні вирази у вигляді інтегралів від рядів з нескінченними межами для індукованого магнітного потоку у вакуумі квантованого масивного зарядженого ферміонного поля в присутності "магнітної" космічної струни у конічному просторі-часі розмірності 2+1.

- За допомогою чисельних методів в просторі-часі розмірності 2+1 досліджено поведінку індукованого магнітного потоку у вакуумі квантованого масивного зарядженого ферміонного поля в присутності "магнітної" космічної струни від значень параметра самоспряженого розширення. Знайдені значення параметра самоспряженого розширення, за яких повний індукований потік є скінченним.

- Показано, що умова скінченності значення індукованого потоку у вакуумі квантованого масивного зарядженого ферміонного поля в присутності "магнітної" космічної струни є недостатньою для визначення фізичних значень параметра самоспряженого розширення. Існує значення параметра самоспряженого розширення при якому індукований потік є скінченним, а квантові ефекти зростають при збільшенні товщини космічної струни, що є нефізичним.

Практичне значення одержаних результатів. Результати представлені в дисертації є важливими для експериментального пошуку легких частинок нової фізики (скалярних, ферміонних та векторних) на прискорювачах в сучасних експериментах типу SHiP (SPS CERN), DUNE (Fermilab) та експериментів на LHC. Отримані результати можуть бути застосовані в астрофізиці для опису прояву ефектів, викликаних топологічними дефектами утвореними у ранньому Всесвіті, а саме космічними струнами з "магнітним" полем калібрувальної групи $U_X(1)$. Результати представлені в дисертації також мають фундаментальне значення, розкриваючи теоретико-польовий прояв ефекту Казимира-Ааронова-Бома.

Публікації. Основні результати роботи викладено у 12 фахових наукових виданнях. Список праць за темою дисертації [1]^a – [12]^a подано після анотації та в додатку А.

Особистий внесок здобувача. У виконаних із співавторами роботах, здобувачеві належить:

- постановка задачі; запис аналітичних виразів для перенормованої індукованої густини енергії; розробка методу чисельного розрахунку поляризації вакууму масивного зарядженого поля матерії в присутності космічної струни, що моделюється непроникливою для полів матерії

трубкою скінченного радіуса з "магнітним" полем; проведення чисельного розрахунку поляризації вакууму [1]^a.

- постановка задачі; розв'язок рівняння, що пов'язує елементи юкавівської матриці з параметрами активних нейтрино; проведення чисельних розрахунків; підготовка рукопису статті [2]^a.

- проведення чисельного розрахунку індукованої густини енергії та повної енергії вакууму масивного зарядженого поля матерії в присутності космічної струни, що моделюється непроникливою для полів матерії трубкою скінченного радіуса з "магнітним" полем в (2+1)-вимірному просторі-часі; доведення незалежності повної індукованої енергії вакууму скалярного поля від сталої зв'язку скалярного поля з кривизною простору-часу [3]^a.

- проведення чисельного розрахунку індукованої густини енергії та повної енергії вакууму масивного зарядженого поля матерії в присутності космічної струни, що моделюється непроникливою для полів матерії трубкою скінченного радіуса з "магнітним" полем в $(d+1)$-вимірному просторі-часі; отримання аналітичних виразів для величини, аналога сили Казимира, що намагається збільшити радіус непроникливої трубки з "магнітним" полем; чисельний розрахунок величини, аналога сили Казимира [4]^a.

- постановка задачі; проведення чисельного розрахунку індукованого струму, магнітного поля та магнітного потоку у вакуумі скалярного поля у випадку простору-часу розмірності $2+1$ та $3+1$ [5]^a.

- проведення чисельного розрахунку індукованого струму та магнітного потоку у вакуумі ферміонного поля; знаходження значень параметра самоспряженого розширення дираковського гамільтоніана, при

яких індукований магнітний потік є скінченним; доведення, що умова скінченності значення індукованого потоку є недостатньою для визначення фізичних значень параметра самоспряженого розширення; знаходження значення параметра самоспряженого розширення при якому індукований потік є скінченним, а квантові ефекти зростають при збільшенні товщини космічної струни, що є нефізичним [6][a].

- проведення розрахунків утворення скалярів в розпадах B та D мезонів; проведення розрахунків утворення скалярів в результаті фотонної взаємодії при розсіянні протонів на ядрах мішені [7][a].

- проведення аналітичних розрахунків; перевірка коректності проведення чисельних розрахунків; аналіз та інтерпретація результатів; підготовка рукопису статті [8][a].

- розрахунок петльової діаграми, що визначає взаємодію векторного бозона (розширення СМ зі взаємодією типу Черна-Саймонса) з кварками різних ароматів; запис в спрощеному вигляді ефективного лагранжіану взаємодії векторного бозона з кварками різних ароматів; розрахунок ймовірності народження векторних бозонів з розпадів нейтральних каонів; підготовка рукопису статті [9][a].

- проведення чисельних розрахунків індукованого магнітного потоку; доведення необхідності врахування внеску зв'язаних станів; знаходження значень енергії зв'язаних станів та їх внеску в індукований магнітний потік; трактовка поведінки індукованого магнітного потоку за наявності зв'язаних станів в системі [10][a].

- постановка задачі; проведення чисельних розрахунків густини індукованого вакуумного струму у випадку простору-часу розмірності $2+1$ та $3+1$; підготовка рукопису статті [11][a].

- постановка задачі; запис аналітичних виразів для перенормованої індукованої густини енергії; перевірка коректності проведення чисельних розрахунків індукованої густини енергії; підготовка рукопису статті [12][a].

Апробація результатів дисертації. Основні результати досліджень доповідалися на наукових семінарах кафедри квантової теорії поля та космомікрофізики фізичного факультету Київського національного університету імені Тараса Шевченка та наукових конференціях:

- Міжнародна конференція молодих вчених та аспірантів "ІЕФ, 2011", Інститут Електронної Фізики НАН України (Україна, Ужгород, 24-27 травня 2011 р).
- III Young Scientists Conference Modern Problems of Theoretical Physics. 21-23 December 2011. Bogolyubov Institute for Theoretical Physics of the NAS of Ukraine, Kyiv, Ukraine.
- 20-th Open Young Scientists' Conference on Astronomy and Space Physics. April 22-27, 2013, Kyiv, Ukraine.
- International Conference on p-Adic Mathematical Physics and its Applications (Belgrade, Serbia, 07-12 September 2015).
- 3-rd Walter THIRRING International School "Fundamentals of Astroparticle and Quantum Physics" , 17 - 23 September 2017, BITP, Kyiv, Ukraine.
- The International Conference "CERN-Ukraine Cooperation: Current State and Prospects" (Institute for Scintillation Materials NAS of Ukraine, Kharkiv, 15-17 May, 2018).
- New trends in high-energy physics, 21-th International conference organized by the Bogolyubov Institute for Theoretical Physics, National Academy

of Sciences of Ukraine, held in Odessa (Ukraine) on May 12–18, 2019.

- XI Bolyai-Gauss-Lobachevsky Conference: Non-Euclidean, Non- Commutative Geometry and Quantum Physics. May 19-24, 2019, Bogolyubov Institute for Theoretical Physics, Kyiv (Ukraine).

- X Young Scientists Conference Modern Problems of Theoretical Physics. 23- 24 December 2019. Bogolyubov Institute for Theoretical Physics of the NAS of Ukraine, Kyiv, Ukraine.

- XI Young Scientists Conference Modern Problems of Theoretical Physics. 21-23 December 2020. Bogolyubov Institute for Theoretical Physics of the NAS of Ukraine, Kyiv, Ukraine.

РОЗДІЛ 1

Пошук проявів частинок нової фізики

1.1. Феноменологія скалярного порталу на масштабі в декілька ГеВ

Published for SISSA by Springer

Received: May 13, 2019
Revised: September 25, 2019
Accepted: November 14, 2019
Published: November 27, 2019

Phenomenology of GeV-scale scalar portal

Iryna Boiarska,[a] **Kyrylo Bondarenko,**[b] **Alexey Boyarsky,**[b] **Volodymyr Gorkavenko,**[c] **Maksym Ovchynnikov**[b] **and Anastasia Sokolenko**[d]

[a] *Discovery Center, Niels Bohr Institute, Copenhagen University, Blegdamsvej 17, DK-2100, Copenhagen, Denmark*
[b] *Intituut-Lorentz, Leiden University, Niels Bohrweg 2, 2333 CA, Leiden, The Netherlands*
[c] *Department of Physics, Taras Shevchenko National University of Kyiv, 64 Volodymyrs'ka str. 01601, Kyiv, Ukraine*
[d] *Department of Physics, University of Oslo, Box 1048, NO-0371, Oslo, Norway*

E-mail: boiarska@nbi.ku.dk, bondarenko@lorentz.leidenuniv.nl, boyarsky@lorentz.leidenuniv.nl, gorkavol@gmail.com, ovchynnikov@lorentz.leidenuniv.nl, anastasia.sokolenko@fys.uio.no

Abstract: We review and revise the phenomenology of the scalar portal — a new scalar particle with the mass in GeV range that mixes with the Higgs boson. In particular, we consider production channels $B \to SK_1(1270)$ and $B \to SK_0^*(700)$ and show that their contribution is significant. We extend the previous analysis by comparing the production of scalars from decays of mesons, of the Higgs bosons and direct production via proton bremsstrahlung, deep inelastic scattering and coherent scattering on nuclei. Relative efficiency of the production channels depends on the energy of the beam and we consider the energies of DUNE, SHiP and LHC-based experiments. We present our results in the form directly suitable for calculations of experimental sensitivities.

Keywords: Beyond Standard Model, Higgs Physics

ArXiv ePrint: 1904.10447

https://doi.org/10.1007/JHEP11(2019)162

JHEP11(2019)162

Contents

1 Introduction **1**

2 Scalar production **1**
2.1 Mixing with the Higgs boson 1
2.2 Quartic coupling 10

3 Scalar decays **12**

4 Conclusion **15**

A Effective interactions **16**
A.1 Photons and gluons 16
A.2 Nucleons 17
A.3 Flavor changing effective Lagrangian 19

B Scalar production from mesons **19**
B.1 Inclusive production 20
B.2 Scalar production in two-body mesons decays 21
B.3 Scalar production in leptonic decays of mesons 21

C DIS **22**

D Scalar production in proton bremsstrahlung **24**
D.1 Splitting probability derivation 25

E Scalar production in photon fusion **28**

F Form-factors for the flavor changing neutral current meson decays **31**
F.1 Scalar and pseudoscalar final meson state 31
F.1.1 Pseudoscalar 31
F.1.2 Scalar 32
F.2 Vector and pseudovector final meson state 33
F.2.1 Vector 33
F.2.2 Pseudo-vector 34
F.3 Tensor final meson state 35

G Production from mesons through quartic coupling **36**

H Decays of a scalar **37**
H.1 Decay into leptons and photons 37
H.2 Decays into quarks and gluons 37

JHEP11(2019)162

1 Introduction

We review and revise the phenomenology of the scalar portal — a gauge singlet scalar particle S that couples to the Higgs boson and can play a role of a mediator between the Standard model and a dark sector (see e.g. [1–3]) or be involved in the cosmological inflation [4–6]. We focus here on the mass range $\lesssim 10$ GeV (see however section 2.2 for a discussion of larger masses).

The interaction of the S particle with the Standard model particles is similar to the interaction of a light Higgs boson but is suppressed by a small mixing angle θ. Namely, the Lagrangian of the scalar portal is

$$\mathcal{L} = \mathcal{L}_{\rm SM} + \frac{1}{2}\partial_\mu S \partial^\mu S + (\alpha_1 S + \alpha_2 S^2)(H^\dagger H) - \frac{m_S^2}{2} S^2. \tag{1.1}$$

After the electroweak symmetry breaking the Higgs doublet gains a non-zero vacuum expectation value v. As a result, the SHH interaction (1.1) provides a mass mixing between S and the Higgs boson h. Transforming the Higgs field into the mass basis, $h \to h + \theta S$, one arrives at the following interaction of S with the SM fermions and gauge bosons:

$$\mathcal{L}^S_{\rm SM} = -\theta \frac{m_f}{v} S \bar{f} f + 2\theta \frac{m_W^2}{v} S W^+ W^- + \theta \frac{m_Z^2}{v} S Z^2 + \alpha \left(\frac{1}{4v} S^2 h^2 + \frac{1}{2} S^2 h \right), \tag{1.2}$$

where $\alpha \equiv 2\alpha_2 v$. These interactions also mediate effective couplings of the scalar to photons, gluons, and flavor changing quark operators, see figure 1. Additionally, the effective proton-scalar interaction that originates from the interaction of scalars with quarks and gluons (see figure 2) will also be relevant for our analysis. The effective Lagrangian for these interactions is discussed in appendix A.

Searches for light scalars have been previously performed by CHARM, LHCb and Belle [7, 8], CMS [9] and ATLAS [10, 11] experiments. Significant progress in searching for light scalars can be achieved by the proposed and planned intensity-frontier experiments SHiP [12–14], CODEX-b [15], MATHUSLA [16–21], FASER [22–24], SeaQuest [25], NA62 [26–28], DUNE [29].

The phenomenology of light GeV-like scalars has been studied in [1, 5, 8, 30–33], and in [34–43] in the context of a light Higgs boson. However, in the literature, there are still conflicting results, both for the scalar production and decay. In this work, we reanalyze the phenomenology of light scalars and present the results in the form directly suitable for experimental sensitivity estimates.

2 Scalar production

2.1 Mixing with the Higgs boson

In this section, we will discuss the scalar production channels that are defined by the mixing between a scalar and the Higgs boson.

In proton-proton or proton-nucleus collisions, a scalar particle: (a) can be emitted by the proton, (b) produced from photon-photon, gluon-gluon or quark-antiquark fusion

JHEP11(2019)162

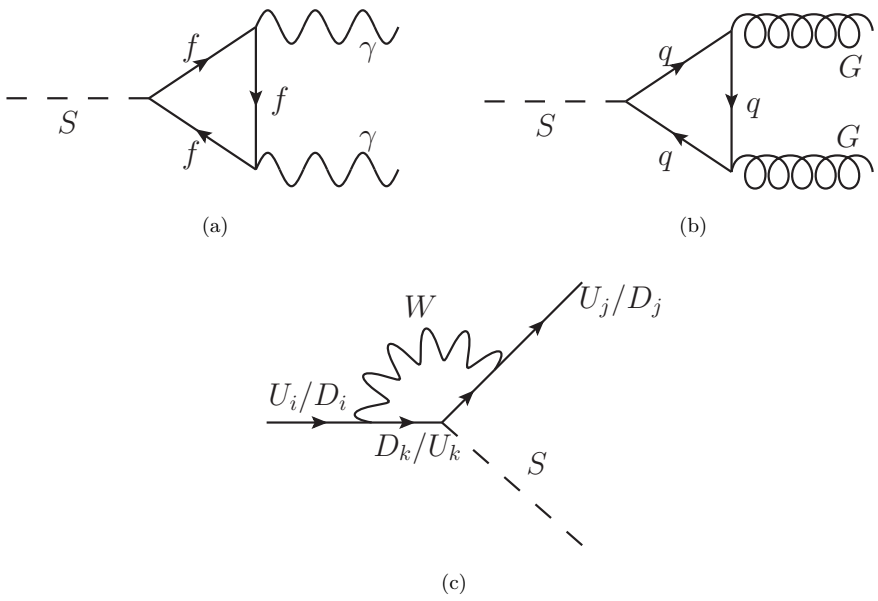

Figure 1. Examples of effective interactions of the scalar with photons (a), gluons (b), and flavor changing quark operators (c). (See appendix A for details.)

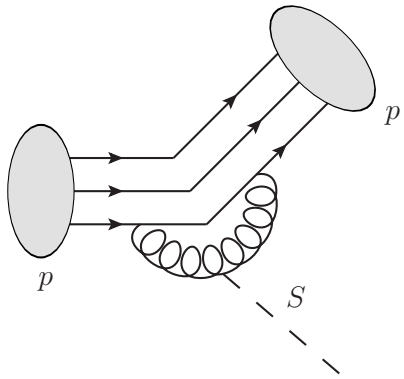

Figure 2. An example of a diagram for the effective interaction of a proton with a scalar, see appendix A.2 for details.

in proton-proton or proton-nucleus interactions or (c) produced in the decay of the secondary particles, see figure 3. Let us compare these three types of the scalar production mechanisms depending on the collision energy and the scalar mass. In the following we will present the results for three referent proton-proton center-of-mass energies: $\sqrt{s_{pp}} \approx 16$ GeV (corresponding to the beam energy of the DUNE experiment), $\sqrt{s_{pp}} \approx 28$ GeV (SHiP) and $\sqrt{s_{pp}} = 13$ TeV (LHC).

JHEP11(2019)162

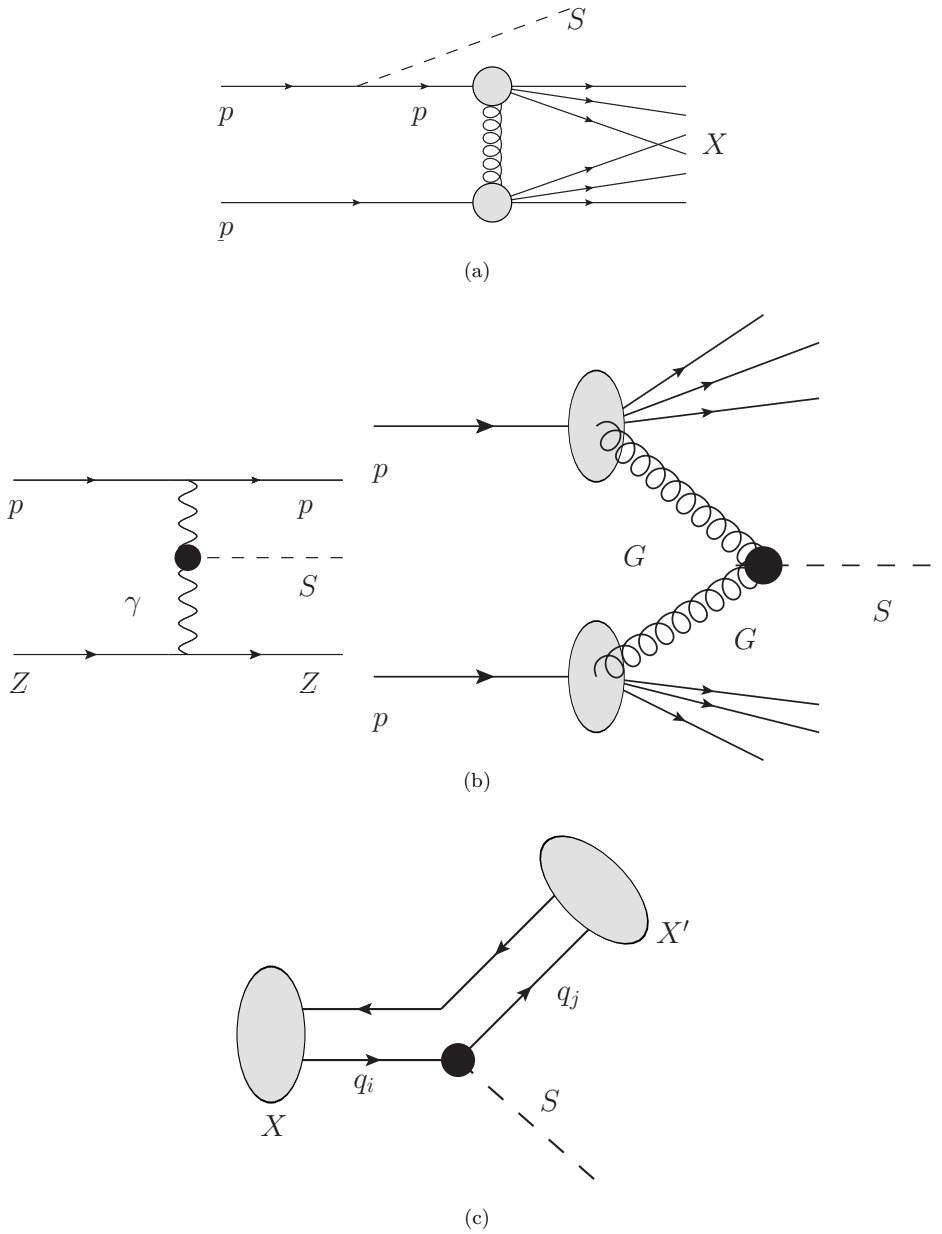

Figure 3. Example diagrams for the main production channels of a scalar S production in proton-nucleus collisions: proton bremsstrahlung (a), photon and gluon fusion (b), decay of secondary mesons (c).

Experiment	DUNE ($\sqrt{s_{pp}} = 16$ GeV)	SHiP ($\sqrt{s_{pp}} = 28$ GeV)	LHC ($\sqrt{s_{pp}} = 13$ TeV)
$W_{GG}(m_S = 2\text{ GeV})$	$1.2 \cdot 10^3$	$1.4 \cdot 10^3$	$6.2 \cdot 10^{10}$
$W_{GG}(m_S = 5\text{ GeV})$	$1.5 \cdot 10^{-1}$	7.9	$3.9 \cdot 10^{10}$

Table 1. Factors W_{GG} (see eq. (2.2)) for the DUNE, SHiP and LHC experiments.

The proton bremsstrahlung (the case (a)): is a process of a scalar emission by a proton in proton-proton interaction. For small masses of scalars, $m_S < 1\,\text{GeV}$, this is a usual bremsstrahlung process described by elastic nucleon-scalar interaction with a coupling constant $\theta g_{\text{SNN}} \sim \theta m_p/v$, see appendix A.2. However, the probability of elastic interaction decreases with the scalar mass and we need to take into account inelastic processes. The probability for the bremsstrahlung is

$$P_{\text{brem}} = \theta^2 g_{\text{SNN}}^2 \mathcal{P}_{\text{brem}}(m_S, s_{pp}), \tag{2.1}$$

where $\mathcal{P}_{\text{brem}}$ is a proton bremsstrahlung probability for the case $\theta = g_{\text{SNN}} = 1$ (see appendix D). This quantity varies from 10^{-2} for DUNE and SHiP to 10^{-1} for the LHC, see appendix D.[1]

For the case (b) we have to distinguish photon-photon fusion that can occur for an arbitrary transferred momentum and, therefore, an arbitrary scalar mass (as electromagnetic interaction is long-range), and gluons or quark-antiquarks fusion (the so-called deep inelastic scattering processes (DIS)), which is effective only for $m_S \gtrsim 1$ GeV. The scalar production in the DIS process can be estimated as $P_{\text{DIS}} = (\sigma_{\text{DIS},G} + \sigma_{\text{DIS},q})/\sigma_{pp}$, where σ_{pp} is the total proton-proton cross section and $\sigma_{\text{DIS},X}$ is the cross section of scalar production in the DIS process,

$$\sigma_{\text{DIS},G} \sim \frac{\theta^2 \alpha_s^2(m_S) m_S^2}{s_{pp} v^2} W_{GG}(m_S, s_{pp}), \quad \sigma_{\text{DIS},q} \sim \frac{\theta^2 m_q^2}{s_{pp} v^2} W_{q\bar{q}}(m_S, s_{pp}). \tag{2.2}$$

Here, $\sqrt{s_{pp}}$ is the center-of-mass energy of colliding protons and W_{XX} given by eq. (C.11) is a dimensionless combinatorial factor that, roughly, counts the number of the parton pairs in two protons that can make a scalar. The values of W_{XX} factors for some scalar masses and experimental energies are given in table 1. In figure 4 we show the ratio between cross sections of gluon-gluon and quark-antiquark fusion. We see that quark fusion is relevant only for low scalar masses, while for $m_S \gtrsim 2\,\text{GeV}$ the gluon fusion dominates for all collision energies considered.

In the case of *the production of a scalar in photon fusion*, the most interesting process is the coherent scattering on the whole nucleus, as its cross section is enhanced by a factor Z^2, where Z is the charge of the nucleus. The electromagnetic process $p + Z \to p + Z + S$ involves the effective $S\gamma\gamma$ vertex proportional to $\theta\alpha_{\text{EM}}$, see appendix A.1. The probability of the process is $P_{\gamma\text{ fus}} = \sigma_{\gamma\text{ fus}}/\sigma_{pZ}$, where the fusion cross section $\sigma_{\gamma\text{ fus}}$ has a structure

[1] In this estimate we neglect possible effects of QCD scalar resonances that could significantly enhance scalar production for some scalar masses.

JHEP11(2019)162

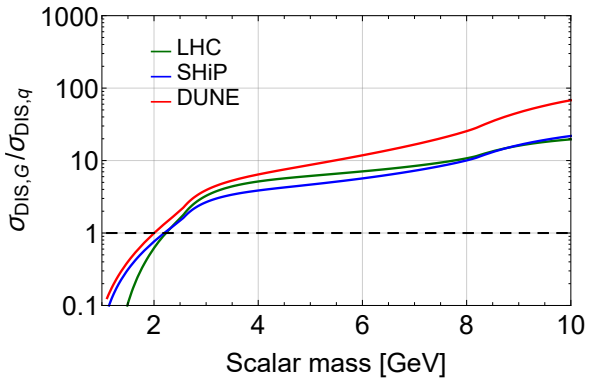

Figure 4. The ratio of cross sections of the scalar production in deep inelastic scattering via gluon and quark fusion. The dashed line corresponds to a ratio equal to unity. "LHC", "SHiP" and "DUNE" denote correspondingly the results for the proton-proton center-of-mass energies $\sqrt{s_{pp}} =$ 13 TeV, $\sqrt{s_{pp}} = 28$ GeV and $\sqrt{s_{pp}} = 16$ GeV.

similar to that of gluon fusion (2.2):

$$\sigma_{\gamma\text{ fus}} \sim 10^{-2} \frac{\theta^2 Z^2 \alpha_{\rm EM}^4 m_S^2}{v^2 s_{pZ}} W_{\rm coh}, \tag{2.3}$$

where $\sqrt{s_{pZ}}$ is the CM energy of the proton and nucleus, and $W_{\rm coh}$ given by eq. (E.8) is a dimensionless combinatorial factor that counts the number of pair of photons that can form a scalar. It ranges from 10^6 for the DUNE energies to 10^{14} for the LHC energies.

Let us compare the probabilities of photon fusion and proton bremsstrahlung,

$$\frac{P_{\gamma\text{ fus}}}{P_{\rm brem}} \sim 10^{-2} \frac{Z^2}{s_{pZ}\sigma_{pZ}} \frac{\alpha_{\rm EM}^4}{g_{\rm SNN}^2} \frac{m_S^2}{v^2} \frac{W_{\rm coh}}{\mathcal{P}_{\rm brem}} \sim \tag{2.4}$$

$$\sim 10^{-15} \frac{(100\text{ GeV})^2}{s_{pp}} \frac{Z^2}{A^{1.77}} \left(\frac{m_S}{1\text{ GeV}}\right)^2 \frac{W_{\rm coh}}{\mathcal{P}_{\rm brem}} \lesssim 10^{-4} \tag{2.5}$$

for all three energies considered. Here we used $s_{pZ} \approx A s_{pp}$, where A is the nucleus mass number. The proton-nucleus cross section σ_{pZ} weakly depends on energy and can be estimated as $\sigma_{pZ} \simeq 50$ mb $A^{0.77}$ [44, 45]. This ratio is smaller than 10^{-4} for all energies and scalar masses of interest. Next, comparing the probabilities of the production in photon fusion and in DIS, we obtain

$$\frac{P_{\gamma\text{ fus}}}{P_{\rm DIS}} \sim \frac{Z^2 \alpha_{\rm EM}^4}{\alpha_s^2} \frac{s_{pp}}{s_{pZ}} \frac{\sigma_{pp}}{\sigma_{pZ}} \frac{W_{\rm coh}}{W_{\rm DIS}} \sim 10^{-8} \frac{Z^2}{A^{1.77}} \frac{W_{\rm coh}}{W_{\rm DIS}} \lesssim 10^{-4}, \tag{2.6}$$

where we used that $s_{pZ}/s_{pp} \approx A$ and $W_{\rm coh}/W_{\rm DIS} \lesssim 1$ for all three energies considered, see appendix E. The proton-proton cross section also depends on the energy weakly, and we can estimate $\sigma_{pZ}/\sigma_{pp} \sim A^{0.77}$ (see appendix D).

We conclude that the scalar production in photon fusion is always sub-dominant for the considered mass range of scalar masses and beam energies.

JHEP11(2019)162

Let us now compare gluon fusion and proton bremsstrahlung with the *production from secondary mesons (type (c))*. The latter can be roughly estimated using "inclusive production", i.e. production from the decay of a free heavy quark, without taking into account that in reality this quark is a part of different mesons with different masses. This is only an order of magnitude estimate that breaks down for $m_S \gtrsim m_q - \Lambda_{\rm QCD}$, so it can be used only for D and B mesons. We will see however that such an estimate is sufficient to conclude that for the energies of SHiP and LHC the production from mesons dominates and we need to study it in more details (see more detailed analysis below).

The inclusive branching $\mathrm{BR}_{\rm incl}(X_{Q_i} \to X_{Q_j} S)$ can be estimated using the corresponding quark level process $Q_i \to Q_j S$. To minimize QCD uncertainty we follow [16, 43] and estimate the inclusive branching ratio as

$$\mathrm{BR}_{\rm incl}(X_{Q_i} \to X_{Q_j} S) \simeq \frac{\Gamma(Q_i \to Q_j S)}{\Gamma(Q_i \to Q' e \bar{\nu}_e)} \times \mathrm{BR}_{\rm incl}(X \to X_{Q'} e \bar{\nu}_e), \tag{2.7}$$

where $\Gamma(Q_i \to Q' e \bar{\nu}_e)$ is the semileptonic decay width of a quark Q_i calculated using the Fermi theory and $\mathrm{BR}_{\rm incl}(X \to X_{Q'} e \bar{\nu}_e)$ is the experimentally measured inclusive branching ratio. As both the quark decay widths in (2.7) get the QCD corrections, their total effect in (2.7) is expected to be minimal [43]

For D and B mesons decays the inclusive production probabilities are [19, 43]

$$P_D \sim 2\chi_{c\bar{c}} \times \mathrm{BR}(c \to Su) \sim 6 \cdot 10^{-11}\ \theta^2 \chi_{c\bar{c}} \left(1 - \frac{m_S^2}{m_c^2}\right)^2, \tag{2.8}$$

$$P_B \sim 2\chi_{b\bar{b}} \times \mathrm{BR}(b \to Ss) \sim 13\ \theta^2 \chi_{b\bar{b}} \left(1 - \frac{m_S^2}{m_b^2}\right)^2, \tag{2.9}$$

where $\chi_{q\bar{q}}$ is the production fraction of the $q\bar{q}$ pair in pp collisions, see table 2. The difference in 10^{-11} orders of magnitude is mostly coming from $(m_b/m_t)^4 \sim 10^{-7}$ and $|V_{ub}|^2/|V_{ts}|^2 \sim 10^{-2}$ (see appendix A.3 for details). In fact for D mesons the leptonic decay $D \to Se\nu$ with $\mathrm{BR}(D \to Se\nu) \sim 5 \cdot 10^{-9}\theta^2$ is more important than (2.8), see appendix B.3 for details. We see that the production from D mesons may be important only if the number of B mesons is suppressed by 10^9 times, which is possible only if the center-of-mass energy of p-p collisions is close to the $b\bar{b}$ pair production threshold.

Let us compare the production from B mesons with the production from proton bremsstrahlung and DIS. Using eqs. (2.1), (2.2) and (2.9) for masses of scalar below b quark kinematic threshold we get

$$\frac{P_{\rm brem}}{P_B} \sim \frac{g_{\rm SNN}^2}{\mathrm{BR}(b \to Ss)} \frac{\mathcal{P}_{\rm brem}}{\chi_{b\bar{b}}} \sim 10^{-7} \frac{\mathcal{P}_{\rm brem}}{\chi_{b\bar{b}}}, \tag{2.10}$$

$$\frac{P_{\rm DIS}}{P_B} \sim 10^{-6} \frac{1}{s_{pp}\sigma_{pp}} \left(\frac{m_S}{1\ \mathrm{GeV}}\right)^2 \frac{W_{GG}(m_S, s_{pp})}{\chi_{b\bar{b}}}. \tag{2.11}$$

The ratios (2.11) and (2.10) depend on the center-of-mass energy of the experiment (see tables 1 and 2).

We conclude that for the experiments with high beam energies, like SHiP or LHC, the most relevant production channel is a production of scalars from secondary mesons.

JHEP11(2019)162

Experiment	DUNE ($\sqrt{s_{pp}} = 16$ GeV)	SHiP ($\sqrt{s_{pp}} = 28$ GeV)	LHC ($\sqrt{s_{pp}} = 13$ TeV)
$\chi_{c\bar{c}}$	$1.0 \cdot 10^{-4}$	$3.9 \cdot 10^{-3}$	$2.9 \cdot 10^{-2}$
$\chi_{b\bar{b}}$	$1.0 \cdot 10^{-10}$	$2.7 \cdot 10^{-7}$	$8.6 \cdot 10^{-3}$

Table 2. Production fractions of the $q\bar{q}$ pair, $\chi_{q\bar{q}} = \sigma_{q\bar{q}}/\sigma_{pp}$, for the DUNE, SHiP and LHC experiments. We took the production fractions for the DUNE and SHiP experiments from [46, 47]. To estimate the production fractions for the LHC, we calculated the total cross section of B and D production using FONLL [48] and took the total cross section of the pp collisions at the LHC energies from [44].

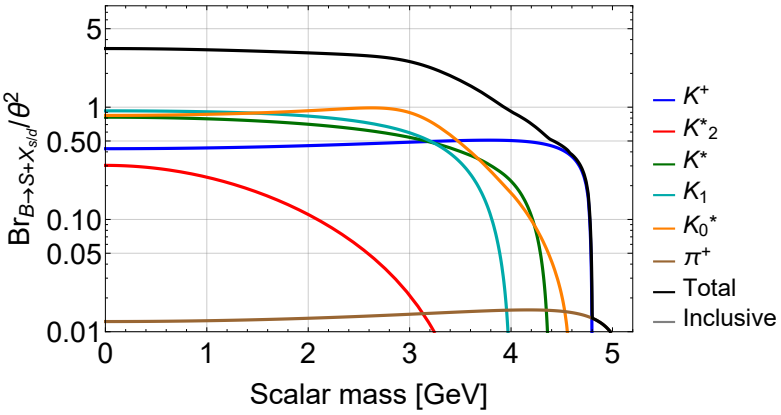

Figure 5. Branching ratios of the 2-body decays $B^+ \to SX_{s/d}$, where X_q is a hadron that contains a quark q. By the K^* channel, we denote the sum of the branching ratios for $K^*(892)$, $K^*(1410)$, $K^*(1680)$ final states, by K_0^* — for $K_0^*(700)$, $K_0^*(1430)$, and by K_1 — for $K_1(1270)$, $K_1(1400)$. The "Inclusive" line corresponds to the branching ratio (2.7) obtained using the free quark model.

For experiments with smaller energies like, e.g., DUNE the dominant channel is the direct production of scalars in proton bremsstrahlung and in DIS.

Production from decays of different mesons. Let us discuss the production of scalars from decays of mesons in more details. The calculation of branching ratios for two-body decays of mesons is summarized in appendix B.2. Above we made an estimate for the cases of D and B mesons that are the most efficient production channels for larger masses of S. Instead, for scalar masses $m_S < m_K - m_\pi$ the main production channel is the decay of kaons, $K \to S\pi$, see table 3 with the relevant information about these production channels. Numerically, the branching ratio of the production from kaons is suppressed by 3 orders of magnitude in comparison to the branching ratio of the production from B mesons, but for the considered energies the number of kaons is at least 10^3 times larger than the number of B mesons.

For scalar masses $m_K - m_\pi < m_S < m_B$ the main scalar production channel from hadrons is the production from B mesons. Inclusive estimate at the quark level, that we

JHEP11(2019)162

Process	BR$(m_S = 0)/\theta^2$	Closing mass [GeV]	Appendix
$K^\pm \to S\pi^\pm$	$1.7 \cdot 10^{-3}$	0.350	F.1.1
$K_L^0 \to S\pi^0$	$7 \cdot 10^{-3}$	0.360	F.1.1
$B^\pm \to SK_1^\pm(1270)$	$(9.1^{+3.6}_{-4.0}) \cdot 10^{-1}$	3.82	F.2.2
$B^\pm \to SK_0^{*,\pm}(700)$	$7.6 \cdot 10^{-1}$	4.27	F.1.2
$B^\pm \to SK^{*,\pm}(892)$	$(4.7^{+0.9}_{-0.8}) \cdot 10^{-1}$	4.29	F.2.1
$B^\pm \to SK^\pm$	$(4.3^{+1.1}_{-1.0}) \cdot 10^{-1}$	4.79	F.1.1
$B^\pm \to SK_2^{*,\pm}(1430)$	$3.0 \cdot 10^{-1}$	3.85	F.3
$B^\pm \to SK^{*,\pm}(1410)$	$(2.1^{+0.6}_{-1.1}) \cdot 10^{-1}$	3.57	F.2.1
$B^\pm \to SK^{*,\pm}(1680)$	$(1.3^{+0.5}_{-0.4}) \cdot 10^{-1}$	3.26	F.2.1
$B^\pm \to SK_0^{*,\pm}(1430)$	$8.1 \cdot 10^{-2}$	3.82	F.1.2
$B^\pm \to SK_1^\pm(1400)$	$(1.6^{+0.6}_{-1.1}) \cdot 10^{-2}$	2.28	F.2.2
$B^\pm \to S\pi^\pm$	$(1.3^{+0.3}_{-0.3}) \cdot 10^{-2}$	5.14	F.1.1

Table 3. Properties of the main production channels of a scalar S from kaons and B mesons through the mixing with the Higgs boson. *First column*: decay channels; *Second column*: branching ratios of 2-body meson decays evaluated at $m_S = 0$ using formula (B.9) and normalized by θ^2. For B mesons the numerical values are given for $B^\pm$ mesons; in the case of B^0 meson all the given branching ratios should be multiplied by a factor of 0.93 that comes from the difference in total decay widths of $B^\pm$ and B^0 mesons [44]. Uncertainties (where available) follow from uncertainties in meson transition form-factors; *Third column*: effective closing mass, i.e. a mass of a scalar at which the branching ratio of the channel decreases by a factor of 10; *Fourth column*: a reference to the appendix with details about form-factors used.

made above (see eq. (2.9)), contains an unknown QCD uncertainty and completely breaks down for scalar masses $m_b - m_S \simeq \Lambda_{\rm QCD}$. Below we discuss therefore decays of different mesons containing the b quark $B \to X_{s/d}S$. We consider kaon and its resonances as the final states X_s:

- Pseudoscalar meson K;
- Scalar mesons $K_0^*(700), K_0^*(1430)$ (here assuming that $K_0^*(700)$ is a di-quark state);
- Vector mesons $K^*(892), K^*(1410), K^*(1680)$;
- Axial-vector mesons $K_1(1270), K_1(1400)$;
- Tensor meson $K_2^*(1430)$.

We also consider the meson $X_d = \pi$. Although the rate of the corresponding process $B \to \pi S$ is suppressed in comparison to the rate of $B \to X_s S$, it may be important since it has the largest kinematic threshold $m_S \lesssim m_B - m_\pi$.

We calculate the branching ratios BR$(B^+ \to X_{s/d}S)$ at $m_S \ll m_K$ using eq. (B.9) and give the results in table 3. The main uncertainty of this approach is related to form factors describing meson transitions $X_{Q_i} \to X'_{Q_j}$, see appendix F for details. They are calculated theoretically using approaches of light cone fum rules and covariant quark model,

JHEP11(2019)162

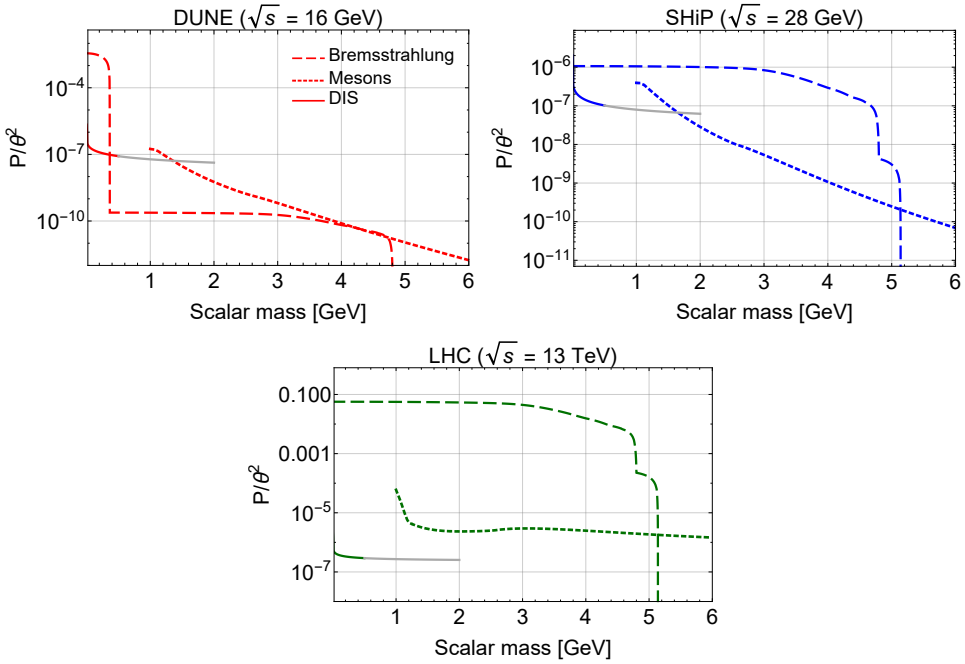

Figure 6. The probabilities of a scalar production in proton bremsstrahlung process (2.1) (solid lines), DIS process (2.2) (dotted lines) and decays of B mesons (dashed lines) versus the scalar mass. "LHC", "SHiP" and "DUNE" denote correspondingly results for the proton-proton center-of-mass energies $\sqrt{s_{pp}} = 13$ TeV, $\sqrt{s_{pp}} = 28$ GeV and $\sqrt{s_{pp}} = 16$ GeV. The gray line corresponds to the extrapolation of the bremsstrahlung production probability assuming unit value of the proton elastic form-factor, see text for details.

and indirectly fixed using experimental data on rare mesons decays [49–53]. The errors given in table 3 result from uncertainties in the meson transition form-factors $F_{BX_{s/d}}$ (see appendix F). Since $F_{BX_{s/d}}$ are the same for B^+ and B^0 mesons, the branching ratios $\mathrm{BR}(B^0 \to X'^0 S)$ differ from $\mathrm{BR}(B^0 \to X^0_{s/d} S)$ only by the factor $\Gamma_{B^+}/\Gamma_{B^0} \approx 0.93$.

The values of the branching ratios for the processes $B \to KS$, $B \to K^*S$ are found to be in good agreement with results from the literature [31, 32]. We conclude that the most efficient production channels of light scalars with $m_S \lesssim 3$ GeV are decays $B \to K_0^* S$, $B \to K_1 S$ and $B \to K^* S$; the channel $B \to KS$, considered previously in the literature, is sub-dominant.

Summing over all final K states, in the limit $m_S \ll m_B$ for the total branching ratio we have

$$\mathrm{BR}(B \to S X_s) \equiv \sum_{X_s} \mathrm{BR}(B \to S X_s) \approx 3.3^{+0.8}_{-0.7}\, \theta^2. \tag{2.12}$$

Using the estimate (2.9), for the ratio of the central value of the branching ratio (2.12) and the inclusive branching ratio at $m_S \ll m_B$ we find

$$\mathrm{BR}(B \to S X_s)/\mathrm{BR}_{\mathrm{incl}}(B \to S X_s) \approx 0.5. \tag{2.13}$$

JHEP11(2019)162

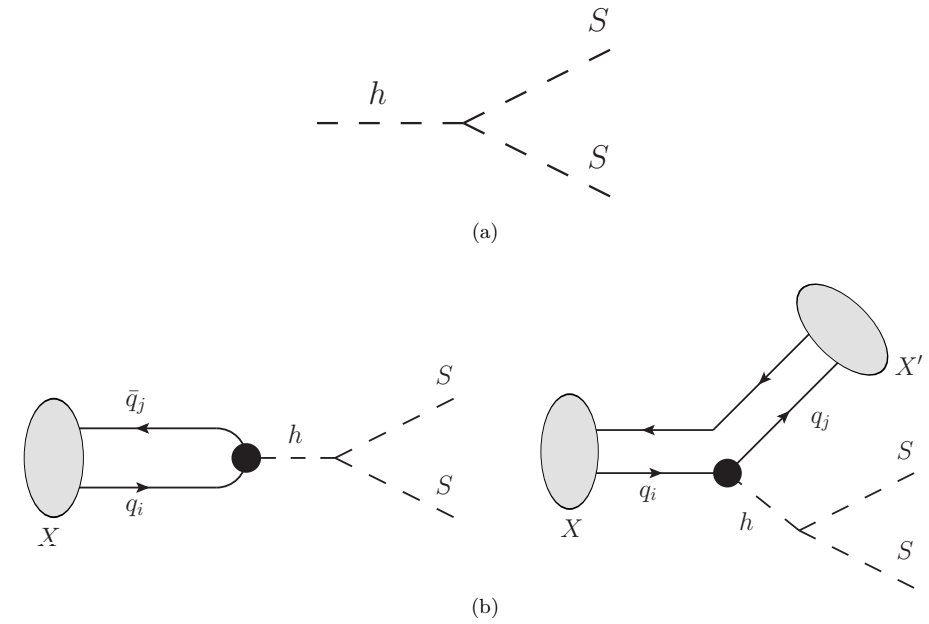

Figure 7. Diagrams for the production channels of a scalar S through a quartic coupling: decay of the Higgs boson (a), decays of mesons (b).

Provided that the inclusive estimate of the branching ration has a large uncertainty, we believe that eq. (2.13) suggests that we have taken into account all main decay channels of this type.

Our results are summarized in table 3 and figure 5. We have found that the channels with K^*, K_0^* and K_1 give the main contribution to the production branching ratio for small scalar masses $m_S \lesssim 3$ GeV, while for larger masses the main channel is decay to K. The comparison between the probability of the production from mesons and our estimates for bremsstrahlung and DIS for three center of mass energies are shown in figure 6.

2.2 Quartic coupling

Above we discussed the production of scalars only through the mixing with the Higgs boson. One more interaction term in the Lagrangian (1.2),

$$\mathcal{L}_{\text{quartic}} = \frac{\alpha}{2} S^2 h, \tag{2.14}$$

(the so-called "quartic coupling" that originates from the term $S^2 H^\dagger H$ in the Lagrangian (1.1)) affects the production of scalars from decays of mesons and opens an additional production channel — production from Higgs boson decays, see figure 7.

JHEP11(2019)162

The production from the Higgs boson (case (a)) can be important for high-energy experiments like LHC. The branching ratio is

$$\mathrm{BR}(h \to SS) = \frac{\alpha^2 |\boldsymbol{p}_S|}{16\pi m_h^2 \Gamma_h} \approx 2.0 \cdot 10^{-2} \left(\frac{\alpha}{1\ \mathrm{GeV}}\right)^2 \sqrt{1 - \frac{4m_S^2}{m_h^2}}, \tag{2.15}$$

where $\boldsymbol{p}_S$ is a momentum of a scalar in the rest frame of the Higgs boson and we used the SM decay width of the Higgs boson $\Gamma_h \approx 4\,\mathrm{MeV}$ [54]. If the decay length of the scalar is large enough $c\gamma\tau_S \gtrsim 1$ m this decay channel manifests itself at ATLAS and CMS experiments as an invisible Higgs boson decay. The invisible Higgs decay is constrained at CMS [9], the 2σ upper bound is

$$\mathrm{BR}(h \to \mathrm{invis.}) < 0.19. \tag{2.16}$$

This puts an upper bound $\alpha < 3.1\,\mathrm{GeV}$ for the scalar masses $m_S < m_h/2$.

The production probability $P_{h\to SS} = \chi_h \times \mathrm{BR}(h \to SS)$, where χ_h is a production fraction of the Higgs bosons. Comparing with the production from B mesons for a scalar mass below the B threshold estimated by the inclusive production (2.9) we get

$$\frac{P_{h\to SS}}{P_B} \sim 10^{-3} \frac{1}{\theta^2} \left(\frac{\alpha}{1\ \mathrm{GeV}}\right)^2 \frac{\chi_h}{\chi_{b\bar{b}}} \sim 10^{-10} \frac{1}{\theta^2} \left(\frac{\alpha}{1\ \mathrm{GeV}}\right)^2, \tag{2.17}$$

where we used $\chi_h \sim 10^{-9}$ for the LHC energy [55] and $\chi_{b\bar{b}} \sim 10^{-2}$ (see table 2).

Also, *the quartic coupling generates new channels of scalar production in meson decays (case (b))*. In addition to the process $X \to X'S$ shown in figure 3(c) the quartic coupling enables also additional processes $X \to SS$ and $X \to X'SS$ shown in figure 7(b) [1, 31, 56–59].

First, let us make a simple comparison between the branching ratios for the scalar production from mesons in the case of mixing with the Higgs boson and quartic coupling. Comparing Feynman diagrams in figures 3(c) and 7(b) we see that for the case $m_S \ll m_X$

$$\frac{\mathrm{BR}(X \to X'SS)}{\mathrm{BR}(X \to X'S)} \sim \frac{\alpha^2 m_X^2}{\theta^2 m_h^4} \sim 10^{-9} \frac{1}{\theta^2} \left(\frac{\alpha}{1\ \mathrm{GeV}}\right)^2 \left(\frac{m_X}{1\ \mathrm{GeV}}\right)^2, \tag{2.18}$$

$$\frac{\mathrm{BR}(X \to SS)}{\mathrm{BR}(X \to X'S)} \sim \frac{\alpha^2 f_X^2}{\theta^2 m_h^4} \sim 10^{-9} \frac{1}{\theta^2} \left(\frac{\alpha}{1\ \mathrm{GeV}}\right)^2 \left(\frac{f_X}{1\ \mathrm{GeV}}\right)^2, \tag{2.19}$$

where f_X is a meson's decay constant (see appendix G).

The channel $X \to X'SS$ is very similar to the channel $X \to X'S$ from figure 3(c). By the same reasons, this process is strongly suppressed for D-mesons and is efficient only for kaons and B mesons.

The decay $X \to SS$ is possible only for K^0, D^0, B^0 and B_s^0 due to conservation of charges. The production from D^0 mesons is strongly suppressed by the same reason as above (small Yukawa constant and CKM elements in the effective interaction, see appendix A.3).

Our results for the branching ratio of the scalar production from mesons decays in the case of the quartic coupling are presented in table 4 and in figure 8, the formulas for the branching ratios and details of calculations are given in appendix G. The results are shown for the value of coupling constant $\alpha = 1\,\mathrm{GeV}$ which corresponds to the Higgs boson branching ratio $\mathrm{BR}(h \to SS) \approx 0.02$ (see eq. (2.15)).

JHEP11(2019)162

Process	BR($m_S = 0$)	Closing mass [GeV]	Appendix
$K_L^0 \to SS$	$4.4 \cdot 10^{-13}$	0.252	G
$K_L^0 \to SS\pi^0$	$6.6 \cdot 10^{-15}$	0.140	F.1.1
$K^\pm \to SS\pi^\pm$	$1.4 \cdot 10^{-15}$	0.136	F.1.1
$K_S^0 \to SS$	$7.8 \cdot 10^{-16}$	0.252	G
$K_S^0 \to SS\pi^0$	$1.2 \cdot 10^{-17}$	0.140	F.1.1
$B_s \to SS$	$4.0 \cdot 10^{-10}$	2.670	G
$B^\pm \to SSK^\pm$	$1.4 \cdot 10^{-10}$	1.998	F.1.1
$B^\pm \to SSK_0^{*,\pm}(700)$	$1.2 \cdot 10^{-10}$	1.621	F.1.2
$B^\pm \to SSK_1^\pm(1270)$	$(1.2^{+0.5}_{-0.5}) \cdot 10^{-10}$	1.478	F.2.2
$B^\pm \to SSK^{*,\pm}(892)$	$9.1 \cdot 10^{-11}$	1.701	F.2.1
$B^\pm \to SSK_0^{*,\pm}(1430)$	$3.5 \cdot 10^{-11}$	1.621	F.1.2
$B^\pm \to SSK^{*,\pm}(1410)$	$(1.9^{+0.6}_{-0.5}) \cdot 10^{-11}$	1.358	F.2.1
$B^\pm \to SSK_2^{*,\pm}(1430)$	$2.5 \cdot 10^{-11}$	1.499	F.3
$B_0 \to SS$	$1.1 \cdot 10^{-11}$	2.624	G
$B^\pm \to SSK^{*,\pm}(1680)$	$(9.9^{+0.4}_{-0.3}) \cdot 10^{-12}$	1.240	F.2.1
$B^\pm \to SS\pi^\pm$	$(4.7^{+1.2}_{-1.1}) \cdot 10^{-12}$	2.149	F.1.1
$B^\pm \to SSK_1^\pm(1400)$	$(7.3^{+0.3}_{-0.3}) \cdot 10^{-13}$	1.545	F.2.2

Table 4. Properties of the main production channels of a scalar S from kaons and B mesons through quartic coupling (2.14). *First column*: decay channels; *Second column*: branching ratios of 2-body meson decays evaluated at $m_S = 0$ and $\alpha = 1$ GeV, see eqs. (G.7), (G.8). For B mesons the numerical values are given for $B^\pm$ mesons; in the case of decays of B^0 mesons, all the given branching ratios should be multiplied by a factor 0.93 that comes from the difference in total decay widths of $B^\pm$ and B^0 mesons [44]. Uncertainties (where available) follow from uncertainties in meson transition form-factors; *Third column*: effective closing mass, i.e. a mass of a scalar at which the branching ratio of the channel decreases by a factor of 10. *Fourth column*: a reference to appendix with details about form-factors used.

3 Scalar decays

The main decay channels of the scalar are decays into photons, leptons and hadrons, see appendix H. In the mass range $m_S \lesssim 2m_\pi$ the scalar decays into photons, electrons and muons, see appendix H.1.

For masses small enough compared to the cutoff $\Lambda_{\rm QCD} \approx 1$ GeV, ChPT (Chiral Perturbation Theory) can be used to predict the decay width into pions [34]. For masses of order $m_S \gtrsim \Lambda_{\rm QCD}$ a method making use of dispersion relations was employed in [35–37] to compute hadronic decay rates. As it was pointed out in [33] and later in [30], the reliability of the dispersion relation method is questionable for $m_S \gtrsim 1$ GeV because of lack of the experimental data on meson scattering at high energies and unknown contribution of scalar hadronic resonances, which provides significant theoretical uncertainties. To have a concrete benchmark — although in the light of the above the result should be taken with a grain of salt — we use the decay width into pions and kaons from [32], see figure 9,

JHEP11(2019)162

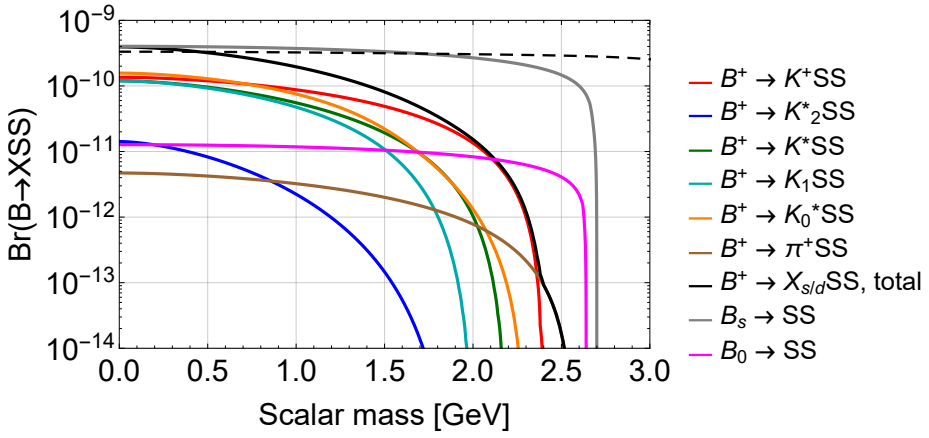

Figure 8. Branching ratios of decays $B^+ \to SSX_{s/d}$ and $B \to SS$, where X_q is a hadron that contains a quark q, versus the scalar mass. By the K^* channel, we denote the sum of the branching ratios for $K^*(892)$, $K^*(1410)$, $K^*(1680)$ final states, by K_0^* — for $K_0^*(700)$, $K_0^*(1430)$, and by K_1 — for $K_1(1270)$, $K_1(1400)$. The values of the branching ratios are given at $\alpha = 1$ GeV.

which combines the next-to-leading order ChPT with the analysis of dispersion relations for the recent experimental data. For the ratio of the decay widths into neutral and charged mesons we have

$$\Gamma_{S\to\pi^0\pi^0}/\Gamma_{S\to\pi^+\pi^-} = 1/2, \quad \Gamma_{S\to K^0\bar{K}^0}/\Gamma_{S\to K^+K^-} = 1. \tag{3.1}$$

For scalar masses above $f_0(1370)$ the channel $S \to 4\pi$ becomes important and should be taken into account [60]. The decay width of this channel is currently not known; its contribution can be approximated by a toy-model formula [32]

$$\Gamma_{\text{multi-meson}} = C\theta^2 m_S^3 \beta_{2\pi}, \quad \beta_{2\pi} = \sqrt{1-(4m_\pi)^2/m_S^2}, \tag{3.2}$$

where a dimensional constant C is chosen so that the total decay width is continuous at large m_S that will be described by perturbation QCD, see figure 10.

For $m_S \geq \Lambda_S^{\text{pert}} \simeq 2-4\,\text{GeV}$ hadronic decays of a scalar can be described perturbatively using decays into quarks and gluons, see appendix H.2. Currently, the value of Λ_S^{pert} is not known because of lack of knowledge about scalar resonances which can mix with S and enhance the scalar decay width. In [32] the value of Λ_S^{pert} is set to 2 GeV, in [5] it is $\Lambda_S^{\text{pert}} = 2.5$ GeV, while in [19] its value is $\Lambda_S^{\text{pert}} = 2m_D$. This scale certainly should above the mass of the heaviest known scalar resonance $f_0(1710)$, so in this work we choose $\Lambda_S^{\text{pert}} = 2\,\text{GeV}$.

The summary of branching ratios of various decay channels of the scalar and the total lifetime of the scalar is shown in figure 10.

JHEP11(2019)162

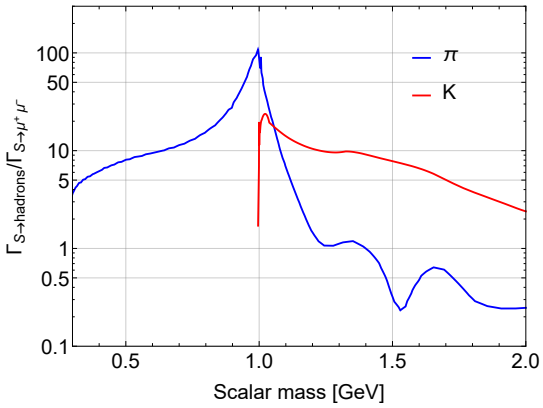

Figure 9. The ratio of the decay widths of a light scalar into pions, kaons and into muons obtained in [32]. We summed over all final meson states, i.e. for decays into pions we summed over $\pi^+\pi^-, \pi^0\pi^0$. A peak in the decay width corresponding to the channel $S \to \pi\pi$ around $m_S \simeq 1$ GeV is caused by the narrow $f_0(980)$ resonance.

Channel	Open, MeV	Rel. from, MeV	Rel. to, MeV	Max BR, %	Formula
$S \to 2\gamma$	0	0	1.02	100	(H.2)
$S \to e^+e^-$	1.02	1.02	212	≈ 100	(H.1)
$S \to \mu^+\mu^-$	211	211 and 1668	564 and 2527	≈ 100	(H.1)
$S \to \pi^+\pi^-$	279	280	1163	65.5	Figure 9
$S \to 2\pi^0$	270	280	1163	32.8	Figure 9
$S \to K^+K^-$	987	996	$\Lambda_S^{\rm pert} = 2000$	36.8	Figure 9
$S \to K^0\bar{K}^0$	995	1004	$\Lambda_S^{\rm pert} = 2000$	36.8	Figure 9
$S \to 4\pi$	550	1210	$\Lambda_S^{\rm pert} = 2000$	52.4	(3.2)
$S \to GG$	275	$\Lambda_S^{\rm pert} = 2000$	4178	68.6	(H.10)
$S \to s\bar{s}$	990	$\Lambda_S^{\rm pert} = 2000$	3807	42.5	(H.3)
$S \to \tau^+\tau^-$	3560	3608	—	45.7	(H.1)
$S \to c\bar{c}$	3740	3797	—	50.6	(H.3)

Table 5. Relevant scalar decay channels. Only channels with the branching ratio above 1% covering the scalar mass range up to 10 GeV are shown. The gray line corresponds to the fake multi-meson channel, see discussion in text. *Columns*: (1) the scalar decay channel. (2) The scalar mass at which the channel opens; (3) The scalar mass starting from which the channel becomes relevant (contributes larger than 10%); (4) The scalar mass above which the channel contributes less than 10%; "—" means that the channel is still relevant at $m_S = 10$ GeV; (5) The maximal branching ratio of the channel for $m_S < 10$ GeV; (6) Reference to the formula (or figure in case of decays into pions and kaons) for the decay width of the channel.

JHEP11(2019)162

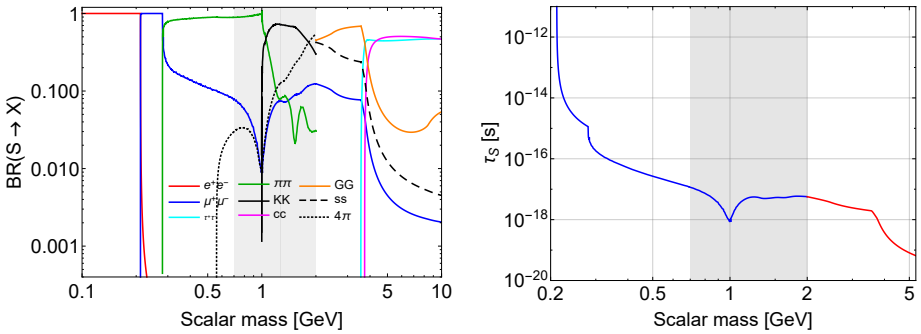

Figure 10. Left panel: branching ratios of decays of a scalar S as a function of its mass. For decays into hadrons up to $m_S = 2$ GeV we used results from [32], while for decays into hadrons in the mass range $m_S > 2$ GeV we used perturbative decays into quarks and gluons (see section H.2). In order to match these two regimes, we added a toy-model contribution to the total decay width that imitates multi-meson decay channels, see eq. (3.2). Right panel: the lifetime of a scalar S as a function of its mass with the mixing angle $\theta^2 = 1$. Solid blue line denotes the lifetime calculated using decays into leptons, kaons and pions from [32] and fictitious multi-meson channel, see eq. (3.2), while solid red line — the lifetime obtained using decays into quarks and gluons within the framework of perturbative QCD. The filled gray regions on the plot correspond to the domain of the scalar masses for which there are significant theoretical uncertainties in hadronic decays.

4 Conclusion

In this paper, we have reviewed and revised the phenomenology of the scalar portal, a simple extension of the Standard Model with a scalar S that is not charged under the SM gauge group, for masses of scalar $m_S \lesssim 10\,\text{GeV}$. We considered three examples of experimental setup that correspond to DUNE (with proton-proton center of mass energy $\sqrt{s_{pp}} \approx 16\,\text{GeV}$), SHiP ($\sqrt{s_{pp}} \approx 28\,\text{GeV}$) and LHC based experiments ($\sqrt{s_{pp}} = 13\,\text{TeV}$).

Interactions of a scalar S with the Standard Model can be induced by the mixing with the Higgs boson and the interaction Sh^2 (the "quartic coupling"), see Lagrangian (1.1). The mixing with the Higgs boson is relevant for a scalar production and decay, while the quartic coupling could be important only for the scalar production.

For the scalar production through the mixing with the Higgs boson, we have explicitly compared decays of secondary mesons, proton bremsstrahlung, photon-photon fusion, and deep inelastic scattering. For the energy of the SHiP experiment, the most relevant production channel is the production in decays of secondary mesons, specifically kaons and B mesons. For smaller energies (corresponding in our examples to the DUNE experiment) the situation is more complicated, and direct production channels from $p-p$ collisions (proton bremsstrahlung, deep inelastic scattering) give the main contribution to the production of scalars, see figure 6.

Our results for various channels of the scalar production from mesons via mixing with the Higgs boson are summarized in table 3 and in figure 5. The results for decays $B \to KS$, $B \to K^*(892)S$ agree with the references [1, 2, 5, 8, 31, 32], while other decay channels have not been studied in these papers.

JHEP11(2019)162

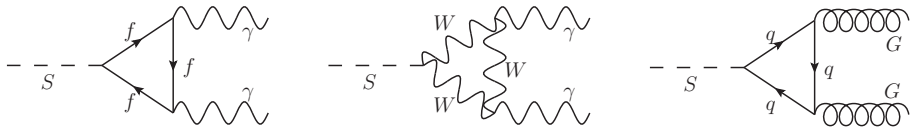

Figure 11. Diagrams of the interaction of the scalar S with photons and gluons.

For the LHC based experiments, an important contribution to the production of scalars is given by the production in decays of Higgs bosons that may be possible due to non-zero quartic coupling. This production channel, when allowed by the energy of an experiment, allows to search for scalars that are heavier than B mesons. It may also significantly increase the experimental sensitivity in the region of the lower bound of the sensitivity curve, where production through the mixing with the Higgs boson is less efficient.

Also the quartic coupling gives rise to meson decay channels $X \to SS$ and $X \to X'SS$ that are important for scalar masses $m_S \lesssim m_B/2$. Our results for these channels are presented in table 4 and in figure 8.

The description of scalar decays is significantly affected by two theoretical uncertainties: (i) the decay width of a scalar into mesons like $S \to \pi\pi$ and $S \to KK$ (that may be uncertain more than by an order of magnitude for masses of a scalar around 1 GeV) and (ii) the uncertainty in the scale $\Lambda_S^{\rm pert}$ at which perturbative QCD description can be used. As a benchmark, for decays into mesons we use results of [32] and choose $\Lambda_s^{\rm pert} = 2$ GeV, but we stress that the correct result is not really known for such masses. The main properties of scalar decays are summarized in table 5 and figure 10.

Acknowledgments

We thank O. Ruchayskiy, F. Bezrukov, J. Bluemlein, A. Manohar, A. Monin for fruitful discussions and J.-L. Tastet for careful reading of the manuscript. This project has received funding from the European Research Council (ERC) under the European Union's Horizon 2020 research and innovation program (GA 694896).

A Effective interactions

A.1 Photons and gluons

The effective lagrangian of the interaction of S with photons and gluons is generated by the diagrams 11. It reads

$$\mathcal{L} = \theta S C_{S\gamma\gamma} \frac{\alpha_{\rm EM}}{4\pi v} F_\gamma F_{\mu\nu} F^{\mu\nu} + \theta S C_{SGG} \frac{\alpha_s}{4\pi v} F_G \sum_a G^a_{\mu\nu} G^{\mu\nu,a}. \tag{A.1}$$

Here the effective vertices F_γ, F_G are [5, 61]

$$F_\gamma = \sum_{l=e,\mu,\tau} F_l + N_c \sum_q F_q + F_W, \quad F_G = \sum_q F_q, \tag{A.2}$$

JHEP11(2019)162

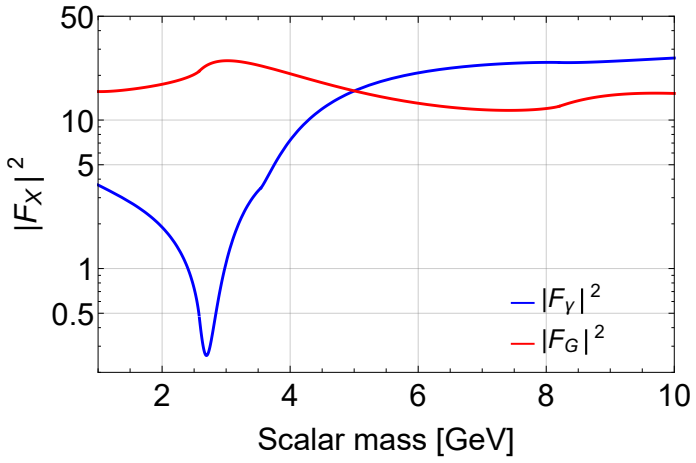

Figure 12. Dependence of the photon and gluon loop factors (A.2) on the scalar mass.

where

$$F_f(l_f) = -2l_f(1 + (1 - l_f)x^2(l_f)),$$
$$F_W = 2 + 3l_W(1 + (2 - l_W)x^2(l_W)), \qquad l_X = 4m_X^2/m_S^2, \tag{A.3}$$

and

$$x(l) = \begin{cases} \arctan\left(\dfrac{1}{\sqrt{l-1}}\right), & l > 1, \\ \dfrac{1}{2}\left(\pi + i\ \ln\left[\dfrac{1+\sqrt{1-l}}{1-\sqrt{1-l}}\right]\right), & l < 1 \end{cases} \tag{A.4}$$

Their behavior in dependence on the scalar mass is shown in figure 12. The values of the constants C_{SGG} and $C_{S\gamma\gamma}$ vary in the literature. Namely, in [5] they are $C_{S\gamma\gamma} = 1, C_{SGG} = 1/\sqrt{8}$. From the other side, in [61] predicts $|C_{S\gamma\gamma}| = 1/2, |C_{SGG}| = 1/4$. Calculating the decay branching ratio of the Higgs boson into two photons, we found that the value $C_{S\gamma\gamma} = 1/2$ is consistent with experimental results for the signal strength of the process $p + p \to h + X,\ h \to \gamma\gamma$ [62].[2] The gluon loop factor in the triangle diagram 11 differs from the photon loop factor by the factor $\mathrm{tr}[t_a t_a] = \frac{1}{2}$, where t_a is the QCD gauge group generators, and therefore $C_{Sgg} = 1/4$.

A.2 Nucleons

Consider the low-energy interaction Lagrangian between the nucleons N and the scalar:

$$\mathcal{L}_{\mathrm{SNN}} = g_{\mathrm{SNN}}\theta S\bar{N}N \tag{A.5}$$

The coupling g_{SNN} is defined as

$$g_{\mathrm{SNN}} \equiv \frac{1}{v}\lim_{p\to p'}\langle N(p)|\sum_q m_q\bar{q}q|N(p')\rangle \equiv \frac{1}{v}\langle N|\sum_q m_q\bar{q}q|N\rangle, \tag{A.6}$$

[2] We used the Higgs boson decay width $\Gamma_{h,\mathrm{SM}} = 4$ MeV.

where the shorthand notation $\langle N|\ldots|N\rangle \equiv \lim_{p\to p'}\langle N(p)|\ldots|N(p')\rangle$ was used. The applicability of the effective interaction (A.5) is $m_S^2 \lesssim r_N^{-2} \simeq 1\ \mathrm{GeV}^2$. Above this scale the elastic SNN vertex competes with the inelastic processes on partonic level and hence it is suppressed.

For energy scales of order of the nucleon mass, the u, d, s quarks are light, while the c, b, t quarks are heavy. Therefore, the latter can contribute to the effective coupling (A.6) only through effective interactions involving the lighs quarks and gluons. The latter can be obtained using the heavy quarks expansion [63, 64]. Keeping only the leading $1/m_{q_{\mathrm{heavy}}}$ term, for the effective interaction operator we obtain [65]

$$\sum_{q=c,b,t} m_q\bar{q}q \to -n_{\mathrm{heavy}}\cdot\frac{\alpha_s}{12\pi}G^a_{\mu\nu}G^{\mu\nu,a} + O\left(\frac{1}{m^2_{q_{\mathrm{heavy}}}}\right). \tag{A.7}$$

Here α_s is the QCD interaction constant evaluated on the scale of the hadronic mass, $G^a_{\mu\nu}$ is the gluon strength tensor and $n_{\mathrm{heavy}} = 3$ is the number of the heavy quarks. Therefore, in the leading order of $1/m_{q_{\mathrm{heavy}}}$ expansion the coupling (A.6) takes the form [65, 66]

$$g_{\mathrm{SNN}} = \frac{\theta}{v}\langle N|\sum_{q=u,d,s} m_q\bar{q}q - n_{\mathrm{heavy}}\frac{\alpha_s}{12\pi}G^a_{\mu\nu}G^{\mu\nu,a}|N\rangle. \tag{A.8}$$

The last expression we can written in terms of the nucleon mass m_N,

$$m_N \equiv \langle N|\theta_{\mu\mu}|N\rangle, \tag{A.9}$$

where $\theta_{\mu\mu}$ is the trace of the stress-energy tensor in the QCD [65]

$$\theta_{\mu\mu} = \sum_{q=u,d,s} m_q\bar{q}q + \frac{\beta_s}{4\alpha_s}G^a_{\mu\nu}G^{\mu\nu,a}, \tag{A.10}$$

where β_s is the QCD β function,

$$\beta_s = -\left(9 - \frac{2}{3}n_{\mathrm{heavy}}\right)\frac{\alpha_s^2}{2\pi}, \tag{A.11}$$

in the leading order by α_s. Therefore, we get [65, 66]

$$g_{\mathrm{SNN}} = \frac{2}{9}\frac{m_N}{v}\left(1 + \frac{7}{2}\sum_{q=u,d,s}\frac{m_q}{m_N}\langle N|\bar{q}q|N\rangle\right). \tag{A.12}$$

The numerical value is $g_{\mathrm{SNN}} \approx 1.2\cdot 10^{-3}$ [67].

In order to incorporate effects of non-zero momentum transfer q^2 in the SNN vertex, we need to take into account an scalar nucleon form-factor $F_{N,S}(q^2)$:

$$g_{\mathrm{SNN}} \to g_{\mathrm{SNN}}F_{N,S}(q^2), \quad F_{N,S}(0) = 1. \tag{A.13}$$

We have not found any paper discussing the form-factor $F_{N,S}$. From general ground we expect that it incorporates a mixing with scalar resonances f_0 which causes peaks at $q^2 = m^2_{f_0}$. For large momentum transfers $F_{N,S}$ should vanish.

JHEP11(2019)162

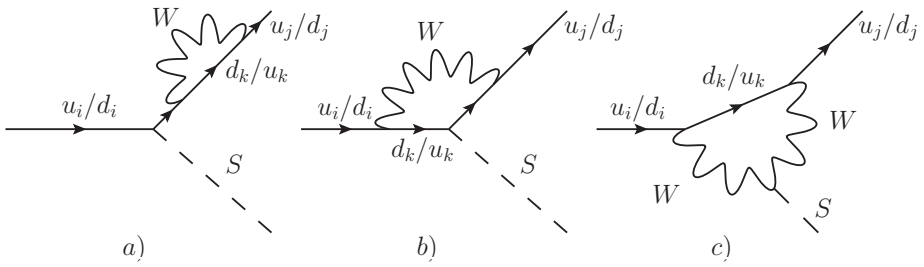

Figure 13. Diagrams of the production of the scalar S in flavor changing quarks transitions in the unitary gauge.

ξ_{ij}	ξ_{ds}	ξ_{uc}	ξ_{db}	ξ_{sb}
Value	$3.3 \cdot 10^{-6}$	$1.4 \cdot 10^{-9}$	$7.9 \cdot 10^{-5}$	$3.6 \cdot 10^{-4}$

Table 6. Numerical values of ξ_{ij} constants in effective Lagrangian (A.14).

A.3 Flavor changing effective Lagrangian

A light scalar S can be produced from a hadron via flavor changing quarks transitions (see diagrams in figure 13). The flavor changing amplitude was calculated using different techniques in many papers [38–43]. The corresponding effective Lagrangian of flavor changing quark interactions with the S particle is

$$\mathcal{L}_{\text{eff}}^{Sqq} = \theta \, \frac{S}{v} \sum_{i,j} \xi_{ij} m_{Q_j} \bar{Q}_i P_R Q_j + h.c., \tag{A.14}$$

where Q_i and Q_j are both upper or lower quarks and $P_R \equiv (1 + \gamma_5)/2$ is a projector on the right chiral state. The effective coupling ξ_{ij} is defined as

$$\xi_{ij} = \frac{3 G_F \sqrt{2}}{16\pi^2} \sum_k V_{ki}^* m_k^2 V_{kj}, \tag{A.15}$$

where Q_k are the lower quarks if Q_i and Q_j are the upper and vice versa, V_{ij} are the elements of the CKM matrix, and G_F is the Fermi constant. One power of the quark mass in the expression for ξ comes from the $h\bar{q}q$ coupling, while another one comes from the helicity flip on the quark line in the diagrams in figure 13. Because of such behavior, the quark transition generated by the Lagrangian (A.14) is more probable for lower quarks than for upper ones, since the former goes through the virtual top quark. Numerical values of some of ξ_{ij} constants are given in table 6.

B Scalar production from mesons

In the scalar production from hadron decays, the main contribution comes from the lightest hadrons in each flavor, which are mesons.[3] The list of the main hadron candidates is the

[3]Indeed, if X is the lightest hadron in the family, it could decay *only* through weak interaction, so it has small decay width Γ_X (in comparison to hadrons that could decay through electromagnetic or strong

JHEP11(2019)162

following (the information is given in the format "Hadron name (quark contents, mass in MeV)"):

- s-mesons $K^-(s\bar{u}, 494)$, $K^0_{S,L}(s\bar{d}, 498)$;
- c-mesons $D^0(c\bar{u}, 1865)$, $D^+(c\bar{d}, 1870)$, $D_s(c\bar{s}, 1968)$, $J/\psi(c\bar{c}, 3097)$;
- b-mesons $B^-(b\bar{u}, 5279)$, $B^0(b\bar{d}, 5280)$, $B_s(b\bar{s}, 5367)$, $B_c(b\bar{c}, 6276)$, $\Upsilon(b\bar{b}, 9460)$.

The production of a scalar from mesons is possible through the flavor changing neutral current A.3, so the production from D_s, J/ψ, B_s, B_c and Υ mesons does not have any advantage with respect to the production from D^0, D^+, B^- and B^0, while their amount at any experiment is significantly lower. Therefore, we will discuss below only production from later mesons.

B.1 Inclusive production

The decay widths for the processes $Q_i \to Q_j S$, $Q_i \to Q' e \bar{\nu}_e$ are

$$\Gamma_{Q_i \to Q_j + S} = \frac{|\mathcal{M}_{Q_i \to Q_j S}|^2}{8\pi m_b} \frac{|\boldsymbol{p}_S|}{m_b} \approx |\xi_{bs}|^2 \frac{m_b^3 \left(1 - \frac{m_S^2}{m_b^2}\right)^2}{32\pi v^2} \theta^2, \tag{B.1}$$

$$\begin{aligned} \Gamma_{Q_i \to Q_k + e + \bar{\nu}_e} &= \frac{1}{(2\pi)^3} \int_{m_{Q_k}^2}^{m_{Q_i}^2} ds_{Q_k e} \int_{s_{e\nu,\min}}^{s_{e\nu,\max}} ds_{e\nu} \frac{|\mathcal{M}_{Q_i \to Q_k + e + \bar{\nu}_e}|^2}{32 m_{Q_i}^3} \\ &\approx \frac{G_F^2 |V_{Q_i Q_k}|^2 m_{Q_i}^5}{192\pi^3} \times f(m_{Q_k}/m_{Q_i}), \end{aligned} \tag{B.2}$$

where $\boldsymbol{p}_S$ is the S particle momentum at the rest frame of the meson X,

$$|\boldsymbol{p}_S| = \frac{\sqrt{(m_X^2 - (m_S + m_{X'})^2)((m_X^2 - (m_S - m_{X'})^2)}}{2m_X}, \tag{B.3}$$

the integration limits are

$$s_{e\nu,\min} = 0, \quad s_{e\nu,\max} = m_{Q_i}^2 + m_{Q_i}^2 - s_{Q_k e} - \frac{m_{Q_i}^2 m_{Q_k}^2}{s_{Q_k e}}, \tag{B.4}$$

and

$$f(m_{Q_k}/m_{Q_i}) = \left(1 - 8\frac{m_{Q_k}^2}{m_{Q_i}^2} - 24\frac{m_{Q_k}^4}{m_{Q_i}^4} \ln\left(\frac{m_{Q_k}}{m_{Q_i}}\right) + 8\frac{m_{Q_k}^6}{m_{Q_i}^6} - \frac{m_{Q_k}^8}{m_{Q_i}^8}\right) \approx 1/2 \tag{B.5}$$

is the phase space factor.

interactions). The probability of light scalar production from hadron is inversely proportional to hadron decay width thus the light scalar production from the lightest hadrons is the most efficient.

JHEP11(2019)162

B.2 Scalar production in two-body mesons decays

Let us consider exclusive 2-body decay of a meson

$$X_{Q_i} \to X'_{Q_j} + S, \tag{B.6}$$

corresponding to the transition $Q_i \to Q_j + S$. Here and below, X_Q denotes a meson which contains a quark Q.

The Feynman diagram of the process is shown in figure 3(c). Using the Lagrangian (A.14), for the matrix element we have

$$\mathcal{M}(X_{Q_i} \to S X'_{Q_j}) = \frac{\theta}{2}\frac{m_{Q_i}}{v} \times \xi_{ij} \times M_{XX'}(m_S^2), \tag{B.7}$$

where

$$M_{XX'}((p_X - p_{X'})^2) \equiv \langle X'(p_{X'})|\bar{Q}_i(1+\gamma_5)Q_j|X(p_X)\rangle \tag{B.8}$$

is the matrix element of the transition $X_{Q_i} \to X'_{Q_j}$. Expressions for these matrix elements for different initial and final mesons are given in appendix F. So, we can calculate the branching fraction of the corresponding process by the formula [44]

$$\mathrm{BR}(X_{Q_i} \to X'_{Q_j} + S) = \frac{1}{\Gamma_X}\theta^2 \frac{|\xi_{ij}|^2 m_{Q_i}^2 |M_{XX'}(m_S^2)|^2}{32\pi v^2}\frac{|\boldsymbol{p}_S|}{m_X^2}, \tag{B.9}$$

where Γ_X is the decay width of the meson X. We use the lifetimes of mesons from [44].

For the kaons, the only possible 2-body decay is the process

$$K \to \pi + S \tag{B.10}$$

There are 3 types of the kaons — $K^\pm, K_L^0, K_S^0$. Although the decay width for each of them is by given by the same loop factor, ξ_{sd}, the branching ratios differ. The first reason is that these kaons have different decay widths. The second reason is that the K_S^0 is approximately the CP-even eigenstate. Therefore the decay $K_S^0 \to \pi S$ is proportional to the CKM CP-violating phase and is strongly suppressed [41]. Further we assume that the corresponding branching ratio vanishes. See table 3 for the branching ratios of $K_L^0, K^\pm$.

B.3 Scalar production in leptonic decays of mesons

Consider the process $X \to Se\nu$. Its branching ratio is [68, 69]

$$\mathrm{BR}(X \to Se\nu) = \frac{\sqrt{2}G_F m_X^4}{96\pi^2 m_\mu^2 (1 - m_\mu^2/m_h^2)^2} \times \mathrm{BR}(X \to \mu\nu)\left(\frac{7}{9}\right)^2 f\left(\frac{m_S^2}{m_X^2}\right), \tag{B.11}$$

where $f(x) = (1-8x+x^2)(1-x^2) - 12x^2 \ln x$. The values of the branching ratios for different types of the mesons are shown in table 7. However, although for the D this channel enhances the production in $\simeq \mathcal{O}(100)$ times, the production from D is still sub-dominant.

JHEP11(2019)162

Meson	$\mathrm{BR}(h \to Se\nu)/f\,(x)\,\theta^2$
$D \to Se\nu$	$5.2 \cdot 10^{-9}$
$K \to Se\nu$	$4.1 \cdot 10^{-8}$
$B \to Se\nu$	$< 7.4 \cdot 10^{-10}$

Table 7. Branching ratios of 3-body meson decay. From experimental data we have only upper bound on the $\mathrm{BR}(B \to \mu\nu)$, so we put upper bound on $B \to Se\nu$ decay.

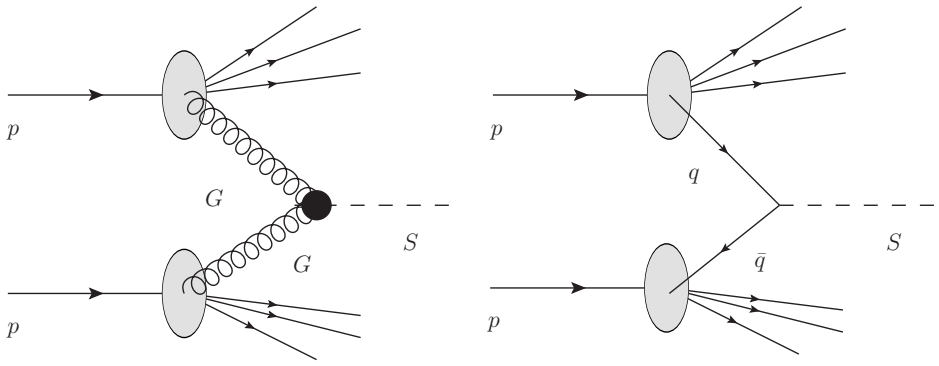

Figure 14. The diagrams of the production of the scalar in deep inelastic scattering.

C DIS

The scalar production in the DIS is driven by the interaction with the quarks and gluons:

$$\mathcal{L} = S\theta \sum_q \frac{m_q}{v}\bar{q}q + \theta\frac{S\alpha_s}{16\pi v}F_G(m_S)G^a_{\mu\nu}G^{\mu\nu,a}, \tag{C.1}$$

where F_G is a loop factor being of order of $|F_G|^2 \simeq 10-20$ for the scalars in the mass range $m_S \lesssim 10$ GeV (see appendix A.1). Processes of the scalar production in DIS are quark and gluon fusions:

$$q + \bar{q} \to S, \quad G + G \to S \tag{C.2}$$

Corresponding diagrams are shown in figure 14 and the matrix elements are

$$\mathcal{M}(GG \to S) = 4\frac{F_G(m_S)\alpha_s}{16\pi}\frac{\theta}{v}[(k_2^\mu \cdot k_1^\nu) - g^{\mu\nu}(k_1 \cdot k_2)]\epsilon_\mu(k_1)\epsilon_\nu(k_2), \tag{C.3}$$

$$i\mathcal{M}(q\bar{q} \to S) = \overline{v}(k_2)\left(\frac{-i\theta\overline{m}_q}{v}\right)u(k_1). \tag{C.4}$$

The differential cross section is given by

$$d\sigma(s_{YY}) = \frac{(2\pi)^4}{4}\frac{\overline{|\mathcal{M}(YY \to S)|^2}}{\sqrt{(k_1 \cdot k_2)^2}}d\Phi(k_1 + k_2, p_S) = \frac{\pi\overline{|\mathcal{M}(YY \to S)|^2}}{m_S^2}\delta(s_{YY} - m_S^2), \tag{C.5}$$

where Y denotes a quark/antiquark or a gluon, $\overline{|\mathcal{M}(GG \to S)|^2}$ is the squared matrix element averaged over gluon or quark polarizations and

$$d\Phi(k_1 + k_2, p_S) = \delta^4(k_1 + k_2 - p_S)\frac{d^3\boldsymbol{p}_S}{(2\pi)^3 2E_s}. \tag{C.6}$$

The hard cross sections for the gluon and quark fusions are thus

$$\sigma_G(s_{GG}) = \delta(s_{GG} - m_S^2)\frac{|F_G(m_S)|^2\alpha_s^2\theta^2 m_S^2}{128\pi v^2}, \tag{C.7}$$

$$\sigma_q(s_{qq}) = \frac{\pi}{m_S^2}\delta(s_{qq} - m_S^2)\frac{\theta^2\overline{m}_q^2}{2v^2}m_S^2. \tag{C.8}$$

Using hard cross sections (C.8) and (C.7), one can calculate the total cross section of the production in DIS as

$$\sigma_{\mathrm{DIS},Y} = g_Y \int \sigma_Y(s) f_{Y_1}(\sqrt{s_{Y_1Y_2}}, x_1) f_{Y_2}(\sqrt{s_{Y_1Y_2}}, x_2) dx_1 dx_2. \tag{C.9}$$

Here, $f_Y(Q, x)$ is the parton distribution function (pdf) of the parton Y carrying the momentum fraction x at the scale Q. $g_q = 2, g_G = 1$; g_q is a combinatorial factor taking into account that the quark/antiquark producing a scalar can be stored in both of colliding protons.

The result is

$$\sigma_{\mathrm{DIS},q}(s) = \frac{\pi}{m_S^2}\frac{\theta^2\overline{m}_q^2 m_S^2}{2v^2 s} \times W_{q\bar{q}},\ \sigma_{\mathrm{DIS},G}(s) = \theta^2\frac{|F_G(m_S)|^2\alpha_s^2(m_S)m_S^2}{128\pi s v^2} \times W_{GG}. \tag{C.10}$$

Here, s denotes the pp CM energy, $\overline{m}_q$ is the $\overline{\mathrm{MS}}$ quark mass at the scale m_S, and

$$W_{XX}(s, m_S) \equiv \int_{m_S^2/s}^1 \frac{dx}{x} f_X(m_S, x) f_X\left(m_S, \frac{m_S^2}{sx}\right) \tag{C.11}$$

is the partonic weight of the process. Since the partonic model breaks down at scales $Q \lesssim 1$ GeV, the description of the scalar production in DIS presented in this section is valid only for scalars with masses $m_S \gtrsim 1$ GeV. For numerical estimates we have used LHAPDF package [70] with CT10NLO pdf set [71].

The main contribution to the DIS cross section comes from gluons. To see this, let us compare the gluon cross section $\sigma_{\mathrm{DIS},G}$ with the s-quark cross section $\sigma_{\mathrm{DIS},S}$, which is the largest quark cross section.[4] Their ratio is

$$\frac{\sigma_{\mathrm{DIS},G}}{\sigma_{\mathrm{DIS},s}} \approx 0.6\left(\frac{\alpha_s(m_S)}{0.4}\right)^2\frac{|F_G(m_S)|^2}{20} \times \left(\frac{m_S}{1\text{ GeV}}\right)^2\frac{W_{GG}}{W_{ss}}. \tag{C.12}$$

The product $|F_G|^2\alpha_s^2$ changes with m_S relatively slowly, and therefore the ratio (C.12) is determined by the product $(m_S/1\text{ GeV})^2 W_{GG}/W_{ss}$. It is larger than one for the masses $m_S \gtrsim 2$ GeV in broad CM energy range, see figure 4.

[4] Indeed, the quark cross sections are proportional to the Yukawa constant squared y_q^2, and the large ratio $(y_s/y_{u,d})^2$ compensates smaller partonic weight $W_{ss}/W_{u,d}$.

JHEP11(2019)162

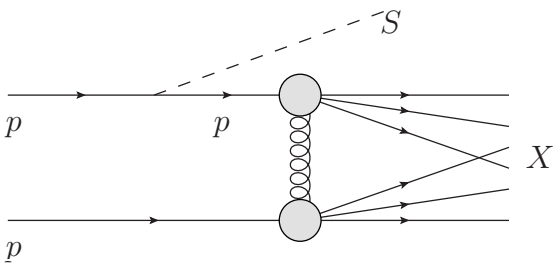

Figure 15. A diagram of the production of a scalar in the proton bremsstrahlung process.

Having the cross sections (C.10), we calculate the DIS probability as

$$P_{\rm DIS} = \frac{\sum_q \sigma_{{\rm DIS},q} + \sigma_{{\rm DIS},G}}{\sigma_{pp}}, \tag{C.13}$$

where for the total proton-proton cross section σ_{pp} we used the data from [44].

D Scalar production in proton bremsstrahlung

A scalar S can be produced through the SNN vertex (see section A.2) in proton-proton bremsstrahlung process

$$p + p \to S + X, \tag{D.1}$$

with the diagram of the process shown in figure 15. Corresponding probability can be estimated using generalized Weizsacker-Williams method, allowing to express the cross section of the given process by the cross section of its sub-process [72–78]. Namely, let us denote the momentum of the incoming proton in the rest frame of the target proton by p_p, the fraction of p_p carried by S as z and the transverse momentum of S as p_T. Then, under conditions

$$\frac{p_T^2}{4p_p^2} \ll z(1-z)^2, \quad \frac{m_S^2}{4p_p^2} \ll z(1-z), \quad \frac{m_p^2}{4p_p^2} \ll \frac{(1-z)^2}{z} \tag{D.2}$$

the differential production cross section of S production can be written as (see appendix D.1)

$$d\sigma_{\rm brem} \approx \sigma_{pp_t}(s') \times P_{p\to pS}(p_T, z) dp_T^2 dz, \tag{D.3}$$

where we denoted a target proton as p_t, σ_{pp_t} is the total p-p cross section, $s' = 2m_p p_p(1-z) + 2m_p^2$ and the differential splitting probability of the proton to emit a scalar is

$$P_{p\to pS}(p_T, z) \approx |F_{pS}(m_S^2)|^2 \frac{g_{\rm SNN}^2 \theta^2}{8\pi^2} z \frac{m_p^2(2-z)^2 + p_T^2}{(m_p^2 z^2 + m_S^2(1-z) + p_T^2)^2}, \tag{D.4}$$

with $g_{\rm SNN}$ being low-energy proton-scalar coupling, and F_{pS} the scalar-proton form-factor, see appendix A.2.

JHEP11(2019)162

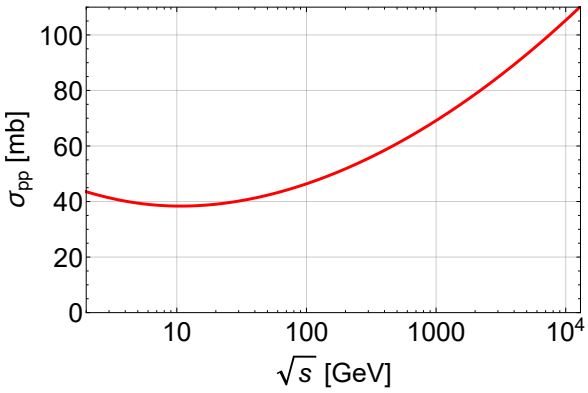

Figure 16. Proton-proton total cross section as a function of the center of mass energy $\sqrt{s_{pp}}$.

For the total pp cross section we use experimental fit

$$\sigma_{pp}(s) = Z + B\ln^2\left(\frac{s}{s_0}\right) + C_1\left(\frac{s_1}{s}\right)^{\eta_1} - C_2\left(\frac{s_1}{s}\right)^{\eta_2}, \tag{D.5}$$

where $Z = 35.45$ mb, $B = 0.308$ mb, $C_1 = 42.53$ mb, $C_2 = 33.34$ mb, $\sqrt{s_0} = 5.38$ GeV, $\sqrt{s_1} = 1$ GeV, $\eta_1 = 0.458$ and $\eta_2 = 0.545$ [44]. This cross section is shown in figure 16, where we see that it is almost constant for a wide range of energies.

The total cross section can be written in the form

$$\sigma_{\text{brem}} = g_{\text{SNN}}^2\theta^2|F_{pS}(m_S^2)|^2\sigma_{pp}(s)\mathcal{P}_{\text{brem}}(s, m_S), \tag{D.6}$$

where

$$\mathcal{P}_{\text{brem}}(s, m_S) = \frac{1}{g_{\text{SNN}}^2\theta^2}\int dp_T^2 dz P_{p\to pS}(p_T, z)\frac{\sigma_{pp}(s')}{\sigma_{pp}(s)}. \tag{D.7}$$

The domain of the definition of p_T and z is determined by the conditions (D.2). For definiteness, we fix the domain of integration by the requirement

$$\frac{m_S^2(1-z) + m_p^2 z^2 + p_T^2}{4p_p^2 z(1-z)^2} < 0.1. \tag{D.8}$$

The probability of a scalar production in proton bremsstrahlung is

$$P_{\text{brem}} = \frac{\sigma_{\text{brem}}}{\sigma_{pp}(s)} \approx g_{\text{SNN}}^2\theta^2|F_{pS}(m_S^2)|^2\mathcal{P}_{\text{brem}}(s, m_S), \tag{D.9}$$

where s is the CM energy of two protons. We show its dependence on the scalar mass and the incoming beam energy in figure 17.

D.1 Splitting probability derivation

Following the approach described in [72], let us consider the process (D.1) within the old-fashioned perturbation theory. The corresponding diagrams are shown in figure 18. The

JHEP11(2019)162

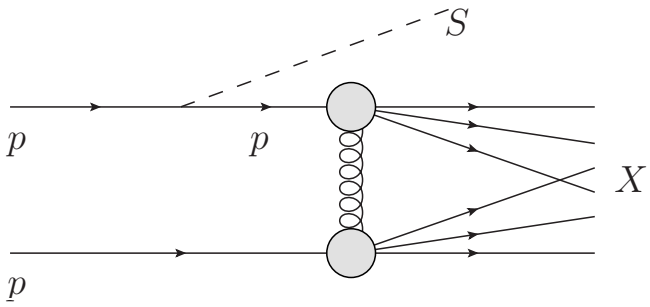

Figure 17. The probability of the production of a scalar S in bremsstrahlung process versus the scalar mass.

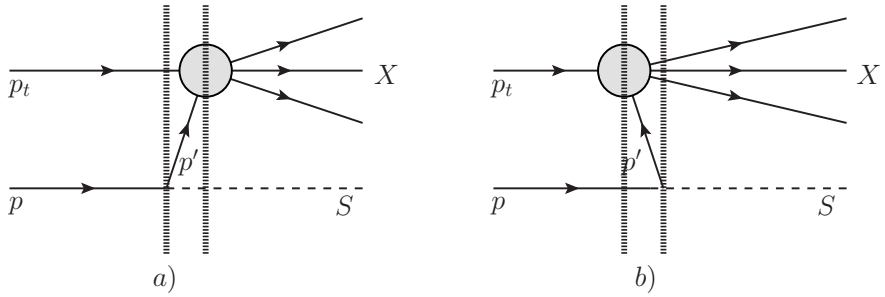

Figure 18. The lowest order old-fashioned perturbation theory diagrams for the bremsstrahlung process (D.1). Vertical dotted lines denote the intermediate states.

matrix element has the form $\mathcal{V}_{pp_t\to SX} = \mathcal{V}_a + \mathcal{V}_b$, where

$$\mathcal{V}_a = \frac{\mathcal{M}_{p\to p'S}\mathcal{M}_{p'p_t\to X}}{2E_{p'}(E_{p'}+E_S-E_p)}\bigg|_{\boldsymbol{p}_{p'}=\boldsymbol{p}_p-\boldsymbol{p}_S}, \quad \mathcal{V}_b = \frac{\mathcal{M}_{p_t\to p'X}\mathcal{M}_{p'p\to S}}{2E_{p'}(E_p+E_{p'}-E_S)}\bigg|_{\boldsymbol{p}_{p'}=\boldsymbol{p}_p-\boldsymbol{p}_S}. \tag{D.10}$$

Here, $\mathcal{M}$ denotes Lorentz-invariant amplitude of the processes. There exists a kinematic domain at which $|\boldsymbol{M}_b| \ll |\boldsymbol{M}_a|$. Namely, let us consider an ultrarelativistic incoming p, and write the 4-momenta of p, S and intermediate p' as

$$P_p^\mu = \left(p_p + \frac{m_p^2}{p_p^2}, \mathbf{0}, p_p\right), \tag{D.11}$$

$$P_S^\mu = \left(p_p z + \frac{p_T^2+m_S^2}{2p_p z}, \boldsymbol{p}_T, z p_p\right), \tag{D.12}$$

$$P_{p'}^\mu = \left((1-z)p_p + \frac{m_p^2+p_T^2}{2p_p(1-z)}, -\boldsymbol{p}_T, (1-z)p_p\right), \tag{D.13}$$

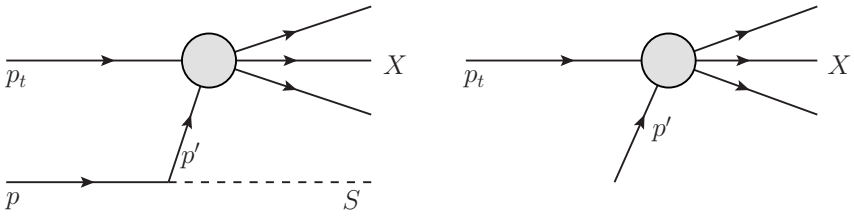

Figure 19. Diagrams the bremsstrahlung process (D.1) (left) and its sub-process $pp_t \to X$ describing a proton-proton collision (right).

where p_T is a transverse momentum of S and z is a fraction of a parallel momentum carried by S. Then the energy denominators in (D.10) are

$$\Delta E_a = E_{p'} + E_S - E_p \approx \frac{p_T^2 + (1-z)m_S^2 + z^2 m_p^2}{2p_p z(1-z)}, \quad \Delta E_b = E_p + E_{p'} - E_S \approx 2p_p(1-z). \tag{D.14}$$

Assuming that $\Delta E_a \ll \Delta E_b$ we can neglect the matrix element $\mathcal{V}_b$.

Once we neglect $\mathcal{V}_b$, it is possible to relate the differential cross section of the process (D.1) to the total pp scattering cross section. Indeed, let us consider a corresponding process $pp_t \to X$, which is a sub-process of (D.1) obtained by removing the in p line and out S line, see figure 19. The matrix element for this process is simply

$$\mathcal{V}_{pp_t \to S} = \mathcal{M}_{pp_t \to X}. \tag{D.15}$$

Using (D.10), (D.15), for the corresponding differential cross sections we obtain

$$d\sigma_{pp_t \to SX} = \frac{1}{4E_p E_{p_t}} \frac{|\mathcal{M}_{p\to p'S}|^2 |\mathcal{M}_{p' p_t \to X}|^2}{(2E_{p'})^2 (E_{p'} + E_S - E_p)^2} \times (2\pi)^4 \delta^{(4)}\left(p_p + p_{p_t} - p_S - \sum_X p_X\right) \frac{d^3\boldsymbol{p}_S}{(2\pi)^3 2E_S} \times \prod_X \frac{d^3\boldsymbol{p}_X}{(2\pi)^3 2E_X}, \tag{D.16}$$

$$d\sigma_{p' p_t \to X} = \frac{1}{4E_{p'} E_{p_t}} |\mathcal{M}_{p' p_t \to X}|^2 \times (2\pi)^4 \delta^{(4)}\left(p_{p'} + p_{p_t} - \sum_X p_X\right) \prod_X \frac{d^3\boldsymbol{p}_X}{(2\pi)^3 2E_X} \tag{D.17}$$

Neglecting the difference in the energy conservation arguments in the delta-functions that are of order $\mathcal{O}(m_{p/S}^2/p_p^2, p_T^2/p_p^2)$, we can relate these two cross sections as

$$d\sigma_{pp_t \to SX} = dP_{p\to p'S}(z, p_T) d\sigma_{p' p_t \to X}(p_T, z), \tag{D.18}$$

where we introduced differential splitting probability $dP_{p\to p'S}$:

$$dP_{p\to p'S}(p_T, z) \equiv 2 \frac{|\mathcal{M}_{p\to p'S}|^2}{4E_p E_{p'}(E_{p'} + E_S - E_p)^2} \frac{d^3\boldsymbol{p}_S}{(2\pi)^3 2E_S}. \tag{D.19}$$

Here a factor of 2 is combinatorial factor taking into account that a scalar can be produced from both the legs of colliding protons.

JHEP11(2019)162

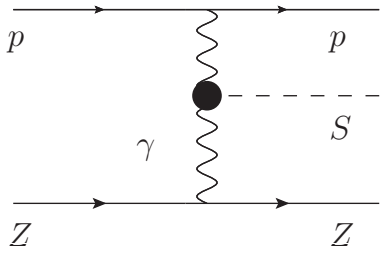

Figure 20. A diagram of the production of a scalar in photon fusion.

Integrating the differential cross section (D.18) over the momenta of the final states particles X and summing over all possible sets $\{X\}$, we finally arrive at

$$d\sigma_{pp_t\to SX} \approx P_{p\to p'S}(z, p_T) dp_T^2 dz \sigma_{pp}(s'), \tag{D.20}$$

where $s' \approx 2m_p p_p(1-z) + 2m_p^2$,[5] and $\sigma_{pp}(s')$ is the total proton-proton cross section.

Let us now find explicit expression for the splitting probability (D.19). Using the expressions (D.2), we find

$$\frac{d^3\boldsymbol{p}_S}{(2\pi)^3 2E_S} \approx \frac{dp_T^2 dz}{16\pi^2 z}, \quad |\mathcal{M}_{p\to pS}|^2 \approx 2g_{\text{SNN}}^2\theta^2 |F_{pS}(m_S^2)|^2 (m_p^2 + (P_p \cdot P_{p'})). \tag{D.21}$$

Finally, we arrive at

$$P_{p\to p'S} \approx \frac{g_{\text{SNN}}^2\theta^2 |F_{pS}(m_S^2)|^2}{8\pi^2} z \frac{m_p^2(2-z)^2 + p_T^2}{(m_p^2 z^2 + m_S^2(1-z) + p_T^2)^2}. \tag{D.22}$$

E Scalar production in photon fusion

A scalar can be produced elastically in pp collisions through the $S\gamma\gamma$ vertex (see appendix A.1). The production process is

$$p + Z \to p + Z + S, \tag{E.1}$$

with the corresponding diagram shown in figure 20. To find the number of produced scalars in the photon fusion, we will use the equivalent photon approximation (EPA), which provides a convenient framework for studying processes involving photons emitted from fast-moving charges [79–81]. The basic idea of the EPA is a replacement of the charged particle Y in the initial and final state, that interacts through the virtual photon carrying the virtuality q and the fraction of charge's energy x, by the almost real photon with a distribution $n_Y(x; q^2)$ that depends on the type of the charged particle, see figure 21. The magnitude of the momentum transfer carried by the virtual photon can be approximated as

$$q^2 \approx \frac{q_t^2 + x^2 m_Y^2}{1-x}, \tag{E.2}$$

[5] Here we neglected the p_T dependence in σ_{pp}.

JHEP11(2019)162

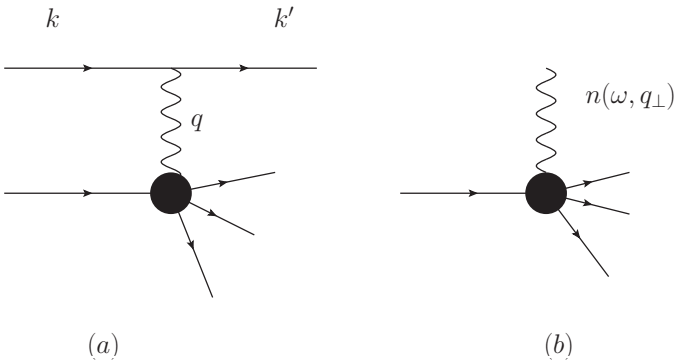

Figure 21. The idea of the equivalent photon approximation. If a charge with the momentum k, emitting the virtual photon with the virtuality q, is ultrarelativistic, then the cross section of the process (a) can be expressed in terms of the cross section of the process (b). The remained effect of the charge is the distribution function $n_{\text{charge}}(x, q^2)$, where x is the energy fraction carried by photon.

where q_t is the transverse component of the spatial momentum of the photon with respect to the spatial momentum of the particle Y, and m_Y is the mass of Y. Conditions for validity of the EPA are $x \ll 1$ and $q_t \lesssim x m_Y$ [81]. The distribution $n_Y(x, q_t^2)$ of the emitted photons can be described by

$$n_Y(x; q_t^2) = \frac{\alpha_{\text{EM}}}{2\pi} \frac{1 + (1-x)^2}{x(q_t^2 + x^2 m_X^2)} \left[\frac{q_t^2}{q_t^2 + x^2 m_Y^2} D_Y(q^2) + \frac{x^2}{2} C_Y(q^2) \right], \tag{E.3}$$

where $C(q^2), D(y^2)$ are appropriate form-factors. We take the proton and nucleus form-factors from [81].

Within the EPA, we approximate the cross section of the process (E.1) by

$$\sigma_{pZ \to SpZ} = \int dx_1 dx_2 d\vec{q}_{1t}^{\,2} d\vec{q}_{2t}^{\,2} \gamma_p(q_{1t}^2, x_1) \gamma_Z(q_{2t}^2, x_2) \sigma_{\gamma\gamma \to S}(s_{\gamma\gamma}). \tag{E.4}$$

Here

$$\sigma_{\gamma\gamma \to S}(s_{\gamma\gamma}) = \frac{\pi}{m_S^2} \frac{|F_\gamma(m_S)|^2 \alpha_{\text{EM}}^2 \theta^2 m_S^4}{256\pi^2 v^2} \delta(s_{\gamma\gamma} - m_S^2) \equiv \frac{1}{x_1} \Sigma_{\gamma\gamma} \frac{\delta\left(x_2 - \frac{m_S^2}{x_1 s_{pZ}}\right)}{x_1 s_{pY}}, \tag{E.5}$$

where $s_{\gamma\gamma} = (q_1 + q_2)^2 \approx 4 x_1 x_2 E_p^{\text{CM}} E_Y^{\text{CM}} \approx x_1 x_2 s_{pY}$, and

$$\Sigma_{\gamma\gamma} = \theta^2 \frac{|F_\gamma|^2 \alpha_{\text{EM}}^2 m_S^2}{256\pi v^2 s_{pZ}}. \tag{E.6}$$

Let us discuss the boundaries of integration in eq. (E.4). Following [81], for the upper limit of q we choose $q_{\max} = 1$ GeV for the maximal virtuality of a photon emitter by the proton and $q_{\max} = 4.49/R_1$ for a photon emitted by the nucleus. Using (E.2), we get $x_{p,max} \approx 0.63$, $x_{Z,max} = 0.018$. The lower bound on q, it is given by the kinematic

JHEP11(2019)162

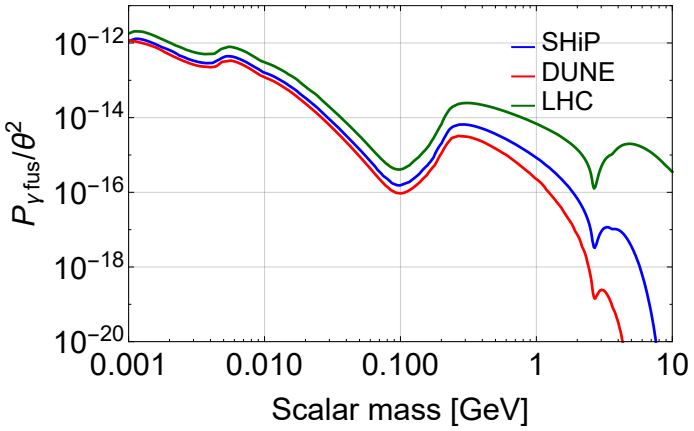

Figure 22. The production probabilities of the scalar in photon fusion process versus the scalar mass. We consider Mo nucleus ($Z = 42$, $A = 96$).

threshold for the S particle production. For the nucleus, there is additional constraint $q^2 \gtrsim r_s^{-2}$, where $r_s \simeq 10$ keV is the inverse radius of the electron shell (at larger scales the nucleus is screened by electrons).

Substituting the photon fusion cross section (E.5) into (E.4), for the pZ cross section we get

$$\sigma_{pZ\to pZS} = Z^2\alpha_{\mathrm{EM}}^2\Sigma_{\gamma\gamma} \times W_{\mathrm{coh}}, \tag{E.7}$$

where

$$W_{\gamma\ \mathrm{fusion}} = \frac{(2\pi)^2}{Z^2\alpha_{\mathrm{EM}}^2}\int_0^{q_{1t,\max}} q_{1t}\,dq_{1t}\int_0^{q_{2t,\max}} q_{2t}\,dq_{2t} \times \int_{\frac{m_S^2}{x_{2,max}s_{pZ}}}^{x_{1,max}} \frac{dx_1}{x_1}\,\gamma_p(x_1,q_{1t})\gamma_Z\left(\frac{m_S^2}{x_1 s_{pZ}},q_{2t}\right) \tag{E.8}$$

is the integrated form-factor. Here we simplified the integration domain for p_t assuming $q_{1t,\max}, q_{2t,\max} = 1$ GeV, since the integrand is nonzero only in some region of parameters within the integration area, and therefore by increasing of integration limits we will not affect the result.

The production probability is calculated using the cross section (E.7) as

$$P_{\gamma\ \mathrm{fusion}} = \frac{\sigma_{pZ\to pZS}}{\sigma_{pZ}}, \tag{E.9}$$

where $\sigma_{pZ} \approx 53\ A^{0.77}$ mb is the total pZ cross section, with A being the mass number of the nucleus target [45].

The dependence of $P_{\gamma\ \mathrm{fusion}}$ on the scalar mass and collision energy is shown in figure 22.

JHEP11(2019)162

F Form-factors for the flavor changing neutral current meson decays

Consider matrix elements

$$M_{XX'}^{P=P'} = \langle X'(p_{X'})|\bar{Q}_j Q_i|X(p_X)\rangle, \quad M_{XX'}^{P\neq P'} = \langle X'(p_{X'})|\bar{Q}_j\gamma_5 Q_i|X(p_X)\rangle \tag{F.1}$$

describing transitions of mesons $X(Q_i) \to X'(Q_j)$ in the case of the same and opposite parities P, P' correspondingly. These matrix elements can be related to the matrix elements

$$M_{XX'}^{\mu} \equiv \langle X'(p_{X'})|\bar{Q}_i\gamma^\mu Q_j|X(p_X)\rangle, \quad M_{XX'}^{\mu 5} \equiv \langle X'(p_{X'})|\bar{Q}_i\gamma^\mu\gamma_5 Q_j|X(p_X)\rangle \tag{F.2}$$

describing the weak charged current mediating mesons transition $X \to X'$. To derive the relation, we follow [82] in which a relation for pseudoscalar transition X' was obtained. We generalize this approach to the arbitrary final-state meson. We first notice that

$$M_{XX'}^{P=P'} \equiv \frac{1}{m_{Q_i} - M_{Q_j}}\langle X'(p_{X'})|\bar{Q}_j \not{p}_Q Q_i|X(p_X)\rangle, \tag{F.3}$$

$$M_{XX'}^{P\neq P'} \equiv \frac{1}{m_{Q_i} + m_{Q_j}}\langle X'(p_{X'})|\bar{Q}_j\gamma_5 \not{p}_Q Q_i|X(p_X)\rangle, \tag{F.4}$$

where $p_Q^\mu \equiv p_{Q_i}^\mu - p_{Q_j}^\mu$ and we used the Dirac equation for free quarks. Using then the identity

$$\bar{Q}_j \not{p}_Q Q_i \equiv \hat{P}_\mu \bar{Q}_j\gamma^\mu Q_i \equiv [\hat{P}_\mu, \bar{Q}_j\gamma^\mu Q_i], \tag{F.5}$$

where $\hat{P}_\mu \equiv i\partial_\mu$ is the momentum operator, we find

$$\begin{aligned} M_{XX'}^{P=P'} &= \frac{1}{m_{Q_i} - m_{Q_j}}\langle X'(p_{X'})|[\hat{P}_\mu,\ \bar{Q}_j\gamma^\mu Q_i]|X(p_X)\rangle \\ &= -\frac{1}{m_{Q_i} - m_{Q_j}}(p_X - p_{X'})_\mu\langle X'(p_{X'})|\bar{Q}_j\gamma^\mu Q_i|X(p_X)\rangle \equiv -\frac{1}{m_{Q_i} - m_{Q_j}}q^\mu M_\mu, \end{aligned} \tag{F.6}$$

where $q_\mu \equiv p_{X'\mu} - p_{X\mu}$; for deriving the expression we have acted by $\hat{P}_\mu$ on the meson states $|X\rangle, |X'\rangle$. Similarly, for $P \neq P'$ we find

$$M_{XX'}^{P\neq P'} = -\frac{1}{m_{Q_i} + m_{Q_j}}q^\mu M_{XX\mu}^5 \tag{F.7}$$

Further we will assume that X is a pseudoscalar, and therefore transitions in pseudoscalar, pseudovector mesons X' are parity even, while transitions in scalar, vector and tensor mesons are parity odd.

F.1 Scalar and pseudoscalar final meson state

F.1.1 Pseudoscalar

In the case of the pseudoscalar meson, $X' = P$, we have [83]

$$\begin{aligned} M_{XP}^\mu &= \langle P(p_P)|\bar{Q}_i\gamma^\mu Q_j|X(p_X)\rangle \\ &= \left[(p_X + p_P)^\mu - \frac{m_X^2 - m_P^2}{q^2}q^\mu\right] f_1^{XP}(q^2) + \frac{m_X^2 - m_P^2}{q^2}q^\mu f_0^{XP}(q^2), \end{aligned} \tag{F.8}$$

where $q = p_X - p_P$.

JHEP11(2019)162

X, P	$B^{+/0}, K^{+/0}$	$B^{+/0}, \pi^{+/0}$	K, π
$m^X_{\rm fit}$, GeV	6.16	6.16	∞
F_0^{XP}	0.33 ± 0.04	0.258 ± 0.031	0.96

Table 8. Values of the parameters in the form-factor (F.11) for different X, P. We use [50, 84].

Contracting it with q_μ, we obtain

$$q_\mu M^\mu_{XP} = (m_X^2 - m_P^2) f_0^{XP}(q^2) \tag{F.9}$$

Therefore

$$M_{XP} = \frac{m_X^2 - m_P^2}{m_{Q_j} - m_{Q_i}} f_0^{XP}(q^2) \tag{F.10}$$

We take the expression for the form-factor $f_0^{XP}(q^2)$ from [50]:

$$f_0^{XP}(q^2) = \frac{F_0^{XP}}{1 - q^2/(m^X_{\rm fit})^2} \tag{F.11}$$

The values of the parameters $m^X_{\rm fit}$, F_0^{XP} for different X, P are summarized in table 8.

F.1.2 Scalar

For the scalar meson $X' = \tilde{S}$ we have [52]

$$M^\mu_{X\tilde{S}} = -i \left[(p_X + p_{\tilde{S}})^\mu - q^\mu \right] f_+^{X\tilde{S}}(q^2) \tag{F.12}$$

(here we used $f_+(q^2) = -f_-(q^2)$ in eq. (6) of [52]). Similarly to the case $h' = P$,

$$M_{X\tilde{S}} = i \frac{m_X^2 - m_{\tilde{S}}^2 - q^2}{m_{Q_j} + m_{Q_i}} f_+^{X\tilde{S}}(q^2). \tag{F.13}$$

Consider the transition $B \to K_0^* S$. There is an open question whether hypothetical $K_0^*(700)$ is a state formed by two or four quarks, see, e.g. [85], discussions in [52, 86] and references therein. We assume that $K_0^*(700)$ is a di-quark state and $K_0^*(1430)$ is its excited state. There are no experimentally observed decays $B \to K_0^*(700)X$, and therefore there is quite large theoretical uncertainty in determination of the form-factors (see a discussion in [87]). We will use [52], where there are results for $B \to K_0^*(700)$ and $B \to K_0^*(1430)$, and the results for the latter are in good agreement with the experimental data for $B \to K_0^*(1430)\eta'$ decay.

We fit the q^2 dependence of $f_+^{BK_0^*}$ from [52] by the standard pole-like function that is used in the literature discussing the $B \to K_0^*$ transitions (see, e.g., [86]):

$$f_+^{BK_0^*}(q^2) = \frac{F_0^{BK_0^*}}{1 - a\frac{q^2}{m_B^2} + b\left(\frac{q^2}{m_B^2}\right)^2}, \tag{F.14}$$

where $m_B = 5.3$ GeV is the mass of the B^+ meson. The fit parameters are given in table 9.

JHEP11(2019)162

$\tilde{S}$	$F_0^{B\tilde{S}}$	a	b
$K_0^*(700)$	0.46	1.6	1.35
$K_0^*(1430)$	0.17	4.4	6.4

Table 9. Values of the parameters in the form-factor (F.14) for $B = B^+$, $\tilde{S} = K_0^{*0}(700)$, $K_0^*(1430)$. We used [52].

F.2 Vector and pseudovector final meson state

F.2.1 Vector

For the vector final state, $X' = V$, we have [49, 83]

$$\begin{aligned}\langle V(p_V)|\bar{Q}_i\gamma^\mu\gamma_5 Q_j|X(p_X)\rangle &= (m_X + m_V)\epsilon^{\mu *}(p_V)A_1(q^2) \\ &\quad - (\epsilon^*(p_V)\cdot q)(p_X + p_V)^\mu \frac{A_2(q^2)}{m_X + m_V} \\ &\quad - 2m_V \frac{\epsilon^*(p_V)\cdot q}{q^2} q^\mu (A_3(q^2) - A_0(q^2)),\end{aligned} \tag{F.15}$$

$$\langle V(p_V)|\bar{Q}_i\gamma^\mu Q_j|X(p_X)\rangle = \frac{2V(q^2)}{m_X + m_V} i\epsilon^{\mu\nu\rho\sigma}\epsilon^*_\nu(p_V)p_{X,\rho}p_{V,\sigma}, \tag{F.16}$$

where $\epsilon_\mu(p_V)$ is the polarization vector of the vector meson, and A_i, V are the form-factors. The form-factor A_3 is related to A_1 and A_2 as

$$A_3(q^2) = \frac{m_X + m_V}{2m_V}A_1(q^2) - \frac{m_X - m_V}{2m_V}A_2(q^2) \tag{F.17}$$

Contracting (F.15) and (F.16) with q_μ, we obtain that the vector part of the matrix element vanishes, while for the axial-vector part we find

$$M_{XV} = \langle V(p_V)|\bar{Q}_i\gamma_5 Q_j|X(p_X)\rangle = -\frac{(\epsilon^*(p_V)\cdot p_X)}{m_{Q_i} + m_{Q_j}} 2m_V A_0^{XV}(q^2), \tag{F.18}$$

where we used the relation (F.17). Consider a scalar product $(\epsilon^*(p_V)\cdot p_X)$ in the rest frame of the meson X. In this case only longitudinal polarization of $\epsilon^*_\mu(p_V)$ contributes. Using $\epsilon^{L,*}_\mu(p_V) = \left(\frac{|\boldsymbol{p}_V|}{m_V}, \frac{\boldsymbol{p}_V}{|\boldsymbol{p}_V|}\frac{E_V}{m_V}\right)$ we obtain

$$M_{XV} = -\frac{2m_X|\boldsymbol{p}_V|}{m_{Q_i} + m_{Q_j}} A_0(q^2) \tag{F.19}$$

For the case $B \to K^*(892)$, we follow [49] and parametrize the form-factor as

$$A_0^{BK^*(892)}(q^2) = \frac{r_1}{1 - q^2/m_R^2} + \frac{r_2}{1 - q^2/(m_{\text{fit}}^{A_0})^2}. \tag{F.20}$$

The values of parameters are given in table 10.

For the case $B \to V = K^*(1410), K^*(1680)$, we use an expression for the form-factors [53, 88]:

$$A_0^{BV}(q^2) = \left(1 - \frac{2m_V^2}{m_B^2 + m_V^2 - q^2}\right)\xi_{||}(q^2) + \frac{m_V}{m_B}\xi_\perp(q^2), \tag{F.21}$$

JHEP11(2019)162

V	r_1	r_2	m_R, GeV	$m_{\rm fit}$, GeV	$A_0^{BV}(0)$
$K^*(892)$	1.364	−0.99	m_B^+	$\sqrt{36.8}$	$0.374^{+0.033}_{-0.033}$

Table 10. Values of the parameters in the vector form-factor (F.20) from [49].

V	$\xi_\perp(0)$	$\xi_{\|\|}(0)$	$A_0^{BV}(0)$
$K^*(1410)$	$0.28^{+0.04}_{-0.04}$	$0.22^{+0.03}_{-0.03}$	$0.3^{+0.036}_{-0.036}$
$K^*(1680)$	$0.24^{+0.05}_{-0.05}$	$0.18^{+0.03}_{-0.03}$	$0.22^{+0.04}_{-0.04}$

Table 11. Values of the parameters in the vector form-factors (F.21) from [53, 88].

where

$$\xi_{\perp/||}(q^2) = \frac{\xi_{\perp/||}(0)}{1 - q^2/m_B^2} \tag{F.22}$$

The values of the parameters are given in table 11.

F.2.2 Pseudo-vector

For the pseudo-vector mesons, $X' = A$, the expansion of the matrix elements is similar to (F.15), (F.16), but the expressions for the vector and axial-vector matrix elements are interchanged [89, 90],

$$\begin{aligned}\langle A(p_A)|\bar{Q}_i\gamma^\mu Q_j|X(p_X)\rangle =& (m_X + m_A)\epsilon^{\mu *}(p_A)V_1(q^2) \\ &- (\epsilon^*(p_A)\cdot q)(p_X + p_A)^\mu \frac{V_2(q^2)}{m_X + m_A} \\ &- 2m_A \frac{\epsilon^*(p_A)\cdot q}{q^2} q^\mu (V_3(q^2) - V_0(q^2)),\end{aligned} \tag{F.23}$$

$$\langle A(p_A)|\bar{Q}_i\gamma^\mu\gamma_5 Q_j|X(p_X)\rangle = \frac{2A(q^2)}{m_X + m_A} i\epsilon^{\mu\nu\rho\sigma}\epsilon^*_\nu(p_A)p_{X,\rho}p_{A,\sigma}, \tag{F.24}$$

with the same relation between V_i as for A_i in the case of vector mesons (F.17). We therefore obtain

$$M_{XA} = \frac{2m_X|\boldsymbol{p}_A|}{m_{Q_j} - m_{Q_i}} V_0^{XA}(q^2), \tag{F.25}$$

We will consider two lightest pseudo-vector resonances $K_1(1270), K_1(1400)$, each of which is the mixture of unphysical K_{1A} and K_{1B} states [89],

$$\begin{pmatrix} |K_1(1270)\rangle \\ |K_1(1400)\rangle \end{pmatrix} = \begin{pmatrix} \sin(\theta_{K_1}) & \cos(\theta_{K_1}) \\ \cos(\theta_{K_1}) & -\sin(\theta_{K_1}) \end{pmatrix} \begin{pmatrix} |K_{1A}\rangle \\ |K_{1B}\rangle \end{pmatrix}, \tag{F.26}$$

The form-factors $V_0^{BK_1}$ can be related to the form-factors $V_0^{A/B}$ of the K_{1A}, K_{1B} as

$$V_0^{BK_1(1270)}(q^2) = \frac{1}{m_{K_1(1270)}}\left[\sin(\theta_{K_1})m_{K_{1A}}V_0^A(q^2) + \cos(\theta_{K_1})m_{K_{1B}}V_0^B(q^2)\right], \tag{F.27}$$

$$V_0^{BK_1(1400)}(q^2) = \frac{1}{m_{K_1(1400)}}\left[\cos(\theta_{K_1})m_{K_{1A}}V_0^A(q^2) - \sin(\theta_{K_1})m_{K_{1B}}V_0^B(q^2)\right], \tag{F.28}$$

JHEP11(2019)162

F_0^A	F_0^B	a_A	a_B	b_A	b_B
$0.22^{+0.04}_{-0.04}$	$-0.45^{+0.12}_{-0.08}$	2.4	1.34	1.78	0.69

Table 12. Values of the parameters in the vector form-factors (F.29) from [89].

θ_{K_1}	$m_{K_{1A}}$	$m_{K_{1B}}$	$V_0^{BK_1(1270)}(0)$	$V_0^{BK_1(1400)}(0)$
$-34^\circ \pm 13^\circ$	1.31 GeV	1.34 GeV	$-0.52^{+0.13}_{-0.09}$	$-0.07^{+0.033}_{-0.012}$

Table 13. Values of the parameters in the vector form-factors (F.27), (F.28) from [89].

where

$$V_0^{A/B}(q^2) = \frac{F_0^{A/B}}{1 - a_{A/B}\frac{q^2}{m_B^2} + b_{A/B}\left(\frac{q^2}{m_B^2}\right)^2}. \tag{F.29}$$

The values of all relevant parameters are given in tables 12, 13.

F.3 Tensor final meson state

For the tensor meson, $X' = T$, the expansion of the matrix element is [51, 91]

$$\begin{aligned}\langle T(p_T)|\bar{Q}_i\gamma^\mu\gamma_5 Q_j|X(p_X)\rangle =& (m_X + m_T)\epsilon_T^{\mu *,s}(p_T)A_1(q^2) \\ &- (\epsilon_T^{*,s}(p_T)\cdot q)(p_X + p_T)^\mu \frac{A_2(q^2)}{m_X + m_T} \\ &- 2m_T\frac{\epsilon_T^{*,s}(p_T)\cdot q}{q^2}q^\mu(A_3(q^2) - A_0(q^2))\end{aligned} \tag{F.30}$$

Here, $\epsilon^s_{T\mu}(p_T)$ is a vector defined by

$$\epsilon^s_{T\mu}(p_T) \equiv \frac{1}{m_X}\epsilon^s_{\mu\nu}(p_T)p_X^\nu, \tag{F.31}$$

with $\epsilon^s_{\mu\nu}$ being the polarization tensor of T satisfying $p_\mu\epsilon^{\mu\nu,s}(p) = 0$ and $\epsilon^{\mu\nu,s} = \epsilon^{\nu\mu,s}$, $\epsilon^{\mu,\ s}_{\mu} = 0$. For particular polarizations $s = \pm 2, \pm 1, 0$ we have [91]

$$\epsilon^{\pm 2}_{T\mu} = 0, \quad \epsilon^{\pm 1}_{T\mu} = \frac{1}{m_h\sqrt{2}}(\epsilon^0\cdot p_X)\epsilon^{\pm 1}_\mu, \quad \epsilon^0_{T\mu} = \sqrt{\frac{2}{3}}\frac{\epsilon^0\cdot p_X}{m_X}\epsilon^0_\mu, \tag{F.32}$$

where

$$\epsilon^{\pm 1}_\mu = \frac{1}{\sqrt{2}}(0, \mp 1, i, 0), \quad \epsilon^0_\mu = \frac{1}{m_T}(|\boldsymbol{p}_T|, 0, 0, E_T). \tag{F.33}$$

Repeating the same procedure as in the previous section, we find that to $q_\mu M^{\mu,s}_{XT}$ contributes only the polarization $s = 0$, and therefore

$$M_{XT} = -\frac{q_\mu M^{\mu,0}_{XT}}{m_{Q_i} + m_{Q_j}} = -\frac{1}{m_{Q_i} + m_{Q_j}}\sqrt{\frac{2}{3}}\frac{m_X|\boldsymbol{p}_T|^2}{m_T}2A_0^{XT}(q^2). \tag{F.34}$$

The parametrization of the form-factor A_0^{XT} is [51, 91]

$$A_0^{XT}(q^2) = \frac{F_0^{XT}}{\left(1 - \frac{q^2}{m_X^2}\right)\left(1 - a_T\frac{q^2}{m_X^2} + b_T\left(\frac{q^2}{m_X^2}\right)^2\right)} \tag{F.35}$$

For the transition $B \to K_2^*(1430)$ we use the values $F_0^{BK_2^*} = 0.23$, $a_T = 1.23$, $b_T = 0.76$ from [51].

JHEP11(2019)162

Meson X	B_0	B_s	K_0
f_X, GeV	0.19	0.23	0.16

Table 14. Values of meson decay constants. We use [92] and references therein.

G Production from mesons through quartic coupling

The quartic coupling

$$\mathcal{L}_{\text{quartic}} = \frac{\alpha}{2} h S^2 \tag{G.1}$$

generates new production channels from the mesons

$$X_{Q_i} \to X'_{Q_j} SS, \quad X \to SS, \tag{G.2}$$

that are described by Feynman diagrams in figure 7(b).

The matrix element for decays $X_{Q_i} \to X'_{Q_j} SS$ can be written in terms of the matrix element $M_{XX'}$ of hadronic transitions given by eq. (B.8):

$$\mathcal{M}(X_{Q_i} \to X'_{Q_j} SS) \approx \frac{\alpha}{m_h^2} \frac{m_{Q_i}}{2v} \xi_{ij} M_{XX'}(q^2), \tag{G.3}$$

where q^2 is invariant mass of scalars pair, $M_{XX'}(q^2)$ is the matrix element of hadronic transitions $X_{Q_i} \to X'_{Q_j}$ given by eq. (B.8).

The matrix element for a process $X_{Q_iQ_j} \to SS$ can be expressed in terms of the decay constant f_X of the meson X. Namely, f_X is defined by

$$\langle 0|\bar{Q}_i \gamma_\mu \gamma_5 Q_j|X(p)\rangle \equiv i f_X p_\mu \tag{G.4}$$

Contracting it with p_μ and using the same trick as in eq. (F.6), we obtain

$$\langle 0|\bar{Q}_i \gamma_5 Q_j|X(p)\rangle \equiv -\frac{i f_X m_X^2}{m_{Q_i} - m_{Q_j}} \tag{G.5}$$

Therefore, the matrix element $\mathcal{M}(X_{Q_iQ_j} \to SS)$ is

$$\mathcal{M}(X_{Q_iQ_j} \to SS) = \frac{m_{Q_i} \xi_{ij}}{2v m_h^2} \langle 0|\bar{Q}_i \gamma_5 Q_j|X(p)\rangle \approx i \frac{\alpha f_X m_X^2}{2v m_h^2} \xi_{ij}, \tag{G.6}$$

The values of f_X are summarized in table 14. For the decay width of the process $X_{Q_iQ_j} \to SS$ we find

$$\Gamma(X_{Q_iQ_j} \to SS) = \frac{m_X^3}{v^2} \frac{|\xi_{ij}|^2 f_X^2 \alpha^2}{128\pi m_h^4} \sqrt{1 - \frac{4m_S^2}{m_X^2}} \tag{G.7}$$

The decay width for the process $X_{Q_i} \to X'_{Q_j} SS$ can be calculated using the formulas from appendices B.1. Namely, we have

$$\Gamma_{X_{Q_i} \to X'_{Q_j} SS} = \frac{|\xi_{ij}|^2 m_{Q_i}^2 \alpha^2}{512\pi^3 m_X^3 v^2 m_h^4} \int_{4m_S^2}^{(m_X - m_{X'})^2} |M_{XX'}(q^2)|^2 \sqrt{(E_2^*)^2 - m_S^2} \sqrt{(E_3^*)^2 - |m_{X'}^2} dq^2, \tag{G.8}$$

where q^2 is the squared invariant mass of two scalars, and

$$E_2^* = \frac{\sqrt{q^2}}{2}, \quad E_3^* = \frac{m_X^2 - q^2 - m_{X'}^2}{2\sqrt{q^2}} \tag{G.9}$$

JHEP11(2019)162

H Decays of a scalar

H.1 Decay into leptons and photons

The decay width of the S particle into leptons pair simply follows from the Lagrangian (1.1) and reads

$$\Gamma(S \to l^+ l^-) = \frac{\theta^2 y_f^2 m_S}{8\pi} \beta_l^3, \tag{H.1}$$

where $\beta_l = \left(1 - \frac{4m_l^2}{m_S^2}\right)^{1/2}$. The decay width into photons is

$$\Gamma(S \to \gamma\gamma) = |F_\gamma(m_S)|^2 \left(\frac{\alpha_{\rm EM}}{8\pi}\right)^2 \frac{\theta^2 m_S^3}{8\pi v^2}, \tag{H.2}$$

Where F_γ is given by eq. (A.2).

H.2 Decays into quarks and gluons

The decay width into quarks in leading order in α_s can be obtained directly from the Lagrangian (1.1); the QCD corrections were obtained in [93]. In order to take into account the quark hadronization, we follow [12, 32, 94] and use the mass of the lightest hadron m_{M_q} containing quark q instead of the quark mass m_q in the kinematical factors. The result is

$$\Gamma(S \to \bar{q}q) = N_c \frac{\theta^2 m_S \overline{m}_q^2(m_S)}{8\pi v^2} \left(1 - \frac{4\overline{m}_{M_q}^2}{m_S^2}\right)^{3/2} \left(1 + \Delta_{\rm QCD} + \Delta_t\right), \tag{H.3}$$

where $M_q = K$ for the s quark and D for c quark, the factor $N_c = 3$ stays for the number of the QCD colors,

$$\begin{aligned} \Delta_{\rm QCD} = & 5.67 \frac{\alpha_s(m_S)}{\pi} + (35.94 - 1.36 N_f) \left(\frac{\alpha_s(m_S)}{\pi}\right)^2 \\ & + (164.14 - 25.77 N_f + 0.259 N_f^2) \left(\frac{\alpha_s(m_S)}{\pi}\right)^3, \end{aligned} \tag{H.4}$$

$$\Delta_t = \left(\frac{\alpha_s(m_S)}{\pi}\right)^2 \left(1.57 - \frac{2}{3}\log\frac{m_S^2}{m_t^2} + \frac{1}{9}\log^2\frac{\overline{m}_q^2(m_S)}{m_S^2}\right), \tag{H.5}$$

and the running mass [93] $\overline{m}_q(m_S)$ is given by

$$\overline{m}_q(m_S) = \overline{m}_q(Q) \frac{c(\alpha_s(m_S)/\pi)}{c(\alpha_s(Q)/\pi)}, \tag{H.6}$$

with the coefficient c, which is equal to

$$c(x) = \left(\frac{9}{2}x\right)^{4/9} (1 + 0.895x + 1.371x^2 + 1.952x^3), \qquad \text{for } m_s < m_S < m_c, \tag{H.7}$$

$$c(x) = \left(\frac{25}{6}x\right)^{12/25} (1 + 1.014x + 1.389x^2 + 1.091x^3), \qquad \text{for } m_c < m_S < m_b, \tag{H.8}$$

$$c(x) = \left(\frac{23}{6}x\right)^{12/23} (1 + 1.175x + 1.501x^2 + 0.1725x^3), \qquad \text{for } m_b < m_S < m_t. \tag{H.9}$$

We use the MS-mass at $Q = 2$ GeV scale [95]: $\overline{m}_c = 1.23$ GeV and $\overline{m}_s = 0.0924$ GeV.

JHEP11(2019)162

For decays into gluons, using the effective couplings (C.1), summing over all gluon species (which gives a factor of 8) and including QCD corrections, we obtain [93]

$$\Gamma(S \to GG) = |F_G(m_S)|^2 \left(\frac{\alpha_s}{4\pi}\right)^2 \frac{\theta^2 m_S^3}{8\pi v^2} \left(1 + \frac{m_t^2}{8v^2\pi^2}\right), \tag{H.10}$$

Where F_G is given by eq. (A.2).

JHEP11(2019)162

References

[1] C. Bird, P. Jackson, R.V. Kowalewski and M. Pospelov, *Search for dark matter in $b \to s$ transitions with missing energy*, *Phys. Rev. Lett.* **93** (2004) 201803 [hep-ph/0401195] [INSPIRE].

[2] M. Pospelov, A. Ritz and M.B. Voloshin, *Secluded WIMP dark matter*, *Phys. Lett.* **B 662** (2008) 53 [arXiv:0711.4866] [INSPIRE].

[3] G. Krnjaic, *Probing light thermal dark-matter with a Higgs portal mediator*, *Phys. Rev.* **D 94** (2016) 073009 [arXiv:1512.04119] [INSPIRE].

[4] M. Shaposhnikov and I. Tkachev, *The νMSM, inflation and dark matter*, *Phys. Lett.* **B 639** (2006) 414 [hep-ph/0604236] [INSPIRE].

[5] F. Bezrukov and D. Gorbunov, *Light inflaton hunter's guide*, *JHEP* **05** (2010) 010 [arXiv:0912.0390] [INSPIRE].

[6] F. Bezrukov and D. Gorbunov, *Light inflaton after LHC8 and WMAP9 results*, *JHEP* **07** (2013) 140 [arXiv:1303.4395] [INSPIRE].

[7] K. Schmidt-Hoberg, F. Staub and M.W. Winkler, *Constraints on light mediators: confronting dark matter searches with B physics*, *Phys. Lett.* **B 727** (2013) 506 [arXiv:1310.6752] [INSPIRE].

[8] J.D. Clarke, R. Foot and R.R. Volkas, *Phenomenology of a very light scalar (100 MeV $< m_h <$ 10 GeV) mixing with the SM Higgs*, *JHEP* **02** (2014) 123 [arXiv:1310.8042] [INSPIRE].

[9] CMS collaboration, *Search for invisible decays of a Higgs boson produced through vector boson fusion in proton-proton collisions at $\sqrt{s} = 13$ TeV*, *Phys. Lett.* **B 793** (2019) 520 [arXiv:1809.05937] [INSPIRE].

[10] ATLAS collaboration, *Search for invisible decays of a Higgs boson using vector-boson fusion in pp collisions at $\sqrt{s} = 8$ TeV with the ATLAS detector*, *JHEP* **01** (2016) 172 [arXiv:1508.07869] [INSPIRE].

[11] ATLAS collaboration, *Search for invisible Higgs boson decays in vector boson fusion at $\sqrt{s} = 13$ TeV with the ATLAS detector*, *Phys. Lett.* **B 793** (2019) 499 [arXiv:1809.06682] [INSPIRE].

[12] S. Alekhin et al., *A facility to search for hidden particles at the CERN SPS: the SHiP physics case*, *Rept. Prog. Phys.* **79** (2016) 124201 [arXiv:1504.04855] [INSPIRE].

[13] SHiP collaboration, *A facility to search for hidden particles (SHiP) at the CERN SPS*, arXiv:1504.04956 [INSPIRE].

[14] SHiP collaboration, *Sensitivity of the SHiP experiment to Heavy Neutral Leptons*, *JHEP* **04** (2019) 077 [arXiv:1811.00930] [INSPIRE].

[15] V.V. Gligorov, S. Knapen, M. Papucci and D.J. Robinson, *Searching for long-lived particles: a compact detector for exotics at LHCb*, *Phys. Rev.* **D 97** (2018) 015023 [arXiv:1708.09395] [INSPIRE].

[16] D. Curtin et al., *Long-lived particles at the energy frontier: the MATHUSLA physics case*, *Rept. Prog. Phys.* **82** (2019) 116201 [arXiv:1806.07396] [INSPIRE].

[17] J.P. Chou, D. Curtin and H.J. Lubatti, *New detectors to explore the lifetime frontier*, *Phys. Lett.* **B 767** (2017) 29 [arXiv:1606.06298] [INSPIRE].

[18] D. Curtin and M.E. Peskin, *Analysis of long lived particle decays with the MATHUSLA detector*, *Phys. Rev.* **D 97** (2018) 015006 [arXiv:1705.06327] [INSPIRE].

[19] J.A. Evans, *Detecting hidden particles with MATHUSLA*, *Phys. Rev.* **D 97** (2018) 055046 [arXiv:1708.08503] [INSPIRE].

[20] J.C. Helo, M. Hirsch and Z.S. Wang, *Heavy neutral fermions at the high-luminosity LHC*, *JHEP* **07** (2018) 056 [arXiv:1803.02212] [INSPIRE].

[21] MATHUSLA collaboration, *MATHUSLA: a detector proposal to explore the lifetime frontier at the HL-LHC*, arXiv:1901.04040 [INSPIRE].

[22] J.L. Feng, I. Galon, F. Kling and S. Trojanowski, *ForwArd Search ExpeRiment at the LHC*, *Phys. Rev.* **D 97** (2018) 035001 [arXiv:1708.09389] [INSPIRE].

[23] J.L. Feng, I. Galon, F. Kling and S. Trojanowski, *Dark Higgs bosons at the ForwArd Search ExpeRiment*, *Phys. Rev.* **D 97** (2018) 055034 [arXiv:1710.09387] [INSPIRE].

[24] F. Kling and S. Trojanowski, *Heavy neutral leptons at FASER*, *Phys. Rev.* **D 97** (2018) 095016 [arXiv:1801.08947] [INSPIRE].

[25] A. Berlin, S. Gori, P. Schuster and N. Toro, *Dark sectors at the Fermilab SeaQuest Experiment*, *Phys. Rev.* **D 98** (2018) 035011 [arXiv:1804.00661] [INSPIRE].

[26] SHiP collaboration, *Prospects of the SHiP and NA62 experiments at CERN for hidden sector searches*, *PoS* **NuFact2017** (2017) 139 [arXiv:1712.01768] [INSPIRE].

[27] NA62 collaboration, *Search for heavy neutral lepton production in K^+ decays*, *Phys. Lett.* **B 778** (2018) 137 [arXiv:1712.00297] [INSPIRE].

[28] M. Drewes, J. Hajer, J. Klaric and G. Lanfranchi, *NA62 sensitivity to heavy neutral leptons in the low scale seesaw model*, *JHEP* **07** (2018) 105 [arXiv:1801.04207] [INSPIRE].

[29] LBNE collaboration, *The long-baseline neutrino experiment: exploring fundamental symmetries of the universe*, in the proceedings of the *Snowmass 2013: Workshop on Energy Frontier*, June 30–July 3, Seattle, U.S.A. (2013), arXiv:1307.7335.

[30] F. Bezrukov, D. Gorbunov and I. Timiryasov, *Uncertainties of hadronic scalar decay calculations*, arXiv:1812.08088 [INSPIRE].

[31] B. Batell, M. Pospelov and A. Ritz, *Multi-lepton signatures of a hidden sector in rare B decays*, *Phys. Rev.* **D 83** (2011) 054005 [arXiv:0911.4938] [INSPIRE].

JHEP11(2019)162

[32] M.W. Winkler, *Decay and detection of a light scalar boson mixing with the Higgs boson*, *Phys. Rev.* **D 99** (2019) 015018 [arXiv:1809.01876] [INSPIRE].

[33] A. Monin, A. Boyarsky and O. Ruchayskiy, *Hadronic decays of a light Higgs-like scalar*, *Phys. Rev.* **D 99** (2019) 015019 [arXiv:1806.07759] [INSPIRE].

[34] M.B. Voloshin, *Once again about the role of gluonic mechanism in interaction of light Higgs boson with hadrons*, *Sov. J. Nucl. Phys.* **44** (1986) 478 [INSPIRE].

[35] S. Raby and G.B. West, *The branching ratio for a light Higgs to decay into $\mu^+\mu^-$ pairs*, *Phys. Rev.* **D 38** (1988) 3488 [INSPIRE].

[36] T.N. Truong and R.S. Willey, *Branching ratios for decays of light Higgs bosons*, *Phys. Rev.* **D 40** (1989) 3635 [INSPIRE].

[37] J.F. Donoghue, J. Gasser and H. Leutwyler, *The decay of a light Higgs boson*, *Nucl. Phys.* **B 343** (1990) 341 [INSPIRE].

[38] R.S. Willey and H.L. Yu, *The decays $K^\pm \to \pi^\pm \ell^+ \ell^-$ and limits on the mass of the neutral Higgs boson*, *Phys. Rev.* **D 26** (1982) 3287 [INSPIRE].

[39] R.S. Willey, *Limits on light Higgs bosons from the decays $K^\pm \to \pi^\pm \ell^- \ell^+$*, *Phys. Lett.* **B 173** (1986) 480 [INSPIRE].

[40] B. Grzadkowski and P. Krawczyk, *Higgs particle effects in flavor changing transitions*, *Z. Phys.* **C 18** (1983) 43 [INSPIRE].

[41] H. Leutwyler and M.A. Shifman, *Light Higgs particle in decays of K and η mesons*, *Nucl. Phys.* **B 343** (1990) 369 [INSPIRE].

[42] H.E. Haber, A.S. Schwarz and A.E. Snyder, *Hunting the Higgs in B Decays*, *Nucl. Phys.* **B 294** (1987) 301 [INSPIRE].

[43] R.S. Chivukula and A.V. Manohar, *LImits on a light Higgs boson*, *Phys. Lett.* **B 207** (1988) 86 [*Erratum ibid.* **B 217** (1989) 568] [INSPIRE].

[44] Particle Data Group collaboration, *Review of Particle Physics*, *Phys. Rev.* **D 98** (2018) 030001 [INSPIRE].

[45] J. Carvalho, *Compilation of cross sections for proton nucleus interactions at the HERA energy*, *Nucl. Phys.* **A 725** (2003) 269 [INSPIRE].

[46] C. Lourenco and H.K. Wohri, *Heavy flavour hadro-production from fixed-target to collider energies*, *Phys. Rept.* **433** (2006) 127 [hep-ph/0609101] [INSPIRE].

[47] SHiP collaboration, *Heavy flavour cascade production in a beam dump*, CERN-SHiP-NOTE-2015-009 (2015).

[48] M. Cacciari, M. Greco and P. Nason, *The p_T spectrum in heavy flavor hadroproduction*, *JHEP* **05** (1998) 007 [hep-ph/9803400] [INSPIRE].

[49] P. Ball and R. Zwicky, *$B_{d,s} \to \rho, \omega, K^*, \phi$ decay form-factors from light-cone sum rules revisited*, *Phys. Rev.* **D 71** (2005) 014029 [hep-ph/0412079] [INSPIRE].

[50] P. Ball and R. Zwicky, *New results on $B \to \pi, K, \eta$ decay formfactors from light-cone sum rules*, *Phys. Rev.* **D 71** (2005) 014015 [hep-ph/0406232] [INSPIRE].

[51] H.-Y. Cheng and K.-C. Yang, *Charmless hadronic B decays into a tensor meson*, *Phys. Rev.* **D 83** (2011) 034001 [arXiv:1010.3309] [INSPIRE].

JHEP11(2019)162

[52] Y.-J. Sun, Z.-H. Li and T. Huang, *$B_{(s)} \to S$ transitions in the light cone sum rules with the chiral current*, *Phys. Rev.* **D 83** (2011) 025024 [arXiv:1011.3901] [INSPIRE].

[53] C.-D. Lu and W. Wang, *Analysis of $B \to K_J^*(\to K\pi)\mu^+\mu^-$ in the higher kaon resonance region*, *Phys. Rev.* **D 85** (2012) 034014 [arXiv:1111.1513] [INSPIRE].

[54] A. Denner et al., *Standard model Higgs-boson branching ratios with uncertainties*, *Eur. Phys. J.* **C 71** (2011) 1753 [arXiv:1107.5909] [INSPIRE].

[55] LHC Higgs Cross Section Working Group collaboration, *Handbook of LHC Higgs Cross Sections: 3. Higgs Properties*, arXiv:1307.1347 [INSPIRE].

[56] C. Bird, R.V. Kowalewski and M. Pospelov, *Dark matter pair-production in $b \to s$ transitions*, *Mod. Phys. Lett.* **A 21** (2006) 457 [hep-ph/0601090] [INSPIRE].

[57] C.S. Kim, S.C. Park, K. Wang and G. Zhu, *Invisible Higgs decay with $B \to K\nu\bar{\nu}$ constraint*, *Phys. Rev.* **D 81** (2010) 054004 [arXiv:0910.4291] [INSPIRE].

[58] X.-G. He, S.-Y. Ho, J. Tandean and H.-C. Tsai, *Scalar dark matter and standard model with four generations*, *Phys. Rev.* **D 82** (2010) 035016 [arXiv:1004.3464] [INSPIRE].

[59] A. Badin and A.A. Petrov, *Searching for light dark matter in heavy meson decays*, *Phys. Rev.* **D 82** (2010) 034005 [arXiv:1005.1277] [INSPIRE].

[60] B. Moussallam, *$N(f)$ dependence of the quark condensate from a chiral sum rule*, *Eur. Phys. J.* **C 14** (2000) 111 [hep-ph/9909292] [INSPIRE].

[61] M. Spira, *Higgs boson production and decay at hadron colliders*, *Prog. Part. Nucl. Phys.* **95** (2017) 98 [arXiv:1612.07651] [INSPIRE].

[62] ATLAS, CMS collaboration, *Measurements of the Higgs boson production and decay rates and constraints on its couplings from a combined ATLAS and CMS analysis of the LHC pp collision data at $\sqrt{s} = 7$ and 8 TeV*, *JHEP* **08** (2016) 045 [arXiv:1606.02266] [INSPIRE].

[63] A.I. Vainshtein, V.I. Zakharov and M.A. Shifman, *A possible mechanism for the $\Delta T = 1/2$ rule in nonleptonic decays of strange particles*, *JETP Lett.* **22** (1975) 55 [INSPIRE].

[64] E. Witten, *Heavy quark contributions to deep inelastic scattering*, *Nucl. Phys.* **B 104** (1976) 445 [INSPIRE].

[65] M.A. Shifman, A.I. Vainshtein and V.I. Zakharov, *Remarks on Higgs boson interactions with nucleons*, *Phys. Lett.* **B 78** (1978) 443.

[66] H.-Y. Cheng, *Low-energy interactions of scalar and pseudoscalar Higgs bosons with baryons*, *Phys. Lett.* **B 219** (1989) 347 [INSPIRE].

[67] H.-Y. Cheng and C.-W. Chiang, *Revisiting scalar and pseudoscalar couplings with nucleons*, *JHEP* **07** (2012) 009 [arXiv:1202.1292] [INSPIRE].

[68] S. Dawson, *Higgs boson production in semileptonic K and π decays*, *Phys. Lett.* **B 222** (1989) 143 [INSPIRE].

[69] H.-Y. Cheng and H.-L. Yu, *Are there really no experimental limits on a light Higgs boson from kaon decay?*, *Phys. Rev.* **D 40** (1989) 2980 [INSPIRE].

[70] A. Buckley et al., *LHAPDF6: parton density access in the LHC precision era*, *Eur. Phys. J.* **C 75** (2015) 132 [arXiv:1412.7420] [INSPIRE].

[71] H.-L. Lai et al., *New parton distributions for collider physics*, *Phys. Rev.* **D 82** (2010) 074024 [arXiv:1007.2241] [INSPIRE].

JHEP11(2019)162

[72] G. Altarelli and G. Parisi, *Asymptotic freedom in parton language*, *Nucl. Phys.* **B 126** (1977) 298 [INSPIRE].

[73] J. Blümlein and J. Brunner, *New exclusion limits on dark gauge forces from proton Bremsstrahlung in beam-dump data*, *Phys. Lett.* **B 731** (2014) 320 [arXiv:1311.3870] [INSPIRE].

[74] J. Blumlein and J. Brunner, *New exclusion limits for dark gauge forces from beam-dump data*, *Phys. Lett.* **B 701** (2011) 155 [arXiv:1104.2747] [INSPIRE].

[75] M.-S. Chen and P.M. Zerwas, *Equivalent-particle approximations in electron and photon processes of higher order QED*, *Phys. Rev.* **D 12** (1975) 187 [INSPIRE].

[76] K.J. Kim and Y.-S. Tsai, *Improved Weizsacker-Williams method and its application to lepton and W boson pair production*, *Phys. Rev.* **D 8** (1973) 3109 [INSPIRE].

[77] S. Frixione, M.L. Mangano, P. Nason and G. Ridolfi, *Improving the Weizsacker-Williams approximation in electron-proton collisions*, *Phys. Lett.* **B 319** (1993) 339 [hep-ph/9310350] [INSPIRE].

[78] V.N. Baier, V.S. Fadin and V.A. Khoze, *Quasireal electron method in high-energy quantum electrodynamics*, *Nucl. Phys.* **B 65** (1973) 381 [INSPIRE].

[79] V.M. Budnev, I.F. Ginzburg, G.V. Meledin and V.G. Serbo, *The two photon particle production mechanism. Physical problems. Applications. Equivalent photon approximation*, *Phys. Rept.* **15** (1975) 181 [INSPIRE].

[80] A.D. Martin and M.G. Ryskin, *The photon PDF of the proton*, *Eur. Phys. J.* **C 74** (2014) 3040 [arXiv:1406.2118] [INSPIRE].

[81] B. Döbrich et al., *ALPtraum: ALP production in proton beam dump experiments*, *JHEP* **02** (2016) 018 [arXiv:1512.03069] [INSPIRE].

[82] C. Bobeth, T. Ewerth, F. Krüger and J. Urban, *Analysis of neutral Higgs boson contributions to the decays $\bar{B}(s) \to \ell^+\ell^-$ and $\bar{B} \to K\ell^+\ell^-$*, *Phys. Rev.* **D 64** (2001) 074014 [hep-ph/0104284] [INSPIRE].

[83] D. Ebert, R.N. Faustov and V.O. Galkin, *Exclusive nonleptonic decays of B mesons*, *Phys. Rev.* **D 56** (1997) 312 [hep-ph/9701218] [INSPIRE].

[84] W.J. Marciano and Z. Parsa, *Rare kaon decays with "missing energy"*, *Phys. Rev.* **D 53** (1996) R1.

[85] ETM collaboration, *Lattice investigation of the tetraquark candidates a0(980) and kappa*, PoS(LATTICE 2012)161 [arXiv:1211.5002] [INSPIRE].

[86] H.-Y. Cheng, C.-K. Chua, K.-C. Yang and Z.-Q. Zhang, *Revisiting charmless hadronic B decays to scalar mesons*, *Phys. Rev.* **D 87** (2013) 114001 [arXiv:1303.4403] [INSPIRE].

[87] A. Issadykov, M.A. Ivanov and S.K. Sakhiyev, *Form factors of the B-S-transitions in the covariant quark model*, *Phys. Rev.* **D 91** (2015) 074007 [arXiv:1502.05280] [INSPIRE].

[88] H. Hatanaka and K.-C. Yang, *Radiative and semileptonic B decays involving the tensor meson $K_2^*(1430)$ in the standard model and beyond*, *Phys. Rev.* **D 79** (2009) 114008 [arXiv:0903.1917] [INSPIRE].

[89] V. Bashiry, *Lepton polarization in $B \to K_1\ell^+\ell^-$ decays*, *JHEP* **06** (2009) 062 [arXiv:0902.2578] [INSPIRE].

JHEP11(2019)162

[90] H. Hatanaka and K.-C. Yang, $K_1(1270)$–$K_1(1400)$ *mixing angle and new-physics effects in* $B \to K_1 \ell^+ \ell^-$ *decays*, *Phys. Rev.* **D 78** (2008) 074007 [arXiv:0808.3731] [INSPIRE].

[91] R.-H. Li, C.-D. Lu and W. Wang, *Branching ratios, forward-backward asymmetries and angular distributions of* $B \to K_2^* l^+ l^-$ *in the standard model and new physics scenarios*, *Phys. Rev.* **D 83** (2011) 034034 [arXiv:1012.2129] [INSPIRE].

[92] Q. Chang, X.-N. Li, X.-Q. Li and F. Su, *Decay constants of pseudoscalar and vector mesons with improved holographic wavefunction*, *Chin. Phys.* **C 42** (2018) 073102 [arXiv:1805.00718] [INSPIRE].

[93] M. Spira, *QCD effects in Higgs physics*, *Fortsch. Phys.* **46** (1998) 203 [hep-ph/9705337] [INSPIRE].

[94] J.F. Gunion, H.E. Haber, G.L. Kane and S. Dawson, *The Higgs hunter's guide*, *Front. Phys.* **80** (2000) 1 [INSPIRE].

[95] F. Sanfilippo, *Quark masses from lattice QCD*, PoS(LATTICE 2014)014 [arXiv:1505.02794] [INSPIRE].

JHEP11(2019)162

1.2. Народження бозонів Черна-Саймонса в розпадах мезонів

IOP Publishing Journal of Physics G: Nuclear and Particle Physics
J. Phys. G: Nucl. Part. Phys. **49** (2022) 085003 (29pp) https://doi.org/10.1088/1361-6471/ac77a7

Production of Chern–Simons bosons in decays of mesons

Yuliia Borysenkova[1], Pavlo Kashko[1,2], Mariia Tsarenkova[1], Kyrylo Bondarenko[3,4] and Volodymyr Gorkavenko[1,*]

[1] Department of Physics, Taras Shevchenko National University of Kyiv, 64 Volodymyrs'ka str. 01601, Kyiv, Ukraine
[2] École Polytechnique Fédérale de Lausanne (EPFL), CH-1015 Lausanne, Switzerland
[3] SISSA, International School for Advanced Studies, Via Bonomea 265, I-34136 Trieste, Italy
[4] IFPU, Institute for Fundamental Physics of the Universe, Via Beirut 2, 34151, Trieste, Italy

E-mail: yuliya.borisenckova@gmail.com, kashko.pavlo@gmail.com, ters.mar@gmail.com, kyrylo.bondarenko@gmail.com and gorkavol@gmail.com

Received 1 February 2022, revised 26 May 2022
Accepted for publication 10 June 2022
Published 30 June 2022

Abstract

We consider the effective interaction of quarks with a new GeV-scale vector particle that couples to electroweak gauge bosons by the so-called effective Chern–Simons (CS) interaction. We call this particle the CS boson. We construct effective Lagrangian of the CS boson interaction with quarks of two different flavors. This interaction is given by a divergent loop diagram, however, it turns out that the divergent part is equal to zero as a consequence of the CKM matrix unitarity in the SM. Therefore, we are able to predict effective interaction of the CS boson with quarks of different flavors without introducing new unknown parameters to the model, using only parameters of the initial effective Lagrangian. Our result shows that the effective interaction of the CS boson with down-type quarks is sufficiently stronger compared with up-type quarks. Based on our results, we give a prediction for the production of CS bosons in mesons decays. Branching fractions were obtained for the main reactions of the CS production in meson decays. The results obtained will be useful for searching for the long-lived GeV-scale CS boson in intensity frontier experiments.

Keywords: beyond standard model, extensions of gauge sector, Chern–Simons theories, rare decays

*Author to whom any correspondence should be addressed.

1. Introduction

Despite all the successes of the standard model (SM), see e.g. [1], there are some phenomena that cannot be solved within the SM. These include baryon asymmetry of the Universe (see e.g. [2–4]), dark matter (see e.g. [5–7]), and neutrino oscillations (see e.g. [8–10]). In addition to these well-established phenomena, it should be noted that there is a number of observed parameters that are difficult to explain. For example, the strong CP problem (as to why the degree of CP violation in the QCD is unobservably small, see e.g. [11, 12]), the Higgs hierarchy problem (as to why quantum corrections to the Higgs mass cancel well, see e.g. [13, 14]), stability of the SM vacuum (top quark Yukawa coupling and the Higgs mass are very close to its critical value, see e.g. [15, 16]), the cosmological constant and dark energy (as to why the cosmological constant is so small, see e.g. [17]). Therefore, one can conclude that the SM is an incomplete theory and it requires an extension. Moreover, the existence of 'hidden' sectors with particles of new physics seems plausible.

Many of the aforementioned phenomena can be explained by an extension of the SM by beyond standard model (BSM) particles. The values of their masses can be in very different ranges. For example, small neutrino masses, dark matter, and baryon asymmetry of the Universe can be explained by new particles with masses from the sub-eV scale up to the GUT scale, see e.g. [9, 18]. The fact that we do not observe BSM particles in accelerator experiments has two possible explanations. Either these particles are too massive to be produced at modern accelerators like the LHC, or they feebly interact with SM particles. If BSM particles are heavy enough, then to search for them we need more powerful, more expensive accelerators and energy frontier experiments, see e.g. [19, 20]. But the case of light but feebly interacting BSM particles is very topical for the experimental search for new physics right now. To search for them, we need intensity frontier experiments with high-intensity particle beams and large detectors, see e.g. [21, 22]. Several such intensity frontier experiments have been proposed in recent years: MATHUSLA [23], FACET [24], FASER [25, 26], SHiP [27, 28], NA62 [29–31], DUNE [32, 33], etc.

Searching for new physics, one should keep in mind that among the hidden particles there must be particles that solve the above-mentioned SM problems. However, the hidden sector may also contain particles that are not directly related to the solution of an SM problem. That is why it is important to look for manifestations of new physics particles at all accessible energy scales. In this work we will be interested in GeV-scale feebly interacting new particles.

The properties of the new light particles are not yet known. They can be scalars (e.g. [34–36]), pseudoscalars (axion-like particles), see e.g. [37–40], vectors (e.g. [41–43]), or fermions (e.g. [44–47]). Each of these options requires thorough study. Discussion of their possible interactions with SM particles (portals) and the available experimental constraints are given e.g. in reviews [23, 28].

In this paper, we will be interested in consideration of the Chern–Simons (CS) portal, which, in our opinion, has received insufficient attention especially concerning experimental search for the CS particles. In this portal a new vector particle X_μ couples with the SM gauge fields by the so-called effective CS interaction in the form of four-dimension operators [48]:

$$\begin{aligned}\mathcal{L}_{\rm CS} = {} & c_z \epsilon^{\mu\nu\lambda\rho} X_\mu Z_\nu \partial_\lambda Z_\rho + c_\gamma \epsilon^{\mu\nu\lambda\rho} X_\mu Z_\nu \partial_\lambda A_\rho \\ & + \left\{ c_w \epsilon^{\mu\nu\lambda\rho} X_\mu W^-_\nu \partial_\lambda W^+_\rho + \text{h.c.} \right\}, \end{aligned} \tag{1}$$

where A_μ is the electromagnetic field; $W^\pm_\mu$ and Z_μ are fields of the weak interaction; $\epsilon^{\mu\nu\lambda\rho}$ is the Levi-Civita symbol ($\epsilon^{0123} = +1$) and c_z, c_γ, c_w are some dimensionless independent

coefficients. Coefficients c_z and c_γ are real, but c_w can be complex. As one can see, there is no direct interaction of the CS vector boson X_μ with fields of the matter. It should be noted that Lagrangian (1) does not contain term $\epsilon^{\mu\nu\lambda\rho}X_\mu A_\nu \partial_\lambda A_\rho$ which is not gauge invariant with respect to the electromagnetic $U(1)$ group.

The interest in the CS model is due to the fact that the CS interaction is derived by an anomaly cancellation. This way is theoretically attractive because the contribution of extremely heavy fermions (not available for direct search at accelerators) to anomaly cancellation remains unsuppressed at low energies [49, 50]. These heavy fermions can act as mediators and induce observable interaction of the SM particles with new light vector particles from the 'hidden' sector. A detailed explanation of the origin of the CS interactions (1), including using of a toy UV model, can be found in [48]. The CS interactions appear in various theoretical models, including extra dimensions and the string theory, see [51–60]. In addition to the need to study the CS theory as one of the possible extensions of the SM, the presence of the Levi-Civita symbol indicates the possible effects of violation of CP invariance in the CS theory, and perhaps the CS boson will be useful in solving some of the SM problems. On the other hand, if the CS boson is discovered, this will unequivocally indicate the presence of new physics at high energy scales. It is important to note that the CS boson was included in the proposal of the SHiP experiment [28].

In order to start looking for the CS boson in experiments, one needs to know the main channels of the CS boson production and decay. In this paper we will consider only the production of GeV-scale CS bosons. We will limit ourselves only to the case of the CS boson production in the decays of different types of mesons. To do this, we will consider loop interaction of the CS boson with the SM fermions and construct the effective Lagrangian of the CS bosons interaction with two different quarks. This will allow us to find more effective channels for the production of CS bosons and bring us closer to the experimental search for CS bosons.

The paper is organized as follows: in section 2 we discuss theoretical aspects of the CS model. In section 3 we obtain the effective Lagrangian of the CS boson interaction with different quarks; in section 4 we consider the CS boson production in mesons decays. The summary and final discussion are given in section 5. Necessary technical clarifications and details about form-factors used are given in appendices.

2. Chern–Simons model

The simplest case of the SM extension with non-trivial anomaly cancellation that involves the electromagnetic $U_{\rm EM}(1)$ gauge group requires small parameters of the photon mass or millicharge of new particles, see [61–64]. These parameters are strongly restricted, see e.g. [65–68], and suppress any visible effects. We get a similar situation when considering non-trivial anomaly cancellation in the electroweak sector of the SM. The small parameter, in this case, is the sum of the electric charges of the electron and the proton, which is also limited to a very small value [69, 70].

To avoid the need to deal with very small parameters of the models that suppress any visible effects it is interesting to consider extension of the SM by an additional gauge group, see e.g. [71] and references therein. In particular, Lagrangian (1) can be obtained in $U_X(1)$ gauge field extension of the SM to the general theory with $SU_C(3) \times SU_W(2) \times U_Y(1) \times U_X(1)$ symmetry. One should also add to the theory heavy new chiral fermions that interact both with the gauge field of $U_X(1)$ and with the SM gauge fields. Herewith the SM fermions are not charged with respect to the $U_X(1)$ group [64].

Lagrangian (1) has $U_{\rm EM}(1)$ gauge invariance, but unfortunately we need at least six-dimension operators [28, 48] to restore $U_Y(1) \times SU_W(2)$ invariance:

$$\mathcal{L}_1 = \frac{C_Y}{\Lambda_Y^2} \cdot X_\mu (\mathfrak{D}_\nu H)^\dagger H B_{\lambda\rho} \cdot \epsilon^{\mu\nu\lambda\rho} + \text{h.c.}, \tag{2}$$

$$\mathcal{L}_2 = \frac{C_{SU(2)}}{\Lambda_{SU(2)}^2} \cdot X_\mu (\mathfrak{D}_\nu H)^\dagger F_{\lambda\rho} H \cdot \epsilon^{\mu\nu\lambda\rho} + \text{h.c.}, \tag{3}$$

where Λ_Y, $\Lambda_{SU(2)}$ are new scales of the theory; C_Y, $C_{SU(2)}$ are new dimensionless coupling constants; H—scalar field of the Higgs doublet; $B_{\mu\nu} = \partial_\mu B_\nu - \partial_\nu B_\mu$, $F_{\mu\nu} = -ig\sum_{i=1}^{3} \frac{\tau^i}{2} V^i_{\mu\nu}$—field strength tensors of the $U_Y(1)$ and $SU_W(2)$ gauge fields.

It is convenient to rewrite the coefficients before operators of dimension-6 as $C_Y/\Lambda_Y^2 = C_1/v^2$ and $C_{SU(2)}/\Lambda_{SU(2)}^2 = C_2/v^2$, where $C_1 = c_1 + \mathrm{i}c_{1\mathrm{i}}$ and $C_2 = c_2 + \mathrm{i}c_{2\mathrm{i}}$ are dimensionless coefficients, v is the vacuum expectation value of the Higgs field. In this case Lagrangians (2) and (3) after the electroweak symmetry breaking generate Lagrangian of three fields interactions (1) with coefficients in unitary gauge:

$$c_z = -c_{1\mathrm{i}} g' + \frac{c_2}{2} g^2, \tag{4}$$

$$c_\gamma = c_{1\mathrm{i}} g + \frac{c_2}{2} g g', \tag{5}$$

$$c_w = \frac{c_2 + \mathrm{i}c_{2\mathrm{i}}}{2} g^2 \equiv \Theta_{W1} + \mathrm{i}\Theta_{W2}. \tag{6}$$

In [28] it was pointed out that from dimension-6 operators (2) and (3) follows $c_z/c_\gamma = \tan\theta_W$. However, we see from relations (4)–(6) that ratio c_z/c_γ depends on two unknown parameters $c_{1\mathrm{i}}$ and c_2. It is evident that the ratio of these quantities has a simple form only in the particular case when the real part of the parameter C_2 is zero ($c_z/c_\gamma = -\tan\theta_W$), or the imaginary part of the parameter C_1 is zero ($c_z/c_\gamma = \cot\theta_W$). As one can see, relations (4)–(6) allow us to write a relation between the real part of parameter C_2 and c_z, c_γ that gives $\Theta_{W1} = \cos^2\theta_W(c_z + \tan\theta_W c_\gamma)$. It is also interesting that the real part of parameter C_1 (parameter c_1) is not included into (4)–(6) and the imaginary part of parameter C_2 (parameter Θ_{W2}) is an independent parameter.

It should be noted that relations (4)–(6) and corresponding conclusions are valid only in the assumptions that the CS theory is derived only by dimension-6 operators (2) and (3). But it may turn out that the main or a significant contribution to Lagrangian (1) comes from higher dimension operators. So, following [28], below we will consider c_z, c_γ, c_w as independent dimensionless parameters.

3. Effective interaction of the CS boson with different quarks

Lagrangian (1) gives diagrams of the CS boson loop interactions with two SM fermions presented in figure 1. Since we want to consider the CS boson production in decays of mesons we only need diagrams (c) and (d), where a heavy initial particle decays in a light particle with the production of the CS boson. It means we can consider in Lagrangian (1) only the interaction of the CS boson with W bosons and put $c_z = c_\gamma = 0$ for simplicity.

Certainly, one can present four fermion interaction with the CS boson without loop, see figure 2, but this interaction will be suppressed by G_F^2 and, as it will be shown in section 3.3, can be neglected compared to the loop interaction of the CS boson with two fermions.

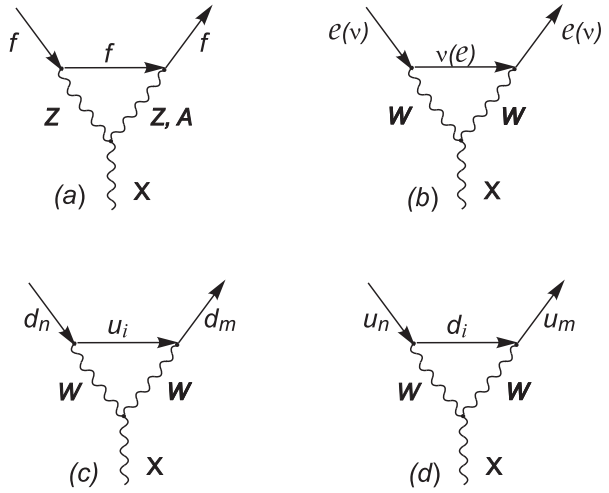

Figure 1. CS boson loop interactions with two fermions of the SM.

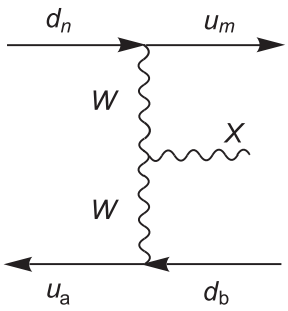

Figure 2. Interaction of the CS boson with four fermions.

3.1. Interaction of the CS boson with two different down-type quarks

Computation of the loop diagram for the interaction of the CS boson with down-type quarks gives us, see figure A1 and appendix A, the following amplitude of the heavy down-type quark (d_n) decay into light down-type quark (d_m) and the CS boson in the unitary gauge:

$$M_{fi} = -\mathrm{i}\frac{g^2}{2}\sum_{i=u,c,t} V^{+}_{d_m i} V_{i d_n}\, \overline{d_m}(p')\gamma^{\mu}_{(i)} d_n(p)\epsilon^{*\lambda_X}_{\mu}, \tag{7}$$

where $\gamma^{\mu}_{(i)}$ has a rather cumbersome form

$$
\begin{aligned}
Y^{\mu}_{(i)} = \hat{\Lambda}_0 \Big\{ & 2(x+y-1)\left\{\Theta_{W1}(2y-1) - \mathrm{i}\Theta_{W2}\right\} - 2y\left\{\Theta_{W1}(1-2x-2y)\right. \\
& \left. + \mathrm{i}\Theta_{W2}\right\} - \frac{x}{M_W^2}\left[c_w^*\left\{(2x+2y-1)m^2 + ym'^2 - 3y(pp')\right\}\right. \\
& + 2\Theta_{W1}\left\{(x+y)^2m^2 + y^2m'^2 - 2y(x+y)(pp')\right\} \\
& \left. + 2\mathrm{i}\Theta_{W2}\left\{(x+y)m^2 - 2y(pp')\right\}\right] \Big\} p'_\lambda \gamma_\rho p_\nu \hat{P}_L \epsilon^{\mu\nu\lambda\rho} \\
& + \hat{\Lambda}_0 m' y \left\{\Theta_{W1}((1-2x-2y)p + (2y-1)p')_\lambda \right. \\
& \left. + \mathrm{i}\Theta_{W2}(p-p')_\lambda\right\} \gamma_\rho\gamma_\nu \hat{P}_L \epsilon^{\mu\nu\lambda\rho} \\
& + \hat{\Lambda}_1 \Big\{ -\mathrm{i}\Theta_{W1}\gamma_\rho\gamma_\lambda\gamma_\nu - \frac{p'_\lambda\gamma_\rho p_\nu}{M_W^2}\left[-\Theta_{W2}\right. \\
& \left. + \mathrm{i}\Theta_{W1}(1+6x)\right] \Big\} \hat{P}_L \epsilon^{\mu\nu\lambda\rho} \\
+ \hat{\Lambda}_0 \Big\{ & -(x+y-1)m\left\{\Theta_{W1}[(1-2x-2y)p + (2y-1)p']_\lambda \right. \\
& \left. + \mathrm{i}\Theta_{W2}(p-p')_\lambda\right\}\gamma_\rho\gamma_\nu + \frac{xmm'}{M_W^2}\left[\Theta_{W1}(1-x)\right. \\
& \left. + \mathrm{i}\Theta_{W2}(2y+x-1)\right] p'_\lambda\gamma_\rho p_\nu \Big\} \hat{P}_R \epsilon^{\mu\nu\lambda\rho} \\
& - \hat{\Lambda}_1 \frac{m}{2M_W^2}\mathrm{i}c_w(p-p')_\lambda\gamma_\rho\gamma_\nu\hat{P}_R\epsilon^{\mu\nu\lambda\rho}, \qquad (8)
\end{aligned}
$$

integral operators $\hat{\Lambda}_{0(1)}$ are defined as

$$\hat{\Lambda}_0 = \mathrm{i}\frac{\pi^2}{(2\pi)^4}\int_0^1 \mathrm{d}x \int_0^{1-x} \mathrm{d}y \, \frac{1}{D(m_i)}, \qquad (9)$$

$$\hat{\Lambda}_1 = -\frac{\pi^2}{(2\pi)^4}\int_0^1 \mathrm{d}x \int_0^{1-x} \mathrm{d}y \, \ln\frac{\Lambda^2 x}{D(m_i)}, \qquad (10)$$

here

$$D(m_i) = xm_i^2 + (1-x)M_W^2 + xy(M_X^2 + m^2 - m'^2) - x(1-x)m^2 - y(1-y)M_X^2, \quad (11)$$

$\hat{P}_{R(L)}$—projection operators on the right(left)-handed chirality states, p is the four-momentum and m is the mass of the initial down-type quark (d_n), p' is the four-momentum and m' is the mass of the final down-type quark (d_m), m_i is the mass of the virtual up-type u_i quark, M_W and M_X are the masses of the W and CS vector bosons, Λ is the regularization parameter that should be set to infinity.

The divergent part of $Y^{\mu}_{(i)}$ is hidden in the operator $\hat{\Lambda}_1$ (10). We can extract in this operator singular and finite parts:

$$\hat{\Lambda}_1 = \hat{\Lambda}_1^{\mathrm{sing}} + \hat{\Lambda}_1^{\mathrm{fin}} = -\frac{\pi^2}{(2\pi)^4}\int_0^1 \mathrm{d}x \int_0^{1-x} \mathrm{d}y \, \left\{\ln\frac{\Lambda^2 x}{\mu^2} - \ln\frac{D(m_i)}{\mu^2}\right\}, \qquad (12)$$

where μ is some parameter with the dimension of mass. It should be noted that operator Λ_1^{sing} does not depend on the mass of the virtual quark in the loop (m_i) and it acts on an expression that does not depend on m_i too. So, after summation over the all virtual quarks in (7) we get a term proportional to

$$\sum_{i=u,c,t} V^+_{d_m i} V_{i d_n} \ln \frac{\Lambda^2 x}{M_W^2} = (V^+ V)_{d_m d_n} \ln \frac{\Lambda^2 x}{M_W^2} = 0, \quad m \neq n,$$

due to the unitarity of the CKM-matrix in the SM. So, in the expression (8) we can replace operator $\hat{\Lambda}_1$ by finite operator $\hat{\Lambda}_1^{\text{fin}}$

$$\hat{\Lambda}_1^{\text{fin}} = \frac{\pi^2}{(2\pi)^4} \int_0^1 \mathrm{d}x \int_0^{1-x} \mathrm{d}y \ln \frac{D(m_i)}{\mu^2}. \tag{13}$$

With the help of the unitary condition for the CKM-matrix, it is not difficult to show that the amplitude of the process does not depend on the value of the parameter μ, see appendix A. In the following, we will put $\mu = M_W$ for the convenience of computations. It should be noted that the established fact of the divergent part of the CS boson loop interaction with quarks of two different flavors being zero (as a consequence of the CKM matrix unitarity in the SM) is consistent with the results of [59, 60].

An explicit form of the $Y^{\mu}_{(i)}$ can be obtained after applying the operators $\hat{\Lambda}_0$, $\hat{\Lambda}_1^{\text{fin}}$ and performing summation over the virtual up-type quarks in (8), see appendix B. The amplitude of a heavy down-type quark (d_n) (with mass m and four-momentum p) decay into a light down-type quark (d_m) (with mass m' and four-momentum p') and the CS boson in the unitary gauge (7) is convenient to present in the form

$$M_{fi} = -\mathrm{i} \frac{g^2}{32\pi^2} \frac{m_t^2}{M_W^2} V^+_{d_m t} V_{t d_n} \overline{d_m}(p') J^{\mu,d}(p, p') d_n(p) \epsilon^{*\lambda_X}_{\mu}, \tag{14}$$

where m_t is mass of the top quark and

$$\begin{aligned} J^{\mu} = \Bigg(& a_L^d \hat{P}_R \gamma_\rho \gamma_\lambda \gamma_\nu \hat{P}_L + b_L^d \frac{p'_\lambda p_\nu}{M_W^2} \hat{P}_R \gamma_\rho \hat{P}_L + c_L^d \frac{m' p'_\lambda}{M_W^2} \hat{P}_L \gamma_\rho \gamma_\nu \hat{P}_L \\ & + d_L^d \frac{m' p_\lambda}{M_W^2} \hat{P}_L \gamma_\rho \gamma_\nu \hat{P}_L + b_R^d \frac{m m'}{M_W^2} \frac{p'_\lambda p_\nu}{M_W^2} \hat{P}_L \gamma_\rho \hat{P}_R \\ & + c_R^d \frac{m p'_\lambda}{M_W^2} \hat{P}_R \gamma_\rho \gamma_\nu \hat{P}_R + d_R^d \frac{m p_\lambda}{M_W^2} \hat{P}_R \gamma_\rho \gamma_\nu \hat{P}_R \Bigg) \epsilon^{\mu\nu\lambda\rho}. \end{aligned} \tag{15}$$

Coefficients in (15) in the first approximation can be considered independent of the masses of down-type quarks. They can be computed numerically, but we also managed to find the analytical expression for these coefficients with less than 1% difference from their values obtained numerically, see appendix B. The values of the coefficients are given in table 1. Coefficients at Θ_{W1} are imaginary with sufficient accuracy, but coefficients at Θ_{W2} are real. Taking into account that near the coefficients $b^d_{L,R}$, $c^d_{L,R}$, $d^d_{L,R}$ there are suppressing factors, one can see that the main contribution to (15) comes from the term a^d_L (if $\Theta_{W1} \neq 0$). It should be noted that coefficient a^d_L depends only on one parameter (Θ_{W1}) unlike almost all other coefficients depending on both parameters: Θ_{W1} and Θ_{W2}.

Table 1. Coefficients in the expression for the amplitude of a heavy quark decay into a down-type quark and the CS boson in (15). Superscript d stands for the decay of down-type quark $d_n \to d_m + X$, superscript up is for the decay of up-type quark $c \to u + X$.

Coeff.	Value	Coeff.	Value $\cdot 10^6$
a_L^d	$-0.13\mathrm{i}\Theta_{W1}$	a_L^{up}	$(-0.98 + 1.13\mathrm{i})\Theta_{W1}$
b_L^d	$-0.61\mathrm{i}\Theta_{W1} + 0.13\Theta_{W2}$	b_L^{up}	$(-6.4 + 7.4\mathrm{i})\Theta_{W1} - (1.1 + 0.98\mathrm{i})\Theta_{W2}$
c_L^d	$0.008\mathrm{i}\Theta_{W1} - 0.033\Theta_{W2}$	c_L^{up}	$(0.27–0.31\mathrm{i})\Theta_{W1} + (0.57 + 0.49\mathrm{i})\Theta_{W2}$
d_L^d	$0.02\mathrm{i}\Theta_{W1} + 0.033\Theta_{W2}$	d_L^{up}	$(0.38–0.44\mathrm{i})\Theta_{W1} - (0.57 + 0.49\mathrm{i})\Theta_{W2}$
b_R^d	$-0.028\mathrm{i}\Theta_{W1}$	b_R^{up}	$(-0.64 + 0.75\mathrm{i})\Theta_{W1}$
c_R^d	$0.086\mathrm{i}\Theta_{W1} - 0.098\Theta_{W2}$	c_R^{up}	$(0.87 - \mathrm{i})\theta_{W1} + (1.1 + 0.98\mathrm{i})\Theta_{W2}$
d_R^d	$-0.058\mathrm{i}\Theta_{W1} + 0.098\Theta_{W2}$	d_R^{up}	$(-0.23 + 0.25\mathrm{i})\Theta_{W1} - (1.1 + 0.98\mathrm{i})\Theta_{W2}$

3.2. Interaction of the CS boson with two different up-type quarks

Let us now consider the interaction of the CS boson with up-type quarks. The amplitude of a heavy up-type quark (u_n) decay into a light up-type quark (u_m) and the CS boson in the unitary gauge is given by

$$M_{fi} = -\mathrm{i}\frac{g^2}{2}\sum_{i=d,s,b} V^+_{iu_m} V_{u_n i}\,\overline{u_m}(p')Y^\mu_{(i)}u_n(p)\epsilon^{*\lambda_X}_\mu, \tag{16}$$

where $Y^\mu_{(i)}$ is defined in (8). However, in this case p is the four-momentum and m is mass of the initial up-type quark (u_n), p' is the four-momentum and m' is mass of the final up-type quark (u_m), m_i is mass of the virtual down-type quark (d_i).

It should be noted that mass of the virtual down-type quark (d_i) in $Y^\mu_{(i)}$ is included only in function $D(m_i)$ (11), but for all virtual down-type quarks $m_i \ll M_W$. So, in the first approximation function $D(m_i)$ can be considered independent of the mass of virtual down-type quark m_i and can be taken as $D(m_i) = (1 - x)M_W^2$. It means that $Y^\mu_{(i)} \approx Y^\mu$ and

$$\sum_{i=d,s,b} V^+_{u_m i} V_{iu_n}\, Y^\mu_{(i)} \approx Y^\mu \sum_{i=d,s,b} V^+_{u_m i} V_{iu_n} = 0, \quad m \neq n. \tag{17}$$

Thus, in the first approximation the amplitude of a heavy up-type quark (u_n) decay into a light up-type quark (u_m) and the CS boson is zero. If we perform accurate calculations and present the amplitude in the form similar to the case of the down-type quarks:

$$M_{fi} = -\mathrm{i}\frac{g^2}{32\pi^2}\frac{m_i^2}{M_W^2}V^+_{st}V_{tb}\overline{u_m}(p')J^{\mu,\mathrm{up}}u_n(p)\epsilon^{*\lambda_X}_\mu, \tag{18}$$

where $J^{\mu,\mathrm{up}}$ has form (15), but with coefficients with superscript up, we get values presented in the table 1.

3.3. Lagrangian of the effective interaction of the CS boson with two different quarks

After analyzing the data in table 1 one can conclude that the production of CS bosons in decays of up-type quarks is substantially suppressed in comparison with the production of CS bosons in decays of down-type quarks.

If parameter Θ_{W1} is nonzero, then the main contribution for the CS boson production from down-type quarks comes from the term $a_L^d = -\mathrm{i}a\,\Theta_{W1}$, see (15). Using relation

$$\epsilon^{\alpha\mu\nu\rho}\gamma_\mu\gamma_\nu\gamma_\rho = 6\mathrm{i}\gamma^\alpha\gamma^5, \tag{19}$$

one can write the effective Lagrangian of the GeV-scale CS boson interaction with different down-type quarks in the form

$$\mathcal{L}^{\rm CS}_{\rm quarks} = \sum_{m<n} \Theta_{W1} \left(C_{mn}\, \overline{d_m}\, \gamma^\mu\, \hat{P}_L\, d_n X_\mu + C^+_{nm}\, \overline{d_n}\, \gamma^\mu\, \hat{P}_L\, d_m X_\mu \right), \tag{20}$$

where the summation occurs over the generations of quarks,

$$C_{mn} = \frac{3a}{2\sqrt{2}\pi^2}\, G_F m_t^2\, V^+_{d_m t} V_{t d_n} \tag{21}$$

and

$$|C_{sb}| = 1.97 \times 10^{-4}, \qquad |C_{db}| = 4.43 \times 10^{-5}, \qquad |C_{\rm ds}| = 1.77 \times 10^{-6}. \tag{22}$$

Interaction of the GeV-scale CS boson with up-type quarks can be neglected. These results are consistent with the results of [59, 60].

There are two points to pay attention to. First, Lagrangian (20) is valid only for the GeV-scale CS boson interaction with different quarks. The case of the CS boson interaction with the same quarks must be considered separately. In the last case, we cannot eliminate divergences in the loop integral using only the condition of the CKM-matrix unitarity. Second, Lagrangian (20) is slightly similar to the interaction Lagrangian of quarks with W bosons in the SM. As in the case of the SM the term $\overline{d_m}\, \gamma^\mu\, \hat{P}_L\, d_n X_\mu$ has no symmetry under the separate action of charge conjugation ($\hat{C}$) and parity transformation ($\hat{P}$) operators. But this term will have symmetry under the simultaneous action of charge conjugation and parity transformation operators

$$\hat{C}\hat{P}\overline{d_m}\, \gamma^\mu\, \hat{P}_L\, d_n X_\mu = \overline{d_n}\, \gamma^\mu\, \hat{P}_L\, d_m X_\mu, \tag{23}$$

if we impose a reasonable condition

$$\hat{C}\hat{P} X_\mu = -X^\mu. \tag{24}$$

Thus, having analyzed the effective Lagrangian (20), we come to the conclusion that the CS boson has no well-defined symmetry under the separate action of charge conjugation ($\hat{C}$) and parity transformation ($\hat{P}$) operators, but is even under the simultaneous action of $\hat{C}\hat{P}$ transformation like Z boson.

As in the case of the interaction Lagrangian of quarks with W bosons in the SM, the effective Lagrangian (20) will be $\hat{C}\hat{P}$ invariant only if matrix C_{mn} is real.

4. The CS boson production in decays of mesons

Since the CS boson interaction with up-type quarks is strongly suppressed, we will consider only production of CS bosons from mesons containing b or s quarks. Such lightest mesons are B mesons and $K^\pm$, K^0_S, K^0_L mesons.

Dominant reactions of the B meson decay with the CS boson production are two-body decays into pseudoscalar mesons (K and π mesons); scalar mesons $K^{0*}(700)$ and $K^{0*}(1430)$; vector mesons $K^*(892)$, $K^*(1410)$, $K^*(1680)$; pseudovector mesons $K_1(1270)$ and $K_1(1400)$; tensor final meson state $K_2(1430)$.

For the initial kaons states, the only possible two-body decay with the CS boson production is the process

$$K \to \pi + X. \tag{25}$$

There are three types of kaons—$K^{\pm}, K^0_L, K^0_S$. Although the decay width for each of them is given by the same loop factor (C^d_{sd}) the branching ratios differ. The first reason is that these kaons have different decay widths. The second reason is that π^0 meson is the *CP*-odd eigenstate, K^0_S is approximately the *CP*-even eigenstate, and K^0_L is approximately the *CP*-odd eigenstate. The *CP* parity of the final state in the reaction $K^0_L \to \pi^0 X$ is $(-1)^L (CP)_{\pi^0} (CP)_X = +1$ (since the total angular momentum of the initial meson is zero, the final particles must have orbital angular momentum $L = 1$). Therefore, the decay width of the reaction $K^0_L \to \pi^0 X$ is proportional to the CKM *CP*-violating phase [72, 73].

Branching of the two-body meson decay $h \to h' + X$ is defined as

$$Br(h \to h' X) = \frac{1}{\Gamma_h} \frac{|M_{h\to h'X}|^2}{8\pi M_h^2} |\vec{k}|, \tag{26}$$

where

$$|\vec{k}| = \frac{\sqrt{\lambda(M_h^2, M_{h'}^2, M_X^2)}}{2M_h} \tag{27}$$

and $\lambda(x, y, z) = x^2 + y^2 + z^2 - 2xy - 2yz - 2zx$ is the Källén function [74].

The amplitude of the decay of a containing d_n quark h meson into a containing d_m quark h' meson and the CS boson has form, see (20),

$$M_{h\to h'X} = \Theta_{1W} C_{mn} \langle h'(p')|\bar{d}_m \gamma^\mu \hat{P}_L d_n |h(p)\rangle \epsilon^{*\lambda_X}_\mu, \tag{28}$$

where the absolute values of C_{mn} are given by (21). In the case of decay of K^0_S, K^0_L mesons, one has to be more careful due to the presence of a certain CP parity in them, namely

$$M_{K^0_L\to\pi^0 X} = \Theta_{1W}\, \mathrm{Im}[C_{\mathrm{ds}}]\, \langle \pi^0(p')) \, |\bar{d}\gamma^\mu \hat{P}_L s|K^0_S(p)\rangle \, \epsilon^{*\lambda_X}_\mu, \tag{29}$$

$$M_{K^0_S\to\pi^0 X} = \Theta_{1W}\, \mathrm{Re}[C_{\mathrm{ds}}]\, \langle \pi^0(p')) \, |\bar{d}\gamma^\mu \hat{P}_L s|K^0_L(p)\rangle \, \epsilon^{*\lambda_X}_\mu, \tag{30}$$

where $\mathrm{Re}[C_{ds}] = -1.62 \times 10^{-6}$ and $\mathrm{Im}[C_{ds}] = -6.69 \times 10^{-7}$.

The average over meson states $\langle h'(p')) \, |\bar{d}_m \gamma^\mu \hat{P}_L d_n |h(p)\rangle$ can be obtained with help of formalism summarized e.g. in [36].

In the rest frame of the initial h meson we have $p = (M_h, 0)$. It decays into the h' meson and the CS boson with momentums

$$p' = (E', -\vec{k}), \qquad p_X = (E_X, \vec{k}), \qquad p_X = p - p'. \tag{31}$$

where direction of spatial vector $\vec{k}$ is arbitrary, but module $|\vec{k}|$ is defined by (27). Let us guide Z-axis along the spatial momentum of the CS boson, then four-vector of the CS boson polarisation is defined as

$$\epsilon^{(\pm)}_X = (0, 1, \mp \mathrm{i}, 0)/\sqrt{2}, \qquad \epsilon^{(0)}_X = \left(|\vec{k}|, 0, 0, E_X\right)/M_X, \tag{32}$$

where $\epsilon^{(\pm)}_X$ corresponds to the spin projection ± 1 and $\epsilon^{(0)}_X$ corresponds to zero spin projection on the momentum direction.

If $\langle h'(p')) \, |\bar{d}_n \gamma^\mu \hat{P}_L d_m |h(p)\rangle$ depends only on p^μ or p'^μ, then only the longitudinal component of the CS boson polarisation gives contribution into the amplitude of the reaction because $\epsilon^{(\pm)}_X p = \epsilon^{(\pm)}_X p' = 0$. It will be useful to write also

Table 2. Properties of the main production channels of the CS boson from kaons and B mesons. *First column*: decay channels; *second column*: type of final mesons; *third column*: branching ratios of two-body meson decays evaluated at $m_X \to 0$ and normalized by θ^2_{W1}. For B mesons the numerical values are given for $B^\pm$ mesons; in the case of B^0 meson all the given branching ratios should be multiplied by a factor of 0.93 that comes from the difference in total decay widths of $B^\pm$ and B^0 mesons [70]; *fourth column*: closing mass, i.e. the difference between the masses of the initial and the final mesons; *fifth column*: a reference to the appendix with details about form-factors used.

Process	Final meson	$\lim_{m_X\to 0}\left(\frac{m_X}{1\ \mathrm{GeV}}\right)^2 \frac{Br(m_X)}{\theta^2_{W1}}$	Closing mass (GeV)	Appendix
$K^\pm \to X\pi^\pm$	Pseudo scalar	2.49×10^1	0.35	Appendix C.1
$K^0_L \to X\pi^0$	Pseudo scalar	1.56×10^1	0.36	Appendix C.1
$K^0_S \to X\pi^0$	Pseudo scalar	1.61×10^{-1}	0.36	Appendix C.1
$B^\pm \to X\pi^\pm$	Pseudo scalar	2.37×10^2	5.14	Appendix C.1
$B^\pm \to XK^\pm$	Pseudo scalar	7.73×10^3	4.79	Appendix C.1
$B^\pm \to XK^{*,\pm}_0(700)$	Scalar	1.43×10^4	4.46	Appendix C.2
$B^\pm \to XK^{*,\pm}(892)$	Vector	9.14×10^3	4.39	Appendix C.3.1
$B^\pm \to XK^\pm_1(1270)$	Pseudo vector	1.72×10^4	4.01	Appendix C.3.2
$B^\pm \to XK^\pm_1(1400)$	Pseudo vector	2.34×10^2	3.88	Appendix C.3.2
$B^\pm \to XK^{*,\pm}(1410)$	Vector	3.99×10^3	3.86	Appendix C.3.1
$B^\pm \to XK^{*,\pm}_0(1430)$	Scalar	1.85×10^3	3.85	Appendix C.2
$B^\pm \to XK^{*,\pm}_2(1430)$	Tensor	6.03×10^3	3.85	Appendix C.4
$B^\pm \to XK^{*,\pm}(1680)$	Vector	2.53×10^3	3.56	Appendix C.3.1

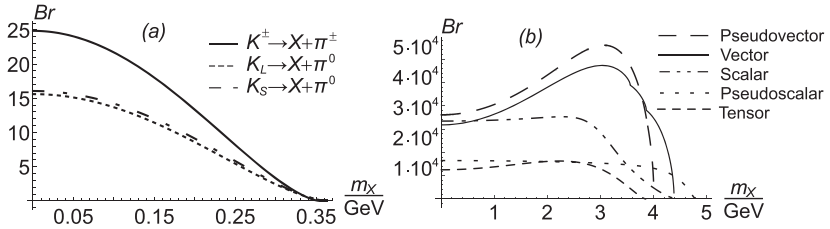

Figure 3. Dependence of the branching $Br = \theta^{-2}_{W1}\left(\frac{m_X}{1\ \mathrm{GeV}}\right)^2 Br(h \to h'X)$ of reactions of the CS boson production on the CS boson mass: (a)—reaction of the CS boson production in two-body decays of charged K mesons and neutral K^0_L, K^0_S mesons (values of the branching for the reaction $K^0_S \to \pi^0 + X$ are multiplied by 10^2); (b)—reaction of the CS boson production in two-body decays of charged B mesons (contributions over the (pseudo)scalar, (pseudo)vector and tensor channels of the B meson decays are summed up).

$$\epsilon^{(0)}_X\, p = \epsilon^{(0)}_X\, p' = |\vec{k}|\frac{M_h}{M_X}, \quad \epsilon^{(0)}_X\, p_X = 0. \tag{33}$$

Results for the branchings for the corresponding reactions are presented in table 2, where for the decays of the B mesons we took into account only the lightest final excited K meson states from its scalar, pseudoscalar, vector, pseudovector and tensor states. The branching dependencies on the CS boson mass for decays of charged K mesons and neutral K^0_L, K^0_S mesons are shown in figure 3(a). The branching dependencies on the CS boson mass for decays of charged B mesons are shown in figure 3(b), where, for clarity, we have summed up the contributions

over the (pseudo)scalar, (pseudo)vector and tensor channels. Because of the inverse quadratic divergence of the amplitude of meson decay at small masses of the CS boson (it originates from its longitudinal component), values of the reaction branchings are presented for quantity $\lim_{m_X\to 0}\left(\frac{m_X}{1\ \mathrm{GeV}}\right)^2\frac{Br(m_X)}{\theta_{W1}^2}$. Main contribution to the uncertainties in the presents results follows from uncertainties in meson transition form-factors. Our results are consistent with the results of [60], where some of the reactions we considered had been calculated.

5. Summary

The goal of our study was to describe the production of the new GeV-scale vector particle X_μ (CS boson) in the decays of mesons starting from the effective interaction of this boson with electroweak gauge bosons (1).

We consider the loop interaction of the CS boson with quarks of different flavors through W bosons. In this case, see figures 1(c) and (d), we have the CS boson interaction with two down-type or two up-type quarks. We have shown that the divergent terms in the calculation of loop diagrams are automatically canceled out due to the unitarity of the CKM matrix, see appendix A. Unfortunately, this result is valid only for the CS boson interaction with quarks of different flavors. The case of the interaction of the CS boson with two identical quarks or with leptons requires a separate, more accurate consideration and some renormalization scheme, which is the subject of further research.

We have shown that the interaction of the CS boson with up-type quarks is sufficiently suppressed compared with down-type quarks. This is due to the fact that when the up-type quarks interact with the CS boson, the masses of the virtual down-type quarks in the loop are small compared to the W boson mass. As a result, in the first approximation, there is no dependence of the loop terms on the mass of virtual down-type quarks and interaction of up-type quarks is suppressed by the condition of the unitarity of the CKM matrix.

We construct the effective Lagrangian of the CS boson interaction with two different down-type quarks (20). It turned out that the effective Lagrangian depends only on one of two unknown couplings (Θ_{W1}) of the CS boson interaction with W boson, see (1). It should be noted that in the interaction of the CS boson with quarks (20), the CS boson behaves like a CP even particle, see (24).

We consider the production of the CS boson in decays of mesons. Since CS bosons interact effectively only with down-type quarks, they can be produced in decays of mesons containing b or s quarks. Such lightest mesons are B mesons and $K^\pm$ mesons. Due to the contribution of longitudinal polarization of the CS boson, the decay width of the reactions increases with decreasing boson mass as M_X^{-2}. So, for convenience, we computed quantity $\theta_{W1}^{-2}\left(\frac{m_X}{1\ \mathrm{GeV}}\right)^2 Br(h\to h'X)$.

We consider the production of the CS bosons in decays of charged K mesons and neutral K_L^0, K_S^0 mesons. In the case of decays of K_L^0, K_S^0 mesons, we took into account that these particles have certain CP parity and the CS boson is a CP even particle. As a result, we found that reaction $K_L^0\to\pi^0+X$ has the greatest branching among the reactions of the CS boson production in decays of kaons. The branching of the reaction $K_S^0\to\pi^0+X$ is suppressed in $\sim 10^3$ times compared to the reaction $K_L^0\to\pi^0+X$, see table 2 and figure 3(a).

We consider dominant reactions of the CS bosons production in two-body decays of B meson into pseudoscalar mesons (K and π mesons); scalar mesons $K^{0*}(700)$ and $K^{0*}(1430)$; vector mesons $K^*(892)$, $K^*(1410)$, $K^*(1680)$; pseudovector mesons $K_1(1270)$ and $K_1(1400)$; tensor final meson state $K_2(1430)$. Results for the branching of the corresponding reactions are presented in table 2 for a very small mass of the CS boson. Dependence of the branching of

the CS boson production on its mass is presented in figure 3(b), where, for clarity, we summed up the contributions over the (pseudo)scalar, (pseudo)vector and tensor channels. As one can see, channels of the CS boson production with the greatest branching are decays of B mesons into pseudovector, vector and scalar mesons for the CS boson mass up to $m_X \simeq 3$ GeV, into pseudovector and vector mesons for 3 GeV $\lesssim m_X \lesssim 4$ GeV, vector and pseudoscalar mesons for 4 GeV $\lesssim m_X \lesssim 4.37$ GeV, and pseudoscalar mesons for 4.37 GeV $\lesssim m_X \lesssim 4.79$ GeV. The greatest branching of the CS boson production up to $m_X \simeq 3.8$ GeV is that of channel $B^{\pm} \to XK_1^{\pm}(1270)$, but other channels are also important and cannot be neglected.

The results of our research will be helpful for the construction of the sensitivity region and the search for the GeV-scale long-lived CS boson at intensity frontier experiments such as MATHUSLA [23], FACET [24], FASER [25, 26], NA62 [29–31], DUNE [32, 33], etc. Especially considering that the CS boson was already included in the SHiP experiment proposal [28].

Acknowledgments

The authors are grateful to Alexey Boyarsky and Oleg Ruchayskiy for fruitful discussions and helpful comments. We also wish to express thanks to Oleg Barabash for helpful consultations.

Data availability statement

All data that support the findings of this study are included within the article (and any supplementary files).

Appendix A. Computation of the loop diagram for CS boson interaction with different down-type quarks

The amplitude of a heavy down-type quark (d_n) decay into a light down-type quark (d_m) and the CS boson X_μ in the unitary gauge can be presented as

$$M_{fi} = -\mathrm{i}\frac{g^2}{2}\sum_{i=u,c,t} V^{+}_{d_m i} V_{i d_n}\, \overline{d_m}(p')\hat{P}_R I^{\mu}_{(i)} \hat{P}_L d_n(p) \epsilon^{*\lambda_X}_{\mu}, \tag{A.1}$$

where $\hat{P}_{R(L)}$—projection operators on the right(left)-handed chirality states and in the unitary gauge $I^{\mu}_{(i)}$ has form

$$\begin{aligned} I^{\mu}_{(i)} &= \int \frac{\mathrm{d}^4 k}{(2\pi)^4} \gamma^{\alpha} G(p-k) D_{\alpha\rho}(k-p_X) \left[c_\omega (k-p_X)_\lambda \right. \\ &\quad \left. + c^{*}_{\omega} k_\lambda\right] D_{\nu\beta}(k) \gamma^{\beta} \epsilon^{\mu\nu\lambda\rho} \\ &= \hat{A}(k)\gamma^{\alpha}\left[m_i + (\not{p} - \not{k})\right]\left[g_{\alpha\rho} - \frac{(k-p_X)_\alpha (k-p_X)_\rho}{M_W^2}\right]\left[c_\omega (k-p_X)_\lambda \right. \\ &\quad \left. + c^{*}_{\omega} k_\lambda\right]\left[g_{\beta\nu} - \frac{k_\beta k_\nu}{M_W^2}\right]\gamma^{\beta}\epsilon^{\mu\nu\lambda\rho}, \end{aligned} \tag{A.2}$$

where m_i is the mass of the u_i quark and integral operator $\hat{A}$ is defined as

$$\hat{A}(k) = \int \frac{\mathrm{d}^4 k}{(2\pi)^4 F(k)}, \qquad F(k) = \left[m_i^2 - (p-k)^2\right]\left[M_W^2 - (k-p')^2\right]\left[M_W^2 - k^2\right]. \quad \text{(A.3)}$$

Relation (A.2) can be further simplified with the help of the following identities:

$$\hat{P}_R(a + b\gamma_i)\hat{P}_L = b\hat{P}_R\gamma_i\hat{P}_L, \quad \hat{P}_R\gamma_i\gamma_j\hat{P}_L = 0. \quad \text{(A.4)}$$

We use the technique of α (Schwinger) representation, see e.g. [75], namely relations

$$\frac{1}{m^2 - k^2 - \mathrm{i}\varepsilon} = \mathrm{i}\int_0^\infty \mathrm{d}\alpha\, \mathrm{e}^{\mathrm{i}\alpha(k^2 - m^2 + \mathrm{i}\varepsilon)}, \quad \varepsilon \to 0, \quad \text{(A.5)}$$

$$\int_{-\infty}^{\infty} \mathrm{d}^4 k\, \mathrm{e}^{\mathrm{i}(Ak^2 + 2Bk)} = \frac{\pi^2}{\mathrm{i}} \cdot \frac{1}{A^2}\, \mathrm{e}^{-\mathrm{i}\frac{B^2}{A}}, \quad \text{(A.6)}$$

$$\int_{-\infty}^{\infty} \mathrm{d}^4 k\, \mathrm{e}^{\mathrm{i}(Ak^2 + 2Bk)} k^\nu = \frac{\pi^2}{\mathrm{i}} \cdot \frac{1}{A^2}\, \mathrm{e}^{-\mathrm{i}\frac{B^2}{A}} \left[-\frac{B^\nu}{A}\right], \quad \text{(A.7)}$$

$$\int_{-\infty}^{\infty} \mathrm{d}^4 k\, \mathrm{e}^{\mathrm{i}(Ak^2 + 2Bk)} k^\nu k^\mu = \frac{\pi^2}{\mathrm{i}} \cdot \frac{1}{A^2}\, \mathrm{e}^{-\mathrm{i}\frac{B^2}{A}} \left[\frac{2B^\nu B^\mu + \mathrm{i}A g^{\mu\nu}}{2A^2}\right], \quad \text{(A.8)}$$

$$\int_{-\infty}^{\infty} \mathrm{d}^4 k\, \mathrm{e}^{\mathrm{i}(Ak^2 + 2Bk)} k^\nu k^\mu k^\lambda = \frac{\pi^2}{\mathrm{i}} \cdot \frac{1}{A^2}\, \mathrm{e}^{-\mathrm{i}\frac{B^2}{A}} \times \left[-\frac{4B^\mu B^\nu B^\lambda + 2\mathrm{i}A\left[g^{\mu\nu}B^\lambda + g^{\mu\lambda}B^\nu + g^{\nu\lambda}B^\mu\right]}{4A^3}\right]. \quad \text{(A.9)}$$

With the help of this technique, we can get the following relations:

$$K^{(0)} = \hat{A}\cdot 1 = \frac{\mathrm{i}\pi^2}{(2\pi)^4}\int_0^1 \mathrm{d}x \int_0^{1-x} \mathrm{d}y \frac{1}{D(m_i)}, \quad \text{(A.10)}$$

$$K^{(1)}_\alpha = \hat{A}k_\alpha = \frac{\mathrm{i}\pi^2}{(2\pi)^4}\int_0^1 \mathrm{d}x \int_0^{1-x} \mathrm{d}y \frac{(xp + yp_X)_\alpha}{D(m_i)}, \quad \text{(A.11)}$$

$$K^{(2)}_{\alpha\beta} = \hat{A}k_\alpha k_\beta = \frac{\mathrm{i}\pi^2}{(2\pi)^4}\int_0^1 \mathrm{d}x \int_0^{1-x} \mathrm{d}y \times \left[\frac{(xp + yp_X)_\alpha (xp + yp_X)_\beta}{D(m_i)} - \frac{g_{\alpha\beta}}{2}\ln\frac{\Lambda^2 x}{D(m_i)}\right], \quad \text{(A.12)}$$

where Λ is some constant with dimension of mass (it should be put to infinity in the end of the computation, $\Lambda \to \infty$) and function $D(m_i)$ is defined by (11).

If we introduce integral operators $\hat{\Lambda}_{0(1)}$ (9) and (10) and notation $\mathcal{P} = xp + yp_X$, we can rewrite relation (A.10)–(A.12) as

$$K^{(0)} = \hat{\Lambda}_0, \qquad K^{(1)}_i = \hat{\Lambda}_0 \mathcal{P}_i, \qquad K^{(2)}_{i\bar{\lambda}} = \hat{\Lambda}_0 \mathcal{P}_{\bar{\lambda}} \mathcal{P}_i + \frac{\mathrm{i}}{2} g_{\bar{\lambda}i} \hat{\Lambda}_1. \quad \text{(A.13)}$$

It will be useful also to give the relation

$$K_i^{(3)} = \hat{A}k^2 k_i = -\hat{\Lambda}_0 \mathcal{P}^2 \mathcal{P}_i - 3\mathrm{i}\hat{\Lambda}_1 \mathcal{P}_i. \tag{A.14}$$

Using the relations obtained above, we can get

$$\begin{aligned} I_{(i)}^{\mu} = \hat{\Lambda}_0 \Big\{ & \gamma_\rho (\hat{\mathcal{P}} - \hat{p}) \gamma_\nu \left\{ \Theta_{W1} (p_X - 2\mathcal{P})_\lambda + \mathrm{i}\Theta_{W2} p_{X,\lambda} \right\} \\ & + \frac{p_{X,\lambda}}{M_W^2} \mathcal{P}_\nu \gamma_\rho \left[c_w^* \left\{ (p\mathcal{P}) + \hat{p}_X \hat{\mathcal{P}} - \hat{p}_X \hat{p} \right\} + 2\Theta_{W1} \mathcal{P}^2 \right. \\ & \left. + 2\mathrm{i}\Theta_{W2} \hat{p} \hat{\mathcal{P}} \right] \Big\} \epsilon^{\mu\nu\lambda\rho} + \hat{\Lambda}_1 \Big\{ - \mathrm{i}\Theta_{W1} \gamma_\rho \gamma_\lambda \gamma_\nu \\ & + \frac{p_{X,\lambda}}{M_W^2} \left[\mathrm{i} \frac{c_w^*}{2} \gamma_\rho \hat{p} \gamma_\nu + 6\mathrm{i}\Theta_{W1} \gamma_\rho \mathcal{P}_\nu - \Theta_{W2} \gamma_\rho \hat{p} \gamma_\nu \right] \Big\} \epsilon^{\mu\nu\lambda\rho}. \end{aligned} \tag{A.15}$$

The divergent part of this relation is hidden in the integral operator $\hat{\Lambda}_1$, see (10), but we can distinguish in this operator singular and finite parts (12) and replace operator $\hat{\Lambda}_1$ by finite operator $\hat{\Lambda}_1^{\mathrm{fin}}$ (13), see section 3.1.

With help of the unitary condition for the CKM matrix, it is not difficult to show that the amplitude of the process does not depend on the value of μ. Indeed, for reaction $b \to s + X$ we have $V_{su}^+ V_{ub} = -(V_{st}^+ V_{tb} + V_{ct}^+ V_{cb})$ and

$$\begin{aligned} & \sum_{i=u,c,t} V_{si}^+ V_{ib} \hat{\Lambda}_1^{\mathrm{fin}} F(x, y, \{p\}) \\ & \quad \sim \int_0^1 \mathrm{d}x \int_0^{1-x} \mathrm{d}y \sum_{i=u,c,t} V_{si}^+ V_{ib} \ \ln \frac{D(m_i)}{\mu^2} F(x, y, \{p\}) \\ & \quad = \int_0^1 \mathrm{d}x \int_0^{1-x} \mathrm{d}y \left[V_{st}^+ V_{tb} \left(\ln \frac{D(m_t)}{\mu^2} - \ln \frac{D(m_u)}{\mu^2} \right) \right. \\ & \qquad \left. + V_{sc}^+ V_{cb} \left(\ln \frac{D(m_c)}{\mu^2} - \ln \frac{D(m_u)}{\mu^2} \right) \right] F(x, y, \{p\}) \\ & \quad = \int_0^1 \mathrm{d}x \int_0^{1-x} \mathrm{d}y \left[V_{st}^+ V_{tb} \ \ln \frac{D(m_t)}{D(m_u)} + V_{sc}^+ V_{cb} \ \ln \frac{D(m_c)}{D(m_u)} \right] F(x, y, \{p\}). \end{aligned} \tag{A.16}$$

In the following, we will put $\mu = M_W$ for the convenience of computations.

Instead of momentum p_X, it is better to use the momentums of quarks $p_X \to p - p'$. It will allow us to use relations $\bar{d}_m(p')\hat{p}' = m'\bar{d}_m(p')$ and $\hat{p}d_n(p) = m d_n(p)$ and, in particular, to get

$$\begin{aligned} & \bar{d}_m(p')\hat{P}_R \gamma_{\bar{\rho}} \hat{p} \gamma_{\bar{\nu}} \hat{P}_L d_n(p) \\ & \qquad = \bar{d}_m(p')\hat{P}_R [2\gamma_{\bar{\rho}} \, p_{\bar{\nu}}] \hat{P}_L d_n(p) - \bar{d}_m(p')\hat{P}_R [m_b \gamma_{\bar{\rho}} \gamma_{\bar{\nu}}] \hat{P}_R d_n(p), \\ & \bar{d}_m(p')\hat{P}_R \gamma_{\bar{\rho}} \hat{p}' \gamma_{\bar{\nu}} \hat{P}_L d_n(p) \\ & \qquad = \bar{d}_m(p')\hat{P}_R [2p'_{\bar{\rho}} \gamma_{\bar{\nu}}] \hat{P}_L d_n(p) - \bar{d}_m(p')\hat{P}_L [m_s \gamma_{\bar{\rho}} \gamma_{\bar{\nu}}] \hat{P}_L d_n(p), \\ & \bar{d}_m(p')\hat{P}_R \gamma_{\bar{\rho}} \hat{p}' \hat{p} \hat{P}_L d_n(p) \\ & \qquad = \bar{d}_m(p')\hat{P}_R [2m_b \, p'_{\bar{\rho}}] \hat{P}_R d_n(p) - \bar{d}_m(p')\hat{P}_L [m_s m_b \gamma_{\bar{\rho}}] \hat{P}_R d_n(p), \end{aligned}$$

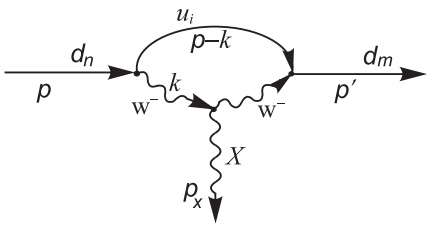

Figure A1. Interaction of the CS boson with two down-type quarks via loop diagram.

where m is the mass of the initial down-type quark (d_n) and m' is the mass of the final down-type quark (d_m). After this substitution, we finally get the relation $Y^{\mu}_{(i)} = \hat{P}_R I^{\mu}_{(i)} \hat{P}_L$ (8).

Appendix B. Coefficients in the amplitude of the CS boson interaction with different down-type quarks

Let us perform summation over virtual quarks and integration over the variables x and y in (7) and (8). For simplicity of notation we consider only decay of the b quark into s quark and the CS boson. First, it is more convenient to compute detached terms that are included in (7) such as

$$A_0 = \sum_{i=u,c,t} V^+_{si} V_{ib} \hat{\Lambda}_0, \qquad A_{0f} = \sum_{i=u,c,t} V^+_{si} V_{ib} \hat{\Lambda}_0 f,$$
$$A_1 = \sum_{i=u,c,t} V^+_{si} V_{ib} \hat{\Lambda}^{\text{fin}}_1, \qquad A_{1f} = \sum_{i=u,c,t} V^+_{si} V_{ib} \hat{\Lambda}^{\text{fin}}_1 f. \tag{B.1}$$

To do it analytically, we will make an estimation, taking into account that $M_W^2 \gg m^2, m'^2, M_X^2$, and simplify relation (11) to the form:

$$D(m_i) = \begin{cases} D_{uc} = (1-x)M_W^2 & \text{for } i = u, c \text{ quarks}, \\ D_t = (1 + (t_w - 1)x)M_W^2 & \text{for } i = t \text{ quark}, \end{cases} \tag{B.2}$$

where $t_w = m_t^2/M_W^2$. Then one can easily obtain quite simple relations e.g.

$$A_0 = \frac{\mathrm{i}\pi^2}{(2\pi)^4} \frac{1}{M_W^2} \left\{ V^+_{su} V_{ub} + V^+_{sc} V_{cb} + V^+_{st} V_{tb} \frac{1 - t_w + t_w \ln\ t_w}{(t_w - 1)^2} \right\}; \tag{B.3}$$

$$A_{0x} = \frac{\mathrm{i}\pi^2}{(2\pi)^4} \frac{1}{2M_W^2} \left\{ V^+_{su} V_{ub} + V^+_{sc} V_{cb} + V^+_{st} V_{tb} \frac{t_w^2 - 1 - 2t_w \ln\ t_w}{(t_w - 1)^3} \right\}; \tag{B.4}$$

$$A_1 = -\frac{1}{4} \frac{\pi^2}{(2\pi)^4} \left\{ V^+_{su} V_{ub} + V^+_{sc} V_{cb} - V^+_{st} V_{tb} \frac{2t_w^2 \ln\ t_w - 1 + 4t_w - 3t_w^2}{(t_w - 1)^2} \right\}. \tag{B.5}$$

From the unitarity condition $(V^+V)_{sb} = 0$, one can conclude $V^+_{su}V_{ub} + V^+_{sc}V_{cb} = -V^+_{st}V_{tb}$ and write

$$A_0 = -\frac{\mathrm{i}\pi^2}{(2\pi)^4}\,\frac{V^+_{st}V_{tb}}{M_W^2}\,t_w\,\frac{t_w - 1 - \ln\,t_w}{(t_w-1)^2}; \tag{B.6}$$

$$A_{0x} = -\frac{\mathrm{i}\pi^2}{(2\pi)^4}\,\frac{V^+_{st}V_{tb}}{M_W^2}\,t_w\,\frac{3 + (t_w-4)t_w + 2\,\ln\,t_w}{2(t_w-1)^3}; \tag{B.7}$$

$$A_{0y} = -\frac{\mathrm{i}\pi^2}{(2\pi)^4}\,\frac{V^+_{st}V_{tb}}{M_W^2}\,t_w\,\frac{t_w^2 - 1 - 2t_w\,\ln\,t_w}{4(t_w-1)^3}; \tag{B.8}$$

$$A_{0x^2} = -\frac{\mathrm{i}\pi^2}{(2\pi)^4}\,\frac{V^+_{st}V_{tb}}{M_W^2}\,t_w\,\frac{2t_w^3 - 9t_w^2 + 18t_w - 11 - 6\,\ln\,t_w}{6(t_w-1)^4}; \tag{B.9}$$

$$A_{0y^2} = -\frac{i\pi^2}{(2\pi)^4}\,\frac{V^+_{st}V_{tb}}{M_W^2}\,t_w\,\frac{1 - 6t_w + 3t_w^2 + 2t_w^3 - 6t_w^2\,\ln\,t_w}{18(t_w-1)^4}; \tag{B.10}$$

$$A_{0xy} = -\frac{\mathrm{i}\pi^2}{(2\pi)^4}\,\frac{V^+_{st}V_{tb}}{M_W^2}\,t_w\,\frac{2 + 3t_w - 6t_w^2 + t_w^3 + 6t_w\,\ln\,t_w}{12(t_w-1)^4}; \tag{B.11}$$

$$A_{0x^3} = -\frac{\mathrm{i}\pi^2}{(2\pi)^4}\,\frac{V^+_{st}V_{tb}}{M_W^2}\,t_w\,\frac{25 - 48t_w + 36t_w^2 - 16t_w^3 + 3t_w^4 + 12\,\ln\,t_w}{12(t_w-1)^5}; \tag{B.12}$$

$$A_{0x^2y} = -\frac{\mathrm{i}\pi^2}{(2\pi)^4}\,\frac{V^+_{st}V_{tb}}{M_W^2}\,t_w\,\frac{-3 - 10t_w + 18t_w^2 - 6t_w^3 + t_w^4 - 12t_w\,\ln\,t_w}{24(t_w-1)^5}; \tag{B.13}$$

$$A_{0y^2x} = -\frac{\mathrm{i}\pi^2}{(2\pi)^4}\,\frac{V^+_{st}V_{tb}}{M_W^2}\,t_w\,\frac{-1 + 8t_w - 8t_w^3 + t_w^4 + 12t_w^2\,\ln\,t_w\,]}{36(t_w-1)^5}; \tag{B.14}$$

$$A_1 = \frac{\pi^2}{(2\pi)^4}\,V^+_{st}V_{tb}\,t_w\,\frac{1 - t_w + t_w\,\ln\,t_w}{2(t_w-1)^2}; \tag{B.15}$$

$$A_{1x} = \frac{\pi^2}{(2\pi)^4}\,V^+_{st}V_{tb}\,t_w\,\frac{2(t_w-1) + (t_w-3)t_w\,\ln\,t_w}{6(t_w-1)^3}. \tag{B.16}$$

Denoting

$$A_{0\alpha} = -\mathrm{i}\frac{\pi^2}{(2\pi)^4}V^+_{st}V_{tb}\,t_w\,\frac{a_{0\alpha}}{M_W^2}, \qquad A_{1\alpha} = \frac{\pi^2}{(2\pi)^4}\,V^+_{st}V_{tb}\,t_w\,a_{1\alpha}, \tag{B.17}$$

where the subscript α is some combination of x and y (or empty index), we get values for dimensionless coefficients $a_{0\alpha}$, $a_{1\alpha}$, see table B1. As one can see, these coefficients do not depend on the down-type quarks which were at the beginning and at the end of the reaction.

Now we can write relations for coefficients in (15):

$$a_L^d = -\mathrm{i}\,a_1\Theta_{W1}, \tag{B.18}$$

$$c_L^d = \mathrm{i}(a_{0y} - 2a_{0y^2})\Theta_{W1} - a_{0y}\Theta_{W2}, \tag{B.19}$$

$$d_L^d = \mathrm{i}(2a_{0xy} - a_{0y} + 2a_{0y^2})\Theta_{W1} + a_{0y}\Theta_{W2}, \tag{B.20}$$

$$b_R^d = -\mathrm{i}\,(a_{0x} - a_{0x^2})\Theta_{W1} + (a_{0x^2} + 2a_{0xy} - a_{0x})\Theta_{W2}, \tag{B.21}$$

Table B1. Numerical values of the coefficients $a_{0\alpha}$ and $a_{1\alpha}$.

a_0	a_{0x}	a_{0y}	a_{0x^2}	a_{0xy}	a_{0y^2}	a_{0x^3}	a_{0x^2y}	a_{0y^2x}	a_1	a_{1x}
0.16	0.094	0.033	0.066	0.014	0.012	0.051	0.0076	0.0042	0.13	0.066

$$c_R^d = \mathrm{i}\left(a_0 - a_{0x} + 2a_{0xy} - 3a_{0y} + 2a_{0y^2} + \frac{a_1}{2}\right)\Theta_{W1} - \left(a_0 - a_{0x} - a_{0y} + \frac{a_1}{2}\right)\Theta_{W2}, \tag{B.22}$$

$$d_R^d = \mathrm{i}\left(-a_0 + 3a_{0x} - 2a_{0x^2} - 4a_{0xy} + 3a_{0y} - 2a_{0y^2} - \frac{a_1}{2}\right)\Theta_{W1} + \left(a_0 - a_{0x} - a_{0y} + \frac{a_1}{2}\right)\Theta_{W2}. \tag{B.23}$$

We also write separately the most cumbersome coefficient

$$b_L^d = \frac{\mathrm{i}}{2}\left[(a_{0xy} - 2a_{0x} + 4(a_{0x^2} + a_{0x^3} + a_{0x^2y}))\frac{m^2}{M_W^2} + (4a_{0x^2y} + 3a_{0xy} + 4a_{0xy^2})\frac{M_X^2}{M_W^2} - (4a_{0x^2y} + a_{0xy})\frac{m'^2}{M_W^2} - 4(a_0 - a_{0x}) - 16(a_{0xy} - a_{0y} + a_{0y^2}) - 2a_1 - 12a_{1x}\right]\Theta_{W1}$$

$$+ \left[2a_0 - 4a_{0y} + a_1 - 2a_{0x} - \left(a_{0x} - \frac{a_{0xy}}{2}\right)\frac{m^2}{M_W^2} + \frac{3a_{0xy}}{2}\frac{m'^2}{M_W^2} - \frac{a_{0xy}}{2}\frac{M_X^2}{M_W^2}\right]\Theta_{W2}. \tag{B.24}$$

In the case of GeV-scale CS bosons the terms suppressed by factor $\sim M_W^{-2}$ can be neglected and we get

$$b_L^d = \frac{\mathrm{i}}{2}\left[-4(a_0 - a_{0x}) - 16(a_{0xy} - a_{0y} + a_{0y^2}) - 2a_1 - 12a_{1x}\right]\Theta_{W1} + \left[2a_0 - 4a_{0y} + a_1 - 2a_{0x}\right]\Theta_{W2}. \tag{B.25}$$

The numerical values of these coefficients are presented in table 1.

Appendix C. Decays of mesons with the CS boson production

C.1. Decay into mesons of the same parity

Let us consider here the production of the CS boson in decays of B mesons into K, π mesons and decays of K mesons into π mesons.

In the case of a decay of one meson into another meson with the same parity, we have the following relation for the averaging the quark current over the meson states:

$$2\langle h'(p')|\bar{Q}_i\gamma^\mu\hat{P}_L Q_j|h(p)\rangle = \langle h'(p')|\bar{Q}_i\gamma^\mu Q_j|h(p)\rangle$$
$$= \left[(p+p')^\mu - \frac{m_P^2 - m_{P'}^2}{q^2}q^\mu\right] f_+^{hh'}(q^2) + \frac{m_P^2 - m_{P'}^2}{q^2}q^\mu f_0^{hh'}(q^2), \quad \text{(C.1)}$$

where q is the momentum transfer to h' meson, namely $q = p - p'$, $q^2 = M_X^2$.

Using relations (28) and (33) one can get the amplitude of the an h meson decay (pseudomeson, P) into an h' meson (with the same parity) and the CS boson:

$$M_{P\to P'X} = \Theta_{1W} C_{mn} |\vec{k}| \frac{M_h}{M_X} f_+^{hh'}(M_X^2). \quad \text{(C.2)}$$

Thus, we will be interested only in the $f_+^{hh'}$ form-factor. It should be noted that in the case of K_S^0, K_L^0 mesons with a certain CP parity, we have to use the real or the imaginary part of the coefficient C_{ds}, see (29) and (30).

We take form-factors $f_+^{hh'}(q^2)$ for the decays of B mesons from [76], where they were given with the help of pole parametrizations:

$$f_+^{hh'}(q^2) = \frac{r_1}{1 - q^2/m_1^2} + \frac{r_2}{1 - q^2/m_{\text{fit}}^2}, \quad \text{(C.3)}$$

$$f_+^{hh'}(q^2) = \frac{r_1}{1 - q^2/m_1^2} + \frac{r_2}{\left(1 - q^2/m_1^2\right)^2}. \quad \text{(C.4)}$$

The last relation is used for the case when m_{fit} gets too close to m_1.

Form-factors for the decay of K meson are discussed in detail in [70].

We use form-factors $f_+^{hh'}(q^2)$ for the decays of $K^\pm$ mesons in the form of a quadratic expansion:

$$f_+^{hh'}(q^2) = f_+^{hh'}(0)\left(1 + \lambda'_+\frac{q^2}{m_{\text{fit}}^2} + \frac{\lambda''_+}{2}\left(\frac{q^2}{m_{\text{fit}}^2}\right)^2\right). \quad \text{(C.5)}$$

We take values of the parameters λ'_+ and λ''_+ from [70], which are the averaged over the values given in [77–79].

For the decays of K_L^0 mesons we take form-factors $f_+^{hh'}(q^2)$ in the form of the quadratic expansion (C.5) too. We take values of the parameters λ'_+ and λ''_+ from [70], which are the averaged over the values given in [80–82], assuming $\mu - e$ universality.

The values of the parameters in (C.3)–(C.5) are summarized in table C1.

For the decays of K_S^0 mesons we take form-factors $f_+^{hh'}(q^2)$ in the form of a linear expansion:

$$f_+^{hh'}(q^2) = f_+^{hh'}(0)\left(1 + \lambda_+\frac{q^2}{m_{\text{fit}}^2}\right), \quad \text{(C.6)}$$

where values of the parameters $f(0) = 0.96$ and $\lambda_+ = 3.39 \times 10^{-2}$ were taken from [83].

C.2. Decays into mesons of another parity

Let us consider here the production of the CS boson in the decays of B mesons into $K^{0*}(700)$, $K^{0*}(1430)$ mesons.

Table C1. Fit parameters for equations (C.3)–(C.5). Here m_1 is the meson mass in the corresponding channel: $m_1^\pi = m_{B^*} = 5.32$ GeV and $m_1^K = m_{B_s^*} = 5.41$ GeV.

	r_1	r_2	$(m_1)^2$	$m^2_{\rm fit}$
$f_+^{B\pi}$	0.744	−0.486	$(m_1^\pi)^2$	40.73
f_+^{BK}	0.162	0.173	$(m_1^K)^2$	—
	$f(0)$	λ'_+	λ''_+	$m^2_{\rm fit}$
$f_+^{K^\pm\pi}$	0.96	2.59×10^{-2}	1.86×10^{-3}	$m^2_{\pi^+}$
$f_+^{K^0_L\pi}$	0.96	2.4×10^{-2}	2×10^{-3}	$m^2_{\pi^+}$

Table C2. Values of the parameters in the form-factor parameterization (C.9) for $B = B^+$, $S = K_0^{*0}(700)$, $K_0^*(1430)$ in regions $q^2 < 11$ GeV^2 and $q^2 < 8$ GeV^2 correspondingly. We used figure 3 of [84] to find interpolation coefficients of (C.9).

S	F_0^{BS}	a	b
$K_0^*(700)$	0.466	1.501	1.026
$K_0^*(1430)$	0.181	4.293	6.450

In the case of a decay of one meson into another meson with different parity we get

$$2\langle h'(p')|\bar{Q}_i\gamma^\mu \hat{P}_L Q_j|h(p)\rangle = -\left[(p+p')^\mu - q^\mu\right] f_+^{hh'}(q^2) = -2p'^\mu f_+^{hh'}(q^2), \tag{C.7}$$

where we used $f_+(q^2) = -f_-(q^2)$ in (C.1), [84].

There is an open question whether hypothetical $K_0^*(700)$ is a state formed by two or four quarks, see, e.g. [85], discussions in [84, 86] and references therein. In this paper, we will do the same as we did in [36], namely, we assume that $K_0^*(700)$ is a di-quark state and $K_0^*(1430)$ is its excited state. There are no experimentally observed decays of B meson into $K_0^*(700)$, and therefore there is quite a large theoretical uncertainty in the determination of the form-factors (see the discussion in [87]). We will use [84], where there are results for $B \to K_0^*(700)$ and $B \to K_0^*(1430)$, and the results for the latter are in good agreement with the experimental data for $B \to K_0^*(1430)\eta'$ decay.

Using relations (28) and (33) one can get the amplitude of an h meson decay (pseudomeson, P) into an h' meson (scalar meson, S) and the CS boson:

$$M_{P\to SX} = -\Theta_{1W} C_{mn} |\vec{k}| \frac{M_h}{M_X} f_+^{hh'}(M_X^2). \tag{C.8}$$

We take $f_+^{BK_0^*}(q^2)$ from [84] in the form of a pole-like function:

$$f_+^{BK_0^*}(q^2) = \frac{F_0^{BK_0^*}}{1 - a\frac{q^2}{m_B^2} + b\left(\frac{q^2}{m_B^2}\right)^2}, \tag{C.9}$$

where $m_B = 5.3$ GeV is the mass of the B^+ meson. The fit parameters are given in table C2.

C.3. Vector and pseudovector final meson state

C.3.1. Vector. Let us consider here the production of the CS boson in the decays of B mesons into vector states $B \to K^*(892), K^*(1410), K^*(1680)$. Since the total angular momentum of the B meson is zero, two final vector particles must have zero total angular momentum.

For the vector final state, $h' = V$, we have [88, 89]

$$\langle V(p')|\bar{Q}_i\gamma^\mu\gamma_5 Q_j|h(p)\rangle = (M_h + M_V)\epsilon_V^{\mu*}(p')A_1(q^2) - (\epsilon_V^*(p')\cdot q) \times (p+p')^\mu \frac{A_2(q^2)}{M_h+M_V} - 2M_V\frac{\epsilon_V^*(p')\cdot q}{q^2}q^\mu(A_3(q^2)-A_0(q^2)), \tag{C.10}$$

$$\langle V(p')|\bar{Q}_i\gamma^\mu Q_j|h(p)\rangle = \frac{2V(q^2)}{M_h+M_V}\mathrm{i}\epsilon^{\mu\nu\rho\sigma}\epsilon^*_{V,\nu}(p')p_\rho p'_\sigma, \tag{C.11}$$

where $\epsilon_V^\mu(p')$ is the polarization vector of the vector meson, and A_i, V are the form-factors. The form-factor A_3 is related to A_1 and A_2 as

$$A_3(q^2) = \frac{M_h+M_V}{2M_V}A_1(q^2) - \frac{M_h-M_V}{2M_V}A_2(q^2). \tag{C.12}$$

The amplitude of an h meson decay into a vector V meson and the CS boson has form

$$\begin{aligned} M_{h\to VX}(\lambda_V,\lambda_X) &= \Theta_{W1}g^2C_{mn}\langle V(p',\lambda_V)|\bar{d}_n\gamma^\mu\hat{P}_L d_m|h(p)\rangle\epsilon^{*\lambda_X}_{X,\mu} \\ &= -\Theta_{W1}\frac{g^2C_{mn}}{2}\Bigg[-\frac{2V(q^2)}{M_h+M_V}\mathrm{i}\epsilon^{\mu\nu\rho\sigma}\epsilon^{\lambda_X*}_{X,\mu}\epsilon^{\lambda_V*}_{V,\nu}p_\rho p'_\sigma \\ &\quad + (M_h+M_V)(\epsilon_V^{\lambda_V*}\cdot\epsilon_X^{\lambda_X*})A_1(q^2) \\ &\quad - (\epsilon_V^{\lambda_V*}\cdot q)(\epsilon_X^{\lambda_X*}\cdot(p+p'))\frac{A_2(q^2)}{M_h+M_V} \\ &\quad - 2M_V\frac{\epsilon_V^{\lambda_V*}\cdot q}{q^2}(\epsilon_X^{\lambda_X*}\cdot q)(A_3(q^2)-A_0(q^2))\Bigg], \end{aligned} \tag{C.13}$$

where $\epsilon_V^{\lambda_V*}$ and $\epsilon_X^{\lambda_X*}$ correspond to the polarizations of the vector meson (V_μ) and the CS boson (X_μ).

In the rest frame of the h meson $p = (M_h, 0)$ we have relations (31). Let us guide Z-axis along the spatial momentum of the CS boson $\vec{k}$, then the other vector particle will move in the opposite direction. In this case, four-vectors of the polarizations for the CS boson or the vector particle have form

$$\begin{aligned} \epsilon^{(\pm)}_{X(V)} &= \frac{1}{\sqrt{2}}(0,1,\mp\mathrm{i},0), \qquad \epsilon^{(0)}_X = \frac{1}{M_X}\left(|\vec{k}|,0,0,E_X\right), \\ \epsilon^{(0)}_V &= \frac{1}{M_V}\left(|\vec{k}|,0,0,-E_V\right), \end{aligned} \tag{C.14}$$

where $\epsilon^{(\pm)}$ corresponds to the spin projection ±1 and $\epsilon^{(0)}$ corresponds to zero spin projection on Z-axis.

Using (C.14) one can get (33) and the following relations for different polarizations of vector particles:

$$\epsilon_V^{(0)*}\cdot p = |\vec{k}|\frac{M_h}{M_V}, \qquad \epsilon_V^{(0)*}\cdot p' = 0,$$
$$\epsilon_V^{(0)*}\cdot\epsilon_X^{(0)*} = \frac{\vec{k}^2 + E_X E_V}{M_X M_V}, \qquad \epsilon_V^{(+)*}\cdot\epsilon_X^{(-)*} = \epsilon_V^{(-)*}\cdot\epsilon_X^{(+)*} = -1, \tag{C.15}$$

where module $|\vec{k}|$ is defined by (26).

Consider now the following convolution $\epsilon^{\mu\nu\rho\sigma}\epsilon^*_{X,\mu}\epsilon^*_{V,\nu}(p')p_\rho p'_\sigma$. Due to the fact that only the 0 and 3 components of the momentums p and p' are nonzero, only the 1 and 2 components of polarization vectors can be used. These components are zero for the longitudinal polarization of the vector particles, so the contribution from longitudinal polarizations is absent, but the contribution from transversal opposite polarizations is nonzero:

$$\epsilon^{\mu\nu\rho\sigma}\epsilon^{(\pm)*}_{X,\mu}\epsilon^{(\mp)*}_{V,\nu}p_\rho p'_\sigma = (p_0p'_3 - p_3p'_0)\left(\epsilon^{(\pm)*}_{X,1}\epsilon^{(\mp*)}_{V,2} - \epsilon^{(\pm)*}_{X,2}\epsilon^{(\mp)*}_{V,1}\right), \tag{C.16}$$

namely

$$\epsilon^{\mu\nu\rho\sigma}\epsilon^{(+)*}_{X,\mu}\epsilon^{(-)*}_{V,\nu}p_\rho p'_\sigma = -\mathrm{i}M_h|\vec{k}|, \qquad \epsilon^{\mu\nu\rho\sigma}\epsilon^{(-)*}_{X,\mu}\epsilon^{(+)*}_{V,\nu}p_\rho p'_\sigma = +\mathrm{i}M_h|\vec{k}|. \tag{C.17}$$

So, we get the following nonzero amplitudes of the reaction:

$$M_{h\to VX}(+,-) = -\Theta_{1W}\frac{C_{mn}}{2}\left[\frac{2M_h|\vec{k}|}{M_h+M_V}V(q^2) - (M_h+M_V)A_1(q^2)\right], \tag{C.18}$$

$$M_{h\to VX}(-,+) = \Theta_{1W}\frac{C_{mn}}{2}\left[\frac{2M_h|\vec{k}|}{M_h+M_V}V(q^2) + (MM_V)A_1(q^2)\right], \tag{C.19}$$

$$M_{h\to VX}(0,0) = -\Theta_{1W}\frac{C_{mn}}{2}\left[(M_h+M_V)\frac{\vec{k}^2+E_XE_V}{M_XM_V}A_1(q^2) - 2\frac{\vec{k}^2M_h^2}{M_VM_X}\frac{A_2(q^2)}{M_h+M_V}\right], \tag{C.20}$$

and

$$\sum_{\text{polarizations}}|M_{h\to VX}|^2 = \Theta_{1W}^2\frac{|C_{mn}|^2}{4}\left[\frac{8M_h^2\vec{k}^{\,2}}{(M_h+M_V)^2}V^2(q^2) + 2(M_h+M_V)^2A_1^2(q^2) + \left((M_h+M_V)\frac{\vec{k}^2+E_XE_V}{M_XM_V}A_1(q^2) - \frac{2M_h^2\vec{k}^2}{M_VM_X(M_h+M_V)}A_2(q^2)\right)^2\right]. \tag{C.21}$$

Table C3. Values of parameters of the vector form-factors (C.22)–(C.24) for the decay of a B meson into $K^*(892)$ [88].

form-factors	r_1	r_2	m_R (GeV)	$m_{\rm fit}$ (GeV)	$q^2=0$
$V(q^2)$	0.923	−0.511	5.32	$\sqrt{49.40}$	0.411
$A_1(q^2)$	—	0.29	—	$\sqrt{40.38}$	0.292
$A_2(q^2)$	−0.084	0.342	—	$\sqrt{52.00}$	0.259

For the case of the decay of a B meson into $K^*(892)$, we follow [88] and parametrize the form-factor V and A_0 as

$$F(q^2) = \frac{r_1}{1 - q^2/m_R^2} + \frac{r_2}{1 - q^2/m_{\rm fit}^2}, \tag{C.22}$$

form-factor A_1 as

$$F(q^2) = \frac{r_2}{1 - q^2/m_{\rm fit}^2}, \tag{C.23}$$

and form-factor A_2 as

$$F(q^2) = \frac{r_1}{1 - q^2/m_{\rm fit}^2} + \frac{r_2}{\left(1 - q^2/m_{\rm fit}^2\right)^2}. \tag{C.24}$$

The values of the corresponding parameters are given in table C3.

For the case of the decay of a B meson into $K^*(1410)$, $K^*(1680)$, we use another parametrization for the form-factors [90, 91]:

$$A_0(q^2) = \left(1 - \frac{2M_V^2}{M_h^2 + M_V^2 - q^2}\right)\zeta_\parallel(q^2) + \frac{M_V}{M_h}\zeta_\perp(q^2), \tag{C.25}$$

$$A_1(q^2) = \frac{2E_V}{M_h + M_V}\zeta_\perp(q^2) = \frac{M_h^2 + M_V^2 - q^2}{M_h(M_h + M_V)}\zeta_\perp(q^2), \tag{C.26}$$

$$A_2(q^2) = \left(1 + \frac{M_V}{M_h}\right)\left[\zeta_\perp(q^2) - \frac{2M_hM_V}{M_h^2 + M_V^2 - q^2}\zeta_\parallel(q^2)\right], \tag{C.27}$$

$$V(q^2) = \left(1 + \frac{M_V}{M_h}\right)\zeta_\perp(q^2), \tag{C.28}$$

where

$$\zeta_{\perp/\parallel}(q^2) = \frac{\zeta_{\perp/\parallel}(0)}{1 - q^2/M_h^2}. \tag{C.29}$$

The values of the corresponding parameters are given in table C4.

C.3.2. Pseudo-vector. For the case of pseudo-vector mesons, $h' = A$, one has to interchange the expressions for the vector and axial-vector matrix elements (C.10) and (C.11), see [92, 93]:

$$\langle A(p')|\bar{Q}_i\gamma^\mu Q_j|h(p)\rangle = (M_h + M_A)\epsilon_A^{\mu*}(p')V_1(q^2) - (\epsilon_A^*(p')\cdot q)(p + p')^\mu \times \frac{V_2(q^2)}{M_h + M_A} - 2M_A\frac{\epsilon_A^*(p')\cdot q}{q^2}q^\mu(V_3(q^2) - V_0(q^2)), \tag{C.30}$$

Table C4. Values of parameters in the vector form-factors (C.25)–(C.28) for the decay of a B meson into $K^*(1410)$, $K^*(1680)$, [90, 91].

V	$\zeta_\perp(0)$	$\zeta_\parallel(0)$
$K^*(1410)$	0.28	0.22
$K^*(1680)$	0.24	0.18

$$\langle A(p')|\bar{Q}_i\gamma^\mu\gamma_5 Q_j|h(p)\rangle = \frac{2A(q^2)}{M_h+M_A}\mathrm{i}\epsilon^{\mu\nu\rho\sigma}\epsilon^*_{A,\nu}(p')p_\rho p'_\sigma, \tag{C.31}$$

with the same relation between V_i as for A_i in the case of vector mesons (C.12).

Expression (C.21) in this case takes form

$$\sum_{\text{polarizations}}|M_{h\to AX}|^2 = \Theta_{1W}^2\frac{|C_{mn}|^2}{4}\left[\frac{8M_h^2\vec{k}^2}{(M_h+M_A)^2}A^2(q^2)\right.$$
$$+2(M_h+M_A)^2V_1^2(q^2)+\left((M_h+M_A)\frac{\vec{k}^2+E_XE_A}{M_XM_A}V_1(q^2)\right.$$
$$\left.\left.-\frac{2M_h^2\vec{k}^2}{M_AM_X(M_h+M_A)}V_2(q^2)\right)^2\right]. \tag{C.32}$$

We will consider decays of B mesons in two lightest pseudo-vector resonances $K_1(1270)$, $K_1(1400)$, each of which is a mixture of unphysical K_{1A} and K_{1B} states [92],

$$\begin{pmatrix}|K_1(1270)\rangle\\|K_1(1400)\rangle\end{pmatrix} = \begin{pmatrix}\sin(\theta_{K_1}) & \cos(\theta_{K_1})\\ \cos(\theta_{K_1}) & -\sin(\theta_{K_1})\end{pmatrix}\begin{pmatrix}|K_{1A}\rangle\\|K_{1B}\rangle\end{pmatrix}. \tag{C.33}$$

The form-factors $V_i^{BK_1}$ and A^{BK_1} can be related to the appropriate form-factors of the K_{1A} and K_{1B} states as

$$A^{BK_1(1270)}(q^2) = \sin(\theta_{K_1})\frac{m_B+m_{K_1(1270)}}{m_B+m_{K_{1A}}}A^{K_{1A}}(q^2)$$
$$+\cos(\theta_{K_1})\frac{m_B+m_{K_1(1270)}}{m_B+m_{K_{1B}}}A^{K_{1B}}(q^2), \tag{C.34}$$

$$A^{BK_1(1400)}(q^2) = \cos(\theta_{K_1})\frac{m_B+m_{K_1(1400)}}{m_B+m_{K_{1A}}}A^{K_{1A}}(q^2)$$
$$-\sin(\theta_{K_1})\frac{m_B+m_{K_1(1400)}}{m_B+m_{K_{1B}}}A^{K_{1B}}(q^2), \tag{C.35}$$

$$V_2^{BK_1(1270)}(q^2) = \sin(\theta_{K_1})\frac{m_B+m_{K_1(1270)}}{m_B+m_{K_{1A}}}V_2^{K_{1A}}(q^2)$$
$$+\cos(\theta_{K_1})\frac{m_B+m_{K_1(1270)}}{m_B+m_{K_{1B}}}V_2^{K_{1B}}(q^2), \tag{C.36}$$

Table C5. Form-factors for $B \to K_{1A}, K_{1B}$ transitions are fitted to the three-parameter form in (C.40), see [93].

F	$F(0)$	a	b	F	$F(0)$	a	b
$V_1^{BK_{1A}}$	0.34	0.635	0.211	$V_1^{BK_{1B}}$	−0.29	0.729	0.074
$V_2^{BK_{1A}}$	0.41	1.51	1.18	$V_2^{BK_{1B}}$	−0.17	0.919	0.855
$A^{BK_{1A}}$	0.45	1.60	0.974	$A^{BK_{1B}}$	−0.37	1.72	0.912

$$V_2^{BK_1(1400)}(q^2) = \cos(\theta_{K_1})\frac{m_B + m_{K_1(1400)}}{m_B + m_{K_{1A}}} V_2^{K_{1A}}(q^2) - \sin(\theta_{K_1})\frac{m_B + m_{K_1(1400)}}{m_B + m_{K_{1B}}} V_2^{K_{1B}}(q^2), \tag{C.37}$$

$$V_1^{BK_1(1270)}(q^2) = \sin(\theta_{K_1})\frac{m_B + m_{K_{1A}}}{m_B + m_{K_1(1270)}} V_1^{K_{1A}}(q^2) + \cos(\theta_{K_1})\frac{m_B + m_{K_{1B}}}{m_B + m_{K_1(1270)}} V_1^{K_{1B}}(q^2), \tag{C.38}$$

$$V_1^{BK_1(1400)}(q^2) = \cos(\theta_{K_1})\frac{m_B + m_{K_{1A}}}{m_B + m_{K_1(1400)}} V_1^{K_{1A}}(q^2) - \sin(\theta_{K_1})\frac{m_B + m_{K_{1B}}}{m_B + m_{K_1(1400)}} V_1^{K_{1B}}(q^2), \tag{C.39}$$

where we take $\theta_{K_1} = -34^\circ$, $m_{K_{1A}} = 1.31\,\text{GeV}$, $m_{K_{1B}} = 1.34\,\text{GeV}$ and the momentum dependence of all form-factors is parameterized as

$$F(q^2) = \frac{F(0)}{1 - a\frac{q^2}{m_B^2} + b\left(\frac{q^2}{m_B^2}\right)^2}. \tag{C.40}$$

The values of all relevant parameters are given in table C5.

C.4. Tensor final meson state

Let us consider here the production of the CS boson in the decays of B mesons into tensor state $K_2^*(1430)$. For the tensor meson, $h' = T$, the expansions of the matrix elements are similar to (C.10) and (C.11), see [94, 95],

$$\langle T(p')|\bar{Q}_i\gamma^\mu\gamma_5 Q_j|h(p)\rangle = (M_h + M_T)\epsilon_T^{\mu *,s}(p')A_{T1}(q^2) - (\epsilon_T^{*,s}(p')\cdot q) \times (p+p')^\mu \frac{A_{T2}(q^2)}{M_h + M_T} - 2M_T\frac{\epsilon_T^{*,s}(p')\cdot q}{q^2}q^\mu(A_{T3}(q^2) - A_{T0}(q^2)), \tag{C.41}$$

$$\langle T(p')|\bar{Q}_i\gamma^\mu Q_j|h(p)\rangle = \frac{2T(q^2)}{M_h + M_T}\mathrm{i}\epsilon^{\mu\nu\rho\sigma}\epsilon_{T,\nu}^{*,s}(p')p_\rho p'_\sigma, \tag{C.42}$$

with the same relation between A_{Ti} as for A_i in the case of vector mesons (C.12). So, the amplitude of the h meson decay into a tensor T meson and the CS boson has form like (C.13):

$$\begin{aligned} M_{h\to TX}(s,\lambda_X) &= \Theta_{1W} C_{mn} \langle T(p',s)|\bar{d}_n \gamma^\mu \hat{P}_L d_m|h(p)\rangle \epsilon^{*\lambda_X}_{X,\mu} \\ &= -\Theta_{1W}\frac{C_{mn}}{2}\left[-\frac{2T(q^2)}{M_h+M_T}\mathrm{i}\epsilon^{\mu\nu\rho\sigma}\epsilon^{\lambda_X *}_{X,\mu}\epsilon^{s*}_{T,\nu}p_\rho p'_\sigma \right. \\ &\quad + (M_h+M_T)(\epsilon^{s*}_T\cdot\epsilon^{\lambda_X *}_X)A_{1T}(q^2) - (\epsilon^{s*}_T\cdot q)(\epsilon^{\lambda_X *}_X\cdot(p+p'))\\ &\quad \left.\times\frac{A_{2T}(q^2)}{M_h+M_T} - 2M_T\frac{\epsilon^{s*}_T\cdot q}{q^2}(\epsilon^{\lambda_X *}_X\cdot q)(A_{3T}(q^2)-A_{0T}(q^2))\right], \end{aligned} \tag{C.43}$$

where $\epsilon^{\lambda_X *}_X$ corresponds to the CS boson polarization, $s=\pm2,\pm1,0$ are the polarization states of the tensor meson and $\epsilon^s_{T\mu}(p')$ is a vector defined by

$$\epsilon^s_{T\mu}(p') \equiv \frac{1}{M_h}\epsilon^s_{\mu\nu}(p')p^\nu, \tag{C.44}$$

where $\epsilon^s_{\mu\nu}$ is the polarization tensor of T meson satisfying conditions $p_\mu\epsilon^{\mu\nu,s}(p)=0$ and $\epsilon^{\mu\nu,s} = \epsilon^{\nu\mu,s}$, $\epsilon^{\mu,s}_\mu = 0$. Tensor $\epsilon^s_{\mu\nu}$ can be constructed with the help of a spin-1 polarization vectors:

$$\begin{aligned} &\epsilon^{(\pm2)}_{\mu\nu} = \epsilon^{(\pm)}_\mu\epsilon^{(\pm)}_\nu, \qquad \epsilon^{(\pm1)}_{\mu\nu} = \frac{1}{\sqrt{2}}[\epsilon^{(\pm)}_\mu\epsilon^{(0)}_\nu + \epsilon^{(\pm)}_\nu\epsilon^{(0)}_\mu], \\ &\epsilon^{(0)}_{\mu\nu} = \frac{1}{\sqrt{6}}[\epsilon^{(+)}_\mu\epsilon^{(-)}_\nu + \epsilon^{(+)}_\nu\epsilon^{(-)}_\mu] + \sqrt{\frac{2}{3}}\epsilon^{(0)}_\mu\epsilon^{(0)}_\nu. \end{aligned} \tag{C.45}$$

In the case of the rest frame of an h meson we have $p=(M_h,0)$ and relations (31). We can guide the CS boson to move along Z-axis and the tensor meson to move in the opposite direction. In this case we can choose spin-1 polarization vectors for the tensor meson as

$$\epsilon^{(0)}_\mu = \frac{1}{M_T}(|\vec{k}|,0,0,-E_T), \qquad \epsilon^{(\pm)}_\mu = \frac{1}{\sqrt{2}}(0,1,\mp\mathrm{i},0), \tag{C.46}$$

then we get

$$\epsilon^{\pm2}_{T\mu} = 0, \qquad \epsilon^{\pm1}_{T\mu} = \frac{|\vec{k}|}{\sqrt{2}M_T}\epsilon^{(\pm)}_\mu, \qquad \epsilon^0_{T\mu} = \sqrt{\frac{2}{3}}\frac{|\vec{k}|}{M_T}\epsilon^{(0)}_\mu, \tag{C.47}$$

where module $|\vec{k}|$ is defined by (26).

So, the amplitude of the reaction is zero for $s=\pm2$. Using relations (C.15), (C.17) and (C.47) we get

$$M_{h\to TX}(+,-) = -\Theta_{1W}\frac{C_{mn}}{2}\frac{|\vec{k}|}{\sqrt{2}M_T}\left[\frac{2M_h|\vec{k}|}{M_h+M_T}T(q^2) - (M_h+M_T)A_{1T}(q^2)\right], \tag{C.48}$$

$$M_{h\to TX}(-,+) = \Theta_{1W}\frac{C_{mn}}{2}\frac{|\vec{k}|}{\sqrt{2}M_T}\left[\frac{2M_h|\vec{k}|}{M_h+M_T}T(q^2) + (M_h+M_T)A_{1T}(q^2)\right]. \tag{C.49}$$

Table C6. Values of the form-factors' parameters for transition $B \to K_2^*(1430)$, [94].

F	$F(0)$	a	b	F	$F(0)$	a	b
$T^{BK_2^*}$	0.29	2.17	2.22	$A_0^{BK_2^*}$	0.23	1.23	0.74
$A_1^{BK_2^*}$	0.22	1.42	0.50	$A_2^{BK_2^*}$	0.21	1.96	1.79

$$M_{h\to TX}(0,0) = -\Theta_{1W}\frac{C_{mn}}{2}\sqrt{\frac{2}{3}}\frac{|\vec{k}|}{M_T}\left[(M_h+M_T)\frac{\vec{k}^2+E_XE_T}{M_XM_T}A_{1T}(q^2) - 2\frac{\vec{k}^2M_h^2}{M_TM_X}\frac{A_{2T}(q^2)}{M_h+M_T}\right], \tag{C.50}$$

and

$$\sum_{\text{polarizations}}|M_{h\to TX}|^2 = \Theta_{1W}^2\frac{|C_{mn}|^2}{4}\frac{\vec{k}^2}{M_T^2}\left[\frac{1}{2}\left(\frac{8M_h^2\vec{k}^2}{(M_h+M_T)^2}T^2(q^2) + 2(M_h+M_T)^2A_{1T}^2(q^2)\right) + \frac{2}{3}\left((M_h+M_T)\frac{\vec{k}^2+E_XE_T}{M_XM_T}A_{1T}\times(q^2) - \frac{2M_h^2\vec{k}^2}{M_TM_X(M_h+M_T)}A_{2T}(q^2)\right)^2\right]. \tag{C.51}$$

The parametrization of the form-factors T and A_{1T}, A_{2T} is taken from [94, 95]

$$F_0^{XT}(q^2) = \frac{F_0^{hT}}{1 - a_T\frac{q^2}{M_h^2} + b_T\left(\frac{q^2}{M_h^2}\right)^2}, \tag{C.52}$$

where the corresponding parameters are given in table C6.

ORCID iDs

Yuliia Borysenkova https://orcid.org/0000-0003-1040-2815
Pavlo Kashko https://orcid.org/0000-0002-7050-7152
Mariia Tsarenkova https://orcid.org/0000-0002-8645-7233
Kyrylo Bondarenko https://orcid.org/0000-0001-6983-7667
Volodymyr Gorkavenko https://orcid.org/0000-0002-9468-5105

References

[1] Altarelli G 2013 (arXiv:1303.2842)
[2] Steigman G 1976 *Annu. Rev. Astron. Astrophys.* **14** 339–72
[3] Riotto A and Trodden M 1999 *Annu. Rev. Nucl. Part. Sci.* **49** 35–75
[4] Canetti L, Drewes M and Shaposhnikov M 2012 *New J. Phys.* **14** 095012

[5] Peebles P J E 2015 *Proc. Natl Acad. Sci.* **112** 2246
[6] Lukovic V, Cabella P and Vittorio N 2014 *Int. J. Mod. Phys.* A **29** 1443001
[7] Bertone G and Hooper D 2018 *Rev. Mod. Phys.* **90** 045002
[8] Bilenky S M and Petcov S T 1987 *Rev. Mod. Phys.* **59** 671
Bilenky S M and Petcov S T 1989 *Rev. Mod. Phys.* **61** 169 (erratum)
Bilenky S M and Petcov S T 1988 *Rev. Mod. Phys.* **60** 575 (erratum)
[9] Strumia A and Vissani F 2006 (arXiv:hep-ph/0606054)
[10] de Salas P F, Forero D V, Ternes C A, Tórtola M and Valle J W F 2018 *Phys. Lett.* B **782** 633–40
[11] Czarnecki A and Krause B 1997 *Phys. Rev. Lett.* **78** 4339–42
[12] Kim J E and Carosi G 2010 *Rev. Mod. Phys.* **82** 557–601
Kim J E and Carosi G 2019 *Rev. Mod. Phys.* **91** 049902 (erratum)
[13] Schmaltz M and Tucker-Smith D 2005 *Annu. Rev. Nucl. Part. Sci.* **55** 229–70
[14] Wells J D 2017 *Synthese* **194** 477–90
[15] Degrassi G, Di Vita S, Elias-Miro J, Espinosa J R, Giudice G F, Isidori G and Strumia A 2012 *J. High Energy Phys.* JHEP08(2012)098
[16] Bezrukov F and Shaposhnikov M 2015 *J. Exp. Theor. Phys.* **120** 335–43
[17] Padmanabhan T 2003 *Phys. Rep.* **380** 235–320
[18] Rubakov V A and Gorbunov D S 2017 *Introduction to the Theory of the Early Universe: Hot Big Bang Theory* (Singapore: World Scientific)
[19] Golling T *et al* 2016 (arXiv:1606.00947)
[20] Abada A *et al* (FCC) 2019 *Eur. Phys. J.* C **79** 474
[21] Beacham J *et al* 2020 *J. Phys. G: Nucl. Part. Phys.* **47** 010501
[22] Lanfranchi G, Pospelov M and Schuster P 2021 *Annu. Rev. Nucl. Part. Sci.* **71** 279–313
[23] Curtin D *et al* 2019 *Rep. Prog. Phys.* **82** 116201 (arXiv:1806.07396)
[24] Cerci S *et al* 2021 (arXiv:2201.00019)
[25] Ariga A *et al* (FASER) 2018 (arXiv:1811.10243)
[26] Ariga A *et al* (FASER) 2019 *Phys. Rev.* D **99** 095011
[27] Anelli M *et al* (SHiP) 2015 (arXiv:1504.04956)
[28] Alekhin S *et al* 2016 *Rep. Prog. Phys.* **79** 124201
[29] Mermod P (SHiP) 2017 *PoS NuFact2017* p 139 (arXiv:1712.01768)
[30] Gil G *et al* (NA62) 2018 *Phys. Lett.* B **778** 137–45 (arXiv:1712.00297)
[31] Drewes M, Hajer J, Klaric J and Lanfranchi G 2018 *J. High Energy Phys.* JHEP07(2018)105
[32] Acciarri R *et al* (DUNE) 2015 (arXiv:1512.06148)
[33] Abi B *et al* (DUNE) 2021 *Eur. Phys. J.* C **81** 322 (arXiv:2008.12769)
[34] Patt B and Wilczek F 2006 arXiv:hep-ph/0605188
[35] Bezrukov F and Gorbunov D 2010 *J. High Energy Phys.* JHEP05(2010)010
[36] Boiarska I, Bondarenko K, Boyarsky A, Gorkavenko V, Ovchynnikov M and Sokolenko A 2019 *J. High Energy Phys.* JHEP11(2019)162
[37] Peccei R D and Quinn H R 1977 *Phys. Rev. Lett.* **38** 1440–3
[38] Weinberg S 1978 *Phys. Rev. Lett.* **40** 223–6
[39] Wilczek F 1978 *Phys. Rev. Lett.* **40** 279–82
[40] Choi K, Im S H and Shin C S 2020 (arXiv:2012.05029)
[41] Okun L B 1982 *Sov. Phys. JETP* **56** 502
[42] Holdom B 1986 *Phys. Lett.* B **166** 196–8
[43] Langacker P 2009 *Rev. Mod. Phys.* **81** 1199–228
[44] Asaka T and Shaposhnikov M 2005 *Phys. Lett.* B **620** 17–26
[45] Asaka T, Blanchet S and Shaposhnikov M 2005 *Phys. Lett.* B **631** 151–6
[46] Bondarenko K, Boyarsky A, Gorbunov D and Ruchayskiy O 2018 *J. High Energy Phys.* JHEP11(2018)032
[47] Boyarsky A, Drewes M, Lasserre T, Mertens S and Ruchayskiy O 2019 *Prog. Part. Nucl. Phys.* **104** 1–45
[48] Antoniadis I, Boyarsky A, Espahbodi S, Ruchayskiy O and Wells J D 2010 *Nucl. Phys.* B **824** 296–313
[49] D'Hoker E and Farhi E 1984 *Nucl. Phys.* B **248** 59–76
[50] D'Hoker E and Farhi E 1984 *Nucl. Phys.* B **248** 77
[51] Antoniadis I, Kiritsis E and Tomaras T N 2000 *Phys. Lett.* B **486** 186–93
[52] Corianò C, Irges N and Kiritsis E 2006 *Nucl. Phys.* B **746** 77–135
[53] Irges N, Coriano C and Morelli S 2008 *Nucl. Phys.* B **789** 133–74

[54] Anastasopoulos P, Bianchi M, Dudas E and Kiritsis E 2006 *J. High Energy Phys.* JHEP11(2006)057
[55] Anastasopoulos P, Fucito F, Lionetto A, Pradisi G, Racioppi A and Stanev Y S 2008 *Phys. Rev.* D **78** 085014
[56] Harvey J A, Hill C T and Hill R J 2008 *Phys. Rev.* D **77** 085017
[57] Dudas E, Mambrini Y, Pokorski S and Romagnoni A 2009 *J. High Energy Phys.* JHEP08(2009)014
[58] Kumar J, Rajaraman A and Wells J D 2008 *Phys. Rev.* D **77** 066011
[59] Dror J A, Lasenby R and Pospelov M 2017 *Phys. Rev. Lett.* **119** 141803
[60] Dror J A, Lasenby R and Pospelov M 2017 *Phys. Rev.* D **96** 075036
[61] Boyarsky A, Ruchayskiy O and Shaposhnikov M 2005 *Phys. Rev.* D **72** 085011
[62] Boyarsky A, Ruchayskiy O and Shaposhnikov M 2005 *Phys. Lett.* B **626** 184–94
[63] Antoniadis I, Boyarsky A and Ruchayskiy O 2006 (arXiv:hep-ph/0606306)
[64] Antoniadis I, Boyarsky A and Ruchayskiy O 2008 *Nucl. Phys.* B **793** 246–59
[65] Williams E R, Faller J E and Hill H A 1971 *Phys. Rev. Lett.* **26** 721–4
[66] Tu L-C, Luo J and Gillies G T 2005 *Rep. Prog. Phys.* **68** 77–130
[67] Davidson S, Campbell B and Bailey D 1991 *Phys. Rev.* D **43** 2314–21
[68] Davidson S, Hannestad S and Raffelt G 2000 *J. High Energy Phys.* JHEP05(2000)003
[69] Marinelli M and Morpurgo G 1984 *Phys. Lett.* B **137** 439–42
[70] Zyla P A *et al* (Particle Data Group) 2020 *Prog. Theor. Exp. Phys.* **2020** 083C01
[71] Hewett J and Rizzo T G 1989 *Phys. Rep.* **183** 193
[72] Gunion J F, Haber H E, Kane G L and Dawson S 1990 *The Higgs Hunter's Guide* 1st edn (Boca Raton: CRC Press)
[73] Leutwyler H and Shifman M A 1990 *Nucl. Phys.* B **343** 369–97
[74] Källén G 1964 *Elementary Particle Physics* (Reading, MA: Addison-Wesley)
[75] Bogolyubov N N and Shirkov D V 1983 *Quantum Fields* (San Francisco: Benjamin Cummings)
[76] Ball P and Zwicky R 2005 *Phys. Rev.* D **71** 014015
[77] Yushchenko O P *et al* 2004 *Phys. Lett.* B **589** 111–7 (arXiv:hep-ex/0404030)
[78] Yushchenko O P *et al* (OKA) 2018 *JETP Lett.* **107** 139–42 (arXiv:1708.09587)
[79] Batley J R *et al* (NA48/2) 2018 *J. High Energy Phys.* **10** 150 (arXiv:1808.09041)
[80] Lai A *et al* (NA48) 2004 *Phys. Lett.* B **604** 1–10 (arXiv:hep-ex/0410065)
[81] Alexopoulos T *et al* (KTeV) 2004 *Phys. Rev.* D **70** 092007
[82] Ambrosino F *et al* (KLOE) 2006 *Phys. Lett.* B **636** 166–72
[83] Ambrosino F *et al* (KLOE) 2006 *Phys. Lett.* B **636** 173–82
[84] Sun Y J, Li Z H and Huang T 2011 *Phys. Rev.* D **83** 025024
[85] Daldrop J, Alexandrou C, Brida M D, Gravina M, Scorzato L, Urbach C and Wagner M (ETM) 2012 *PoS LATTICE2012* p 161 (arXiv:1211.5002)
[86] Cheng H-Y, Chua C-K, Yang K-C and Zhang Z-Q 2013 *Phys. Rev.* D **87** 114001
[87] Issadykov A, Ivanov M A and Sakhiyev S K 2015 *Phys. Rev.* D **91** 074007
[88] Ball P and Zwicky R 2005 *Phys. Rev.* D **71** 014029
[89] Ebert D, Faustov R N and Galkin V O 1997 *Phys. Rev.* D **56** 312–20
[90] Hatanaka H and Yang K C 2009 *Phys. Rev.* D **79** 114008
[91] Lu C D and Wang W 2012 *Phys. Rev.* D **85** 034014
[92] Bashiry V 2009 *J. High Energy Phys.* JHEP06(2009)062
[93] Hatanaka H and Yang K C 2008 *Phys. Rev.* D **78** 074007
[94] Cheng H Y and Yang K C 2011 *Phys. Rev.* D **83** 034001
[95] Li R H, Lu C D and Wang W 2011 *Phys. Rev.* D **83** 034034

1.3. Обмеження на юкавівські параметри в нейтринній модифікації СМ

Eur. Phys. J. C
DOI 10.1140/epjc/s10052-010-1488-y

THE EUROPEAN PHYSICAL JOURNAL C

Regular Article - Theoretical Physics

Some constraints on the Yukawa parameters in the neutrino modification of the Standard Model (*νMSM*) and CP-violation

Volodymyr M. Gorkavenko[a], **Stanislav I. Vilchynskiy**[b]

Department of Physics, Taras Shevchenko National University of Kyiv, 64 Volodymyrs'ka St., Kyiv 01601, Ukraine

Received: 27 April 2010 / Revised: 19 July 2010

Abstract The equations connecting elements of the Yukawa matrix to elements of the active neutrino mass matrix in the *νMSM* theory (an extension of the Standard Model by a singlet of three right-handed neutrinos) was analyzed, and explicit relations for the ratio of the Yukawa matrix elements and elements of the active neutrino mass matrix were obtained. This relation can be used for getting more accurate constraints on the model parameters. Particularly, with the help of the obtained results we investigated CP-violating phase in the *νMSM* theory. We demonstrate that even in the case when elements of the active neutrino mass matrix are real the baryon asymmetry can be generated also.

1 Introduction

The Standard Model (SM) [1–3] of the electroweak and the strong interactions is one of the greatest successes of the physics. It describes correctly the processes with participation of elementary particles to energy scale ∼100 GeV and for individual processes to several TeV. It predicted a number of particles, the overwhelming majority of which has been observed. However, it is well known that the SM does not account for several phenomena in particle physics, astrophysics and cosmology. Namely: the SM does not provide the dark matter candidate; the SM does not explain neutrino oscillations and the baryon asymmetry of the Universe; the SM cannot solve the strong CP problem in particle physics, the primordial perturbations problem and the horizon problem in cosmology, etc.

The solutions of the above mentioned problems of the SM need some new physics between the electroweak and the Planck scales. An important challenge for the theoretical physics is to see if it is possible to solve them using only the extensions of the SM below the electroweak scale [4].

The SM is the renormalized theory which is based on $SU(3) \times SU(2) \times U(1)$ gauge group and contains three generations fermions. The left-handed components of fermions form the weak isospin doublets relative to the $SU(2)$ group, and the right-handed components of all fermions except neutrinos are singlets of the weak isospin. The absence of the right-handed neutrino fields in the SM is due to the fact that neutrinos are considered as massless particles. However, the recent experimental discovery of the neutrino oscillation phenomenon [5, 6] (transitions between neutrinos of different flavors) is a proof that neutrinos have a nonzero mass. The current data show that the mass squared differences of active neutrino $\Delta m^2_{\text{atm}} = (2.5 \pm 0.2) \times 10^{-3}$ eV^2 and $\Delta m^2_{\text{sol}} = (8.0 \pm 0.3) \times 10^{-5}$ eV^2.

One of the simplest and the most promising ways of modification of the SM is an extension of the fermionic sector by adding the singlet of right-handed neutrinos, which do not take part in the SM gauge interactions.[1] The consequence of the existence of two distinct scales Δm^2_{atm} and Δm^2_{sol} is that number of right-handed neutrinos must be greater than or equal to two. The introduction of only two right-handed neutrinos leads to the emergence of 11 new parameters in the modified theory, which may be able to explain the available experimental data on the oscillations of active neutrinos. In this case the model predicts the existence of two massive active neutrinos and one massless neutrino, which does not contradict the available experimental data. However, the extension of the SM by only two right-handed neutrinos does not solve the remaining problems of the SM, in particular, does not explain the nature of the dark matter [7, 8].

It turns out that introduction of three right-handed neutrinos with masses smaller than electroweak scale can provide explanations of the experimental data in particle physics, astrophysics, and cosmology. This model (called *νMSM*)

[a] e-mail: gorka@univ.kiev.ua
[b] e-mail: sivil@univ.kiev.ua

[1] This is why these neutrinos are called sterile neutrinos. The left-handed neutrinos of the SM are called active neutrinos.

Published online: 16 November 2010

[7, 9] is the simplest extension[2] of the SM, which can explain simultaneously some of phenomena of the new physics without a new energy scale. Moreover, the parameters of the model (it contains 18 new parameters—three Majorana neutrino masses, three Dirac neutrino masses, six mixing angles and six CP-violating phases) can be chosen in such a way that the physics above the electroweak scale is not altered, while the following three phenomena beyond the SM are explained.

(a) All data on the neutrino oscillations can be fitted. The smallness of the neutrino masses is explained by the Type I of the "see-saw" mechanism [10].
(b) Parameters of two heavier neutrinos can be chosen to allow baryogenesis. The masses of these particles can still be chosen below the electroweak scale.
(c) The lightest sterile neutrino can be intensively produced in the early universe and have cosmologically long lifetime. So, it might be a viable dark matter candidate.

The topical problem is the determination of the parameters of the *νMSM*. One of the purpose of this work is to obtain restrictions on the values of the Yukawa's matrix elements from the *νMSM* equations that connect elements of the Yukawa's matrix with elements of the active neutrinos mass matrix.

Since neutrinos in the SM are massless particles, the only source of CP-symmetry violation in weak interactions is a single complex element of the Kabbibo–Kobayashi–Maskawa matrix, which describes the mixing between the quarks of different generations. Due to the existence of neutrinos with nonzero masses it becomes possible to mix different generations of neutrinos. Moreover, in the *νMSM* the mix between active and sterile neutrino is possible too. So, there is another possible source of generation of CP-symmetry violation and the *νMSM* theory has a much richer structure than the SM.

Another purpose of this work is to study CP violation in the frame of the *νMSM* theory. As was shown in [7], effect of the CP violation on the baryogenesis in the *νMSM* theory can be expressed through the CP-violating factor δ_{CP}. This factor includes the above mentioned CP-violating phases. The baryon asymmetry is proportional to δ_{CP}. An applicable expression for δ_{CP} was obtained in [14]. Investigation of this expression is the second goal of the work.

The paper is organized as follows. The first section contains basic relations and some results obtained in the *νMSM*. In the second section of the paper the *νMSM* equations are analyzed in detail, and the explicit relations for ratio of the Yukawa matrix elements through the elements of active neutrino mass matrix are obtained. Using results of the second section the CP-violating factor is analyzed in the third section.

2 The basic relations and some results of the *νMSM*

In the *νMSM* [7, 9] the following terms are added to the Lagrangian of the SM (without taking into account the kinetic terms):

$$\begin{aligned}\mathcal{L}^{\mathrm{ad}} &= -F_{\alpha I}\bar{L}_{\alpha}\tilde{\Phi}\nu_{IR} - \frac{M_{IJ}}{2}\bar{\nu}^{c}_{IR}\nu_{JR} + h.c.\\ &= -\frac{h+v}{\sqrt{2}}\bar{\nu}_{\alpha L}F_{\alpha I}\nu_{IR} - \bar{\nu}^{c}_{IR}\frac{M_{IJ}}{2}\nu_{JR} + h.c.,\end{aligned} \tag{2.1}$$

where index $\alpha = e, \mu, \tau$ corresponds to the active neutrino flavors, indices I, J run from 1 to 3, L_{α} is for the lepton doublet, ν_{IR} the field functions of the sterile right-handed neutrinos, the superscript "c" means charge conjugation, $F_{\alpha I}$ is for the new (neutrino) matrix of the Yukawa constants, M_{IJ} for the Majorana mass matrix of the right-handed neutrinos, Φ for the field of the Higgs doublet in the unitary gauge, $\tilde{\Phi} = i\sigma_2\Phi^*$, h is for the neutral Higgs field and the parameter v determines minimum of the Higgs field potential ($v \cong 247$ GeV).

In the SM the mass of fermions are generated due to interactions of fermions fields with scalar Higgs field. The structure of the SM is such that after spontaneous symmetry breaking the neutrino remains to be a massless particle.[3] The SM does not contain Dirac mass term $\sim\bar{\nu}_L \cdot \nu_R$ due to the absence in theory the right-handed neutrinos, and the Majorana mass term $\sim\bar{\nu}^{c}_L \cdot \nu_L$ is forbidden by $SU(2)_L$ invariance. The assumption about the existence of the right-handed neutrinos leads to the appearance of the Dirac as well as Majorana mass terms in the Lagrangian, which in the general case have the form (see, e.g., [15])

$$\mathcal{L}^{\mathrm{DM}} = -\left(\overline{(N_L)^c}\,\frac{M^{\mathrm{DM}}}{2}\,N_L + h.c.\right), \tag{2.2}$$

where

$$\begin{aligned}&N_L = \begin{pmatrix}\nu_L\\ \nu^c_R\end{pmatrix}; \qquad N^c_L = \begin{pmatrix}\nu^c_L\\ \nu_R\end{pmatrix};\\ &M^{\mathrm{DM}} = \begin{pmatrix}M_L & M_D^T\\ M_D & M_R\end{pmatrix}.\end{aligned} \tag{2.3}$$

[2] Various possibilities to incorporate neutrino masses in the theory are discussed, e.g., in [11, 12].

[3] There is a possibility to introduce the mass of neutrino after the electroweak symmetry breaking with help of the effective dimension 5 non-renormalizable operator $\frac{\lambda_{ij}}{\Lambda}(L_i\Phi)^T(L_j\Phi)$, $i, j = e, \mu, \tau$, where L is the $SU(2)$ lepton doublets, Λ is the cutoff high-energy scale [13]. This operator breaks lepton number and can be obtained from (2.1) by integrating out heavy right-handed neutrinos.

Comparing mass terms in (2.1) with (2.2) one can see

$$M_L = 0, \qquad M_D = F^+ \frac{v}{\sqrt{2}}, \qquad M_R = M^*, \tag{2.4}$$

where M, F are square matrix of the third order with elements $F_{\alpha I}$ and M_{IJ} (2.1).

As it was shown in [7, 9], the parameters of the νMSM can be chosen in such a way to simultaneously explain the neutrino oscillations, the baryon asymmetry and to determine the nature of the dark matter. This requires the existence of two right-handed neutrinos with large practically the same masses ($\gtrsim$100 MeV) and one right-handed neutrino with a relatively small mass.[4]

In zero approximation the extended Lagrangian $\mathcal{L}_{\nu MSM}$ is assumed to be invariant under $U(1)_e \times U(1)_\mu \times U(1)_\tau$ transformations, that provides preservation of the e, μ, τ lepton numbers separately as in the SM. In addition, it is assumed that two heavy sterile neutrinos interact with the active neutrinos, but the third (lightest) sterile neutrino does not interact.[5] This assumption can be realized by following matrix $M^{\rm DM}$ [16]:

$$M_L^{(0)} = 0; \qquad M_R^{(0)} = \begin{pmatrix} 0 & 0 & 0 \\ 0 & 0 & M \\ 0 & M & 0 \end{pmatrix},$$
$$M_D^{(0)+} = \frac{v}{\sqrt{2}} \begin{pmatrix} 0 & h_{12} & 0 \\ 0 & h_{22} & 0 \\ 0 & h_{32} & 0 \end{pmatrix}, \tag{2.5}$$

where M is real and h_{12}, h_{22}, h_{32} are complex quantities.

In this approximation we have two massive right-handed neutrinos with equal mass M, the third right-handed neutrino is massless, and all active neutrinos have a zero mass, which is in contradiction with observable data. To adjust it next small terms are added to the matrix M_R and M_D [16]:

$$M_L^{(1)} = 0; \qquad M_R^{(1)} = \begin{pmatrix} m_{11} e^{-i\alpha} & m_{12} & m_{13} \\ m_{12} & m_{22} e^{-i\beta} & 0 \\ m_{13} & 0 & m_{33} e^{-i\gamma} \end{pmatrix};$$
$$M_D^{(1)+} = \frac{v}{\sqrt{2}} \begin{pmatrix} h_{11} & 0 & h_{13} \\ h_{21} & 0 & h_{23} \\ h_{31} & 0 & h_{33} \end{pmatrix}, \tag{2.6}$$

where m_{ij} ($m_{ij} \ll M$) are real, but elements of first and second columns ($|h_{i1}| \ll |h_{k2}|$, $|h_{i3}| \ll |h_{k2}|$) are in general complex elements.

These corrections break $U(1)_e \times U(1)_\mu \times U(1)_\tau$-symmetry, lead to the appearance of a small mass of the third right-handed neutrino, and remove the mass degeneracy for two heavy right-handed neutrinos. It ensures the appearance of extra small masses of the active neutrinos and nonzero mixing angles among them.

As is well known [15], the mass part of the Lagrangian (2.2) can be diagonalized by the transition from the basis of the gauge functions N_L to the basis of the mass functions n_L using an unitary matrix V, namely $N_L = V n_L$, so

$$\bar{N}_L = \bar{n}_L V^+; \qquad N_L^c = (V^+)^T n_L^c; \qquad \overline{N}_L^c = \overline{(n_L)^c} V^T, \tag{2.7}$$

where V (6×6) is a product of two matrices $V = WU$.

The W matrix is introduced for the block diagonalization of the $M^{\rm DM}$ matrix [17]. The explicit form of the W matrix can be approximately found in the "see-saw" approach due to the smallness of matrix $\varepsilon = M_R^{-1} M_D \ll 1$:

$$W = \begin{pmatrix} 1 - \frac{1}{2}\varepsilon^+\varepsilon & \varepsilon^+ \\ -\varepsilon & 1 - \frac{1}{2}\varepsilon\varepsilon^+ \end{pmatrix}. \tag{2.8}$$

In this approximation the result of the block diagonalization has the form

$$W^T M^{\rm DM} W = \begin{pmatrix} -M_D^T M_R^{-1} M_D & 0 \\ 0 & M_R \end{pmatrix}$$
$$= \begin{pmatrix} M_{\rm light} & 0 \\ 0 & M_{\rm heavy} \end{pmatrix}, \tag{2.9}$$

where matrices $M_{\rm light}$ and $M_{\rm heavy}$ are the mass matrices of the active and the sterile neutrinos correspondingly. Note that the elements of the matrix $M_{\rm light}$ and accordingly the masses of the active neutrinos are completely determined by elements of the matrices M_D and M_R.

The U matrix has the form

$$U = \begin{pmatrix} U_1 & 0 \\ 0 & U_2 \end{pmatrix}, \tag{2.10}$$

where matrices $U_{(1,2)}$ (each of them are (3×3) matrix) are chosen for the diagonalization of block matrix $W^T M^{\rm DM} W$

$$m = {\rm diag}(m_1, m_2, \ldots, m_6) = V^T M V$$
$$= U^T W^T M W U = \begin{pmatrix} U_1^T M_{\rm light} U_1 & 0 \\ 0 & U_2^T M_{\rm heavy} U_2 \end{pmatrix}. \tag{2.11}$$

There is a standard parametrization [5] for $U_{(1,2)}$:

$$U_{(1,2)} = \begin{pmatrix} c_{12}c_{13} & c_{13}s_{12} & s_{13}e^{-i\delta} \\ -s_{12}c_{23} - c_{12}s_{23}s_{13}e^{i\delta} & c_{12}c_{23} - s_{12}s_{23}s_{13}e^{i\delta} & s_{23}c_{13} \\ s_{12}s_{23} - c_{12}c_{23}s_{13}e^{i\delta} & -c_{12}s_{23} - s_{12}c_{23}s_{13}e^{i\delta} & c_{23}c_{13} \end{pmatrix}$$
$$\times \begin{pmatrix} e^{i\alpha_1/2} & 0 & 0 \\ 0 & e^{i\alpha_2/2} & 0 \\ 0 & 0 & 1 \end{pmatrix}, \tag{2.12}$$

[4] For the time being the allowed region for the mass of the lightest sterile neutrino is $(1 \div 50)$ KeV [4].

[5] The lightest neutrino is the dark matter candidate in the νMSM, just because it does not have to interact with other particles of the SM.

where $c_{ij} = \cos\theta_{ij}$, $s_{ij} = \sin\theta_{ij}$, $\theta_{12}, \theta_{13}, \theta_{23}$ are the three mixing angles; δ is the Dirac phase, and α_1, α_2 are the Majorana phases. The angles θ_{ij} can be in the region $0 \le \theta_{ij} \le \pi/2$, phases $\delta, \alpha_1, \alpha_2$ vary from 0 to 2π. Each of the matrices $U_{(1)}$ and $U_{(2)}$ contains its own, independent angles and phases.

Thus, the determination of the masses of active and sterile neutrinos is reduced to the diagonalization of the matrix (2.9), where diagonalization can be carried out separately for the matrices M_{light} and M_{heavy}. Since the matrix M_{light} and M_{heavy} are not Hermitian, it is more appropriate to find eigenvalues of Hermitian matrices $M^{+}_{\text{light}} M_{\text{light}}$ and $M^{+}_{\text{heavy}} M_{\text{heavy}}$ by solving corresponding equations. The found eigenvalues are the square of eigenvalues of the matrices M_{light} and M_{heavy}.

In the approximation when the elements of the first column of the Yukawa matrix are neglected and $M \gg m_{ij}$, the mass of the lightest active neutrino is zero. The nondiagonal mass matrix of the active neutrinos has the form [16]

$$[M_{\text{light}}]_{\alpha\beta} = \eta(h_{\beta 3}h_{\alpha 2} + h_{\alpha 3}h_{\beta 2}), \quad \text{where } \eta = v^2/2M \tag{2.13}$$

and eigenvalues

$$m_{2,3} = \eta\big(F_2 F_3 \pm |h^{+}h|_{23}\big), \tag{2.14}$$

where $F_2^2 = [h^{+}h]_{22}$, $F_3^2 = [h^{+}h]_{33}$, $F_2 F_3 = M(m_2 + m_3)/v^2$.

On the other hand, the elements of the matrix M_{light} are defined by masses and mixing matrix $U_{(1)}$ of the active neutrinos [15]:

$$[M_{\text{light}}]_{\alpha\beta} = m_1 U^{*}_{(1)i1} U^{*}_{(1)j1} + m_2 U^{*}_{(1)i2} U^{*}_{(1)j2} + m_3 U^{*}_{(1)i3} U^{*}_{(1)j3}. \tag{2.15}$$

The elements of the mixing matrix $U_{(1)}$ are known (unfortunately with a considerable inaccuracy) from the neutrino oscillation experiments (see, e.g., [5, 6]). Parameters of the matrix $U_{(1)}$ (2.12) are presented in Table 1.

Table 1 Experimental constraints on the parameters of active neutrinos

Central value	99% confidence interval
$\lvert\Delta m^2_{12}\rvert = (8.0 \pm 0.3) \times 10^{-5}$ eV^2	(7.2–8.9) $\times 10^{-5}$ eV^2
$\lvert\Delta m^2_{23}\rvert = (2.5 \pm 0.2) \times 10^{-3}$ eV^2	(2.1–3.1) $\times 10^{-3}$ eV^2
$\tan^2\theta_{12} = 0.45 \pm 0.05$	$30^\circ < \theta_{12} < 38^\circ$
$\sin^2 2\theta_{23} = 1.02 \pm 0.04$	$36^\circ < \theta_{23} < 54^\circ$
$\sin^2 2\theta_{13} = 0 \pm 0.05$	$\theta_{13} < 10^\circ$

3 The ratio of the Yukawa matrix elements in the *νMSM*

The system of (2.13) connects elements of the second and the third columns of the Yukawa sterile neutrinos matrix with elements of the active neutrinos matrix and has infinite number of solutions. Indeed, the replacement of h_{i2} to zh_{i2} and h_{i3} to h_{i3}/z (z is an arbitrary complex number) does not change the system (2.13).

But the system of (2.13) has a good solutions for the ratio of the Yukawa matrix elements. Indeed, if we take h_{13}, h_{23}, and h_{33} from the equations for the diagonal elements of M_{light} and substitute it into equations for the off-diagonal elements of M_{light} we get

$$\begin{cases} M_{12} = \frac{1}{2}(M_{22}\frac{h_{12}}{h_{22}} + M_{11}\frac{h_{22}}{h_{12}}), \\ M_{13} = \frac{1}{2}(M_{33}\frac{h_{12}}{h_{32}} + M_{11}\frac{h_{32}}{h_{12}}), \\ M_{23} = \frac{1}{2}(M_{33}\frac{h_{22}}{h_{32}} + M_{22}\frac{h_{32}}{h_{22}}), \end{cases} \tag{3.1}$$

with the obvious solutions

$$\begin{cases} A_{12} = \frac{M_{12}}{M_{22}}(1 \pm \sqrt{1 - \frac{M_{11}M_{22}}{M_{12}{}^2}}), \\ A_{13} = \frac{M_{13}}{M_{33}}(1 \pm \sqrt{1 - \frac{M_{11}M_{33}}{M_{13}{}^2}}), \\ A_{23} = \frac{M_{23}}{M_{33}}(1 \pm \sqrt{1 - \frac{M_{22}M_{33}}{M_{23}{}^2}}), \end{cases} \tag{3.2}$$

for the ratio of the second column elements of the Yukawa matrix

$$A_{12} = h_{12}/h_{22}; \qquad A_{13} = h_{12}/h_{32}; \qquad A_{23} = h_{22}/h_{32}. \tag{3.3}$$

The ratio of the third column elements of the Yukawa matrix can be easily obtained from the equations for the diagonal elements of M_{light}:

$$\frac{h_{23}}{h_{13}} = A_{12}\frac{M_{22}}{M_{11}}; \qquad \frac{h_{33}}{h_{13}} = A_{13}\frac{M_{33}}{M_{11}}. \tag{3.4}$$

So, in the approximation when (2.13) is valid the ratio of the Yukawa matrix elements depends only on the active neutrino mass matrix.

Though formally there are eight different choices for the solutions, only four are independent. For example, if we fix the sign before the square roots in the expressions for A_{12} and A_{13} then A_{23} is unambiguously determined by the relation

$$A_{23} = A_{13}/A_{12}. \tag{3.5}$$

It should be emphasized that solutions (3.2) do not allow one to find elements of the Yukawa matrix but only its ratio:[6]

$$\frac{\{h_{12};h_{22};h_{32}\}}{F_2}=\frac{e^{i\cdot\arg(h_{12})}}{\sqrt{1+|A_{12}|^{-2}+|A_{13}|^{-2}}}\times\left\{1;A_{12}^{-1};A_{13}^{-1}\right\},\tag{3.6}$$

$$\frac{\{h_{13};h_{23};h_{33}\}}{F_3}=\frac{e^{i\cdot\arg(h_{13})}}{\sqrt{1+|A_{12}\frac{M_{22}}{M_{11}}|^2+|A_{13}\frac{M_{33}}{M_{11}}|^2}}\times\left\{1;A_{12}\frac{M_{22}}{M_{11}};A_{13}\frac{M_{33}}{M_{11}}\right\},\tag{3.7}$$

where phases of h_{12}, h_{13} are connected by condition

$$\arg(h_{12})+\arg(h_{13})=\arg(M_{11})\tag{3.8}$$

and $A_{12}, A_{13}, M_{11}, M_{22}, M_{33}$ are definitely expressed via parameters of the active neutrino mass matrix. Since the system of (2.13) is written in the approximation $m_1=0$, the phase α_1 is excluded from all expressions (see (2.12) and (2.15)). In this approximation only seven parameters of active neutrinos are used: two mass m_2, m_3; three mixing angles $\theta_{12}, \theta_{13}, \theta_{23}$; one Dirac δ and one Majorana α_2 CP-violating phases.

To know straight values of the Yukawa matrix elements we have to know in addition two arbitrary parameters[7] of Yukawa matrix, e.g., absolute value and phase of an arbitrary Yukawa matrix element or quantities ξ and ϵ from (4.3).

It can be shown that (for fixed values of the active neutrino parameters) there are only two choices[8] for placing of the signs in the expressions for A_{12}, A_{13}, A_{23} (3.2) which are not inconsistent with condition (3.5). These two variants are distinguished from each other by simultaneous replacement of the sign in front of square roots in the expressions for A_{12}, A_{13}, A_{23}. It can be shown that such replacement of the signs leads to interchanging and conjugating of the relation between elements of the second and the third columns of the Yukawa matrix, notably $h_{22}/h_{12}\leftrightarrow h_{23}^*/h_{13}^*$, $h_{32}/h_{12}\leftrightarrow h_{33}^*/h_{13}^*$.

The solutions of (2.13) can be analyzed numerically. Really, using condition (3.5) for setting correct signs in (3.2), we can straightly find the ratio of elements of the second ($|h_{22}/h_{12}|=A_{12}^{-1}$; $|h_{32}/h_{12}|=A_{13}^{-1}$) and the third ($|h_{23}/h_{13}|=A_{12}\frac{M_{22}}{M_{11}}$; $|h_{33}/h_{13}|=A_{13}\frac{M_{33}}{M_{11}}$) columns of the Yukawa matrix for every fixed point in the space of values $m_2, m_3, \theta_{12}, \theta_{13}, \theta_{23}, \alpha_2, \delta$.

In the case of the normal hierarchy the masses of active neutrinos increase with increasing their numbers ($m_1<m_2<m_3$). In the νMSM $m_1=0$, so we take central values $m_2=\sqrt{|\Delta m_{12}^2|}=0.009$ eV, $m_3=\sqrt{|\Delta m_{23}^2|}=0.05$ eV. The phases δ, α_2 vary in range from $-\pi$ to π, the angles $\theta_{12}, \theta_{13}, \theta_{23}$ vary in accordance with Table 1. With help of the numerical analysis we found the minimum and the maximum values for the ratio of elements of the second column of the Yukawa matrix and obtained $0.65\lesssim|h_{32}/h_{12}|\lesssim 24.2$, $1.4\lesssim|h_{22}/h_{12}|\lesssim 29.6$. Also, we found values of $(|h_{22}/h_{12}|;\ |h_{32}/h_{12}|)$ and $(\mathrm{Arg}[h_{22}/h_{12}];\ \mathrm{Arg}[h_{32}/h_{12}])$ for 10^4 points in the space of values $\theta_{12}, \theta_{13}, \theta_{23}, \alpha_2, \delta$. Results of calculations are demonstrated in Fig. 1.

It should be noted that if one arbitrary takes a point in the space of values $\theta_{12}, \theta_{13}, \theta_{23}, \alpha_2, \delta$ there is a strong probability that $|h_{32}/h_{12}|$ and $|h_{22}/h_{12}|$ will lie in range from 1 to 10 and it is improbable that ratio of the Yukawa couplings will be greater than ten. The values of the phase differences $\mathrm{Arg}[h_{32}/h_{12}]$ and $\mathrm{Arg}[h_{22}/h_{12}]$ lie not in the full region $[-\pi,\pi]$ but only in a closed compact region (Fig. 1b).

In the case of the inverse hierarchy the masses of active neutrinos increase with reducing their numbers ($m_1>m_2>m_3$) but the νMSM predicts $m_1=0$. In order to conform it we can swap the mass state m_3 and m_1 with help of additional rotation via unitary anti-diagonal matrix $\tilde{U}$: $U_{(1)}\to U_{(1)}\tilde{U}$ where $U_{(1)}$ is the mixing matrix of the active neutrinos (2.12). Assuming $m_1=0$, we get central values $m_2=m_3=\sqrt{|\Delta m_{23}^2|}=0.05$ eV and found the same quantities for the same range of values θ_{12}, θ_{13}, $\theta_{23}, \alpha_2, \delta$ like in the case of normal hierarchy. In this case the ratio of elements of the second column of the Yukawa matrix lies in range $0\le|h_{32}/h_{12}|\lesssim 3.2$, $1.1\lesssim|h_{22}/h_{12}|\lesssim 4.3$. The points in the space of values $\theta_{12}, \theta_{13}, \theta_{23}$, α_2, δ are demonstrated by Fig. 2.

In this case the boundary great values of the elements ratio are improbable too. The ratio $|h_{32}/h_{12}|$ can be equal to zero because of $|h_{32}/h_{12}|=A_{12}^{-1}\sim M_{12}$ and M_{12} can be equal zero in allowed range of parameters (Table 1) under condition $m_1=m_2$. So, in contrast to the case of the normal hierarchy, elements $|h_{i2}|$ can be of different order of magnitude. Similarly to the case of the normal hierarchy, the phase differences $\mathrm{Arg}[h_{32}/h_{12}]$ and $Arg[h_{22}/h_{12}]$ lies in closed compact region (Fig. 2b).

In the case of normal and inverse hierarchies the graphical representation of ratio of the third column elements $(|h_{33}/h_{13}|;\ |h_{23}/h_{13}|)$ is identical to Figs. 1a, 2a. The corresponding representation of the phase differences $(\mathrm{Arg}[h_{33}/h_{13}];\ \mathrm{Arg}[h_{23}/h_{13}])$ is identical to Figs. 1b, 2b but in the region $[0;2\pi]$.

[6] It can be shown that our results (3.6), (3.7) coincide with results of [14] where the ratios of the elements were obtained in the particular case $\theta_{13}\to 0$, $\theta_{23}\to\pi/4$.

[7] Only the relation between absolute values of the elements of the second and third columns of the Yukawa matrix $\epsilon=F_3/F_2$ was used as an additional relation in [16]. It allows one to find out only the absolute values of the Yukawa's elements.

[8] This assertion is always true, except the special case of the parameters when at least one radical expression in (3.2) is zero.

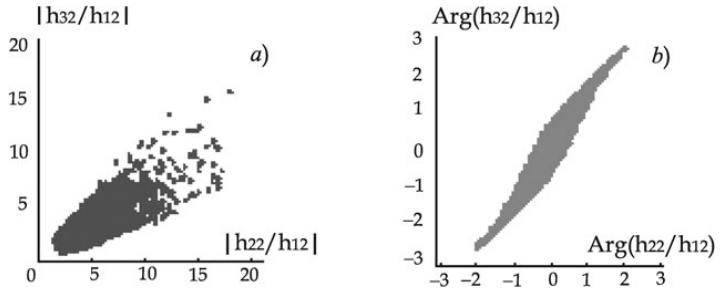

Fig. 1 The ratio of modules (**a**) and difference of phases (**b**) of the second column elements of the Yukawa matrix in the case of the normal hierarchy

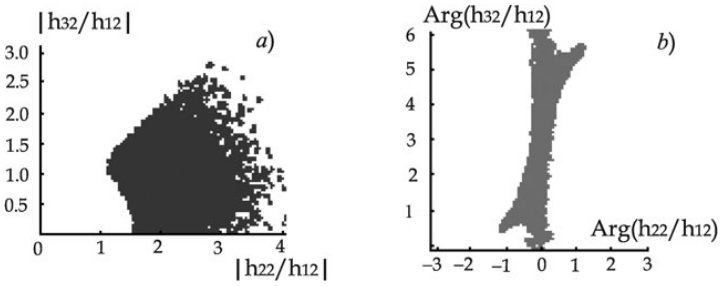

Fig. 2 The ratio of modules (**a**) and difference of phases (**b**) of the second column elements of the Yukawa matrix in the case of the inverse hierarchy

The obtained constraints on the possible values of ratio of the Yukawa sterile neutrinos matrix elements are determined by the current data on active neutrino parameters. When the inaccuracy of the active neutrino parameters will decrease the constraints will be improved too. Obtained results can be useful for getting more accurate predictions of the *νMSM* theory particularly for the investigation of the baryon asymmetry.

As one can see, there are four independent variants of solutions of (2.13). It should be noted that even in the case when the masses and mixture angles of active neutrinos are known exactly we will be not able to say which of these variants of the solutions are realized. To known it we need the values of phases of the active neutrinos matrix U_1. For fixed values of the all active neutrino matrix parameters the quantity of the possible solutions reduces to two that corresponds to interchanging and conjugating of the relation between elements of the second and the third columns of the Yukawa matrix. It is closely related to the symmetry of (2.13) under replacing the elements of the second column of the Yukawa matrix by elements of the third column. In this case two variants of solutions in principle can be distinguished experimentally with help of measurement of the mixture angles between active and sterile neutrinos.

4 CP-violation in the *νMSM*

As is known [18], in order that the baryon asymmetry generated from the initial charge symmetric state of the hot Universe, the next conditions must be satisfied simultaneously: (a) baryon number non-conservation; (b) C- and CP-violation; (c) deviations from thermal equilibrium.

In the field theory the Lagrangian under CP-transformations turns into the Lagrangian with complex conjugated couplings. If theory contains couplings with unremovable phases, then this theory is not CP-invariant. The unique source of CP-violation in the SM is one complex element in the Cabibbo–Kobayashi–Maskawa mixing matrix of quarks. In the *νMSM* theory, owing to massiveness of neutrinos, there is mixing among different generations of neutrinos and therefore there is additional possible source of CP-symmetry violation. This theory has a possibility of the baryon asymmetry generation due to existence of CP-violating oscillations of active neutrinos into sterile. Such oscillations change the full lepton number of a system and create lepton asymmetry that transforms into the baryon asymmetry with the help of the electroweak sphalerons [4, 19–22].

To analyze CP-symmetry violation in the *νMSM* we use relation for the CP-violating factor [14]

$$\delta_{\mathrm{CP}} = \frac{1}{F_2^6}\Big[\mathrm{Im}\big(h^+h\big)_{23}\sum_{\alpha}\big(|h_{\alpha 2}|^4 - |h_{\alpha 3}|^4\big) - \big(F_2^2 - F_3^2\big) \times \sum_{\alpha}\big(|h_{\alpha 2}|^2 + |h_{\alpha 3}|^2\big)\,\mathrm{Im}[h^*_{\alpha 2}h_{\alpha 3}]\Big]. \tag{4.1}$$

The solutions (3.2) allow us to express the last relation through the parameters of the active neutrinos. We get

$$\delta_{\rm CP}(\xi,\varepsilon) = |M_{11}|^{-1} C^{-3}\big[\varepsilon\big(\mathrm{Im}\big[e^{-2i\xi}A\big]B - CD\big) + \varepsilon^3(C_1 D - C D_1) + \varepsilon^5\big(C_1 D_1 - B_1\,\mathrm{Im}\big[e^{-2i\xi}A\big]\big)\big], \tag{4.2}$$

where there is dependence on only two parameters of the Yukawa matrix

$$\xi = \arg[h_{12}], \qquad \varepsilon = |h_{13}/h_{12}| = \epsilon\sqrt{C/C_1}, \tag{4.3}$$

and following notations are used:

$$\epsilon = F_3/F_2; \qquad A = M_{11} + \frac{A_{12}}{A_{12}^*}M_{22} + \frac{A_{13}}{A_{13}^*}M_{33};$$

$$B = 1 + |A_{12}|^{-4} + |A_{13}|^{-4};$$

$$C = 1 + |A_{12}|^{-2} + |A_{13}|^{-2};$$

$$B_1 = 1 + \left|A_{12}\frac{M_{22}}{M_{11}}\right|^4 + \left|A_{13}\frac{M_{33}}{M_{11}}\right|^4;$$

$$C_1 = 1 + \left|A_{12}\frac{M_{22}}{M_{11}}\right|^2 + \left|A_{13}\frac{M_{33}}{M_{11}}\right|^2;$$

$$D = \mathrm{Im}\big[e^{-2i\xi}M_{11}\big] + |A_{12}|^{-2}\,\mathrm{Im}\left[e^{-2i\xi}\frac{A_{12}}{A_{12}^*}M_{22}\right] + |A_{13}|^{-2}\,\mathrm{Im}\left[e^{-2i\xi}\frac{A_{13}}{A_{13}^*}M_{33}\right];$$

$$D_1 = \mathrm{Im}\big[e^{-2i\xi}M_{11}\big] + \left|\frac{M_{22}}{M_{11}}A_{12}\right|^2\mathrm{Im}\left[e^{-2i\xi}\frac{A_{12}}{A_{12}^*}M_{22}\right] + \left|\frac{M_{33}}{M_{11}}A_{13}\right|^2\mathrm{Im}\left[e^{-2i\xi}\frac{A_{13}}{A_{13}^*}M_{33}\right].$$

Numerical analysis of the relation (4.2) confirms the general properties of the CP-violating factor (4.1) obtained in [14]:

(1) Sign of the CP-violating factor and correspondingly the sign of the baryon asymmetry cannot be determined by only the elements of the active neutrino matrix.
(2) If $\epsilon \to 0$, then $\delta_{\rm CP} \sim \epsilon$ and also tends to zero.
(3) The CP-violating factor cannot be equal zero[9] when $\epsilon = 1$.
(4) The CP-violating factor cannot be equal zero (see footnote 9) when $\theta_{13} = 0$ and $\theta_{23} = \pi/4$.
(5) In the case of inverse hierarchy the CP-violating factor cannot be equal zero (see footnote 9) when $m_1 = m_2$, $\theta_{13} = 0$, $\theta_{23} = \pi/4$.

[9]For some particular values of mixing angles and phases $\delta_{\rm CP}$ may be zero. This values of the parameters can be found numerically.

The range of values of all parameters in the relation (4.2) is known.[10] This allows one to estimate bounds of possible values of the CP-violating factor. For the case of normal hierarchy we have $|\delta_{\rm CP}| \lesssim 0.27$, for the case of inverse—$|\delta_{\rm CP}| \lesssim 0.08$.

As one can see from (4.1) the CP-violating factor may be nonzero only in the case when Yukawa matrix elements have an imaginary part. The solutions (3.2) allow one to consider the possibility of the baryon asymmetry generation in the case when mixing matrix $U_{(1)}$ and, correspondingly to (2.15), the mass matrix of the active neutrino $M_{\rm light}$ are real. It is easy to see that for real matrix $U_{(1)}$ (2.12) the following minors of the matrix $M_{\rm light} = U_{(1)}^* m U_{(1)}^+$ (here $m = \mathrm{diag}(0, m_2, m_3)$) are not negative:

$$\begin{cases} M_{11}M_{22} - M_{12}^2 = m_2 m_3(\sin\theta_{13}\cos\theta_{12}\cos\theta_{23} - \sin\theta_{12}\sin\theta_{23})^2 \geq 0; \\ M_{11}M_{33} - M_{13}^2 = m_2 m_3(\sin\theta_{13}\cos\theta_{12}\sin\theta_{23} + \sin\theta_{12}\cos\theta_{23})^2 \geq 0; \\ M_{22}M_{33} - M_{23}^2 = m_2 m_3\cos^2\theta_{13}\cos^2\theta_{12} \geq 0. \end{cases} \tag{4.4}$$

If the values of the mixing angles are defined by Table 1 all the above minors are positive. In this case the ratio of Yukawa's elements (3.3), (3.4) and, consequently, the Yukawa's elements are complex numbers. So, we can expect that CP-violating factor can be nonzero.

The direct numerical analysis of the CP-violating factor (4.2) confirms this assumption. Furthermore, if one takes arbitrary a point in the space of values θ_{12}, $\theta_{13}, \theta_{23}, \xi, \varepsilon$ ($\delta = \alpha_2 = 0$) there is a strong probability that the CP-violating factor will be nonzero.[11] Thus, even in the case when active neutrino mass matrix $M_{\rm light}$ is real the electroweak generation of the baryon asymmetry can be realized also.

The CP-violating factor is a complicated function of parameters of the active neutrino matrix and the Yukawa matrix. The analysis of this factor is accentuated by fact that for fixed point in space of active neutrino parameters one needs to take appropriate variant of solutions of (2.13). The investigation of manifestation of the different variants of solutions (3.2) on the CP-violating factor is an interesting task for future.

5 Conclusions

The *νMSM* is the minimal neutrino modification of the SM that can explain simultaneously neutrino oscillations, generation of the baryon asymmetry, and the nature of dark matter.

[10]The bounds of values of the mixing angles are defined by Table 1, the phases are in the region $[0, 2\pi]$, $7 \times 10^{-5} < \epsilon < 1$ [14].

[11]The equation for zero CP-violating factor (4.2) has a fine-tuning solutions in space of the mentioned parameters.

There are strong conditions on the parameters of the *νMSM* that can be experimentally checked. For the time being observable data, obtained from the missions XMM-Newton, Chandra, INTEGRAL, Suzaku, reveal no signs of existence of the sterile neutrino in predicted by the *νMSM* and instrumentally allowed region (see [4] and references there). But new investigations are planed (for example, project Xenia [23]) that will continue to inspect theoretically allowed region of the model parameters.

Obtained in this paper exact solutions of the *νMSM* equations connect elements of the Yukawa matrix with elements of the active neutrino mass matrix and will be useful for analysis, data processing, and getting more accurate constraints on the model parameters.

The analysis of the ratio of the Yukawa matrix elements demonstrates that in the case of normal hierarchy elements of second (h_{i2}) and third (h_{i3}) columns are the same order of magnitude. But in the case of inverse hierarchy the magnitudes of elements can considerably vary from each other in the column.

CP-violating phase in the SM is parameter of the Cabibbo–Kobayashi–Maskawa matrix and it is known from observable data. In contrast to it the CP-violating factor (δ_{CP}) in the *νMSM* is effective parameter that is present in the expression for the baryon asymmetry. Therefore the CP-violating factor in the *νMSM* has a sophisticated structure as a function of the Yukawa matrix parameters.

Obtained solutions (3.2) allow one to get expression for the CP-violating factor (4.1) through the parameters of the active neutrinos and two parameters of the Yukawa matrix. Due to this the bounds of possible values of the CP-violating factor were estimated. It should be noted that in the case of the inverse hierarchy the maximum of $|\delta_{\mathrm{CP}}|$ is considerably smaller (fourfold) as compared to the case of normal hierarchy.

As is known, the phases of the active neutrino mixing matrix cannot be measured for the time being. It was shown that in any case (even if these phases are zero) the CP-violating factor can be nonzero and the baryon asymmetry generation is possible. The fact of the matter is that the elements of the Yukawa matrix are complex when the elements of the active neutrino mixing matrix are real.

As it was mentioned above the *νMSM* provides a candidate for dark matter particle with mass M_1 in the range $(1\div 50)$ KeV. It is the lightest sterile neutrino that is produced due to the resonant active-sterile neutrino oscillations in the presence of lepton asymmetry [14, 24]. It requires the high mass degeneracy of two other heavier neutrinos and leads to the fine-turning problem [14, 25].

It should be noted that modifications of the *νMSM* can provide other production mechanisms of the lightest sterile neutrino due to interactions with other particles [26–29] or primordial Higgs-inflation [30]. It applies some additional constraints on the parameters of the *νMSM* (see, also, [25]) and changes the mass range of the lightest sterile neutrino. The change of only M_1 has no action on the results of the present work but the additional terms in the Lagrangians of such theories can modify (2.13) that should be taken into account for investigations of the constraints in such theories.

Acknowledgements We would like to thank A. Boyarsky, O. Ruchayskiy, D. Iakubovskyi and M. Shaposhnikov for the idea of treating this subject, and for useful comments and discussions. This work has been supported by the Swiss Science Foundation (grant SCOPES 2010-2012, No. IZ73Z0_128040).

References

1. S. Weinberg, Phys. Rev. Lett. **19**, 1264 (1967)
2. S.L. Glashow, Nucl. Phys. **22**, 579 (1961)
3. A. Salam, in *Proceedings of the Nobel Symposium Held 1968 at Lerum*, Sweden, Stockholm (1968), pp. 367–377
4. A. Boyarsky, O. Ruchayskiy, M. Shaposhnikov, Ann. Rev. Nucl. Part. Sci. **59**, 191 (2009)
5. Particle Data Group. http://pdg.lbl.gov
6. A. Strumia, F. Vissani, arXiv:hep-ph/0606054
7. T. Asaka, S. Blanchet, M. Shaposhnikov, Phys. Lett. B **631**, 151 (2005)
8. M. Shaposhnikov, Prog. Theor. Phys. **122**(1), 185 (2009)
9. T. Asaka, M. Shaposhnikov, Phys. Lett. B **620**, 17 (2005)
10. R.N. Mohapatra, A.Y. Smirnov, Ann. Rev. Nucl. Sci. **56**, 569 (2006)
11. S.F. King, Rep. Prog. Phys. **67**, 107 (2004)
12. G. Altarelli, F. Feruglio, New J. Phys. **6**, 106 (2004)
13. S. Weinberg, Phys. Rev. Lett. **43**, 1566 (1979)
14. M. Shaposhnikov, arXiv:0804.4542
15. S. Bilenky, S. Petcov, Rev. Mod. Phys. **59**(3), 671 (1987)
16. M. Shaposhnikov, Nucl. Phys. B **763**, 49 (2007)
17. S. Bilenky, C. Giunti, W. Grimus, Prog. Part. Nucl. Phys. **43**, 1 (1999)
18. A.D. Sakharov, JETP Lett. **5**, 24 (1967)
19. E.K. Akhmedov, V.A. Rubakov, A.Y. Smirnov, Phys. Rev. Lett. **81**, 1359 (1998)
20. V.A. Kuzmin, V.A. Rubakov, M.E. Shaposhnikov, Phys. Lett. B **155**, 36 (1985)
21. V.A. Kuzmin, V.A. Rubakov, M.E. Shaposhnikov, Phys. Lett. B **191**, 171 (1987)
22. S.Y. Khlebnikov, M.E. Shaposhnikov, Phys. Lett. B **387**, 817 (1996)
23. J.W. den Herder et al., arXiv:0906.1788
24. X. Shi, G.M. Fuller, Phys. Rev. Lett. **82**, 2832 (1999)
25. A. Roy, M. Shaposhnikov, arXiv:1006.4008
26. M. Shaposhnikov, I. Tkachev, Phys. Lett. B **639**, 414 (2006)
27. A. Kusenko, Phys. Rev. Lett. **97**, 241301 (2006)
28. A. Anisimov, Y. Bartocci, F.L. Bezrukov, Phys. Lett. B **671**, 211 (2009)
29. F. Bezrukov, D. Gorbunov, J. High Energy Phys. **05**, 010 (2010)
30. F. Bezrukov, D. Gorbunov, M. Shaposhnikov, J. Cosmol. Astropart. Phys. **0906**, 029 (2009)

1.4. Народження масивних нейтрино з правою кіральністю у 3-частинкових розпадах мезонів

IOP Publishing Journal of Physics G: Nuclear and Particle Physics
J. Phys. G: Nucl. Part. Phys. **48** (2021) 105001 (24pp) https://doi.org/10.1088/1361-6471/ac1394

Production of GeV-scale heavy neutral leptons in three-body decays. Comparison with the PYTHIA approach

V M Gorkavenko*, Yu R Borysenkova and M S Tsarenkova

Faculty of Physics, Taras Shevchenko National University of Kyiv, 64, Volodymyrs'ka str., Kyiv 01601, Ukraine

E-mail: gorkavol@gmail.com

Received 21 March 2021, revised 26 June 2021
Accepted for publication 12 July 2021
Published 24 August 2021

Abstract

Despite the undeniable success of the standard model of particle physics (SM), there are some phenomena that the SM cannot explain. These phenomena indicate that the SM has to be modified. One of the possible ways to extend the SM is to introduce heavy neutral leptons (HNLs). To search for HNLs in intensity Frontier experiments, one has to consider HNL production both in two-body and three-body decays of some mesons. We verified the possibility of using the parton level PYTHIA default matrix elements (without the form-factor formalism) to calculate HNL production in three-body semileptonic decays of B and D mesons in the experimentally interesting mass range of the produced HNLs. We conclude that this approach is quite suitable for the estimation of the sensitivity region for HNLs in the intensity Frontier experiments, provided one uses suitable parton level PYTHIA default matrix elements. Our study was driven by the usage of such an approximation by the SHiP collaboration. We conclude that in this case the parton level PYTHIA default matrix elements could have been chosen more appropriately.

Keywords: physics beyond the standard model, intensity frontier experiment, HNL

1. Introduction

The standard model of particle physics (SM) [1–3] is a theory that describes with high precision the processes of electroweak and strong interactions with the participation of elementary particles. It is consistent up to a very high energy scale (perhaps up to the Planck scale) and

*Author to whom any correspondence should be addressed.

it is verified in numerous accelerator experiments up to energy ~ 15 TeV. However, the SM fails to explain some phenomena such as massiveness of neutrinos (see e.g. [4, 5]), dark matter (for reviews see e.g. [6–8]), dark energy [9], baryon asymmetry of the Universe [10], etc. Therefore, the SM is an incomplete theory and it requires an extension. One has to suggest the existence of 'hidden' sectors with particles of new physics.

It turns out that the mentioned SM problems can be theoretically solved by extending the SM by new particles that can be either heavy or light. Indeed, neutrino oscillations and the smallness of the active neutrino masses can be explained with the help of new particles with sub-eV mass as well as with the help of heavy particles of the GUT scale, see e.g. [11]. The same may be said about the baryon asymmetry of the Universe and dark matter problems: physics at very different scales can be responsible for them, see e.g. [12].

So, two possible answers can be formulated to the question 'why do we not observe particles of new physics in experiments?' The first answer is the following. The new particles are very heavy and cannot be produced in modern accelerators like the LHC. To detect them one has to build more powerful and more expensive accelerators (we need energy Frontier experiments). However, there is another possibility. The particles of new physics can be light (with a mass below or of the order of the electroweak scale) that feebly interact with the SM particles. The last case is very interesting for the experimental search for new physics right now, see e.g. [13]. To search for rare interactions of feebly interacting hypothetical particles, the intensity Frontier experiments are needed. These experiments aim to create high-intensity particle beams and use large detectors [14]. Several such intensity Frontier experiments have been proposed in recent years: DUNE [15], NA62 [16–18], SHiP [19, 20], etc.

We do not know what are the properties of the new particles. They can be new scalars, pseudoscalars, vectors or fermions, see [19, 21] for a review. Each of these options has to be tested in experiments. From a theoretical point of view, there are three possible choices of the new renormalized Lagrangian of the interaction of new particles with the SM particles. These interactions are called portals. There are scalar (e.g. [22–24]), vector (e.g. [25–27]) and heavy neutral leptons (HNLs) renormalized portals. It means the new interaction can be observed at any energy scale, including that below the EW scale. There are also other portals of high-dimensional operators such as the portal of pseudoscalar particles (axion-like particles), see e.g. [28–30] and [31] for a review, or Chern–Simons like (parity odd) interaction of electroweak gauge bosons with a new vector field (e.g. [32, 33]). The lower the energy scale is, the less important these interactions will be.

In this paper, we consider extending the SM by neutrino singlets with right chirality, which extremely faintly interact with the SM particles. Such right-handed neutrinos are called sterile neutrinos or HNLs.

Interest in the HNL modification of the SM is conditioned by the model's ability to explain the smallness of active neutrino masses (due to large values of the sterile neutrino masses M_I or small values of Yukawa elements $F_{\alpha I}$) and to describe the generation of the matter-antimatter asymmetry of the Universe due to CP violation in the model [34]. It was shown that Majorana masses of HNLs can be GeV scale [35–37] to explain baryon asymmetry of the Universe.

In 2005 the neutrino minimal standard model (νMSM) model was proposed [36, 38]. In this model, the SM is extended by three right-handed neutrinos (HNLs) with masses smaller than the electroweak scale. It was shown that 18 new parameters of the model can be chosen in such a way as to simultaneously solve problems of neutrino oscillations, baryon asymmetry in the Universe, and dark matter. In this case, the νMSM model requires the existence of two right-handed neutrinos with practically the same masses ($\gtrsim$100 MeV) and one right-handed neutrino with a relatively small mass in the keV region, see [39] for a review. The lightest right-handed neutrino is a long-lived particle, a dark matter candidate. In 2014 the possible

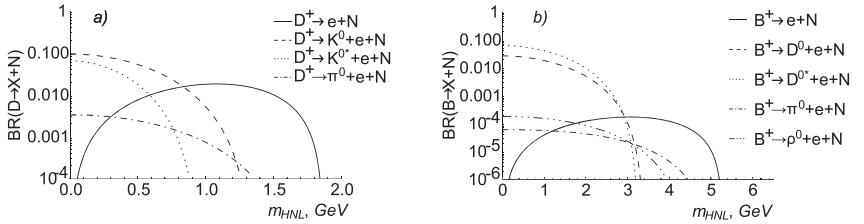

Figure 1. Dominant branching ratios of HNL production from charged D (figure (a)) and B (figure (b)) mesons, see [43] for details. Here $U_e = 1$, $U_\mu = U_\tau = 0$.

manifestation of the lightest right-handed neutrino with mass 7 keV was found in x-ray spectra of the Andromeda galaxy and the Perseus galaxy cluster [40, 41].

That is why the HNL extension of the SM attracts a lot of attention and interest. This modification of the SM is especially interesting for GeV-scale HNLs that can be in principle detected in the intensity Frontier experiments [14, 19].

A model-independent phenomenological approach is used in the experimental search for HNLs, assuming the existence of only one HNL and considering that the other HNLs do not affect the analysis. For simplicity of analysis, restrictions are imposed on only two free parameters of the model: Majorana mass of the appropriate HNL (m_N) and the mixing angle of the interaction of this HNL with only one active neutrino of flavor α (U_α). While it is usually assumed that the mixing angles of interaction with other active neutrinos are zero.

It should be noted that the results of previous numerous experiments almost completely closed the region for HNLs with masses below the mass of kaon, see [19, 42] for details. Therefore, HNLs with mass $m_N \gtrsim 0.5$ GeV are of interest to us. The phenomenology of GeV-scale HNLs was considered e.g. in [43]. A recent computation of the sensitivity region for HNL search in the SHiP experiment was performed in [44].

If we consider the most important production channels of HNLs in the fixed target intensity Frontier experiments (such as NA62, SHiP or DUNE), we see that they are the semileptonic decays of D, D_s mesons, B, B_s, B_c mesons and decays of τ leptons, see [43]. It should be noted that an essential contribution to HNL production is given by three-body decays of the mentioned particles, see figure 1, where we present branchings for decays of D and B mesons as an example. Branchings for decays of other mesons can be found in [43].

Taking into account that the number of the produced D mesons is sufficiently greater than the number of the produced B mesons in proton-target collisions (e.g. $\sim 10^{17}$ and $\sim 10^{13}$ correspondingly for 5 years of SHiP experiment operation [43]), it is obvious that HNLs production from B mesons decay can be neglected for HNLs with masses $m_N \lesssim 2$ GeV.

So, three-body decays of mesons with τ leptons in the final state are either forbidden (for the decays of D mesons) or ineffective (for the decays of B mesons). We will denote the final states of charged leptons as $\ell = e,\ \mu$.

In the SHiP collaboration paper [44] computation of the three-body semileptonic decay contributions ($h \to h' + \ell + N$) for the formation of the sensitivity region for HNLs was based on PYTHIA 8. PYTHIA is a general purpose collision event generator [45], that can be modified to embody new simulations with an arbitrarily good approximation in principle. However, the three-body decay contributions to the sensitivity region built in [44] were computed with use of the parton level PYTHIA default matrix elements without additional tuning. This can be

clearly seen by looking at their program code[1]. It motivated us to verify the accuracy of this approach.

The fact is that for the description of the semileptonic decays of D mesons PYTHIA uses a default matrix element

$$|M_{\rm fi}|^2 = (p_h p_\ell)(p_\nu p_{h'}) \tag{1}$$

and for description of the semileptonic decays of B mesons PYTHIA uses a default matrix element

$$|M_{\rm fi}|^2 = (p_h p_\nu)(p_\ell p_{h'}). \tag{2}$$

Explicit form of these matrix elements is given in the PYTHIA 6.4 manual [46]. The current version, PYTHIA 8, uses the same matrix elements without change. Our further computations are valid for PYTHIA 6 as well as for PYTHIA 8.

However, for accurate consideration we need to use at least form-factors of meson transitions. In this paper, we analyze the relevancy of the usage of the parton level default PYTHIA matrix elements in the SHiP collaboration paper [44] for the computation of the contributions of the three-body decays of B and D mesons to the sensitivity region.

As it was pointed out in [19] HNLs can be produced in τ lepton decays and these decays are important in case of dominant mixing with the τ flavor. The main three-body decay channels of τ leptons are decays into elementary particles $\tau \to N\ell_\alpha\bar{\nu}_\alpha$ and $\tau \to \nu_\tau\ell_\alpha N$, where $\alpha = e,\ \mu$. In contrast to meson decays, which must be described using the form-factor formalism, these decays can be directly described by the PYTHIA formalism.

The paper is organized in the following way. In section 2 we consider a general formalism of the neutrino modification to the SM. In section 3 we formulate a general strategy to get the domain of parameters that allows hidden particles to be detected in the intensity Frontier experiments. In section 4 we get the general definition of a probability density function (PDF) for the production of particles with a certain value of energy in three-body decays. In sections 5 and 6 we present the exact matrix elements for the three-body decays of mesons. In section 7 we compare PDFs for HNL production in three-body decays of mesons (in the own reference frame of the mesons) computed using the parton level PYTHIA default matrix elements and the exact ones. In section 8 we derive the energy and polar angle distribution functions of the produced HNLs in the laboratory reference frame. In section 9 we find the probability of a produced HNL to fall on the detector. In section 10 we estimate the probability of a produced HNL to decay inside the vacuum tank before the detector. Finally, the results are summarized in section 11. Useful kinematic relations for HNLs in the different reference frames are outlined in appendix A.

2. Neutrino modification of the SM. Heavy neutral leptons

Renormalized interaction of the right-handed neutrinos with the SM particles (HNL portal) is similar to the Yukawa interaction of left-handed quark doublets with singlets of the right-handed quarks in the SM, namely:

$$\mathcal{L}_{\rm int} = -\left(F_{\alpha I}\bar{L}_\alpha\tilde{H}N_I + \text{h.c.}\right), \tag{3}$$

[1] The calculations of the SHiP collaboration were carried out with the use of the FairShip software framework. The program code is in open access, see https://github.com/ShipSoft/FairShip.

where $\alpha = e,\ \mu, \tau$, the index I is from 1 to the full number of the sterile neutrinos (n), L_α—the doublet of the leptons of α-generation, N_I—a right-handed sterile neutrino, $F_{\alpha I}$—a new matrix of dimensionless Yukawa couplings, $\tilde{H} = \mathrm{i}\sigma_2 H^*$.

Conditions of invariance of the Lagrangian (3) to the transformations of the gauge groups of the SM demand the corresponding charges of the sterile neutrinos to be zero. Therefore, sterile neutrinos are not charged relative to the gauge groups of the SM, which justifies their name.

After the electroweak symmetry breaking, Lagrangian (3) in the unitary gauge looks as follows:

$$\mathcal{L}_{\text{int}} = -\left(M^D_{\alpha I}\bar{\nu}_\alpha N_I + \text{h.c.}\right), \qquad M^D_{\alpha I} = \frac{v}{\sqrt{2}}F_{\alpha I}, \tag{4}$$

where $v \approx 246$ GeV is the vacuum expectation value of the Higgs field, $M^D_{\alpha I}$—Dirac mass terms.

Considering sterile neutrinos as neutral Majorana particles, we can write the full Lagrangian of the modified neutrino sector of the SM in the form

$$\mathcal{L}_{\nu,N} = \mathrm{i}\bar{\nu}_k\partial\!\!\!/\nu_k + \mathrm{i}\bar{N}_I\partial\!\!\!/N_I - \left(M^D_{\alpha I}\bar{\nu}_\alpha N_I + \frac{M_I}{2}\bar{N}_I{}^c N_I + \text{h.c.}\right), \tag{5}$$

where M_I is the Majorana mass of Ith sterile neutrino. Imposing the condition $M^D_{I\alpha}/M_I \ll 1$, one can perform the diagonalization of the neutrino mass matrix, see e.g. [11, 47], and get the mass matrix of the active neutrinos

$$(M^{\text{active}}_\nu)_{\alpha\beta} = -\sum_{I=1}^{n}\frac{M^D_{I\alpha}M^D_{I\beta}}{M_I}. \tag{6}$$

The mass matrix for the sterile neutrinos will remain almost unchanged. This mechanism is known as the seesaw mechanism[2], see e.g. [54, 55].

As a result of the neutrino states mixture, the active neutrino states become superposition of the mass states of the active and sterile neutrinos

$$\nu_L = \left(1 - \frac{1}{2}U^+U\right)V_1\nu_{mL} + U^+V_2N^c, \tag{7}$$

where $U_{I\alpha} = M^D_{I\alpha}/M_I$ ($U = M^{-1}M^D$) is a so-called mixing angle ($U_{I\alpha} \ll 1$), V_1—a unitary matrix for diagonalization of the active neutrino mass matrix, V_2—a unitary matrix for diagonalization of the sterile neutrino mass matrix (it can be taken as a unit matrix in our case). It means that sterile neutrinos interact with the SM particles similarly to active neutrinos:

$$\begin{aligned}\mathcal{L}_{\text{int}} = &-\frac{g}{2\sqrt{2}}W^+_\mu\sum_{I,\alpha}\bar{N}^c{}_I U_{I\alpha}\gamma^\mu(1-\gamma_5)\ell^-_\alpha \\ &-\frac{g}{4\,\cos\,\theta_W}Z_\mu\sum_{I,\alpha}\bar{N}^c{}_I U_{I\alpha}\gamma^\mu(1-\gamma_5)\nu_\alpha + \text{h.c.}\end{aligned} \tag{8}$$

It should be noted that the extension of the SM by HNLs gives an additional source of CP-symmetry violation in the theory, see e.g. [56].

[2] This mechanism is called type-I seesaw mechanism because there are other ways to explain small neutrino masses, see e.g. [11, 48]. In the type-II seesaw mechanism an extra SU(2) triplet scalar is introduced [49–52], in the type-III seesaw mechanism an extra fermion in the adjoint of SU(2) is added to the model [53].

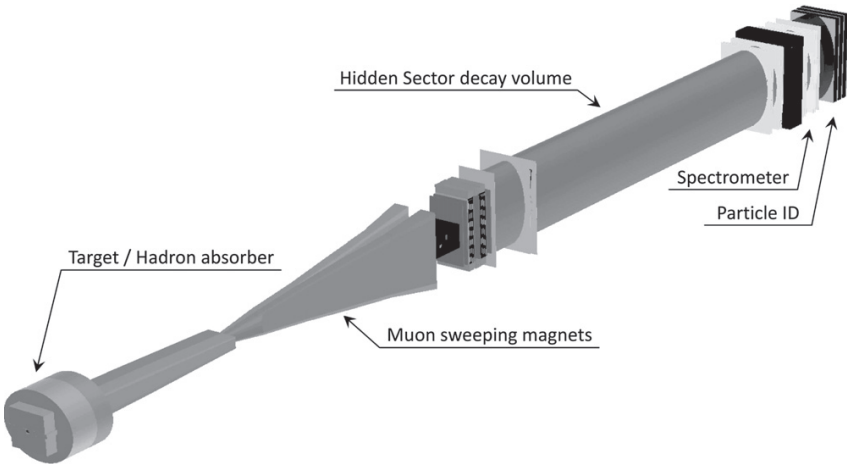

Figure 2. General scheme of the SHiP facility.

3. General strategy

At first, let us remind the general principles of the intensity Frontier experiments operation on the example of an intended experiment SHiP [57], see figure 2. A beam line from the CERN SPS accelerator will transmit 400 GeV protons at the SHiP. A proton beam will strike in a molybdenum and tungsten fixed target at a center-of-mass energy $E_{\rm CM} \approx 27$ GeV. A great number of light SM particles and hadrons will be produced under such collisions. Hidden particles are expected to be predominantly produced in the decays of the produced hadrons.

The main concept of the SHiP functioning is the following. Almost all the produced SM particles should be either trapped by an absorber or deflected in a magnetic field (muons). Remaining events with the SM particles can be rejected using specially developed cuts. If hidden particles decay into SM particles inside the decay volume, the latter will be detected. It will mean the existence of hidden particles.

We can estimate the number of hidden particles that can be detected as

$$N_{\rm det} = N_{\rm BSM} \cdot \epsilon_{\rm tot} \cdot P_{\rm decay}. \tag{9}$$

This relation allows us to find a range of parameters (m_N, θ_α), when HNLs can be detected. It is a region where $N_{\rm det} \geqslant N_{\rm det}^{\rm thr}$. Value $N_{\rm det}^{\rm thr}$ is the threshold number of the detected particles when we can affirm the discovery of HNLs. It depends on the characteristics of the experiment facilities and the background level.

Let us explain the meaning of the constituent factors in (9). Factor $N_{\rm BSM}$ is the number of hidden particles produced during all the time of the SHiP experiment operation. Factor $\epsilon_{\rm tot}$ is the product of the following factors $\epsilon_{\rm geom} \cdot Br_{\rm vis} \cdot \epsilon_{\rm det}$, where $\epsilon_{\rm geom}$ is the probability of a produced HNL to move towards the detector, $\epsilon_{\rm det}$ is the probability of the detector to register visible particles, $Br_{\rm vis}$ is the branching of HNL decay into channels, visible for the detectors. Factor $P_{\rm decay}$ is the probability of a produced HNL to decay in the volume of the vacuum tank before the detectors.

Therefore, to validate the accuracy of the computation with use of the parton level PYTHIA default matrix elements of the contribution of the produced in the three-body decays HNLs to the sensitivity region we have to consider only two factors in (9), namely ϵ_{geom} and P_{decay}.

The probability for the produced HNLs to move towards the detector (ϵ_{geom}) can be easily found if we know the distribution function of these particles. The probability of the HNLs to decay inside the vacuum tank before the detector is

$$P_{\text{decay}} = \mathrm{e}^{-\frac{L\Gamma}{\gamma\beta}} - \mathrm{e}^{-\frac{(L+\Delta L)\Gamma}{\gamma\beta}}, \tag{10}$$

where L is the distance from the target to the vacuum tank, ΔL—the length of the vacuum tank, γ is the Lorentz factor, β—the velocity of the particle and Γ—the decay width of HNLs. Thus, P_{decay} depends on the energy distribution function of HNLs, HNL's lifetime, geometry of the experiment, and the coupling constant.

Therefore, to compute both ϵ_{geom} and P_{decay} we need the energy-angle distribution functions of the produced HNLs. One can easily get these functions in the rest frame of the initial meson. Using the energy-angle distribution of the initial mesons, we can get the distribution functions of HNLs in the laboratory reference frame. We assume that in the initial meson's rest frame the production of HNLs is isotropic.

4. Probability density function for particles produced in a three-body decay

Let us consider a three-body decay $A \to B + C + N$, where A, B, C are some particles (with masses m_A, m_B, m_C) and N is a sterile neutrino with mass m_N.

If the decaying particle (A) is a scalar (or we average over its spin states), the differential decay width of the three-body decay in the rest frame of the A particle is defined as, see e.g. [58],

$$\mathrm{d}\Gamma = \frac{|M_{\text{fi}}|^2}{8m_A(2\pi)^3}\,\mathrm{d}E_N\,\mathrm{d}E_B. \tag{11}$$

The full partial decay width for this channel is given as

$$\Gamma(A \to BCN) = \int\limits_{E_N^{\min}}^{E_N^{\max}} \mathrm{d}E_N \int\limits_{E_B^{\min}(E_N)}^{E_B^{\max}(E_N)} \mathrm{d}E_B\, \frac{|M_{\text{fi}}|^2}{8m_A(2\pi)^3}, \tag{12}$$

where the boundaries of integration can be found from condition

$$E_N^{2\ \max/\min} = m_N^2 + \vec{p}_N^{\,2\ \max/\min} = m_N^2 + \vec{p}_B{}^2 + \vec{p}_C{}^2 \pm 2|\vec{p}_B|\,|\vec{p}_C|, \tag{13}$$

that can be rewritten as the solution of equation

$$\begin{aligned} E_N^{2\ \max/\min} &= m_N^2 + E_B^2 - m_B^2 + (m_A - E_N - E_B)^2 \\ &\quad - m_C^2 \pm 2\sqrt{(E_B^2 - m_B^2)((m_A - E_N - E_B)^2 - m_C^2)}, \end{aligned} \tag{14}$$

namely

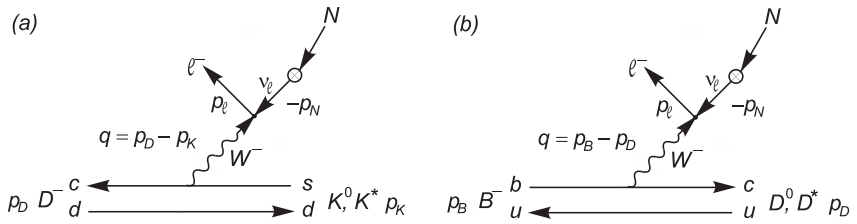

Figure 3. Diagram of the semileptonic decays: (a) decay of pseudoscalar meson D^- into pseudoscalar meson K^0 or vector meson $K^*(892)$, (b) decay of pseudoscalar meson B^- into pseudoscalar meson D^0 or vector meson $D^*(2007)^0$.

$$E_B^{\max/\min}(E_N) = \frac{(m_A - E_N)(w^2 + m_B^2 - m_C^2)}{2w^2} \pm \sqrt{E_N^2 - m_N^2}\,\frac{\sqrt{\lambda(w^2, m_B^2, m_C^2)}}{2w^2}, \tag{15}$$

where $w^2 = m_A^2 + m_N^2 - 2E_N m_A$ and $\lambda(x, y, z) = x^2 + y^2 + z^2 - 2xy - 2yz - 2zx$ is the Källén function [59].

As one can see, two functions $E_{B\max/\min}(E_N)$ in (15) define the upper and lower boundaries of the region with the allowed values of energy. These functions coincide at the minimal and maximum values of the energy E_N that can be found from the condition for the changing sign term being zero. We get

$$E_N^{\min} = m_N, \quad E_N^{\max} = \frac{m_A^2 + m_N^2 - (m_B + m_C)^2}{2m_A}. \tag{16}$$

Taking into account (12), we get the probability density function (PDF) for the production of HNLs with a certain value of energy (E_N) in the form

$$\mathrm{pdf}(E_N) = \frac{1}{\Gamma(A \to BCN)} \int\limits_{E_B^{\min}(E_N)}^{E_B^{\max}(E_N)} \mathrm{d}E_B\, \frac{|M_{\mathrm{fi}}|^2}{8m_A(2\pi)^3}. \tag{17}$$

5. HNL production in semileptonic decays of *B* and *D* mesons into pseudoscalar mesons

Decay of an electrically charged pseudoscalar meson h into an electrically neutral pseudoscalar meson h', a charged lepton and an HNL ($h \to h' + \ell + N$) is derived by weak interaction, see figure 3. The amplitude of the reaction is

$$M_{\mathrm{fi}} = \theta_\alpha \frac{G_F}{\sqrt{2}} V_{ij}^* \bar{\ell}_\alpha \gamma^\nu (1 - \gamma^5) N \langle h'(p')|\bar{Q}_i \gamma_\nu (1 - \gamma^5) Q_j|h(p)\rangle, \tag{18}$$

where averaging over the axial quark current gives zero, but averaging over vector quark current can be presented as

Table 1. Best fit parameters for the form-factors (21) of $B \to D$ transitions [61].

f	$M_{\rm pole}$ (GeV)	a_0	a_1	a_2
f_+^{BD}	∞	0.909	−7.11	66
f_0^{BD}	∞	0.794	−2.45	33

$$\mathcal{W}_\nu = \langle h'(p')|\bar{Q}_i\gamma_\nu Q_j|h(p)\rangle = \left[(p+p')_\nu - \frac{m_h^2-m_{h'}^2}{q^2}q_\nu\right] f_+^{hh'}(q^2) + \frac{m_h^2-m_{h'}^2}{q^2}q_\nu f_0^{hh'}(q^2), \tag{19}$$

where $f_+^{hh'}(q^2)$ and $f_0^{hh'}(q^2)$ are the form-factors for hh' transitions.

For $|M_{\rm fi}|^2$ summarized over the helicities of the final particles, we have

$$\overline{|M_{\rm fi}|^2} = 4\theta_\alpha^2 G_F^2 |V_{ij}|^2 \left[2(m_h^2 - m_{h'}^2) f_0^{hh'}(q^2)\,(k\mathcal{W}) - 2(k\mathcal{W})^2 - (qk)\mathcal{W}^2 + m_N^2\mathcal{W}^2\right], \tag{20}$$

where m_h, $m_{h'}$ are the masses of the corresponding mesons, m_N—the mass of the sterile neutrino.

For consideration of reaction $B^\pm \to D^0 + \ell^\pm + N$ we use a popular parametrization for form-factors of mesons, namely the Bourrely–Caprini–Lellouch (BCL) parametrization [60] that takes into account the analytic properties of the form-factors (see e.g. [61, 62]),

$$f(q^2) = \frac{1}{1 - q^2/M_{\rm pole}^2}\sum_{n=0}^{N-1} a_n \left[\left(z(q^2)\right)^n - (-1)^{n-N}\frac{n}{N}\left(z(q^2)\right)^N\right], \tag{21}$$

where function $z(q^2)$ is defined via

$$z(q^2) \equiv \frac{\sqrt{t_+ - q^2} - \sqrt{t_+ - t_0}}{\sqrt{t_+ - q^2} + \sqrt{t_+ - t_0}} \tag{22}$$

with

$$t_+ = (m_h + m_{h'})^2. \tag{23}$$

The choice of t_0 and the pole mass $M_{\rm pole}$ varies from group to group that performs the analysis. In this work we follow the FLAG collaboration [61] and take

$$t_0 = (m_h + m_{h'})\left(\sqrt{m_h} - \sqrt{m_{h'}}\right)^2. \tag{24}$$

The coefficients a_n^+ and a_n^0 are then fitted to the experimental data or lattice results. Their best fit parameter values are given in table 1.

For consideration of reaction $D^\pm \to K^0 + \ell^\pm + N$ we use the parametrization for form-factors of mesons given in [63]:

$$f(q^2) = \frac{f(0) - c(z(q^2) - z_0)\left(1 + \frac{z(q^2)+z_0}{2}\right)}{1 - Pq^2}, \tag{25}$$

where $z(q^2)$ is defined by (22) and $z_0 = z(0)$. The best fit parameter values are given in table 2.

Table 2. Best fit parameters for the form-factors (25) of $D \to K$ transitions [63].

f	$f(0)$	c	$P(\mathrm{GeV}^{-2})$
f_+^{DK}	0.7647	0.066	0.224
f_0^{DK}	0.7647	2.084	0

6. HNL production in semileptonic decays of *B* and *D* mesons into vector mesons

Let us consider production of HNLs in semileptonic decays of B and D mesons into vector mesons, namely $B^{\pm} \to D^*(2007)^0 + \ell^{\pm} + N$ and $D^{\pm} \to K^*(892) + \ell^{\pm} + N$.

Decay of an electrically charged pseudoscalar meson h into an electrically neutral vector meson h'_V, a charged lepton and an HNL ($h \to h'_V + \ell + N$) is derived by weak interaction, see figure 3. The amplitude of the reaction is similar to (18), where there is contribution from both the vector and the axial parts of the quark current $\bar{Q}_i\gamma_\nu(1-\gamma^5)Q_j = V_\nu - A_\nu$, see [43]:

$$\begin{aligned}\langle h'_V(\epsilon,p')|V_\mu|h(p)\rangle &= \mathrm{i}g(q^2)\varepsilon_{\mu\alpha\sigma\rho}\epsilon^{*\alpha}(p+p')^\sigma(p-p')^\rho \\ &= \mathrm{i}2g(q^2)\varepsilon_{\mu\alpha\sigma\rho}\epsilon^{*\alpha}p'^{\,\sigma}p^\rho = \mathrm{i}\mathbb{V}_\mu, \end{aligned} \tag{26}$$

$$\begin{aligned}\langle h'_V(\epsilon,p')|A_\mu|h(p)\rangle &= f(q^2)\epsilon^*_\mu + a_+(q^2)(\epsilon^*\cdot p)(p+p')_\mu \\ &\quad + a_-(q^2)(\epsilon^*\cdot p)(p-p')_\mu = \mathbb{A}_\mu, \end{aligned} \tag{27}$$

and ϵ_μ is the polarization vector of the vector meson.

For $|M_{\mathrm{fi}}|^2$ summarized over the helicities and polarization states of the final particles, we have

$$\overline{|M_{\mathrm{fi}}|^2} = 4\theta_\alpha^2 G_F^2 |V_{ij}|^2 \sum_\lambda R^{\mu\nu}[\mathbb{V}_\nu\mathbb{V}^*_\mu + \mathbb{A}_\nu\mathbb{A}^*_\mu + \mathrm{i}(\mathbb{A}_\nu\mathbb{V}^*_\mu - \mathbb{V}_\nu\mathbb{A}^*_\mu)], \tag{28}$$

where λ is the polarization state of the vector meson and

$$R^{\mu\nu} = (q^\nu - k^\nu)k^\mu - (qk)g^{\nu\mu} + m_N^2 g^{\nu\mu} + (q^\mu - k^\mu)k^\nu - \mathrm{i}q_i k_j \varepsilon^{ij\nu\mu}. \tag{29}$$

Summation over the polarization states of the vector meson can be performed directly using the relation

$$\sum_\lambda \varepsilon^*_\alpha(p')\varepsilon_\beta(p') = -\left(g_{\alpha\beta} - \frac{p'_\alpha p'_\beta}{m^2_{h'_V}}\right). \tag{30}$$

We get

$$\begin{aligned}\sum_\lambda R^{\mu\nu}\mathbb{V}_\nu\mathbb{V}^*_\mu &= 8g^2(q^2)\left\{m_B^2[(p'k)^2 - m_D^2(qk)]\right. \\ &\quad \left. + m_D^2(pk)^2 + (pp')[-2(p'k)(pk) + (pp')(qk)]\right\}, \end{aligned} \tag{31}$$

$$\sum_\lambda R^{\mu\nu}\mathrm{i}(\mathbb{A}_\nu\mathbb{V}^*_\mu - \mathbb{V}_\nu\mathbb{A}^*_\mu) = 8g(q^2)f(q^2)[m_B^2(p'k) + m_D^2(pk) - (p'k + pk)(pp')], \tag{32}$$

Table 3. First part of the table with parameters of the form-factors (39)–(41) of B and D mesons decays into vector mesons [64–66].

h, h'	$f_V^{hh'}$	$f_{A_0}^{hh'}$	$f_{A_1}^{hh'}$	$f_{A_2}^{hh'}$	$\sigma_V^{hh'}$	$\sigma_{A_0}^{hh'}$	$\sigma_{A_1}^{hh'}$	$\sigma_{A_2}^{hh'}$
D, K^*	1.03	0.76	0.66	0.49	0.27	0.17	0.30	0.67
B, D^*	0.76	0.69	0.66	0.62	0.57	0.59	0.78	1.40

$$\sum_\lambda R^{\mu\nu}\mathbb{A}_\mu\mathbb{A}^*_\nu = -R^2(m_N^2 - qk)\left(m_B^2 - \frac{(pp')^2}{m_D^2}\right) + \frac{2(kR)(kR - qR)}{m_D^2} + 2f(q^2)\left[(kQ)(qR) + (kR)(qQ - 2kQ) + (RQ)(m_N^2 - qk)\right] + f^2(q^2)\left(\frac{2(p'k)(p'p - p'k)}{m_D^2} - m_N^2 + qk - 2p'k\right), \tag{33}$$

where

$$R_\mu = a_+(q^2)(p + p')_\mu + a_-(q^2)(p - p')_\mu, \qquad Q_\nu = \frac{(pp')}{m_D^2}p'_\nu - p_\nu. \tag{34}$$

Form-factors $f(q^2)$, $g(q^2)$, $a_\pm(q^2)$ can be found from the dimensionless linear combinations [64–66]:

$$V^{hh'}(q^2) = (m_h + m_{h'})\, g^{hh'}(q^2), \tag{35}$$

$$A_0^{hh'}(q^2) = \frac{1}{2m_{h'}}\left(f^{hh'}(q^2) + q^2 a_-^{hh'}(q^2) + \left(m_h^2 - m_{h'}^2\right) a_+^{hh'}(q^2)\right), \tag{36}$$

$$A_1^{hh'}(q^2) = \frac{f^{hh'}(q^2)}{m_h + m_{h'}}, \tag{37}$$

$$A_2^{hh'}(q^2) = -(m_h + m_{h'})\, a_+^{hh'}(q^2), \tag{38}$$

that can be parameterized as

$$V^{hh'}(q^2) = \frac{f_V^{hh'}}{1 - q^2/(M_V^h)^2[1 - \sigma_V^{hh'}q^2/(M_V^h)^2 - \xi_V^{hh'}q^4/(M_V^h)^4]}, \tag{39}$$

$$A_0^{hh'}(q^2) = \frac{f_{A_0}^{hh'}}{1 - q^2/(M_P^h)^2[1 - \sigma_{A_0}^{hh'}q^2/(M_V^h)^2 - \xi_{A_0}^{hh'}q^4/(M_V^h)^4]}, \tag{40}$$

$$A_{1/2}^{hh'}(q^2) = \frac{f_{A_{1/2}}^{hh'}}{1 - \sigma_{A_{1/2}}^{hh'}q^2/(M_V^h)^2 - \xi_{A_{1/2}}^{hh'}q^4/(M_V^h)^4}. \tag{41}$$

The best fit values of parameters are given in papers [64–66]. The parameters f and σ are given in table 3. The parameters ξ and the pole masses M_V, M_P are given in table 4, where $m_{D_s} = 1.969, m_{D_s^*} = 2.112, m_{B_c} = 6.275, m_{B_c^*} = 6.331$. The mass for B_c^* was taken from theoretical prediction [67].

Table 4. Second part of the table with parameters of the form-factors (39)–(41) of B and D mesons decays into vector mesons [64–66].

h, h'	$\xi_V^{hh'}$	$\xi_{A_0}^{hh'}$	$\xi_{A_1}^{hh'}$	$\xi_{A_2}^{hh'}$	M_P^h (GeV)	M_V^h (GeV)
D, K^*	0	0	0.20	0.16	m_{D_s}	$m_{D_s^*}$
B, D^*	0	0	0	0.41	m_{B_c}	$m_{B_c^*}$

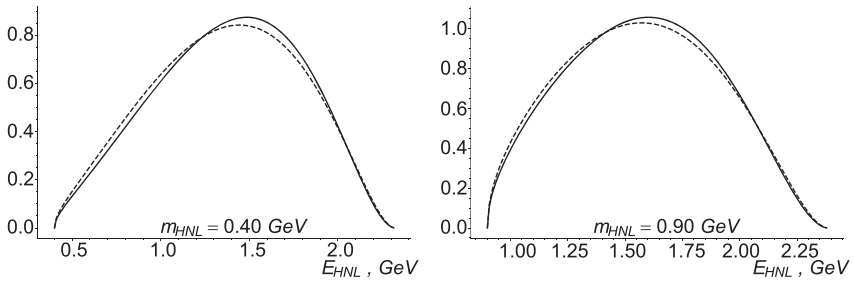

Figure 4. Probability density functions (PDF) for the energy of HNLs (in the rest frame of the initial meson) produced in the reaction $B^\pm \to D^0 + \ell^\pm + N$ computed exactly (solid line) and with the PYTHIA default matrix element for decays of B meson (2) (dashed line).

7. PDF for HNLs produced in three-body decays

In this paper, we consider HNL production in three-body decays of pseudoscalar B and D mesons into other pseudoscalar mesons, namely $B^\pm \to D^0 + \ell^\pm + N$ and $D^\pm \to K^0 + \ell^\pm + N$. Also we consider HNL production in three-body decays of pseudoscalar B and D mesons into vector mesons, namely $B^\pm \to D^*(2007)^0 + \ell^\pm + N$ and $D^\pm \to K^*(892) + \ell^\pm + N$. Two cases of leptons ($\ell = e,\ \mu$) in the final states are practically indistinguishable because of the small masses of electron and muon as compared with the masses of mesons in the reactions.

Let us compare the probability density function in the own frame of the initial meson for production of HNLs with a certain energy (E_N) computed with the help of relation (17) for the exact matrix elements (see section 5 and section 6) and for the parton level PYTHIA default matrix elements, see (1) and (2).

We see that the PDF computed exactly for the reaction of HNL production in the decay of the pseudoscalar meson B into the pseudoscalar meson D^0 is in good agreement with the PDF computed with the PYTHIA default matrix element for the decay of B mesons (2), see figure 4. But the PDF computed exactly for the reaction of the B meson decay into a vector meson $B^\pm \to D^*(2007)^0 + \ell^\pm + N$ is in good agreement not with the PDF computed with the PYTHIA default matrix element for decays of B mesons (2), but with the PDF computed with the PYTHIA default matrix element for decays of D mesons (1), see figure 5.

We see that the PDF computed exactly for the reaction of HNL production in the decay of the pseudoscalar meson D into the pseudoscalar meson K^0 is in good agreement not with the PDF computed with the PYTHIA default matrix element of the D meson decays (1), but with the PDF computed with the PYTHIA default matrix element for decays of B mesons (2), see figure 6. But the PDF computed exactly for the reaction of D meson decay into a vector meson

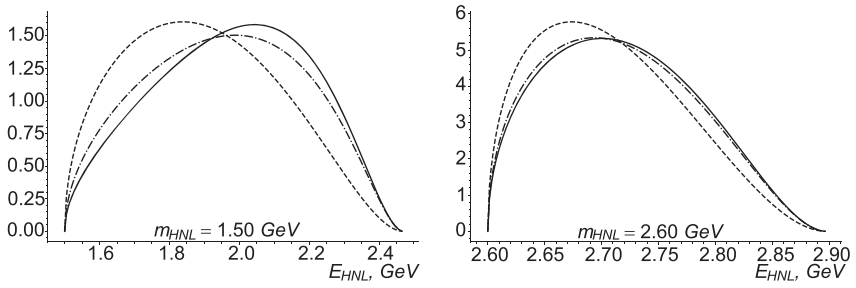

Figure 5. PDF for the energy of HNLs (in the rest frame of the initial meson) produced in the reaction $B^{\pm} \to D^{*}(2007)^{0} + \ell^{\pm} + N$ computed exactly (solid line), with the PYTHIA default matrix element for decays of B meson (2) (dashed line) and with the PYTHIA default matrix element for decays of D meson (1) (dot-dashed line).

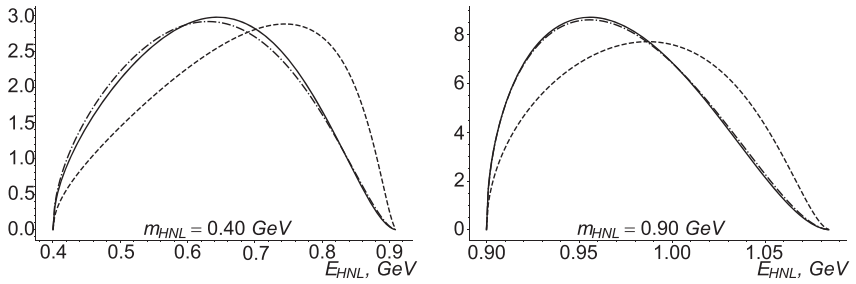

Figure 6. PDF for the energy of HNLs (in the rest frame of the initial meson) produced in the reaction $D^{\pm} \to K^{0} + \ell^{\pm} + N$ computed exactly (solid line) and with the PYTHIA default matrix element for decays of D meson (1) (dashed line) and with the PYTHIA default matrix element for decays of B meson (2) (dot-dashed line).

$D^{\pm} \to K^{*}(892) + \ell^{\pm} + N$ is in good agreement with the PDF computed with the PYTHIA default matrix element for decays of D mesons (1), see figure 7.

The result, at least for the initial B and D mesons, can be summarized as follows. The parton level PYTHIA default matrix element (2) works well for a pseudoscalar meson three-body decay into a pseudoscalar meson, a charged lepton and an HNL. The parton level PYTHIA default matrix element (1) works well for a pseudoscalar meson three-body decay into a vector meson, a charged lepton and an HNL.

An intriguing question is how the sufficiently large difference in the PDFs will affect the quantities necessary for calculating the sensitivity region, namely ϵ_{geom} and P_{decay}. We consider this question in sections 9 and 10.

8. Distribution functions

Data *Datah* for distribution of the produced h mesons (h stands for B or D mesons) in proton-target collisions (along axis z) in the SHiP experiment over the energy (E_h) and polar angle (θ_h) values were kindly provided by the SHIP collaboration. These data were obtained by using a

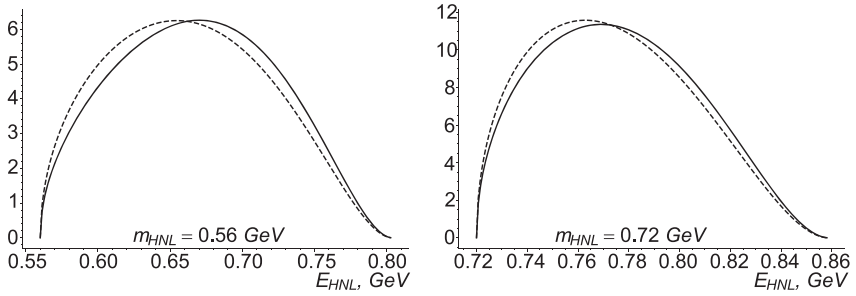

Figure 7. PDF for the energy of HNLs (in the rest frame of the initial meson) produced in the reaction $D^{\pm} \to K^*(892) + \ell^{\pm} + N$ computed exactly (solid line) and with the PYTHIA default matrix element for decays of D meson (1) (dashed line).

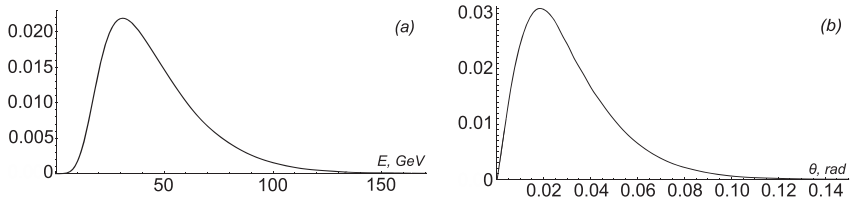

Figure 8. PDF for energy (a) and polar angle (b) in the laboratory frame for HNLs with mass 2.6 GeV produced in the reaction $B^{\pm} \to D^*(2007)^0 + \ell^{\pm} + N$.

tuned PYTHIA 6.4, see [68] for more details. In the following calculations, a data array with $a_B = 6.27 \times 10^5$ elements of type (E_B, θ_B) and a data array with $a_D = 10^6$ elements of type (E_D, θ_D) are used.

We use these data to calculate the distribution functions for the energy (E_N^{lab}) and the polar angle (θ_N^{lab}) of the produced HNLs in the laboratory frame with the help of Monte-Carlo simulation. Kinematic relations for HNLs between the laboratory and h meson's own reference frames are presented in appendix A. Corresponding relations contain dependence on two parameters of the h meson in the laboratory reference frame (the energy E_h and the polar angle θ_h) and four parameters of the HNL in the own reference frame of the h meson (the mass of the HNL m_N, the energy of the HNL E_N^{cm}, the polar and azimuth angles of the HNL θ_N^{cm}, φ_N^{cm}).

It should be noted that in the h meson's own reference frame, the energy of the HNL is defined by the energy probability distribution function (17), but directions of motion of the produced HNL are equiprobable because of the isotropic property of the h meson decay. So we take these parameters ($y = \cos\,\theta_N^{\text{cm}}$ and φ_N^{cm}) with randomly chosen values. A set of values (E_h, θ_h) is taken from the elements of *Datah* with a serial number that is taken in a random way. Thus we receive data (*DataN*) in a form $(E_N^{\text{lab}}, \theta_N^{\text{lab}})$.

Using the obtained data, we can now derive PDF and cumulative distribution functions for energy and polar angle for HNLs and for the initial h mesons also. As an example, we present the PDFs for energy and polar angle (computed via the matrix element from section 6) in the laboratory reference frame for HNLs with mass 2.6 GeV produced in reaction $B^{\pm} \to D^*(2007)^0 + \ell^{\pm} + N$, see figure 8.

Using the definition of the median value as a value corresponding to the cumulative distribution function equal to 1/2, we get the median values of energy and polar angle for the initial B and D mesons produced in the SHiP experiment, namely $\overline{E_B} \simeq 80$ GeV, $\overline{\theta_B} \simeq 0.022$ and $\overline{E_D} \simeq 16.5$ GeV, $\overline{\theta_D} \simeq 0.022$.

For the produced HNLs the corresponding median values depend on their masses and the reaction of their production. As an example, for an HNL with mass 2.6 GeV produced in the reaction $B^- \to D^*(2007)^0 + e^- + N$, see figure 8, the median values of energy and polar angle in the laboratory reference frame are $\overline{E_N} \simeq 40$ GeV and $\overline{\theta_N} \simeq 0.026$.

9. Factor ϵ_{geom}

In this section we consider the probability of a produced HNL to move toward the detector (ϵ_{geom}). To do this, we have to find the probability of the polar angle θ_N^{lab} of the produced HNL to be less than the angular size of the detector e.g. for the SHiP experiment $\theta_{\text{detector}} = 0.028$. It is just the value of the cumulative distribution function ($F_{N,\theta}$) for the polar angle of the HNL in the laboratory frame

$$\epsilon_{\text{geom}}(m_N) = F_{N,\theta}(m_N) = \int_0^{\theta_{\text{detector}}} \text{pdf}(m_N, \theta)\text{d}\theta, \tag{42}$$

where $\text{pdf}(m_N, \theta)$ is the PDF on polar angle θ of the HNL. Value of ϵ_{geom} depends on the mass of the HNL and the matrix element for its production.

The result of our computations can be presented in the following way. Factor ϵ_{geom} computed exactly (with the help of matrix elements presented in section 5 and section 6) for the reactions $B^\pm \to D^0 + \ell^\pm + N$ and $D^\pm \to K^*(892) + \ell^\pm + N$ is in good agreement (the relative difference is of order 1%–2% in the area to the right of the vertical dashed line) with factor ϵ_{geom} computed with the help of the parton level PYTHIA default matrix elements for decays of B and D mesons correspondingly, see line 1B of figure 9(a) and line 2D of figure 9(b). But for the reactions $B^\pm \to D^*(2007)^0 + \ell^\pm + N$ and $D^\pm \to K^0 + \ell^\pm + N$ it is more preferable to use the parton level PYTHIA default matrix elements for decays of D and B mesons correspondingly, see line 2D of figure 9(a) and line 1B of figure 9(b). It should be noted that a similar situation was for computations of PDFs in section 7. We emphasize that in figure 9(b) the experimentally interesting area is $m_{\text{HNL}} \gtrsim 0.5$ GeV (to the right of the vertical dashed line) and in figure 9(a) it is $m_{\text{HNL}} \gtrsim 2$ GeV (to the right of the vertical dashed line), see section 1.

As one can see from figure 9 the probabilities of a produced HNL to move towards the detector coincide ($\epsilon_{\text{geom}}^{\text{PYTH}} = \epsilon_{\text{geom}}$) for an HNL with the maximum kinetically allowed value of the mass. This is how it should be. In the case when an HNL has the maximum value of mass, the initial hadron in its own reference frame decays into three motionless particles. All these particles in the laboratory frame will move in the direction of the initial meson regardless of the matrix element type.

10. Factor P_{decay}

The number of the produced HNLs that can be detected during the period of the SHIP operation is defined by (9). This relation allows us to find the region of parameters (m_N, U_α), with which HNLs can be detected.

Behavior of the lower bound of this region for coupling constant (θ) can be estimated analytically. In this case arguments of the exponents in P_{decay} (10) are small and approximation

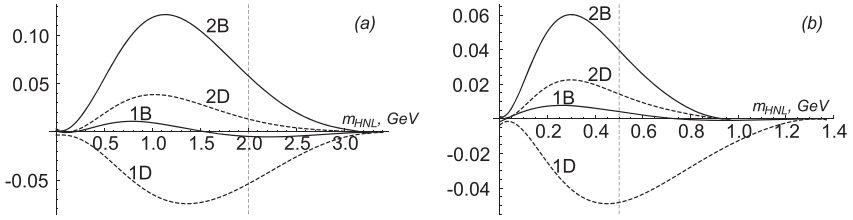

Figure 9. We present ratio $\frac{\epsilon^{\rm PYTH}_{\rm geom}-\epsilon_{\rm geom}}{\epsilon_{\rm geom}}$ for the produced HNLs. Figure (a) corresponds to the B meson decays (lines 1B and 1D: $B^{\pm}\to D^0+\ell^{\pm}+N$, lines 2B and 2D: $B^{\pm}\to D^*(2007)^0+\ell^{\pm}+N$). Figure (b) corresponds to the D meson decays (lines 1D and 1B: $D^{\pm}\to K^0+\ell^{\pm}+N$, lines 2D and 2B: $D^{\pm}\to K^*(892)+\ell^{\pm}+N$). Dashed line corresponds to computations via the PYTHIA matrix element (1). Solid line corresponds to computations via the PYTHIA matrix element (2). We are only interested in the area to the right of the vertical dashed line.

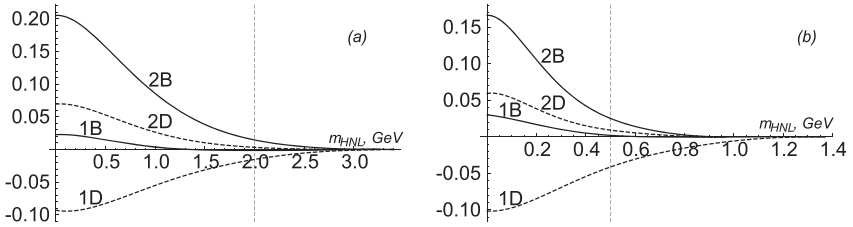

Figure 10. We present ratio $\frac{P^{\rm PYTH}_{\rm decay}-P_{\rm decay}}{P_{\rm decay}}$ for the produced HNLs. Figure (a) corresponds to the B meson decays (lines 1B and 1D: $B^{\pm}\to D^0+\ell^{\pm}+N$, lines 2B and 2D: $B^{\pm}\to D^*(2007)^0+\ell^{\pm}+N$). Figure (b) corresponds to the D meson decays (lines 1D and 1B: $D^{\pm}\to K^0+\ell^{\pm}+N$, lines 2D and 2B: $D^{\pm}\to K^*(892)+\ell^{\pm}+N$). Dashed line corresponds to computations via the PYTHIA matrix element (1). Solid line corresponds to computations via the PYTHIA matrix element (2). We are only interested in the area to the right of the vertical dashed line.

$e^x\simeq 1+x$ can be used and we get

$$P_{\rm decay}\approx \Delta L\cdot\Gamma\cdot X(E_N/m_N), \tag{43}$$

where $X(u)=(u^2-1)^{-1/2}$.

With the help of (43) we can easily obtain the ratio of $P_{\rm decay}$ computed for the exact matrix elements (see sections 5 and 6) and for the matrix elements in the PYTHIA approximation, see (1) and (2):

$$\frac{P^{\rm PYTH}_{\rm decay}}{P_{\rm decay}}=\frac{\tilde X^{\rm PYTH}(E_N/m_N)}{\tilde X(E_N/m_N)}, \tag{44}$$

where $\tilde X$ is the median value of the corresponding function X. The median value of the function X was found by computing the median of the set of the X-function values produced by Monte Carlo simulations, see section 8.

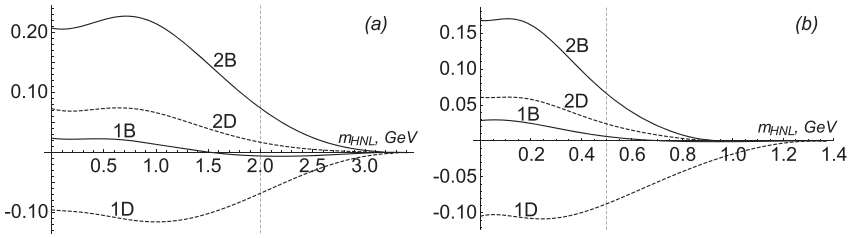

Figure 11. We present ratio $\frac{\epsilon_{\rm geom}^{\rm PYTH} P_{\rm decay}^{\rm PYTH} - \epsilon_{\rm geom} P_{\rm decay}}{\epsilon_{\rm geom} P_{\rm decay}}$ for HNLs produced in the three-body decays of mesons for the default PYTHIA matrix elements. Figure (a) corresponds to the B meson decays (lines 1B and 1D: $B^{\pm} \to D^0 + \ell^{\pm} + N$, lines 2B and 2D: $B^{\pm} \to D^*(2007)^0 + \ell^{\pm} + N$). Figure (b) corresponds to the D meson decays (lines 1D and 1B: $D^{\pm} \to K^0 + \ell^{\pm} + N$, lines 2D and 2B: $D^{\pm} \to K^*(892) + \ell^{\pm} + N$). Dashed line corresponds to computations via the PYTHIA matrix element (1). Solid line corresponds to computations via the PYTHIA matrix element (2). We are only interested in the area to the right of the vertical dashed line.

The results of our computations are similar to the results of the analysis of the $\epsilon_{\rm geom}$ factor. Factor $P_{\rm decay}$ computed exactly (with the help of the matrix elements presented in section 5) for the reactions $B^{\pm} \to D^0 + \ell^{\pm} + N$ is in good agreement (the relative difference is about 1% for $m_N \gtrsim 2$ GeV) with factor $P_{\rm decay}$ computed with the help of the parton level PYTHIA default matrix elements (2) for decays of B mesons, see line 1B of figure 10(a). Factor $P_{\rm decay}$ computed exactly (with the help of the matrix elements presented in section 6) for the reactions $D^{\pm} \to K^*(892) + \ell^{\pm} + N$ is in agreement (the relative difference less than 3% for $m_N \gtrsim 0.5$ GeV) with factor $P_{\rm decay}$ computed with the help of the parton level PYTHIA default matrix elements (1) for decays of D mesons, see line 2D of figure 10(b).

It should be noted that for the reactions $B^{\pm} \to D^*(2007)^0 + \ell^{\pm} + N$ and $D^{\pm} \to K^0 + \ell^{\pm} + N$ it is more preferable to use the parton level PYTHIA default matrix elements for decays of D and B mesons correspondingly, see line 2D of figure 10(a) and line 1B of figure 10(b). As in the case with $\epsilon_{\rm geom}$ we are only interested in the area to the right of the vertical dashed line.

11. Conclusions

There are some indisputable phenomena that point to the fact that the SM has to be modified and complemented by a new particle (particles). We are sure that new physics exists, but we do not know where to search for it. There are many theoretical possibilities to modify the SM, namely by scalar, pseudoscalar, vector, pseudovector, or fermion particles of new physics. These particles may be substantially heavier than the energy scale of the present colliders. However, they may also be light (with mass less than the electroweak scale) and feebly interact with the SM particles.

In this paper, we consider the HNL extension of the SM. We analyzed the relevance of using the parton level PYTHIA default matrix elements without additional tuning for describing GeV-scale HNL production in the most important three-body decays of B, D mesons that is a topical question for construction of the sensitivity region for the experimental search for HNLs. Our study was driven by the use of such an approximation in the SHiP collaboration paper [44]. We consider this question concerning the SHiP experiment, but our results are also applicable to other intensity Frontier experiments.

Some general conclusions can now be drawn. The computations of the three-body decays of τ leptons with HNL production in the PYTHIA approximation coincide with the exact computations, but the parton level PYTHIA default matrix elements for describing the three-body decays of mesons are just similar to the matrix elements for free quark electroweak decays. Despite this, we have shown that this PYTHIA approximation has the right to be used for construction of the sensitivity region for the experimental search for HNLs, provided one uses the suitable parton level PYTHIA default matrix elements.

We consider the case of three-body decays of B and D mesons into a light meson, an HNL and either an electron or a muon. These two cases of leptons in the final state are practically indistinguishable because of the small electron and muon masses as compared with the masses of mesons in the reactions. Reactions with τ leptons in the final state are either forbidden (for the decays of D mesons) or ineffective (as it was pointed in the introduction HNL production from B meson decays can be neglected for HNLs with masses $m_N \lesssim 2$ GeV).

As it was shown in section 3, explicit form of matrix elements for HNL production in a three-body decay affects factors ϵ_{geom} and P_{decay} (probabilities of the produced HNL to move toward the detector and to decay inside the vacuum tank before the detectors correspondingly) in the relation (9) that defines the sensitivity region of the intensity Frontier experiments.

In sections 9 and 10 we conducted a detailed analysis of factors ϵ_{geom} and P_{decay}. Summing up the results of this analysis, one can conclude that for the description of HNL production in a three-body decay of a pseudoscalar meson into another pseudoscalar meson ($B^{\pm} \to D^0 + \ell^{\pm} + N$ and $D^{\pm} \to K^0 + \ell^{\pm} + N$) the parton level PYTHIA matrix element (2) is better to use. For the description of HNL production in a three-body decay of a pseudoscalar meson into a vector meson ($B^{\pm} \to D^*(2007)^0 + \ell^{\pm} + N$ and $D^{\pm} \to K^*(892) + \ell^{\pm} + N$) the parton level PYTHIA matrix element (1) is better to use.

Actually, it is more important to analyze the product $\epsilon_{\text{geom}} \cdot P_{\text{decay}}$, which is included in the relation (9) that defines the sensitivity region for HNLs. Considering other factors in (9) fixed, this allows us to obtain the total error of the quantity N_{det}, which directly defines the accuracy of the sensitivity region construction. We demonstrate the discrepancies for $\epsilon_{\text{geom}} \cdot P_{\text{decay}}$ in figure 11. We emphasize that in figure 11(b) the experimentally interesting area is $m_{\text{HNL}} \gtrsim 0.5$ GeV (region to the left of the vertical dashed line is almost completely closed by experiments [19, 42]) and in figure 11(a) the interesting area is $m_{\text{HNL}} \gtrsim 2$ GeV, where the production of HNLs in B mesons decays is effective, see section 1.

One can see that if we use default matrix element (2) for both the considered decays of B meson (into $D^*(2007)$ as well as into D^0), we get quite a large maximum discrepancy $\simeq 7.3\%$ for the reaction $B^{\pm} \to D^*(2007)^0 + \ell^{\pm} + N$, see line 2B of figure 11(a). Similarly, if we use default matrix element (1) for decays of D meson into K^0 as well as into $K^*(892)$ we get quite a large maximum discrepancy $\simeq 8.8\%$ for reaction $D^{\pm} \to K^0 + \ell^{\pm} + N$, see line 1D of figure 11(b). This is just the case implemented by the SHiP collaboration.

We come to the conclusion that if, for some reasons, under computations for HNL production in three-body decays of mesons only default matrix elements are used, without additional tuning, it must be done in a more reasonable way. The most suitable choice of the parton level PYTHIA default matrix elements (1) and (2) is as shown by lines 1B and 2D for figures 11(a) and (b). With this choice, one can get, among all the considered B and D meson decays, the smallest difference with the exact matrix element for the reaction $D^{\pm} \to K^0 + \ell^{\pm} + N$ (the relative difference less than 0.6%), while the largest irremovable difference is for the reaction $D^{\pm} \to K^*(892) + \ell^{\pm} + N$ (the relative difference less than 2.4%).

To summarize, it can be noted at least for the initial B and D mesons that the parton level PYTHIA default matrix element (2) works well for a pseudoscalar meson three-body decay into a pseudoscalar meson, a charged lepton and an HNL. The parton level PYTHIA default

matrix element (1) works well for a pseudoscalar meson three-body decay into a vector meson, a charged lepton and an HNL. The interesting question of the possibility of generalizing this statement for other initial meson states requires further investigation.

It is important to note that the results of our research apply not only to physics beyond the SM but also for the SM processes of semileptonic decays of mesons, see figure 11 at zero HNL mass.

In no case should our research be considered as a call to use only the parton level PYTHIA default matrix elements instead of accurate calculations using additional tuning for PYTHIA. We just checked the possibility and correctness of using the default matrix elements approach.

Acknowledgments

The authors are grateful to Alexey Boyarsky for the statement of the problem and to Kyrylo Bondarenko for a useful discussion and helpful comments.

Data availability statement

The data that support the findings of this study are available upon reasonable request from the authors.

Appendix A. Useful kinematic relations for the HNLs in the different reference frames

Let us consider an h meson with mass m_h and a given four-momentum $(E_h,\ \vec{p}_h)$ in the laboratory reference frame. Its velocity in this reference frame (the origin of coordinates is at the point of proton-target collisions, axis z is directed to the center of detector) is

$$\vec{V}_h^{\,\mathrm{lab}} = |\vec{V}_h^{\,\mathrm{lab}}|\,\vec{e}_h^{\,\mathrm{lab}}, \tag{A.1}$$

where

$$|\vec{V}_h^{\,\mathrm{lab}}| = |\vec{p}_h|\left(m_h^2 + \vec{p}_h^{\,2}\right)^{-1/2}, \qquad \vec{e}_h^{\,\mathrm{lab}} = (\sin\theta_h\cos\varphi_h, \sin\theta_h\sin\varphi_h, \cos\theta_h). \tag{A.2}$$

θ_h and φ_h are the polar and azimuth angles of the h meson's velocity vector in spherical coordinate system.

The absolute value of the HNL's velocity in the center-of-mass system of the produced particles (own reference frame of the initial h meson) is

$$\vec{V}_N^{\,\mathrm{cm}} = |\vec{V}_N^{\,\mathrm{cm}}|\,\vec{e}_N^{\,\mathrm{cm}}, \tag{A.3}$$

where

$$|\vec{V}_N^{\,\mathrm{cm}}| = |\vec{p}_{N,\mathrm{cm}}|\left(m_N^2 + \vec{p}_{N,\mathrm{cm}}^{\,2}\right)^{-1/2},$$
$$\vec{e}_N^{\,\mathrm{cm}} = (\sin\theta_N^{\mathrm{cm}}\cos\varphi_N^{\mathrm{cm}}, \sin\theta_N^{\mathrm{cm}}\sin\varphi_N^{\mathrm{cm}}, \cos\theta_N^{\mathrm{cm}}). \tag{A.4}$$

θ_N^{cm} and φ_N^{cm} are the polar and azimuth angles of the HNL's velocity vector in the center-of-mass system. It should be noted that in the center-of-mass system of the produced particles the decay of the h meson is isotropic and the angles θ_N^{cm} and φ_N^{cm} can be arbitrary.

To find the value and the direction of the HNL's velocity in the laboratory reference frame we have to find the components of $\vec{V}_N^{\rm cm}$ that are parallel and perpendicular to the direction of $\vec{V}_h^{\rm lab}$, namely $\vec{V}_{N,\parallel}^{\rm cm}$ and $\vec{V}_{N,\perp}^{\rm cm}$.

It is obvious that $\vec{V}_{N,\parallel}^{\rm cm} = V_{N,\parallel}^{\rm cm}\,\vec{e}_h^{\rm lab}$, where

$$\begin{aligned} V_{N,\parallel}^{\rm cm} &= |\vec{V}_N^{\rm cm}|\,\vec{e}_h^{\rm lab}\cdot\vec{e}_N^{\rm cm} \\ &= |\vec{V}_N^{\rm cm}|(\sin\,\theta_N^{\rm cm}\,\sin\,\theta_h\,\cos(\varphi_h-\varphi_N^{\rm cm})+\cos\,\theta_N^{\rm cm}\,\cos\,\theta_h) \end{aligned} \tag{A.5}$$

is the projection of vector $\vec{V}_N^{\rm cm}$ on the direction $\vec{e}_h^{\rm lab}$. Its value can be either positive or negative.

Consider now vector $\vec{V}_{N,\perp}^{\rm cm} = |\vec{V}_{N,\perp}^{\rm cm}|\,\vec{e}_{N,\perp}^{\rm cm}$, where

$$|\vec{V}_{N,\perp}^{\rm cm}| = |\vec{V}_N^{\rm cm}|\,|\vec{e}_N^{\rm cm}\times\vec{e}_h^{\rm lab}|. \tag{A.6}$$

Vector $\vec{V}_{N,\perp}^{\rm cm}$ has to lie in the plane of vectors $\vec{V}_N^{\rm cm}$ and $\vec{V}_h^{\rm lab}$. The equation of this plane is $\vec{n}\cdot(\vec{r}-\vec{r}_0)=0$, where $\vec{n}$ is the normal vector of the plane $\vec{n}=\vec{e}_N^{\rm cm}\times\vec{e}_h^{\rm lab}$ and $\vec{r}-\vec{r}_0$ is vector lying in the plane. Radii $\vec{r}$ and $\vec{r}_0$ are meant to be taken with a base in the center of target. We put $\vec{r}_0$ (point of the h meson decay) to be a zero vector, because the distance between the point of production of meson and the point of its decay is very small compared with the distance from the target to the detector. As the vector $\vec{r}$ we can use the unit vector of direction $\vec{e}_{N,\perp}^{\rm cm}$.

Components of the unit vector $\vec{e}_{N,\perp}^{\rm cm} = (\tilde{\alpha},\tilde{\beta},\tilde{\gamma})$ have to satisfy the following equations

$$\begin{cases} \vec{e}_h^{\rm lab}\cdot\vec{e}_{N,\perp}^{\rm cm} = \tilde{\alpha}\,\sin\,\theta_h\,\cos\,\varphi_h+\tilde{\beta}\,\sin\,\theta_h\,\sin\,\varphi_h+\tilde{\gamma}\,\cos\,\theta_h=0, \\ n_x\tilde{\alpha}+n_y\tilde{\beta}+n_z\tilde{\gamma}=0, \\ \tilde{\alpha}^2+\tilde{\beta}^2+\tilde{\gamma}^2=1. \end{cases} \tag{A.7}$$

One can get the solution in the form $\vec{e}_{N,\perp}^{\rm cm} = \vec{N}/|\vec{N}|$, where $\vec{N}=(\alpha,\beta,\gamma)$,

$$\begin{aligned} \alpha &= \cos\,\theta_N^{\rm cm}\,\cos\,\theta_h\,\sin\,\theta_h\,\cos\,\varphi_h \\ &\quad -\sin\,\theta_N^{\rm cm}\left(\cos^2\theta_h\,\cos\,\varphi_N^{\rm cm}+\sin^2\theta_h\,\sin(\varphi_h-\varphi_N^{\rm cm})\sin\,\varphi_h\right), \\ \beta &= \cos\,\theta_N^{\rm cm}\,\cos\,\theta_h\,\sin\,\theta_h\,\sin\,\varphi_h \\ &\quad -\sin\,\theta_N^{\rm cm}\left(\cos^2\theta_h\,\sin\,\varphi_N^{\rm cm}-\sin^2\theta_h\,\sin(\varphi_h-\varphi_N^{\rm cm})\cos\,\varphi_h\right), \\ \gamma &= \sin\,\theta_h\left(\cos\,\theta_h\,\sin\,\theta_N^{cm}\,\cos(\varphi_h-\varphi_N^{\rm cm})-\sin\,\theta_h\,\cos\,\theta_N^{\rm cm}\right), \end{aligned} \tag{A.8}$$

and the normalized coefficient $|\vec{N}|$ is equal to $|\vec{e}_N^{\rm cm}\times\vec{e}_h^{\rm lab}|$. The obtained solution has ambiguity, because the system of equation (A.7) is invariant under simultaneous change of sign of all the vector's components. This ambiguity can be removed under the following condition. If scalar product $\vec{N}\cdot\vec{V}_N^{\rm cm}$ is positive the sign of vector $\vec{N}$ is correct, otherwise the sign of vector $\vec{N}$ has to be changed.

So, vector $\vec{V}_{N,\perp}^{\rm cm}$ is simply defined as

$$\vec{V}_{N,\perp}^{\rm cm} = \alpha|\vec{V}_{N,\perp}^{\rm cm}|\,\vec{e}_{N,\perp}^{\rm cm} = \alpha|\vec{V}_{N,\perp}^{\rm cm}|\,\vec{N}/|\vec{N}|, \qquad \alpha=\mathrm{sgn}[\vec{N}\cdot\vec{e}_N^{\rm cm}]. \tag{A.9}$$

Now we can find the value and the direction of the HNL's velocity in the laboratory reference frame

$$V_{N,\parallel}^{\rm lab} = \frac{|\vec{V}_h^{\rm lab}| + V_{N,\parallel}^{\rm cm}}{1 + V_{N,\parallel}^{\rm cm}\,|\vec{V}_h^{\rm lab}|}, \qquad \vec{V}_{N,\parallel}^{\rm lab} = V_{N,\parallel}^{\rm lab}\,\vec{e}_h^{\rm lab} \tag{A.10}$$

$$|\vec{V}_{N,\perp}^{\rm lab}| = |\vec{V}_{N,\perp}^{\rm cm}|\frac{\sqrt{1-|\vec{V}_h^{\rm lab}|^2}}{1 + \vec{V}_{N,\parallel}^{\rm cm}|\vec{V}_h^{\rm lab}|}, \qquad \vec{V}_{N,\perp}^{\rm lab} = \alpha|\vec{V}_N^{\rm cm}|\vec{N}, \tag{A.11}$$

$$|\vec{V}_N^{\rm lab}| = \sqrt{|\vec{V}_{N,\parallel}^{\rm lab}|^2 + |\vec{V}_{N,\perp}^{\rm lab}|^2}. \tag{A.12}$$

The components of the HNL's velocity vector $\vec{V}_N^{\rm lab}$ are

$$\begin{aligned}
(\vec{V}_N^{\rm lab})_x &= V_{N,\parallel}^{\rm lab}(\vec{e}_h^{\rm lab})_x + \alpha|\vec{V}_N^{cm}|(\vec{N})_x = |\vec{V}_N^{\rm lab}|\,\sin\,\theta_N^{\rm lab}\,\cos\,\varphi_N^{\rm lab},\\
(\vec{V}_N^{\rm lab})_y &= V_{N,\parallel}^{\rm lab}(\vec{e}_h^{\rm lab})_y + \alpha|\vec{V}_N^{\rm cm}|(\vec{N})_y = |\vec{V}_N^{\rm lab}|\,\sin\,\theta_N^{\rm lab}\,\sin\,\varphi_N^{\rm lab},\\
(\vec{V}_N^{\rm lab})_z &= V_{N,\parallel}^{\rm lab}(\vec{e}_h^{\rm lab})_z + \alpha|\vec{V}_N^{cm}|(\vec{N})_z = |\vec{V}_N^{\rm lab}|\,\cos\,\theta_N^{\rm lab},
\end{aligned} \tag{A.13}$$

where $(\vec{e}_h^{\rm lab})_i$ and $(\vec{N})_i$ are the components of vectors (A.2) and (A.8) and $\theta_N^{\rm lab}$, $\varphi_N^{\rm lab}$ are the angles of the HNL's velocity vector in the laboratory reference frame. The energy of the HNL in the laboratory reference frame is

$$E_N^{\rm lab} = m_N\left(1 - |\vec{V}_N^{\rm lab}|^2\right)^{-1/2}. \tag{A.14}$$

In this paper we assume that the experiment facility has a cylindrical symmetry. Therefore, the azimuth angle of the h meson in the laboratory reference frame can be set to zero ($\varphi_h = 0$). The energy $E_N^{\rm lab}$ and the direction of the HNL's velocity ($\theta_N^{\rm lab}$, $\varphi_N^{\rm lab}$) in the laboratory reference frame are defined only by six parameters: the energy E_h and the polar angle θ_h of the h meson in the laboratory reference frame, the two angles ($\theta_N^{\rm cm}$ and $\varphi_N^{\rm cm}$), the mass m_N and the energy $E_N^{\rm cm}$ of the produced HNL in the center-of-mass system of the produced particles (own reference frame of the h meson).

ORCID iDs

V M Gorkavenko https://orcid.org/0000-0002-9468-5105
Yu R Borysenkova https://orcid.org/0000-0003-1040-2815

References

[1] Glashow S L 1961 Partial-symmetries of weak interactions *Nucl. Phys.* **22** 579
[2] Weinberg S 1967 A model of leptons *Phys. Rev. Lett.* **19** 1264
[3] Salam A 1968 Weak and electromagnetic interactions *Proc. of 8th Nobel Symp.* ed N Svartholm (Stockholm: Almquist and Wiksells) p 367
[4] Bilenky S M 2014 Neutrino oscillations: brief history and present status *Proc. 22nd Int. Baldin Seminar on High Energy Physics Problems, Relativistic Nuclear Physics and Quantum Chromodynamics, (ISHEPP 2014)* (Dubna, Russia 15–20 September 2014) (arXiv:1408.2864)

[5] de Salas P F, Forero D V, Ternes C A, Tórtola M and Valle J W F 2018 Status of neutrino oscillations 2018: 3σ hint for normal mass ordering and improved CP sensitivity *Phys. Lett.* B **782** 633
[6] Peebles P J E 2013 Dark matter *Proc. Nat. Acad. Sci.* **112** 2246
[7] Lukovic V, Cabella P and Vittorio N 2014 Dark matter in cosmology *Int. J. Mod. Phys.* A **29** 1443001
[8] Bertone G and Hooper D 2018 A history of dark matter *Rev. Mod. Phys.* **90** 045002
[9] Brax P 2018 What makes the Universe accelerate? A review on what dark energy could be and how to test it *Rep. Prog. Phys.* **81** 016902
[10] Steigman G 1976 Observational tests of antimatter cosmologies *Annu. Rev. Astron. Astrophys.* **14** 339
[11] Strumia A and Vissani F 2010 Neutrino masses and mixings and… (arXiv:0606054 [hep-ph])
[12] Gorbunov D S and Rubakov V A 2011 *Introduction to the Theory of the Early Universe: Hot Big Bang Theory* (Singapore: World Scientific)
[13] Gorkavenko V M 2019 Search for hidden particles in intensity frontier experiment SHiP *Ukr. J. Phys.* **64** 689
[14] Beacham J *et al* 2020 Physics beyond colliders at CERN: beyond the standard model working group report *J. Phys. G: Nucl. Part. Phys.* **47** 010501
[15] Adams C *et al* (LBNE Collaboration) 2014 The long-baseline neutrino experiment: exploring fundamental symmetries of the universe (arXiv:1307.7335)
[16] Mermod P (SHiP Collaboration) 2017 Hidden sector searches with SHiP and NA62 *2017 Int. Workshop on Neutrinos from Accelerators (NuFact17)* (Uppsala, Sweden 25–30 September 2017) (Uppsala University Main Building) (arXiv:1712.01768)
[17] Cortina Gil E *et al* (NA62 Collaboration) 2018 Search for heavy neutral lepton production in K^+ decays *Phys. Lett.* B **778** 137
[18] Drewes M, Hajer J, Klaric J and Lanfranchi G 2018 NA62 sensitivity to heavy neutral leptons in the low scale seesaw model *J. High Energy Phys.* JHEP07(2018)105
[19] Alekhin S *et al* 2016 A facility to search for hidden particles at the CERN SPS: the SHiP physics case *Rep. Prog. Phys.* **79** 124201
[20] Anelli M *et al* (SHiP Collaboration) 2015 A facility to search for hidden particles (SHiP) at the CERN SPS (arXiv:1504.04956)
[21] Curtin D *et al* 2019 Long-lived particles at the energy frontier: the MATHUSLA physics case *Rep. Prog. Phys.* **82** 116201
[22] Patt B and Wilczek F 2006 Higgs-field portal into hidden sectors (arXiv:hep-ph/0605188)
[23] Bezrukov F and Gorbunov D 2010 Light inflaton Hunter's guide *J. High Energy Phys.* JHEP05(2010)010
[24] Boiarska I, Bondarenko K, Boyarsky A, Gorkavenko V, Ovchynnikov M and Sokolenko A 2019 Phenomenology of GeV-scale scalar portal *J. High Energy Phys.* JHEP11(2019)162
[25] Okun L B 1982 Limits of electrodynamics: paraphotons? *Sov. Phys. - JETP* **56** 502 https://inspirehep.net/literature/177918
[26] Holdom B 1986 Two U(1)'s and ϵ charge shifts *Phys. Lett.* B **166** 196
[27] Langacker P 2009 The physics of heavy Z′ gauge bosons *Rev. Mod. Phys.* **81** 1199
[28] Peccei R D and Quinn H R 1977 CP conservation in the presence of pseudoparticles *Phys. Rev. Lett.* **38** 1440
[29] Weinberg S 1978 A new light boson? *Phys. Rev. Lett.* **40** 223
[30] Wilczek F 1978 Problem of strong p and t invariance in the presence of instantons *Phys. Rev. Lett.* **40** 279
[31] Choi K, Im S H and Shin C S 2020 Recent progress in physics of axions or axion-like particles (arXiv:2012.05029)
[32] Anastasopoulos P, Bianchi M, Dudas E and Kiritsis E 2006 Anomalies, anomalous U(1)'s and generalized Chern-Simons terms *J. High Energy Phys.* JHEP11(2006)057
[33] Antoniadis I, Boyarsky A, Espahbodi S, Ruchayskiy O and Wells J D 2010 Anomaly driven signatures of new invisible physics at the large hadron collider *Nucl. Phys.* B **824** 296
[34] Fukugita M and Yanagida T 2002 Resurrection of grand unified theory baryogenesis *Phys. Rev. Lett.* **89** 131602
[35] Akhmedov E K, Rubakov V A and Smirnov A Y 1998 Baryogenesis via neutrino oscillations *Phys. Rev. Lett.* **81** 1359
[36] Asaka T and Shaposhnikov M 2005 The νMSM, dark matter and baryon asymmetry of the universe *Phys. Lett.* B **620** 17

[37] Shaposhnikov M 2008 The νMSM, leptonic asymmetries, and properties of singlet fermions *J. High Energy Phys.* JHEP08(2008)008
[38] Asaka T, Blanchet S and Shaposhnikov M 2005 The νMSM, dark matter and neutrino masses *Phys. Lett.* B **631** 151
[39] Boyarsky A, Ruchayskiy O and Shaposhnikov M 2009 The role of sterile neutrinos in cosmology and astrophysics *Annu. Rev. Nucl. Part. Sci.* **59** 191
[40] Boyarsky A, Ruchayskiy O, Iakubovskyi D and Franse J 2014 Unidentified line in X-ray spectra of the Andromeda galaxy and Perseus galaxy cluster *Phys. Rev. Lett.* **113** 251301
[41] Bulbul E, Markevitch M, Foster A, Smith R K, Loewenstein M and Randall S W 2014 Detection of an unidentified emission line in the stacked x-ray spectrum of galaxy clusters *Astrophys. J.* **13** 789
[42] Bondarenko K, Boyarsky A, Klaric J, Mikulenko O, Ruchayskiy O, Syvolap V and Timiryasov I 2021 An allowed window for heavy neutral leptons below the kaon mass (arXiv:2101.09255)
[43] Bondarenko K, Boyarsky A, Gorbunov D and Ruchayskiy O 2018 Phenomenology of GeV-scale heavy neutral leptons *J. High Energy Phys.* JHEP11(2018)032
[44] Ahdida C 2019 Sensitivity of the SHiP experiment to heavy neutral leptons *J. High Energy Phys.* JHEP02(2019)077
[45] Sjöstrand T, Mrenna S and Skands P 2008 A brief introduction to PYTHIA 8.1 *Comput. Phys. Commun.* **178** 852
[46] Sjöstrand T, Mrenna S and Skands P 2006 PYTHIA 6.4 physics and manual *J. High Energy Phys.* JHEP05(2006)026
[47] Bilenky S M and Petcov S T 1987 Massive neutrinos and neutrino oscillations *Rev. Mod. Phys.* **59** 671
[48] Ma E 1998 Pathways to naturally small neutrino masses *Phys. Rev. Lett.* **81** 1171
[49] Lazarides G, Shafi Q and Wetterich C 1981 Proton lifetime and fermion masses in an SO(10) model *Nucl. Phys.* B **181** 287
[50] Mohapatra R N and Senjanović G 1981 Neutrino masses and mixings in gauge models with spontaneous parity violation *Phys. Rev.* D **23** 165
[51] Schechter J and Valle J W F 1980 Neutrino masses in SU(2) $\otimes$ U(1) theories *Phys. Rev.* D **22** 2227
[52] Ma E and Sarkar U 1998 Neutrino masses and leptogenesis with heavy Higgs triplets *Phys. Rev. Lett.* **80** 5716
[53] Foot R, Lew H, He X-G and Joshi G C 1989 See-saw neutrino masses induced by a triplet of leptons *Z. Phys.* C **44** 441
[54] Mohapatra R N and Senjanović G 1980 Neutrino mass and spontaneous parity nonconservation *Phys. Rev. Lett.* **44** 912
[55] Yanagida T 1980 Horizontal symmetry and masses of neutrinos *Prog. Theor. Phys.* **64** 1103
[56] Gorkavenko V M and Vilchynskiy S I 2010 Some constraints on the Yukawa parameters in the neutrino modification of the Standard Model (νMSM) and CP-violation *Eur. Phys. J.* C **70** 1091
[57] Ahdida C *et al* 2019 The experimental facility for the search for hidden particles at the CERN SPS *J. Instrum.* **14** P03025
[58] Tanabashi M *et al* (Particle Data Group) 2019 *Phys. Rev.* D **98** 030001
[59] Källén G 1964 *Elementary Particle Physics* (*Addison-Wesley Series in Advanced Physics*) (Reading, MA: Addison-Wesley)
[60] Bourrely C, Lellouch L and Caprini I 2009 Model-independent description of $B \to \pi \ell \nu$ decays and a determination of $|V_{ub}|$ *Phys. Rev.* D **79** 013008
Bourrely C, Lellouch L and Caprini I 2010 *Phys. Rev.* D **82** 099902
[61] Aoki S *et al* 2020 FLAG review 2019: Flavour Lattice Averaging Group (FLAG) *Eur. Phys. J.* C **80** 113
[62] Na H, Bouchard C M, Lepage G P, Monahan C and Shigemitsu J 2015 $B \to D \ell \nu$ form factors at non-zero recoil and extraction of $|V_{cb}|$ *Phys. Rev.* D **92** 054510
Na H, Bouchard C M, Lepage G P, Monahan C and Shigemitsu J 2016 *Phys. Rev.* D **93** 119906
[63] Lubicz V, Riggio L, Salerno G, Simula S and Tarantino C 2017 Scalar and vector form factors of $D \to \pi(K) \ell \nu$ decays with $N_f = 2 + 1 + 1$ twisted fermions *Phys. Rev.* D **96** 054514
Lubicz V, Riggio L, Salerno G, Simula S and Tarantino C 2017 *Phys. Rev.* D **99** 099902
Lubicz V, Riggio L, Salerno G, Simula S and Tarantino C 2019 *Phys. Rev.* D **100** 079901
[64] Ebert D, Faustov R N and Galkin V O 2007 Analysis of semileptonic B decays in the relativistic quark model *Phys. Rev.* D **75** 074008

[65] Faustov R N and Galkin V O 2014 Relativistic description of weak decays of Bs mesons *AIP Conf. Proc.* **1701** 050020
[66] Melikhov D and Stech B 2000 Weak form factors for heavy meson decays: an update *Phys. Rev.* D **62** 014006
[67] Mathur N, Padmanath M and Lewis R 2016 Charmed-bottom mesons from lattice QCD *PoS LATTICE2016* p 100
[68] Dijkstra H and Ruf T (SHiP Collaboration) 2015 Heavy flavour cascade production in a beam dump *CERN-SHiP-NOTE-2015-009*

РОЗДІЛ 2

Поляризація енергії у вакуумі топологічним струноподібним об'єктом

2.1. Індукування енергії у вакуумі скалярного поля матерії у випадку граничної умови типу Діріхле

J. Phys. A: Math. Theor. **43** (2010) 175401 (12pp) doi:10.1088/1751-8113/43/17/175401

Polarization of the vacuum of a quantized scalar field by an impenetrable magnetic vortex of finite thickness

V M Gorkavenko[1], Yu A Sitenko[2] and O B Stepanov[1]

[1] Department of Physics, Taras Shevchenko National University of Kyiv, 64 Volodymyrs'ka str., Kyiv 01601, Ukraine
[2] Bogolyubov Institute for Theoretical Physics, National Academy of Sciences of Ukraine, 14-b Metrologichna str., Kyiv 03680, Ukraine

E-mail: gorka@univ.kiev.ua

Received 25 November 2009, in final form 2 March 2010
Published 13 April 2010
Online at stacks.iop.org/JPhysA/43/175401

Abstract
We consider the effect of the magnetic field background in the form of a tube of the finite transverse size on the vacuum of the quantized charged massive scalar field which is subject to the Dirichlet boundary condition at the tube. It is shown that if the Compton wavelength associated with the scalar field considerably exceeds the transverse size of the tube, then the vacuum energy which is finite and periodic in the value of the magnetic flux enclosed in the tube is induced on a plane transverse to the tube. Some consequences for generic features of the vacuum polarization in the cosmic-string background are discussed.

PACS numbers: 11.27.+d, 11.10.Kk, 11.15.Tk

1. Introduction

The emergence of calculable and detectable vacuum energy as a consequence of imposing external boundary conditions in quantum field theory was predicted more than 60 years ago by Casimir [1]. Since then the vacuum energy of fluctuating quantum fields that are subject to boundary conditions has been studied in various setups (see, e.g., reviews in [2–4]). Usually, the boundary manifold is chosen to be noncompact disconnected (e.g. two parallel infinite plates, as generically in [1]) or closed compact (e.g. box or sphere); see [2–4].

In the present paper, we shall consider the boundary manifold which is noncompact connected and has the form of an infinite tube in three-dimensional space. As has been first demonstrated by Aharonov and Bohm [5] in the framework of first-quantized theory, the magnetic flux enclosed in such a tube affects the properties of quantum matter outside the tube. This effect which is named after them has no analogues in classical physics and is characterized by the periodic dependence on the value of the flux, vanishing at integer multiples of the London flux value, while being maximal at half of the London flux value.

In the framework of second-quantized theory, one is interested in the vacuum polarization effects which are induced outside the tube by the magnetic flux enclosed in the tube. In particular, the question is whether the vacuum energy is induced. If this is the case, then this may be denoted as the Casimir–Bohm–Aharonov effect (see also [6]).

It should be noted that initially [5] the Bohm–Aharonov effect was considered under the assumption that the transverse size of the tube is zero, which corresponds to the singular magnetic vortex configuration. Taking into account the finite transverse size of the tube was an important task, since in reality a vortex-forming solenoid is of finite width[3]. This task was fulfilled once before, see [7, 8]. Although, unlike the case of a singular vortex, the quantum-mechanical problem in the case of a finite-thickness vortex is not exactly solvable, a thorough analysis has been carried out, and, in particular, it has been shown that the Bohm–Aharonov effect disappears at a sufficiently large thickness of an impenetrable magnetic vortex [7].

Returning to quantum field theory, and, appropriately, to the Casimir–Bohm–Aharonov effect, we note that up to now this effect was considered for the case of a singular magnetic vortex only [6, 9–11]. Therefore, the aim of the present paper is to make a first step in the study of the dependence on the thickness of an impenetrable magnetic vortex. It should be noted that vacuum polarization effects which are induced by magnetic fluxes of finite thickness were considered by different authors, see [12–16]. However, these authors are concerned with the case when there is no boundary at all and the region of the flux is penetrable for the quantized matter fields; therefore, the obtained results have no relation neither to the Casimir, nor to the Bohm–Aharonov effects. In the present paper we shall show that, similar to the Bohm–Aharonov effect, the Casimir–Bohm–Aharonov effect disappears at a sufficiently large thickness of the vortex. The second-quantized matter will be represented by the charged massive scalar field.

In the next section a general definition of the vacuum energy density for the quantized scalar field is reviewed and a starting expression for its renormalized value is given. In section 3 this value is calculated numerically in the case of $(2+1)$-dimensional space-time. Finally, the results are summarized and discussed in section 4.

2. Vacuum energy density

The operator of the quantized charged scalar field is represented in the form

$$\Psi(x^0, \boldsymbol{x}) = \sum\!\!\!\!\!\!\int_{\lambda} \frac{1}{\sqrt{2E_\lambda}} \left[\mathrm{e}^{-\mathrm{i}E_\lambda x^0} \psi_\lambda(\boldsymbol{x})\, a_\lambda + \mathrm{e}^{\mathrm{i}E_\lambda x^0} \psi_{-\lambda}(\boldsymbol{x})\, b_\lambda^\dagger \right], \tag{1}$$

where $a_\lambda^\dagger$ and a_λ $\left(b_\lambda^\dagger \text{ and } b_\lambda\right)$ are the scalar particle (antiparticle) creation and destruction operators satisfying commutation relations; the wavefunctions $\psi_\lambda(\mathbf{x})$ form a complete set of solutions to the stationary Klein–Gordon equation

$$(-\nabla^2 + m^2)\psi_\lambda(\boldsymbol{x}) = E_\lambda^2 \psi(\boldsymbol{x}), \tag{2}$$

where ∇ is the covariant derivative in an external (background) field and m is the mass of the scalar particle; λ is the set of parameters (quantum numbers) specifying the state; $E_\lambda = E_{-\lambda} > 0$ is the energy of the state; the symbol $\sum\!\!\!\!\!\!\int_{\lambda}$ denotes summation over discrete and integration (with a certain measure) over continuous values of λ.

[3] Also, a real solenoid is of finite length. However, in the case when the width of the solenoid is much smaller than its length and the motion of a quantum-mechanical particle is confined to a plane which is transverse to the solenoid, the effects of the width prevail over the effects of the length.

We are considering the static background in the form of the cylindrically symmetric magnetic vortex of finite thickness; hence, the covariant derivative is $\mathbf{\nabla} = \boldsymbol{\partial} - \mathrm{i}e\boldsymbol{V}$ with the vector potential possessing only one nonvanishing component given by

$$V_\varphi = \Phi/2\pi \tag{3}$$

outside the vortex; here, Φ is the vortex flux and φ is the angle in the polar (r, φ) coordinates on a plane which is transverse to the vortex. The Dirichlet boundary condition on the edge $(r = r_0)$ of the vortex is imposed on the scalar field:

$$\psi_\lambda|_{r=r_0} = 0, \tag{4}$$

i.e. quantum matter is assumed to be perfectly reflected from the thence impenetrable vortex. Provided the orthonormalization condition is satisfied,

$$\int \mathrm{d}^3x\ \psi^*_\lambda \psi_{\lambda'} = \langle\lambda|\lambda'\rangle, \tag{5}$$

the solution to (2) and (4) in the case of the impenetrable magnetic vortex of thickness $2r_0$ takes the form

$$\psi_{knk_z}(\boldsymbol{x}) = (2\pi)^{-1}\,\mathrm{e}^{\mathrm{i}k_z z}\,\mathrm{e}^{\mathrm{i}n\varphi}\beta_n(kr_0) \times [Y_{|n-e\Phi/2\pi|}(kr_0)J_{|n-e\Phi/2\pi|}(kr) - J_{|n-e\Phi/2\pi|}(kr_0)Y_{|n-e\Phi/2\pi|}(kr)], \tag{6}$$

where z is the coordinate along the vortex,

$$\beta_n(kr_0) = \left[Y^2_{|n-e\Phi/2\pi|}(kr_0) + J^2_{|n-e\Phi/2\pi|}(kr_0)\right]^{-1/2}, \tag{7}$$

and $0 < k < \infty$, $-\infty < k_z < \infty$, $n \in \mathbb{Z}$ ($\mathbb{Z}$ is the set of integer numbers); $J_\mu(u)$ and $Y_\mu(u)$ are the Bessel functions of order μ of the first and second kinds. It should be noted that the vortex can be obviously generalized to d-dimensional space by adding extra $d-3$ longitudinal coordinates to z; then factor $(2\pi)^{-1}\,\mathrm{e}^{\mathrm{i}k_z z}$ is changed to $(2\pi)^{\frac{1-d}{2}}\,\mathrm{e}^{\mathrm{i}\boldsymbol{k}_z \boldsymbol{z}}$, where $\boldsymbol{z}$ is the $(d-2)$-dimensional vector which is orthogonal to the (r, φ)-plane in d-dimensional space.

In general, the vacuum energy density is determined as the vacuum expectation value of the time–time component of the energy–momentum tensor, that is given formally by the expression

$$\varepsilon = \langle\mathrm{vac}|(\partial_0\Psi^+\partial_0\Psi + \partial_0\Psi\partial_0\Psi^+)|\mathrm{vac}\rangle = \sum\!\!\!\!\!\!\int_\lambda E_\lambda \psi^*_\lambda(\boldsymbol{x})\,\psi_\lambda(\boldsymbol{x}), \tag{8}$$

which is ill-defined, suffering from the ultraviolet divergencies: the momentum integral corresponding to the last expression in (8) diverges as p^{d+1} for $p \to \infty$. The well-defined quantity is obtained with the use of regularization and then renormalization procedures (see, e.g., [3]). As to regularization, one employs conventionally either heat-kernel or zeta-function methods (see, e.g., [2]). As to renormalization, it has been shown [17] that, for a specific configuration of a vortex through the excluded region, it suffices, irrespective of the number of spatial dimensions, to perform one subtraction, namely to subtract the contribution corresponding to the absence of the vortex. This fact owes to the symmetry in the problem, being of rather general nature. It is consistent, for instance, with a more recent result obtained in a quite different setup in paper [18], where the Casimir energy per unit length for n non-overlapping parallel cylinders of infinite length in three-dimensional space is shown to be directly related (without the need of an extra subtraction or an extra counter-term) to the Casimir energy for n non-overlapping discs in two-dimensional space.

Thus, the renormalized vacuum energy density in the case of the finite-thickness vortex takes the form

$$\varepsilon_{\mathrm{ren}} = (2\pi)^{1-d}\int \mathrm{d}^{d-2}k_z \int_0^\infty \mathrm{d}k\, k\left(\boldsymbol{k}_z^2 + k^2 + m^2\right)^{1/2}[S(kr, kr_0) - S(kr, kr_0)|_{\Phi=0}], \tag{9}$$

where, in view of (6),

$$S(kr, kr_0) = \sum_{n\in\mathbb{Z}} \beta_n^2(kr_0)[Y_{|n-e\Phi/2\pi|}(kr_0)J_{|n-e\Phi/2\pi|}(kr) - J_{|n-e\Phi/2\pi|}(kr_0)Y_{|n-e\Phi/2\pi|}(kr)]^2. \tag{10}$$

Owing to the infinite range of summation, the last expression is periodic in the flux Φ with period equal to $2\pi e^{-1}$, i.e. it depends on the quantity

$$F = \frac{e\Phi}{2\pi} - \left[\!\left[\frac{e\Phi}{2\pi}\right]\!\right], \tag{11}$$

where $[[u]]$ is the integer part of quantity u (i.e. the integer which is less than or equal to u).

Let us rewrite (10) in the form

$$S(kr, kr_0) = S_0(kr) + S_1(kr, kr_0), \tag{12}$$

where $S_0(kr)$ corresponds to the appropriate series in the case of the vacuum polarization by a singular magnetic vortex [9–11]:

$$S_0(kr) = \sum_{n=0}^{\infty}\left[J_{n+F}^2(kr) + J_{n+1-F}^2(kr)\right] = \int_0^{kr} \mathrm{d}\tau[J_F(\tau)J_{-1+F}(\tau) + J_{-F}(\tau)J_{1-F}(\tau)], \tag{13}$$

and $S_1(kr, kr_0)$ is a correction term due to the finite thickness of a vortex:

$$\begin{aligned} S_1(kr, kr_0) = 2\sum_{n=0}^{\infty}\Bigg[& J_{n+F}(kr_0)Y_{n+F}(kr)\frac{J_{n+F}(kr_0)Y_{n+F}(kr) - Y_{n+F}(kr_0)J_{n+F}(kr)}{J_{n+F}^2(kr_0) + Y_{n+F}^2(kr_0)} \\ & + J_{n+1-F}(kr_0)Y_{n+1-F}(kr)\frac{J_{n+1-F}(kr_0)Y_{n+1-F}(kr) - Y_{n+1-F}(kr_0)J_{n+1-F}(kr)}{J_{n+1-F}^2(kr_0) + Y_{n+1-F}^2(kr_0)}\Bigg] \\ & - \sum_{n=0}^{\infty}\Bigg[J_{n+F}^2(kr_0)\frac{J_{n+F}^2(kr) + Y_{n+F}^2(kr)}{J_{n+F}^2(kr_0) + Y_{n+F}^2(kr_0)} \\ & + J_{n+1-F}^2(kr_0)\frac{J_{n+1-F}^2(kr) + Y_{n+1-F}^2(kr)}{J_{n+1-F}^2(kr_0) + Y_{n+1-F}^2(kr_0)}\Bigg]. \end{aligned} \tag{14}$$

In the absence of the magnetic flux in the tube we have

$$S(kr, kr_0)|_{\Phi=0} = \tilde{S}_0 + \tilde{S}_1(kr, kr_0), \tag{15}$$

where

$$\tilde{S}_0 = J_0^2(kr) + 2\sum_{n=1}^{\infty} J_n^2(kr) = 1, \tag{16}$$

and a correction term due to the finite thickness of an empty tube:

$$\begin{aligned} \tilde{S}_1(kr, kr_0) = 2\Bigg[& J_0(kr_0)Y_0(kr)\frac{J_0(kr_0)Y_0(kr) - Y_0(kr_0)J_0(kr)}{J_0^2(kr_0) + Y_0^2(kr_0)} \\ & + 2\sum_{n=1}^{\infty} J_n(kr_0)Y_n(kr)\frac{J_n(kr_0)Y_n(kr) - Y_n(kr_0)J_n(kr)}{J_n^2(kr_0) + Y_n^2(kr_0)}\Bigg] \\ & - \Bigg[J_0^2(kr_0)\frac{J_0^2(kr) + Y_0^2(kr)}{J_0^2(kr_0) + Y_0^2(kr_0)} + 2\sum_{n=1}^{\infty} J_n^2(kr_0)\frac{J_n^2(kr) + Y_n^2(kr)}{J_n^2(kr_0) + Y_n^2(kr_0)}\Bigg]. \end{aligned} \tag{17}$$

Thus, vacuum energy density (9) depends on F (11), i.e. it is periodic in the flux Φ with a period equal to $2\pi e^{-1}$. Moreover, relation (9) is symmetric under the substitution $F \to 1 - F$,

vanishing at $F \to 0$ ($F \to 1$) and, perhaps, attaining its maximal value at $F = 1/2$.[4] Relations (13) and (14) are simplified at $F = 1/2$:

$$S_0(kr)|_{\Phi=\pi e^{-1}} = \frac{2}{\pi}\int_0^{2kr} \frac{\mathrm{d}\tau}{\tau}\sin\tau, \tag{18}$$

and

$$S_1(kr, kr_0)|_{\Phi=\pi e^{-1}} = 2\sum_{n=0}^{\infty} \frac{J^2_{n+\frac{1}{2}}(kr_0)\left[Y^2_{n+\frac{1}{2}}(kr) - J^2_{n+\frac{1}{2}}(kr)\right] - 2J_{n+\frac{1}{2}}(kr_0)Y_{n+\frac{1}{2}}(kr_0)J_{n+\frac{1}{2}}(kr)Y_{n+\frac{1}{2}}(kr)}{J^2_{n+\frac{1}{2}}(kr_0) + Y^2_{n+\frac{1}{2}}(kr_0)}. \tag{19}$$

Since it is hardly possible to evaluate sums in (14) and (17) analytically, our further analysis will employ numerical calculation. In the following we restrict ourselves to the case of $F = 1/2$ and $d = 2$, when the expression for the vacuum energy density takes the form

$$\varepsilon_{\mathrm{ren}} = \frac{1}{2\pi}\int_0^{\infty} \mathrm{d}k\, k(k^2 + m^2)^{1/2} G(kr, kr_0), \tag{20}$$

where

$$G(kr, kr_0) = S(kr, kr_0)|_{\Phi=\pi e^{-1}} - S(kr, kr_0)|_{\Phi=0}. \tag{21}$$

3. Numerical evaluation of the vacuum energy density

We rewrite (20) in the dimensionless form

$$r^3\varepsilon_{\mathrm{ren}} = \frac{1}{2\pi}\int_0^{\infty} \mathrm{d}z\, z\sqrt{z^2 + \left(\frac{mr_0}{\lambda}\right)^2}\, G(z, \lambda z), \tag{22}$$

where $\lambda = r_0/r$, $\lambda \in [0, 1]$. Let us point out some analytical properties of the integrand function in (22): it vanishes at the edge of the vortex

$$\lim_{\lambda\to 1} G(z, \lambda z) = 0; \tag{23}$$

at large distances from the vortex the case of a singular vortex is recovered:

$$\lim_{\lambda\to 0} G(z, \lambda z) = S_0(z)|_{\Phi=\pi e^{-1}} - \tilde{S}_0; \tag{24}$$

at small values of z one gets

$$G(z, \lambda z)|_{z\to 0} = -[\ln(\lambda)/\ln(\lambda z)]^2. \tag{25}$$

Numerical analysis indicates that in the calculation of the function $G(z, \lambda z)$ one can use series in (17) and (19) with finite limits, namely for calculating $G(z, \lambda z)$ at point $z = z'$ it is enough to cut off the summation limits by $n = [[z' + 30]]$. In this case the relative error is

$$\left|\frac{G(z, \lambda z)|_{n\in(0,[[z+30]])} - G(z, \lambda z)}{G(z, \lambda z)}\right| < \delta(\lambda), \qquad \delta(\lambda) < 10^{-17}, \qquad \lambda \in [1/10, 9/10]. \tag{26}$$

It can be shown that the envelope of $G(z, \lambda z)$ is an exponentially decreasing function at large z, see figure 1. So, for the finite-thickness magnetic vortex we can compute values of the

[4] At least, this is certainly true in the case of the singular vortex both for the Bohm–Aharonov [5] and the Casimir–Bohm–Aharonov [6, 9–11] effects.

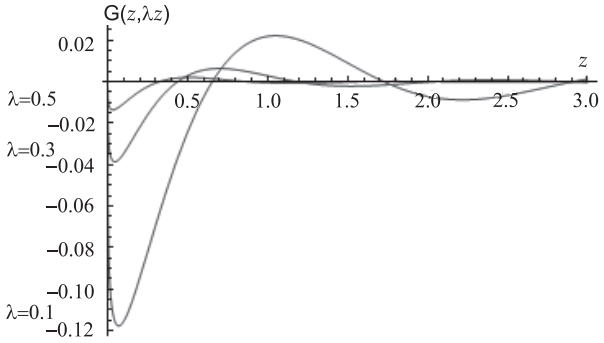

Figure 1. Behaviour of $G(z, \lambda z)$ at different values of λ.

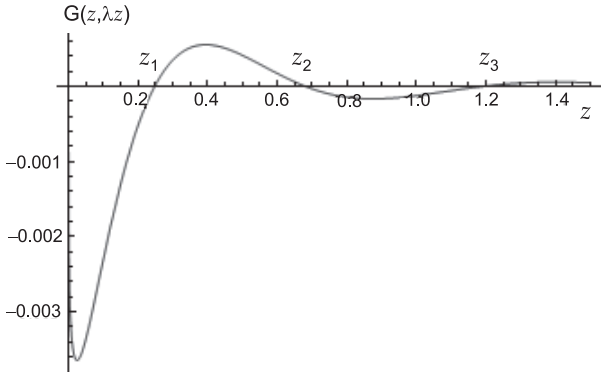

Figure 2. The location of roots of $G(z, \lambda z)$ at $\lambda = 0.7$.

dimensionless quantity $r^3\varepsilon_{\text{ren}}$ (22) for different (not very small) values of λ. To do this, we have to be able to perform integration in (22) with high precision. This is carried out in the following way.

As one can see from figure 2, the function $G(z, \lambda z)$ is negative from $z = 0$ to the first function root at $z = z_1$ ($z_1 \neq 0$). So, the appropriate integral in (22) is negative. The subsequent roots are denoted by z_2, z_3, etc. Because of the decreasing character of the envelope function the integral from z_1 to z_3 will be positive. It is useful to define a period of the function $G(z, \lambda z)$ as an interval between two next to neighbouring roots, i.e. from z_1 to z_3, from z_3 to z_5 and so on. Then the full integral in (22) will be a sum of the negative integral from $z = 0$ to $z = z_1$ and a multitude of positive integrals over subsequent periods. In the case of sufficiently small transverse size of the tube ($mr_0 < 0.1$) the integrals over some finite number of first periods may be negative but thereupon they become and remain positive also.

For small z ($z \lesssim 20$) we make a direct integration of the function $G(z, \lambda z)$ over periods using 25 digits of precision in internal computations.

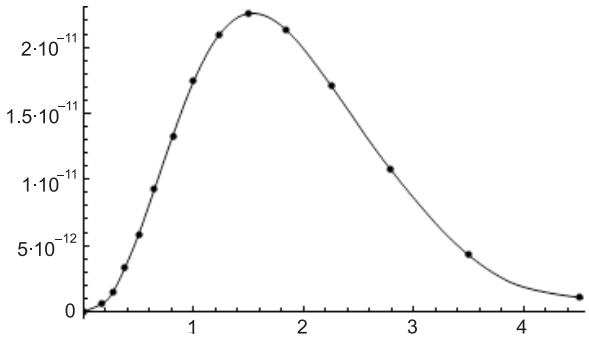

Figure 3. $r^3\varepsilon_{\rm ren}$ at $mr_0 = 3/2$ as a function of x.

For large z we make integration for each period separately. To carry this out we create a table of values of the function $G(z, \lambda z)$ for a separate period and replace this function by a more simple function in the form

$$G_{\rm int}(z, \lambda z) = a\frac{{\rm e}^{-bz}}{z^c}\frac{A_q(z^2)}{B_q(z^2)}\sin(kz + j\ln z + \phi_0), \tag{27}$$

where the sine function ensures that roots of $G_{\rm int}(z, \lambda z)$ coincide with roots of $G(z, \lambda z)$; $A_q(y)$ and $B_q(y)$ are q-degree polynomials, q can be 3, 4 or 5; all unknown parameters can be found from an interpolation procedure. We allow a relative error of interpolation to be

$$\left|\frac{G_{\rm int}(z, \lambda z) - G(z, \lambda z)}{G(z, \lambda z)}\right| < 10^{-8} \tag{28}$$

for each period. The function $G_{\rm int}(z, \lambda z)$ can be immediately integrated with the required accuracy. In this way we made integration up to $z \simeq 100/\lambda$ with an absolute accuracy up to 10^{-17}.

With the help of the above procedure we obtain a table of contributions from integration over each period, extrapolate this table to infinity and after that we find the full integral in (22) as a sum of the negative integral over first period(s), a multitude of positive integrals over periods up to $z \simeq 100/\lambda$ and an interpolation term. The absolute accuracy of the obtained result is 10^{-13}. It should be noted that nearly 99% of the integral value in (22) is obtained by direct calculation and only nearly 1% is the contribution from the interpolation.

The dimensionless quantity $r^3\varepsilon_{\rm ren}$ (22) is a function of two dimensionless parameters, mr_0 and mr. Using the above-described procedure, we calculate $r^3\varepsilon_{\rm ren}$ at several values of mr_0 as a function of the dimensionless distance from the edge of the vortex, $x = m(r - r_0)$, in the range $0 < x < 3mr_0$. Further increase of the distance from the vortex results in a significant increment of computational time, because there the envelope of $G(z, \lambda z)$ fails to be a sufficiently decreasing function as it is at smaller distances. The results of our numerical calculations are presented in figures 3–7, where $r^3\varepsilon_{\rm ren}$ is along the ordinate axis and x is along the abscissa axis; solid lines are interpolating the dots that have been calculated.

The typical behaviour of $r^3\varepsilon_{\rm ren}$ is clearly illustrated in cases $mr_0 \geqslant 1$ by figures 3 and 4. The vacuum energy density is zero at the edge of the vortex (at $x = 0$), starts increasing by some power law x^α with $\alpha > 1$, reaches maximum at $x \sim 1$ and decreases at larger distances to zero (probably exponentially as ${\rm e}^{-x}$). However, as mr_0 decreases, the available range of x is

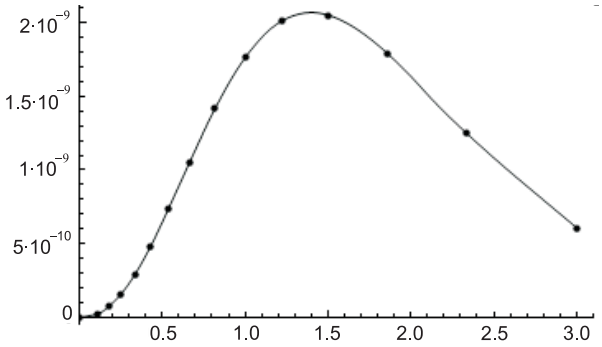

Figure 4. $r^3\varepsilon_{\rm ren}$ at $mr_0 = 1$ as a function of x.

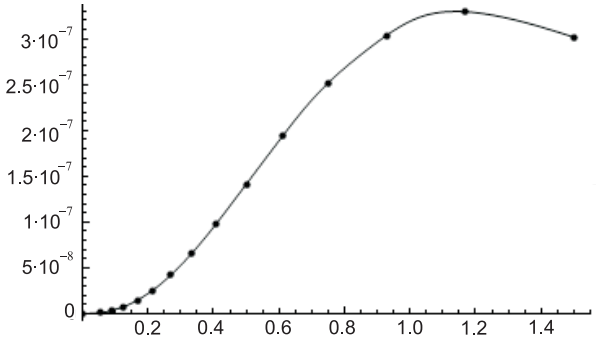

Figure 5. $r^3\varepsilon_{\rm ren}$ at $mr_0 = 1/2$ as a function of x.

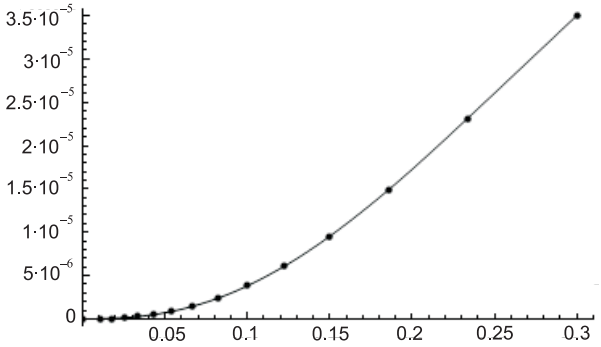

Figure 6. $r^3\varepsilon_{\rm ren}$ at $mr_0 = 10^{-1}$ as a function of x.

shrunk due to above-mentioned restriction $x < 3mr_0$. In the case of $mr_0 = 1/2$ a maximum at $x \sim 1$ is clearly seen (figure 5), and a following decrease to zero may be anticipated. In the

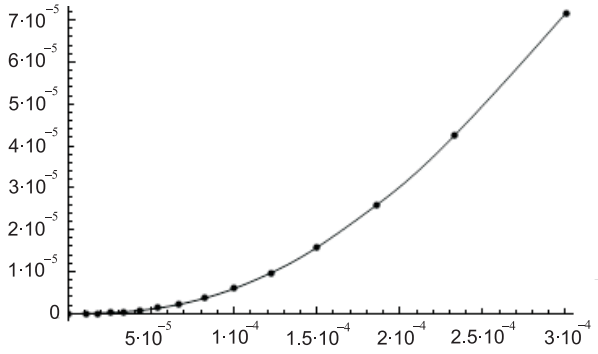

Figure 7. $r^3\varepsilon_{\rm ren}$ at $mr_0 = 10^{-4}$ as a function of x.

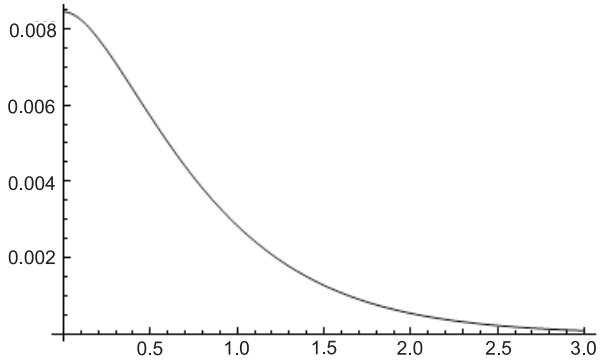

Figure 8. $r^3\varepsilon_{\rm ren}$ at $r_0 = 0$ as a function of mr.

cases of $mr_0 = 10^{-1}$ (figure 6) and $mr_0 = 10^{-4}$ (figure 7) one may suppose that there will be a maximum at $x \sim 1$ and a following decrease to zero. But, one can be sure for certain from figures 3–7 that the vacuum energy density decreases to zero as x^α with $\alpha > 1$ at $x \to 0$.

As to values of the vacuum energy density, they are rapidly decreasing as the parameter mr_0 increases and becomes more than unity. Namely, the maximal values of $r^3\varepsilon_{\rm ren}$ are 3.3×10^{-7} at $mr_0 = 1/2$ (figure 5), 2.1×10^{-9} at $mr_0 = 1$ (figure 4) and 2.2×10^{-11} at $mr_0 = 3/2$ (figure 3). These should be compared with much larger values which are already attained below maxima in figures 6 and 7: 3.5×10^{-5} at $mr_0 = 10^{-1}$ and 7×10^{-5} at $mr_0 = 10^{-4}$. It should be noted that, in the case of the singular vortex ($mr_0 = 0$), the maximal value of $r^3\varepsilon_{\rm ren}$ is $(12\pi^2)^{-1} \approx 8.5 \times 10^{-3}$ [9]; the appropriate plot of $r^3\varepsilon_{\rm ren}$ as a function of mr is taken from [11] and is presented in figure 8. Thus, one may suppose that, in the case of the vortex with thickness in the range $0 < mr_0 < 10^{-4}$, the maximal value of $r^3\varepsilon_{\rm ren}$ will be somewhere in the range 10^{-4}–10^{-3}. For more clarity, the results of figures 6 and 7 are plotted as functions of variable $r/r_0 = \lambda^{-1}$ in figure 9. Note that, as mr_0 falls by three orders from 10^{-1} to 10^{-4}, quantity $r^3\varepsilon_{\rm ren}$ changes by factor 2 only. This should be compared with $r^3\varepsilon_{\rm ren}$ at $m = 0$, which is plotted as a function of r/r_0 in figure 10; the latter plot coincides actually with that corresponding to $mr_0 = 10^{-4}$ in figure 9. It should be noted also that at sufficiently small

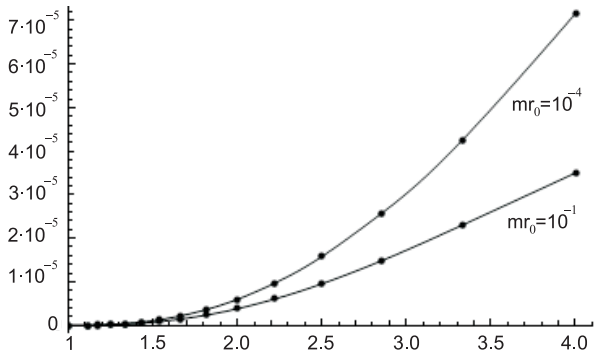

Figure 9. $r^3\varepsilon_{\rm ren}$ at the smallest values of mr_0 as a function of r/r_0.

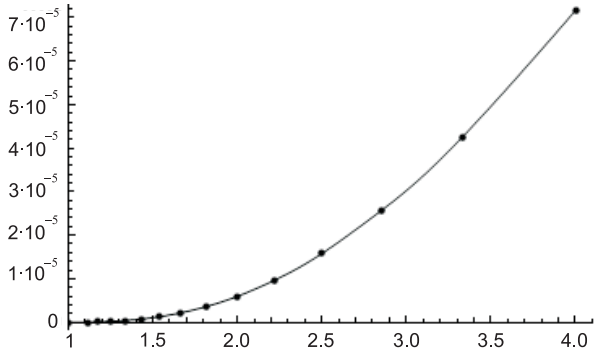

Figure 10. $r^3\varepsilon_{\rm ren}$ at $m = 0$ as a function of r/r_0.

distances from the vortex edge (at $r - r_0 \ll m^{-1}$) the behaviour of $r^3\varepsilon_{\rm ren}$ coincides with that in the $m = 0$ case.

4. Discussion of the results

We have studied the influence of finite thickness of the impenetrable magnetic vortex on the vacuum polarization of the quantized charged massive scalar field. Since units $c = \hbar = 1$ are used, the London flux value is $2\pi e^{-1}$, and we show that induced vacuum energy density (9) is periodic in the value of the vortex flux Φ, vanishing at integer multiples of the London flux value (at $\Phi = 2\pi n e^{-1}$) and being presumably maximal at half of the London flux value (at $\Phi = \pi(2n+1)e^{-1}$). If the vortex thickness decreases, $r_0 \to 0$, or a distance from the vortex increases, $r - r_0 \to \infty$, then the contribution of $S_1(kr, kr_0)$ (14) and $\tilde{S}_1(kr, kr_0)$ (17) to (9) tends smoothly to zero, and the vacuum energy density converges with that induced by the singular magnetic vortex.

Our numerical analysis of the vortex thickness effects has been carried out for the case of the vortex flux equal to half of the London flux value; the quantized scalar field is confined to a plane which is orthogonal to the vortex. As follows from this analysis, the vacuum

polarization actually disappears, when the transverse size of the vortex (r_0) exceeds the Compton wavelength of the scalar particle (m^{-1}): the maximal value of the induced vacuum energy density falls by two orders from $2.6 \times 10^{-10} m^3$ to $1.4 \times 10^{-12} m^3$ as mr_0 increases from 1 to 3/2.

This result should be compared with the influence of the vortex thickness on the conventional Bohm–Aharonov effect. In the framework of first-quantized theory, one considers elastic scattering of a quantum-mechanical charged particle on the impenetrable magnetic vortex of thickness $2r_0$. The incident wave is characterized by momentum p, so the dimensionless parameter of the problem is pr_0. In the long-wavelength limit, $pr_0 \to 0$, scattering converges with scattering on the singular magnetic vortex [8]. Since the short-wavelength limit, $pr_0 \to \infty$, corresponds to the case when quasi-classical approximation is applicable, one would anticipate that the purely quantum effect, as is the Bohm–Aharonov one, disappears in this limit. As it has been shown in [7], this anticipation is indeed confirmed, and scattering in the $pr_0 \to \infty$ limit converges with scattering of a classical point particle on the impenetrable tube, being independent of the enclosed magnetic flux.

In the framework of second-quantized theory, one considers the vacuum polarization in the background of the impenetrable magnetic vortex. The appropriate dimensionless parameter is mr_0, and, as we have shown in the present paper, the Casimir–Bohm–Aharonov effect disappears in the $mr_0 \to \infty$ limit becoming actually negligible at $mr_0 > 3/2$.

In the case of the singular magnetic vortex, the induced vacuum energy density diverges at the location of the vortex [6, 9–11]. As it has been shown in the present paper, this divergence is unphysical, disappearing when thickness of the impenetrable magnetic vortex is taken into account: under the Dirichlet condition for the quantized field (4), the induced vacuum energy density is vanishing as $(r - r_0)^\alpha$ with $\alpha > 1$ at the edge of the vortex. Therefore, the vacuum energy which is induced on the whole transverse plane,

$$E_{\mathrm{ren}} = 2\pi \int_{r_0}^{\infty} \mathrm{d}r\, r \varepsilon_{\mathrm{ren}}, \tag{29}$$

is finite, contrary to the case of the singular vortex when it is infinite. Although we are unaware of the value of E_{ren}, the maximal value of $\varepsilon_{\mathrm{ren}}$ is estimated to be somewhat of the order of $10^{-3} m^3$ if $mr_0 < 10^{-4}$.

A brief discussion of polarization of the vacuum of the quantized massless scalar field is in order. In this case, the induced vacuum energy density is zero at the edge of the vortex, starts increasing as $(r - r_0)^\alpha$ with $\alpha > 1$ (see figure 10), reaches its maximum and then decreases with asymptotics $(12\pi^2 r^3)^{-1}$ [9–11]. Induced vacuum energy (29) is finite in this case also.

The finite-thickness vortex can be formed as a topological defect appearing after a phase transition with spontaneous breakdown of the gauge symmetry [19]. Such a structure under the name of a cosmic string [20, 21] is currently discussed in various contexts in cosmology and astrophysics, see, e.g., [22, 23]. The cosmic string is characterized by the flux $2\pi e_{\mathrm{H}}^{-1}$, where e_{H} is the coupling constant of the Higgs scalar field to the string-forming gauge field; the transverse size of the string is of the order of correlation length m_{H}^{-1}, where m_{H} is the mass of the Higgs scalar field. Then, as it follows from our consideration in the present paper, the cosmic string can polarize the vacuum of quantum matter only in the case when the mass of the matter field is much less than that of the Higgs field, $m \ll m_{\mathrm{H}}$. For instance, the cosmic string which is formed at the grand unification scale can polarize the vacuum of the electroweak theory, whereas the would-be cosmic string corresponding to the electroweak symmetry breaking has no impact on the vacuum of quantum matter at the grand unification scale.

Acknowledgments

YAS acknowledges the support from the State Foundation for Fundamental Research under project F28.2/083 'Application of the string theory and the field theory methods to the study of nonlinear phenomena in low-dimensional systems' and from the National Academy of Science of Ukraine under project 10/07-N 'Study of physical properties of nanomaterials for electronics, photonics, spintronics and information technologies'.

References

[1] Casimir H B G 1948 *Proc. Kon. Ned. Akad. Wetenschap* B **51** 793
Casimir H B G 1953 *Physica* **19** 846
[2] Elizalde E 1995 *Ten Physical Applications of Spectral Zeta Functions* (Berlin: Springer)
[3] Mostepanenko V M and Trunov N N 1997 *The Casimir Effect and Its Applications* (Oxford: Clarendon)
[4] Bordag M, Mohideen U and Mostepanenko V M 2001 *Phys. Rep.* **353** 1
[5] Aharonov Y and Bohm D 1959 *Phys. Rev.* **115** 485
[6] Sitenko Yu A and Babansky A Yu 1998 *Mod. Phys. Lett.* A **13** 379
[7] Olariu S and Iovitzu Popescu I 1985 *Rev. Mod. Phys.* **57** 339
[8] Skarzhinsky V D 1986 *Trudy FIAN Proc. Lebedev. Inst.* **167** 139 (In Russian)
[9] Sitenko Yu A and Babansky A Yu 1998 *Phys. Atom. Nucl.* **61** 1594
[10] Sitenko Yu A and Gorkavenko V M 2003 *Ukrainian J. Phys.* **48** 1286
[11] Sitenko Yu A and Gorkavenko V M 2003 *Phys. Rev.* D **67** 085015
[12] Fry M P 1996 *Phys. Rev.* D **54** 6444
[13] Dunne G and Hall T M 1998 *Phys. Lett.* B **419** 322
[14] Bordag M and Kirsten K 1999 *Phys. Rev.* D **60** 105019
[15] Langfeld K, Moyaerts L and Gies H 2002 *Nucl. Phys.* B **646** 158
[16] Graham N, Khemani V, Quandt M, Schroeder O and Weigel H 2005 *Nucl. Phys.* B **707** 233
[17] Babansky A Yu and Sitenko Yu A 1999 *Theor. Math. Phys.* **120** 876
[18] Wirzba A 2008 *J. Phys. A: Math. Theor.* **41** 164003
[19] Abrikosov A A 1957 *Sov. Phys.—JETP* **5** 1174
[20] Vilenkin A and Shellard E P S 1994 *Cosmic Strings and Other Topological Defects* (Cambridge: Cambridge University Press)
[21] Hindmarsh M B and Kibble T W B 1995 *Rep. Prog. Phys.* **58** 477
[22] Polchinski J 2005 *Int. J. Mod. Phys.* A **20** 3413
[23] Sazhin M V, Khovanskaya O S, Capaccioli M, Longo L, Paolillo M, Covone G, Grogin N A and Schreier E J 2007 *Mon. Not. R. Astron. Soc.* **376** 1731

2.2. Індукування енергії у вакуумі скалярного поля матерії у випадку граничної умови Неймана

https://doi.org/10.15407/ujpe67.10.715

V.M. GORKAVENKO,[1] T.V. GORKAVENKO,[1] YU.A. SITENKO,[2,3]
M.S. TSARENKOVA [1]

[1] Taras Shevchenko National University of Kyiv, Ukraine
(64, Volodymyrs'ka Str., Kyiv 01601, Ukraine)
[2] Bogolyubov Institute for Theoretical Physics, Nat. Acad. of Sci. of Ukraine
(14-b, Metrologichna Str., Kyiv 03143, Ukraine)
[3] Donostia International Physics Center
(4, Paseo Manuel de Lardizabal, 20018 Donostia-San Sebastán, Gipuzkoa, Spain)

INDUCED VACUUM ENERGY DENSITY OF QUANTUM CHARGED SCALAR MATTER IN THE BACKGROUND OF AN IMPENETRABLE MAGNETIC TUBE WITH THE NEUMANN BOUNDARY CONDITION

We consider the vacuum polarization of a charged scalar matter field outside the tube with magnetic flux inside. The tube is impenetrable for quantum matter, and the perfectly rigid (Neumann) boundary condition is imposed at its surface. We write expressions for the induced vacuum energy density for the case of a space with arbitrary dimension and for an arbitrary value of the magnetic flux. We do the numerical computation for the case of a half-integer flux value in the London flux units and the (2 + 1)-dimensional space-time. We show that the induced vacuum energy of the charged scalar matter field is induced, if the Compton wavelength of the matter field exceeds the transverse size of the tube considerably. We show that the vacuum energy is periodic in the value of the magnetic flux of the tube, providing a quantum-field-theoretical manifestation of the Aharonov–Bohm effect. The dependencies of the induced vacuum energy upon the distance from the center of the tube for different values of its thickness are obtained. The results are compared to those obtained earlier in the case of the perfectly reflecting (Dirichlet) boundary condition. It is shown that the value of the induced vacuum energy density in the case of the Neumann boundary condition is greater than in the case of the Dirichlet boundary condition.

K e y w o r d s: vacuum polarization, Aharonov–Bohm effect, Casimir effect.

1. Introduction

More than 70 years ago, it was shown by Casimir [1] that the presence of external boundaries leads to changes in the vacuum energy density. First, two perfectly conducting plates at a very tiny distance apart were considered. It was shown that the difference between the vacuum expectation values leads to the emergence of a force of interaction between the plates. Since then, many setups with different shapes of boundaries' and materials have been considered. The boundary manifolds are usually chosen as a disconnected noncompact object (as the infinite plates) or, in other cases, a closed compact object (as a box or a sphere), see, e.g., [2–4]. However, there is another case that is interesting of its own accord: a connected noncompact object (e.g., an infinite tube).

As shown by Aharonov and Bohm in the framework of the first-quantized theory, see [5], the magnetic flux inside a cylindrical tube impenetrable for the matter field can interact with quantum matter outside the tube. The consequences arising from it in the framework of the second-quantized theory are the polarization of the vacuum and the induction of the vacuum current and magnetic flux outside the tube. The effect of the boundary condition at the surface of the impenetrable tube and the magnetic flux inside the tube on the vacuum of the matter field outside the tube has the name of the Casimir–Bohm–Aharonov effect [6]. The boundary condition

in this setup affects the matter field outside the tube essentially.

It should be noted the problem of vacuum polarization outside the impenetrable magnetic tube has numerous physical applications. In astrophysics, it can be considered as a model of the cosmic strings, that may have appeared in the early Universe as a result of phase transitions with spontaneous gauge symmetry breaking [7–10]. In condensed matter physics, it can be considered as a model of Abrikosov–Nielsen–Olesen vortex in superconductors of the second group, see, e.g., [11, 12] or as disclinations in nanoconical structures, see, e.g., [13–16].

It should be noted that, initially, the Bohm–Aharonov effect was considered under the assumption that the transverse size of the tube is zero, which corresponds to the singular magnetic vortex, see, e.g., [6, 17–25].

In this paper, we will consider the case of charged scalar matter. In the case of finite transverse size, impenetrable magnetic tube boundary conditions can be generically parametrized with the use of a family of boundary conditions of the Robin type

$$(\cos\theta\,\psi+\sin\theta\,r\partial_r\psi)|_{r_0}=0. \tag{1}$$

Here, the cases $\theta=0$ and $\theta=\pi/2$ correspond to the Dirichlet and Neumann boundary conditions, respectively. For the induced vacuum energy, the case of the Dirichlet boundary condition was considered in [26–28]. For the induced vacuum current and magnetic flux, the case of the Dirichlet boundary condition was considered in [29], the case of the Neumann boundary condition was considered in [30], and the general case for the arbitrary value of the parameter θ was considered in [31].

In this paper, we will focus on the vacuum polarization of the charged scalar matter outside the impenetrable finite-thickness magnetic tube with the Neumann boundary condition at its surface.

The paper is organized as follows. In the second section, we provide a general definition of the induced renormalized vacuum energy density for the quantized charged scalar field in the case of d-dimensional space. In the third section, using numerical methods, we compute the value of the induced vacuum energy density in the simplest case of $(2+1)$-dimensional space-time, namely outside the impenetrable tube (it is a ring in the 2-dimensional space) of radius r_0 and a magnetic flux inside it. In the fourth section, we summarize and discuss the results.

2. Energy Density

The Lagrangian for a complex scalar field ψ in the $(d+1)$-dimensional space-time has form

$$\mathcal{L}=(\nabla_\mu\psi)^*\,(\nabla^\mu\psi)-m^2\psi^*\psi, \tag{2}$$

where ∇_μ is the covariant derivative, and m is the mass of the scalar field. The operator of the quantized charged scalar field is represented in the form

$$\Psi(x^0,\mathbf{x})=\sum\!\!\!\!\!\!\int_\lambda \frac{1}{\sqrt{2E_\lambda}}\times \\ \times\left[e^{-iE_\lambda x^0}\psi_\lambda(\mathbf{x})\,a_\lambda+e^{iE_\lambda x^0}\psi^*_\lambda(\mathbf{x})\,b^\dagger_\lambda\right]. \tag{3}$$

Here, $a^\dagger_\lambda$ and a_λ ($b^\dagger_\lambda$ and b_λ) are the scalar particle (antiparticle) creation and annihilation operators satisfying the commutation relation; λ is the set of parameters (quantum numbers) specifying the state; $E_\lambda=E_{-\lambda}>0$ is the energy of the state; symbol $\sum\!\!\!\!\!\!\int_\lambda$ denotes the summation over discrete and the integration (with a certain measure) over continuous values of λ; wave functions $\psi_\lambda(\mathbf{x})$ are the solutions to the stationary equation of motion,

$$\left\{-\boldsymbol{\nabla}^2+m^2\right\}\psi_\lambda(\mathbf{x})=E^2_\lambda\psi(\mathbf{x}), \tag{4}$$

$\boldsymbol{\nabla}$ is the covariant differential operator in an external (background) field.

We are considering a static background in the form of a cylindrically symmetric gauge flux tube with finite transverse size. The coordinate system is chosen in such a way that the tube is along the z axis. The tube in the 3-dimensional space is obviously generalized to the $(d-2)$-tube in the d-dimensional space by adding extra $d-3$ dimensions as longitudinal ones. The covariant derivative is $\nabla_0=\partial_0$, $\boldsymbol{\nabla}=\boldsymbol{\partial}-\mathrm{i}\tilde{e}\,\mathbf{V}$ with $\tilde{e}$ being the coupling constant of dimension $m^{(3-d)/2}$, and the vector potential possessing only one nonvanishing component is given by

$$V_\varphi=\Phi/2\pi, \tag{5}$$

outside the tube; here, Φ is the value of the gauge flux inside the $(d-2)$-tube, and φ is the angle in polar (r,φ) coordinates on a plane that is transverse to the tube. The Neumann boundary condition at the

surface of the tube ($r = r_0$) is imposed on the scalar field:

$$\partial_r \psi_\lambda|_{r=r_0} = 0, \tag{6}$$

i.e., the surface of the flux tube is a perfectly rigid boundary for the matter field.

The solution of (4) satisfying the boundary condition (6) outside the impenetrable tube of radius r_0 takes the form

$$\psi_{kn\mathbf{p}}(\mathbf{x}) = (2\pi)^{(1-d)/2} e^{i\mathbf{p}\mathbf{x}_{\mathbf{d-2}}} e^{in\varphi} \Omega_{|n-\tilde{e}\Phi/2\pi|}(kr, kr_0), \tag{7}$$

where

$$\Omega_\rho(u,v) = \frac{Y'_\rho(v)J_\rho(u) - J'_\rho(v)Y_\rho(u)}{\left[J'^2_\rho(v) + Y'^2_\rho(v)\right]^{1/2}}, \tag{8}$$

and $0 < k < \infty$, $-\infty < p^j < \infty$ ($j = \overline{1, d-2}$), $n \in \mathbb{Z}$ ($\mathbb{Z}$ is the set of integer numbers), $J_\rho(u)$ and $Y_\rho(u)$ are the Bessel functions of order ρ of the first and second kinds, the prime near the function means a derivative with respect to the function argument. Solutions (7) obey the orthonormalization condition

$$\int\limits_{r>r_0} d^{\,d}\mathbf{x}\, \psi^*_{kn\mathbf{p}}(\mathbf{x}) \psi_{k'n'\mathbf{p}'}(\mathbf{x}) = \\ = \frac{\delta(k-k')}{k}\, \delta_{n,n'}\, \delta^{d-2}(\mathbf{p}-\mathbf{p}'). \tag{9}$$

The standard definition for vacuum energy density is the vacuum expectation value of the time-time component of the energy-momentum tensor

$$\varepsilon = \langle \mathrm{vac}| \left(\partial_0\Psi^+\partial_0\Psi + \partial_0\Psi\partial_0\Psi^+\right) |\mathrm{vac}\rangle = \\ = \sum\!\!\!\!\!\!\int_\lambda E_\lambda \psi^*_\lambda(\mathbf{x})\, \psi_\lambda(\mathbf{x}). \tag{10}$$

This relation suffers from ultraviolet divergencies. The well-defined quantity is obtained with the help of the regularization and then renormalization procedures, see, e.g., [3].

For the regularization, one can use the zeta-function method, see, e.g., [2, 32, 33], i.e., by inserting the inverse energy in a sufficiently high power

$$\varepsilon_{reg}(s) = \sum\!\!\!\!\!\!\int_\lambda E_\lambda^{-2s} \psi^*_\lambda(\mathbf{x})\, \psi_\lambda(\mathbf{x}). \tag{11}$$

The sums (integrals) are convergent in the case of $\mathrm{Re}\, s > d/2$. Thus, the summation (integration) is performed in this case, and then the result will be analytically continued to the case of $s = -1/2$.

In our case, the magnetic field configuration in the excluded region, irrespective of the number of spatial dimensions, the renormalization procedure is reduced to making one subtraction, namely to subtract the contribution corresponding to the absence of the magnetic flux, see [24].

Now, to compute the vacuum expectation value of the energy density, we have to substitute (7) into (11) and then obtain

$$\varepsilon_{\mathrm{ren}}(s) = (2\pi)^{1-d} \lim_{s\to -1/2} \int d^{d-2}p \int\limits_0^\infty dk\, k \times \\ \times \left(\mathbf{p}^2 + k^2 + m^2\right)^{-s} \left[S(kr, kr_0, \Phi) - S(kr, kr_0, 0)\right], \tag{12}$$

where

$$S(kr, kr_0, \Phi) = \sum_{n\in\mathbb{Z}} \Omega^2_{|n-\tilde{e}\Phi/2\pi|}(kr, kr_0). \tag{13}$$

Because of the infinite range of summation, the S-function will depend only on the fractional part of the flux

$$F = \frac{\tilde{e}\Phi}{2\pi} - \left[\!\left[\frac{\tilde{e}\Phi}{2\pi}\right]\!\right], \quad (0 \le F < 1), \tag{14}$$

where $[[u]]$ is the integer part of the quantity u (i.e., the integer which is less than or equal to u). So, we get

$$S(kr, kr_0, F) = \\ = \sum_{n=0}^{\infty} [\Omega^2_{n+F}(kr, kr_0) + \Omega^2_{n+1-F}(kr, kr_0)] \tag{15}$$

and conclude that the induced vacuum energy density (12) depends on F, i.e., it is periodic in the flux Φ with a period equal to $2\pi\tilde{e}^{-1}$. Moreover, the value of the induced vacuum energy density is symmetric under the substitution $F \to 1 - F$.

In the absence of a magnetic flux in the tube, the S-function takes the form

$$S(kr, kr_0, 0) = \Omega^2_0(kr, kr_0) + 2\sum_{n=1}^{\infty} \Omega^2_n(kr, kr_0). \tag{16}$$

Unfortunately, the computation of the vacuum energy density in the case of the finite-thickness magnetic tube can not be done analytically because of the complicated form of the ψ-function (7) and requires numerical methods.

3. Numerical Evaluation of Energy Density

In this paper, we will take the simplest situation of the $(2+1)$-dimensional space-time and consider the induced vacuum energy density outside the impenetrable tube (it is a ring in the 2-dimensional space) of radius r_0 with the Neumann boundary condition at its edge and with half-integer values of the magnetic flux $F = 1/2$ inside the tube. At this flux value, we expect the maximal effect of vacuum polarization by analogy with the case of singular magnetic vortex, see, e.g., [6, 25]. Based on the results of [26–28] on the computation of the induced vacuum energy density outside the magnetic impenetrable tube with the Dirichlet boundary condition at its edge, we can conclude that we can immediately take $s = -1/2$ in (12).

Let us now briefly discuss the main ideas of numerical calculations. Expression (12) is finite and can be evaluated numerically because of the possibility to restrict the upper limit of integration and summation in it. To make numerical computations in this case, it is better to use, instead of (12), the following relation for the dimensionless quantity

$$r^3\varepsilon_{\rm ren} = \frac{1}{2\pi}\int\limits_0^{z_{\max}} dz z\sqrt{z^2+\left(\frac{mr_0}{\lambda}\right)^2}\times$$
$$\times\sum_{n=0}^{n_{\max}(z)}[2\Omega^2_{n+1/2}(z,\lambda z)-\Omega^2_n(z,\lambda z)-\Omega^2_{n+1}(z,\lambda z)], \tag{17}$$

where we introduced a dimensionless variables

$$kr = z, \quad \lambda = r_0/r, \quad \lambda\in[0,1]. \tag{18}$$

The case of $\lambda = 1$ corresponds to $r = r_0$, i.e., the point on the boundary of the tube, the case of $\lambda = 0$ corresponds to the point on the infinity $r\to\infty$ or the case of a singular tube ($r_0 = 0$).

The necessary number of terms for the summation ($n_{\max}(z)$) is defined at the fixed value of the parameter z from the condition that the summation result with a high precision did not change with an increase in the number of terms.

For small values of z, we make a direct integration of the function in (17). For large values of z, we use another approach. The integrand function in this case is a quasiperiodic [1] oscillating function (with the change of sign) with the slowly decreasing amplitude with increasing its argument. So, it is convenient to integrate over these periods separately with the right value of the parameter $n_{\max}(z)$. In such a way we get a falling series, each element of which is the value of the integral over the single period of the function. Getting a sufficiently large number of the elements of the series, we stop integrating and interpolate the series forward. The final result of the integration is the sum of the integral for small values of z, the sum of the explicitly counted elements of the series, and the sum of interpolated series. If the contribution to the overall integration result from the sum of the interpolated series is a few percent or less, then the computation result can be considered reliable. In the next step, we compute $r^3\varepsilon_{\rm ren}$ (17) for different values of the parameter λ and interpolate the obtained results.

It should be noted that, in the case of a singular magnetic vortex, the analytic expressions for the induced vacuum energy density can be obtained [23, 25]. For the case of a $(2+1)$-dimensional space-time and a half-integer magnetic flux value $F = 1/2$, it is expressed in terms of the Macdonald function $K_\rho(u)$ and modified Struve function $L_\rho(u)$

$$r^3\varepsilon^{\rm sing}_{\rm ren} = \frac{x^3}{3\pi^2}\left\{\frac{\pi}{2}+\frac{K_0(2x)}{2x}-\left(1-\frac{1}{2x^2}\right)K_1(2x)-\right.$$
$$\left.-\pi x\left[K_0(2x)L_{-1}(2x)+K_1(2x)L_0(2x)\right]\right\}, \tag{19}$$

where $x = mr$.

The result of our computation for the induced vacuum energy density outside the impenetrable magnetic tube with the Neumann boundary condition at its edge is presented in Fig. 1 as a function of the dimensionless distance from the center of the tube (mr) for the different values of the dimensionless tube radius (mr_0). For the comparison, we demonstrate also the induced vacuum energy density for the case of a singular magnetic vortex.

It is of interest also to compare the obtained induced vacuum energy density with the case of vacuum polarization outside an impenetrable magnetic tube with perfectly reflecting (Dirichlet) boundary condition at its edge. The results of the comparison are presented in Fig. 2.

4. Summary

We obtained a general relation for the computation of the vacuum polarization of the quantized charged

[1] Value of the period slowly decreases, as the function argument increases.

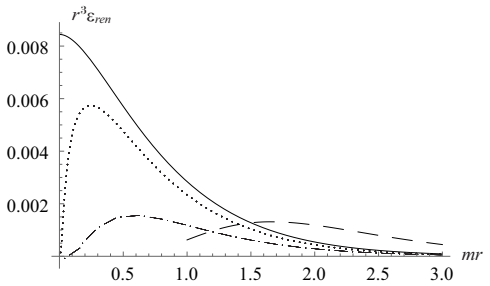

Fig. 1. Induced vacuum energy density of the charged scalar matter outside the impenetrable magnetic tube with the Neumann boundary condition at its edge for the (2+1)-dimensional space time and a half-integer magnetic flux value $F = 1/2$. Dotted line corresponds to the case of the dimensionless tube radius $mr_0 = 0.01$, dash-dotted line to the case of $mr_0 = 0.1$ and the dashed line corresponds to the induced vacuum energy density multiplied by 200, and $mr_0 = 1$. Solid line corresponds to the case of a singular magnetic vortex

scalar field in the background of a $(d-1)$-tube (it is an infinitely long tube for $d = 3$ and a ring for $d = 2$) with a static magnetic field inside in the flat $(d+1)$-dimensional space-time in the case where the tube is impenetrable for the scalar field and obeys perfectly rigid (Neumann) boundary conditions at its surface. We showed that the induced vacuum energy, in this case, (15) depends periodically on the magnetic flux inside the tube with a period equal to $2\pi\tilde{e}^{-1}$. The effect of the vacuum polarization disappears for an integer value of the magnetic flux $\Phi = 2\pi n\tilde{e}^{-1}$, $n \in \mathbb{Z}$. Thus, the induced vacuum energy depends only on the fractional part of the magnetic flux. We can see the manifestation of the Casimir–Bohm–Aharonov effect [6] in this case.

Our results confirm the statement that the Casimir–Bohm–Aharonov effect is due to the condition of the impenetrability of the tube for the matter field. Otherwise, namely in the case where a quantized matter penetrates into the region with a magnetic field, the dependence of the induced vacuum polarization effect on the magnetic flux is not periodic: the effect is determined by the value of the total magnetic flux in the tube, see, e.g., [34–40].

In the simplest case of the (2 + 1)-dimensional space-time, with the help of numerical methods, we compute the value of the vacuum energy density of the quantized charged scalar field outside the impenetrable tube of radius r_0 with the Neumann boundary

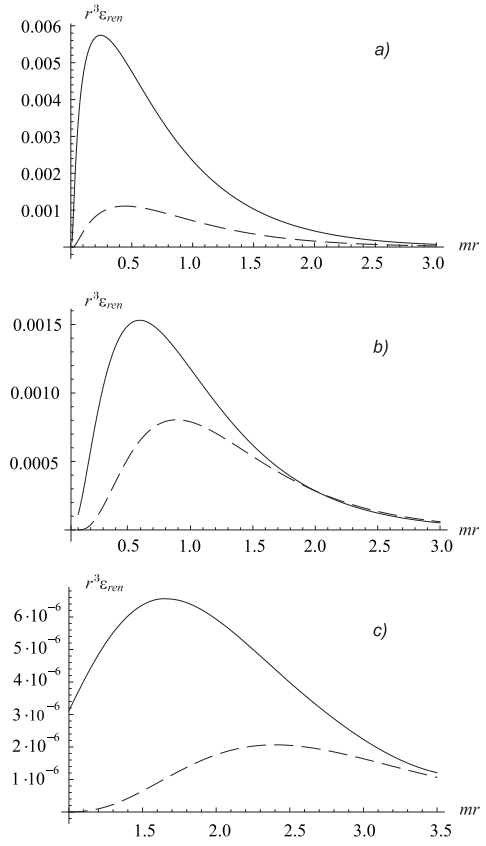

Fig. 2. Comparison of the induced vacuum energy density of the charged scalar matter outside the impenetrable magnetic tube with the Neumann (solid line) and Dirichlet (dashed line) boundary conditions at its edge for the case of a $(2+1)$-dimensional space-time and a half-integer magnetic flux value $F = 1/2$: $mr_0 = 0.01$ (a), $mr_0 = 0.1$ and the dashed line corresponds to the induced vacuum energy density multiplied by 10 (b), $mr_0 = 1$ and dashed line corresponds to the induced vacuum energy density multiplied by 1000 (c)

conditions at its edge. We chose a half-integer value of the magnetic flux $F = 1/2$ inside the tube. At this flux value, we expect the maximal effect of the vacuum polarization by analogy with the case of a singular magnetic vortex, see, e.g., [6, 25]. Without the regularization procedure, we made computations of the vacuum energy, but due to its renormalization by subtracting the contribution corresponding to the absence of the magnetic flux, see (17).

The results of our computations are presented in Fig. 1. One can see that, at the same dimensionless distance from the center of the tube (mr), the vacuum polarization effect is the largest in the case of the singular magnetic vortex and the exponentially quickly decrease with the growth of the tube radius. It should be noted that the effect of the vacuum polarization becomes negligible, when the radius of the tube is of order or more than the Compton wavelength of the matter field ($mr_0 \gtrsim 1$).

The comparison of the vacuum polarization in the case of the perfectly rigid (Neumann) and perfectly reflecting (Dirichlet) boundary conditions at the tube edge is presented in Fig. 2. One can see that, for the tubes of the same thickness, the vacuum polarization effect is always the largest in the case of the Neumann boundary condition. This result is in agreement with the result in [30] in the case of induced magnetic flux.

We need to pay attention to that the convergence of the integral under the computation of the induced vacuum energy density (17) in the case of the Neumann boundary condition at the tube edge is weaker than that in the case of the Dirichlet boundary condition. The complexity of the computations strongly increases with decreasing the tube thickness. We conclude that relation (17) based on the direct usage of the field solutions (7) is not suitable for the computations of the vacuum polarization outside the impenetrable thin tube ($mr_0 \ll 1$). In this case, more appropriate, in our opinion, should be the technique of computation with the help of a transformation in the complex plane, when the Bessel functions $J_\nu(y)$ and $Y_\nu(y)$ transform to the modified Bessel $I_\nu(y)$ and Macdonald $K_\nu(y)$ functions, see, e.g., [31].

The work of Yu.A.S. was supported by the National Academy of Sciences of Ukraine (Project No. 0122U000886).

1. H.B.G. Casimir. On the attraction between two perfectly conducting plates. *Proc. Kon. Ned. Akad. Wetenschap B* **51**, 793 (1948); *Physica* **19**, 846 (1953).
2. E. Elizalde. *Ten Physical Applications of Spectral Zeta Functions* (Springer-Verlag, 1995) [ISBN: 3-540-60230-5].
3. V.M. Mostepanenko, N.N. Trunov. *The Casimir effect and its applications* (Clarendon Press, 1997).
4. M. Bordag, U. Mohideen, V.M. Mostepanenko. New developments in the Casimir effect. *Phys. Rept.* **353**, 1 (2001).
5. Y. Aharonov, D. Bohm. Significance of Electromagnetic potentials in the quantum theory. *Phys. Rev.* **115**, 485 (1959).
6. Yu.A. Sitenko, A.Yu. Babansky. The Casimir–Aharonov–Bohm effect? *Mod. Phys. Lett. A* **13** (5), 379 (1998).
7. T.W.B. Kibble. Some implications of a cosmological phase transition. *Phys. Rep.* **67**, 183 (1980).
8. A. Vilenkin. Cosmic strings. *Phys. Rev. D* **24**, 2082 (1981).
9. A. Vilenkin, E.P.S. Shellard. *Cosmic Strings and Other Topological Defects* (Cambridge Univ. Press, Cambridge UK, 1994).
10. M.B. Hindmarsh, T.W.B. Kibble. Cosmic strings. *Rep. Progr. Phys.* **58**, 477 (1995).
11. A.A. Abrikosov. On the magnetic properties of superconductors of the second group. *Sov. Phys.-JETP* **5**, 1174 (1957).
12. H.B. Nielsen, P. Olesen. Vortex-line models for dual strings. *Nucl. Phys. B* **61**, 45 (1973).
13. A. Krishnan, E. Dujardin, M.M.J. Treacy, J. Hugdahl, S. Lynum, T.W. Ebbesen. Graphitic cones and the nucleation of curved carbon surfaces. *Nature* **388**, 451 (1997).
14. Yu.A. Sitenko, N.D. Vlasii. Electronic properties of graphene with a topological defect. *Nucl. Phys. B* **787**, 241 (2007).
15. S.N. Naess, A. Elgsaeetter, G. Helgesen, K.D. Knudsen. Carbon nanocones: Wall structure and morphology. *Sci. Technol. Adv. Mat.* **10**, 065002 (2009).
16. Yu.A. Sitenko, V.M. Gorkavenko. Properties of the ground state of electronic excitations in carbon-like nanocones. *Low Temp. Phys.* **44**, 1261 (2018) [Fiz. Nizk. Temp. 44, 1618 (2018)].
17. E.M. Serebrianyi. Vacuum polarization by magnetic flux: The Aharonov–Bohm effect. *Theor. Math. Phys.* **64**, 846 (1985) [*Teor. Mat. Fiz.* **64**, 299 (1985)].
18. P. Gornicki. Aharonov-bohm effect and vacuum polarization. *Ann. Phys. (N.Y.)* **202**, 271 (1990).
19. E.G. Flekkoy, J.M. Leinaas. Vacuum currents around a magnetic flux string. *Intern. J. Mod. Phys. A* **06**, 5327 (1991).
20. R.R. Parwani, A.S. Goldhaber. Decoupling in (2+1)-dimensional QED? *Nucl. Phys. B* **359**, 483 (1991).
21. Yu.A. Sitenko. Self-adjointness of the Dirac hamiltonian and fermion number fractionization in the background of a singular magnetic vortex. *Phys. Lett. B* **387**, 334 (1996).
22. Yu.A. Sitenko. Self-adjointness of the Dirac hamiltonian and vacuum quantum numbers induced by a singular external field. *Phys. Atom. Nucl.* **60**, 2102 (1997) [*Yad. Fiz.* **60**, 2285 (1997)].
23. Yu.A. Sitenko, A.Yu. Babansky. Effects of boson-vacuum polarization by a singular magnetic vortex. *Phys. Atom. Nucl.* **61**, 1594 (1998) [*Yad. Fiz.* **61**, 1706 (1998)].
24. A.Yu. Babanskii, Ya.A. Sitenko. Vacuum energy induced by a singular magnetic vortex. *Theor. Math. Phys.* **120**, 876 (1999).
25. Yu.A. Sitenko, V.M. Gorkavenko. Induced vacuum energy-momentum tensor in the background of a $(d-2)$-brane in

$(d+1)$-dimensional space-time. *Phys. Rev. D* **67**, 085015 (2003).

26. V.M. Gorkavenko, Yu.A. Sitenko, O.B. Stepanov. Polarization of the vacuum of a quantized scalar field by an impenetrable magnetic vortex of finite thickness. *J. Phys. A: Math. Theor.* **43**, 175401 (2010).
27. V.M. Gorkavenko, Yu.A. Sitenko, O.B. Stepanov. Vacuum energy induced by an impenetrable flux tube of finite radius. *Int. J. Mod. Phys. A* **26**, 3889 (2011).
28. V.M. Gorkavenko, Yu.A. Sitenko, O.B. Stepanov. Casimir energy and force induced by an impenetrable flux tube of finite radius. *Int. J. Mod. Phys. A* **28**, 1350161 (2013).
29. V.M. Gorkavenko, I.V. Ivanchenko, Yu.A. Sitenko. Induced vacuum current and magnetic field in the background of a vortex. *Int. J. Mod. Phys. A* 31, 1650017 (2016).
30. V.M. Gorkavenko, T.V. Gorkavenko, Yu.A. Sitenko, M.S. Tsarenkova. Induced vacuum current and magnetic flux in quantum scalar matter in the background of a vortex defect with the Neumann boundary condition. *Ukr. J. Phys.* **67**, 3 (2022).
31. Yu.A. Sitenko, V.M. Gorkavenko, M.S. Tsarenkova. Magnetic flux in the vacuum of quantum bosonic matter in the cosmic string background. *Phys. Rev. D* **106**, 105010 (2022).
32. J.S. Dowker, R. Critchley. Effective Lagrangian and energy-momentum tensor in de Sitter space. *Phys. Rev. D.* **13**, 3224 (1976).
33. S.W. Hawking. Zeta function regularization of path integrals in curved spacetime. *Commun. Math. Phys.* **55**, 133 (1977).
34. D. Cangemi, G. Dunne, E. D'Hoker. Effective energy for $(2+1)$-dimensional QED with semilocalized static magnetic fields: A solvable model. *Phys. Rev. D.* **52**, 3163 (1995).
35. M.P. Fry. QED in inhomogeneous magnetic fields. *Phys. Rev. D* **54**, 6444 (1996).
36. G. Dunne and T.M. Hall. An exact QED_{3+1} effective action. *Phys. Lett. B* **419**, 322 (1998).
37. M. Bordag and K. Kirsten. The ground state energy of a spinor field in the background of a finite radius flux tube. *Phys. Rev. D* **60**, 105019 (1999).
38. M. Scandurra. Vacuum energy in the presence of a magnetic string with a delta function profile. *Phys. Rev. D.* **62**, 085024 (2000).
39. K. Langfeld, L. Moyaerts, H. Gies. Fermion induced quantum action of vortex systems. *Nucl. Phys. B* **646**, 158 (2002).
40. N. Graham, V. Khemani, M. Quandt, O. Schroeder, H. Weigel. Quantum QED flux tubes in 2+1 and 3+1 dimensions. *Nucl. Phys. B* **707**, 233 (2005).

Received 24.11.22

В.М. Горкавенко, Т.В. Горкавенко,
Ю.А. Ситенко, М.С. Царенкова

ІНДУКОВАНА ГУСТИНА ЕНЕРГІЇ ВАКУУМУ КВАНТОВАНОЇ ЗАРЯДЖЕНОЇ СКАЛЯРНОЇ МАТЕРІЇ В ПРИСУТНОСТІ НЕПРОНИКНОЇ МАГНІТНОЇ ТРУБКИ З ГРАНИЧНОЮ УМОВОЮ ТИПУ НЕЙМАНА

В роботі досліджується поляризація вакууму зарядженого скалярного поля матерії зовні трубки, яка містить магнітний потік та є непроникливою для квантованої матерії. На поверхні трубки накладено граничну умову типу Неймана. Записано вирази для індукованої густини енергії вакууму у випадку простору довільної вимірності та при довільному значенні магнітного потоку. Проведено чисельні розрахунки для випадку напівцілого значення магнітного потоку в одиницях Лондона у $(2+1)$-вимірному просторі-часі. Показано, що індукування енергії вакууму зарядженої скалярної матерії відбувається за умови, якщо комптонівська довжина хвилі поля матерії набагато перевищує поперечний розмір трубки. Показано, що енергія вакууму періодична по відношенню до значення магнітного потоку в трубці, що є квантовотеоретичним проявом ефекту Ааронова–Бома. Отримано залежності індукованої енергії вакуума від відстані до центру трубки при різних значеннях товщини трубки. Отримані результати було порівняно з результатами, отриманими раніше для випадку граничної умови типу Діріхле. Показано, що значення індукованої густини енергії вакууму у випадку граничної умови типу Неймана більші, ніж у випадку граничної умови типу Діріхле.

Ключові слова: поляризація вакууму, ефект Ааронова–Бома, ефект Казимира.

2.3. Поляризація вакууму скалярного поля матерії з урахуванням сталої зв'язку скалярного поля з кривизною простору-часу

International Journal of Modern Physics A
Vol. 26, No. 22 (2011) 3889–3899

DOI: 10.1142/S0217751X11054346

VACUUM ENERGY INDUCED BY AN IMPENETRABLE FLUX TUBE OF FINITE RADIUS

V. M. GORKAVENKO
Department of Physics, Taras Shevchenko National University of Kyiv, 64 Volodymyrs'ka str., Kyiv 01601, Ukraine
gorka@univ.kiev.ua

YU. A. SITENKO
Bogolyubov Institute for Theoretical Physics, National Academy of Sciences of Ukraine, 14-b Metrologichna str., Kyiv 03680, Ukraine
yusitenko@bitp.kiev.ua

O. B. STEPANOV
Bogolyubov Institute for Theoretical Physics, National Academy of Sciences of Ukraine, 14-b Metrologichna str., Kyiv 03680, Ukraine
pnd@ukr.net

Received 10 June 2011

We consider the effect of the magnetic field background in the form of a tube of the finite transverse size on the vacuum of the quantized charged massive scalar field which is subject to the Dirichlet boundary condition at the edge of the tube. The vacuum energy is induced, being periodic in the value of the magnetic flux enclosed in the tube. The dependence of the vacuum energy density on the distance from the tube and on the coupling to the space-time curvature scalar is comprehensively analyzed.

Keywords: Vacuum polarization; Casimir effect; magnetic vortex.

PACS numbers: 11.27.+d, 11.10.Kk, 11.15.Tk

1. Introduction

The energy which is induced in the vacuum of quantized matter fields that are subject to boundary conditions has been studied intensively over more than six decades since Casimir[1] predicted a force between grounded metal plates, see reviews in Refs. 2 and 3. The induced vacuum energy in bounded spaces gives rise to a macroscopic force between bounding surfaces. The Casimir force between grounded metal plates has now been measured quite accurately and agrees with his predictions, see, e.g. Refs. 4 and 5, as well as other publications cited in Refs. 2 and 3.

In the present paper we study the vacuum energy which is induced by boundary conditions in space that is not bounded but, instead, is not simply connected, being

an exterior to a straight infinitely long tube. This setup is inspired by the famous Aharonov-Bohm effect,[6] and we are interested in polarization of the vacuum which is due to imposing a boundary condition at the edge of the tube carrying magnetic flux lines inside itself.

Throughout the present paper, we restrict ourselves to the case of quantized scalar matter. A peculiarity of this case is that the energy-momentum tensor depends on the coupling (ξ) of the scalar field to the scalar curvature of space-time even then when space-time is flat. If scalar field is massless, then conformal invariance of the theory is achieved at $\xi = \xi_c$, where[7–9]

$$\xi_c = \frac{d-1}{4d}\,, \tag{1}$$

and d is the spatial dimension; note that ξ_c varies from 0 to 1/4 when d varies from 1 to ∞. Up to now the study was restricted to the case of a singular magnetic vortex only,[10–13] i.e. when the transverse size of the flux-carrying tube is neglected. Therefore, the aim of the present paper is to take account of nonzero transverse size of the flux-carrying tube (for a preliminary study, see Ref. 14).

2. Vacuum Energy Density

The operator of the quantized charged scalar field is represented in the form

$$\Psi(x^0,\vec{x}) = \sum\!\!\!\!\!\!\int_{\lambda} \frac{1}{\sqrt{2E_\lambda}} \left[e^{-\mathrm{i}E_\lambda x^0}\psi_\lambda(\mathbf{x})\,a_\lambda + e^{\mathrm{i}E_\lambda x^0}\psi_{-\lambda}(\mathbf{x})\,b_\lambda^\dagger\right], \tag{2}$$

where $a_\lambda^\dagger$ and a_λ ($b_\lambda^\dagger$ and b_λ) are the scalar particle (antiparticle) creation and destruction operators satisfying commutation relations; wave functions $\psi_\lambda(\mathbf{x})$ form a complete set of solutions to the stationary Klein-Gordon equation

$$\left(-\boldsymbol{\nabla}^2 + m^2\right)\psi_\lambda(\mathbf{x}) = E_\lambda^2\psi(\mathbf{x}), \tag{3}$$

$\boldsymbol{\nabla}$ is the covariant derivative in an external (background) field and m is the mass of the scalar particle; λ is the set of parameters (quantum numbers) specifying the state; $E_\lambda = E_{-\lambda} > 0$ is the energy of the state; symbol $\sum\!\!\!\!\!\!\int_{\lambda}$ denotes summation over discrete and integration (with a certain measure) over continuous values of λ.

We are considering the static background in the form of the cylindrically symmetric magnetic vortex of finite thickness, hence the covariant derivative is $\boldsymbol{\nabla} = \boldsymbol{\partial} - \mathrm{i}e\mathbf{V}$ with the vector potential possessing only one nonvanishing component given by

$$V_\varphi = \Phi/2\pi \tag{4}$$

outside the vortex; here Φ is the vortex flux and φ is the angle in the polar (r,φ) coordinates on a plane which is transverse to the vortex. The Dirichlet boundary condition on the edge ($r = r_0$) of the vortex is imposed on the scalar field:

$$\psi_\lambda|_{r=r_0} = 0, \tag{5}$$

i.e. quantum matter is assumed to be perfectly reflected from the thence impenetrable vortex. Provided the orthonormalization condition is satisfied,

$$\int d^3x \psi^*_\lambda \psi_{\lambda'} = \langle \lambda | \lambda' \rangle, \tag{6}$$

the solution to (3) and (5) in the case of the impenetrable magnetic vortex of thickness $2r_0$ takes form

$$\psi_{knk_z}(\mathbf{x}) = (2\pi)^{-1} e^{\mathrm{i}k_z z} e^{\mathrm{i}n\varphi} \beta_n(kr_0) \times [Y_{|n-e\Phi/2\pi|}(kr_0) J_{|n-e\Phi/2\pi|}(kr) - J_{|n-e\Phi/2\pi|}(kr_0) Y_{|n-e\Phi/2\pi|}(kr)], \tag{7}$$

where z is the coordinate along the vortex,

$$\beta_n(kr_0) = \left[Y^2_{|n-e\Phi/2\pi|}(kr_0) + J^2_{|n-e\Phi/2\pi|}(kr_0) \right]^{-1/2}, \tag{8}$$

and $0 < k < \infty$, $-\infty < k_z < \infty$, $n \in \mathbb{Z}$ ($\mathbb{Z}$ is the set of integer numbers); $J_\mu(u)$ and $Y_\mu(u)$ are the Bessel functions of order μ of the first and second kinds.

In general, the vacuum energy density is determined as the vacuum expectation value of the time-time component of the energy-momentum tensor, that is given formally by expression

$$\varepsilon = \langle \mathrm{vac} | \left[\partial_0 \Psi^\dagger \partial_0 \Psi + \partial_0 \Psi \partial_0 \Psi^\dagger - (\xi - 1/4) \boldsymbol{\nabla}^2 (\Psi^\dagger \Psi + \Psi \Psi^\dagger) \right] | \mathrm{vac} \rangle = \sum\!\!\!\!\!\!\int_\lambda E_\lambda \psi^*_\lambda(\mathbf{x}) \, \psi_\lambda(\mathbf{x}) - (\xi - 1/4) \boldsymbol{\nabla}^2 \sum\!\!\!\!\!\!\int_\lambda E^{-1}_\lambda \psi^*_\lambda(\mathbf{x}) \, \psi_\lambda(\mathbf{x}). \tag{9}$$

In the following we shall restrict our consideration to the plane $z = 0$ which is orthogonal to the vortex.

Thus, the renormalized vacuum energy density in the case of the finite-thickness vortex takes form

$$\varepsilon_{ren} = \frac{1}{2\pi} \left\{ \int_0^\infty dk \, k \left(k^2 + m^2 \right)^{1/2} [S(kr, kr_0) - S(kr, kr_0)|_{\Phi=0}] - (\xi - 1/4) \triangle \int_0^\infty dk \, k \left(k^2 + m^2 \right)^{-1/2} [S(kr, kr_0) - S(kr, kr_0)|_{\Phi=0}] \right\}, \tag{10}$$

where, in view of (7),

$$S(kr, kr_0) = \sum_{n \in \mathbb{Z}} \beta^2_n(kr_0) \times \left[Y_{|n-e\Phi/2\pi|}(kr_0) J_{|n-e\Phi/2\pi|}(kr) - J_{|n-e\Phi/2\pi|}(kr_0) Y_{|n-e\Phi/2\pi|}(kr) \right]^2, \tag{11}$$

and $\triangle = \partial^2_r + r^{-1} \partial_r$ is the transverse radial part of the laplacian.

Owing to the infinite range of summation, the last expression is periodic in flux Φ with a period equal to $2\pi e^{-1}$, i.e. it depends on quantity

$$F = \frac{e\Phi}{2\pi} - \left[\left[\frac{e\Phi}{2\pi} \right] \right], \tag{12}$$

where $[[u]]$ is the integer part of quantity u (i.e. the integer which is less than or equal to u).

Let us rewrite (11) in the form

$$S(kr, kr_0) = S_0(kr) + S_1(kr, kr_0), \tag{13}$$

where $S_0(kr)$ corresponds to the appropriate series in the case of the vacuum polarization by a singular magnetic vortex:[11–13]

$$\begin{aligned} S_0(kr) &= \sum_{n=0}^{\infty} \left[J^2_{n+F}(kr) + J^2_{n+1-F}(kr) \right] \\ &= \int_0^{kr} d\tau \left[J_F(\tau) J_{-1+F}(\tau) + J_{-F}(\tau) J_{1-F}(\tau) \right], \end{aligned} \tag{14}$$

and $S_1(kr, kr_0)$ is a correction term due to the finite thickness of a vortex:

$$\begin{aligned} S_1(kr, kr_0) = 2 \sum_{n=0}^{\infty} \Bigg[& J_{n+F}(kr_0) Y_{n+F}(kr) \\ & \times \frac{J_{n+F}(kr_0) Y_{n+F}(kr) - Y_{n+F}(kr_0) J_{n+F}(kr)}{J^2_{n+F}(kr_0) + Y^2_{n+F}(kr_0)} \\ + J_{n+1-F}(kr_0) Y_{n+1-F}(kr) & \frac{J_{n+1-F}(kr_0) Y_{n+1-F}(kr) - Y_{n+1-F}(kr_0) J_{n+1-F}(kr)}{J^2_{n+1-F}(kr_0) + Y^2_{n+1-F}(kr_0)} \Bigg] \\ - \sum_{n=0}^{\infty} \Bigg[& J^2_{n+F}(kr_0) \frac{J^2_{n+F}(kr) + Y^2_{n+F}(kr)}{J^2_{n+F}(kr_0) + Y^2_{n+F}(kr_0)} \\ & + J^2_{n+1-F}(kr_0) \frac{J^2_{n+1-F}(kr) + Y^2_{n+1-F}(kr)}{J^2_{n+1-F}(kr_0) + Y^2_{n+1-F}(kr_0)} \Bigg]. \end{aligned} \tag{15}$$

In the absence of the magnetic flux in the tube we have

$$S(kr, kr_0)|_{\Phi=0} = \tilde{S}_0 + \tilde{S}_1(kr, kr_0), \tag{16}$$

where

$$\tilde{S}_0 = J^2_0(kr) + 2 \sum_{n=1}^{\infty} J^2_n(kr) = 1, \tag{17}$$

and a correction term due to the finite thickness of an empty tube:

$$\begin{aligned} \tilde{S}_1(kr, kr_0) = 2 \Bigg[& J_0(kr_0) Y_0(kr) \frac{J_0(kr_0) Y_0(kr) - Y_0(kr_0) J_0(kr)}{J^2_0(kr_0) + Y^2_0(kr_0)} \\ & + 2 \sum_{n=1}^{\infty} J_n(kr_0) Y_n(kr) \frac{J_n(kr_0) Y_n(kr) - Y_n(kr_0) J_n(kr)}{J^2_n(kr_0) + Y^2_n(kr_0)} \Bigg] \\ - \Bigg[& J^2_0(kr_0) \frac{J^2_0(kr) + Y^2_0(kr)}{J^2_0(kr_0) + Y^2_0(kr_0)} + 2 \sum_{n=1}^{\infty} J^2_n(kr_0) \frac{J^2_n(kr) + Y^2_n(kr)}{J^2_n(kr_0) + Y^2_n(kr_0)} \Bigg]. \end{aligned} \tag{18}$$

Thus, vacuum energy density (10) depends on F (12), i.e. it is periodic in flux Φ with a period equal to $2\pi e^{-1}$. Moreover, relation (10) is symmetric under substitution $F \to 1-F$, vanishing at $F \to 0$ ($F \to 1$) and, perhaps, attaining its maximal value at $F = 1/2$.[a] Relations (14) and (15) are simplified at $F = 1/2$:

$$S_0(kr)|_{\Phi=\pi e^{-1}} = \frac{2}{\pi} \int\limits_0^{2kr} \frac{d\,\tau}{\tau} \sin\tau, \tag{19}$$

and

$$S_1(kr, kr_0)|_{\Phi=\pi e^{-1}} = 2\sum_{n=0}^{\infty} \left\{ \frac{J^2_{n+\frac{1}{2}}(kr_0)\left[Y^2_{n+\frac{1}{2}}(kr) - J^2_{n+\frac{1}{2}}(kr)\right]}{J^2_{n+\frac{1}{2}}(kr_0) + Y^2_{n+\frac{1}{2}}(kr_0)} \right.$$
$$\left. - \frac{2J_{n+\frac{1}{2}}(kr_0)Y_{n+\frac{1}{2}}(kr_0)J_{n+\frac{1}{2}}(kr)Y_{n+\frac{1}{2}}(kr)}{J^2_{n+\frac{1}{2}}(kr_0) + Y^2_{n+\frac{1}{2}}(kr_0)} \right\}. \tag{20}$$

Since it is hardly possible to evaluate sums in (15) and (18) analytically, our further analysis will employ numerical calculation. In the following we restrict ourselves to the case of $F = 1/2$, when the expression for the vacuum energy density takes form

$$\varepsilon_{ren} = \frac{1}{2\pi} \left\{ \int\limits_0^{\infty} dk\, k \left(k^2 + m^2\right)^{1/2} G(kr, kr_0) \right.$$
$$\left. -(\xi - 1/4)\triangle \int\limits_0^{\infty} dk\, k \left(k^2 + m^2\right)^{-1/2} G(kr, kr_0) \right\}, \tag{21}$$

where

$$G(kr, kr_0) = S(kr, kr_0)|_{\Phi=\pi e^{-1}} - S(kr, kr_0)|_{\Phi=0}. \tag{22}$$

3. Numerical Evaluation of the Vacuum Energy Density

Following Ref. 14 we rewrite (21) in the dimensionless form

$$r^3\varepsilon_{ren} = \alpha_+(mr_0, mr) - (\xi - 1/4)r^3\triangle \frac{\alpha_-(mr_0, mr)}{r}, \tag{23}$$

where

$$\alpha_\pm(mr_0, mr) = \frac{1}{2\pi} \int\limits_0^{\infty} dz\, z \left[z^2 + \left(\frac{mr_0}{\lambda}\right)^2\right]^{\pm 1/2} G(z, \lambda z), \tag{24}$$

[a]At least, this is certainly true in the case of the singular vortex both for the Aharonov-Bohm[6] and the Casimir-Aharonov-Bohm[10–13] effects.

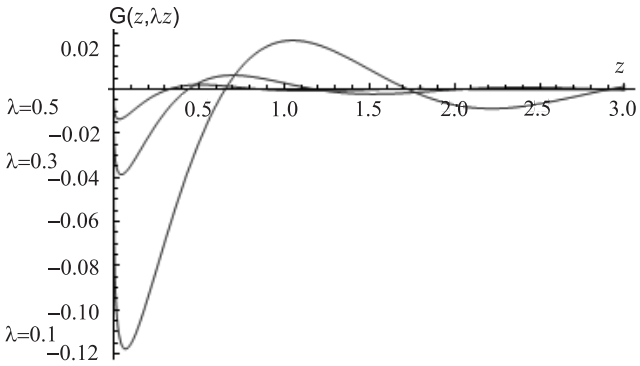

Fig. 1. Behavior of $G(z, \lambda z)$ at different values of λ.

and $\lambda = r_0/r$, $\lambda \in [0, 1]$. Let us point out some analytical properties of the integrand function in (23): it vanishes at the edge of the vortex

$$\lim_{\lambda \to 1} G(z, \lambda z) = 0 \tag{25}$$

at large distances from the vortex the case of a singular vortex is recovered

$$\lim_{\lambda \to 0} G(z, \lambda z) = S_0(z)|_{\Phi = \pi e^{-1}} - \tilde{S}_0. \tag{26}$$

At small values of z one gets

$$G(z, \lambda z)|_{z \to 0} = -[\ln(\lambda)/\ln(\lambda z)]^2. \tag{27}$$

Numerical analysis indicates that in the calculation of function $G(z, \lambda z)$ one can use series in (18) and (20) with finite limits, namely for calculation $G(z, \lambda z)$ at point $z = z'$ it is enough to cut off the summation limits by some value n that can be found from condition

$$\left| \frac{G(z, \lambda z)|_n - G(z, \lambda z)|_N}{G(z, \lambda z)} \right| < \delta(\lambda), \quad \delta(\lambda) < 10^{-17}, \tag{28}$$

where N is a big number $N \sim 10^2$, $n < N$. It can be shown that the envelope of $G(z, \lambda z)$ is exponentially decreasing function at large z, see Fig. 1. So, for the finite-thickness magnetic vortex we can compute values of dimensionless quantity $r^3 \varepsilon_{ren}$ (23) for different values of λ. To do this, we have to be able to perform integration in (23) with high precision. We make it in a following way.

As one can see from Fig. 2, the function $G(z, \lambda z)$ is negative from $z = 0$ to the first function root at $z = z_1$ ($z_1 \neq 0$). So, the appropriate integral in (21) is negative. The subsequent roots are denoted by z_2, z_3, etc. Because of decreasing character of the envelope function the integral from z_1 to z_3 will be positive. It is useful to define a period of function $G(z, \lambda z)$ as an interval between two next to neighboring roots, i.e. from z_1 to z_3, from z_3 to z_5, and so on. Then the full integral in (21) will be a sum of the negative integral from $z = 0$ to $z = z_1$ and a multitude of positive integrals over subsequent periods. In the case of sufficiently

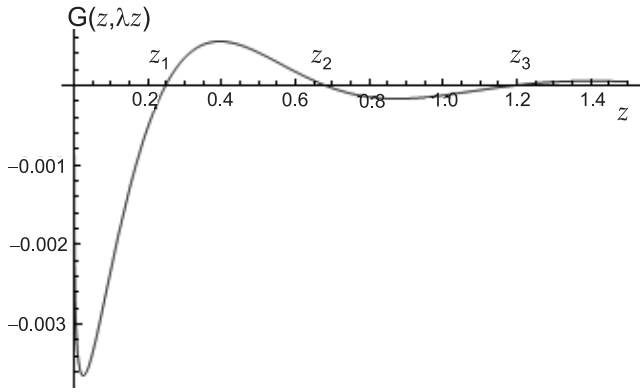

Fig. 2. The location of roots of $G(z, \lambda z)$ at $\lambda = 0.7$.

small transverse size of the tube ($mr_0 \ll 1$) the integrals over some finite number of first periods may be negative but thereupon they become and remain positive also.

For small z we make a direct integration of function $G(z, \lambda z)$ over periods. For large z we make integration for each period separately. To do it we create a table of values of function $G(z, \lambda z)$ for a separate period and replace this function by a more simple function in the form

$$G_{int}(z, \lambda z) = a \frac{e^{-bz}}{z^c} \frac{A_q(z^2)}{B_q(z^2)} \sin(kz + j \ln z + \phi_0), \tag{29}$$

where sine function ensures that roots of $G_{int}(z, \lambda z)$ coincide with roots of $G(z, \lambda z)$; $A_q(y)$ and $B_q(y)$ are q-degree polynomials, q can be $3, 4$ or 5; all unknown parameters can be found from an interpolation procedure. We allow a relative error of interpolation to be

$$\left| \frac{G_{int}(z, \lambda z) - G(z, \lambda z)}{G(z, \lambda z)} \right| < 10^{-8} \tag{30}$$

for each period. The function $G_{int}(z, \lambda z)$ can be immediately integrated with the required accuracy.

With the help of the above procedure we obtain a table of contributions from integration over each period, extrapolate this table to infinity, and after that we find the full integral in (21) as a sum of the negative integral over first period(s), a multitude of positive integrals over periods and an interpolation term.

For α_+ function we estimate the relative error of the obtained result as 0.1%. It should be noted that nearly 95 % of the integral value is obtained by direct calculation and only nearly 5% is the contribution from the interpolation. The integration in α_- function is performed more quickly and with a higher accuracy, as compared to the case of α_+ function, because of its more rapid decreasing at large distances. In this case the contribution from the interpolation can be 10^{-3}% from the final value of integration.

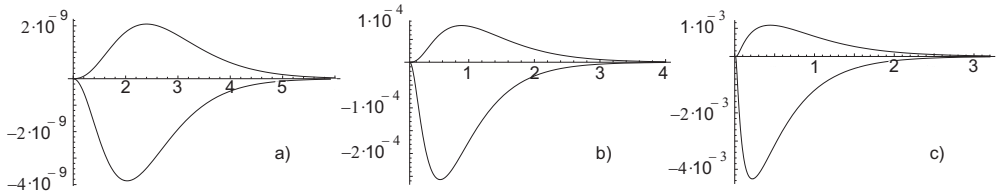

Fig. 3. Behavior of the $\alpha_+(x_0, x)$ (positive) and the $\alpha_-(x_0, x)$ (negative) functions for the case of a) $x_0 = 1$, b) $x_0 = 10^{-1}$, c) $x_0 = 10^{-2}$. The variable x ($x > x_0$) is along the abscissa axis.

Dimensionless quantity $r^3\varepsilon_{ren}$ (23) can be interpreted as a function of two dimensionless parameters, mr_0 and mr. Using the above described procedure, we calculate α_+ and α_- functions at fixed values of mr_0 ($mr_0 = 1; 10^{-1}; 10^{-2}$) at some set of points of dimensionless distance from the center of the vortex. This allows us to obtain coefficients (which are different for different values of mr_0) of the interpolation function that is found in the form

$$\alpha_\pm(x_0, x) = \left[\pm e^{-2x} x^{1\mp 1/2}\right] \left[\left(\frac{x - x_0}{x}\right)^2 \frac{P_3^\pm(x - x_0)}{x^3}\right] \frac{Q_3^\pm(x^2)}{x^6}, \quad x > x_0, \quad (31)$$

where $x = mr$, $x_0 = mr_0$ and $P_n^\pm, Q_n^\pm$ — are polynomials of n-th order. First factor in the square bracket in (31) describes the large distance behavior of the appropriate functions in the case of the singular vortex,[13] second factor in the square bracket is an asymptotic at small distances from the edge of the tube, and the last factor is the intermediate part of the function. Since the flux tube is impenetrable, the $\alpha_\pm$ functions are zero at $x \leq x_0$. Behavior of the dimensionless $\alpha_\pm$ functions is presented on Fig. 3.

We define function

$$\tilde{\alpha}_-(x_0, x) = r^3 \triangle \left(\frac{\alpha_-(x_0, x)}{r}\right) = \alpha_-(x_0, x) - x\frac{\partial \alpha_-(x_0, x)}{\partial x} + x^2 \frac{\partial^2 \alpha_-(x_0, x)}{\partial x^2} \quad (32)$$

and present its behavior on Fig. 4.

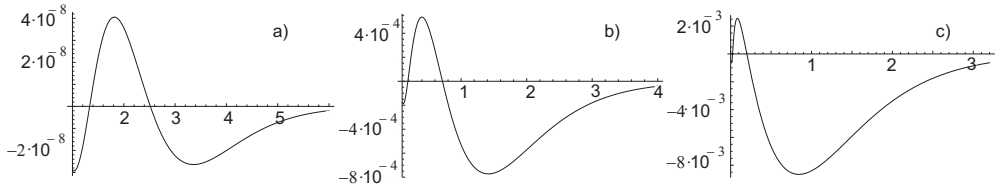

Fig. 4. Behavior of the $\tilde{\alpha}_-(x_0, x)$ function for the case of a) $x_0 = 1$, b) $x_0 = 10^{-1}$, c) $x_0 = 10^{-2}$. The variable x ($x > x_0$) is along the abscissa axis.

Now we can construct the dimensionless vacuum energy density at different values of the coupling to the space-time curvature scalar:

$$r^3\varepsilon_{ren} = \alpha_+(x_0, x) - (\xi - 1/4)\tilde{\alpha}_-(x_0, x). \quad (33)$$

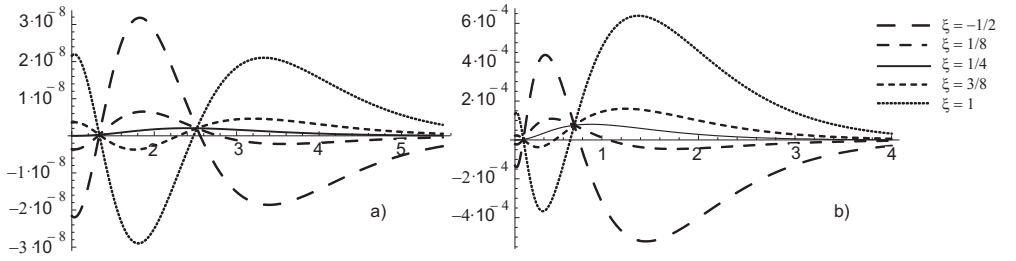

Fig. 5. The dimensionless vacuum energy density $r^3\varepsilon_{ren}(x_0, x)$ at different values of the coupling to the space-time curvature scalar for the case of a) $x_0 = 1$, b) $x_0 = 10^{-1}$. The variable x $(x > x_0)$ is along the abscissa axis.

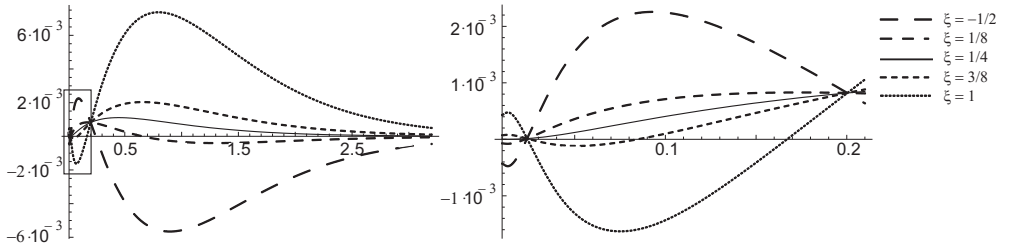

Fig. 6. The dimensionless vacuum energy density $r^3\varepsilon_{ren}(x_0, x)$ at different values of the coupling to the space-time curvature scalar for the case of $x_0 = 10^{-2}$. The region in a rectangle on the left figure is seen in the scaled-up form on the right figure. The variable x $(x > x_0)$ is along the abscissa axis.

Its behavior is presented on Fig. 5 and Fig. 6. The case of the singular magnetic vortex[13] is presented on Fig. 7.

The analytical form of the vacuum energy density allows us to obtain the total induced vacuum energy

$$E = \int_0^{2\pi} d\varphi \int_{r_0}^{\infty} \varepsilon_{ren}\, r dr = 2\pi m \left[\int_{x_0}^{\infty} \frac{\alpha_+(x_0, x)}{x^2}\, dx - (\xi - 1/4) \int_{x_0}^{\infty} \frac{\tilde{\alpha}_-(x_0, x)}{x^2}\, dx \right]. \tag{34}$$

The integral over the $\tilde{\alpha}_-$ function (32) can be taken by parts, yielding

$$\int_{x_0}^{\infty} \frac{\tilde{\alpha}_-(x_0, x)}{x^2}\, dx = - \left. \frac{\partial \alpha_-(x_0, x)}{\partial x} \right|_{x=x_0}. \tag{35}$$

In this respect the question about the small distance behavior of the α_- function is very important. We have made a numerical calculations at small distances from the tube $(x - x_0 \sim 10^{-6} x_0)$ and confirm the quadratic behavior near the edge of the tube (31) $\lim\limits_{x \to x_0} \alpha_-(x_0, x) \sim (x - x_0)^2$. So, quantity (35) is zero, and the $\tilde{\alpha}_-$ function affects only the local properties of the vacuum energy density. The total

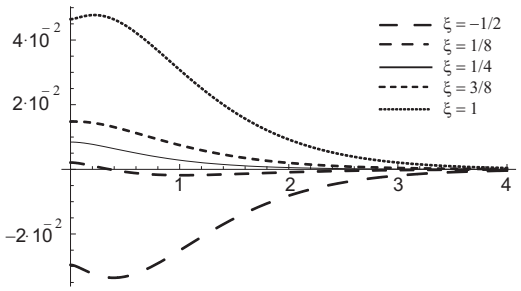

Fig. 7. The dimensionless vacuum energy density $r^3\varepsilon_{ren}(x_0, x)$ at different values of the coupling to the space-time curvature scalar for the case of the singular magnetic vortex.

vacuum energy is defined exclusively by the α_+ function and is independent of ξ:

$$E = 2\pi m \int\limits_{x_0}^{\infty} \frac{\alpha_+(x_0, x)}{x^2}\, dx. \tag{36}$$

The total vacuum energy (in $2\pi m$ units) of the impenetrable flux tube is 6.94×10^{-10}, 1.65×10^{-4}, and 1.06×10^{-2} for the case of $x_0 = 1$, $x_0 = 10^{-1}$, $x_0 = 10^{-2}$ correspondingly. It should be noted that the total energy is infinite[13] in the case of a singular magnetic vortex.

The induced vacuum energy density in the units of m^3 is presented on Fig. 8. The results for the case of $\xi = 1/4$ are vanishingly small as compared to cases of other values of ξ, so they are not visible on Fig. 8.

4. Discussion

In the present paper we have considered the energy density which is induced in the vacuum outside a magnetic flux enclosed into an impenetrable tube of finite radius r_0. Whereas the induced vacuum energy density is divergent at small distances as r^{-3} when the radius is neglected ($r_0 = 0$), see Fig. 7, it becomes finite when the radius is taken into account. A very characteristic feature is the appearance of oscillations in the vicinity of the tube, see Fig. 5 and Fig. 6. Another peculiarity is that curves corresponding to different values of ξ are symmetric with respect to the curve corresponding to $\xi = 1/4$, the latter yielding the minimal absolute values of the vacuum energy density, see also Fig. 8. The maximal values of the vacuum

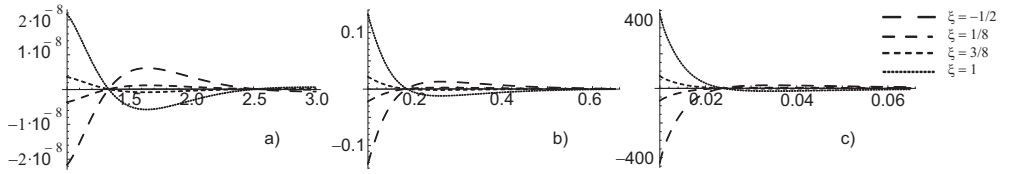

Fig. 8. The vacuum energy density $\varepsilon_{ren}(x_0, x)$ (in m^3 units) at different values of the coupling to the space-time curvature scalar for the case of a) $x_0 = 1$, b) $x_0 = 10^{-1}$, c) $x_0 = 10^{-2}$.

energy density are becoming hardly observable for $mr_0 > 1$, however, they are quite conspicuous for $mr_0 < 10^{-2}$. This result was obtained earlier,[14] but a completely new result concerns the behavior at large distances from the tube (up to $200\, r_0$), as well as at different values of ξ. It should be noted that the vacuum energy density in the vicinity of the tube is negative at $\xi < 1/4$, including the important cases of conformal coupling $\xi = 1/8$ [see (1) at $d = 2$] and minimal coupling $\xi = 0$.

Since the vacuum energy density is finite, the total vacuum energy, see (34), is finite as well. We show that the latter is positive and independent of ξ. Being negligible in the case of $mr_0 \gtrsim 1$, it produces an appreciable effect of order of $10^{-2}m$ in the case of $mr_0 = 10^{-2}$.

Acknowledgments

Yu.A.S. would like to thank the Organizers of the 8th Friedmann Seminar in Rio de Janeiro for kind hospitality during this extremely interesting and inspiring meeting. The work was supported in part by the Ukrainian FRSF grant F40.2/108 "Application of string theory and field theory methods to nonlinear phenomena is low dimensional systems".

References

1. H. B. G. Casimir, *Proc. Kon. Ned. Akad. Wetenschap B* **51**, 793 (1948); *Physica* **19**, 846 (1953).
2. K. A. Milton, *The Casimir Effect: Physical Manifistations of Zero-Point Energy* (World Scientific, Singapore, 2001).
3. M. Bordag, G. L. Klimchitskaya, U. Mohideen and V.M. Mostepanenko, *Advances in the Casimir Effect* (Oxford University Press, Oxford, 2009).
4. S. K. Lamoreax, *Phys. Rev. Lett.* **78**, 5 (1997).
5. G. Bressi, G. Carugno, R. Onofrio and G. Ruoso, *Phys. Rev. Lett.* **88**, 041804 (2002).
6. Y. Aharonov and D. Bohm, *Phys. Rev.* **115**, 485 (1959).
7. R. Penrose, in: *Relativity, Groups and Topology*, eds. B. S. DeWitt and C. DeWitt (Gordon and Breach, New York, 1964).
8. N. A. Chernikov and E. A. Tagirov, *Ann. Inst. Henri Poincare A* **9**, 109 (1968).
9. C. G. Callan, S. Coleman, and R. Jackiw, *Ann. Phys. (N.Y.)* **59**, 42 (1970).
10. Yu. A. Sitenko and A. Yu. Babansky, *Mod. Phys. Lett. A* **13**, 379 (1998).
11. Yu. A. Sitenko and A. Yu. Babansky, *Phys. Atom. Nucl.* **61**, 1594 (1998).
12. Yu. A. Sitenko and V. M. Gorkavenko, *Ukrainian J. Phys.* **48**, 1286 (2003).
13. Yu. A. Sitenko and V.M. Gorkavenko, *Phys. Rev. D* **67**, 085015 (2003).
14. V. M. Gorkavenko, Yu. A. Sitenko and O. B. Stepanov, *J. Phys. A: Math. Theor.* **43**, 175401 (2010).

2.4. Поляризація вакууму скалярного поля матерії в просторі-часі довільної розмірності

International Journal of Modern Physics A
Vol. 28, No. 31 (2013) 1350161 (17 pages)

DOI: 10.1142/S0217751X13501613

CASIMIR ENERGY AND FORCE INDUCED BY AN IMPENETRABLE FLUX TUBE OF FINITE RADIUS

VOLODYMYR M. GORKAVENKO
Department of Physics, Taras Shevchenko National University of Kyiv,
64/13 Volodymyrska str., Kyiv 01601, Ukraine
gorka@univ.kiev.ua

YURII A. SITENKO* and OLEXANDER B. STEPANOV†
Bogolyubov Institute for Theoretical Physics, National Academy of Sciences of Ukraine,
14-b Metrologichna str., Kyiv 03680, Ukraine
**yusitenko@bitp.kiev.ua*
†*pnd_@ukr.net*

Received 3 June 2013
Accepted 11 November 2013
Published 11 December 2013

A perfectly reflecting (Dirichlet) boundary condition at the edge of an impenetrable magnetic-flux-carrying tube of nonzero transverse size is imposed on the charged massive scalar matter field which is quantized outside the tube. We show that the vacuum polarization effects outside the tube give rise to a macroscopic force acting at the increase of the tube radius (if the magnetic flux is held steady). The Casimir energy and force are periodic in the value of the magnetic flux, being independent of the coupling to the space–time curvature scalar. We conclude that a topological defect of the vortex type can polarize the vacuum of only those quantum fields that have masses which are much less than a scale of the spontaneous symmetry breaking.

Keywords: Vacuum polarization; Casimir effect; magnetic vortex.

PACS numbers: 11.10.Kk, 04.60.Kz, 11.15.Tk, 11.27.+d

1. Introduction

Polarization of the vacuum of quantum matter fields under the influence of boundary conditions was studied intensively over more than six decades since Casimir[1,2] predicted a force between grounded metal plates: the prediction was that the induced vacuum energy in bounded spaces gave rise to a macroscopic force between bounding surfaces, see reviews in Refs. 3 and 4. The Casimir force between grounded metal plates has now been measured quite accurately and agrees with the theoretical predictions, see e.g. Refs. 5 and 6, as well as other publications cited in Refs. 3 and 4.

In the present paper, we consider the vacuum energy which is induced by boundary conditions in space that is not bounded but, instead, is not simply connected, being an exterior to a straight infinitely long tube. This setup is inspired by the famous Aharonov–Bohm effect,[7] and we are interested in polarization of the vacuum which is due to imposing a boundary condition at the edge of the tube carrying magnetic flux lines inside itself; this may be denoted as the Casimir–Aharonov–Bohm effect (see also Ref. 8).

The vacuum polarization effects which are due to imposing boundary conditions of various types at the cylindrical surfaces were extensively discussed in the literature, see Refs. 9–14. In general, the Casimir effect in the presence of a single smooth object (cylinder or sphere) is rather different from that in the presence of two disjoint ones (e.g. plates): new divergences appear, and to tame them one has to sum contributions of quantized matter from both sides of the boundary surface, still this does not help to get rid completely of divergences, see Ref. 4 and references therein. In view of this, the conventional prescription which is to subtract vacuum energy of empty Minkowski space–time becomes insufficient for obtaining the meaningful results. Some authors[15,16] assert that there is no Casimir effect at all in this case. Our concern will not be in the case of an empty tube but, instead, in the case of a tube filled with the magnetic flux lines. We shall follow the author of Ref. 17 who proposes to define the Casimir energy for physical systems divided into classes: the difference in vacuum energy of any two systems within the same class should be finite, then the *finite* Casimir energy has the universal interpretation as a vacuum energy with respect to the vacuum energy of a certain reference system which is common for the whole class. We define a class of physical systems corresponding to the charged matter field which is quantized outside an impenetrable tube with the magnetic flux taking different values; the case of zero flux can be chosen as the reference system. As we shall show, the Casimir energy for this class is unambiguous and finite.

A magnetic flux tube is formed inside a long current-carrying solenoid or simply a magnetized whisker made of a ferromagnetic material, and its effect on the outside vacuum can be studied in laboratory. Otherwise, a flux tube can be formed as a topological defect of the vortex type, appearing after a phase transition with spontaneous breakdown of the gauge symmetry:[18,19] the condition of its appearance is that the first homotopy group of the group space of the broken symmetry group be nontrivial. The vortex is characterized by flux $2\pi\hbar ce_H^{-1}$, where e_H is the coupling constant of the Higgs scalar field to the vortex-forming gauge field; the transverse size of the vortex is of the order of correlation length $\hbar(m_H c)^{-1}$, where m_H is the mass of the Higgs scalar field. The issue of vortices is widely discussed in condensed matter physics (e.g. Abrikosov vortices in superconductors, see Ref. 20), as well as in astrophysics and cosmology (e.g. cosmic strings, see Refs. 21 and 22). While considering the effect of the vortices on the vacuum of the surrounding quantum matter, the following two circumstances should be kept in mind: (1) the phase with broken symmetry exists outside the vortex which is topological defect, and the

vacuum is to be defined only where the phase exists, hence the quantum matter field does not penetrate inside the vortex, obeying a boundary condition at its edge, (2) the coupling constant (e) of the quantum matter field to the vortex-forming gauge field differs, in general, from e_H (e.g. $e = e_H/2$ for normal excitations in superconductors).

A simplifying assumption consists in a neglect of a transverse size of the flux tube, i.e. in a use of an approximation of an infinitely thin singular thread. Energy density and other components of the energy–momentum tensor, which are induced in the background of a singular magnetic thread, were studied in Ref. 23 (see also Refs. 8 and 24). The quantum matter field obeys the regularity condition at the location of the thread, and the vacuum polarization effects are periodic in the value of the magnetic flux with the period equal to the London flux quantum ($2\pi\hbar ce^{-1}$); the absolute value of the induced vacuum energy density is maximal at half of the London flux quantum. A shortcoming of the approximation of a singular thread is the power divergence of the induced vacuum energy–momentum tensor in the vicinity of the thread, and, as a consequence, neither Casimir energy (i.e. the induced vacuum energy per unit length of the thread) nor Casimir force can be defined in this approximation.

The transverse size of the magnetic flux tube was taken into account in Refs. 25–29, where it was shown that the induced vacuum energy per unit length of the tube depends on the configuration of the magnetic field inside the tube, being quadratic in the flux for sufficiently smooth configurations. However, these authors were concerned with the case when the region of the flux was penetrable for the quantum matter field; therefore, their results have no relation to the Casimir–Aharonov–Bohm effect. When the quantum matter field is excluded from the region of the flux (that is appropriate for the interpretation of the flux tube as a topological defect), then the vacuum polarization effects become independent of the details of the magnetic field configuration and depend periodically on the whole flux;[30–32] meanwhile the contribution to both the Casimir energy and force which is due to the magnetic flux in the excluded region is well-defined. In the following quantum matter will be represented by the charged massive scalar field. As we shall see, the vacuum energy which is induced outside the flux tube gives rise to a macroscopic force acting at the increase of the tube radius, if the magnetic flux is held steady. Although the induced vacuum energy density depends on the coupling of the scalar field to the space–time curvature scalar, the Casimir energy and force will be shown to be independent of this coupling.

In the next section, we define the renormalized induced vacuum energy density in the background of an impenetrable flux tube and review briefly the obtained earlier results as to its behavior in a plane, i.e. when the spatial dimension along the tube is ignored. The Casimir energy and force in a plane are considered in Sec. 3. The longitudinal dimensions are added in Sec. 4 where we find the Casimir energy and force in the most general case of a $(d-2)$-tube in d-dimensional space. The obtained results are summarized and discussed in Sec. 5.

2. Vacuum Energy Density

The temporal component of the energy–momentum tensor for the quantized charged scalar field $\Psi(x)$ in flat space–time is given by expression

$$T_{00}(x) = \frac{1}{2}\big[\partial_0\Psi^\dagger, \partial_0\Psi\big]_+ - \frac{1}{4}\big[\partial_0^2\Psi^\dagger, \Psi\big]_+ - \frac{1}{4}\big[\Psi^\dagger, \partial_0^2\Psi\big]_+ - \left(\xi - \frac{1}{4}\right)\boldsymbol{\nabla}^2\big[\Psi^\dagger, \Psi\big]_+ , \tag{1}$$

where $\boldsymbol{\nabla}$ is the covariant spatial derivative involving both affine and bundle connections and the field operator in the case of a static (ultrastatic) background takes the form

$$\Psi(x^0, \mathbf{x}) = \sum\!\!\!\!\!\!\int_\lambda \frac{1}{\sqrt{2E_\lambda}}\Big[e^{-\mathrm{i}E_\lambda x^0}\psi_\lambda(\mathbf{x})a_\lambda + e^{\mathrm{i}E_\lambda x^0}\psi_{-\lambda}(\mathbf{x})b_\lambda^\dagger\Big]; \tag{2}$$

units $\hbar = c = 1$ are used, $a_\lambda^\dagger$ and a_λ ($b_\lambda^\dagger$ and b_λ) are the scalar particle (antiparticle) creation and destruction operators satisfying commutation relations; wave functions $\psi_\lambda(\mathbf{x})$ form a complete set of solutions to the stationary Klein–Gordon equation

$$\big(-\boldsymbol{\nabla}^2 + m^2\big)\psi_\lambda(\mathbf{x}) = E_\lambda^2\psi(\mathbf{x}), \tag{3}$$

m is the mass of the scalar particle; λ is the set of parameters (quantum numbers) specifying the state; $E_\lambda = E_{-\lambda} > 0$ is the energy of the state; symbol $\sum\!\!\!\!\!\!\int_\lambda$ denotes summation over discrete and integration (with a certain measure) over continuous values of λ.

As is known for a long time,[33–35] the energy–momentum tensor depends on parameter ξ which couples Ψ to the scalar curvature of space–time even in the case of the vanishing curvature, see (1); conformal invariance is achieved in the limit of vanishing mass ($m = 0$) at $\xi = (d-1)(4d)^{-1}$, where d is the spatial dimension. Consequently, the density of the induced vacuum energy which is given formally by expression

$$\varepsilon = \langle \mathrm{vac}|T_{00}(x)|\mathrm{vac}\rangle = \sum\!\!\!\!\!\!\int_\lambda E_\lambda\psi_\lambda^*(\mathbf{x})\,\psi_\lambda(\mathbf{x}) - \left(\xi - \frac{1}{4}\right)\boldsymbol{\nabla}^2\sum\!\!\!\!\!\!\int_\lambda E_\lambda^{-1}\psi_\lambda^*(\mathbf{x})\psi_\lambda(\mathbf{x}), \tag{4}$$

depends on ξ as well. This poses a question: whether physically measurable effects (e.g. the Casimir force) can be dependent on ξ?

In the present paper, we are considering a static background in the form of the cylindrically symmetric magnetic flux tube of finite transverse size, hence the covariant derivative is $\boldsymbol{\nabla} = \boldsymbol{\partial} - \mathrm{i}e\mathbf{V}$ with the vector potential possessing only one nonvanishing component given by

$$V^\varphi = \frac{\Phi}{2\pi}, \tag{5}$$

outside the tube; here Φ is the value of the magnetic flux and φ is the angle in polar (r, φ) coordinates on a plane which is transverse to the tube.

The vacuum polarization depends on the choice of a boundary condition at the edge of the tube ($r = r_0$). We impose, as in Refs. 30–32, the Dirichlet boundary condition:

$$\psi_\lambda|_{r=r_0} = 0\,, \tag{6}$$

i.e. quantum matter is assumed to be perfectly reflected from the thence impenetrable flux tube. Other possible choices of a boundary condition will be considered elsewhere.

The solution to (3) outside the magnetic flux tube can be obtained in terms of the cylindrical functions. The formal expression (4) for the vacuum energy density has to be renormalized by subtracting the contribution corresponding to the zero flux. The tube in three-dimensional space can be obviously generalized to the $(d-2)$-tube in d-dimensional space by adding extra $d-3$ dimensions as longitudinal ones. Thus, we obtain (for details see Refs. 30 and 31):

$$\varepsilon_{\rm ren} = (2\pi)^{1-d} \int d^{d-2}\mathbf{k}_z \int_0^\infty dk\, k \left(\sqrt{\mathbf{k}_z^2 + k^2 + m^2} - \frac{\xi - 1/4}{\sqrt{\mathbf{k}_z^2 + k^2 + m^2}} \triangle \right) \times \left[S(kr, kr_0) - S(kr, kr_0)|_{\Phi=0} \right], \tag{7}$$

where

$$S(kr, kr_0) = \sum_{n\in\mathbb{Z}} \frac{\left[Y_{|n-e\Phi/2\pi|}(kr_0) J_{|n-e\Phi/2\pi|}(kr) - J_{|n-e\Phi/2\pi|}(kr_0) Y_{|n-e\Phi/2\pi|}(kr) \right]^2}{Y^2_{|n-e\Phi/2\pi|}(kr_0) + J^2_{|n-e\Phi/2\pi|}(kr_0)}\,, \tag{8}$$

$\mathbb{Z}$ is the set of integer numbers, $J_\mu(u)$ and $Y_\mu(u)$ are the Bessel and the Neumann functions of order μ, the integration over the components of the $(d-2)$-dimensional momentum $\mathbf{k}_z$ ranges from $-\infty$ to ∞, and $\triangle = \partial_r^2 + r^{-1}\partial_r$ is the radial part of the Laplacian operator on the plane which is orthogonal to the $(d-2)$-tube.

Owing to the infinite range of summation, the last expression is periodic in flux Φ with a period equal to $2\pi e^{-1}$, i.e. the London flux quantum (in units $c = \hbar = 1$). Our further analysis concerns the case of $\Phi = (2n+1)\pi e^{-1}$ when each of the integrals in (7) is the most distinct from zero. Introducing function

$$G(kr, kr_0) = S(kr, kr_0)|_{\Phi=\pi e^{-1}} - S(kr, kr_0)|_{\Phi=0}\,, \tag{9}$$

we rewrite (7) in the case of $d = 2$ in the dimensionless form

$$r^3 \varepsilon_{\rm ren} = \alpha_+(mr_0, mr) - \left(\xi - \frac{1}{4}\right) r^3 \triangle \frac{\alpha_-(mr_0, mr)}{r}\,, \tag{10}$$

where

$$\alpha_\pm(mr_0, mr) = \frac{1}{2\pi} \int_0^\infty dz\, z \left[z^2 + \left(\frac{mr_0}{\lambda} \right)^2 \right]^{\pm 1/2} G(z, \lambda z) \tag{11}$$

and $\lambda = r_0/r$ ($\lambda \in [0, 1]$).

Functions α_+ and α_- were numerically calculated at a set of different distances from the axis of the tube in Refs. 31 and 32 where it was shown that the results can be approximated by the interpolation function in the form

$$\alpha_\pm(x_0,x)=\left[\pm e^{-2x}x^{1\mp 1/2}\right]\left[\left(\frac{x-x_0}{x}\right)^2\frac{P_3^\pm(x-x_0)}{x^3}\right]\frac{Q_3^\pm(x^2)}{R_3^\pm(x^2)}\,,\quad x>x_0\,,\qquad(12)$$

where $x=mr$, $x_0=mr_0$ and $P_n^\pm(y)$, $Q_n^\pm(y)$, $R_n^\pm(y)$ are polynomials in y of the nth order with the x_0-dependent coefficients. First factor in square bracket in (12) describes the large distance behavior in the case of the zero-radius tube (singular thread), second factor in square bracket is an asymptotics at small distances from the edge of the tube and the last quotient is the intermediate part. Since the flux tube is impenetrable, the $\alpha_\pm$ functions vanish at $x\leq x_0$.

For the α_+ function we estimate the relative error of the obtained result as 0.1%. It should be noted that nearly 95% of the integral value is obtained by direct calculation and only nearly 5% is the contribution from the interpolation. The integration in the case of the α_- function is performed more quickly and with a higher accuracy, as compared to the case of the α_+ function, because the former tends to zero more rapidly at large distances. In this case the contribution from the interpolation can be estimated as 10^{-3}% from the total value.

We define function[31]

$$\begin{aligned}\tilde{\alpha}_-(x_0,x)&=r^3\triangle\frac{\alpha_-(x_0,x)}{r}\\&=\alpha_-(x_0,x)-x\frac{\partial\alpha_-(x_0,x)}{\partial x}+x^2\frac{\partial^2\alpha_-(x_0,x)}{\partial x^2}\end{aligned}\qquad(13)$$

and construct the dimensionless vacuum energy density at different values of the coupling to the space–time curvature scalar (ξ) in the form:

$$r^3\varepsilon_{\rm ren}=\alpha_+(x_0,x)-\left(\xi-\frac{1}{4}\right)\tilde{\alpha}_-(x_0,x)\,.\qquad(14)$$

The behavior of $\alpha_\pm$, $\tilde{\alpha}_-$ and $r^3\varepsilon_{\rm ren}$ as functions of the distance from the axis of the tube for different values of r_0 and ξ was analyzed in Refs. 30 and 31. Of primary interest is the behavior at the decrease of the tube radius. It seems plausible that this case becomes more similar to the case of the tube of zero radius (singular thread). However, there are some peculiarities in the behavior in the vicinity of the tube, and we discuss them following Ref. 32. Let us first recall the exact expressions corresponding to the case of the singular magnetic thread (see Ref. 23):

$$\begin{aligned}\alpha_+(0,x)=\frac{x^3}{3\pi^2}\Bigg\{&\frac{\pi}{2}-2xK_0(2x)-K_1(2x)+\frac{K_2(2x)}{2x}\\&-\pi x[K_0(2x)L_1(2x)+K_1(2x)L_0(2x)]\Bigg\}\,,\end{aligned}\qquad(15)$$

$$\alpha_-(0,x) = \frac{x}{\pi^2}\Big\{\frac{\pi}{2} - 2xK_0(2x) - K_1(2x) - \pi x[K_0(2x)L_1(2x) + K_1(2x)L_0(2x)]\Big\}, \tag{16}$$

$$\tilde{\alpha}_-(0,x) = -\frac{x}{\pi^2}[2xK_0(2x) + K_1(2x)], \tag{17}$$

where $K_\nu(u)$ and $L_\nu(u)$ are the Macdonald and the modified Struve functions of order ν. Consequently, in the vicinity of a thread one gets

$$\alpha_+(0,x) = \frac{1-3x^2}{12\pi^2}, \qquad x \ll 1, \tag{18}$$

$$\alpha_-(0,x) = -\frac{1-\pi x + (3-2\gamma-2\ln x)x^2}{2\pi^2} + O(x^3), \quad x \ll 1, \tag{19}$$

$$\tilde{\alpha}_-(0,x) = -\frac{1}{2\pi^2} + \frac{1+2\gamma+2\ln x}{2\pi^2}\,x^2 + O(x^3), \qquad x \ll 1, \tag{20}$$

where γ is the Euler constant. Using the latter relations, we get asymptotics of the renormalized vacuum energy density at small distances from the singular magnetic thread

$$r^3\varepsilon_{\rm ren}^{\rm sing} = \frac{1}{12\pi^2} - \frac{x^2}{4\pi^2} - \left(\xi - \frac{1}{4}\right) \times \left(-\frac{1}{2\pi^2} + \frac{1+2\gamma+2\ln x}{2\pi^2}x^2\right) + O(x^3), \quad x \ll 1. \tag{21}$$

In contrast to (18) and (19), the $\alpha_\pm(x_0,x)$ functions in the case of nonzero radius are vanishing quadratically in the vicinity of the tube, see Ref. 31,

$$\alpha_\pm(x_0,x)|_{x\to x_0} \sim O[(x-x_0)^2]. \tag{22}$$

To be more precise, we assume the asymptotics in the form, cf. (12),

$$\alpha_\pm(x_0,x) = \pm\frac{(x-x_0)^2}{x^2} f_\pm(x_0,x), \tag{23}$$

then one gets

$$\tilde{\alpha}_-(x_0,x) = -(x-x_0)^2\frac{\partial^2}{\partial x^2}f_-(x_0,x) + \left(1 - 6\frac{x_0}{x} + 5\frac{x_0^2}{x^2}\right)x\frac{\partial}{\partial x}f_-(x_0,x) - \left(1 - 8\frac{x_0}{x} + 9\frac{x_0^2}{x^2}\right)f_-(x_0,x), \tag{24}$$

with $\tilde{\alpha}_-(x_0,x_0) = -2f_-(x_0,x_0)$.

The $f_\pm(x_0,x)$ functions are adjusted as

$$f_+(0,x) = \frac{1-3x^2}{12\pi^2}, \qquad x \ll 1, \tag{25}$$

$$f_-(0,x) = \frac{1-\pi x + (3-2\gamma-2\ln x)x^2}{2\pi^2}, \quad x \ll 1. \tag{26}$$

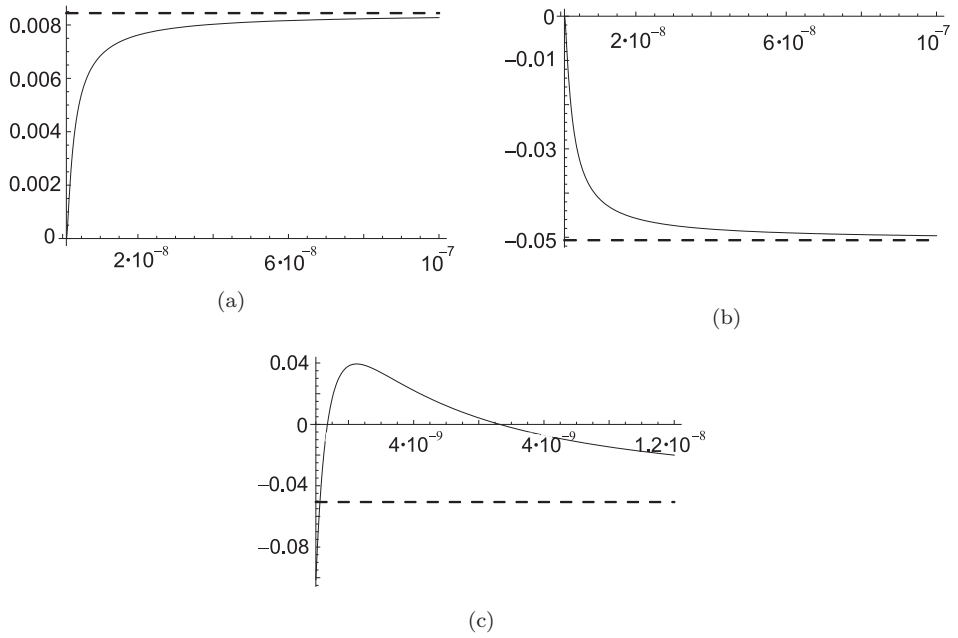

Fig. 1. The behavior of the constituents of the dimensionless vacuum energy density at small distances from the tube: (a) α_+, (b) α_- and (c) $\tilde{\alpha}_-$ for the case of $x_0 = 10^{-9}$ (solid line). The behavior of the corresponding functions for the case of a singular magnetic thread is presented by a dashed line. Variable x ($x > x_0$) is along the abscissa axis.

consequently, one gets

$$\tilde{\alpha}_-(x_0,x)\big|_{\substack{x_0\to 0\\ x\to x_0}} = -\frac{1}{2\pi^2} + \frac{1+2\gamma+2\ln x}{2\pi^2}x^2 + \frac{4-\pi x}{\pi^2 x}x_0 + \frac{-9+4\pi x-7x^2+2\gamma x^2+2x^2\ln x}{2\pi^2 x^2}x_0^2\,. \tag{27}$$

The asymptotical behavior of the $\alpha_\pm$ and $\tilde{\alpha}_-$ functions with the use of (23)–(27) is presented in Fig. 1 for the case of a sufficiently small value of x_0. It should be noted that the $f_\pm(x_0,x)$ functions depend strongly on x_0.

3. Total Vacuum Energy and the Casimir Force in a Plane

The total vacuum energy which is induced in a plane outside the magnetic flux region is

$$E_2 = 2\pi m\left[\int_{x_0}^{\infty}\frac{\alpha_+(x_0,x)}{x^2}\,dx - \left(\xi-\frac{1}{4}\right)\int_{x_0}^{\infty}\frac{\tilde{\alpha}_-(x_0,x)}{x^2}\,dx\right]. \tag{28}$$

In view of the relation

$$\int_{x_0}^{\infty}\frac{\tilde{\alpha}_-(x_0,x)}{x^2}\,dx = -x\frac{\partial}{\partial x}\left(\frac{\alpha_-(x_0,x)}{x}\right)\Big|_{x=x_0} \tag{29}$$

which follows from (13), and relations (23) and (26), we conclude that the total vacuum energy is independent of the coupling to the space–time curvature scalar (ξ):

$$E_2 = m\mathcal{D}(mr_0)\,, \tag{30}$$

where

$$\mathcal{D}(x_0) = 2\pi \int_{x_0}^{\infty} \frac{\alpha_+(x_0, x)}{x^2}\, dx\,. \tag{31}$$

This is in contrast to the case of the singular magnetic thread, when the total induced vacuum energy is divergent and ξ-dependent (see Ref. 23):

$$E_2^{\rm sing} \equiv \int_0^{2\pi} d\varphi \int_0^{\infty} \varepsilon_{\rm ren}^{\rm sing} r\, dr \sim 4m\left(\xi - \frac{1}{12}\right) \int_0 \frac{dx}{x^2}\,. \tag{32}$$

It is curious that the vacuum energy in this case is finite at $\xi = 1/12$, being equal to

$$\begin{aligned} E_2^{\rm sing}|_{\xi=1/12} &= \frac{2m}{3\pi} \int_0^{\infty} \left\{ \frac{\pi}{2} - \left(2x + \frac{1}{2x}\right) K_0(2x) - K_1(2x) \right. \\ &\quad \left. - \pi x [K_0(2x) L_1(2x) + K_1(2x) L_0(2x)] \right\} x\, dx \\ &= -0.01989 \times 2\pi m\,, \end{aligned} \tag{33}$$

and taking the negative value.

Although vacuum energy E_2 (30) is finite, its value grows infinitely as x_0 tends to zero (see (23) and (25)):

$$E_2|_{x_0 \to 0} = m\left[\frac{1}{18\pi x_0} - \frac{x_0}{\pi} \ln x_0 + O(x_0^3)\right], \tag{34}$$

which is in accordance with the divergence of the vacuum energy in the case of the singular magnetic thread. To be more precise, relation (29) fails to yield zero in the case $x_0 = 0$, and, therefore, the divergence of the vacuum energy in the latter case becomes ξ-dependent.

We present the values of vacuum energy E_2 (30) for several values of the tube radius in the second row of the Table 1.

Table 1. Values of the dimensionless vacuum energy at several values of mr_0.

x_0	3/2	1	1/2	10^{-1}	10^{-2}	10^{-3}
E_2/m	$3.15 \cdot 10^{-11}$	$4.363 \cdot 10^{-9}$	$1.299 \cdot 10^{-6}$	$1.038 \cdot 10^{-3}$	0.0666	0.933
E_3/m^2	$3.577 \cdot 10^{-12}$	$5.942 \cdot 10^{-10}$	$2.411 \cdot 10^{-7}$	$4.162 \cdot 10^{-4}$	0.119	12.704

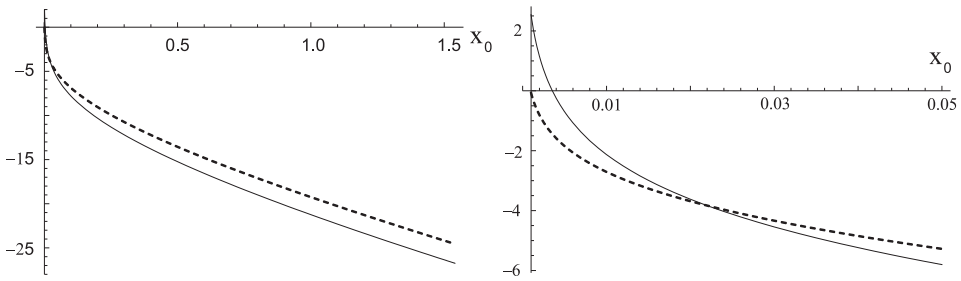

Fig. 2. The logarithm of the induced vacuum energy in the plane as a function of the tube radius starting from $x_0 = 10^{-3}$: $\ln \frac{E_2}{m}$ is given by a dashed curve and $\ln \frac{E_3}{m^2}$ (see Sec. 4) is given by a solid curve.

These results are also given in Fig. 2 in a logarithmic scale, where the dots corresponding to the data in Table 1 are joined with the help of an interpolation function $\eta(x_0) = \ln \frac{E_2}{m}$, which, for the range $x_0 > 10^{-3}$, can be taken in the form

$$\eta(x_0) = -a - x_0^b P_n(x_0) - \big(c + x_0^d Q_n(x_0)\big) \ln x_0 \,, \tag{35}$$

where a, b, c, d are the positive constants and $P_n(x_0)$, $Q_n(x_0)$ are polynomials in x_0 of the nth order.

To change the radius of the flux tube one has to apply a work that is equal to the change of the total vacuum energy which is induced outside the tube. In the case of the infinitely small change of the radius one has

$$\delta E_2 = 2\pi P_2 r_0 \delta r_0 \,, \tag{36}$$

where P_2 can be interpreted as the vacuum pressure which acts from the outside to the inside of the tube

$$P_2 = \frac{1}{2\pi r_0} \frac{dE_2}{dr_0} = \frac{m^3}{2\pi x_0} \mathcal{D}'(x_0) \,, \tag{37}$$

$\mathcal{D}'(x_0) = \frac{d}{dx_0} \mathcal{D}(x_0)$, and the value of the magnetic flux inside the tube is assumed to remain unchanged.

This results in the Casimir force acting from the inside to the outside of the tube

$$F_2 = -2\pi r_0 P_2 = -m^2 \mathcal{D}'(x_0) \,. \tag{38}$$

As the tube radius tends to zero, the Casimir force grows infinitely:

$$F_2 = m^2 \left(\frac{1}{18\pi x_0^2} - \frac{1}{\pi} (\ln x_0 + 1) + O(x_0^2) \right) . \tag{39}$$

The behavior of the Casimir force is presented in Fig. 3.

As one can see, the Casimir force tends to increase the radius of the tube and to minimize the induced vacuum energy of the quantized scalar field. As to the energy stored inside the tube, it is the purely classical energy of the magnetic field. Its behavior at the increase of the tube radius as the magnetic flux is held constant

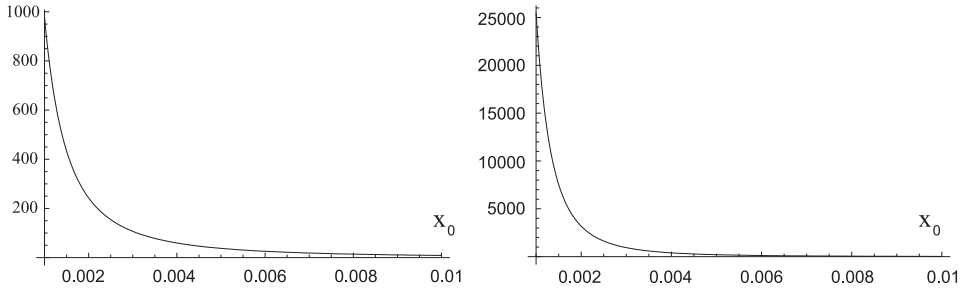

Fig. 3. The Casimir force as a function of the tube radius in the range $10^{-3} < x_0 < 10^{-2}$: F_2/m^2 is on the left and F_3/m^3 (see Sec. 4) is on the right.

can be different depending on the details of the magnetic field configuration. Mild assumptions as to the smoothness of the configuration yield that the energy is either constant or decreasing at most as $\sim r_0^{-2}$.

4. Generalization to Higher than Two Dimensions

In d-dimensional space, we define the vacuum energy which is induced outside a $(d-2)$-tube in a plane orthogonal to it:

$$E_d = \int_0^{2\pi} d\varphi \int_{r_0}^{\infty} dr\, r\varepsilon_{\rm ren}\,, \tag{40}$$

where $\varepsilon_{\rm ren}$ is given by (7). Generalizing relation (29) we obtain relation

$$\int_{r_0}^{\infty} dr\, r\Delta \int d^{d-2}\mathbf{k}_z \int_0^{\infty} \frac{dk\, k}{\sqrt{\mathbf{k}_z^2+k^2+m^2}}[S(kr,kr_0)-S(kr,kr_0)|_{\Phi=0}]$$
$$= -\left\{r\partial_r \int d^{d-2}\mathbf{k}_z \int_0^{\infty} \frac{dk\, k}{\sqrt{\mathbf{k}_z^2+k^2+m^2}}[S(kr,kr_0)-S(kr,kr_0)|_{\Phi=0}]\right\}\Big|_{r=r_0}. \tag{41}$$

The right-hand side of (41) is obviously vanishing due to relation

$$[r\partial_r S(kr,kr_0)]|_{r=r_0} = 0\,, \tag{42}$$

stemming from the definition of $S(kr,kr_0)$, see (8). Consequently, the Casimir energy, i.e. the induced vacuum energy per unit length of the $(d-2)$-tube, is independent of the coupling to the space–time curvature scalar

$$E_d = (2\pi)^{2-d}\int_{r_0}^{\infty} dr\, r \int d^{d-2}\mathbf{k}_z \int_0^{\infty} dk\, k\sqrt{\mathbf{k}_z^2+k^2+m^2}$$
$$\times\,[S(kr,kr_0)-S(kr,kr_0)|_{\Phi=0}]\,. \tag{43}$$

Changing the order of integration over r and $\mathbf{k}_z$, we relate E_d to the total induced vacuum energy in the $d=2$ case, E_2 (30):

$$E_d = m^{d-1}\frac{(4\pi)^{1-d/2}}{\Gamma(d/2)}\int_0^{\infty} du\sqrt{1+u^{2/(d-2)}}\,\mathcal{D}\big(x_0\sqrt{1+u^{2/(d-2)}}\big)\,, \tag{44}$$

where $u = (|\mathbf{k}_z| r_0)^{d-2}$, $\Gamma(y)$ is the Euler gamma function, and

$$\mathcal{D}(y) = \int_y^\infty \frac{dx}{x^2} \int_0^\infty dz\, z\sqrt{z^2+x^2}\left[S\left(z, z\frac{y}{x}\right) - S\left(z, z\frac{y}{x}\right)\Big|_{\Phi=0}\right], \tag{45}$$

is generalizing (31) to arbitrary values of the flux.

Similarly to the $d = 2$ case we define the Casimir force acting from the inside to the outside of the $(d-2)$-tube along the radial direction

$$F_d = -\frac{dE_d}{dr_0}, \tag{46}$$

and relate it to the Casimir force in the $d = 2$ case, F_2 (38):

$$F_d = -m^d \frac{(4\pi)^{1-d/2}}{\Gamma(d/2)} \int_0^\infty du\big(1+u^{2/(d-2)}\big)\mathcal{D}'\big(x_0\sqrt{1+u^{2/(d-2)}}\big). \tag{47}$$

It should be emphasized that relations (44) and (47) are valid for arbitrary values of the flux. The finiteness of integrals in (44) and (47) is due to the sufficiently strong decrease of $\mathcal{D}(x_0)$ and $\mathcal{D}'(x_0)$ at $x_0 \gg 1$, which was demonstrated for $\Phi = (2n+1)\pi e^{-1}$ in the previous section.

Changing the integration variable in (44) and (47), we get

$$E_d = \frac{2}{r_0^{d-1}} \frac{(4\pi)^{1-d/2}}{\Gamma\big(\frac{d-2}{2}\big)} \int_{x_0}^\infty dv\, v^2\big(v^2-x_0^2\big)^{\frac{d-4}{2}}\mathcal{D}(v), \tag{48}$$

$$F_d = -\frac{2}{r_0^{d}} \frac{(4\pi)^{1-d/2}}{\Gamma\big(\frac{d-2}{2}\big)} \int_{x_0}^\infty dv\, v^3\big(v^2-x_0^2\big)^{\frac{d-4}{2}}\mathcal{D}'(v), \tag{49}$$

where the latter in the case of $d > 3$, after integration by parts, takes form

$$F_d = \frac{2}{r_0^{d}} \frac{(4\pi)^{1-d/2}}{\Gamma\big(\frac{d-2}{2}\big)} \int_{x_0}^\infty dv\, v^2\big(v^2-x_0^2\big)^{\frac{d-6}{2}}[(d-1)v^2-3x_0^2]\mathcal{D}(v). \tag{50}$$

At $x_0 \ll 1$, we obtain

$$F_d = \frac{d-1}{r_0}E_d = \frac{C_\Phi(d)}{r_0^d}, \quad r_0 \ll m^{-1}, \tag{51}$$

where

$$C_\Phi(d) = 2\frac{(4\pi)^{1-d/2}}{\Gamma\big(\frac{d-2}{2}\big)}(d-1)\int_0^\infty dv\, v^{d-2}\mathcal{D}(v), \quad d > 2, \tag{52}$$

is monotonically decreasing with the increase of d. The numerical estimate of $C(d)$ at $\Phi = (2n+1)\pi e^{-1}$ in the range $3 \le d \le 10$ yields that it can be well approximated as

$$C_\Phi(d) = (d-1)d^{10.025}\exp\left(\frac{44.76}{d} - 3d - 28.097\right), \tag{53}$$

where a decisive factor is e^{-3d}. In the following we shall use a rough, but quite suitable for a further analysis, approximation

$$C_\Phi(d) \approx (d-1)e^{-2.7d-4}\,, \tag{54}$$

that is valid for $d \leq 10$.

In view of (54) and relation

$$\frac{1}{d-2}\int_{x_0}^{\infty} dv\, v(v^2-x_0^2)^{\frac{d-2}{2}}[2\mathcal{D}'(v)+v\mathcal{D}''(v)] \leq (d-1)\int_0^{\infty} dv\, v^{d-2}\mathcal{D}(v)\,, \tag{55}$$

where the equality sign corresponds to sufficiently small values of x_0, we find that the dimensionless force, $m^{-d}F_d$, as a function of d at $\Phi = (2n+1)\pi e^{-1}$ can be approximated as

$$m^{-d}F_d \approx (d-1)e^{-4}e^{-d(\ln x_0+2.7)}\,. \tag{56}$$

Thus, the dimensionless force increases with d at $x_0 < e^{-2.7}$ and decreases with d at $x_0 > e^{-2.7}$.

In the $d=3$ case, we get

$$\begin{aligned} E_3 &= \frac{m^2}{\pi}\int_0^{\infty} du\sqrt{1+u^2}\mathcal{D}\big(x_0\sqrt{1+u^2}\big) \\ &= -\frac{1}{\pi r_0^2}\int_{x_0}^{\infty} dv\sqrt{v^2-x_0^2}[\mathcal{D}(v)+v\mathcal{D}'(v)] \end{aligned} \tag{57}$$

and

$$\begin{aligned} F_3 &= -\frac{m^3}{\pi}\int_0^{\infty} du(1+u^2)\mathcal{D}'\big(x_0\sqrt{1+u^2}\big) \\ &= \frac{1}{\pi r_0^3}\int_{x_0}^{\infty} dv\, v\sqrt{v^2-x_0^2}[2\mathcal{D}'(v)+v\mathcal{D}''(v)]\,. \end{aligned} \tag{58}$$

We present the values of Casimir energy E_3 (57) at $\Phi = (2n+1)\pi e^{-1}$ ($n \in \mathbb{Z}$) for several values of the tube radius in the third row of Table 1. These results are also given in Fig. 2 in a logarithmic scale, where the dots corresponding to the data in Table 1 are joined with help of an interpolation function similarly to that as in the previous section; the comparison is made with the $d=2$ case. Casimir force F_3 (58) is presented on the right of Fig. 3 and compared with Casimir force F_2 (38); the former attains a considerable value of $2.54\times 10^4 \times m^3$ at $r_0 = 10^{-3}m^{-1}$.

At $x_0 \ll 1$, restoring constants $\hbar$ and c, we obtain

$$F_3 = \frac{2}{r_0}E_3 = \frac{\hbar c}{r_0^3}\,C_\Phi(3)\,, \quad r_0 \ll m^{-1}\,, \tag{59}$$

where, see (52),

$$C_\Phi(3) = \frac{2}{\pi}\int_0^{\infty} dv\, v\mathcal{D}(v)\,. \tag{60}$$

Let us compare Casimir force F_3 (59) with the force caused by the classical magnetic field inside the tube. Assuming the uniformity of the magnetic field filling completely the tube, $B = \Phi/(\pi r_0^2)$, one obtains an expression for the classical energy per unit length of the tube, $E^{(\mathrm{class})} = \Phi^2/(2\pi r_0^2)$, which can be rewritten in terms of London flux quantum $\Phi_0 = 2\pi\hbar c e^{-1}$ and fine structure constant $\alpha = e^2(4\pi\hbar c)^{-1}$:

$$E^{(\mathrm{class})} = \frac{\hbar c}{r_0^2}\frac{\Phi^2}{\Phi_0^2}\frac{1}{2\alpha}\,. \tag{61}$$

The classical force which tends to decrease energy (61) by increasing the tube radius under the steady magnetic flux filling completely the tube is

$$F^{(\mathrm{class})} = -\frac{d}{dr_0}E^{(\mathrm{class})} = \frac{\hbar c}{r_0^3}\frac{\Phi^2}{\Phi_0^2}\frac{1}{\alpha}\,. \tag{62}$$

Comparing this with Casimir force F_3 (59), we recall that $C_\Phi(3)$ is a periodic function of the magnetic flux, vanishing at $\Phi = n\Phi_0$. Even the maximal value of $C_\Phi(3)$ which is achieved at $\Phi = (n+1/2)\Phi_0$ and is equal to $2.545\cdot 10^{-5}$, see (54), is more than million times smaller than the value of the corresponding factor, $\Phi^2/(\Phi_0^2\alpha)$, in (62): taking $\Phi = \Phi_0/2$ one obtains value $(4\alpha)^{-1} \approx 34.2$ for this factor.

However, as it was already noted, the classical force acting from the inside of the tube depends strongly on the detailed form of the magnetic field configuration: it decreases if the magnetic field is decreasing in the vicinity of the tube edge. For instance, in the case of the magnetic field concentrated wholly inside a tube of smaller radius, the classical force acting to extend the tube of larger radius disappears at all, and only the Casimir force from the outside vacuum is left in this capacity.

5. Summary

In the present paper, we consider the vacuum polarization effects which are induced in charged scalar matter by a magnetic flux enclosed in an impenetrable finite-radius tube; a perfectly reflecting (Dirichlet) boundary condition is imposed at the edge of the tube. The previous analysis of the induced vacuum energy density in the $d = 2$ case[30,31] was extended down to the values of the tube radius as small as $r_0 = 10^{-3}\hbar(mc)^{-1}$ in Ref. 32, where it was shown that contrary to the case of a singular magnetic thread ($r_0 = 0$), the vacuum energy density is finite everywhere, but its behavior is very similar to that in the $r_0 = 0$ case, except the behavior in the vicinity of the tube, where peculiar oscillations appear. The case of $r_0 < 10^{-3}\hbar(mc)^{-1}$ is analyzed indirectly by combining the numerical and analytical estimates, and the difference between the $r_0 = 0$ and $r_0 = 10^{-9}\hbar(mc)^{-1}$ cases is illustrated in Fig. 1.

These two circumstances (the finiteness and at the same time the similarity to the case of a singular thread) which are proven in the $d = 2$ case have far-reaching consequences that allow us to determine the *finite* Casimir energy in the case of space of arbitrary dimension, as long as the tube radius is taken into account. We

find that the Casimir energy, i.e. the vacuum energy per unit length of the $(d-2)$-tube, is positive and independent of the coupling to the space–time curvature scalar (ξ), notwithstanding the ξ-dependence of the vacuum energy density and its lack of positivity. The functional dependence of the Casimir energy on the tube radius for the magnetic flux equal to half of the London flux quantum is numerically estimated for the range $10^{-3}\hbar(mc)^{-1} < r_0 < 1.5\hbar(mc)^{-1}$, and the results for the $d = 2$ and $d = 3$ cases are presented in Table 1 and in Fig. 2. The Casimir energy is negligible for $r_0 \sim \hbar(mc)^{-1}$, being of order $10^{-10} \times m^{d-1}c^d\hbar^{2-d}$ for $d = 2, 3$ and even less for larger d, but it increases considerably with the decrease of the tube radius.

The Casimir energy gives rise to the Casimir force which is directed from the inside to the outside of the tube along its normal. The force is ξ-independent as well as the Casimir energy. The force acts at the increase of the tube radius and the decrease of the Casimir energy, if the magnetic flux is held steady. The behavior of the force as a function of the tube radius in the $d = 2$ and $d = 3$ cases for the magnetic flux equal to half of the London flux quantum is illustrated in Fig. 3. The force takes considerable values at small values of the tube radius and actually disappears otherwise: in the $d = 3$ case it is, e.g. $2.54 \times 10^4 \times m^3c^4\hbar^{-2}$ at $r_0 = 10^{-3}\hbar(mc)^{-1}$ and $10^{-3} \times m^3c^4\hbar^{-2}$ at $r_0 = 10^{-1}\hbar(mc)^{-1}$.

It should be noted that we consider the case of the Casimir force caused by a magnetic flux enclosed by a boundary where the Dirichlet boundary condition is imposed. The force is periodic in the flux value with a period equal to the London flux quantum, attaining its maximal value at $\Phi = (n + 1/2)\Phi_0$ and vanishing at $\Phi = n\Phi_0$ ($n \in \mathbb{Z}$). A general conclusion which is valid for arbitrary spatial dimension $d \geq 2$ is that the Casimir energy and force at $r_0 \ll \hbar(mc)^{-1}$, when they take considerable values, are actually the same as they are in the case of the massless scalar field, see (34), (39) and (51); the massive case becomes formally distinct from the massless one at larger values of the tube radius, when the Casimir energy and force take negligible values. The Casimir force and energy increase with d at smaller r_0, when they are considerable, while decrease with d at larger r_0, when they are negligible, see (56); even the comparison of numerical calculations for the $d = 2$ and $d = 3$ cases reveals this fact, see Table 1 and Fig. 2.

Whereas in the case of parallel plates the pure action of the Casimir force to minimize the Casimir energy leads to a collapse, the pure action of the Casimir force to minimize the Casimir energy in the case of a flux tube leads not to a collapse but to an expansion of the tube in the transverse direction. Note that the classical energy of the constant magnetic flux inside the tube is most likely to be constant or decreasing maximally as r_0^{-2} with the expansion of the tube radius, see (61). Thus, the Casimir force tends to smear both quantum and classical effects of the flux tube. The vacuum polarization is quite negligible at $mcr_0 > \hbar$, whereas it becomes noticeable at $mcr_0 \ll \hbar$. If the flux tube is interpreted as a topological defect of the vortex type, then the vacuum polarization in its background is absent when the mass of the Higgs field ($m_H \sim \hbar(r_0c)^{-1}$) does not exceed the mass of the quantum matter field, $m_H \lesssim m$. Vacuum polarization is essential for the quantum

matter field with the mass which is much less than the Higgs mass, $m \ll m_H$; since $\Phi = 2\pi\hbar c e_H^{-1}$ for the topological defect case, the effect is maximal when the coupling of the Higgs field to the gauge field is twice the coupling of the quantum matter field to the gauge field, $e_H = 2e$ (e.g. the Higgs field describing the Cooper pair in a superconductor). In particular, we can arrive at a conclusion that a cosmic string which has been formed at the grand unification scale polarizes the vacuum of the present-day quantum matter, but it has no effect on the vacuum of matter fields with masses which are comparable to the scale of grand unification.

Acknowledgments

The work was partially supported by special program "Microscopic and phenomenological models of fundamental physical processes in micro- and macroworld" of the Department of Physics and Astronomy of the National Academy of Sciences of Ukraine and by the ICTP — SEENET-MTP grant PRJ-09 "Strings and Cosmology." V. M. Gorkavenko and Yu. A. Sitenko acknowledge the support from the State Agency for Science, Innovations and Informatization of Ukraine under the SFFR-BRRFR grant F54.1/019.

References

1. H. B. G. Casimir, *Proc. Kon. Ned. Akad. Wetenschap B* **51**, 793 (1948).
2. H. B. G. Casimir, *Physica* **19**, 846 (1953).
3. K. A. Milton, *The Casimir Effect*: *Physical Manifestations of Zero-Point Energy* (World Scientific, 2001).
4. M. Bordag, G. L. Klimchitskaya, U. Mohideen and V. M. Mostepanenko, *Advances in the Casimir Effect* (Oxford University Press, Oxford, 2009).
5. S. K. Lamoreax, *Phys. Rev. Lett.* **78**, 5 (1997).
6. G. Bressi, G. Carugno, R. Onofrio and G. Ruoso, *Phys. Rev. Lett.* **88**, 041804 (2002).
7. Y. Aharonov and D. Bohm, *Phys. Rev.* **115**, 485 (1959).
8. Yu. A. Sitenko and A. Yu. Babansky, *Mod. Phys. Lett. A* **13**, 379 (1998).
9. L. L. DeRaad, Jr. and K. A. Milton, *Ann. Phys.* (*N.Y.*) **136**, 229 (1981).
10. P. Gosdzinsky and A. Romeo, *Phys. Lett. B* **441**, 265 (1998).
11. N. Graham, R. L. Jaffe, V. Khemani, M. Quandt, M. Scandurra and H. Weigel, *Phys. Lett. B* **572**, 196 (2003).
12. S. A. Fulling, *J. Phys. A*: *Math. Theor.* **36**, 6857 (2003).
13. G. Barton, *Phys. Rev. D* **73**, 065018 (2006).
14. I. Cavero-Pelaez, K. A. Milton and K. Kirsten, *J. Phys. A*: *Math. Theor.* **40**, 3607 (2007).
15. A. Bulgac, P. Magierski and A. Wirzba, *Phys. Rev. D* **73**, 025007 (2006).
16. A. Wirzba, *J. Phys. A*: *Math. Theor.* **41**, 164003 (2008).
17. M. Schaden, *Phys. Rev. A* **73**, 042102 (2006).
18. A. A. Abrikosov, *Sov. Phys. – JETP* **5**, 1174 (1957).
19. H. B. Nielsen and P. Olesen, *Nucl. Phys. B* **61**, 45 (1973).
20. R. P. Huebener, *Magnetic Flux Structure in Superconductors* (Springer-Verlag, Berlin, 1979).
21. A. Vilenkin and E. P. S. Shellard, *Cosmic Strings and Other Topological Defects* (Cambridge University Press, Cambridge, 1994).

22. M. B. Hindmarsh and T. W. B. Kibble, *Rep. Prog. Phys.* **58**, 477 (1995).
23. Yu. A. Sitenko and V. M. Gorkavenko, *Phys. Rev. D* **67**, 085015 (2003).
24. Yu. A. Sitenko and A. Yu. Babansky, *Phys. Atom. Nucl.* **61**, 790 (1998).
25. G. Dunne and T. M. Hall, *Phys. Lett. B* **419**, 322 (1998).
26. M. Bordag and K. Kirsten, *Phys. Rev. D* **60**, 105019 (1999).
27. M. P. Fry, *Int. J. Mod. Phys. A* **17**, 936 (2002).
28. K. Langfeld, L. Moyaerts and H. Gies, *Nucl. Phys. B* **646**, 158 (2002).
29. N. Graham, V. Khemani, M. Quandt, O. Schroeder and H. Weigel, *Nucl. Phys. B* **707**, 233 (2005).
30. V. M. Gorkavenko, Yu. A. Sitenko and O. B. Stepanov, *J. Phys. A*: *Math. Theor.* **43**, 175401 (2010).
31. V. M. Gorkavenko, Yu. A. Sitenko and O. B. Stepanov, *Int. J. Mod. Phys. A* **26**, 3889 (2011).
32. V. M. Gorkavenko, Yu. A. Sitenko and O. B. Stepanov, *Ukr. J. Phys.* **58**, 424 (2013).
33. R. Penrose, *Relativity, Groups and Topology*, eds. B. S. DeWitt and C. DeWitt (Gordon and Breach, New York, 1964).
34. N. A. Chernikov and E. A. Tagirov, *Ann. Inst. Henri Poincaré A* **9**, 109 (1968).
35. C. G. Callan, S. Coleman and R. Jackiw, *Ann. Phys.* (*N.Y.*) **59**, 42 (1970).

РОЗДІЛ 3

Індукування магнітного потоку топологічним дефектом

3.1. Індукування у вакуумі скалярного поля. Гранична умова типу Діріхле

International Journal of Modern Physics A
Vol. 31, No. 6 (2016) 1650017 (11 pages)

DOI: 10.1142/S0217751X16500172

Induced vacuum current and magnetic field in the background of a vortex

Volodymyr M. Gorkavenko

Department of Physics, Taras Shevchenko National University of Kyiv, 64 Volodymyrs'ka str., Kyiv 01601, Ukraine
gorka@univ.kiev.ua

Iryna V. Ivanchenko[*,‡] and Yurii A. Sitenko[*,†,§]

[*] *Bogolyubov Institute for Theoretical Physics, National Academy of Sciences of Ukraine, 14-b Metrologichna str., Kyiv 03680, Ukraine*
[†] *Institute for Theoretical Physics, University of Bern, Sidlerstrasse 5, CH-3012 Bern, Switzerland*
[‡] *iiv.ivanchenko@gmail.com*
[§] *sitenko@itp.unibe.ch*

Received 13 December 2015
Revised 8 January 2016
Accepted 11 January 2016
Published 18 February 2016

A topological defect in the form of the Abrikosov–Nielsen–Olesen vortex is considered as a gauge-flux-carrying tube that is impenetrable for quantum matter. Charged scalar matter field is quantized in the vortex background with the perfectly reflecting (Dirichlet) boundary condition imposed at the side surface of the vortex. We show that a current circulating around the vortex and a magnetic field directed along the vortex are induced in the vacuum, if the Compton wavelength of the matter field exceeds considerably the transverse size of the vortex. The vacuum current and magnetic field are periodic in the value of the gauge flux of the vortex, providing a quantum-field-theoretical manifestation of the Aharonov–Bohm effect. The total flux of the induced vacuum magnetic field attains notable finite values even for the Compton wavelength of the matter field exceeding the transverse size of the vortex by just three orders of magnitude.

Keywords: Vacuum polarization; vortex; current; magnetic flux.

PACS numbers: 11.27.+d, 11.10.Kk, 03.70.+k

1. Introduction

Spontaneous breakdown of continuous symmetries gives rise to topological defects (texture solitons) of various kinds. In particular, if the first homotopy group of the

group space of the broken symmetry group is nontrivial, then a linear topological defect known as the Abrikosov–Nielsen–Olesen (ANO) vortex[1,2] is formed. The vortex is described classically in terms of a spin-0 (Higgs) field which condenses and a spin-1 field which corresponds to the spontaneously broken gauge group; the former is coupled to the latter in the minimal way with constant $\tilde{e}_H$. The transverse size of the vortex is of the order of the correlation length, $\hbar(m_H c)^{-1}$, where m_H is the mass of the condensate field. Single-valuedness of the condensate field and finiteness of the vortex energy implement that the vortex flux is related to $\tilde{e}_H$: $\Phi = \oint d\mathbf{x}\,\mathbf{A}(\mathbf{x}) = 2\pi\hbar c\tilde{e}_H^{-1}$, where $\mathbf{A}(\mathbf{x})$ is the vector potential of the spin-1 gauge field, and the integral is over a path enclosing the vortex tube once. The quantized matter field is coupled minimally to the spin-1 field with constant $\tilde{e}$; thus quantum effects in the background of the ANO vortex depend on the value of $\tilde{e}\Phi$. The case of $\tilde{e}_H = 2\tilde{e}$ ($\Phi = \pi\hbar c\tilde{e}^{-1}$, half of the London flux quantum) is realized in ordinary Bardeen–Cooper–Schrieffer superconductors where the Cooper-pair field condenses and, in addition, there are normal electron (pair-breaking) excitations, see Ref. 3; the cases of fractional values of $\tilde{e}_H/(2\tilde{e})$ can be realized in chiral superfluids, liquid crystals and quantum liquids, see Refs. 4 and 5.

An issue of ANO vortices under the name of cosmic strings is widely discussed in the context of astrophysics and cosmology for more than three decades.[6,7] The formation of such topological defects during the cosmological expansion is predicted in most interesting models of high energy physics, providing an important link between cosmology and particle physics, see Ref. 8. Cosmic strings serve as plausible sources of detectable gravitational waves, high-energy cosmic rays and gamma-ray bursts.[9–11]

While considering the effect of the ANO vortices on the vacuum of quantum matter, the following circumstance should be kept in mind: the phase with broken symmetry exists outside the vortex and the vacuum is to be defined only there; hence the quantum matter field is not permitted to penetrate inside the vortex, obeying a boundary condition at its side surface. Further, we shall assume that the interaction between the ANO vortex and the quantum matter field is mediated by the vector potential of the vortex-forming spin-1 field only. The direct coupling between the vortex-forming spin-0 field and the quantum matter field can be neglected. The latter is consistent with the requirement that the Compton wavelength of the quantum matter field is much larger than the transverse size of the vortex, and this requirement will be substantiated in the course of this study. Thus, the ANO vortex has no effect on the surrounding matter in the framework of classical theory, and such an effect, if exists, is of purely quantum nature. The effect should be denoted as a quantum-field-theoretical manifestation of the famous Aharonov–Bohm effect,[12] see Ref. 13, and is characterized by the periodic dependence on the value of the vortex flux, Φ, with the period equal to the London flux quantum, $2\pi\hbar c\tilde{e}^{-1}$.

In this paper, we shall study the current and the magnetic field which are induced in the vacuum of the quantized charged scalar matter field by the ANO vortex. These vacuum characteristics were considered previously in the approximation

neglecting the transverse size of the vortex, see Refs. 14 and 15 and references therein. The aim of this study is to take account for the nonvanishing transverse size. We follow the lines of Refs. 16–19 where the Casimir energy and force in the background of the ANO vortex are studied. The quantized matter field is assumed to vanish at the side surface of the vortex, and the tension spread over the vortex is neglected; natural units $\hbar = c = 1$ will be used in the following.

2. Induced Vacuum Current and Total Magnetic Flux

We start with Lagrangian for a complex scalar field ψ in $(d+1)$-dimensional space–time

$$\mathcal{L} = (\nabla_\mu \psi)^* (\nabla^\mu \psi) - m^2 \psi^* \psi \,, \tag{1}$$

where ∇_μ is the covariant derivative and m is the mass of the scalar field. The operator of a second-quantized scalar field can be represented in the form

$$\Psi(x^0, \mathbf{x}) = \sum\!\!\!\!\!\!\int_\lambda \frac{1}{\sqrt{2E_\lambda}} \left[e^{-\mathrm{i}E_\lambda x^0} \psi_\lambda(\mathbf{x}) a_\lambda + e^{\mathrm{i}E_\lambda x^0} \psi^*_\lambda(\mathbf{x}) b^\dagger_\lambda \right]; \tag{2}$$

$a^\dagger_\lambda$ and a_λ ($b^\dagger_\lambda$ and b_λ) are the scalar particle (antiparticle) creation and destruction operators satisfying commutation relations

$$\left[a_\lambda, a^+_{\lambda'} \right]_- = \left[b_\lambda, b^+_{\lambda'} \right]_- = \langle \lambda' | \lambda \rangle \,; \tag{3}$$

λ is the set of parameters (quantum numbers) specifying the state; wave functions $\psi_\lambda(\mathbf{x})$ form a complete set of solutions to the stationary Klein–Fock–Gordon equation

$$(-\boldsymbol{\nabla}^2 + m^2)\psi_\lambda(\mathbf{x}) = E^2_\lambda \psi(\mathbf{x}) \,, \tag{4}$$

$E_\lambda = E_{-\lambda} > 0$ is the energy of the state; symbol $\sum\!\!\!\!\!\!\int_\lambda$ denotes summation over discrete and integration (with a certain measure) over continuous values of λ.

In this paper, we are considering a static background in the form of the cylindrically symmetric gauge flux tube of the finite transverse size. The coordinate system is chosen in such a way that the tube is along the z-axis. The tube in three-dimensional space is obviously generalized to the $(d-2)$-tube in d-dimensional space by adding extra $d-3$ dimensions as longitudinal ones. The covariant derivative is $\nabla_0 = \partial_0$, $\boldsymbol{\nabla} = \boldsymbol{\partial} - \mathrm{i}\tilde{e}\mathbf{V}$ with $\tilde{e}$ being the coupling constant of dimension $m^{(3-d)/2}$ and the vector potential possessing only one nonvanishing component given by

$$V_\varphi = \frac{\Phi}{2\pi} \,, \tag{5}$$

outside the tube; here, Φ is the value of the gauge flux inside the $(d-2)$-tube and φ is the angle in polar (r, φ) coordinates on a plane which is transverse to the tube. The Dirichlet boundary condition at the side surface of the tube ($r = r_0$) is imposed on the scalar field

$$\psi_\lambda|_{r=r_0} = 0 \,, \tag{6}$$

i.e. the quantum matter is assumed to be perfectly reflected from the thence impenetrable flux tube.

The solution to (4) and (6) outside the impenetrable tube of radius r_0 takes form

$$\psi_{kn\mathbf{p}}(\mathbf{x}) = (2\pi)^{(1-d)/2} e^{\mathrm{i}\mathbf{p}\mathbf{x}_{d-2}} e^{\mathrm{i}n\varphi} \Omega_{|n-\tilde{e}\Phi/2\pi|}(kr, kr_0)\,, \tag{7}$$

where

$$\Omega_\rho(u,v) = \frac{Y_\rho(v)J_\rho(u) - J_\rho(v)Y_\rho(u)}{\left[J_\rho^2(v) + Y_\rho^2(v)\right]^{1/2}}\,, \tag{8}$$

and $0 < k < \infty$, $-\infty < p^j < \infty$ ($j = \overline{1, d-2}$), $n \in \mathbb{Z}$ ($\mathbb{Z}$ is the set of integer numbers), $J_\rho(u)$ and $Y_\rho(u)$ are the Bessel functions of order ρ of the first and second kinds. Solutions (7) obey orthonormalization condition

$$\int_{r>r_0} d^d\mathbf{x}\, \psi^*_{kn\mathbf{p}}(\mathbf{x})\psi_{k'n'\mathbf{p}'}(\mathbf{x}) = \frac{\delta(k-k')}{k}\,\delta_{n,n'}\delta^{d-2}(\mathbf{p}-\mathbf{p}')\,. \tag{9}$$

The vacuum current of scalar field is defined as

$$\mathbf{j}(\mathbf{x}) = \frac{1}{2\mathrm{i}}\langle \mathrm{vac}|\left\{\left[\Psi^+(x^0,\mathbf{x}), \boldsymbol{\nabla}\Psi(x^0,\mathbf{x})\right]_+ - \left[\boldsymbol{\nabla}\Psi^+(x^0,\mathbf{x}), \Psi(x^0,\mathbf{x})\right]_+\right\}|\mathrm{vac}\rangle\,, \tag{10}$$

with $[A,B]_+ = AB + BA$. Using (2) and (7), we get $j_r = \mathbf{j}_{d-2} = 0$ and

$$\begin{aligned} j_\varphi(r) &\equiv x^1 j^2(\mathbf{x}) - x^2 j^1(\mathbf{x}) \\ &= (2\pi)^{1-d} \int d^{d-2}p \int_0^\infty dk\, k(\mathbf{p}^2 + k^2 + m^2)^{-1/2} S(kr, kr_0)\,, \end{aligned} \tag{11}$$

where

$$S(u,v) = \sum_{n\in\mathbb{Z}} \left(n - \frac{\tilde{e}\Phi}{2\pi}\right) \Omega^2_{|n-\tilde{e}\Phi/2\pi|}(u,v)\,. \tag{12}$$

Due to the infinite range of the summation, the last expression is periodic in flux Φ with a period equal to $2\pi\tilde{e}^{-1}$, i.e. it depends on quantity

$$F = \frac{\tilde{e}\Phi}{2\pi} - \left[\!\left[\frac{\tilde{e}\Phi}{2\pi}\right]\!\right], \tag{13}$$

where $[[u]]$ is the integer part of quantity u (i.e. the integer which is less than or equal to u).

Let us rewrite (12) in the form

$$S(u,v) = S_0(u) + S_1(u,v)\,, \tag{14}$$

where

$$S_0(u) = \sum_{n=0}^\infty \left[(n+1-F)J^2_{n+1-F}(u) - (n+F)J^2_{n+F}(u)\right] \tag{15}$$

and

$$S_1(u,v)=\sum_{n=0}^{\infty}[(n+1-F)\Lambda_{n+1-F}(u,v)-(n+F)\Lambda_{n+F}(u,v)]\,, \tag{16}$$

where

$$\Lambda_\rho(u,v)=\frac{J_\rho^2(v)\big[Y_\rho^2(u)-J_\rho^2(u)\big]-2J_\rho(v)J_\rho(u)Y_\rho(v)Y_\rho(u)}{Y_\rho^2(v)+J_\rho^2(v)}\,. \tag{17}$$

Vacuum current j_φ circulating around the $(d-2)$-tube leads to the appearance of the vacuum magnetic field with strength $B^{3\cdots d}$ directed along the $(d-2)$-tube; this is a consequence of the Maxwell equation

$$r\partial_r B_{(I)}^{3\cdots d}(r)=-ej_\varphi(r)\,, \tag{18}$$

where coupling constant e differs in general from $\tilde{e}$. The total flux of the induced vacuum magnetic field across a plane which is orthogonal to the $(d-2)$-tube is defined as

$$\Phi_d^{(I)}=2\pi\int_{r_0}^{\infty}dr\,rB_{(I)}^{3\cdots d}(r) \tag{19}$$

and is given by expression

$$\Phi_d^{(I)}=e\pi\int_{r_0}^{\infty}dr\,rj_\varphi(r)\bigg(1-\frac{r_0^2}{r^2}\bigg)\,. \tag{20}$$

Inserting $j_\varphi(r)$ (11) and changing the order of integration over r and $\mathbf{p}$, we obtain

$$\Phi_d^{(I)}=em^{d-3}\frac{(4\pi)^{(2-d)/2}}{2\Gamma(d/2)}\int_0^{\infty}\frac{du}{\sqrt{1+u^{2/(d-2)}}}\,\mathcal{D}\Big(mr_0\sqrt{1+u^{2/(d-2)}}\Big)\,, \tag{21}$$

where $\Gamma(v)$ is the Euler gamma-function and

$$\mathcal{D}(y)=\int_y^{\infty}dx\bigg(1-\frac{y^2}{x^2}\bigg)\int_0^{\infty}\frac{dz\,z}{\sqrt{z^2+x^2}}\,S\bigg(z,z\frac{y}{x}\bigg)\,. \tag{22}$$

It should be noted that function $\mathcal{D}(y)$ (22) is immediately related to the total induced vacuum magnetic flux in the $d=2$ case

$$\Phi_2^{(I)}=\frac{e}{2m}\,\mathcal{D}(mr_0)\,. \tag{23}$$

Since $S_1(u,0)=0$, one can obtain

$$\mathcal{D}(0)=\int_0^{\infty}dx\int_0^{\infty}\frac{dz\,z}{\sqrt{z^2+x^2}}\,S_0(z)=\frac{1}{3}\,F(1-F)\bigg(F-\frac{1}{2}\bigg)\,, \tag{24}$$

and the total induced vacuum magnetic flux in the $d=2$ case is finite in the limit of a singular (i.e. infinitely thin) vortex filament, $r_0\to 0$:[20,21]

$$\lim_{r_0\to 0}\Phi_2^{(I)}=\frac{e}{6m}\,F(1-F)\bigg(F-\frac{1}{2}\bigg)\,. \tag{25}$$

However, in the $d \geq 3$ cases the situation is different. One gets

$$\Phi_3^{(I)} = \frac{e}{2\pi} \int_0^\infty \frac{du}{\sqrt{1+u^2}}\, \mathcal{D}\big(mr_0\sqrt{1+u^2}\big)\,, \tag{26}$$

which yields[14]

$$\Phi_3^{(I)} \underset{r_0\to 0}{=} -\frac{e}{2\pi}\, \mathcal{D}(0)\ln(mr_0)\,. \tag{27}$$

In the $d > 3$ cases, one gets by changing the integration variable

$$\Phi_d^{(I)} = e r_0^{3-d} \frac{(4\pi)^{(2-d)/2}}{\Gamma\big(\frac{d-2}{2}\big)} \int_{mr_0}^\infty dv \big(v^2 - m^2 r_0^2\big)^{(d-4)/2} \mathcal{D}(v)\,, \tag{28}$$

which yields

$$\Phi_d^{(I)} \underset{r_0\to 0}{=} e r_0^{3-d} \frac{2(2F-1)\sin(F\pi)\Gamma\big(\frac{d-1}{2}+F\big)\Gamma\big(\frac{d+1}{2}-F\big)}{d(d-1)(d-3)(4\pi)^{d/2}\Gamma(d/2)}\,, \quad d>3\,. \tag{29}$$

3. Numerical Analysis of the Induced Vacuum Characteristics

Let us rewrite expression (11) in the $d = 2$ case in the dimensionless form

$$rj_\varphi(r) = \frac{1}{2\pi}\int_0^\infty dz\, z\left[z^2 + \left(\frac{mr_0}{\lambda}\right)^2\right]^{-1/2} S(z,\lambda z)\,, \tag{30}$$

where $\lambda = r_0/r$ ($\lambda \in [0,1]$). In the limit of a singular filament ($r_0 = 0$), expression (30) can be reduced to the following form, see Refs. 20 and 21:

$$rj_\varphi^{\rm sing}(r) = \frac{\sin(F\pi)}{\pi^3}\int_{mr}^\infty dw\, \frac{w^2}{\sqrt{w^2-(mr)^2}} \times \Big\{ w\big[K_{1-F}^2(w) - K_F^2(w)\big] + (2F-1)K_F(w)K_{1-F}(w)\Big\} \tag{31}$$

($K_\rho(u)$ is the Macdonald function of order ρ) with asymptotics

$$rj_\varphi^{\rm sing}(r) = e^{-1} r B_{(I)}^{\rm sing}(r) = -\frac{\tan(F\pi)}{4\pi}\left(F-\frac{1}{2}\right)^2 + O[(mr)^2]\,, \quad mr \ll 1 \tag{32}$$

and

$$rj_\varphi^{\rm sing}(r) = 2me^{-1}r^2 B_{(I)}^{\rm sing}(r) = \frac{\sin(F\pi)}{2\pi}\left(F-\frac{1}{2}\right)\frac{e^{-2mr}}{\sqrt{\pi mr}}\big(1+O[(mr)^{-1}]\big)\,, \quad mr \gg 1\,, \tag{33}$$

where $B_{(I)}^{\rm sing}(r)$ is the vacuum magnetic field which is induced in the $d = 2$ case by a singular vortex filament. The total induced vacuum magnetic flux in this case, see (25), attains the maximal absolute value equal to $|e|/(72\sqrt{3}m)$ at $F = F_\pm$, where

$$F_\pm = \frac{1}{2}\left(1 \pm \frac{1}{\sqrt{3}}\right). \tag{34}$$

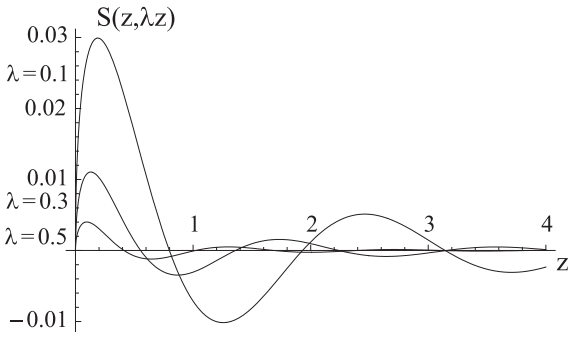

Fig. 1. Behavior of $S(z, \lambda z)$ at different values of λ.

Our primary task is to compute numerically the induced vacuum current in the $d = 2$ case, see (30), at $F = F_{\pm}$, when the integral in (30) is likely to be most distinct from zero. It can be shown that $S(z, \lambda z)$ is an oscillating function with an amplitude that exponentially decreases at large z, see Fig. 1. So, for a vortex tube of nonvanishing radius, we have to compute values of dimensionless quantity rj_{φ} at different values of λ. To do this, we perform high-precision numerical integration in (30) with the help of a technique developed earlier in Refs. 16–19 for the computation of the vacuum energy density which is induced in the $d = 2$ case by a vortex tube of nonvanishing radius. The results can be approximated by an interpolation function in the form

$$rj_{\varphi}(r) = \left[\frac{e^{-2x}}{\sqrt{x}}\right]\left[\left(\frac{x-x_0}{x}\right)^2 \frac{P_3(x-x_0)}{x^3}\right]\frac{Q_3(x^2)}{R_3(x^2)}\,, \quad x > x_0\,, \tag{35}$$

where $x = mr$, $x_0 = mr_0$ and $P_n(y)$, $Q_n(y)$, $R_n(y)$ are polynomials in y of the nth order with the x_0-dependent coefficients. The first factor in the square brackets describes the large distance behavior in the case of a zero-radius tube (filament), the second factor in the square brackets is an asymptotics at small distances from the side surface of the tube and the last factor describes the behavior at intermediate distances. Since the vortex tube is impenetrable, $rj_{\varphi}(r)$ (35) vanishes at $x \leq x_0$.

The results are presented on Fig. 2. The current is negligible for the tube of large radius, i.e. of order of the Compton wavelength and larger, $r_0 \geq m^{-1}$, see Fig. 2(a). But the current in the case of $r_0 \ll m^{-1}$ is comparable with the current in the case of a singular filament; note that the former is always less in value than the latter, see Fig. 2(b).

Of particular interest is the behavior of the induced vacuum current as the tube radius decreases. However, a direct numerical computation in the case of $x_0 < 10^{-3}$ is a rather complicated task, needing a long computational time. To surmount these difficulties, one has to take account for the following two circumstances. On one hand, the case of a singular filament is recovered as the tube radius tends to zero, $r_0 \to 0$. On the other hand, in contrast to (32), the current in the case of

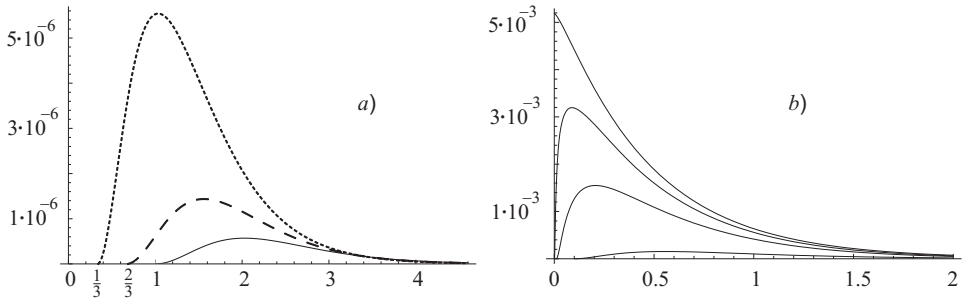

Fig. 2. The dimensionless induced vacuum current (rj_φ) as a function of the dimensionless distance from the axis of the tube (x) for different values of the dimensionless tube radius (x_0): (a) solid line corresponds to $rj_\varphi \cdot 10^2$ for $x_0 = 1$, dashed line corresponds to $rj_\varphi \cdot 10$ for $x_0 = 2/3$ and dotted line corresponds to rj_φ for $x_0 = 1/3$; (b) the cases of a singular filament ($x_0 = 0$) and of a tube with $x_0 = 10^{-3}$, 10^{-2} and 10^{-1} are from up to down on the plot. Variable x is along the abscissa axis.

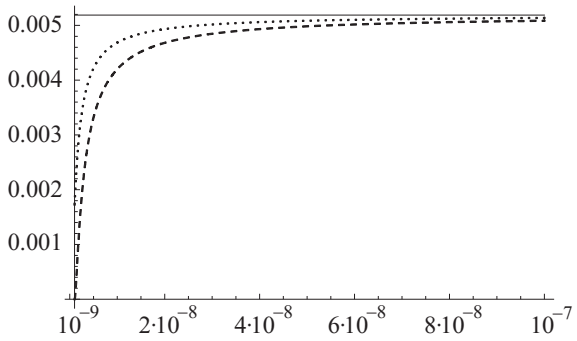

Fig. 3. The expected behavior of the dimensionless induced current (rj_φ, dashed line) and the dimensionless induced magnetic field ($e^{-1}rB_{(I)}$, dotted line) at small distances from the side surface of the tube for the case of $x_0 = 10^{-9}$; solid line corresponds to the case of a singular filament ($x_0 = 0$), see (32). The variable x ($x > x_0$) is along the abscissa axis.

the nonvanishing tube radius vanishes quadratically in the vicinity of the tube, see (35); this is in accordance with the analysis of the $r_0 \to 0$ limit for the solution to the Klein–Fock–Gordon equation.[22,23] Therefore, it is reasonable to assume the following behavior at $r_0 \ll m^{-1}$ and $r - r_0 \ll m^{-1}$:

$$rj_\varphi(r) = \left(\frac{r - r_0}{r}\right)^2 rj_\varphi^{\mathrm{sing}}(r)\,. \tag{36}$$

The expected asymptotic behavior of the current in the case of the extremely small tube radius ($r_0 = 10^{-9}m^{-1}$) is presented in Fig. 3.

Using (18) and (35), we compute numerically $B_{(I)}(r)$, i.e. the induced vacuum magnetic field in the $d = 2$ case. The results are presented in Fig. 4 for the tube radius in the range $10^{-3}m^{-1} \leq r_0 \leq m^{-1}$. As the tube radius decreases, the results approach to the result in the case of a singular filament, excepting the

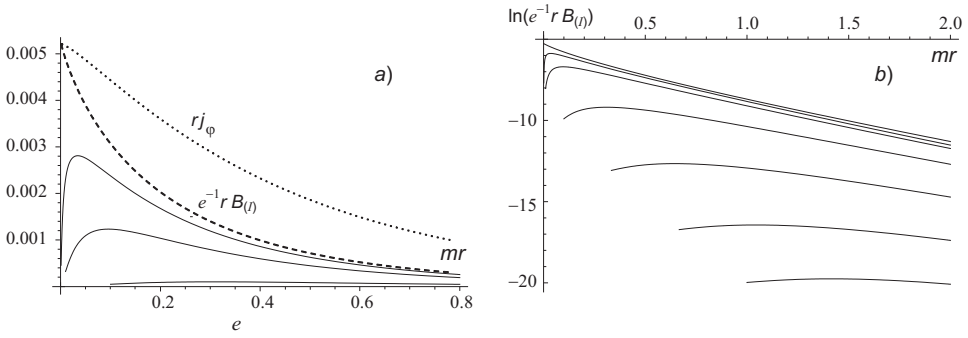

Fig. 4. The dimensionless induced vacuum magnetic field ($e^{-1}rB_{(I)}$) outside of tubes of different radius: (a) the cases of a singular filament (dotted and dashed lines) and tubes with $x_0 = 10^{-3}$, 10^{-2} and 10^{-1} are from up to down; (b) the case of a singular filament and tubes with $x_0 = 10^{-3}$, 10^{-2}, 10^{-1}, 2/3, 1/3 and 1 in logarithmic scale are from up to down.

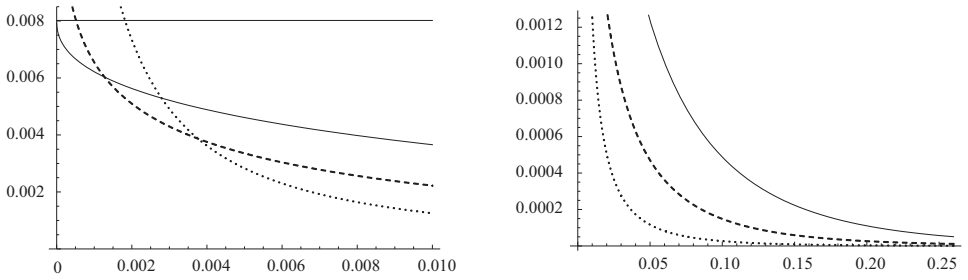

Fig. 5. The dimensionless induced vacuum magnetic flux in spaces of different dimensionality as a function of the dimensionless tube radius (x_0): $e^{-1}m\Phi_2^{(I)}$ — solid line, $e^{-1}\Phi_3^{(I)}$ — dashed line, $(em)^{-1}\Phi_4^{(I)}$ — dotted line. The case of small x_0 is on the left, and the case of large x_0 is on the right. The case of $x_0 = 0$ and $d = 2$ is presented by a horizontal solid line on the left.

region in the vicinity of the tube. The expected asymptotic ($r \to r_0$) behavior of the induced vacuum magnetic field in the case of the extremely small tube radius ($r_0 = 10^{-9}m^{-1}$) is presented in Fig. 3.

Using (21), (22), (30) and (35), we compute numerically the total induced vacuum magnetic flux in the $d = 2, 3, 4$ cases, i.e. $\Phi_2^{(I)}$, $\Phi_3^{(I)}$ and $\Phi_4^{(I)}$. The results are presented in Fig. 5 and in Table 1. In the $d = 2$ case, the absolute value of the flux induced by a filament is always larger than the absolute value of the flux induced by a tube of the nonvanishing radius. As the spatial dimension increases, the induced flux becomes a more strongly decreasing function of the large tube radius ($r_0 \gtrsim m^{-1}$) and a more strongly increasing function of the small tube radius ($r_0 \ll m^{-1}$). Of particular interest is the realistic case of $d = 3$. Whereas the induced flux in the unphysical case of a singular filament is infinite, see (27) and (29) in the limit $r_0 \to 0$, the induced flux in the physical case of a tube of the nonvanishing radius is finite; for instance, it attains a notable value of $0.0065\,e$ at $r_0 = 0.001\,m^{-1}$ at $d = 3$.

Table 1. The dimensionless induced vacuum magnetic flux in cases of dimension $d = 2, 3, 4$ for tubes of different radius.

x_0	1	2/3	1/3	10^{-1}	10^{-2}	10^{-3}
$m\Phi_2^{(I)}/e$	$2.355 \cdot 10^{-8}$	$5.762 \cdot 10^{-7}$	$2.071 \cdot 10^{-5}$	$4.878 \cdot 10^{-4}$	$3.657 \cdot 10^{-3}$	$6.217 \cdot 10^{-3}$
$\Phi_3^{(I)}/e$	$3.07 \cdot 10^{-9}$	$8.829 \cdot 10^{-8}$	$4.129 \cdot 10^{-6}$	$1.483 \cdot 10^{-4}$	$2.223 \cdot 10^{-3}$	$6.547 \cdot 10^{-3}$
$\Phi_4^{(I)}/(me)$	$2.06 \cdot 10^{-10}$	$7.06 \cdot 10^{-9}$	$4.43 \cdot 10^{-7}$	$2.675 \cdot 10^{-5}$	$1.254 \cdot 10^{-3}$	$1.585 \cdot 10^{-2}$

4. Summary

In this paper, we consider the current and the magnetic field which are induced in the vacuum of the quantized charged scalar matter field by a topological defect in the form of the ANO vortex. A perfectly reflecting (Dirichlet) boundary condition is imposed on the matter field at the side surface of the vortex. The induced current is circulating around the vortex, and the induced magnetic field is directed along the vortex. Both the current and the magnetic field are vanishingly small in the case of the vortex transverse size being of the order of or exceeding the Compton wavelength of the matter field (the dimensionless current is less than 10^{-8}, the dimensionless total flux of the magnetic field is less than 10^{-9} in the $d = 3$ case). Together with the results of Refs. 16 and 19 about the Casimir force acting on the vortex side surface, this confirms the conclusion that the vacuum polarization of the quantized matter is almost absent in the case when the mass of the Higgs field (forming the topological defect) is of the order of or less than the mass of the matter field; the vacuum polarization effects are essential for matter fields with masses which are much smaller than a scale of the spontaneous symmetry breaking (Higgs mass). As to the induced vacuum current and magnetic field in the background of the ANO vortex, we show in this paper that they are essential in this latter case, being odd in the value of the vortex flux, Φ, and periodic in this value with the period equal the London flux quantum, $2\pi\tilde{e}^{-1}$; to be more precise, they vanish at $F = 0$, $1/2$ and 1, where F is given by (13), and are of opposite signs in the intervals $0 < F < 1/2$ and $1/2 < F < 1$, with their absolute values being symmetric with respect to the point $F = 1/2$. The current and the magnetic field decrease exponentially at large distances from the vortex, while otherwise they behave similarly to the case of a singular filament (vanishing transverse size) with the exception of a small vicinity of the vortex tube. The latter distinction allows us to eliminate an unphysical divergence which is present at $d \geq 3$ for the total induced vacuum magnetic flux in the case of a singular filament. As long as the nonvanishing transverse size of the vortex is taken into account, the total induced vacuum magnetic flux becomes finite, attaining quite realistic values for the case of the three-dimensional space even at the spontaneous symmetry breaking scale exceeding the mass of the matter field by just three orders of magnitude, see Fig. 5 and Table 1. This can provide a possible mechanism for generating primordial magnetic fields by cosmic strings in early universe.

Acknowledgments

I. V. Ivanchenko and Yu. A. Sitenko acknowledge the support from the National Academy of Science of Ukraine (project No. 0112U000054). The work of V. M. Gorkavenko was supported by the Swiss National Science Foundation Grant SCOPE IZ 7370-152581. The work of Yu. A. Sitenko was supported by the ICTP-SEENET-MTP Grant PRJ-09 "Strings and Cosmology."

References

1. A. A. Abrikosov, *Sov. Phys. – JETP* **5**, 1174 (1957).
2. H. B. Nielsen and P. Olesen, *Nucl. Phys. B* **61**, 45 (1973).
3. R. P. Huebener, *Magnetic Flux Structure in Superconductors* (Springer-Verlag, Berlin, 1979).
4. D. R. Nelson, *Defects and Geometry in Condensed Matter Physics* (Cambridge University Press, Cambridge, 1994).
5. G. E. Volovik, *The Universe in a Helium Droplet* (Clarendon, Oxford, 2003).
6. A. Vilenkin and E. P. S. Shellard, *Cosmic Strings and Other Topological Defects* (Cambridge University Press, Cambridge, 1994).
7. M. B. Hindmarsh and T. W. B. Kibble, *Rep. Prog. Phys.* **58**, 477 (1995).
8. E. J. Copeland and T. W. B. Kibble, *Proc. R. Soc. A* **466**, 623 (2010).
9. V. Berezinsky, B. Hnatyk and A. Vilenkin, *Phys. Rev. D* **64**, 043004 (2001).
10. R. Brandenberger, H. Firouzjahi, J. Karoubi and S. Khosravi, *J. Cosmol. Astropart. Phys.* **01**, 008 (2009).
11. M. G. Jackson and X. Siemens, *J. High Energy Phys.* **06**, 089 (2009).
12. Y. Aharonov and D. Bohm, *Phys. Rev.* **115**, 485 (1959).
13. A. Tonomura, *J. Phys. A*: *Math. Theor.* **43**, 35402 (2010).
14. Yu. A. Sitenko and N. D. Vlasii, *Class. Quantum Grav.* **26**, 195009 (2009).
15. R. Jackiw, A. I. Milstein, S.-Y. Pi and I. S. Terekhov, *Phys. Rev. B* **80**, 033413 (2009).
16. V. M. Gorkavenko, Yu. A. Sitenko and O. B. Stepanov, *J. Phys. A*: *Math. Theor.* **43**, 175401 (2010).
17. V. M. Gorkavenko, Yu. A. Sitenko and O. B. Stepanov, *Int. J. Mod. Phys. A* **26**, 3889 (2011).
18. V. M. Gorkavenko, Yu. A. Sitenko and O. B. Stepanov, *Ukr. J. Phys.* **58**, 424 (2013).
19. V. M. Gorkavenko, Yu. A. Sitenko and O. B. Stepanov, *Int. J. Mod. Phys. A* **28**, 1350161 (2013).
20. Yu. A. Sitenko and A. Yu. Babansky, *Mod. Phys. Lett. A* **13**, 379 (1998).
21. Yu. A. Sitenko and A. Yu. Babansky, *Phys. Atom. Nucl.* **61**, 1594 (1998).
22. V. G. Bagrov, D. M. Gitman and V. B. Tlyachev, *J. Math. Phys.* **42**, 1933 (2001).
23. S. P. Gavrilov, D. M. Gitman, A. A. Smirnov and B. L. Voronov, *Focus on Mathematical Physics Research* (Nova Science Publishers, New York, 2004), pp. 131–168.

3.2. Індукування у вакуумі скалярного поля. Гранична умова типу Неймана

FIELDS AND ELEMENTARY PARTICLES

https://doi.org/10.15407/ujpe67.1.3

V.M. GORKAVENKO,[1] T.V. GORKAVENKO,[1] YU.A. SITENKO,[2] M.S. TSARENKOVA [1]

[1] Taras Shevchenko National University of Kyiv, Ukraine
(64, Volodymyrs'ka Str., Kyiv 01601, Ukraine)
[2] Bogolyubov Institute for Theoretical Physics, Nat. Acad. of Sci. of Ukraine
(14-b, Metrologichna Str., Kyiv 03680, Ukraine)

INDUCED VACUUM CURRENT AND MAGNETIC FLUX IN QUANTUM SCALAR MATTER IN THE BACKGROUND OF A VORTEX DEFECT WITH THE NEUMANN BOUNDARY CONDITION

A topological defect in the form of the Abrikosov–Nielsen–Olesen vortex in the space of an arbitrary dimension is considered as a gauge-flux-carrying tube that is impenetrable for quantum matter. The charged scalar matter field is quantized in the vortex background with the perfectly rigid (Neumann) boundary condition imposed at the side surface of the vortex. We show that a current circulating around the vortex is induced in the vacuum, if the Compton wavelength of the matter field exceeds the transverse size of the vortex considerably. The vacuum current is periodic in the value of the gauge flux of the vortex, providing a quantum-field-theoretical manifestation of the Aharonov–Bohm effect. The vacuum current leads to the appearance of an induced vacuum magnetic flux that, for some values of the tube thickness, exceeds the vacuum magnetic flux induced by a singular vortex filament. The results are compared to those obtained earlier in the case of the perfectly reflecting (Dirichlet) boundary condition imposed at the side surface of the vortex. It is shown that the absolute value of the induced vacuum current and the induced vacuum magnetic flux in the case of the Neumann boundary condition is greater than in the case of the Dirichlet boundary condition.

K e y w o r d s: vacuum polarization, Aharonov–Bohm effect, vortex defect.

1. Introduction

There are many theoretical models in field theory which contain the phenomenon of spontaneous breakdown of symmetries, see, e.g., [1]. This phenomenon gives rise to topological defects of various kinds, see, e.g., [2, 3]. In this paper, we will consider a linear topological defect known as the Abrikosov–Nielsen–Olesen (ANO) vortex in condensed matter physics [4, 5] or a cosmic string in cosmology [2, 6, 7]. This topological object is formed, when the first homotopy group of the group space of the broken symmetry group is nontrivial. Abrikosov vortices are real physical objects in the type-II superconductors [8, 9]. Cosmic strings are currently hypothetical objects, and their possible manifestations such as gravitational waves, high-energy cosmic rays, and gamma-ray bursts are actively searched in the Universe [10–12].

In the classical theory of the ANO vortex, a spin-0 (Higgs) field condenses, and a spin-1 field corresponds to the spontaneously broken gauge group; they are coupled in the minimal way with constant $\tilde{e}_H$. The transverse size of the vortex is of the order

of the correlation length or the Compton wavelength, $\hbar(m_H c)^{-1}$, where m_H is the mass of the condensate field. The physical requirements of single-valuedness of the condensate field and finiteness of the vortex energy result in the following dependence of the vortex flux on $\tilde{e}_H$: $\Phi = \oint d\mathbf{x}\mathbf{A}(\mathbf{x}) = 2\pi\hbar c\tilde{e}_H^{-1}$, where $\mathbf{A}(\mathbf{x})$ is the vector potential of the gauge field, and the integral is over a path enclosing the vortex once. The quantized matter field is coupled minimally to the gauge field with constant $\tilde{e}$. So, the quantum effects in the background of the ANO vortex depend on the value of $\tilde{e}\Phi$.

Since the phase with broken symmetry exists only outside the vortex, the quantum matter field cannot penetrate inside the vortex. We assume further that the interaction between the ANO vortex and the quantized matter field is mediated by the vector potential of the vortex-forming spin-1 field only, and the direct coupling between the vortex-forming spin-0 field and the quantized matter field can be neglected. If so, the ANO vortex does not affect the surrounding matter in the framework of classical theory, and such an influence is of the purely quantum nature. The effect is a quantum-field-theoretical manifestation of the famous Aharonov–Bohm effect [13], see review [14]. It is characterized by the periodic dependence on the value of the vortex flux, Φ, with the period equal to the London flux quantum, $2\pi\hbar c\tilde{e}^{-1}$. A particular case of $\tilde{e}_H = 2\tilde{e}$ ($\Phi = \pi\hbar c\tilde{e}^{-1}$, half of the London flux quantum) is implemented in ordinary superconductors, see, e.g., [8]. Cases of fractional values of the London flux quantum are physically meaningful as well, and can be implemented in chiral superfluids, liquid crystals, and quantum liquids, see [15, 16].

The physical condition of non-penetration of the matter field inside the vortex means the absence of the matter field current through the side surface of the vortex, namely $j_r|_{r_0} = 0$, where r is a radial coordinate which is perpendicular to the side surface, and r_0 is the radius of the vortex. Hence, the ANO vortex can be considered as a magnetic tube of the finite transverse size. In the case of the scalar matter field, the condition of non-penetrability can be satisfied with the use of a family of boundary conditions of the Robin type

$$(\cos\theta\,\psi + \sin\theta\, r\partial_r\psi)|_{r_0} = 0, \tag{1}$$

where θ is some arbitrary parameter. Among all possible values of the parameter θ, two values are prominent. The case of $\theta = 0$ corresponds to the perfectly reflecting (Dirichlet) boundary condition $\psi|_{r_0} = 0$. The case of $\theta = \pi/2$ corresponds the perfectly rigid (Neumann) boundary condition $r\partial_r\psi|_{r_0} = 0$.

In the present paper, we shall study the current which is induced in the vacuum of the quantized charged scalar matter field by the ANO vortex with nonvanishing transverse size with the perfectly rigid (Neumann) boundary condition on its side surface ($\theta = \pi/2$). This current creates a magnetic field in the vacuum, and the total induced vacuum magnetic flux will be studied in detail in what follows. In the case of the ANO vortex of zero transverse size, this problem was solved previously, see [17–19] and references therein. For the case of the finite transverse size of the ANO vortex, the induced vacuum current, magnetic flux, energy and the Casimir force were considered in the [20–24] for the case of the perfectly reflecting (Dirichlet) boundary condition.

It should be noted that, for the quantized fermion matter field, the condition of non-penetration of the matter field inside the finite transverse size ANO vortex has a form different from (1), and it can be parametrized with the help of one parameter in the case of two-dimensional space and four parameters in the case of three-dimensional space. The induced vacuum current and magnetic flux in these cases were considered for all values of parameters in [25–27].

2. Induced Vacuum Current and Total Magnetic Flux

We start with the Lagrangian for a complex scalar field ψ in the $(d+1)$-dimensional space-time

$$\mathcal{L} = (\nabla_\mu\psi)^*(\nabla^\mu\psi) - m^2\psi^*\psi, \tag{2}$$

where ∇_μ is the covariant derivative, and m is the mass of the scalar field. The vacuum current is conventionally defined as

$$\mathbf{j}(\mathbf{x}) = -\mathrm{i}\sum\!\!\!\!\!\!\int_\lambda (2E_\lambda)^{-1} \times$$
$$\times\{\psi_\lambda^*(\mathbf{x})[\boldsymbol{\nabla}\psi_\lambda(\mathbf{x})] - [\boldsymbol{\nabla}\psi_\lambda(\mathbf{x})]^*\psi_\lambda(\mathbf{x})\}, \tag{3}$$

where λ is the set of parameters (quantum numbers) specifying the state, wave functions $\psi_\lambda(\mathbf{x})$ form a complete set of solutions to the stationary Klein–Fock–Gordon equation

$$\left(-\boldsymbol{\nabla}^2 + m^2\right)\psi_\lambda(\mathbf{x}) = E_\lambda^2\psi(\mathbf{x}), \tag{4}$$

$E_\lambda = E_{-\lambda} > 0$ is the energy of the state; symbol $\sum\!\!\!\!\!\!\int\limits_{\lambda}$ denotes summation over discrete and integration (with a certain measure) over continuous values of λ.

In the present paper we are considering a static background in the form of the cylindrically symmetric gauge flux tube of the finite transverse size. The coordinate system is chosen in such a way that the tube is along the z axis. The tube in a 3-dimensional space is obviously generalized to the $(d-2)$-tube in a d-dimensional space by adding extra $d-3$ dimensions as longitudinal ones. The covariant derivative is $\nabla_0 = \partial_0$, $\boldsymbol{\nabla} = \boldsymbol{\partial} - \mathrm{i}\tilde{e}\,\mathbf{V}$ with $\tilde{e}$ being the coupling constant of the dimension $m^{(3-d)/2}$ and the vector potential possessing only one nonvanishing component given by

$$V_\varphi = \Phi/2\pi, \tag{5}$$

outside the tube; here, Φ is the value of the gauge flux inside the $(d-2)$-tube, and φ is the angle in polar (r,φ) coordinates on a plane which is transverse to the tube. The Neumann boundary condition at the side surface of the tube ($r = r_0$) is imposed on the scalar field:

$$\partial_r \psi_\lambda|_{r=r_0} = 0, \tag{6}$$

i.e., the surface of the flux tube is a perfectly rigid boundary for the matter field.

The solution to (4) and (6) outside the impenetrable tube of radius r_0 takes the form

$$\psi_{kn\mathbf{p}}(\mathbf{x}) = (2\pi)^{(1-d)/2} e^{\mathrm{i}\mathbf{p}\mathbf{x}_{\mathbf{d-2}}} e^{\mathrm{i}n\varphi} \Omega_{|n-\tilde{e}\Phi/2\pi|}(kr, kr_0), \tag{7}$$

where

$$\Omega_\rho(u,v) = \frac{Y'_\rho(v)J_\rho(u) - J'_\rho(v)Y_\rho(u)}{\left[J'^2_\rho(v) + Y'^2_\rho(v)\right]^{1/2}}, \tag{8}$$

and $0 < k < \infty$, $-\infty < p^j < \infty$ ($j = \overline{1, d-2}$), $n \in \mathbb{Z}$ ($\mathbb{Z}$ is the set of integer numbers), $J_\rho(u)$ and $Y_\rho(u)$ are the Bessel functions of order ρ of the first and second kinds, the prime near the function means the derivative with respect to the function argument. Solutions (7) obey orthonormalization condition

$$\int\limits_{r>r_0} d^{\,d}\mathbf{x}\, \psi^*_{kn\mathbf{p}}(\mathbf{x}) \psi_{k'n'\mathbf{p}'}(\mathbf{x}) = \\ = \frac{\delta(k-k')}{k}\, \delta_{n,n'}\, \delta^{d-2}(\mathbf{p}-\mathbf{p}'). \tag{9}$$

Using (3) and (7), we get $j_r = \mathbf{j}_{d-2} = 0$ and

$$j_\varphi(r) \equiv x^1 j^2(\mathbf{x}) - x^2 j^1(\mathbf{x}) = (2\pi)^{1-d} \int d^{d-2}p \times \\ \times \int\limits_0^\infty dk\, k(\mathbf{p}^2 + k^2 + m^2)^{-1/2} S(kr, kr_0), \tag{10}$$

where

$$S(u,v) = \sum_{n\in\mathbb{Z}} \left(n - \frac{\tilde{e}\Phi}{2\pi}\right) \Omega^2_{|n-\tilde{e}\Phi/2\pi|}(u,v). \tag{11}$$

Due to the infinite range of the summation, the last expression is periodic in the flux Φ with a period equal to $2\pi\tilde{e}^{-1}$, i.e., it depends on the quantity

$$F = \frac{\tilde{e}\Phi}{2\pi} - \left[\!\left[\frac{\tilde{e}\Phi}{2\pi}\right]\!\right], \tag{12}$$

where $[[u]]$ is the integer part of the quantity u (i.e., the integer which is less than or equal to u).

Let us rewrite (11) in the form

$$S(u,v) = S_0(u) + S_1(u,v), \tag{13}$$

where

$$S_0(u) = \\ = \sum_{n=0}^\infty \left[(n+1-F)\, J^2_{n+1-F}(u) - (n+F)\, J^2_{n+F}(u)\right] \tag{14}$$

and

$$S_1(u,v) = \sum_{n=0}^\infty \left[(n+1-F)\Lambda_{n+1-F}(u,v) - \right. \\ \left. - (n+F)\Lambda_{n+F}(u,v)\right], \tag{15}$$

where

$$\Lambda_\rho(u,v) = \\ = \frac{J'^2_\rho(v)\left[Y^2_\rho(u) - J^2_\rho(u)\right] - 2J'_\rho(v)J_\rho(u)Y'_\rho(v)Y_\rho(u)}{Y'^2_\rho(v) + J'^2_\rho(v)}\,. \tag{16}$$

The vacuum current j_φ circulating around the $(d-2)$-tube leads to the appearance of a vacuum magnetic field with strength $B^{3\ldots d}$ directed along the $(d-2)$-tube; this is a consequence of the Maxwell equation

$$r\partial_r B^{3\ldots d}_{(I)}(r) = -e j_\varphi(r), \tag{17}$$

where the coupling constant e differs in general from $\tilde{e}$. The total flux of the induced vacuum magnetic field across a plane which is orthogonal to the $(d-2)$-tube is defined as

$$\Phi_d^{(I)} = 2\pi \int\limits_{r_0}^{\infty} dr\, r B_{(I)}^{3,\ldots,d}(r) \tag{18}$$

and is given by the expression

$$\Phi_d^{(I)} = e\pi \int\limits_{r_0}^{\infty} dr\, r j_\varphi(r) \left(1 - \frac{r_0^2}{r^2}\right). \tag{19}$$

Inserting $j_\varphi(r)$ (10) and changing the order of integration over r and $\mathbf{p}$, we get, see [20],

$$\Phi_d^{(I)} = em^{d-3} \frac{(4\pi)^{(2-d)/2}}{2\Gamma(d/2)} \int\limits_0^{\infty} \frac{du}{\sqrt{1+u^{2/(d-2)}}} \times$$
$$\times\, \mathcal{D}(mr_0 \sqrt{1+u^{2/(d-2)}}), \tag{20}$$

where $\Gamma(v)$ is the Euler gamma-function and

$$\mathcal{D}(y) = \int\limits_y^{\infty} dx \left(1 - \frac{y^2}{x^2}\right) \int\limits_0^{\infty} \frac{dz\, z}{\sqrt{z^2+x^2}}\, S\left(z, z\frac{y}{x}\right). \tag{21}$$

It should be noted that the function $\mathcal{D}(y)$ (21) is immediately related to the total induced vacuum magnetic flux in the $d = 2$ case:

$$\Phi_2^{(I)} = \frac{e}{2m}\, \mathcal{D}(mr_0). \tag{22}$$

Since $S_1(u, 0) = 0$, one can obtain

$$\mathcal{D}(0) = \int\limits_0^{\infty} dx \int\limits_0^{\infty} \frac{dz\, z}{\sqrt{z^2+x^2}}\, S_0(z) =$$
$$= \frac{1}{3} F(1-F) \left(F - \frac{1}{2}\right), \tag{23}$$

and the total induced vacuum magnetic flux in the $d = 2$ case is finite in the limit of a singular (i.e., infinitely thin) vortex filament, $r_0 \to 0$ [17]:

$$\lim_{r_0 \to 0} \Phi_2^{(I)} = \frac{e}{6m}\, F(1-F) \left(F - \frac{1}{2}\right). \tag{24}$$

However, in the $d \geq 3$ cases, the total induced magnetic flux becomes infinite in the limit of the infinitely thin vortex filament [18]. In this case, the consideration of the vacuum polarization by the vortex filament of the finite transverse size is especially actual.

3. Numerical Analysis of the Induced Vacuum Characteristics

As one can see from the previous section, in order to find the induced vacuum magnetic flux in the d-dimensional space, we first need to find it in the 2-dimensional space. Unfortunately, this task in the case of a vortex tube of finite transverse size can be solved only by numerical methods.

With this aim, we rewrite expression (10) in the $d = 2$ case in the dimensionless form

$$r j_\varphi(r)\big|_{d=2} = \frac{1}{2\pi} \int\limits_0^{\infty} dz\, z \left[z^2 + \left(\frac{mr_0}{\lambda}\right)^2\right]^{-1/2} S(z, \lambda z), \tag{25}$$

where $\lambda = r_0/r$ ($\lambda \in [0, 1]$).

In the limit of a singular filament ($r_0 = 0$), expression (25) contains only S_0 (14). The summation in (14) can be performed analytically and (25) is reduced to the following form, see [20]:

$$r j_\varphi^{\mathrm{sing}}(r)\big|_{d=2} = \frac{\sin(F\pi)}{\pi^3} \int\limits_{mr}^{\infty} dw \frac{w^2}{\sqrt{w^2-(mr)^2}} \times$$
$$\times \left\{w\left[K_{1-F}^2(w) - K_F^2(w)\right] + (2F-1) K_F(w) K_{1-F}(w)\right\}, \tag{26}$$

where $K_\rho(u)$ is the Macdonald function of order ρ. The total induced vacuum magnetic flux in this case, see (24), attains the maximal absolute value equal to $|e|/(72\sqrt{3}m)$ at $F = F_\pm$, where

$$F_\pm = \frac{1}{2}\left(1 \pm \frac{1}{\sqrt{3}}\right). \tag{27}$$

Next, we will numerically compute the induced vacuum current in the $d = 2$ case at $F = F_+$, when the integral in (25) is likely to be most distinct from zero (note that the current at $F = F_-$ equals to that at $F = F_+$ with the opposite sign). So, for a vortex tube of nonvanishing radius, we have to compute values of dimensionless quantity $r j_\varphi$ at different values of λ. To do this, we perform the high-precision numerical integration in (25) with the help of a technique developed earlier in [20–24]. The results of computation can be approximated by an interpolation function in the form

$$r j_\varphi(r)\big|_{d=2} = \left[\frac{e^{-2x}}{\sqrt{x}}\right] \left[\frac{P_n(x-x_0)}{x^n}\right] \frac{Q_k(x^2)}{R_k(x^2)},\ x > x_0, \tag{28}$$

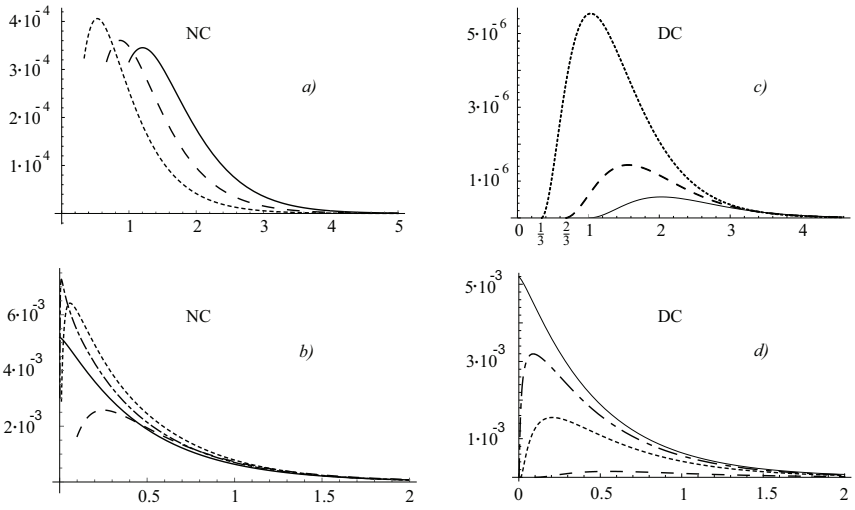

Fig. 1. The dimensionless induced vacuum current (rj_φ) as a function of the dimensionless distance from the axis of the tube (x) for different values of the dimensionless tube radius (x_0) for the case of the Neumann (NC) and the Dirichlet (DC) boundary conditions: (*a*), (*c*) solid line corresponds to $rj_\varphi \times 10^2$ for $x_0 = 1$, dashed line corresponds to $rj_\varphi \times 10$ for $x_0 = 2/3$, and dotted line corresponds to rj_φ for $x_0 = 1/3$; (*b*), (*d*) solid line corresponds to the cases of a singular filament ($x_0 = 0$), dashed line corresponds to $x_0 = 10^{-1}$, dotted line corresponds to $x_0 = 10^{-2,}$ and dash-dotted line corresponds to $x_0 = 10^{-3}$. Variable x is along the abscissa axis

where $x = mr$, $x_0 = mr_0$ and $P_j(y)$, $Q_j(y)$, $R_j(y)$ are polynomials in y of the j-th order with the x_0-dependent coefficients. It turns out that, for the interpolation of data, the most suitable choice of function (28) contains the polynomials with indices $n = 9$ and $k = 4$. The first factor in square brackets describes the large-distance behavior in the case of a zero-radius tube (filament), the second factor in square brackets is an asymptotics at small distances from the side surface of the tube, the last factor describes the behavior at intermediate distances. Since the vortex tube is impenetrable, $rj_\varphi(r)$ (28) vanishes at $x \leq x_0$.

The results in the $d = 2$ case for the induced vacuum current in the case of the Neumann boundary condition are presented on Fig. 1, *a* and Fig. 1, *b*. For comparison, we also present the results for the induced vacuum current in the case of the Dirichlet boundary condition [20], see Fig. 1, *c* and Fig. 1, *d*. As one can see, the current is negligible for the tube of large radius, i.e., of order of the Compton wavelength and greater, $r_0 \geq m^{-1}$, see Fig. 1, *a* and Fig. 1, *c*. One can note that the induced vacuum current in the case of the Neumann boundary condition has a much weaker dependence on the tube thickness x_0 (Fig. 1, *a*) as compared to that in the case of the Dirichlet boundary condition (Fig. 1, *c*). The current in the case of $r_0 \ll m^{-1}$ is comparable with the current in the case of a singular filament, see Fig. 1, *b* and Fig. 1, *d*. It should be noted that, in the case of the Dirichlet boundary condition, the induced vacuum current is always less in value than in the case of a singular filament, see Fig. 1, *d*. It is not true for the case of the Neumann boundary condition, see Fig. 1, *b*. It should be noted that the value of the current in the case of the Neumann boundary condition is greater than the value of the current in the case of the Dirichlet boundary condition at any value of the tube thickness.

Using (19), (21), (22), and (28), we compute numerically the total induced vacuum magnetic flux in the $d = 2$ case for different values of the tube thickness (parameter $x_0 = mr_0$). The results of the computation in the dimensionless form can be approximated by an interpolation function in the form

$$\ln \frac{m\Phi_2^{(I)}}{e} = \ln \mathcal{D}(x_0) = M_1(x_0)\Theta(X - x_0) + \\ + \left[a + bx_0^1 + dx_0^5 + \sqrt{L_2(x_0)}\right]\Theta(x_0 - X), \qquad (29)$$

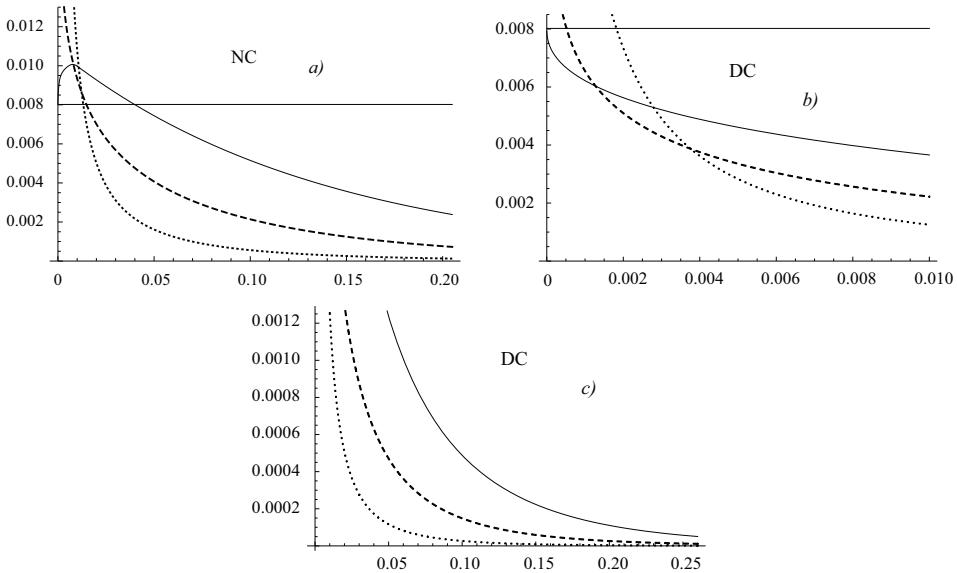

Fig. 2. The dimensionless induced vacuum magnetic flux in spaces of different dimensionality as a function of the dimensionless tube radius (x_0) for the case of the Neumann (NC) and the Dirichlet (DC) boundary conditions: $e^{-1}m\Phi_2^{(I)}$ – solid line, $e^{-1}\Phi_3^{(I)}$ – dashed line, $(em)^{-1}\Phi_4^{(I)}$ – dotted line. The case of $x_0 = 0$ and $d = 2$ is presented by a horizontal solid line

The dimensionless induced vacuum magnetic flux in the cases of dimension $d = 2, 3, 4$ for tubes of different radii and for the case of the Neumann (NC) and Dirichlet (DC) boundary condition

x_0	1	2/3	1/3	10^{-1}	10^{-2}	10^{-3}
$\frac{m}{e}\,\Phi_2^{(I)}$, NC	7.09×10^{-6}	7.79×10^{-5}	9.05×10^{-4}	5.34×10^{-3}	9.92×10^{-3}	0.01
$\frac{m}{e}\,\Phi_2^{(I)}$, DC	2.36×10^{-8}	5.76×10^{-7}	2.07×10^{-5}	4.88×10^{-4}	3.66×10^{-3}	6.22×10^{-3}
$\frac{1}{e}\,\Phi_3^{(I)}$, NC	10^{-6}	1.41×10^{-5}	2.26×10^{-4}	2.14×10^{-3}	9.34×10^{-3}	1.64×10^{-2}
$\frac{1}{e}\,\Phi_3^{(I)}$, DC	3.07×10^{-9}	8.83×10^{-8}	4.13×10^{-6}	1.48×10^{-4}	2.22×10^{-3}	6.55×10^{-3}
$\frac{1}{me}\,\Phi_4^{(I)}$, NC	7.5×10^{-8}	1.3×10^{-6}	3.02×10^{-5}	5.58×10^{-4}	1.08×10^{-2}	1.15×10^{-1}
$\frac{1}{me}\,\Phi_4^{(I)}$, DC	2.06×10^{-10}	7.06×10^{-9}	4.43×10^{-7}	2.68×10^{-5}	1.25×10^{-3}	1.32×10^{-2}

where $M_j(y)$, $L_j(y)$ are polynomials in y of the j-th order, $\Theta(y)$ is the Heaviside step function and $X = = 10^{-2}$. Using (20) and (29), we compute numerically the total induced magnetic flux in the $d = 3, 4$ cases, i.e. $\Phi_3^{(I)}$ and $\Phi_4^{(I)}$. The results for the $d = 2, 3, 4$ cases are presented in Fig. 2, *a* and in Table. For comparison, we also present the results for the induced flux in the case of the Dirichlet boundary condition [20], see Fig. 2, *b* and Fig. 2, *c*.

As one can see, in the case of the Neumann boundary condition (for $d = 2$), there is a region of the tube thickness ($0 < x_0 < 0.4$), where the absolute value of the induced flux is greater than in the case of a singular filament, see Fig. 2, *a*. Whereas the absolute value of the flux induced by a singular filament is always greater than the absolute value of the flux induced by a tube of the nonvanishing radius with the Dirichlet boundary condition, see Fig. 2, *b* and Fig. 2, *c*. One

can see also that the induced flux from a tube with the Neumann boundary condition is greater than the induced flux from a tube with the Dirichlet boundary condition at any value of the tube thickness.

In the case of higher space dimensions, the behavior of the induced flux in the case of the Neumann and Dirichlet boundary conditions is similar, see Fig. 2. For the case of a space with a higher dimension ($d = 4$) at large radii of the tube, the induced flux is a more strongly decreasing function. But, at smaller radii of the tube, the induced flux is a more strongly increasing function compared to that in the case of the space with a smaller dimension ($d = 3$). While the induced flux in the unphysical case of a singular filament is infinite for $d > 2$,, the induced flux in the physical case of a tube of nonvanishing radius is finite. As one see from Table, the absolute value of the flux induced by a tube with the Neumann boundary condition is always greater than the absolute value of the flux induced by a tube with the Dirichlet boundary condition for any dimension of the space.

4. Summary

In the present paper, we have considered the current and the total magnetic flux which are induced in the vacuum of the quantized charged scalar matter field by a topological defect in the form of the ANO vortex in a space of arbitrary dimension. We assume that the ANO vortex is impenetrable for the quantum matter. The perfectly rigid (Neumann) boundary condition is imposed on the matter field at the side surface of the vortex. The same problem was considered previously for the vortex with the perfectly reflecting (Dirichlet) boundary condition on its side surface [20]. So, we compare the results obtained for the Neumann and Dirichlet boundary conditions at the side surface of the vortex.

In both cases of the above- mentioned boundary conditions, the induced current is circulating around the vortex, and it is vanishingly small in the case of the vortex transverse size being of the order of or exceeding the Compton wavelength of the matter field ($x_0 \gtrsim 1$), see Fig. 1, Fig. 2 and Table for the $d = 2, 3, 4$ dimensions of the space. This confirms the previously obtained conclusion [21–24] that the vacuum polarization effects are essential only for matter fields with masses which are much smaller than the scale of the spontaneous symmetry breaking (mass of the Higgs field forming the topological defect).

In both cases of the above- mentioned boundary conditions, the induced vacuum current decreases exponentially at large distances from the vortex. The current and the induced vacuum magnetic flux are odd in the value of the vortex flux, Φ, and periodic in this value with the period equal to the London flux quantum, $2\pi\tilde{e}^{-1}$. They vanish at $F = 0, 1/2, 1$ and are of opposite signs in the intervals $0 < F < 1/2$ and $1/2 < F < 1$, with their absolute values being symmetric with respect to the point $F = 1/2$. In the case of a space of dimension $d > 2$, the account for the finite transverse size of the vortex eliminates an unphysical divergence for the total induced vacuum flux, which takes place in the case of a singular vortex filament.

The visible difference between the cases of the Neumann and Dirichlet boundary conditions lies in the magnitude of the vacuum polarization effects. The absolute value of the induced vacuum current and the induced vacuum magnetic flux in the case of the Neumann boundary condition is greater than that in the case of the Dirichlet boundary condition. In particular, as one can see from Fig. 1, *d* and Fig. 2, *b* for the dimension of the space $d = 2$, the vacuum effects in the case of the Dirichlet boundary condition are always smaller than in the case of a singular vortex filament. However, as one can see from Fig. 1, *b*, for the case of the Neumann boundary condition, the absolute value of the induced vacuum current can exceed the absolute value of the induced vacuum current in the case of a singular vortex filament. Moreover, there is a region of the vortex thickness values ($0 < x_0 < 0.4$), see Fig. 2, *a*, where the absolute value of the induced vacuum magnetic flux is greater than that in the case of a singular vortex filament for the $d = 2$ space.

The work of Yu.A.S. was supported by the National Academy of Sciences of Ukraine (project No. 0122U000886).

1. A.J. Beekman, L. Rademaker, Jasper van Wezel. An introduction to spontaneous symmetry breaking. *SciPost Phys. Lect. Notes* **11**, 1 (2019).
2. A. Vilenkin, E.P.S. Shellard. *Cosmic Strings and Other Topological Defects* (Cambridge University Press, 1994) [ISBN: 0-521-39153-9].
3. R.H. Brandenberger. Topological defects and structure formation. *Int. J. Mod. Phys. A* **09**, 2117 (1994).

4. A.A. Abrikosov. On the magnetic properties of superconductors of the second group. *Sov. Phys.-JETP* **5**, 1174 (1957).
5. H.B. Nielsen, P. Olesen. Vortex-line models for dual strings. *Nucl. Phys. B* **61**, 45 (1973).
6. M.B. Hindmarsh, T.W.B. Kibble. Cosmic strings. *Rep. Prog. Phys.* **58**, 477 (1995).
7. E.J. Copeland, T.W.Kibble. Cosmic strings and superstrings. *Proc. Roy. Soc. A* **466**, 623 (2010).
8. R.P. Huebener. *Magnetic Flux Structure in Superconductors* (Springer-Verlag Berlin Heidelberg, 1979) [ISBN: 978-3-662-02307-5].
9. B. Rosenstein, D. Li. Ginzburg-Landau theory of type II superconductors in magnetic field. *Rev. Mod. Phys.* **82**, 109 (2010).
10. V. Berezinsky, B. Hnatyk, A. Vilenkin. Gamma ray bursts from superconducting cosmic strings. *Phys. Rev. D* **64**, 043004 (2001).
11. R. Brandenberger, H. Firouzjahi, J. Karoubi, S. Khosravi. Gravitational radiation by cosmic strings in a junction. *J. Cosmol. Astropart. Phys.* **01**, 008 (2009).
12. M.G. Jackson, X. Siemens. Gravitational wave bursts from cosmic superstring reconnections. *J. High Energy Phys.* **06**, 089 (2009).
13. Y. Aharonov, D. Bohm. Significance of electromagnetic potentials in the quantum theory. *Phys. Rev.* **115**, 485 (1959).
14. A. Tonomura. The AB effect and its expanding applications. *J. Phys. A: Math. Theor.* **43**, 35402 (2010).
15. D.R. Nelson. *Defects and Geometry in Condensed Matter Physics* (Cambridge University Press, 2002) [ISBN: 0-521-80159-1].
16. G.E. Volovik. *The Universe in a Helium Droplet* (Clarendon, 2003).
17. Yu.A. Sitenko, A.Yu. Babansky. The Casimir–Aharonov–Bohm effect? *Mod. Phys. Lett. A* **13**, 379 (1998).
18. Yu.A. Sitenko, A.Yu. Babansky. Effects of boson-vacuum polarization by a singular magnetic vortex. *Phys. Atom. Nucl.* **61**, 1594 (1998).
19. Yu.A. Sitenko. One-loop effective action for the extended spinor electrodynamics with violation of Lorentz and CPT symmetry. *Phys. Lett. B* **515**, 414 (2001).
20. V.M. Gorkavenko, I.V. Ivanchenko, Yu.A. Sitenko. Induced vacuum current and magnetic field in the background of a vortex. *Int. J. Mod. Phys. A* **31**, 1650017 (2016).
21. V.M. Gorkavenko, Yu.A. Sitenko, O.B. Stepanov. Polarization of the vacuum of a quantized scalar field by an impenetrable magnetic vortex of finite thickness. *J. Phys. A: Math. Theor.* **43**, 175401 (2010).
22. V.M. Gorkavenko, Yu.A. Sitenko, O.B. Stepanov. Vacuum energy induced by an impenetrable flux tube of finite radius. *Int. J. Mod. Phys. A* **26**, 3889 (2011).
23. V.M. Gorkavenko, Yu.A. Sitenko, O.B. Stepanov. Casimir force induced on a plane by an impenetrable flux tube of finite radius. *Ukr. J. Phys.* **58**, 424 (2013).
24. V.M. Gorkavenko, Yu.A. Sitenko, O.B. Stepanov. Casimir energy and force induced by an impenetrable flux tube of finite radius. *Int. J. Mod. Phys. A* **28**, 1350161 (2013).
25. Yu.A. Sitenko, V.M Gorkavenko. Properties of the ground state of electronic excitations in carbon-like nanocones. *Low Temp. Phys.* **44**, 1261 (2018).
26. Yu.A. Sitenko, V.M. Gorkavenko. Induced vacuum magnetic flux in quantum spinor matter in the background of a topological defect in two-dimensional space. *Phys. Rev. D* **100**, 085011 (2019).
27. Yu.A. Sitenko. Induced vacuum magnetic field in the cosmic string background. *Phys. Rev. D* **104**, 045013 (2021).

Received 17.11.21

В.М. Горкавенко, Т.В. Горкавенко,
Ю.А. Ситенко, М.С. Царенкова

ІНДУКОВАНІ ВАКУУМНИЙ СТРУМ ТА МАГНІТНИЙ ПОТІК У КВАНТОВАНІЙ СКАЛЯРНІЙ МАТЕРІЇ В ПРИСУТНОСТІ ВИХРОВОГО ДЕФЕКТУ З ГРАНИЧНОЮ УМОВОЮ ТИПУ НЕЙМАНА

Топологічний дефект у вигляді вихору Абрикосова–Нільсена–Олесена у просторі довільної вимірності розглядається як трубка, що містить потік калібрувального поля та є непроникливою для поля матерії. Квантоване заряджене скалярне поле матерії квантується з урахуванням наявності вихору, на поверхні якого накладено умову типу Неймана. Показано, що навколо вихору індукується вакуумний струм за умови, що комптонівська довжина хвилі поля матерії значно перевищує поперечний розмір вихору. Вакуумний струм є періодичною функцією від потоку калібрувального поля вихору, що є квантово-польовим проявом ефекту Ааронова–Бома. Вакуумний струм викликає появу індукованого вакуумного магнітного потоку, який (за деяких значень товщини трубки) перевищує вакуумний магнітний потік, що індукується сингулярним вихором. Отримані результати були порівняні з результатами, отриманими для випадку, коли на поверхню трубки накладалися граничні умови типу Діріхле. Було показано, що у випадку граничної умови типу Неймана абсолютні значення індукованого вакуумного струму та індукованого вакуумного магнітного потоку перевищують значення відповідних величин у випадку, коли на трубку накладаються граничні умови типу Діріхле.

Ключові слова: вакуумна поляризація, ефект Ааронова–Бома, вихровий дефект.

3.3. Індукування у вакуумі скалярного поля. Гранична умова типу Робена

PHYSICAL REVIEW D **106,** 105010 (2022)

Magnetic flux in the vacuum of quantum bosonic matter in the cosmic string background

Yurii A. Sitenko,[1,2,3] Volodymyr M. Gorkavenko,[4] and Maria S. Tsarenkova[4]

[1]*Bogolyubov Institute for Theoretical Physics, National Academy of Sciences of Ukraine, 14-b Metrologichna Street, Kyiv 03143, Ukraine*

[2]*Van Swinderen Institute for Particle Physics and Gravity, University of Groningen, 4 Nijenborg, Groningen 9747 AG, Netherlands*

[3]*Erwin Schrödinger International Institute for Mathematics and Physics, University of Vienna, 9/2 Boltzmanngassse, Vienna A-1090, Austria*

[4]*Department of Physics, Taras Shevchenko National University of Kyiv, 64 Volodymyrs'ka Street, Kyiv 01601, Ukraine*

(Received 16 August 2022; accepted 18 October 2022; published 14 November 2022)

The relativistic spin-0 matter field is quantized in the background of a straight cosmic string with nonvanishing transverse size. The most general boundary condition ensuring the impenetrability of the matter field into the interior of the cosmic string is shown to be the Robin condition with a boundary parameter varying arbitrarily from point to point of the boundary. The role of the bound states in the spectrum of solutions to the Fock-Klein-Gordon equation is elucidated. We derive, in the general case, an analytic expression for the total magnetic flux, which is induced in the vacuum in the cosmic string background. Further numerical analysis and the requirement of physical plausibility are shown to restrict ambiguity, which is due to the boundary condition. The dependence of the induced vacuum magnetic flux on the string flux and tension, as well as on the transverse size of the string, is analyzed.

DOI: 10.1103/PhysRevD.106.105010

I. INTRODUCTION

Considerable attention is always paid to the study of nonperturbative effects in quantum systems, arising as a consequence of the interaction of quantized fields with various configurations of classical fields. Especially interesting is the influence of configurations with nontrivial topology (domain walls, vortices, monopoles, or, in general, topological defects) on the properties of quantum systems. In the course of spontaneous breaking of a continuous symmetry, a confined region of the false vacuum of the appropriate Higgs field forms a locus of trapped energy, i.e., a topological defect, which can serve as a background for quantum matter fields. There is a need, in this regard, to take into account the finite size of a topological defect and to set up a boundary condition on its edge. An approach might be to employ a family of the most general boundary conditions, ensuring the impenetrability of quantum matter fields into the interior of a topological defect; in mathematical parlance, this means the condition of self-adjointness for the appropriate quantum-mechanical operator of one-particle energy. Then a task is to discover effects that are induced by the topological defect in the ground state of the quantum matter system in the general case, while a further analysis with the requirement of physical plausibility of obtained results is aimed to restrict an arbitrariness in the choice of boundary conditions. In this way, there is a possibility to achieve the unambiguous determination of the influence of the topological defect on quantum matter.

In the present paper, a topological defect in the form of the Abrikosov-Nielsen-Olesen vortex [1,2] is considered. Such defects are known in cosmology and astrophysics under the name of cosmic strings; they emerge in the aftermath of phase transitions with spontaneous gauge symmetry breaking during evolution of the early Universe [3,4]. Cosmic strings, starting from a random tangle, evolve into two different sets: the unstable one, which consists of a variety of string loops decaying by gravitational radiation, and the stable one, which consists of several long, approximately straight strings spanning the horizon; see, e.g., reviews in [5,6]. Although observational bounds predict a negligible contribution of cosmic strings to large scale inhomogeneity, such as the angular distribution in the cosmic microwave background radiation, their evolution brings distinct astrophysical effects, in particular, they

produce detectable gravitational waves [7], gamma-ray bursts [8], and high-energy cosmic rays [9]. The interest in cosmic strings is augmented by theoretical findings that they are demanded in the framework of the superstring theory inspired cosmological models, i.e., the brane-world models of inflation [10–12]. While the Universe undergoes phase transitions at energy scales much higher than the scale of grand unification, such supermassive cosmic strings can be produced, opening new observational windows; see [13,14].

Vortex-type defects are widely discussed in the context of condensed matter physics as well; in particular, they can be viewed as disclinations in nanoconical structures. A development in material science of this century provides a remarkable link between condensed matter and high-energy physics, which is caused to a large extent by the experimental discovery of graphene—a two-dimensional crystalline allotrope formed by a monolayer of carbon atoms [15,16]. It is well established by now that a sheet of graphene is always corrugated and covered by ripples that can be either intrinsic or induced by roughness of a substrate [17]. A single topological defect (disclination) warps a sheet of graphene, rolling it into a nanocone, which is similar to the transverse section of a spatial region out of a cosmic string; see, e.g., [18–21].

Spin-0 quantized fields in various aspects are a subject of study in cosmology and astrophysics. They are present in all unified field theory models, appearing as possible types of matter, in particular, as dilatons and inflatons in the early Universe, as candidates to describe dark matter, and as possible Bose-Einstein condensates. Our purpose is to study the influence of a vortex-type defect on the ground state of the surrounding quantum relativistic bosonic (scalar or pseudoscalar) matter. The induced ground state magnetic flux will be found, and its dependence on the gauge flux and the string tension, as well as on the defect size and the choice of boundary conditions, will be analyzed. We show that the boundary conditions allowing for the existence of bound states are incompatible with the physically plausible behavior of the induced ground state magnetic flux.

In the next section, we define the current and the magnetic field strength that are induced by a cosmic string in the vacuum of quantum relativistic bosonic matter. In Sec. III, we determine the most general boundary condition ensuring the impossibility for matter to penetrate through the edge of the string core and display an appearance of bound states in addition to continuum ones. The analytic expression for the induced vacuum magnetic flux in the general case is derived in Sec. IV. In Sec. V, the numerical study of the analytic expression is carried out, and we show that the range of the boundary parameter values is restricted by requiring the physically plausible behavior for the flux. Finally, the results are summarized and discussed in Sec. VI. The details of derivation of the asymptotics of the flux at small values of the transverse size of the string are given in the Appendix.

II. DEFINITIONS AND PRELIMINARIES

The operator of the second-quantized relativistic spin-0 field in a static (ultrastatic) background is presented as

$$\hat{\Psi}(\mathbf{x},t)=\sum_{\lambda}\frac{1}{\sqrt{2E_\lambda}}[e^{-iE_\lambda t}\psi_\lambda(\mathbf{x})\hat{a}_\lambda+e^{iE_\lambda t}\psi^*_\lambda(\mathbf{x})\hat{b}^\dagger_\lambda], \tag{1}$$

where natural units $\hbar=c=1$ are used, $\hat{a}^\dagger_\lambda$ and $\hat{a}_\lambda$ ($\hat{b}^\dagger_\lambda$ and $\hat{b}_\lambda$) are the spin-0 particle (antiparticle) creation and destruction operators satisfying commutation relations

$$[\hat{a}_\lambda,\hat{a}^\dagger_{\lambda'}]_-=[\hat{b}_\lambda,\hat{b}^\dagger_{\lambda'}]_-=\langle\lambda|\lambda'\rangle, \tag{2}$$

and λ is the set of parameters (quantum numbers) specifying the state; wave functions $\psi_\lambda(\mathbf{x})$ form a complete set of solutions to the stationary Fock-Klein-Gordon equation,

$$[-\boldsymbol{\nabla}^2+m^2+\xi R(\mathbf{x})]\psi_\lambda(\mathbf{x})=E^2_\lambda\psi_\lambda(\mathbf{x}), \tag{3}$$

$\boldsymbol{\nabla}$ is the covariant derivative involving the bundle connection, $R(\mathbf{x})$ is the curvature scalar, $E_\lambda>0$ is the energy of the state, and symbol $\sum_\lambda$ in (1) denotes summation over discrete and integration (with a certain measure) over continuous values of λ. The current that is induced in the vacuum is defined through the vacuum expectation value of the anticommutator of the field operators,

$$\begin{aligned}\mathbf{j}(\mathbf{x})&\equiv\frac{1}{2i}\langle\mathrm{vac}|\{[\hat{\Psi}^\dagger(\mathbf{x},t),\boldsymbol{\nabla}\hat{\Psi}(\mathbf{x},t)]_+\\&\quad-[\boldsymbol{\nabla}\hat{\Psi}^\dagger(\mathbf{x},t),\hat{\Psi}(\mathbf{x},t)]_+\}|\mathrm{vac}\rangle\\&=-i\sum_{\lambda}(2E_\lambda)^{-1}\{\psi^*_\lambda(\mathbf{x})[\boldsymbol{\nabla}\psi_\lambda(\mathbf{x})]-[\boldsymbol{\nabla}\psi_\lambda(\mathbf{x})]^*\psi_\lambda(\mathbf{x})\},\end{aligned} \tag{4}$$

where the vacuum is conventionally defined by relation

$$\hat{a}_\lambda|\mathrm{vac}\rangle=\hat{b}_\lambda|\mathrm{vac}\rangle=0. \tag{5}$$

A straight, infinitely long cosmic string in its rest frame is characterized by two parameters, the gauge flux

$$\Phi=\int_{\mathrm{core}}d\boldsymbol{\sigma}\cdot\boldsymbol{\partial}\times\mathbf{V}(\mathbf{x}) \tag{6}$$

and tension (or linear density of mass)

$$M=\frac{1}{16\pi G}\int_{\mathrm{core}}d\sigma\,R(\mathbf{x}). \tag{7}$$

Here, $\mathbf{V}(\mathbf{x})$ is the vector potential of the gauge field corresponding to the spontaneously broken gauge symmetry, Ç is the gravitational constant, and the integration is over the transverse section of the string core. Without loss of generality, the string core is assumed to have the form of a tube of radius r_0. A tube in three-dimensional space can be obviously generalized to a $(d-2)$ tube in d-dimensional space by adding extra $d-3$ dimensions as longitudinal ones. Space outside the string core is locally flat ($R=0$) but non-Euclidean, with squared length element

$$ds^2 = dr^2 + (1-4\text{Ç}M)^2 r^2 d\varphi + d\mathbf{z}_{d-2}^2, \tag{8}$$

where r and φ are the polar coordinates on a surface that is transverse to the string, and $\mathbf{z}_{d-2}$ are the Cartesian coordinates in the longitudinal directions. Such a space can be denoted as a conical one, since its transverse section is isometric to the surface of a cone with the deficit angle equal to $8\pi\text{Ç}M$. In general, the values of the deficit angle are bounded from above by 2π, whereas they are unbounded from below (surplus angle can be arbitrarily large),

$$-\infty < 8\pi\text{Ç}M < 2\pi. \tag{9}$$

If we return to real cosmic strings in three-dimensional space, then the tension (and, consequently, the deficit angle) surely has to be non-negative; moreover, the observation of discontinuities in the cosmic microwave background radiation imposes the stringent upper bound $M \lesssim 10^{-7}\text{Ç}^{-1}$ (see [22]). However, negative values of M and corresponding saddlelike conical spaces, as well as positive values of M up to $(4\text{Ç})^{-1}$, can be of some physical interest. Various nanoconical structures arise in a diverse set of condensed matter systems known as the Dirac materials, ranging from honeycomb crystalline allotropes (graphene [16], silicene, germanene [23], and phosphorene [24]) to high-temperature cuprate superconductors [25] and topological insulators [26]; in particular, a saddlelike conical space effectively emerges due to a radial disgyration in the A phase of superfluid He3; see [27].

Matter is assumed to interact with a cosmic string in the minimal way; i.e., the covariant derivative takes form $\boldsymbol{\nabla} = \boldsymbol{\partial} - \mathrm{i}\tilde{e}\mathbf{V} + \frac{\mathrm{i}}{2}\boldsymbol{\omega}$, where $\tilde{e}$ is the appropriate coupling constant and $\boldsymbol{\omega}$ is the affine connection. In the gauge with the only one nonvanishing component,

$$V_\varphi = \frac{\Phi}{2\pi}, \tag{10}$$

the Laplace-Beltrami operator takes the form

$$\boldsymbol{\nabla}^2 = r^{-1}\frac{\partial}{\partial r} r \frac{\partial}{\partial r} + (1-4\text{Ç}M)^{-2} r^{-2}\left(\frac{\partial}{\partial\varphi} - \frac{\mathrm{i}\tilde{e}\Phi}{2\pi}\right)^2 + \left(\frac{\partial}{\partial \mathbf{z}_{d-2}}\right)^2, \tag{11}$$

and we obtain the following expression for a general solution to (3), describing a state belonging to the continuous spectrum:

$$\psi_{kn\mathbf{p}}(\mathbf{x}) = (2\pi)^{(1-d)/2} e^{\mathrm{i}\mathbf{p}\cdot\mathbf{z}_{d-2}} e^{\mathrm{i}n\varphi} (1-4\text{Ç}M)^{-1/2} \times [\sin(\mu_n) J_{|n-\tilde{e}\Phi/(2\pi)|/(1-4\text{Ç}M)}(kr) + \cos(\mu_n) Y_{|n-\tilde{e}\Phi/(2\pi)|/(1-4\text{Ç}M)}(kr)], \tag{12}$$

where $0 < k < \infty$, $-\infty < p_j < \infty$ ($j = \overline{1, d-2}$), $E = \sqrt{\mathbf{p}^2 + k^2 + m^2}$, $n \in \mathbb{Z}$ ($\mathbb{Z}$ is the set of integer numbers), and $J_\rho(u)$ and $Y_\rho(u)$ are the Bessel functions of order ρ of the first and second kinds. Parameter μ_n has to be determined from the boundary condition at $r = r_0$; see the next section. In the case of a vanishing transverse size of the string, relation

$$\mu_n|_{r_0=0} = \pi/2 \tag{13}$$

is assumed, then the wave function in this case is regular at $r=0$, obeying orthonormality condition

$$\int d^d\mathbf{x}\sqrt{g}\psi^*_{kn\mathbf{p}}(\mathbf{x})|_{r_0=0}\psi_{k'n'\mathbf{p}'}(\mathbf{x})|_{r_0=0} = \frac{\delta(k-k')}{k}\delta_{n,n'}\delta^{d-2}(\mathbf{p}-\mathbf{p}'). \tag{14}$$

Substituting (12) into (4), we obtain the induced vacuum current due to the contribution of the continuous spectrum, and this part possesses an angular component as the only nonvanishing one,

$$j_\varphi^{(CS)}(r) = \int d^{d-2}\mathbf{p}\int_0^\infty \frac{dkk}{\sqrt{m^2+\mathbf{p}^2+k^2}}\sum_{n\in\mathbb{Z}}\left(n - \frac{\tilde{e}\Phi}{2\pi}\right)|\psi_{kn\mathbf{p}}(\mathbf{x})|^2. \tag{15}$$

It is obvious from (12) and (15) that $j_\varphi^{(CS)}(r)$ is a periodic function of the string flux, Φ (6), with a period equal to $2\pi/\tilde{e}$; i.e., it depends on quantity

$$F = \frac{\tilde{e}\Phi}{2\pi} - \left[\left[\frac{\tilde{e}\Phi}{2\pi}\right]\right], \qquad 0 \leq F < 1 \tag{16}$$

and not on $[[\frac{\tilde{e}\Phi}{2\pi}]]$, where $[[u]]$ denotes the integer part of quantity u. Such a periodicity certainly is a manifestation of the renowned Aharonov-Bohm effect [28,29]. Defining quantity

$$\nu = (1 - 4\text{G}M)^{-1} \tag{17}$$

and inserting (12) into (15), we rewrite the latter as

$$j_{\varphi}^{(CS)}(r) = (2\pi)^{1-d} \int d^{d-2}\mathbf{p} \int_0^{\infty} \frac{dkk}{\sqrt{m^2 + \mathbf{p}^2 + k^2}} \sum_{n\in\mathbb{Z}} \nu(n-F)[\sin^2(\mu_n) J^2_{\nu|n-F|}(kr) + \sin(2\mu_n) J_{\nu|n-F|}(kr) Y_{\nu|n-F|}(kr) + \cos^2(\mu_n) Y^2_{\nu|n-F|}(kr)]. \tag{18}$$

If the angular component of the induced vacuum current is the only nonvanishing one, then the magnetic field strength in the longitudinal directions, $B_{\text{I}}^{3\ldots d}(r)$, is also induced in the vacuum, as a consequence of the Maxwell equation,

$$\frac{r}{\nu}\frac{\partial}{\partial r} B_{\text{I}}^{3\ldots d}(r) = -e j_{\varphi}(r), \tag{19}$$

where e is the electromagnetic coupling constant that, in general, differs from $\tilde{e}$. The total flux of the induced vacuum magnetic field is then given by expression

$$\Phi_{\text{I}} = \nu^{-1} \int_0^{2\pi} d\varphi \int_{r_0}^{\infty} dr\, r B_{\text{I}}^{3\ldots d}(r). \tag{20}$$

Induced vacuum current, as well as consequent magnetic field, in the background of a vortex-type defect attracted attention several decades ago in view of its anticipated relevance to the Aharonov-Bohm effect. In the pioneering study in [30–38], a simplifying unphysical assumption of the vanishing transverse size ($r_0 = 0$) and tension ($M = 0$) of the vortex was employed. It was realized that the total induced vacuum magnetic flux is finite in the $d = 2$ case and infinite in the physically interesting $d = 3$ case. The problem of removing the above restriction, i.e., going over to $r_0 > 0$ and $M \neq 0$, was completely solved for the vacuum of a spin-1/2 quantized matter field in the $d = 2$ case [39] and in the $d = 3$ case [40]. In the present study, we consider the same problem for the vacuum of a spin-0 quantized matter field in the $d \geq 2$ case.

III. SELF-ADJOINTNESS OF THE LAPLACE-BELTRAMI OPERATOR AND CHOICE OF BOUNDARY CONDITIONS

Our attention is drawn to the Laplace-Beltrami operator, because, in the case of relativistic bosonic matter, the relevant quantum-mechanical operator is that of one-particle energy squared, see (3). Defining a scalar product as

$$(\tilde{\chi}, \chi) = \int_X d^d\mathbf{x} \sqrt{g} \tilde{\chi}^* \chi, \tag{21}$$

we get, using integration by parts,

$$(\tilde{\chi}, \boldsymbol{\nabla}^2\chi) = (\boldsymbol{\nabla}^2\tilde{\chi}, \chi) + \int_{\partial X} d\boldsymbol{\sigma} \cdot [\tilde{\chi}^*(\boldsymbol{\nabla}\chi) - (\boldsymbol{\nabla}\tilde{\chi})^*\chi], \tag{22}$$

where ∂X is a hypersurface bounding the d-dimensional spatial region X. Operator $\boldsymbol{\nabla}^2$ is Hermitian (or symmetric in mathematical parlance),

$$(\tilde{\chi}, \boldsymbol{\nabla}^2\chi) = (\boldsymbol{\nabla}^2\tilde{\chi}, \chi), \tag{23}$$

if relation

$$\int_{\partial X} d\boldsymbol{\sigma} \cdot [\tilde{\chi}^*(\boldsymbol{\nabla}\chi) - (\boldsymbol{\nabla}\tilde{\chi})^*\chi] = 0 \tag{24}$$

holds. The latter can be satisfied in various ways by imposing different boundary conditions for χ and $\tilde{\chi}$. However, among the whole variety, there may exist a possibility that a boundary condition for $\tilde{\chi}$ is the same as that for χ; then operator $\boldsymbol{\nabla}^2$ is self-adjoint. The action of a self-adjoint operator on functions of its domain of definition results in functions of the same domain only, and, therefore, a multiple action and functions of such an operator can be consistently defined. The spectral theorem (see, e.g., [41]) is valid for self-adjoint operators only, and this allows one to construct unitary exponents of them; see also [42].

In the case of a connected boundary, condition (24) implies

$$\mathbf{n} \cdot [\tilde{\chi}^*(\boldsymbol{\nabla}\chi) - (\boldsymbol{\nabla}\tilde{\chi})^*\chi]|_{\mathbf{x}\in\partial X} = 0, \tag{25}$$

where $\mathbf{n}$ is the unit normal to boundary ∂X. Defining

$$\chi_{\pm} = \mathbf{n} \cdot \boldsymbol{\nabla}\chi \pm \frac{\text{i}}{\mathbf{n} \cdot \mathbf{x}}\chi, \qquad \tilde{\chi}_{\pm} = \mathbf{n} \cdot \boldsymbol{\nabla}\tilde{\chi} \pm \frac{\text{i}}{\mathbf{n} \cdot \mathbf{x}}\tilde{\chi}, \tag{26}$$

we rewrite (25) as

$$\frac{\mathrm{i}}{2}\mathbf{n}\cdot\mathbf{x}(\tilde{\chi}_+^*\chi_+ - \tilde{\chi}_-^*\chi_-)|_{\mathbf{x}\in\partial X} = 0. \tag{27}$$

The latter condition is satisfied by imposing linear conditions

$$(\chi_- - \Xi\chi_+)|_{\mathbf{x}\in\partial X} = 0, \quad (\tilde{\chi}_- - \Xi\tilde{\chi}_+)|_{\mathbf{x}\in\partial X} = 0, \quad |\Xi|^2 = 1. \tag{28}$$

Using parametrization $\Xi = e^{2i\theta}$, we rewrite (28) as[1]

$$\left[\left(\frac{\cos\theta}{\mathbf{n}\cdot\mathbf{x}} + \sin\theta\,\mathbf{n}\cdot\boldsymbol{\nabla}\right)\chi\right]\Big|_{\mathbf{x}\in\partial X} = 0,$$
$$\left[\left(\frac{\cos\theta}{\mathbf{n}\cdot\mathbf{x}} + \sin\theta\,\mathbf{n}\cdot\boldsymbol{\nabla}\right)\tilde{\chi}\right]\Big|_{\mathbf{x}\in\partial X} = 0. \tag{29}$$

One can recognize that (29) is actually the Robin boundary condition, with $\theta = 0$ corresponding to the Dirichlet condition (perfect reflectivity of the boundary) and $\theta = \pm\pi/2$ corresponding to the Neumann condition (absolute rigidity of the boundary). The condition is periodic in the value of θ with the period equal to π, and the range of θ can be restricted to $-\pi/2 \le \theta < \pi/2$.

Parameter θ can be regarded as the self-adjoint extension parameter. It should be emphasized that the values of this parameter may, in general, vary from point to point on the boundary. In this respect the "number" of self-adjoint extension parameters is infinite; moreover, it is not countable but is of power of a continuum. This distinguishes the case of an extended boundary from the case of an excluded point, when the number of self-adjoint extension parameters is finite, being equal to n^2 for the deficiency index equal to (n, n); see, e.g., [42]. Defining the quantum-mechanical current of matter as

$$\mathbf{J}_\lambda(\mathbf{x}) = -\mathrm{i}\{\psi_\lambda^*(\mathbf{x})[\boldsymbol{\nabla}\psi_\lambda(\mathbf{x})] - [\boldsymbol{\nabla}\psi_\lambda(\mathbf{x})]^*\psi_\lambda(\mathbf{x})\}, \tag{30}$$

we note that imposing the self-adjoint extension condition (29) on ψ_λ results in the vanishing of the normal component of the current at the boundary,

$$\mathbf{n}\cdot\mathbf{J}_\lambda(\mathbf{x})|_{\mathbf{x}\in\partial X} = 0. \tag{31}$$

Thus, the Robin boundary condition with the position-dependent boundary parameter is the most general one ensuring the impenetrability of a connected boundary for a spin-0 matter field. It should be noted that, in the case of a disconnected two-component boundary, the requirement of self-adjointness allows for a penetrable boundary, but the influx of quantum matter through one boundary component has to be equal to its outflux through another one; see [43,44].

In the case of a cosmic string, the boundary condition takes form[2]

$$\left[\left(\cos\theta + \sin\theta\frac{r\partial}{\partial r}\right)\chi\right]\Big|_{r=r_0} = 0,$$
$$\left[\left(\cos\theta + \sin\theta\frac{r\partial}{\partial r}\right)\tilde{\chi}\right]\Big|_{r=r_0} = 0. \tag{32}$$

Imposing this condition on wave function (12), we determine parameter μ_n as

$$\tan\mu_n = -\frac{[(\cot\theta + r\frac{\partial}{\partial r})Y_{\nu|n-F|}(kr)]|_{r=r_0}}{[(\cot\theta + r\frac{\partial}{\partial r})J_{\nu|n-F|}(kr)]|_{r=r_0}}. \tag{33}$$

As was already noted, the values of parameter θ, in general, depend on φ and $\mathbf{z}_{d-2}$. As a consequence, current (18) additionally depends on φ and $\mathbf{z}_{d-2}$ via the dependence of μ_n ($n \in \mathbb{Z}$) on φ and $\mathbf{z}_{d-2}$. To be more precise, we assume the following ansatz for a solution to the stationary Fock-Klein-Gordon equation in the cosmic string background:

$$\psi_{kn\mathbf{p}}(\mathbf{x}) = (2\pi)^{(1-d)/2}e^{i\mathbf{p}\cdot\mathbf{z}_{d-2}}e^{in\varphi}f_n(kr), \tag{34}$$

where function $f_n(kr)$ is the solution to equation

$$\left[-\frac{1}{r}\frac{\partial}{\partial r}r\frac{\partial}{\partial r} + \frac{\nu^2}{r^2}(n-F)^2 - k^2\right]f_n(kr) = 0 \tag{35}$$

and obeys boundary condition

$$\left[\left(\cos\theta + \sin\theta\frac{r\partial}{\partial r}\right)f_n(kr)\right]\Big|_{r=r_0} = 0. \tag{36}$$

Note also that, by taking the limit of $r_0 \to 0$ in (33), we justify assumption (13).

In the case of $\min\{F, 1-F\} < \nu^{-1}\cot\theta < \infty$, in addition to solutions with $k > 0$, see (12), there are solutions with $k = \mathrm{i}\kappa_n$, where κ_n is determined by relation

$$\left[\left(\cos\theta + \sin\theta\frac{r\partial}{\partial r}\right)K_{\nu|n-F|}(\kappa_n r)\right]\Big|_{r=r_0} = 0, \tag{37}$$

$K_\rho(u)$ is the Macdonald function of order ρ. These solutions correspond to bound states on a surface that is transverse to a cosmic string,

[1]Note that, in the case of a disconnected two-component boundary, the most general boundary condition depends on four parameters; see [43].

[2]The impenetrability of the string core, on the one hand, is a consequence of the self-adjointness of the quantum-mechanical operator of energy squared. On the other hand, it is inevitable, since the vacuum of a spin-0 quantized matter field is not defined inside the string core.

$$\psi^{(BS)}_{\kappa_n n\mathbf{p}}(\mathbf{x}) = (2\pi)^{(1-d)/2} e^{i\mathbf{p}\cdot\mathbf{z}_{d-2}} e^{in\varphi} \frac{\sqrt{2\nu}}{r_0} \times [K_{\nu|n-F|+1}(\kappa_n r_0) K_{\nu|n-F|-1}(\kappa_n r_0) - K^2_{\nu|n-F|}(\kappa_n r_0)]^{-1/2} K_{\nu|n-F|}(\kappa_n r). \tag{38}$$

The dependence of κ_n on the value of $\nu|n-F|$ for fixed values of θ is illustrated in Fig. 1. For fixed values of θ and $\mathbf{p}$, there is no more than one bound state for each value of n, and their energies, $E^{(BS)}_n = \sqrt{m^2 + \mathbf{p}^2 - \kappa_n^2}$, are in the gap below the continuum,

$$\sqrt{m^2 + \mathbf{p}^2 - [\cot^2\theta - \nu^2(n-F)^2] r_0^{-2}} < E^{(BS)}_n < \sqrt{m^2 + \mathbf{p}^2}. \tag{39}$$

Note that, in the limit of a vanishing transverse size of the string, wave function (38) vanishes at $\nu|n-F| > 1$, whereas it is novanishing at $\nu|n-F| < 1$.[3]

A variation of θ with φ can be moderate enough, so that a dependence of κ_n on φ can be neglected. Then, substituting (38) into (4), we obtain

$$j^{(BS)}_\varphi(r) = \frac{2(2\pi)^{1-d}}{r_0^2} \int d^{d-2}\mathbf{p} \sum_{n\in\mathbb{Z}} \frac{\nu(n-F)}{\sqrt{m^2 + \mathbf{p}^2 - \kappa_n^2}} \frac{\Theta(\cot\theta - \nu|n-F|) K^2_{\nu|n-F|}(\kappa_n r)}{K_{\nu|n-F|+1}(\kappa_n r_0) K_{\nu|n-F|-1}(\kappa_n r_0) - K^2_{\nu|n-F|}(\kappa_n r_0)}, \tag{40}$$

where

$$\Theta(u) = \left\{ \begin{array}{ll} 1, & u > 0 \\ 0, & u < 0 \end{array} \right\}$$

is the step function. Thus, the induced vacuum current in the cosmic string background is

$$j_\varphi(r) = j^{(CS)}_\varphi(r) + j^{(BS)}_\varphi(r), \tag{41}$$

with $j^{(CS)}_\varphi$ and $j^{(BS)}_\varphi$ given by (18) and (40), respectively. It should be noted that the integral in (40), as well as that in (18), is divergent at $|\mathbf{p}| \to \infty$ (logarithmically at $d = 3$ and as a power at $d > 3$). However, we shall show that these divergences cancel each other in the sum in (41). Note also that a variation of θ with $\mathbf{z}_{d-2}$ can be moderate enough, so that a violation of translational invariance along the longitudinal directions can be regarded as negligible. Then the induced vacuum magnetic field strength is in the longitudinal directions, as is given by (19).

[3]It should be noted that, in the case of an infinitely thin string, the requirement of self-adjointness of the Laplace-Beltrami operator allows for regular and irregular square integrable at $r = 0$ modes. The deficiency index can be (n, n) with $n = 0, 1, 2, \ldots$, depending on the values of ν and F. In particular, it is (2, 2) for $\nu = 1$; see, e.g., [45,46].

IV. INDUCED VACUUM MAGNETIC FLUX: ANALYTIC EXPRESSIONS

We present induced vacuum current $j_\varphi(r)$ (41) as

$$j_\varphi(r) = j^{(a)}_\varphi(r) + j^{(b)}_\varphi(r), \tag{42}$$

where

$$j^{(a)}_\varphi(r) = (2\pi)^{1-d} \int d^{d-2}\mathbf{p} \times \int_0^\infty \frac{dk k}{\sqrt{m^2 + \mathbf{p}^2 + k^2}} \sum_{n\in\mathbb{Z}} \nu(n-F) J^2_{\nu|n-F|}(kr) \tag{43}$$

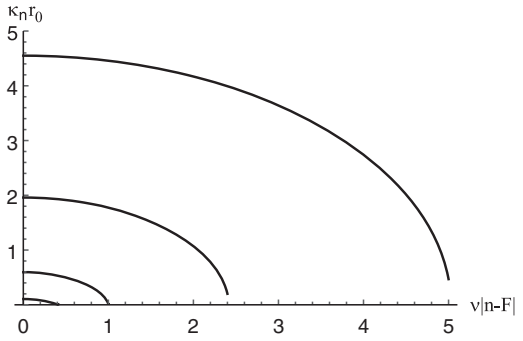

FIG. 1. The value of the root of Eq. (37) as a function of $\nu|n-F|$: curves from top to bottom correspond to $\theta = \pi/16$, $\pi/8, \pi/4, 3\pi/8$.

and

$$j_\varphi^{(b)}(r) = (2\pi)^{1-d}\int d^{d-2}\mathbf{p}\int_0^\infty \frac{dkk}{\sqrt{m^2+\mathbf{p}^2+k^2}}\sum_{n\in\mathbb{Z}}\nu(n-F)$$
$$\times\{\cos^2(\mu_n)[Y^2_{\nu|n-F|}(kr)-J^2_{\nu|n-F|}(kr)]+\sin(2\mu_n)J_{\nu|n-F|}(kr)Y_{\nu|n-F|}(kr)\}+j_\varphi^{(BS)}(r). \tag{44}$$

The Bessel functions $J_\rho(u)$ and $Y_\rho(u)$ in (43) and (44) are expressed through the modified Bessel function $I_\rho(u)$ and the Macdonald function $K_\rho(u)$, and the integration is extended to negative values of k as well, $-\infty < k < \infty$; see [47]. Such an integral can be regarded as the integral over the real axis in the complex k plane. In the case of $j_\varphi^{(a)}(r)$ (43), the integrand as a function of the complex k variable possesses branching points at $k = \pm i\sqrt{m^2+\mathbf{p}^2}$, and the integration path over the real axis is continuously deformed to envelope a cut on the imaginary axis from $i\sqrt{m^2+\mathbf{p}^2}$ to $i\infty$. In this way, we get

$$j_\varphi^{(a)}(r) = \frac{4}{(2\pi)^d}\int d^{d-2}\mathbf{p}\int_{m_{|\mathbf{p}|}}^\infty \frac{dq\,q}{\sqrt{q^2-m^2_{|\mathbf{p}|}}}\sum_{n\in\mathbb{Z}}\nu(n-F)I_{\nu|n-F|}(qr)K_{\nu|n-F|}(qr),$$
$$m_{|\mathbf{p}|} = \sqrt{m^2+\mathbf{p}^2}. \tag{45}$$

Using relation (see [48])

$$I_\rho(u)K_\rho(u) = \frac{1}{2}\int_0^\infty \frac{dy}{y}\exp\left(-\frac{u^2}{2y}-y\right)I_\rho(y)$$

and the Schläfli contour representation for $I_\rho(y)$, one can perform the summation over n and then perform the integrations. The final result,

$$j_\varphi^{(a)}(r) = -\frac{8}{(4\pi)^{(d+1)/2}}\frac{m^{(d+1)/2}}{r^{(d-3)/2}}\left\{\frac{1}{2\pi}\int_0^\infty du K_{(d+1)/2}[2mr\cosh(u/2)]\right.$$
$$\times\frac{\sinh(u/2)}{[\cosh(u/2)]^{(d-1)/2}}\frac{\sin(\nu F\pi)\sinh[\nu(1-F)u]-\sin[\nu(1-F)\pi]\sinh(\nu Fu)}{\cosh(\nu u)-\cos(\nu\pi)}$$
$$\left.+\frac{1}{\nu}\sum_{l=1}^{[[\nu/2]]}K_{(d+1)/2}[2mr\sin(l\pi/\nu)]\frac{\cos(l\pi/\nu)}{[\sin(l\pi/\nu)]^{(d-1)/2}}\sin(2Fl\pi)\right\}, \tag{46}$$

was obtained in [49] for the case of $0 < \nu \le 2$, while additional terms appearing at $\nu > 2$ were obtained in [50]. Further, we get

$$B_I^{3\ldots d(a)}(r) = e\nu\int_r^\infty \frac{dr'}{r'}j_\varphi^{(a)}(r') = -\frac{4e\nu}{(4\pi)^{(d+1)/2}}\left(\frac{m}{r}\right)^{(d-1)/2}\left\{\frac{1}{2\pi}\int_0^\infty du\,K_{(d-1)/2}[2mr\cosh(u/2)]\frac{\sinh(u/2)}{[\cosh(u/2)]^{(d+1)/2}}\right.$$
$$\times\frac{\sin(\nu F\pi)\sinh[\nu(1-F)u]-\sin[\nu(1-F)\pi]\sinh(\nu Fu)}{\cosh(\nu u)-\cos(\nu\pi)}$$
$$\left.+\frac{1}{\nu}\sum_{l=1}^{[[\nu/2]]}K_{(d-1)/2}[2mr\sin(l\pi/\nu)]\frac{\cos(l\pi/\nu)}{[\sin(l\pi/\nu)]^{(d+1)/2}}\sin(2Fl\pi)\right\} \tag{47}$$

and

$$\Phi_I^{(a)} = \frac{2\pi}{\nu}\int_{r_0}^{\infty} dr\, r B_I^{3\ldots d(a)}(r) = -\frac{e}{(4\pi)^{(d-1)/2}}\left(\frac{m}{r_0}\right)^{(d-3)/2}\left\{\frac{1}{2\pi}\int_0^{\infty} du\, K_{(d-3)/2}[2mr_0\cosh(u/2)]\frac{\sinh(u/2)}{[\cosh(u/2)]^{(d+3)/2}}\right.$$
$$\times\frac{\sin(\nu F\pi)\sinh[\nu(1-F)u] - \sin[\nu(1-F)\pi]\sinh(\nu F u)}{\cosh(\nu u)-\cos(\nu\pi)}$$
$$\left.+\frac{1}{\nu}\sum_{l=1}^{[[\nu/2]]} K_{(d-3)/2}[2mr_0\sin(l\pi/\nu)]\frac{\cos(l\pi/\nu)}{[\sin(l\pi/\nu)]^{(d+3)/2}}\sin(2Fl\pi)\right\}. \tag{48}$$

In the case of the vanishing string tension $\nu = 1$, the results for $j_\varphi^{(a)}(r)$ and $B_I^{3\ldots d(a)}(r)$ were obtained more than two decades ago, see [37,38],

$$j_\varphi^{(a)}(r)\Big|_{\nu=1} = \frac{32\sin(F\pi)}{(4\pi)^{(d+3)/2}}\frac{m^{(d+1)/2}}{r^{(d-3)/2}}\int_1^{\infty}\frac{dv}{v^{(d+1)/2}}K_{(d+1)/2}(2mrv)\sinh[(2F-1)\operatorname{arccosh}(v)] \tag{49}$$

and

$$B_I^{3\ldots d(a)}(r)\Big|_{\nu=1} = \frac{16e\sin(F\pi)}{(4\pi)^{(d+3)/2}}\left(\frac{m}{r}\right)^{(d-1)/2}\int_1^{\infty}\frac{dv}{v^{(d+3)/2}}K_{(d-1)/2}(2mrv)\sinh[(2F-1)\operatorname{arccosh}(v)], \tag{50}$$

whereas the flux is given by expression

$$\Phi_I^{(a)}\Big|_{\nu=1} = \frac{4e\sin(F\pi)}{(4\pi)^{(d+1)/2}}\left(\frac{m}{r_0}\right)^{(d-3)/2}\int_1^{\infty}\frac{dv}{v^{(d+5)/2}}K_{(d-3)/2}(2mr_0v)\sinh[(2F-1)\operatorname{arccosh}(v)]. \tag{51}$$

For generic ν, we find out that flux $\Phi_I^{(a)}$ (48) in the limit of a vanishing transverse size of the string is finite in the $d = 2$ case only, while otherwise a divergence occurs,

$$\lim_{r_0\to 0}\Phi_I^{(a)}|_{d=2} = \frac{e}{4m}I_3(F,\nu), \tag{52}$$

$$\Phi_I^{(a)}|_{d=3} \underset{r_0\to 0}{=} \frac{e}{4\pi}[-\ln(mr_0)]I_3(F,\nu), \tag{53}$$

and

$$\Phi_I^{(a)}|_{d>3} \underset{r_0\to 0}{=} \frac{e\Gamma\left(\frac{d-3}{2}\right)}{2(4\pi)^{(d-1)/2}}r_0^{3-d}I_d(F,\nu), \tag{54}$$

where

$$I_d(F,\nu) = -\frac{1}{2\pi}\int_0^{\infty} du\frac{\sinh(u/2)}{[\cosh(u/2)]^d}\frac{\sin(\nu F\pi)\sinh[\nu(1-F)u]-\sin[\nu(1-F)\pi]\sinh(\nu F u)}{\cosh(\nu u)-\cos(\nu\pi)} - \frac{1}{\nu}\sum_{l=1}^{[[\nu/2]]}\frac{\cos(l\pi/\nu)}{[\sin(l\pi/\nu)]^d}\sin(2Fl\pi), \tag{55}$$

and $\Gamma(u)$ is the Euler gamma function. The integration and summation in (55) can be performed in the case of the odd d values; see the Appendix. In particular, we obtain

$$\lim_{r_0\to 0}\Phi_I^{(a)}\Big|_{d=2}=\frac{e}{6m}\left(F-\frac{1}{2}\right)F(1-F)\nu^2, \tag{56}$$

$$\Phi_I^{(a)}\Big|_{d=3}\underset{r_0\to 0}{=}\frac{e}{6\pi}[-\ln(mr_0)]\left(F-\frac{1}{2}\right)F(1-F)\nu^2, \tag{57}$$

$$\Phi_I^{(a)}\Big|_{d=5}\underset{r_0\to 0}{=}\frac{e}{12(2\pi)^2}r_0^{-2}\left(F-\frac{1}{2}\right)F(1-F)\nu^2\left\{\frac{1}{3}+\frac{1}{5}\left[\frac{1}{3}+F(1-F)\right]\nu^2\right\}, \tag{58}$$

$$\Phi_I^{(a)}\Big|_{d=7}\underset{r_0\to 0}{=}\frac{e}{180(2\pi)^3}r_0^{-4}\left(F-\frac{1}{2}\right)F(1-F)\nu^2\left\{\frac{4}{3}+\left[\frac{1}{3}+F(1-F)\right]\nu^2+\frac{1}{7}\left[\frac{1}{3}+F(1-F)+F^2(1-F)^2\right]\nu^4\right\}, \tag{59}$$

$$\begin{aligned}\Phi_I^{(a)}\Big|_{d=9}\underset{r_0\to 0}{=}&\frac{e}{810(2\pi)^4}r_0^{-6}\left(F-\frac{1}{2}\right)F(1-F)\nu^2\left\{4+\frac{49}{15}\left[\frac{1}{3}+F(1-F)\right]\nu^2\right.\\&\left.+\frac{2}{3}\left[\frac{1}{3}+F(1-F)+F^2(1-F)^2\right]\nu^4+\frac{1}{15}\left[\frac{1}{3}+F(1-F)+\frac{10}{9}F^2(1-F)^2+\frac{5}{9}F^3(1-F)^3\right]\nu^6\right\},\end{aligned} \tag{60}$$

and so on; note the positive definiteness of all terms in curly brackets in (58)–(60). Note also that (55) can be calculated exactly for all d values in the case of a vanishing string tension, see [51],

$$I_d(F,1)=\frac{\sin(F\pi)}{2\sqrt{\pi}}\left(F-\frac{1}{2}\right)\frac{\Gamma(\frac{d-1}{2}+F)\Gamma(\frac{d+1}{2}-F)}{\Gamma(\frac{d}{2}+1)\Gamma(\frac{d+1}{2})}. \tag{61}$$

Turning now to the θ-dependent piece of the induced vacuum current, see $j_\varphi^{(b)}(r)$ (44), the integral over k is transformed into the integral over a contour enveloping the upper imaginary semiaxis on the complex k plane. In this way, we get

$$\begin{aligned}j_\varphi^{(b)}(r)=&\frac{8}{(2\pi)^{d+1}}\int d^{d-2}\mathbf{p}\sum_{n\in\mathbb{Z}}\nu(n-F)\sum_{\pm}\left\{\int_0^{m_{|\mathbf{p}|}}\frac{dq\,q}{\sqrt{m_{|\mathbf{p}|}^2-q^2}}e^{\mp i\nu|n-F|\pi}\left[\cos^2(\mu_n)|_{k=\pm iq}\pm\frac{i}{2}\sin(2\mu_n)|_{k=\pm iq}\right]K^2_{\nu|n-F|}(qr)\right.\\&\left.+\int_{m_{|\mathbf{p}|}}^{\infty}\frac{dq\,q}{\sqrt{q^2-m_{|\mathbf{p}|}^2}}e^{\mp i\nu|n-F|\pi}\left[\pm i\cos^2(\mu_n)|_{k=\pm iq}-\frac{1}{2}\sin(2\mu_n)|_{k=\pm iq}\right]K^2_{\nu|n-F|}(qr)\right\}+j_\varphi^{(BS)}(r),\quad m_{|\mathbf{p}|}=\sqrt{m^2+\mathbf{p}^2}.\end{aligned} \tag{62}$$

In view of relation

$$\sum_{\pm}e^{\mp i\nu|n-F|\pi}\left[\cos^2(\mu_n)|_{k=\pm iq}\pm\frac{i}{2}\sin(2\mu_n)|_{k=\pm iq}\right]=-\frac{\pi^2}{\kappa_n r_0^2}\frac{\Theta(\cot\theta-\nu|n-F|)\delta(q-\kappa_n)}{K_{\nu|n-F|+1}(\kappa_n r_0)K_{\nu|n-F|-1}(\kappa_n r_0)-K^2_{\nu|n-F|}(\kappa_n r_0)}, \tag{63}$$

the contribution of the integral over q from 0 to $m_{|\mathbf{p}|}$ cancels $j_\varphi^{(BS)}(r)$ (40). Using relation

$$\sum_{\pm}e^{\mp i\nu|n-F|\pi}\left[\pm i\cos^2(\mu_n)|_{k=\pm iq}-\frac{1}{2}\sin(2\mu_n)|_{k=\pm iq}\right]=-\pi C_{\nu|n-F|}(\theta,qr_0), \tag{64}$$

where

$$C_\rho(\theta,v)=\frac{[(\cot\theta+v\partial_v)I_\rho(v)]}{[(\cot\theta+v\partial_v)K_\rho(v)]}, \tag{65}$$

we obtain the following expression for the remaining piece, after integration over $\mathbf{p}$:

$$j_{\varphi}^{(b)}(r) = -\frac{8}{(4\pi)^{(d+1)/2}}\frac{1}{\Gamma(\frac{d-1}{2})}\int_{m}^{\infty} dq\, q(q^2-m^2)^{(d-3)/2}\sum_{n\in\mathbb{Z}}\nu(n-F)C_{\nu|n-F|}(\theta, qr_0)K^2_{\nu|n-F|}(qr); \tag{66}$$

note that a zero in the denominator of $C_{\rho}(\theta, v)$ (65) is to be treated with the principal value prescription. It should be noted also that terms with $\nu|n-F|<1$ in the integrand of $j_{\varphi}^{(BS)}(r)$ (40), unlike terms with $\nu|n-F|>1$, are finite in the limit of a vanishing transverse size of the string. However, as has been just remarked, they, as well as others, are canceled out, and the θ-dependent piece of the current, as is clear from (65) and (66), is vanishing in this limit,

$$\lim_{r_0\to 0} j_{\varphi}^{(b)}(r) = 0. \tag{67}$$

Further, we get the θ-dependent piece of the induced vacuum magnetic field strength,

$$\begin{aligned} B_I^{3\ldots d(b)}(r) &= e\nu\int_{r}^{\infty}\frac{dr'}{r'}j_{\varphi}^{(b)}(r') \\ &= -\frac{4e\nu}{(4\pi)^{(d+1)/2}}\frac{1}{\Gamma(\frac{d-1}{2})}\int_{m}^{\infty} dq\, q(q^2-m^2)^{(d-3)/2}\sum_{n\in\mathbb{Z}}\mathrm{sgn}(n-F)C_{\nu|n-F|}(\theta, qr_0)[K^2_{\nu|n-F|}(qr)+qrW_{\nu|n-F|}(qr)], \end{aligned} \tag{68}$$

where $\mathrm{sgn}(u)=\Theta(u)-\Theta(-u)$ is the sign function and

$$W_{\rho}(v) = K_{\rho}(v)\frac{d}{d\rho}K_{\rho-1}(v) - K_{\rho-1}(v)\frac{d}{d\rho}K_{\rho}(v); \tag{69}$$

this piece also vanishes in the $r_0\to 0$ limit. Thus, the θ-independent pieces, $j_{\varphi}^{(a)}(r)$ (46) and $B_I^{3\ldots d(a)}(r)$ (47), can be regarded as corresponding to the case of an infinitely thin cosmic string.

As to the appropriate flux,

$$\Phi_I^{(b)} = \frac{1}{\nu}\int_{0}^{2\pi} d\varphi\int_{r_0}^{\infty} dr\, rB_I^{3\ldots d(b)}(r), \tag{70}$$

we obtain the following expression for it:

$$\begin{aligned} \Phi_I^{(b)} = -\frac{2e}{(4\pi)^{(d+1)/2}}\frac{r_0^{3-d}}{\Gamma(\frac{d-1}{2})}\int_{0}^{2\pi} d\varphi\int_{mr_0}^{\infty} dv\, v(v^2-m^2r_0^2)^{(d-3)/2}\sum_{n\in\mathbb{Z}}\mathrm{sgn}(n-F)C_{\nu|n-F|}(\theta, v) \\ \times[\nu|n-F|K_{\nu|n-F|+1}(v)K_{\nu|n-F|-1}(v) - (\nu|n-F|+1)K^2_{\nu|n-F|}(v) - vW_{\nu|n-F|}(v)]. \end{aligned} \tag{71}$$

The total induced vacuum magnetic flux,

$$\Phi_I = \Phi_I^{(a)} + \Phi_I^{(b)}, \tag{72}$$

decreases as the transverse size of the string increases, $r_0\to\infty$. Since, as a consequence of (67), $\Phi_I^{(b)}$ vanishes in the limit of the vanishing transverse size of the string, the behavior of the total flux in this limit is governed by that of $\Phi_I^{(a)}$, and relations (52)–(54) and, consequently, (56)–(60) are relevant for Φ_I. In the case of $\nu^{-1}\cot\theta < \min\{F, 1-F\}$ (in particular, in the cases of Dirichlet and Neumann boundary conditions), the total flux as a function of r_0 does not change sign, being finite for $d=2$ and for $d>2$, except $r_0=0$. In the case of $\nu^{-1}\cot\theta > |n'-F|$ ($n'\in\mathbb{Z}$), the total flux can be rewritten as

$$\Phi_I = -\frac{2e}{(4\pi)^{(d+1)/2}}\frac{r_0^{3-d}}{\Gamma(\frac{d-1}{2})}\int_0^{2\pi} d\varphi \int_{mr_0}^{\infty} dv\, v(v^2-m^2r_0^2)^{(d-3)/2}\sum_{n'\in\mathbb{Z}}\mathrm{sgn}(n'-F)\Theta(\cot\theta-\nu|n'-F|)C_{\nu|n'-F|}(\theta,v)$$
$$\times[\nu|n'-F|K_{\nu|n'-F|+1}(v)K_{\nu|n'-F|-1}(v)-(\nu|n'-F|+1)K^2_{\nu|n'-F|}(v)-vW_{\nu|n'-F|}(v)]+\tilde{\Phi}_I, \tag{73}$$

where terms with the principal value prescription are explicitly exhibited as a finite sum over n'. Coefficient $C_{\nu|n'-F|}(\theta,v)$ changes sign in the vicinity of point $v_{n'}$,

$$C_{\nu|n'-F|}(\theta,v)|_{v\sim v_{n'}} = -(v-v_{n'})^{-1}\{v_{n'}[K_{\nu|n'-F|+1}(v_{n'})K_{\nu|n'-F|-1}(v_{n'})-K^2_{\nu|n'-F|}(v_{n'})]\}^{-1}, \tag{74}$$

where $v_{n'}$ is a root of equation, cf. (37),

$$\left[\left(\cos\theta+\sin\theta\frac{v\partial}{\partial v}\right)K_{\nu|n'-F|}(v)\right]\Big|_{v=v_{n'}}=0. \tag{75}$$

As a consequence of the sign change of $C_{\nu|n'-F|}(\theta,v)$, the total flux in the case of $2\le d\le 3$, as a function of r_0, becomes infinite at points $r_0=m^{-1}v_{n'}$. These peculiarities will be studied in more detail in the next section. Note that the peaks at points $r_0=m^{-1}v_{n'}$ are absent in the case of $d>3$, and thus, in this case, the behavior of terms with a zero in the denominator in (71) is qualitatively the same as that of other ones.

V. INDUCED VACUUM MAGNETIC FLUX: NUMERICAL RESULTS

As is clear from (48) and (71), the induced vacuum magnetic flux is odd under change $F\to 1-F$, where F is defined by (6). In the $d=2$ case, neglecting the transverse size of a cosmic string, one obtains (56) for $\Phi_I^{(a)}$ and zero for $\Phi_I^{(b)}$; thus, the maximal absolute value for the flux is attained at two points that are symmetric with respect to $F=1/2$,

$$F_\pm=\frac{1}{2}\left(1\pm\frac{1}{\sqrt{3}}\right). \tag{76}$$

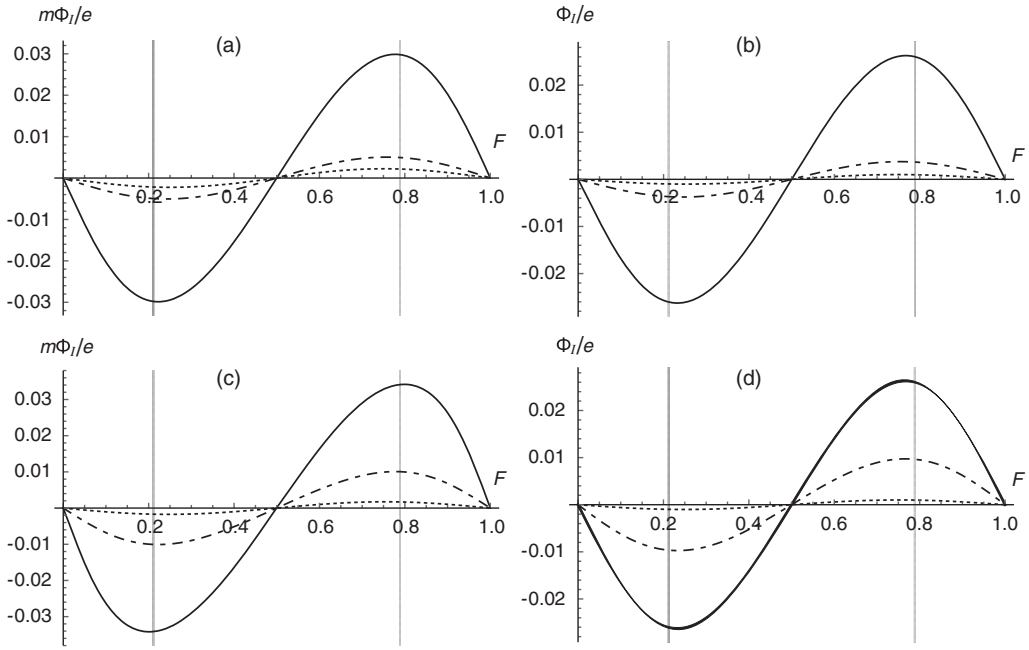

FIG. 2. Dimensionless induced vacuum magnetic flux at $mr_0=10^{-2}$ as a function of F: (a) $\theta=-\pi/4$, $d=2$, (b) $\theta=-\pi/4$, $d=3$, (c) $\theta=-\pi/2$, $d=2$, (d) $\theta=-\pi/2$, $d=3$. Parameter ν takes values 2, 1, and $1/2$ for solid, dash-dotted, and dashed lines, correspondingly; the values for the case of $\nu=1/2$ in (a) and (b) are multiplied by 10; vertical lines correspond to $F=F_\pm$.

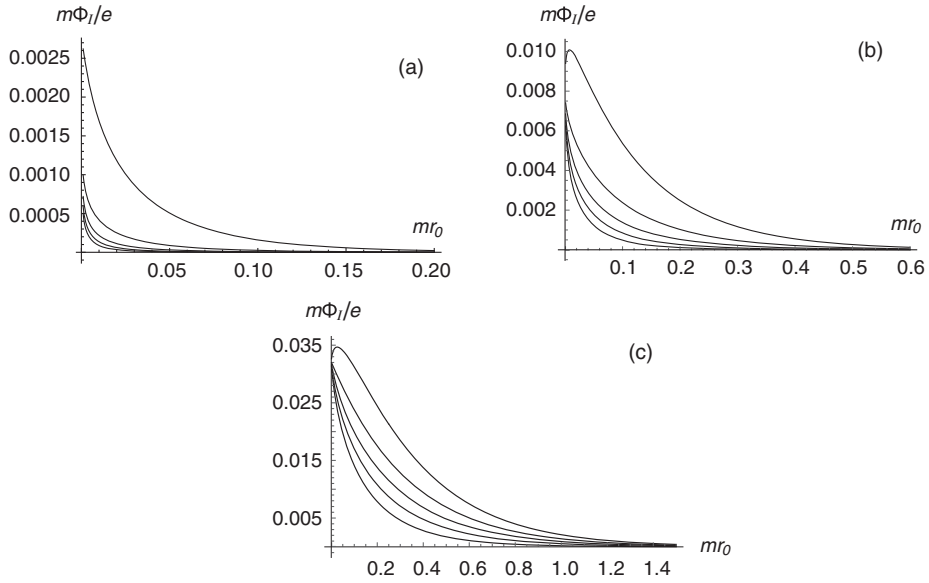

FIG. 3. Dimensionless vacuum flux at $\cot\theta \leq 0$, $F = F_+$, and $d = 2$: (a) $\nu = 1/2$, (b) $\nu = 1$, (c) $\nu = 2$. Parameter θ takes values $-\pi/2$, $-3\pi/8$, $-\pi/4$, $-\pi/8$, 0 from top to bottom.

Such a behavior of the flux as a function of F remains qualitatively the same, when the transverse size of the string is taken into account, although the position of the maximum in the flux absolute value is shifted, depending on r_0, ν, and θ. To illustrate this, we display the F dependence of the dimensionless flux in the $d = 2$ and $d = 3$ cases at $r_0 = 10^{-2}$ m^{-1} and several values of ν and θ in Fig. 2.

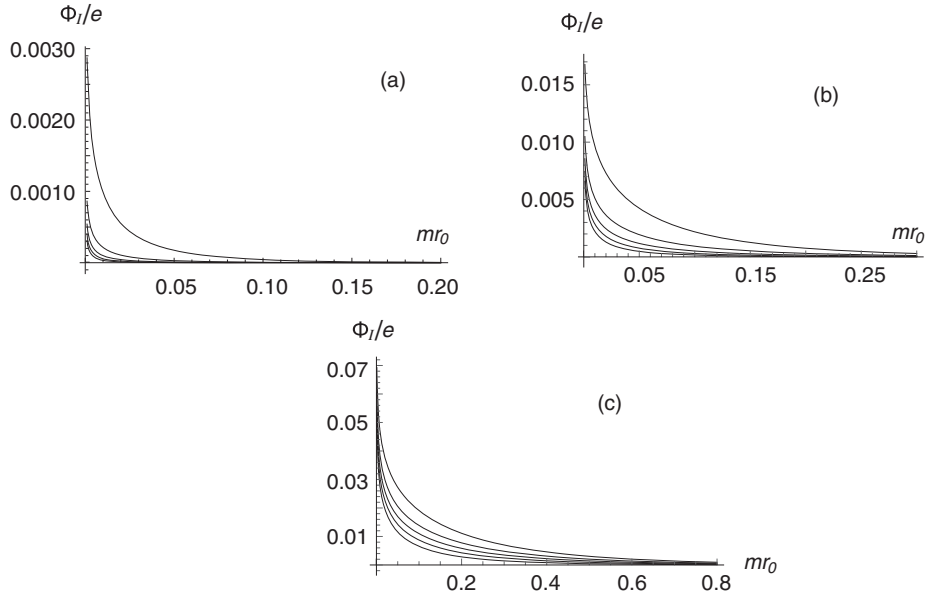

FIG. 4. Dimensionless vacuum flux at $\cot\theta \leq 0$, $F = F_+$, and $d = 3$: (a) $\nu = 1/2$, (b) $\nu = 1$, (c) $\nu = 2$. Parameter θ takes values $-\pi/2$, $-3\pi/8$, $-\pi/4$, $-\pi/8$, 0 from top to bottom.

Fixing $F = F_+$, let us now consider the behavior of induced vacuum magnetic flux as a function of the transverse size of the string. Results at $\cot\theta \leq 0$ in the case of $d = 2$ and several values of ν are presented in Fig. 3. As boundary conditions vary from Dirichlet ($\theta = 0$) to Neumann ($\theta = -\pi/2$), the flux monotonically increases in the region of small mr_0; note a bend near $mr_0 = 0$ in the case of $\theta = -\pi/2$. The region where flux is somewhat essential increases with the increase of ν. A situation is qualitatively the same in the case of $d = 3$, see Fig. 4, with a distinction that flux diverges at $mr_0 \to 0$; see (57). In the realistic case of $\nu \approx 1$, the values of $e^{-1}\Phi_I$ exceeding 10^{-3} are reached at $mr_0 < 5 \times 10^{-2}$ for the Dirichlet condition and at $mr_0 < 25 \times 10^{-2}$ for the Neumann one; note that the case of $\nu = 1$ was considered for the Dirichlet condition in [51] and for the Neumann one in [52].

The situation drastically changes at $0 < \cot\theta < \infty$. The results for flux in the case of $d = 2$ at several values of θ and ν are presented in Figs. 5–7. As positive θ decreases starting from the value of $\pi/2$, more and more terms with a zero in the denominator contribute; see (73). Before integration, as well as after it, these terms change sign, see (74), at the points of zeros that are determined by (75). The integration starts from mr_0, and each time, as increasing mr_0 passes point $v_{n'}$, the principal value prescription becomes decompensated just to the right of these points, giving rise to infinite peaks in the integral. As ν decreases, the number of peaks increases: more values of n' satisfy inequality $\nu^{-1}\cot\theta > |n' - F|$. The situation looks somewhat different in the case of $d = 3$, and the appropriate results for flux are presented in Figs. 8–10. The behavior of integrands containing factors with a zero in the denominator is qualitatively the same with only the distinction that an overall factor of $(v^2 - m^2 r_0^2)^{-1/2}$ is missing in this case. Therefore, a contribution of interval $mr_0 < v < v_{n'}$ might not be sufficient to outweigh a contribution of the opposite sign from $v > v_{n'}$. As a consequence, the flux can be of the same sign from both sides of the infinite peaks at $mr_0 = v_{n'}$.

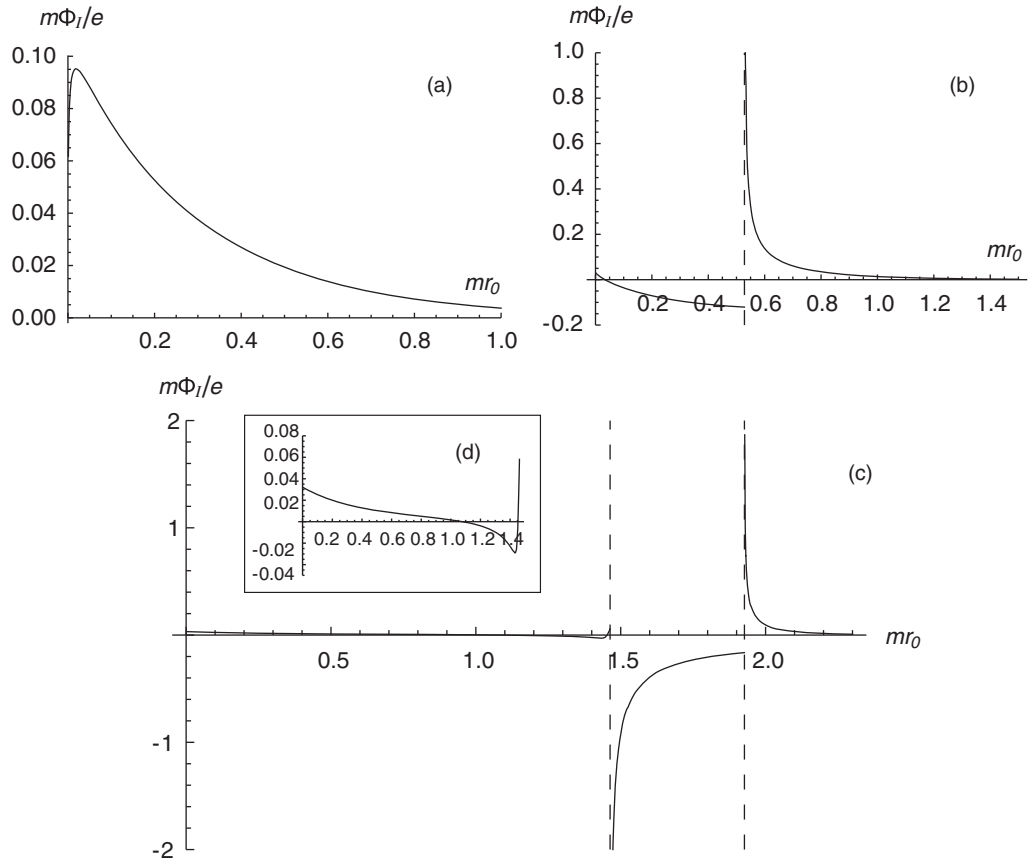

FIG. 5. Dimensionless vacuum flux at $0 < \cot\theta < \infty$, $F = F_+$, $d = 2$, and $\nu = 2$: (a) $\theta = 3\pi/8$, (b) $\theta = \pi/4$, (c) $\theta = \pi/8$, (d) is an enlarged part of (c).

To illustrate this, let us consider the case of $\theta = 3\pi/8$, $F = F_+$, and $\nu = 1$, when the sum over n' in (73) reduces to the only one term, $n' = 1$,

$$G_d(mr_0) = em^{d-3}\int_{mr_0}^{\infty} dv\, g_d(v), \tag{77}$$

where

$$g_d(v) = -\frac{v[v^2(mr_0)^{-2}-1]^{(d-3)/2}}{(4\pi)^{(d-1)/2}\Gamma(\frac{d-1}{2})} C_{F_-}\left(\frac{3\pi}{8}, v\right)[F_- K_{1+F_-}(v)K_{F_+}(v) - (1+F_-)K^2_{F_-}(v) - vW_{F_-}(v)]. \tag{78}$$

We display both (78) and (77) at $d = 2$ and at $d = 3$ in Fig. 11. Although the behavior of $g_2(v)$ and $g_3(v)$ in the vicinity of v_1 is qualitatively the same, the behavior of integrals $G_2(mr_0)$ and $G_3(mr_0)$ differs due to an integrable divergence of $g_2(v)$ at mr_0. Note a symmetry with respect to point $v = v_1$ in the $d = 3$ case; see Figs. 11(b) and 11(d). This signifies that relation $(v - v_1)g_3(v) = 0.0152$ holds with high precision for interval $0.07 < v < 0.09$. Note also that $g_d(v)$ at $d > 3$ is evidently integrable at $v = v_1 = mr_0$.

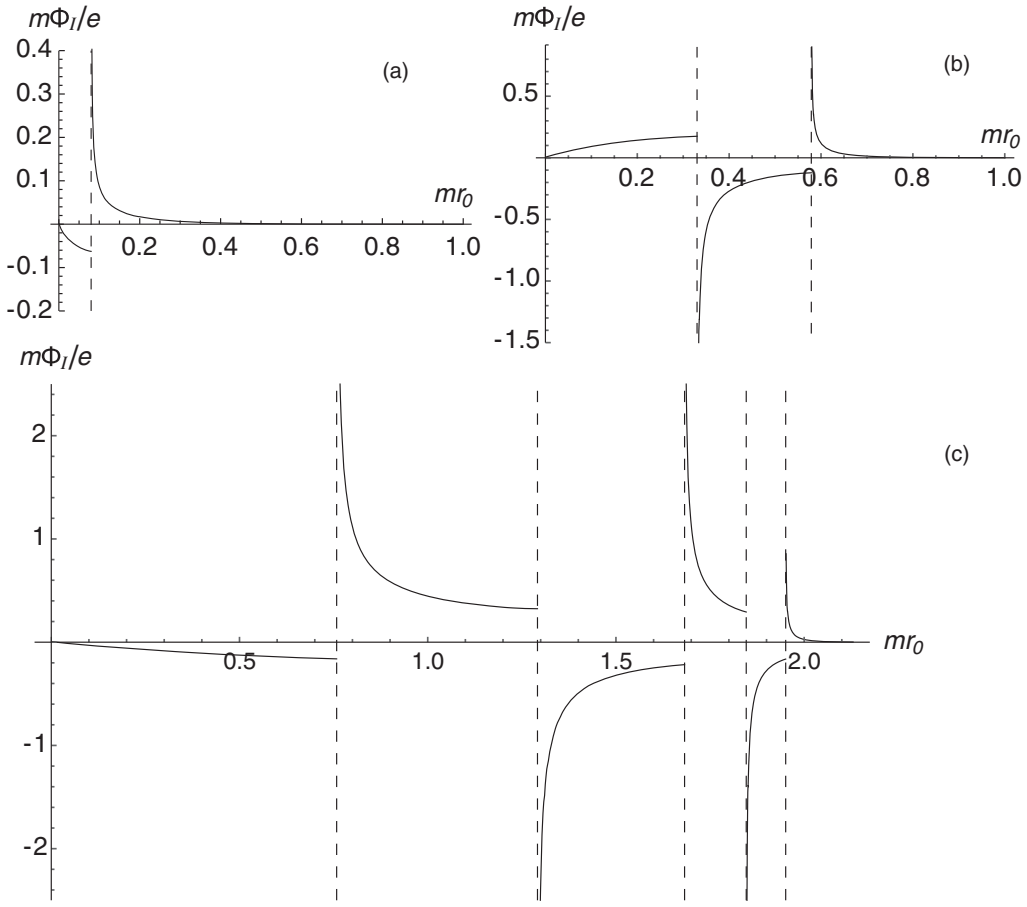

FIG. 6. Dimensionless vacuum flux at $0 < \cot\theta < \infty$, $F = F_+$, $d = 2$, and $\nu = 1$: (a) $\theta = 3\pi/8$, (b) $\theta = \pi/4$, (c) $\theta = \pi/8$.

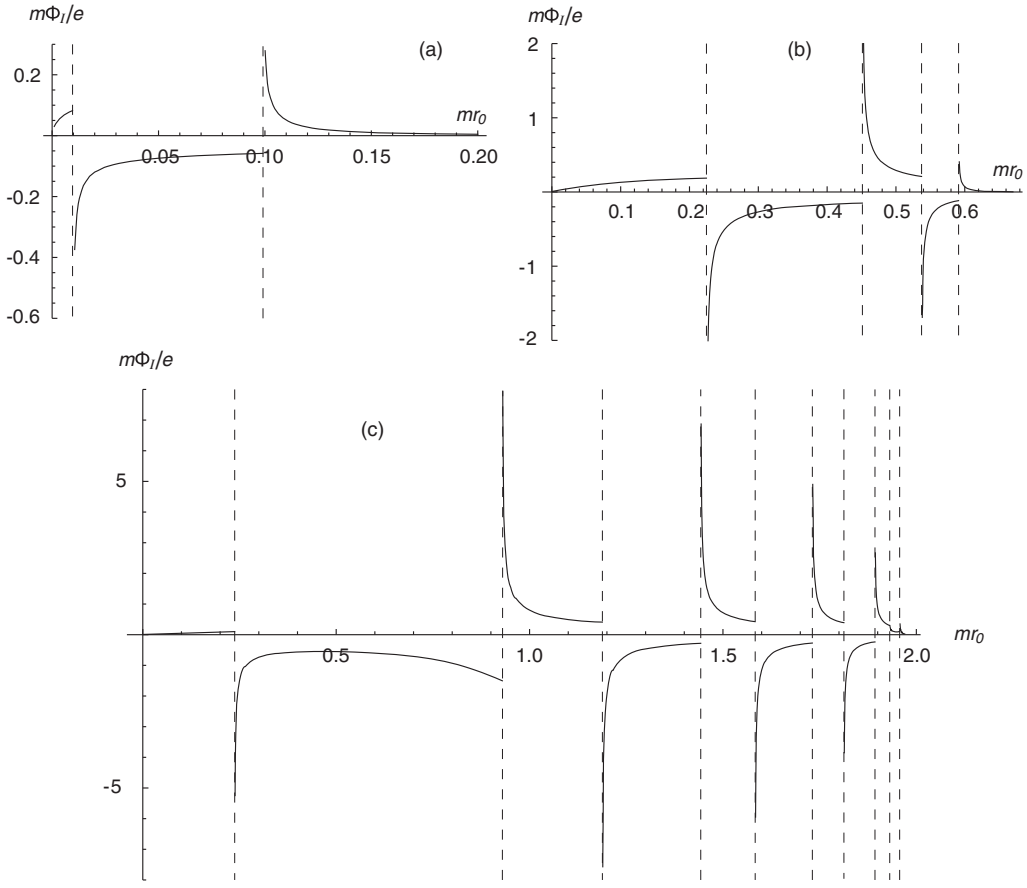

FIG. 7. Dimensionless vacuum flux at $0 < \cot\theta < \infty$, $F = F_+$, $d = 2$, and $\nu = 1/2$: (a) $\theta = 3\pi/8$, (b) $\theta = \pi/4$, (c) $\theta = \pi/8$.

Returning to the total induced vacuum magnetic flux in the $d = 3$ case, see Figs. 4 and 8–10, we note that the infinite peak of the positive sign to the right of point $mr_0 = 0$ exists, although it is hardly visible on some plots due to its narrowness; the numerical calculations start from the minimal value of mr_0 equal to 10^{-3}, and the width of the peak can be less than this value in some cases.

As to the $d \geq 4$ case, the numerical analysis shows that integrals corresponding to separate terms in the sum over n in (71) are infinite due to divergence at $v \to \infty$; see, in particular, (77) at $d \geq 4$. However, due to the sign changing, these divergencies are canceled upon summation of the whole series.

VI. SUMMARY

In the present paper, we have considered a magnetic field that is induced by a cosmic string in the ground state of quantum relativistic bosonic (scalar or pseudoscalar) matter. The transverse size of the string is taken into account, and the string is obviously generalized to a $(d-2)$ tube in d-dimensional space by adding extra $d-3$ dimensions as longitudinal ones. The most general boundary conditions ensuring the impenetrability of matter to the interior of the string is shown to be the Robin condition with one parameter θ varying arbitrarily from point to point of the boundary. Provided that the variation of θ is moderate enough, we find that a current circulating around the string and a magnetic field strength directed along the string are induced in the ground state; they decrease exponentially at large distances from the string. We also find the total induced ground state magnetic flux, which is given by (72), with $\Phi_I^{(a)}$ and $\Phi_I^{(b)}$ given by (48) and (71), respectively. These results provide a field-theoretical realization of the Aharonov-Bohm effect [28,29], since they depend on F (16); i.e., they depend periodically on gauge flux Φ (6) with period equal to $2\pi/\tilde{e}$. The ground state characteristics are smooth continuous functions of F, vanishing at $F = 0, \frac{1}{2}$, and 1, and being odd under change $F \to 1 - F$. They depend on

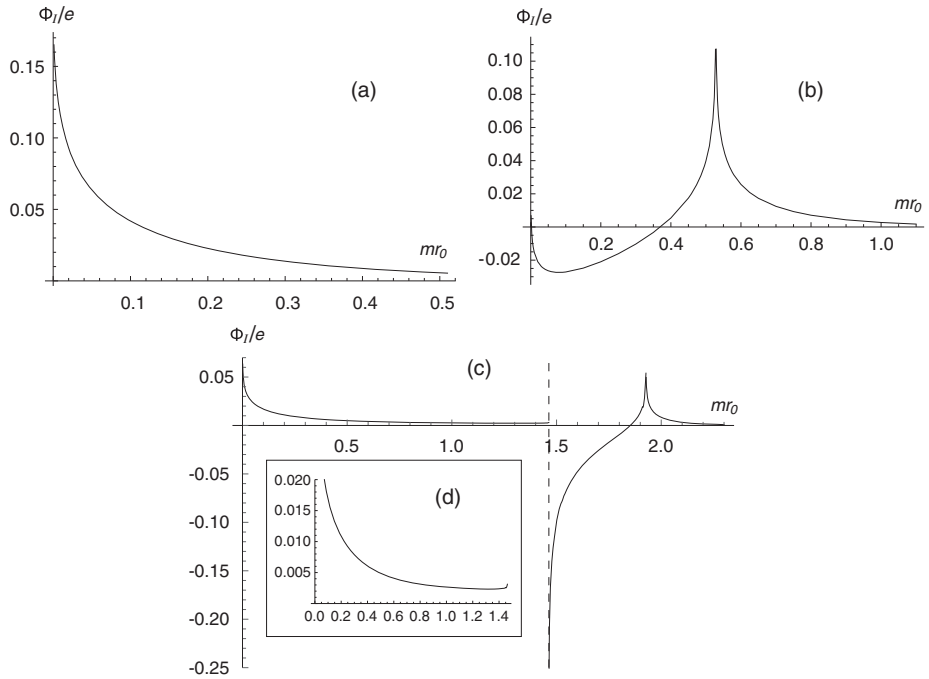

FIG. 8. Dimensionless vacuum flux at $0 < \cot\theta < \infty$, $F = F_+$, $d = 3$, and $\nu = 2$: (a) $\theta = 3\pi/8$, (b) $\theta = \pi/4$, (c) $\theta = \pi/8$, (d) is an enlarged part of (c).

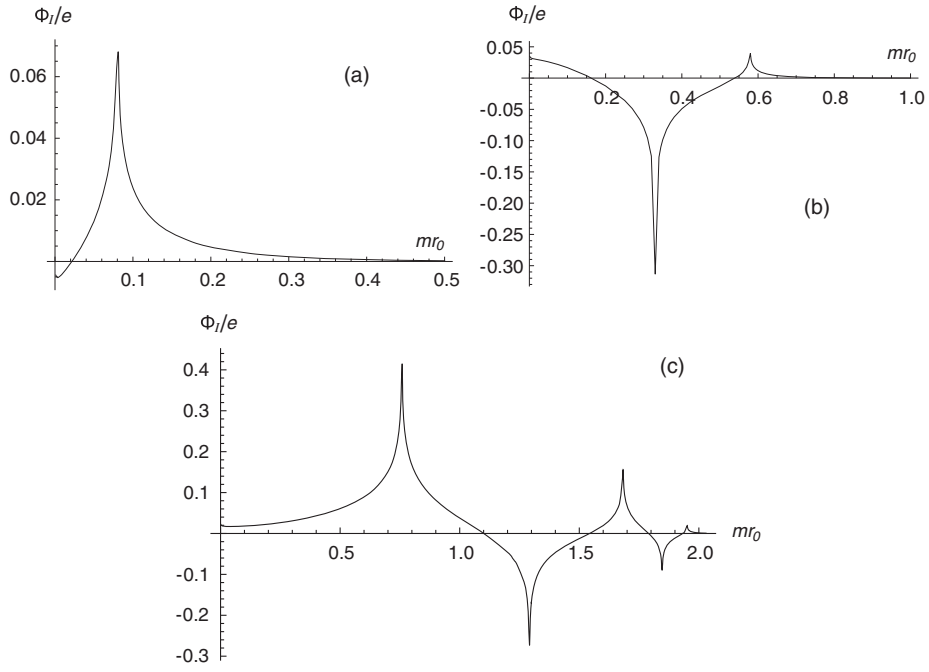

FIG. 9. Dimensionless vacuum flux at $0 < \cot\theta < \infty$, $F = F_+$, $d = 3$, and $\nu = 1$: (a) $\theta = 3\pi/8$, (b) $\theta = \pi/4$, (c) $\theta = \pi/8$.

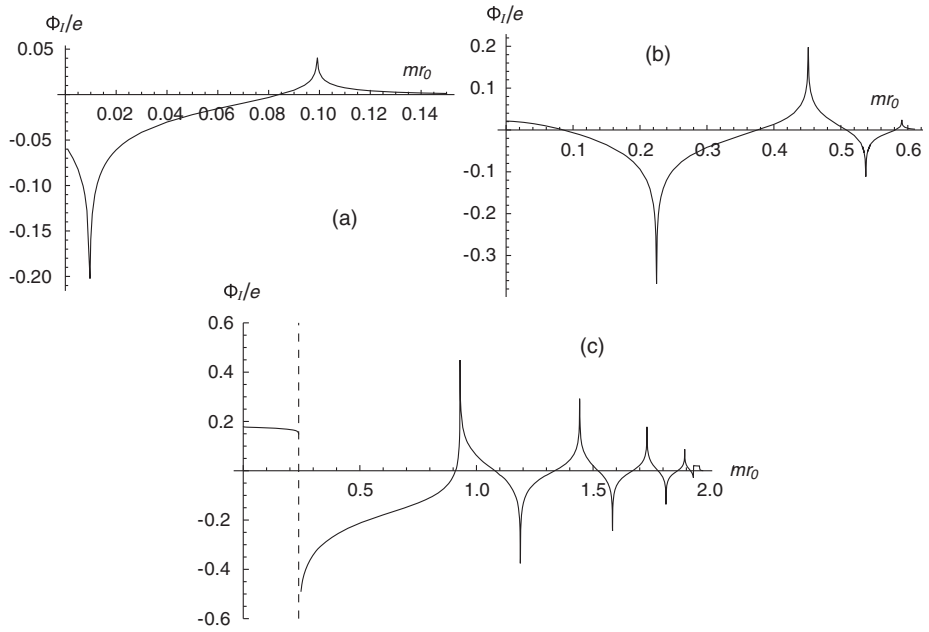

FIG. 10. Dimensionless vacuum flux at $0 < \cot\theta < \infty$, $F = F_+$, $d = 3$, and $\nu = 1/2$: (a) $\theta = 3\pi/8$, (b) $\theta = \pi/4$, (c) $\theta = \pi/8$.

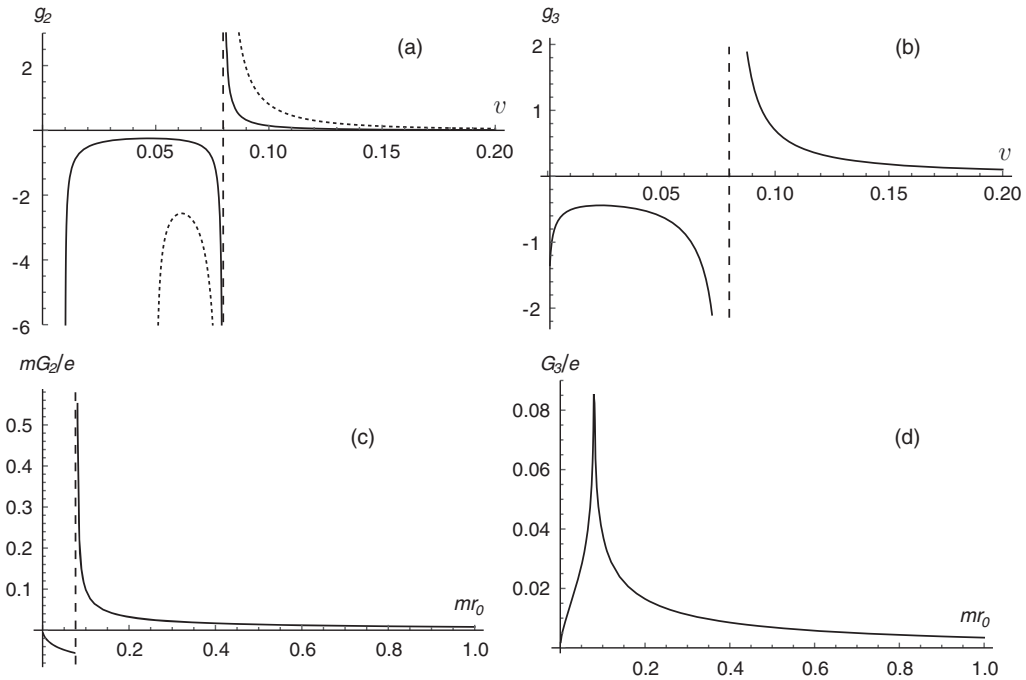

FIG. 11. Eqs. (78) and (77) in the $d = 2$ and $d = 3$ cases: (a) $g_2(v)$, solid and dotted lines correspond to $mr_0 = 10^{-2}$ and $mr_0 = 5 \cdot 10^{-2}$, (b) $g_3(v)$, (c) mG_2/e, (d) G_3/e.

parameter ν (17), which is related to string tension M (7); the range of ν, in general, is $0 < \nu < \infty$; see (9).

It should be noted that, for $0 < \cot\theta < \infty$, in addition to the continuum state solutions to the Fock-Klein-Gordon equation in the cosmic string background, there are solutions corresponding to bound states on a surface that is transverse to the string. We show in the process of calculation of vacuum characteristics that their direct contribution is canceled; see (62) and (63). However, the bound states reveal themselves in the manner of a smoking gun, through zeros in the denominators of coefficients $C_\rho(\theta, v)$ (65), which are to be treated with the principal value prescription when integrated over v. The appearance of these zeros results in a thoroughgoing distinction of the case of $0 < \cot\theta < \infty$ from that of $\cot\theta \leq 0$.

The numerical analysis of the expression for induced vacuum magnetic flux, obtained in Sec. IV, is carried out in Sec. V. Restricting ourselves to constant values of θ, we find that the flux decreases significantly at large values of mr_0. In the case of $\cot\theta \leq 0$, the flux is of the same sign, as mr_0 varies from 0 to ∞, see Figs. 3 and 4; it is finite at $d = 2$ and diverges logarithmically at $d = 3$ in the limit of $mr_0 \to 0$. In contrast to this, the flux in the case of $0 < \cot\theta < \infty$ is a sign changing function of mr_0; see Figs. 5–10. Moreover, it diverges at points $mr_0 = v_{n'}$, where $v_{n'}$ are the above-mentioned zeros in the denominators; see (74) and (75). The number of these points is determined by inequality $\nu^{-1}\cot\theta > |n' - F|$. The position of the rightmost infinite peak of the flux is shifted to region $mr_0 > 1$, as $\nu^{-1}\cot\theta$ increases; for instance, this happens at $\frac{\pi}{4} > \theta > \frac{\pi}{8}$ in the case of $F = F_+$ [where F_+ is given by (76)] and $\frac{1}{2} < \nu < 2$.

Note that, as is clear from the numerical results, the minimal absolute values for the induced vacuum magnetic flux in the cosmic string background are attained with the use of the Dirichlet boundary condition. Hereof, appealing in somewhat sense to an analog of the Occam's razor principle, we can eliminate the variety of boundary conditions by giving preference to that of Dirichlet, as the most plausible one in view of its minimal effect on the vacuum. However, more stringent arguments are given below that allow us to restrict the set of boundary conditions with more definiteness.

The transverse size of a cosmic string is of the order of correlation length, $r_0 \sim m_H^{-1}$, where m_H is the energy scale of spontaneous symmetry breaking, i.e., the mass of the appropriate Higgs boson. It looks hardly plausible that a topological defect (cosmic string) influences surrounding quantum matter with the matter particle mass m exceeding the Higgs particle mass m_H. For instance, a cosmic string that is formed at the grand unification scale can polarize the vacuum of quantum matter in the electroweak model, whereas a would-be cosmic string corresponding to the electroweak symmetry breaking has no impact on the vacuum of quantum matter in the grand unified model. The more implausible is an enormous influence, i.e., infinite peaks in the induced vacuum magnetic flux at $m > m_H$. This reasoning allows us to exclude the range of boundary parameters corresponding to $0 < \cot\theta < \infty$ as that leading to unphysical consequences.

Thus, we are left with the range of boundary parameters corresponding to $\cot\theta \leq 0$, when the induced vacuum magnetic flux attains visible values at $m \ll m_H$; see Figs. 3 and 4. The effect is minimal for the case of the Dirichlet condition $\theta = 0$, slightly and monotonically increasing, as the boundary parameter gradually evolves in value to the Neumann condition $\theta = -\pi/2$. This result has to be compared with that for the case of magnetic field that is induced by a cosmic string in the vacuum of quantum relativistic fermionic matter; see [39,40]. In the latter case, the most general boundary condition involves one at $d = 2$ [39] and four at $d = 3$ [40] parameters varying arbitrarily from point to point of the boundary, and the requirement of finiteness for the induced vacuum magnetic flux removes completely the ambiguity in the choice of boundary conditions. We conclude that the impact of a topological defect (cosmic string) on quantum matter differs significantly for bosons and fermions. If bosons and fermions are assigned to a representation of a supersymmetry group, then this supersymmetry is violated by the vacuum effects in the cosmic string background.

ACKNOWLEDGMENTS

The work of Y. A. S. was supported by the National Academy of Sciences of Ukraine (Project No. 0122-U000886) and by the Special Research Program URF 2022 of the Erwin Schrödinger International Institute for Mathematics and Physics. He thanks E. Pallante for fruitful discussion and critical remarks.

APPENDIX: CASE OF A THIN COSMIC STRING

Only the pieces with superscript (a) are relevant for this case. Starting from $j_\varphi^{(a)}(r)$ (45), we recall that summation

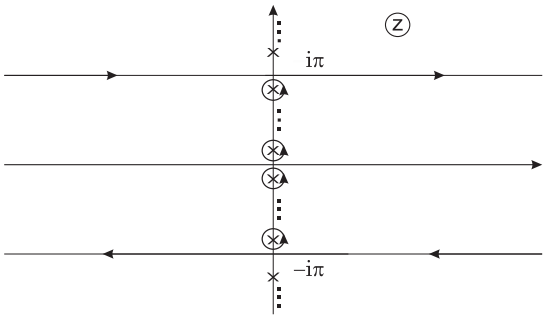

FIG. 12. Singularities of the integrand in (A1) on the complex z plane out of the origin are simple poles on the imaginary axis; they are denoted by crosses. Contour C consists of two horizontal lines and circles around the simple poles with $0 < |\mathrm{Im}\, z| < \pi$.

over n is performed by using the Schläfli contour integral representation for $I_\rho(u)$; see [49] for details. Generically, we obtain

$$j_\varphi^{(a)}(r)=\frac{1}{(4\pi)^{(d+1)/2}}\frac{m^{(d+1)/2}}{r^{(d-3)/2}}\frac{1}{2\pi\mathrm{i}}\int_C\frac{dz}{\left[\sqrt{-\sinh^2(z/2)}\right]^{(d+1)/2}}K_{(d+1)/2}\left[2mr\sqrt{-\sinh^2(z/2)}\right]\frac{\sinh(z)\sinh[\nu(F-\frac{1}{2})z]}{\sinh(\nu z/2)},\quad\text{(A1)}$$

where contour C results from merging two different Schläfli contours for the modified Bessel functions of orders $\nu(n-F)>0$ and $-\nu(n-F)>0$; see Fig. 12. The contribution of horizontal lines yields the integral over u in (46), while the contribution of circles yields the sum over l in (46). Further, we get

$$B_I^{3\ldots d(a)}(r)=\frac{e\nu}{2(4\pi)^{(d+1)/2}}\left(\frac{m}{r}\right)^{(d-1)/2}\frac{1}{2\pi\mathrm{i}}\int_C\frac{dz}{\left[\sqrt{-\sinh^2(z/2)}\right]^{(d+3)/2}}K_{(d-1)/2}\left[2mr\sqrt{-\sinh^2(z/2)}\right]\frac{\sinh(z)\sinh[\nu(F-\frac{1}{2})z]}{\sinh(\nu z/2)}\quad\text{(A2)}$$

and

$$\Phi_I^{(a)}=\frac{e}{8(4\pi)^{(d-1)/2}}\left(\frac{m}{r_0}\right)^{(d-3)/2}\frac{1}{2\pi\mathrm{i}}\int_C\frac{dz}{\left[\sqrt{-\sinh^2(z/2)}\right]^{(d+5)/2}}K_{(d-3)/2}\left[2mr_0\sqrt{-\sinh^2(z/2)}\right]\frac{\sinh(z)\sinh[\nu(F-\frac{1}{2})z]}{\sinh(\nu z/2)}.\quad\text{(A3)}$$

Taking the asymptotics of $\Phi_I^{(a)}$ (A3) at $r_0\to 0$, we obtain (52)–(54), where $I_d(F,\nu)$ is presented as

$$I_d(F,\nu)=\frac{1}{16\pi\mathrm{i}}\int_C\frac{dz}{\left[\sqrt{-\sinh^2(z/2)}\right]^{d+1}}\frac{\sinh(z)\sinh[\nu(F-\frac{1}{2})z]}{\sinh(\nu z/2)}.\quad\text{(A4)}$$

In the case of odd values of d, a singularity of the integrand at $z=0$ is an isolated pole. Contour C in this case can be continuously deformed to encircle the origin, and we get

$$I_{2n+1}(F,\nu)=\frac{(-1)^n}{8\pi\mathrm{i}}\oint dz\frac{\cosh(z/2)\sinh[\nu(F-\frac{1}{2})z]}{[\sinh(z/2)]^{2n+1}\sinh(\nu z/2)}.\quad\text{(A5)}$$

Taking a residue of the simple pole at the origin, we obtain (56)–(60).

[1] A. A. Abrikosov, On the magnetic properties of superconductors of the second group, Sov. Phys. JETP **5**, 1174 (1957).
[2] H. B. Nielsen and P. Olesen, Vortex-line models for dual strings, Nucl. Phys. **B61**, 45 (1973).
[3] T. W. B. Kibble, Some implications of a cosmological phase transition, Phys. Rep. **67**, 183 (1980).
[4] A. Vilenkin, Cosmic strings, Phys. Rev. D **24**, 2082 (1981).
[5] A. Vilenkin and E. P. S. Shellard, *Cosmic Strings and Other Topological Defects* (Cambridge University Press, Cambridge, England, 1994).
[6] M. B. Hindmarsh and T. W. B. Kibble, Cosmic strings, Rep. Prog. Phys. **58**, 477 (1995).
[7] T. Damour and A. Vilenkin, Gravitational radiation from cosmic (super)strings: Bursts, stochastic background, and observational windows, Phys. Rev. D **71**, 063510 (2005).
[8] V. Berezinsky, B. Hnatyk, and A. Vilenkin, Gamma ray bursts from superconducting cosmic strings, Phys. Rev. D **64**, 043004 (2001).
[9] P. Bhattaharjee and G. Sigl, Origin and propagation of extremely high-energy cosmic rays, Phys. Rep. **327**, 109 (2000).
[10] R. Jeannerot, J. Rocher, and M. Sakellariadou, How generic is cosmic string formation in supersymmetric grand unified theories, Phys. Rev. D **68**, 103514 (2003).
[11] G. Dvali and A. Vilenkin, Formation and evolution of cosmic D strings, J. Cosmol. Astropart. Phys. 03 (2004) 010.
[12] J. Polchinski, Cosmic superstrings revisited, Int. J. Mod. Phys. A **20**, 3413 (2005).
[13] M. Sakellariadou, Cosmic strings and cosmic superstrings, Nucl. Phys. B, Proc. Suppl. **192–193**, 68 (2009).

[14] E. J. Copeland and T. W. B. Kibble, Cosmic strings and superstrings, Proc. R. Soc. A **466**, 623 (2010).
[15] K. S. Novoselov, D. Jiang, F. Schedin, T. J. Booth, V. V. Khotkevich, S. V. Morozov, and A. K. Geim, Two-dimensional atomic crystals, Proc. Natl. Acad. Sci. U.S.A. **102**, 10451 (2005).
[16] A. K. Geim and K. S. Novoselov, The rise of graphene, Nat. Mater. **6**, 183 (2007).
[17] M. I. Katsnelson, *Graphene: Carbon in Two Dimensions* (Cambridge University Press, Cambridge, England, 2012).
[18] A. Krishnan, E. Dujardin, M. M. J. Treacy, J. Hugdahl, S. Lynum, and T. W. Ebbesen, Graphitic cones and the nucleation of curved carbon surfaces, Nature (London) **388**, 451 (1997).
[19] Yu. A. Sitenko and N. D. Vlasii, Electronic properties of graphene with a topological defect, Nucl. Phys. **B787**, 241 (2007).
[20] S. N. Naess, A. Elgsaeetter, G. Helgesen, and K. D. Knudsen, Carbon nanocones: Wall structure and morphology, Sci. Technol. Adv. Mater. **10**, 065002 (2009).
[21] Yu. A. Sitenko and V. M. Gorkavenko, Properties of the ground state of electronic excitations in carbon-like nanocones, Fiz. Nizk. Temp. **44**, 1618 (2018) [Low Temp. Phys. **44**, 1261 (2018)].
[22] R. A. Battye, B. Garbrecht, A. Moss, and H. Stoica, Constraints on brane inflation and cosmic strings, J. Cosmol. Astropart. Phys. 01 (2008) 020.
[23] S. Cahangirov, M. Topsakal, E. Akturk, H. Sahin, and S. Ciraci, Two- and One-Dimensional Honeycomb Structures of Silicon and Germanium, Phys. Rev. Lett. **102**, 236804 (2009).
[24] H. Liu, A. T. Neal, Z. Zhu, Z. Luo, X. Xu, D. Tomanek, and P. D. Ye, Phosphorene: An unexplored 2D semiconductor with a high hole mobility, ACS Nano **8**, 4033 (2014).
[25] C. C. Tsuei and J. R. Kirtley, Pairing symmetry in cuprate superconductors, Rev. Mod. Phys. **72**, 969 (2000).
[26] X. L. Qi and S. C. Zhang, Topological insulators and superconductors, Rev. Mod. Phys. **83**, 1057 (2011).
[27] G. E. Volovik, Gravity of monopole and string and the gravitational constant in ^{3}He-A, Pis'ma Zh. Eksp. Teor. Fiz. **67**, 666 (1998) [JETP Lett. **67**, 698 (1998)].
[28] W. Ehrenberg and R. E. Siday, The refractive index in electron optics and the principles of dynamics, Proc. Phys. Soc. London Sect. B **62**, 8 (1949).
[29] Y. Aharonov and D. Bohm, Significance of electromagnetic potentials in the quantum theory, Phys. Rev. **115**, 485 (1959).
[30] E. M. Serebrianyi, Vacuum polarization by magnetic flux: The Aharonov-Bohm effect, Teor. Mat. Fiz. **64**, 299 (1985) [Theor. Math. Phys. **64**, 846 (1985)].
[31] M. G. Alford, J. March-Russel, and F. Wilczek, Enhanced baryon number violation due to cosmic strings, Nucl. Phys. **B328**, 140 (1989).
[32] P. Gornicki, Aharonov-Bohm effect and vacuum polarization, Ann. Phys. (N.Y.) **202**, 271 (1990).
[33] E. G. Flekkoy and J. M. Leinaas, Vacuum currents around a magnetic flux string, Int. J. Mod. Phys. A **06**, 5327 (1991).
[34] R. R. Parwani and A. S. Goldhaber, Decoupling in $(2+1)$-dimensional QED?, Nucl. Phys. **B359**, 483 (1991).
[35] Yu. A. Sitenko, Self-adjointness of the Dirac Hamiltonian and fermion number fractionization in the background of a singular magnetic vortex, Phys. Lett. B **387**, 334 (1996).
[36] Yu. A. Sitenko, Self-adjointness of the Dirac Hamiltonian and vacuum quantum numbers induced by a singular external field, Yad. Fiz. **60**, 2285 (1997) [Phys. At. Nucl. **60**, 2102 (1997)].
[37] Yu. A. Sitenko and A. Yu. Babansky, The Casimir-Aharonov-Bohm effect?, Mod. Phys. Lett. A **13**, 379 (1998).
[38] Yu. A. Sitenko and A. Yu. Babansky, Effects of boson-vacuum polarization by a singular magnetic vortex, Yad. Fiz. **61**, 1706 (1998) [Phys. At. Nucl. **61**, 1594 (1998)].
[39] Yu. A. Sitenko and V. M. Gorkavenko, Induced vacuum magnetic flux in quantum spinor matter in the background of a topological defect in two-dimensional space, Phys. Rev. D **100**, 085011 (2019).
[40] Yu. A. Sitenko, Induced vacuum magnetic field in the cosmic string background, Phys. Rev. D **104**, 045013 (2021).
[41] M. Reed and B. Simon, The Spectral Theorem, in *Methods of Modern Mathematical Physics I. Functional Analysis* (Academic Press, New York, 1980), Chap. VII, pp. 221–248.
[42] M. Reed and B. Simon, *Methods of Modern Mathematical Physics II. Fourier Analysis, Self-Adjointness* (Academic Press, New York, 1975).
[43] Yu. A. Sitenko and S. A. Yushchenko, The Casimir effect with quantized charged scalar matter in background magnetic field, Int. J. Mod. Phys. A **29**, 1450052 (2014).
[44] Yu. A. Sitenko, Influence of quantized massive matter fields on the Casimir effect, Mod. Phys. Lett. A **30**, 1550099 (2015).
[45] R. Adami and A. Teta, On the Aharonov-Bohm effect, Lett. Math. Phys. **43**, 43 (1998).
[46] L. Dabrowski and P. Stovicek, Aharonov-Bohm effect with δ-type interaction, J. Math. Phys. (N.Y.) **39**, 47 (1998).
[47] Yu. A. Sitenko, A. V. Solovyov, and N. D. Vlasii, Induced quantum numbers of a magnetic monopole at finite temperature, Phys. Rev. D **74**, 085009 (2006).
[48] A. P. Prudnikov, Yu. A. Brychkov, and O. I. Marychev, *Integrals and Series: Special Functions* (Gordon and Breach, New York, 1986).
[49] Yu. A. Sitenko and N. D. Vlasii, Induced vacuum current and magnetic field in the background of a cosmic string, Classical Quantum Gravity **26**, 195009 (2009).
[50] E. R. Bezerra de Mello, V. Bezerra, A. A. Saharian, and H. H. Harutyunyan, Vacuum currents induced by a magnetic flux around a cosmic string with finite core, Phys. Rev. D **91**, 064034 (2015).
[51] V. M. Gorkavenko, I. V. Ivanchenko, and Yu. A. Sitenko, Induced vacuum current and magnetic field in the background of a vortex, Int. J. Mod. Phys. A **31**, 1650017 (2016).
[52] V. M. Gorkavenko, T. V. Gorkavenko, Yu. A. Sitenko, and M. S. Tsarenkova, Induced vacuum current and magnetic flux in quantum scalar matter in the background of a vortex defect with the Neumann boundary condition, Ukr. J. Phys. **67**, 3 (2022).

3.4. Індукування у вакуумі спінорного поля. Загальний вигляд граничної умови

PHYSICAL REVIEW D **100,** 085011 (2019)

Induced vacuum magnetic flux in quantum spinor matter in the background of a topological defect in two-dimensional space

Yurii A. Sitenko[1] and Volodymyr M. Gorkavenko[2]

[1]*Bogolyubov Institute for Theoretical Physics, National Academy of Sciences of Ukraine, 14-b Metrologichna strasse, Kyiv 03143, Ukraine*

[2]*Department of Physics, Taras Shevchenko National University of Kyiv, 64 Volodymyrs'ka strasse, Kyiv 01601, Ukraine*

(Received 10 August 2019; published 21 October 2019)

A topological defect in the form of the Abrikosov-Nielsen-Olesen vortex is considered as a gauge-flux-carrying tube that is impenetrable for quantum matter. The relativistic spinor matter field is quantized in the vortex background in $(2+1)$-dimensional conical spacetime, which is a section orthogonal to the vortex axis; the most general set of boundary conditions ensuring the impenetrability of the vortex core is employed. We find the induced vacuum current circulating around the vortex and the induced vacuum magnetic field strength pointing along the vortex axis. The requirement of finiteness and physical plausibility for the total induced vacuum magnetic flux allows us to restrict the variety of admissible boundary conditions. The dependence of the results on the transverse size of the vortex, as well as on the vortex flux and the parameter of conicity, is elucidated. We discuss a significant distinction between the cases of massive and massless quantum spinor matter.

DOI: 10.1103/PhysRevD.100.085011

I. INTRODUCTION

Spontaneous breakdown of continuous symmetries can give rise to topological defects with rather interesting properties. A topological defect in three-dimensional space, which is characterized by the nontrivial first homotopy group, is known as the Abrikosov-Nielsen-Olesen (ANO) vortex [1,2]. The vortex is described classically in terms of a spin-zero (Higgs) field that condenses and a spin-one field corresponding to the spontaneously broken gauge group; the former field is coupled to the latter one in the minimal way with constant $\tilde{e}_{\mathrm{cond}}$. Single valuedness of the condensate field and finiteness of the vortex energy implement that the vortex flux is related to $\tilde{e}_{\mathrm{cond}}$,

$$\Phi = \oint d\mathbf{x}\mathbf{V}(\mathbf{x}) = 2\pi/\tilde{e}_{\mathrm{cond}}, \tag{1.1}$$

where $\mathbf{V}(\mathbf{x})$ is the vector potential of the spin-one gauge field, and the integral is over a path enclosing the vortex tube once (natural units $\hbar = c = 1$ are used). As some amount of energy (mass) is stored in the core of a topological defect, this core is a source of gravity. Such a source in the case of the linear ANO vortex makes the spatial region outside the vortex core to be conical, i.e., with the deficit angle equal to $8\pi G M$: the squared length element in the outer region is

$$ds^2 = dr^2 + \nu^{-2} r^2 d\varphi^2 + dz^2, \tag{1.2}$$

where

$$\nu = (1 - 4GM)^{-1}, \tag{1.3}$$

G is the gravitational constant, and M is the linear density of mass stored in the core. The transverse size of the vortex core is determined by the correlation length, and the quantity M is of the order of the inverse correlation length squared. Since constant G is of order of the Planck length squared, the effects of conicity, which are characterized by the value of the deficit angle, are negligible for vortices in ordinary superconductors. However, topological defects of the type of ANO vortices may arise in a field that is seemingly rather different from condensed matter physics—in cosmology and high-energy physics. This was realized by Kibble [3,4] and Vilenkin [5,6] (see also [7]), and, from the beginning of the 1980s, such topological defects are known under the name of cosmic strings. Cosmic strings with the thickness of the order of the Planck length are definitely ruled out by astrophysical observations, but there remains a room for cosmic strings with the thickness that is more than 3 orders

larger than the Planck length (see, e.g., [8]), although the direct evidence for their existence is lacking.

A recent development in material science also provides an unexpected link between condensed matter and high-energy physics, which is caused to a large extent by the experimental discovery of graphene—a two-dimensional crystalline allotrope formed by a monolayer of carbon atoms [9]. Low-energy electronic excitations in graphene are characterized by dispersion law which is the same as that for Dirac fermions in relativistic field theory, with the only distinction that the velocity of light is changed to the Fermi velocity; see [10,11]. It is well established by now that a sheet of graphene is always corrugated and covered by ripples that can be either intrinsic or induced by roughness of a substrate. A single topological defect (disclination) warps a sheet of graphene, rolling it into a nanocone, which is similar to the transverse section of a spatial region out of a cosmic string; carbon nanocones with deficit angles equal to $N_d\pi/3$ ($N_d = 1, 2, 3, 4, 5$, i.e., $\nu = \frac{6}{5}, \frac{3}{2}, 2, 3, 6$) were observed experimentally (see [12,13] and references therein). Moreover, theory also predicts saddlelike nanocones with the deficit angle taking negative values unbounded from below, $N_d = -1, -2, -3, \ldots, -\infty$, i.e., $\nu = \frac{6}{7}, \frac{3}{4}, \frac{2}{3}, \ldots, 0$, which can be regarded as corresponding to cosmic strings with negative mass density. Note that nanoconical structures may arise as well in a diverse set of condensed matter systems known as the two-dimensional Dirac materials, ranging from honeycomb crystalline allotropes (silicene and germanene [14], phosphorene [15]) to high-temperature cuprate superconductors [16] and topological insulators [17].

While considering the effect of the ANO vortex on the vacuum of quantum matter, the following two circumstances should be kept in mind. First, the phase with broken symmetry exists outside the vortex core and the vacuum is to be defined there. Hence, the quantum matter field does not penetrate inside the core, obeying a boundary condition at its side edge. Second, the impact of the ANO vortex on quantum matter is through a vector potential of the vortex-forming spin-one field, and the quantum matter field is assumed to couple to this vector potential in the minimal way with coupling constant $\tilde{e}$. Hence, the ANO vortex flux has no effect on the surrounding matter in the framework of classical theory, and such an effect, if it exists, is of a purely quantum nature. This phenomenon should be understood as a quantum-field-theoretical manifestation of the famous Aharonov-Bohm effect [18] and is characterized by the periodic dependence on the value of the vortex flux, Φ (1.1), with the period equal to London flux quantum $2\pi/\tilde{e}$.

A crucial task in the study of the effect of the ANO vortex on the vacuum of quantum matter is to elucidate the dependence on a boundary condition at the edge of the vortex core. It seems reasonable to start from the most general set of mathematically admissible boundary conditions and then, after obtaining the outcoming effect, to restrict this set by physically motivated arguments. Another task is to elucidate the dependence on the transverse size of the vortex core. These two tasks will be thoroughly scrutinized and solved in the course of the present study by considering a somewhat simplified case of two-dimensional space[1] being the transverse section of a three-dimensional spatial region out of the ANO vortex.

It should be noted that the current, the condensate, and the energy-momentum tensor that are induced in the vacuum of quantum relativistic spinor matter were considered in the above-described context in [20–22]. However, a particular boundary condition was employed, and the issue of a dependence of the results on the choice of admissible boundary conditions remained undisclosed.

The current and the magnetic field strength, as well as the energy density and the Casimir force, which are induced in the vacuum of quantum relativistic scalar matter at $\nu = 1$ in a space of arbitrary dimension were considered in the above-described context in [23–26]. In these studies the Dirichlet boundary condition was employed; a physical motivation herein is in the assumption of a perfect reflection of quantum matter from the edge of the vortex core.

In the case of quantum relativistic spinor matter, neither the Dirichlet nor the Neumann boundary condition is admissible. A physically motivated demand is the absence of the matter flux across the boundary. In $(2+1)$-dimensional spacetime with a connected boundary, this demand yields a one-parameter family of boundary conditions; see Sec. IV below. Employing such boundary conditions, we shall find the induced vacuum current and the induced vacuum magnetic field strength; further physical arguments will be shown to remove an ambiguity in the choice of boundary conditions.

In the next section we define the current and the magnetic field that are induced in the vacuum of quantum relativistic spinor matter in the background of the ANO vortex of nonzero transverse size. In Sec. III we present the complete set of solutions to the Dirac equation that is relevant to the problem considered. In Sec. IV we choose boundary conditions ensuring the absence of the matter flux across the edge of the vortex core. The induced vacuum current is obtained in Sec. V. In Sec. VI we consider the induced vacuum magnetic field and its total flux with the use of both analytical and numerical methods. Finally, the results are summarized and discussed in Sec. VII. Some details in the derivation of the expression for the induced vacuum current are given in the Appendixes A and B. The case of the infinitely thin vortex

[1]Quantum-field-theoretical models in $(2+1)$-dimensional spacetime play a role of toy models in particle physics and may be relevant to real systems in condensed matter physics. They exhibit a number of interesting features, such as fermion number fractionization, parity violation, and flavor symmetry breaking; for a review see [19].

is reviewed in Appendix C. The results for massless quantum spinor matter are presented in Appendix D.

II. PRELIMINARIES AND DEFINITION OF PHYSICAL CHARACTERISTICS OF THE VACUUM

The operator of the second-quantized spinor field is presented as

$$\Psi(\mathbf{x},t)=\sum\!\!\!\!\!\!\int_{E>0} e^{-iEt}\psi_E(\mathbf{x})a_E+\sum\!\!\!\!\!\!\int_{E<0} e^{-iEt}\psi_E(\mathbf{x})b_E^\dagger, \tag{2.1}$$

where $a_E^\dagger$ and a_E ($b_E^\dagger$ and b_E) are the spinor particle (antiparticle) creation and destruction operators obeying the anticommutation relations, $\psi_E(\mathbf{x})$ is the solution to the stationary Dirac equation,

$$H\psi_E(\mathbf{x})=E\psi_E(\mathbf{x}), \tag{2.2}$$

and symbol $\sum\!\!\!\!\!\!\int$ denotes summation over the discrete part and integration (with a certain measure) over the continuous part of the energy spectrum; ground state $|\mathrm{vac}\rangle$ is conventionally defined by relation

$$a_E|\mathrm{vac}\rangle=b_E|\mathrm{vac}\rangle=0. \tag{2.3}$$

In the case of the ANO vortex background, the Dirac Hamiltonian takes the form

$$H=-i\boldsymbol{\alpha}\cdot\left(\boldsymbol{\partial}-i\tilde{e}\mathbf{V}+\frac{i}{2}\boldsymbol{\omega}\right)+\beta m, \tag{2.4}$$

where ω is the spin connection corresponding to conical space (1.2). The current that is induced in the vacuum is given by expression

$$\begin{aligned}\mathbf{j}(\mathbf{x})&=\langle\mathrm{vac}|\Psi^\dagger(\mathbf{x},t)\boldsymbol{\alpha}\Psi(\mathbf{x},t)|\mathrm{vac}\rangle\\&=-\frac{1}{2}\sum\!\!\!\!\!\!\int \mathrm{sgn}(E)\psi_E^\dagger(\mathbf{x})\boldsymbol{\alpha}\psi_E(\mathbf{x})\end{aligned} \tag{2.5}$$

[$\mathrm{sgn}(u)$ is the sign function, $\mathrm{sgn}(u)=\pm1$ at $u\gtrless 0$]. The magnetic field strength, $\mathbf{B}_\mathrm{I}(\mathbf{x})$, is also induced in the vacuum, as a consequence of the Maxwell equation,

$$\boldsymbol{\partial}\times\mathbf{B}_\mathrm{I}(\mathbf{x})=e\mathbf{j}(\mathbf{x}), \tag{2.6}$$

where the electromagnetic coupling constant, e, differs in general from $\tilde{e}$. The total flux of the induced vacuum magnetic field is

$$\Phi_I=\int d\boldsymbol{\sigma}\cdot\mathbf{B}_\mathrm{I}(\mathbf{x}). \tag{2.7}$$

Since the vacuum of quantum matter exists outside the ANO vortex core, as was already emphasized, an issue of the choice of boundary conditions at the edge of the core is of primary concern. Turning to this issue, let us note first that (2.4) is not enough to define the Hamiltonian operator rigorously in a mathematical sense. To define an operator in an unambiguous way, one has to specify its domain of definition. Let the set of functions ψ be the domain of definition of operator H and the set of functions $\tilde{\psi}$ be the domain of definition of its adjoint, operator $H^\dagger$. Then the operator is Hermitian (or symmetric in mathematical parlance),

$$\int_X d^3x\sqrt{g}\tilde{\psi}^\dagger(H\psi)=\int_X d^3x\sqrt{g}(H^\dagger\tilde{\psi})^\dagger\psi, \tag{2.8}$$

if relation

$$-i\int_{\partial X} d\boldsymbol{\sigma}\cdot\tilde{\psi}^\dagger\boldsymbol{\alpha}\psi=0 \tag{2.9}$$

is valid; here functions $\psi(\mathbf{x})$ and $\tilde{\psi}(\mathbf{x})$ are defined in space X with boundary ∂X. It is evident that condition (2.9) can be satisfied by imposing different boundary conditions for ψ and $\tilde{\psi}$. But, a nontrivial task is to find a possibility that a boundary condition for $\tilde{\psi}$ is the same as that for ψ; then the domain of definition of $H^\dagger$ coincides with that of H, and operator H is self-adjoint (for a review of the Weyl–von Neumann theory of self-adjoint operators see [27,28]). The action of a self-adjoint operator on functions belonging to its domain of definition results in functions of the same kind only, and a multiple action and functions of such an operator, for instance, the resolvent and evolution operators, can consistently be defined. Thus, the requirement of the self-adjointness of operator H (2.4) renders the most general boundary condition at the edge of the vortex core for the solution to the Dirac equation, $\psi_E(\mathbf{x})$.

Note also that relation (2.9), when applied to the solution to the Dirac equation, yields

$$-i\int_{\partial X} d\boldsymbol{\sigma}\cdot\psi_E^\dagger\boldsymbol{\alpha}\psi_E=0 \tag{2.10}$$

or

$$\int_{\partial X} d\boldsymbol{\sigma}\cdot\mathbf{j}=0 \tag{2.11}$$

with $\mathbf{j}(\mathbf{x})$ given by (2.5). If boundary ∂X is connected, then (2.11) is reduced to

$$\boldsymbol{n}\cdot\mathbf{j}|_{\mathbf{x}\in\partial X}=0, \tag{2.12}$$

where $\boldsymbol{n}$ is the unit normal that may be chosen as pointing outward to X. The last relation signifies the impenetrability of ∂X; i.e., the matter field is confined to X.

In the present paper we consider the vacuum polarization effects in $(2+1)$-dimensional spacetime, which is a section orthogonal to the ANO vortex axis, i.e., at $z = \text{const}$. The irreducible representation of the Clifford algebra is chosen in such a way that the Dirac matrices in flat $(2+1)$-dimensional spacetime take the form

$$\alpha^1_{(0)} = -\sigma^2, \qquad \alpha^2_{(0)} = \sigma^1, \qquad \beta = \sigma^3, \tag{2.13}$$

where σ^1, σ^2, and σ^3 are the Pauli matrices (a transition to another inequivalent irreducible representation can be made by changing he sign of β). In the background of the ANO vortex, the only one component of the vector potential and the spin connection is nonvanishing:

$$V_\varphi = \frac{\Phi}{2\pi}, \qquad w_\varphi = \mathrm{i}\frac{\nu-1}{r}\alpha_\varphi\alpha_r, \tag{2.14}$$

and the Dirac Hamiltonian takes the form

$$H = -\mathrm{i}\left[\alpha^r\left(\partial_r + \frac{1-\nu}{2r}\right) + \alpha^\varphi\left(\partial_\varphi - \mathrm{i}\frac{\tilde{e}\Phi}{2\pi}\right)\right] + \beta m, \tag{2.15}$$

where

$$\alpha^r = \alpha_r = \begin{pmatrix} 0 & \mathrm{i}e^{-\mathrm{i}\varphi} \\ -\mathrm{i}e^{\mathrm{i}\varphi} & 0 \end{pmatrix}, \qquad \alpha^\varphi = \frac{\nu}{r}\begin{pmatrix} 0 & e^{-\mathrm{i}\varphi} \\ e^{\mathrm{i}\varphi} & 0 \end{pmatrix},$$
$$\alpha_\varphi = \frac{r^2}{\nu^2}\alpha^\varphi. \tag{2.16}$$

Decomposing function $\psi_E(\mathbf{x})$ as

$$\psi_E(\mathbf{x}) = \sum_{n\in\mathbb{Z}}\begin{pmatrix} f_n(r,E)e^{\mathrm{i}n\varphi} \\ g_n(r,E)e^{\mathrm{i}(n+1)\varphi} \end{pmatrix} \tag{2.17}$$

($\mathbb{Z}$ is the set of integer numbers), we present the Dirac equation as a system of two first-order differential equations for radial functions:

$$\left\{\begin{array}{l} \{-\partial_r + r^{-1}[\nu(n-n_\mathrm{c}) - G]\}f_n(r,E) = (E+m)g_n(r,E) \\ \{\partial_r + r^{-1}[\nu(n-n_\mathrm{c}) + 1 - G]\}g_n(r,E) = (E-m)f_n(r,E) \end{array}\right\}, \tag{2.18}$$

where

$$n_\mathrm{c} = \left[\left|\frac{\tilde{e}\Phi}{2\pi}\right|\right], \qquad F = \left\{\left|\frac{\tilde{e}\Phi}{2\pi}\right|\right\}, \qquad G = \nu\left(F - \frac{1}{2}\right) + \frac{1}{2}, \tag{2.19}$$

$[|u|]$ is the integer part of quantity u (i.e., the integer that is less than or equal to u), and $\{|u|\} = u - [|u|]$ is the fractional part of quantity u, $0 \le \{|u|\} < 1$.

Using (2.16) and (2.17), one gets $j_r = 0$, and the only component of the induced vacuum current,

$$j_\varphi(r) = -\frac{r}{\nu}\sum_{n\in\mathbb{Z}}\mathrm{sgn}(E)f_n(r,E)g_n(r,E), \tag{2.20}$$

is independent of the angular variable. The induced vacuum magnetic field strength is directed along the vortex axis,

$$B_\mathrm{I}(r) = e\nu\int_r^\infty \frac{dr'}{r'}j_\varphi(r'), \tag{2.21}$$

with total flux

$$\Phi_\mathrm{I} = \frac{2\pi}{\nu}\int_{r_0}^\infty drrB_\mathrm{I}(r), \tag{2.22}$$

where it is assumed without a loss of generality that the vortex core has the form of a tube of radius r_0.

III. SOLUTION TO THE DIRAC EQUATION

The solution to the system of equations, (2.18), is given in terms of cylindrical functions. Let us define

$$\begin{pmatrix} f_n^{(\wedge)} \\ g_n^{(\wedge)} \end{pmatrix} = \frac{1}{2}\sqrt{\frac{\nu}{\pi}}\begin{pmatrix} \sqrt{1+m/E}[\sin(\mu^{(\wedge)}_{\nu l+1-G})J_{\nu l-G}(kr) + \cos(\mu^{(\wedge)}_{\nu l+1-G})Y_{\nu l-G}(kr)] \\ \mathrm{sgn}(E)\sqrt{1-m/E}[\sin(\mu^{(\wedge)}_{\nu l+1-G})J_{\nu l+1-G}(kr) + \cos(\mu^{(\wedge)}_{\nu l+1-G})Y_{\nu l+1-G}(kr)] \end{pmatrix}, \tag{3.1}$$

where $l = n - n_\mathrm{c}$, and

$$\begin{pmatrix} f_n^{(\vee)} \\ g_n^{(\vee)} \end{pmatrix} = \frac{1}{2}\sqrt{\frac{\nu}{\pi}}\begin{pmatrix} \sqrt{1+m/E}[\sin(\mu^{(\vee)}_{\nu l'+G})J_{\nu l'+G}(kr) + \cos(\mu^{(\vee)}_{\nu l'+G})Y_{\nu l'+G}(kr)] \\ -\mathrm{sgn}(E)\sqrt{1-m/E}[\sin(\mu^{(\vee)}_{\nu l'+G})J_{\nu l'-1+G}(kr) + \cos(\mu^{(\vee)}_{\nu l'+G})Y_{\nu l'-1+G}(kr)] \end{pmatrix}, \tag{3.2}$$

where $l' = -n + n_\mathrm{c}$; here $J_\rho(u)$ and $Y_\rho(u)$ are the Bessel and Neumann functions of order ρ, $k = \sqrt{E^2 - m^2}$.

In the case of $\nu > 1$ and $0 < F < \frac{1}{2}(1-\frac{1}{\nu})$ $[\frac{1}{2}(1-\nu) < G < 0]$, the complete set of solutions to (2.18) is given by

$$\left.\begin{pmatrix} f_n \\ g_n \end{pmatrix}\right|_{n\geq n_c} = \begin{pmatrix} f_n^{(\wedge)} \\ g_n^{(\wedge)} \end{pmatrix}, \qquad \left.\begin{pmatrix} f_n \\ g_n \end{pmatrix}\right|_{n\leq n_c-1} = \begin{pmatrix} f_n^{(\vee)} \\ g_n^{(\vee)} \end{pmatrix}. \tag{3.3}$$

In the case of $\nu > 1$ and $\frac{1}{2}(1+\frac{1}{\nu}) < F < 1$ $[1 < G < \frac{1}{2}(1+\nu)]$, the complete set of solutions to (2.18) is given by

$$\left.\begin{pmatrix} f_n \\ g_n \end{pmatrix}\right|_{n\geq n_c+1} = \begin{pmatrix} f_n^{(\wedge)} \\ g_n^{(\wedge)} \end{pmatrix}, \qquad \left.\begin{pmatrix} f_n \\ g_n \end{pmatrix}\right|_{n\leq n_c} = \begin{pmatrix} f_n^{(\vee)} \\ g_n^{(\vee)} \end{pmatrix}. \tag{3.4}$$

One can note that both upper and lower components of each mode consist of two terms: one (given by the Bessel function) is vanishing and another one (given by the Neumann function) is diverging in the limit of $r \to 0$.

In the case of $\nu \geq 1$ and $\frac{1}{2}(1-\frac{1}{\nu}) < F < \frac{1}{2}(1+\frac{1}{\nu})$ $(0 < G < 1)$, there is a peculiar mode corresponding to $n = n_c$. This mode can be composed either from the pair of columns

$$\begin{pmatrix} \sqrt{1+m/E}J_{-G}(kr) \\ \mathrm{sgn}(E)\sqrt{1-m/E}J_{1-G}(kr) \end{pmatrix} \quad \text{and} \quad \begin{pmatrix} \sqrt{1+m/E}Y_{-G}(kr) \\ \mathrm{sgn}(E)\sqrt{1-m/E}Y_{1-G}(kr) \end{pmatrix}$$

or from the pair of columns

$$\begin{pmatrix} \sqrt{1+m/E}J_{G}(kr) \\ -\mathrm{sgn}(E)\sqrt{1-m/E}J_{-1+G}(kr) \end{pmatrix} \quad \text{and} \quad \begin{pmatrix} \sqrt{1+m/E}Y_{G}(kr) \\ -\mathrm{sgn}(E)\sqrt{1-m/E}Y_{-1+G}(kr) \end{pmatrix};$$

both terms in the first variant have divergent upper components, whereas both terms in the second variant have divergent lower components. Instead of these variants we choose the following form:

$$\begin{pmatrix} f_{n_c} \\ g_{n_c} \end{pmatrix} = \frac{1}{2}\sqrt{\frac{\nu}{\pi}}\frac{1}{\sqrt{1+\sin(2\mu_{1-G})\cos(G\pi)}} \begin{pmatrix} \sqrt{1+m/E}[\sin(\mu_{1-G})J_{-G}(kr)+\cos(\mu_{1-G})J_{G}(kr)] \\ \mathrm{sgn}(E)\sqrt{1-m/E}[\sin(\mu_{1-G})J_{1-G}(kr)-\cos(\mu_{1-G})J_{-1+G}(kr)] \end{pmatrix}. \tag{3.5}$$

Modes

$$\left.\begin{pmatrix} f_n \\ g_n \end{pmatrix}\right|_{n\geq n_c+1} = \begin{pmatrix} f_n^{(\wedge)} \\ g_n^{(\wedge)} \end{pmatrix}, \qquad \left.\begin{pmatrix} f_n \\ g_n \end{pmatrix}\right|_{n\leq n_c-1} = \begin{pmatrix} f_n^{(\vee)} \\ g_n^{(\vee)} \end{pmatrix} \tag{3.6}$$

together with mode (3.5) comprise the set of all solutions with $|E| > m$ in this case.

In the case of $\frac{1}{2} \leq \nu < 1$ and $\frac{1}{2}(\frac{1}{\nu}-1) < F < \frac{1}{2}(3-\frac{1}{\nu})$ $(1-\nu < G < \nu)$, the set of all solutions with $|E| > m$ is also given by (3.5) and (3.6). In the case of $\frac{1}{2} \leq \nu < 1$ and $0 < F < \frac{1}{2}(\frac{1}{\nu}-1)$ $[\frac{1}{2}(1-\nu) < G < 1-\nu]$, there is an additional peculiar mode:

$$\begin{pmatrix} f_{n_c-1} \\ g_{n_c-1} \end{pmatrix} = \frac{1}{2}\sqrt{\frac{\nu}{\pi}}\frac{1}{\sqrt{1+\sin(2\mu_{1-\nu-G})}} \begin{pmatrix} \sqrt{1+m/E}[\sin(\mu_{1-\nu-G})J_{-\nu-G}(kr)+\cos(\mu_{1-\nu-G})J_{\nu+G}(kr)] \\ \mathrm{sgn}(E)\sqrt{1-m/E}[\sin(\mu_{1-\nu-G})J_{1-\nu-G}(kr)-\cos(\mu_{1-\nu-G})J_{-1+\nu+G}(kr)] \end{pmatrix}. \tag{3.7}$$

Modes

$$\left.\begin{pmatrix} f_n \\ g_n \end{pmatrix}\right|_{n\geq n_c+1} = \begin{pmatrix} f_n^{(\wedge)} \\ g_n^{(\wedge)} \end{pmatrix}, \qquad \left.\begin{pmatrix} f_n \\ g_n \end{pmatrix}\right|_{n\leq n_c-2} = \begin{pmatrix} f_n^{(\vee)} \\ g_n^{(\vee)} \end{pmatrix} \tag{3.8}$$

together with modes (3.5) and (3.7) comprise the set of all solutions with $|E| > m$ in this case. An additional peculiar mode also appears in the case of $\frac{1}{2} \leq \nu < 1$ and $\frac{1}{2}(3-\frac{1}{\nu}) < F < 1$ $[\nu < G < \frac{1}{2}(1+\nu)]$:

$$\begin{pmatrix} f_{n_c+1} \\ g_{n_c+1} \end{pmatrix} = \frac{1}{2}\sqrt{\frac{\nu}{\pi}}\frac{1}{\sqrt{1+\sin(2\mu_{1+\nu-G})}} \begin{pmatrix} \sqrt{1+m/E}[\sin(\mu_{1+\nu-G})J_{\nu-G}(kr)+\cos(\mu_{1+\nu-G})J_{-\nu+G}(kr)] \\ \mathrm{sgn}(E)\sqrt{1-m/E}[\sin(\mu_{1+\nu-G})J_{1+\nu-G}(kr)-\cos(\mu_{1+\nu-G})J_{-1-\nu+G}(kr)] \end{pmatrix}. \tag{3.9}$$

Modes

$$\begin{pmatrix} f_n \\ g_n \end{pmatrix}\Big|_{n\geq n_c+2} = \begin{pmatrix} f_n^{(\wedge)} \\ g_n^{(\wedge)} \end{pmatrix}, \qquad \begin{pmatrix} f_n \\ g_n \end{pmatrix}\Big|_{n\leq n_c-1} = \begin{pmatrix} f_n^{(\vee)} \\ g_n^{(\vee)} \end{pmatrix} \tag{3.10}$$

together with modes (3.5) and (3.9) comprise the set of all solutions with $|E| > m$ in this case. In the case of $0 < \nu < \frac{1}{2}$ there are two and more peculiar modes.

Certainly, the limit of $r \to 0$ is of no sense for vortices of nonzero transverse size. However, it is instructive to discuss an infinitely thin vortex, and we shall touch upon this subject in the rest of the section. Most of the modes in the $r_0 = 0$ case are obtained by putting $\mu_\rho^{(\wedge)} = \mu_\rho^{(\vee)} = \pi/2$ in (3.3), (3.4), (3.6), (3.8), and (3.10); these modes are regular at $r \to 0$. However, peculiar modes (3.5), (3.7), and (3.9) cannot be made regular at $r \to 0$; they are irregular but square integrable. The latter circumstance requires a quest for a self-adjoint extension, and the Weyl–von Neumann theory of deficiency indices (see [27,28]) has to be employed. In the case of $\nu \geq 1$ and $\frac{1}{2}(1-\frac{1}{\nu}) < F < \frac{1}{2}(1+\frac{1}{\nu})$, as well as in the case of $\frac{1}{2} \leq \nu < 1$ and $\frac{1}{2}(\frac{1}{\nu}-1) < F < \frac{1}{2}(3-\frac{1}{\nu})$, when there is one irregular mode, the deficiency index is (1,1), and the one-parametric family of self-adjoint extensions can be introduced with the use of condition

$$\lim_{r\to 0}(mr)^G \cos\left(\frac{\Theta}{2}+\frac{\pi}{4}\right) f_{n_c} = -\lim_{r\to 0}(mr)^{1-G}\sin\left(\frac{\Theta}{2}+\frac{\pi}{4}\right) g_{n_c}, \tag{3.11}$$

where Θ is the self-adjoint extension parameter [29,30]. In view of relations

$$\int_0^\infty dr r J_\rho(kr) J_\rho(k'r) = \frac{\delta(k-k')}{\sqrt{kk'}}, \qquad \rho > -1, \tag{3.12}$$

and

$$\int_0^\infty dr r J_\rho(kr) J_{-\rho}(k'r) = \cos(\rho\pi)\frac{\delta(k-k')}{\sqrt{kk'}}, \qquad -1 < \rho < 1, \tag{3.13}$$

the modes are orthonormalized as the modes corresponding to the continuous spectrum:

$$\int d^2x\sqrt{g}[f_n(r,E)f_n(r,E') + g_n(r,E)g_n(r,E')] = \frac{1}{2}[1+\mathrm{sgn}(EE')]\frac{\delta(k-k')}{\sqrt{kk'}}. \tag{3.14}$$

In addition, there is a bound state at $\cos\Theta < 0$ with energy E_{BS} in the gap between the continuums, $-m < E_{BS} < m$. Its mode is

$$\begin{pmatrix} f_{n_c}^{(BS)} \\ g_{n_c}^{(BS)} \end{pmatrix} = \frac{1}{\pi}\sqrt{\frac{\nu(m^2-E_{BS}^2)\sin(G\pi)}{1+(2G-1)E_{BS}/m}} \times \begin{pmatrix} \sqrt{1+E_{BS}/m}K_G(r\sqrt{m^2-E_{BS}^2}) \\ \sqrt{1-E_{BS}/m}K_{1-G}(r\sqrt{m^2-E_{BS}^2}) \end{pmatrix}, \tag{3.15}$$

and the value of its energy is determined from relation

$$\frac{(1+E_{BS}/m)^{1-G}}{(1-E_{BS}/m)^G} = -2^{1-2G}\frac{\Gamma(1-G)}{\Gamma(G)}\tan\left(\frac{\Theta}{2}+\frac{\pi}{4}\right), \tag{3.16}$$

$\Gamma(u)$ is the Euler gamma function, and $K_\rho(u)$ is the Macdonald function of order ρ. The induced vacuum current and other vacuum polarization effects were comprehensively and exhaustively studied for $\nu = 1$ in [31–35] and for carbon nanocones in [36–39].

In the case of $\frac{1}{2} \leq \nu < 1$ and $0 < F < \frac{1}{2}(\frac{1}{\nu}-1)$, or $\frac{1}{2} \leq \nu < 1$ and $\frac{1}{2}(3-\frac{1}{\nu}) < F < 1$, and other cases, when there are two irregular square integrable modes [of the kind given by the pair of (3.5) and (3.7), or (3.5) and (3.9)], the deficiency index is (2,2), and there are four self-adjoint extension parameters. These cases remain unstudied yet.

IV. SELF-ADJOINTNESS AND CHOICE OF BOUNDARY CONDITIONS

The Dirac Hamiltonian operator in the background of the ANO vortex of nonzero radius r_0 is self-adjoint, if condition

$$\tilde{\psi}^\dagger \alpha^r \psi|_{r=r_0} = 0 \tag{4.1}$$

is valid [see (2.8) and (2.9)] and sets of functions ψ and $\tilde{\psi}$ coincide. Ergo, the quest is for a boundary condition in the form

$$\psi|_{r=r_0} = K\psi|_{r=r_0}, \qquad \tilde{\psi}|_{r=r_0} = K\tilde{\psi}|_{r=r_0}, \tag{4.2}$$

where K is a matrix (element of the Clifford algebra) which without a loss of generality can be chosen to be Hermitian and has to obey conditions

$$[K, \alpha^r]_+ = 0 \tag{4.3}$$

and

$$K^2 = I. \tag{4.4}$$

One can simply go through four linearly independent elements of the Clifford algebra in $(2+1)$-dimensional spacetime, which is a section orthogonal to the ANO vortex axis, and find

$$K = c_1\beta + c_2 \mathrm{i}\beta\alpha^r \tag{4.5}$$

with real coefficients satisfying

$$c_1^2 + c_2^2 = 1. \tag{4.6}$$

Using obvious parametrization

$$c_1 = \sin\theta, \qquad c_2 = \cos\theta,$$

we finally obtain

$$K = \mathrm{i}\beta\alpha^r \mathrm{e}^{-\mathrm{i}\theta\alpha^r}. \tag{4.7}$$

Thus, boundary condition (4.2) with K given by (4.7) is the most general boundary condition ensuring the self-adjointness of the Dirac Hamiltonian operator in the background of the ANO vortex of nonzero radius r_0 in transverse section $z = \text{const}$, and parameter θ can be interpreted as the self-adjoint extension parameter. Value $\theta = 0$ corresponds to the MIT bag boundary condition, which was proposed long ago as the condition ensuring the confinement of the matter field [40]. However, it should be comprehended that a condition with an arbitrary value of θ ensures the confinement equally as well as that with $\theta = 0$.

Imposing boundary condition (4.2) with matrix K (4.7) on the solution to the Dirac equation, $\psi_E(\mathbf{x})$ (2.17), we obtain the condition for the modes,

$$\cos\left(\frac{\theta}{2}+\frac{\pi}{4}\right) f_n(r_0, E) = -\sin\left(\frac{\theta}{2}+\frac{\pi}{4}\right) g_n(r_0, E), \tag{4.8}$$

which allows us to determine their coefficients:

$$\tan(\mu_\rho^{(\wedge)}) = \frac{\cos(\frac{\theta}{2}+\frac{\pi}{4}) kY_{\rho-1}(kr_0) - \sin(\frac{\theta}{2}+\frac{\pi}{4})(m-E)Y_\rho(kr_0)}{-\cos(\frac{\theta}{2}+\frac{\pi}{4}) kJ_{\rho-1}(kr_0) + \sin(\frac{\theta}{2}+\frac{\pi}{4})(m-E)J_\rho(kr_0)}, \tag{4.9}$$

$$\tan(\mu_\rho^{(\vee)}) = \frac{\cos(\frac{\theta}{2}+\frac{\pi}{4})(m+E)Y_\rho(kr_0) - \sin(\frac{\theta}{2}+\frac{\pi}{4}) kY_{\rho-1}(kr_0)}{-\cos(\frac{\theta}{2}+\frac{\pi}{4})(m+E)J_\rho(kr_0) + \sin(\frac{\theta}{2}+\frac{\pi}{4}) kJ_{\rho-1}(kr_0)}, \tag{4.10}$$

$$\tan(\mu_\rho) = \frac{\cos(\frac{\theta}{2}+\frac{\pi}{4}) kJ_{1-\rho}(kr_0) + \sin(\frac{\theta}{2}+\frac{\pi}{4})(m-E)J_{-\rho}(kr_0)}{-\cos(\frac{\theta}{2}+\frac{\pi}{4}) kJ_{\rho-1}(kr_0) + \sin(\frac{\theta}{2}+\frac{\pi}{4})(m-E)J_\rho(kr_0)}. \tag{4.11}$$

Because of condition (4.8), in addition to the continuous spectrum, there is a bound state at $\cos\theta < 0$ for $n = n_c$ [$\nu \geq 1$ and $\frac{1}{2}(1-\frac{1}{\nu}) < F < \frac{1}{2}(1+\frac{1}{\nu})$, or $\frac{1}{2} \leq \nu < 1$], as well as for $n = n_c - 1$ [$\frac{1}{2} \leq \nu < 1$ and $0 < F < \frac{1}{2}(\frac{1}{\nu} - 1)$], or $n = n_c + 1$ [$\frac{1}{2} \leq \nu < 1$ and $\frac{1}{2}(3-\frac{1}{\nu}) < F < 1$]. The bound state modes are

$$\begin{pmatrix} f_{n_c}^{(BS)} \\ g_{n_c}^{(BS)} \end{pmatrix} = \sqrt{\frac{\nu\kappa m}{2\pi r_0}} \{ mK_G(\kappa r_0)K_{1-G}(\kappa r_0) + E_{BS}[\kappa r_0 K_{1-G}^2(\kappa r_0) - \kappa r_0 K_G^2(\kappa r_0) + (2G-1)K_G(\kappa r_0)K_{1-G}(\kappa r_0)] \}^{-1/2} \times \begin{pmatrix} \sqrt{1+E_{BS}/m}\, K_G(\kappa r_0) \\ \sqrt{1-E_{BS}/m}\, K_{1-G}(\kappa r_0) \end{pmatrix}, \tag{4.12}$$

$$\begin{pmatrix} f_{n_c\mp1}^{(BS)} \\ g_{n_c\mp1}^{(BS)} \end{pmatrix} = \sqrt{\frac{\nu\kappa m}{2\pi r_0}} \{ mK_{G\pm\nu}(\kappa r_0)K_{1-G\mp\nu}(\kappa r_0) + E_{BS}[\kappa r_0 K_{1-G\mp\nu}^2(\kappa r_0) - \kappa r_0 K_{G\pm\nu}^2(\kappa r_0) + (2G\pm2\nu-1)K_{G\pm\nu}(\kappa r_0)K_{1-G\mp\nu}(\kappa r_0)] \}^{-1/2} \times \begin{pmatrix} \sqrt{1+E_{BS}/m}\, K_{G\pm\nu}(\kappa r_0) \\ \sqrt{1-E_{BS}/m}\, K_{1-G\mp\nu}(\kappa r_0) \end{pmatrix}, \tag{4.13}$$

where $\kappa = \sqrt{m^2 - E_{BS}^2}$. The bound state energy for $n = n_c$ is determined from relation

$$\sqrt{\frac{1+E_{BS}/m}{1-E_{BS}/m}} = -\frac{K_{1-G}(\kappa r_0)}{K_G(\kappa r_0)} \tan\left(\frac{\theta}{2}+\frac{\pi}{4}\right); \tag{4.14}$$

by changing G to $G \pm \nu$ in (4.14), one obtains the relation for $n = n_c \mp 1$.

Comparing the case of a vortex of nonzero transverse size with that of an infinitely thin one, we conclude that in the first case the total Hamiltonian is extended with the use of the only one self-adjoint extension parameter, whereas in the second case several partial Hamiltonians are extended, and the number of self-adjoint extension parameters can be zero (no need for extension, the operator is essentially self-adjoint), one, four, etc. The values of the self-adjoint extension parameters in the second case can be fixed from the first case by limiting procedure $r_0 \to 0$ [41]. The nonpeculiar modes ($\rho > 1$) in this limit become regular and independent of θ, since, as was already noted,

$$\lim_{r_0\to 0}\mu_\rho^{(\wedge)} = \lim_{r_0\to 0}\mu_\rho^{(\vee)} = \frac{\pi}{2}.$$

The peculiar modes ($0 < \rho < 1$) in this limit become irregular and square integrable, and

$$\lim_{r_0\to 0}\mu_\rho = \begin{cases} \frac{\pi}{2}, & \frac{1}{2} < \rho(\theta \neq \pm\frac{\pi}{2}), \quad 0 < \rho(\theta = \frac{\pi}{2}), \\ \mathrm{sgn}(E)\arctan\left[\sqrt{\frac{1-m/E}{1+m/E}}\tan\left(\frac{\theta}{2}+\frac{\pi}{4}\right)\right], & \rho = \frac{1}{2}, \\ 0, & \rho < \frac{1}{2}(\theta \neq \pm\frac{\pi}{2}), \quad \rho < 1(\theta = -\frac{\pi}{2}). \end{cases} \tag{4.15}$$

Namely in this way, the condition of minimal irregularity [31,32] is obtained, which in the case of the deficiency index equal to (1,1) (i.e., only one peculiar mode) takes the form

$$\Theta = \begin{cases} \frac{\pi}{2}, & \frac{1}{2}(1-\frac{1}{\nu}) < F < \frac{1}{2} \ (\nu \geq 1), \quad \frac{1}{2}(\frac{1}{\nu}-1) < F < \frac{1}{2} \ (\frac{1}{2} < \nu < 1), \\ \theta, & F = \frac{1}{2} \ (\nu \geq \frac{1}{2}), \\ -\frac{\pi}{2}, & \frac{1}{2} < F < \frac{1}{2}(1+\frac{1}{\nu}) \ (\nu \geq 1), \quad \frac{1}{2} < F < \frac{1}{2}(3-\frac{1}{\nu}) \ (\frac{1}{2} < \nu < 1). \end{cases} \tag{4.16}$$

V. INDUCED VACUUM CURRENT

We start with the case of $\nu \geq 1$ and $\frac{1}{2}(1-\frac{1}{\nu}) < F < \frac{1}{2}(1+\frac{1}{\nu})$, or $\frac{1}{2} \leq \nu < 1$ and $\frac{1}{2}(\frac{1}{\nu}-1) < F < \frac{1}{2}(3-\frac{1}{\nu})$, when there is one peculiar mode. Inserting the contribution of the appropriate modes [see (3.1), (3.2), (3.5), (3.6), and (4.12)] to (2.20), we obtain

$$j_\varphi(r) = j_\varphi^{(1)}(r) + j_\varphi^{(2)}(r) + j_\varphi^{(3)}(r), \tag{5.1}$$

where

$$j_\varphi^{(1)}(r) = -\frac{r}{2\pi}\int_0^\infty \frac{dkk^2}{\sqrt{k^2+m^2}}\sum_{l=1}^\infty [J_{\nu l+1-G}(kr)J_{\nu l-G}(kr) - J_{\nu l+G}(kr)J_{\nu l-1+G}(kr)], \tag{5.2}$$

$$\begin{aligned} j_\varphi^{(2)}(r) = -\frac{r}{4\pi}\int_0^\infty \frac{dkk^2}{\sqrt{k^2+m^2}}\sum_{\mathrm{sgn}(E)}\sum_{l=1}^\infty \Big\{ & \cos^2(\mu_{\nu l+1-G}^{(\wedge)})[Y_{\nu l+1-G}(kr)Y_{\nu l-G}(kr) - J_{\nu l+1-G}(kr)J_{\nu l-G}(kr)] \\ & + \frac{1}{2}\sin(2\mu_{\nu l+1-G}^{(\wedge)})[J_{\nu l+1-G}(kr)Y_{\nu l-G}(kr) + Y_{\nu l+1-G}(kr)J_{\nu l-G}(kr)] \\ & - \cos^2(\mu_{\nu l+G}^{(\vee)})[Y_{\nu l+G}(kr)Y_{\nu l-1+G}(kr) - J_{\nu l+G}(kr)J_{\nu l-1+G}(kr)] \\ & - \frac{1}{2}\sin(2\mu_{\nu l+G}^{(\vee)})[J_{\nu l+G}(kr)Y_{\nu l-1+G}(kr) + Y_{\nu l+G}(kr)J_{\nu l-1+G}(kr)]\Big\}, \end{aligned} \tag{5.3}$$

$$\begin{aligned} j_\varphi^{(3)}(r) = -\frac{r}{4\pi}\int_0^\infty \frac{dkk^2}{\sqrt{k^2+m^2}}\sum_{\mathrm{sgn}(E)} & [\tan(\mu_{1-G}) + 2\cos(G\pi) + \cot(\mu_{1-G})]^{-1}[\tan(\mu_{1-G})J_{-G}(kr)J_{1-G}(kr) + J_G(kr)J_{1-G}(kr) \\ & - J_{-G}(kr)J_{-1+G}(kr) - \cot(\mu_{1-G})J_G(kr)J_{-1+G}(kr)] \\ & + \frac{\kappa^2}{4\pi r_0}\frac{[1-\mathrm{sgn}(\cos\theta)]\mathrm{sgn}[\tan(\frac{\theta}{4}+\frac{\pi}{4}) + \frac{K_G(\kappa r_0)}{K_{1-G}(\kappa r_0)}]K_G(\kappa r)K_{1-G}(\kappa r)}{mK_G(\kappa r_0)K_{1-G}(\kappa r_0) + E_{BS}\{\kappa r_0[K_{1-G}^2(\kappa r_0) - K_G^2(\kappa r_0)] + (2G-1)K_G(\kappa r_0)K_{1-G}(\kappa r_0)\}}. \end{aligned} \tag{5.4}$$

In Appendix A, the summation in (5.2) is performed, yielding

$$
\begin{aligned}
j_{\varphi}^{(1)}(r) = & -\frac{r}{2\pi^2}\int_m^{\infty}\frac{dqq^2}{\sqrt{q^2-m^2}}[I_{1-G}(qr)K_G(qr)-I_G(qr)K_{1-G}(qr)] \\
& -\frac{m}{(2\pi)^2}\left\{\int_0^{\infty}\frac{du}{\cosh(u/2)}\left[1+\frac{1}{2mr\cosh(u/2)}\right]e^{-2mr\cosh(u/2)}\right. \\
& \times\frac{\sin(G\pi)\sinh(\nu u)\sinh[(G-\frac{1}{2})u]-\cos(G\pi)\sin(\nu\pi)\cosh[(G-\frac{1}{2})u]}{\cosh(\nu u)-\cos(\nu\pi)} \\
& -\frac{2\pi}{\nu}\sum_{p=1}^{[|\nu/2|]}\left[1+\frac{1}{2mr\sin(p\pi/\nu)}\right]\exp[-2mr\sin(p\pi/\nu)]\frac{\sin[(2G-1)p\pi/\nu]}{\sin(p\pi/\nu)} \\
& \left.-\frac{\pi}{\nu}\left(1+\frac{1}{2mr}\right)e^{-2mr}\cos(G\pi)\delta_{\nu,2N}\right\},
\end{aligned}
\tag{5.5}
$$

where $I_{\rho}(u)$ is the modified Bessel function of order ρ (p and N are the positive integers, $\delta_{\omega,\omega'}$ is the Kronecker symbol, $\delta_{\omega,\omega'}=0$ at $\omega'\neq\omega$, and $\delta_{\omega,\omega}=1$), while (5.3) is transformed to the following expression:

$$
\begin{aligned}
j_{\varphi}^{(2)}(r) = & -\frac{r}{\pi^2}\int_m^{\infty}\frac{dqq^2}{\sqrt{q^2-m^2}}\sum_{l=1}^{\infty}[C_{\nu l+1-G}^{(\wedge)}(qr_0)K_{\nu l+1-G}(qr)K_{\nu l-G}(qr) \\
& -C_{\nu l+G}^{(\vee)}(qr_0)K_{\nu l+G}(qr)K_{\nu l-1+G}(qr)],
\end{aligned}
\tag{5.6}
$$

where

$$
\begin{aligned}
C_{\rho}^{(\wedge)}(v) = & \left\{vI_{\rho}(v)K_{\rho}(v)\tan\left(\frac{\theta}{2}+\frac{\pi}{4}\right)+mr_0[I_{\rho}(v)K_{\rho-1}(v)-I_{\rho-1}(v)K_{\rho}(v)]\right. \\
& \left.-vI_{\rho-1}(v)K_{\rho-1}(v)\cot\left(\frac{\theta}{2}+\frac{\pi}{4}\right)\right\}\left[vK_{\rho}^2(v)\tan\left(\frac{\theta}{2}+\frac{\pi}{4}\right)+2mr_0K_{\rho}(v)K_{\rho-1}(v)\right. \\
& \left.+vK_{\rho-1}^2(v)\cot\left(\frac{\theta}{2}+\frac{\pi}{4}\right)\right]^{-1}
\end{aligned}
\tag{5.7}
$$

and

$$
\begin{aligned}
C_{\rho}^{(\vee)}(v) = & \left\{vI_{\rho}(v)K_{\rho}(v)\cot\left(\frac{\theta}{2}+\frac{\pi}{4}\right)+mr_0[I_{\rho}(v)K_{\rho-1}(v)-I_{\rho-1}(v)K_{\rho}(v)]\right. \\
& \left.-vI_{\rho-1}(v)K_{\rho-1}(v)\tan\left(\frac{\theta}{2}+\frac{\pi}{4}\right)\right\}\left[vK_{\rho}^2(v)\cot\left(\frac{\theta}{2}+\frac{\pi}{4}\right)+2mr_0K_{\rho}(v)K_{\rho-1}(v)\right. \\
& \left.+vK_{\rho-1}^2(v)\tan\left(\frac{\theta}{2}+\frac{\pi}{4}\right)\right]^{-1};
\end{aligned}
\tag{5.8}
$$

note that $C_{\nu l+1-G}^{(\wedge)}(v)\leftrightarrow C_{\nu l+G}^{(\vee)}(v)$ under simultaneous changes $F\to 1-F$ and $\theta\to-\theta$.

In Appendix B, $j_{\varphi}^{(3)}$ (5.5) is transformed to the following expression:

$$
\begin{aligned}
j_{\varphi}^{(3)}(r) = & \frac{r}{2\pi^2}\int_m^{\infty}\frac{dqq^2}{\sqrt{q^2-m^2}}[I_{1-G}(qr)K_G(qr)-I_G(qr)K_{1-G}(qr) \\
& -2C_{1-G}(qr_0)K_G(qr)K_{1-G}(qr)],
\end{aligned}
\tag{5.9}
$$

where

$$C_{1-G}(v)=\left\{v\left[I_{1-G}(v)+\frac{\sin(G\pi)}{\pi}K_{1-G}(v)\right]K_{1-G}(v)\tan\left(\frac{\theta}{2}+\frac{\pi}{4}\right)+mr_0[I_{1-G}(v)K_G(v)\right.$$
$$\left.-I_G(v)K_{1-G}(v)]-v[I_G(v)+\frac{\sin(G\pi)}{\pi}K_G(v)]K_G(v)\cot\left(\frac{\theta}{2}+\frac{\pi}{4}\right)\right\}$$
$$\times\left[vK_{1-G}^2(v)\tan\left(\frac{\theta}{2}+\frac{\pi}{4}\right)+2mr_0K_G(v)K_{1-G}(v)+vK_G^2(v)\cot\left(\frac{\theta}{2}+\frac{\pi}{4}\right)\right]^{-1}; \tag{5.10}$$

note that $C_{1-G}(v)$ changes sign under simultaneous changes $F\to 1-F$ and $\theta\to-\theta$.

Summing (5.5), (5.6), and (5.9), we obtain the final form for the induced vacuum current and express it in terms of F instead of G [see (2.19)],

$$j_\varphi(r)=-\frac{m}{(2\pi)^2}\left\{\int_0^\infty\frac{du}{\cosh(u/2)}\left[1+\frac{1}{2mr\cosh(u/2)}\right]e^{-2mr\cosh(u/2)}\right.$$
$$\times\frac{\cos[\nu(F-\frac{1}{2})\pi]\sinh(\nu u)\sinh[\nu(F-\frac{1}{2})u]+\sin[\nu(F-\frac{1}{2})\pi]\sin(\nu\pi)\cosh[\nu(F-\frac{1}{2})u]}{\cosh(\nu u)-\cos(\nu\pi)}$$
$$-\frac{2\pi}{\nu}\sum_{p=1}^{[|\nu/2|]}\left[1+\frac{1}{2mr\sin(p\pi/\nu)}\right]\exp[-2mr\sin(p\pi/\nu)]\frac{\sin[(2F-1)p\pi]}{\sin(p\pi/\nu)}$$
$$\left.+\frac{\pi}{2N}(-1)^N\sin(2NF\pi)\left(1+\frac{1}{2mr}\right)e^{-2mr}\delta_{\nu,2N}\right\}$$
$$-\frac{r}{\pi^2}\int_m^\infty\frac{dqq^2}{\sqrt{q^2-m^2}}[C_{\frac{1}{2}-\nu(F-\frac{1}{2})}(qr_0)K_{\frac{1}{2}-\nu(F-\frac{1}{2})}(qr)K_{\frac{1}{2}+\nu(F-\frac{1}{2})}(qr)+\Sigma(qr,qr_0)], \tag{5.11}$$

where

$$\Sigma(w,v)=\sum_{l=1}^\infty[C^{(\wedge)}_{\nu(l-F+\frac{1}{2})+\frac{1}{2}}(v)K_{\nu(l-F+\frac{1}{2})+\frac{1}{2}}(w)K_{\nu(l-F+\frac{1}{2})-\frac{1}{2}}(w)$$
$$-C^{(\vee)}_{\nu(l+F-\frac{1}{2})+\frac{1}{2}}(v)K_{\nu(l+F-\frac{1}{2})+\frac{1}{2}}(w)K_{\nu(l+F-\frac{1}{2})-\frac{1}{2}}(w)]. \tag{5.12}$$

The analysis in Appendix A is sufficient to consider cases when there are no peculiar modes. In the case of $\nu>1$ and $0<F<\frac{1}{2}(1-\frac{1}{\nu})$ $[\frac{1}{2}(1-\nu)<G<0]$, we obtain

$$j_\varphi(r)=-\frac{m}{(2\pi)^2}\left\{\int_0^\infty\frac{du}{\cosh(u/2)}\left[1+\frac{1}{2mr\cosh(u/2)}\right]e^{-2mr\cosh(u/2)}\right.$$
$$\times\frac{\cos[\nu(F-\frac{1}{2})\pi]\cosh[\nu(F+\frac{1}{2})u]-\cos[\nu(F+\frac{1}{2})\pi)]\cosh[\nu(F-\frac{1}{2})u]}{\cosh(\nu u)-\cos(\nu\pi)}$$
$$-\frac{2\pi}{\nu}\sum_{p=1}^{[|\nu/2|]}\left[1+\frac{1}{2mr\sin(p\pi/\nu)}\right]\exp[-2mr\sin(p\pi/\nu)]\frac{\sin[(2F-1)p\pi]}{\sin(p\pi/\nu)}$$
$$\left.+\frac{\pi}{2N}(-1)^N\sin(2NF\pi)\left(1+\frac{1}{2mr}\right)e^{-2mr}\delta_{\nu,2N}\right\}$$
$$-\frac{r}{\pi^2}\int_m^\infty\frac{dqq^2}{\sqrt{q^2-m^2}}[C^{(\wedge)}_{\frac{1}{2}-\nu(F-\frac{1}{2})}(qr_0)K_{\frac{1}{2}-\nu(F-\frac{1}{2})}(qr)K_{\frac{1}{2}+\nu(F-\frac{1}{2})}(qr)+\Sigma(qr,qr_0)]. \tag{5.13}$$

In the case of $\nu>1$ and $\frac{1}{2}(1+\frac{1}{\nu})<F<1$ $[1<G<\frac{1}{2}(1+\nu)]$, we obtain

$$
\begin{aligned}
j_\varphi(r) = \frac{m}{(2\pi)^2}\Bigg\{ & \int_0^\infty \frac{du}{\cosh(u/2)}\left[1+\frac{1}{2mr\cosh(u/2)}\right]e^{-2mr\cosh(u/2)} \\
& \times \frac{\cos[\nu(F-\frac{1}{2})\pi]\cosh[\nu(F-\frac{3}{2})u]-\cos[\nu(F-\frac{3}{2})\pi)]\cosh[\nu(F-\frac{1}{2})u]}{\cosh(\nu u)-\cos(\nu\pi)} \\
& + \frac{2\pi}{\nu}\sum_{p=1}^{[|\nu/2|]}\left[1+\frac{1}{2mr\sin(p\pi/\nu)}\right]\exp[-2mr\sin(p\pi/\nu)]\frac{\sin[(2F-1)p\pi]}{\sin(p\pi/\nu)} \\
& - \frac{\pi}{2N}(-1)^N\sin(2NF\pi)\left(1+\frac{1}{2mr}\right)e^{-2mr}\delta_{\nu,2N}\Bigg\} \\
& + \frac{r}{\pi^2}\int_m^\infty \frac{dqq^2}{\sqrt{q^2-m^2}}[C^{(\vee)}_{\frac{1}{2}+\nu(F-\frac{1}{2})}(qr_0)K_{\frac{1}{2}+\nu(F-\frac{1}{2})}(qr)K_{\frac{1}{2}-\nu(F-\frac{1}{2})}(qr)-\Sigma(qr,qr_0)]. \qquad (5.14)
\end{aligned}
$$

Note that both (5.13) and (5.14) consist of two parts: one [with a factor of $m/(2\pi)^2$] is independent of r_0, and another one (with a factor of r/π^2) is vanishing in the limit of $r_0 \to 0$,

$$
j_\varphi(r) = j^{(a)}_\varphi(r) + j^{(b)}_\varphi(r), \qquad j^{(a)}_\varphi(r) = \lim_{r_0\to 0} j_\varphi(r). \qquad (5.15)
$$

It is instructive to present result (5.11) in the same way; evidently, $j^{(a)}_\varphi(r)$ then coincides with the current that is obtained by imposing the condition of minimal irregularity in the case of an infinitely thin vortex [31,32]; see (3.11) and (4.16). We obtain for the decomposition of (5.11) according to (5.15):

$$
\begin{aligned}
j^{(a)}_\varphi(r)|_{F\neq 1/2,\theta\neq\pm\pi/2} = \frac{m}{(2\pi)^2}\Bigg\{ & \mathrm{sgn}\left(F-\frac{1}{2}\right)\int_0^\infty \frac{du}{\cosh(u/2)}\left[1+\frac{1}{2mr\cosh(u/2)}\right]e^{-2mr\cosh(u/2)} \\
& \times \frac{\cos[\nu(F-\frac{1}{2})\pi]\cosh[\nu(|F-\frac{1}{2}|-1)u]-\cos[\nu(|F-\frac{1}{2}|-1)\pi]\cosh[\nu(F-\frac{1}{2})u]}{\cosh(\nu u)-\cos(\nu\pi)} \\
& + \frac{2\pi}{\nu}\sum_{p=1}^{[|\nu/2|]}\left[1+\frac{1}{2mr\sin(p\pi/\nu)}\right]\exp[-2mr\sin(p\pi/\nu)]\frac{\sin[(2F-1)p\pi]}{\sin(p\pi/\nu)} \\
& - \frac{\pi}{2N}(-1)^N\sin(2NF\pi)\left(1+\frac{1}{2mr}\right)e^{-2mr}\delta_{\nu,2N}\Bigg\}, \qquad (5.16)
\end{aligned}
$$

$$
\begin{aligned}
j^{(a)}_\varphi(r)|_{F\neq 1/2,\theta=\pm\pi/2} = \mp\frac{m}{(2\pi)^2}\Bigg\{ & \int_0^\infty \frac{du}{\cosh(u/2)}\left[1+\frac{1}{2mr\cosh(u/2)}\right]e^{-2mr\cosh(u/2)} \\
& \times \frac{\cos[\nu(F-\frac{1}{2})\pi]\cosh[\nu(F-\frac{1}{2}\pm 1)u]-\cos[\nu(F-\frac{1}{2}\pm 1)\pi]\cosh[\nu(F-\frac{1}{2})u]}{\cosh(\nu u)-\cos(\nu\pi)} \\
& \mp \frac{2\pi}{\nu}\sum_{p=1}^{[|\nu/2|]}\left[1+\frac{1}{2mr\sin(p\pi/\nu)}\right]\exp[-2mr\sin(p\pi/\nu)]\frac{\sin[(2F-1)p\pi]}{\sin(p\pi/\nu)} \\
& \pm \frac{\pi}{2N}(-1)^N\sin(2NF\pi)\left(1+\frac{1}{2mr}\right)e^{-2mr}\delta_{\nu,2N}\Bigg\}, \qquad (5.17)
\end{aligned}
$$

$$
j^{(a)}_\varphi(r)|_{F=1/2} = -\frac{\sin\theta}{2\pi^2}\int_m^\infty \frac{dqq^2}{\sqrt{q^2-m^2}}\frac{e^{-2qr}}{q+m\cos\theta}, \qquad (5.18)
$$

$$
j^{(b)}_\varphi(r)|_{F<1/2,\theta\neq-\pi/2} = -\frac{r}{\pi^2}\int_m^\infty \frac{dqq^2}{\sqrt{q^2-m^2}}[C^{(\wedge)}_{\frac{1}{2}-\nu(F-\frac{1}{2})}(qr_0)K_{\frac{1}{2}-\nu(F-\frac{1}{2})}(qr)K_{\frac{1}{2}+\nu(F-\frac{1}{2})}(qr)+\Sigma(qr,qr_0)], \qquad (5.19)
$$

$$
j^{(b)}_\varphi(r)|_{F>1/2,\theta\neq\pi/2} = \frac{r}{\pi^2}\int_m^\infty \frac{dqq^2}{\sqrt{q^2-m^2}}[C^{(\vee)}_{\frac{1}{2}+\nu(F-\frac{1}{2})}(qr_0)K_{\frac{1}{2}+\nu(F-\frac{1}{2})}(qr)K_{\frac{1}{2}-\nu(F-\frac{1}{2})}(qr)-\Sigma(qr,qr_0)], \qquad (5.20)
$$

$$j_{\varphi}^{(b)}(r)|_{F\neq 1/2,\theta=\pm\pi/2} = \mp\frac{r}{\pi^2}\int_m^{\infty}\frac{dqq^2}{\sqrt{q^2-m^2}}\left\{\frac{I_{\frac{1}{2}\pm\nu(\frac{1}{2}-F)}(qr_0)}{K_{\frac{1}{2}\pm\nu(\frac{1}{2}-F)}(qr_0)}K_{\frac{1}{2}+\nu(F-\frac{1}{2})}(qr)K_{\frac{1}{2}-\nu(F-\frac{1}{2})}(qr)\right.$$
$$+\sum_{l=1}^{\infty}\left[\frac{I_{\nu(l-F+\frac{1}{2})\pm\frac{1}{2}}(qr_0)}{K_{\nu(l-F+\frac{1}{2})\pm\frac{1}{2}}(qr_0)}K_{\nu(l-F+\frac{1}{2})+\frac{1}{2}}(qr)K_{\nu(l-F+\frac{1}{2})-\frac{1}{2}}(qr)\right.$$
$$\left.\left.+\frac{I_{\nu(l+F-\frac{1}{2})\mp\frac{1}{2}}(qr_0)}{K_{\nu(l+F-\frac{1}{2})\mp\frac{1}{2}}(qr_0)}K_{\nu(l+F-\frac{1}{2})+\frac{1}{2}}(qr)K_{\nu(l+F-\frac{1}{2})-\frac{1}{2}}(qr)\right]\right\}, \tag{5.21}$$

and

$$j_{\varphi}^{(b)}(r)|_{F=1/2} = -\frac{\sin\theta}{2\pi^2}\int_m^{\infty}\frac{dqq^2}{\sqrt{q^2-m^2}}\left[\frac{e^{-2qr}(e^{2qr_0}-1)}{q+m\cos\theta}+4r\sum_{l=1}^{\infty}\tilde{C}_{\nu l+\frac{1}{2}}(qr_0)K_{\nu l+\frac{1}{2}}(qr)K_{\nu l-\frac{1}{2}}(qr)\right], \tag{5.22}$$

where

$$\tilde{C}_{\nu l+\frac{1}{2}}(v) = \left\{2vK_{\nu l+\frac{1}{2}}(v)K_{\nu l-\frac{1}{2}}(v)+mr_0\cos\theta\left[K^2_{\nu l+\frac{1}{2}}(v)+K^2_{\nu l-\frac{1}{2}}(v)\right]\right\}$$
$$\times\left\{v\cos\theta\left[K^2_{\nu l+\frac{1}{2}}(v)+K^2_{\nu l-\frac{1}{2}}(v)\right]\left[v\cos\theta\left(K^2_{\nu l+\frac{1}{2}}(v)+K^2_{\nu l-\frac{1}{2}}(v)\right)+4mr_0K_{\nu l+\frac{1}{2}}(v)K_{\nu l-\frac{1}{2}}(v)\right]\right.$$
$$\left.+4(v^2\sin^2\theta+m^2r_0^2\cos^2\theta)K^2_{\nu l+\frac{1}{2}}(v)K^2_{\nu l-\frac{1}{2}}(v)\right\}^{-1}, \tag{5.23}$$

and the use is made of relations

$$-\frac{1}{\pi}\cos\left[\nu\left(F-\frac{1}{2}\right)\pi\right]+C_{\frac{1}{2}-\nu(F-\frac{1}{2})}(v) = C^{(\wedge)}_{\frac{1}{2}-\nu(F-\frac{1}{2})} \tag{5.24}$$

and

$$\frac{1}{\pi}\cos\left[\nu\left(F-\frac{1}{2}\right)\pi\right]+C_{\frac{1}{2}-\nu(F-\frac{1}{2})}(v) = -C^{(\vee)}_{\frac{1}{2}+\nu(F-\frac{1}{2})}(v). \tag{5.25}$$

It should be noted that the r_0-independent part of the current in cases $\frac{1}{2}(1-\frac{1}{\nu}) < F < \frac{1}{2}$ and $\frac{1}{2} < F < \frac{1}{2}(1+\frac{1}{\nu})$ ($\nu \geq 1$), or $\frac{1}{2}(\frac{1}{\nu}-1) < F < \frac{1}{2}$ and $\frac{1}{2} < F < \frac{1}{2}(3-\frac{1}{\nu})$ ($\frac{1}{2} \leq \nu < 1$), is independent of θ if $\theta \neq \pm\pi/2$ [see (5.16)], whereas it depends on θ if $\theta = \pm\pi/2$ [see (5.17)]. The latter is distinct from cases of the absence of peculiar modes, when the r_0-independent part of the current is always independent of θ, see the first four lines in (5.13) and (5.14). Note also that limits $F \to 1/2$ and $r_0 \to 0$ in general do not commute. Indeed, we obtain a discontinuity at $F = 1/2$, if limit $r_0 \to 0$ is taken first,

$$\lim_{F\to(1/2)_{\pm}}\lim_{r_0\to 0} j_{\varphi}(r)\Big|_{\theta\neq\pm\pi/2} = \lim_{F\to(1/2)_{\pm}} j_{\varphi}^{(a)}(r)\Big|_{\theta\neq\pm\pi/2} = \pm\frac{m}{2\pi^2}K_1(2mr), \tag{5.26}$$

where the use is made of relation

$$\frac{m}{2}\int_0^{\infty}\frac{du}{\cosh(u/2)}\left[1+\frac{1}{2mr\cosh(u/2)}\right]e^{-2mr\cosh(u/2)} = \int_m^{\infty}\frac{dqq}{\sqrt{q^2-m^2}}e^{-2qr} = mK_1(2mr). \tag{5.27}$$

When the order of limits is reversed, then $j_{\varphi}^{(b)}(r)|_{\theta\neq\pm\pi/2}$ contributes, because of relation

$$\lim_{F\to(1/2)_{\pm}} j_{\varphi}^{(b)}(r)\Big|_{\theta\neq\pm\pi/2} = \mp\frac{m}{2\pi^2}K_1(2mr)-\frac{\sin\theta}{2\pi^2}\int_m^{\infty}\frac{dqq^2}{\sqrt{q^2-m^2}}\frac{e^{2q(r_0-r)}}{q+m\cos\theta}+mO\left[mr_0\left(\frac{r_0}{r}\right)^{2\nu-1}\right], \tag{5.28}$$

which follows from particular cases of (5.24) and (5.25),

$$C_{1/2}^{(\wedge)}(qr_0) = -\frac{1}{\pi} + \frac{q\sin\theta}{q+m\cos\theta}e^{2qr_0}$$

and

$$C_{1/2}^{(\vee)}(qr_0) = -\frac{1}{\pi} - \frac{q\sin\theta}{q+m\cos\theta}e^{2qr_0}.$$

Adding $\lim_{F\to(1/2)_\pm} j_\varphi^{(a)}(r)|_{\theta\neq\pm\pi/2}$ to (5.28) and taking limit $r_0\to 0$, we get

$$\lim_{r_0\to 0}\lim_{F\to(1/2)_\pm} j_\varphi(r)\Big|_{\theta\neq\pm\pi/2} = j_\varphi^{(a)}(r)|_{F=1/2,\theta\neq\pm\pi/2}. \quad (5.29)$$

The limits do commute in special cases only:

$$\lim_{F\to 1/2}\lim_{r_0\to 0} j_\varphi(r)|_{\theta=\pm\pi/2} = \lim_{r_0\to 0}\lim_{F\to 1/2} j_\varphi(r)|_{\theta=\pm\pi/2} = j_\varphi^{(a)}(r)|_{F=1/2,\theta=\pm\pi/2} = \mp\frac{m}{2\pi^2}K_1(2mr); \quad (5.30)$$

the discontinuity at $F=1/2$ is absent in these cases.

We can summarize our results for the current at $F\neq 1/2$ in cases when there is one peculiar mode: (i) $j_\varphi(r)|_{F<1/2,\theta\neq-\pi/2}$ is given by the right-hand side of (5.13) at $\theta\neq-\pi/2$, whereas $j_\varphi(r)|_{F<1/2,\theta=-\pi/2}$ is given by the right-hand side of (5.14) at $\theta=-\pi/2$, and (ii) $j_\varphi(r)|_{F>1/2,\theta\neq\pi/2}$ is given by the right-hand side of (5.14) at $\theta\neq\pi/2$, whereas $j_\varphi(r)|_{F>1/2,\theta=\pi/2}$ is given by the right-hand side of (5.13) at $\theta=\pi/2$. Note also relation

$$j_\varphi(r)|_{F,\theta} = -j_\varphi(r)|_{1-F,-\theta}, \quad (5.31)$$

which holds in all cases considered in the present section.

In the case of $\nu=1$ expression (5.11) takes the form

$$j_\varphi(r)|_{\nu=1} = -\frac{r}{\pi^2}\int_m^\infty \frac{dqq^2}{\sqrt{q^2-m^2}}\left\{\frac{\sin(F\pi)}{\pi}qr[K_{1-F}^2(qr)-K_F^2(qr)] + \left[(2F-1)\frac{\sin(F\pi)}{\pi}+C_{1-F}(qr_0)\right]K_F(qr)K_{1-F}(qr)+\Sigma(qr,qr_0)|_{\nu=1}\right\}, \quad (5.32)$$

where the use is made of (A17) and relation

$$\int_m^\infty \frac{dqq^3}{\sqrt{q^2-m^2}}[K_{1-F}^2(qr)-K_F^2(qr)] = \frac{\pi m}{4r^2}\int_0^\infty \frac{du}{\cosh(u/2)}\left[1+\frac{1}{2mr\cosh(u/2)}\right]e^{-2mr\cosh(u/2)} \times\left\{\tanh(u/2)\sinh\left[\left(F-\frac{1}{2}\right)u\right]-(2F-1)\cosh\left[\left(F-\frac{1}{2}\right)u\right]\right\}. \quad (5.33)$$

Decomposing (5.32) according to (5.15), we get

$$j_\varphi^{(a)}(r)|_{\nu=1,F\neq1/2,\theta\neq\pm\pi/2} = -\frac{r}{\pi^3}\sin(F\pi)\int_m^\infty\frac{dqq^2}{\sqrt{q^2-m^2}}\left\{qr[K_{1-F}^2(qr)-K_F^2(qr)] + \mathrm{sgn}\left(F-\frac{1}{2}\right)(|2F-1|-1)K_F(qr)K_{1-F}(qr)\right\}, \quad (5.34)$$

$$j_\varphi^{(a)}(r)|_{\nu=1,F\neq1/2,\theta=\pm\pi/2} = -\frac{r}{\pi^3}\sin(F\pi)\int_m^\infty\frac{dqq^2}{\sqrt{q^2-m^2}}\{qr[K_{1-F}^2(qr)-K_F^2(qr)] + (2F-1\pm1)K_F(qr)K_{1-F}(qr)\}, \quad (5.35)$$

$j_\varphi^{(a)}(r)|_{\nu=1,F=1/2}$ is given by (5.18), while $j_\varphi^{(b)}(r)|_{\nu=1,F<1/2,\theta\neq-\pi/2}$, $j_\varphi^{(b)}(r)|_{\nu=1,F>1/2,\theta\neq\pi/2}$, $j_\varphi^{(b)}(r)|_{\nu=1,F\neq1/2,\theta=\pm\pi/2}$, and $j_\varphi^{(b)}(r)|_{\nu=1,F=1/2}$ are obtained by putting $\nu=1$ in (5.19), (5.20), (5.21), and (5.22), respectively.

VI. INDUCED VACUUM MAGNETIC FIELD AND ITS FLUX

In the case of $\nu \geq 1$ and $\frac{1}{2}(1-\frac{1}{\nu}) < F < \frac{1}{2}(1+\frac{1}{\nu})$, or $\frac{1}{2} \leq \nu < 1$ and $\frac{1}{2}(\frac{1}{\nu}-1) < F < \frac{1}{2}(3-\frac{1}{\nu})$, we obtain the following expression for B_{I} (2.21):

$$\begin{aligned} B_{\mathrm{I}}(r) = & -\frac{\nu e}{2(2\pi)^2}\frac{1}{r}\left\{\int_0^\infty \frac{du}{\cosh^2(u/2)}\mathrm{e}^{-2mr\cosh(u/2)}\right. \\ & \times \frac{\cos[\nu(F-\frac{1}{2})\pi]\sinh(\nu u)\sinh[\nu(F-\frac{1}{2})u] + \sin[\nu(F-\frac{1}{2})\pi]\sin(\nu\pi)\cosh[\nu(F-\frac{1}{2})u]}{\cosh(\nu u)-\cos(\nu\pi)} \\ & \left. -\frac{2\pi}{\nu}\sum_{p=1}^{[|\nu/2|]}\exp[-2mr\sin(p\pi/\nu)]\frac{\sin[(2F-1)p\pi]}{\sin^2(p\pi/\nu)} + \frac{\pi}{2N}(-1)^N\sin(2NF\pi)\mathrm{e}^{-2mr}\delta_{\nu,2N}\right\} \\ & -\frac{\nu e}{\pi^2}\int_r^\infty dr'\int_m^\infty \frac{dqq^2}{\sqrt{q^2-m^2}}[C_{\frac{1}{2}-\nu(F-\frac{1}{2})}(qr_0)K_{\frac{1}{2}-\nu(F-\frac{1}{2})}(qr')K_{\frac{1}{2}+\nu(F-\frac{1}{2})}(qr') + \Sigma(qr',qr_0)], \end{aligned} \tag{6.1}$$

where $\Sigma(w,v)$ is given by (5.12), while $C_\rho^{(\wedge)}(v)$, $C_\rho^{(\vee)}(v)$, and $C_{1-G}(v)$ are given by (5.7), (5.8), and (5.10), respectively. Expression (6.1) can be decomposed as

$$B_{\mathrm{I}}(r) = B_{\mathrm{I}}^{(a)}(r) + B_{\mathrm{I}}^{(b)}(r), \qquad B_{\mathrm{I}}^{(a)}(r) = \lim_{r_0\to 0} B_{\mathrm{I}}(r), \tag{6.2}$$

where

$$\begin{aligned} B_{\mathrm{I}}^{(a)}(r)|_{F<1/2,\theta\neq-\pi/2} = B_{\mathrm{I}}^{(a)}(r)|_{F>1/2,\theta=\pi/2} = & -\frac{\nu e}{2(2\pi)^2}\frac{1}{r}\left\{\int_0^\infty \frac{du}{\cosh^2(u/2)}\mathrm{e}^{-2mr\cosh(u/2)}\right. \\ & \times \frac{\cos[\nu(F-\frac{1}{2})\pi]\cosh[\nu(F+\frac{1}{2})u] - \cos[\nu(F+\frac{1}{2})\pi)]\cosh[\nu(F-\frac{1}{2})u]}{\cosh(\nu u)-\cos(\nu\pi)} \\ & \left. -\frac{2\pi}{\nu}\sum_{p=1}^{[|\nu/2|]}\exp[-2mr\sin(p\pi/\nu)]\frac{\sin[(2F-1)p\pi]}{\sin^2(p\pi/\nu)} + \frac{\pi}{2N}(-1)^N\sin(2NF\pi)\mathrm{e}^{-2mr}\delta_{\nu,2N}\right\}, \end{aligned} \tag{6.3}$$

$$\begin{aligned} B_{\mathrm{I}}^{(a)}(r)|_{F>1/2,\theta\neq\pi/2} = B_{\mathrm{I}}^{(a)}(r)|_{F<1/2,\theta=-\pi/2} = & \frac{\nu e}{2(2\pi)^2}\frac{1}{r}\left\{\int_0^\infty \frac{du}{\cosh^2(u/2)}\mathrm{e}^{-2mr\cosh(u/2)}\right. \\ & \times \frac{\cos[\nu(F-\frac{1}{2})\pi]\cosh[\nu(F-\frac{3}{2})u] - \cos[\nu(F-\frac{3}{2})\pi)]\cosh[\nu(F-\frac{1}{2})u]}{\cosh(\nu u)-\cos(\nu\pi)} \\ & \left. +\frac{2\pi}{\nu}\sum_{p=1}^{[|\nu/2|]}\exp[-2mr\sin(p\pi/\nu)]\frac{\sin[(2F-1)p\pi]}{\sin^2(p\pi/\nu)} - \frac{\pi}{2N}(-1)^N\sin(2NF\pi)\mathrm{e}^{-2mr}\delta_{\nu,2N}\right\}, \end{aligned} \tag{6.4}$$

$$B_{\mathrm{I}}^{(a)}(r)|_{F=1/2} = -\frac{\nu e\sin\theta}{2\pi^2}\int_m^\infty \frac{dqq^2}{\sqrt{q^2-m^2}}\frac{\Gamma(0,2qr)}{q+m\cos\theta}, \tag{6.5}$$

and

$$\Gamma(z,u) = \int_u^\infty dy y^{z-1}\mathrm{e}^{-y}$$

is the incomplete gamma function. The r_0-dependent part of $B_{\mathrm{I}}(r)$ is given by

$$\begin{aligned} B_{\mathrm{I}}^{(b)}(r)|_{F<1/2,\theta\neq-\pi/2} = & -\frac{\nu e}{\pi^2}\int_r^\infty dr'\int_m^\infty \frac{dqq^2}{\sqrt{q^2-m^2}} \\ & \times\left[C_{\frac{1}{2}-\nu(F-\frac{1}{2})}^{(\wedge)}(qr_0)K_{\frac{1}{2}-\nu(F-\frac{1}{2})}(qr')K_{\frac{1}{2}+\nu(F-\frac{1}{2})}(qr') + \Sigma(qr',qr_0)\right], \end{aligned} \tag{6.6}$$

$$B_{\rm I}^{(b)}(r)|_{F>1/2,\theta\neq\pi/2}=\frac{\nu e}{\pi^2}\int_r^\infty dr'\int_m^\infty\frac{dqq^2}{\sqrt{q^2-m^2}}\times\left[C^{(\vee)}_{\frac{1}{2}+\nu(F-\frac{1}{2})}(qr_0)K_{\frac{1}{2}+\nu(F-\frac{1}{2})}(qr')K_{\frac{1}{2}-\nu(F-\frac{1}{2})}(qr')-\Sigma(qr',qr_0)\right],\tag{6.7}$$

$$\begin{aligned}B_{\rm I}^{(b)}(r)|_{F\neq1/2,\theta=\pm\pi/2}=&\mp\frac{\nu e}{\pi^2}\int_r^\infty dr'\int_m^\infty\frac{dqq^2}{\sqrt{q^2-m^2}}\left\{\frac{I_{\frac{1}{2}\pm\nu(\frac{1}{2}-F)}(qr_0)}{K_{\frac{1}{2}\pm\nu(\frac{1}{2}-F)}(qr_0)}K_{\frac{1}{2}+\nu(F-\frac{1}{2})}(qr')K_{\frac{1}{2}-\nu(F-\frac{1}{2})}(qr')\right.\\&+\sum_{l=1}^\infty\left[\frac{I_{\nu(l-F+\frac{1}{2})\pm\frac{1}{2}}(qr_0)}{K_{\nu(l-F+\frac{1}{2})\pm\frac{1}{2}}(qr_0)}K_{\nu(l-F+\frac{1}{2})+\frac{1}{2}}(qr')K_{\nu(l-F+\frac{1}{2})-\frac{1}{2}}(qr')\right.\\&\left.\left.+\frac{I_{\nu(l+F-\frac{1}{2})\mp\frac{1}{2}}(qr_0)}{K_{\nu(l+F-\frac{1}{2})\mp\frac{1}{2}}(qr_0)}K_{\nu(l+F-\frac{1}{2})+\frac{1}{2}}(qr')K_{\nu(l+F-\frac{1}{2})-\frac{1}{2}}(qr')\right]\right\},\end{aligned}\tag{6.8}$$

$$\begin{aligned}B_{\rm I}^{(b)}(r)|_{F=1/2}=&-\frac{\nu e\sin\theta}{2\pi^2}\int_m^\infty\frac{dqq^2}{\sqrt{q^2-m^2}}\left[\frac{{\rm e}^{2qr_0}-1}{q+m\cos\theta}\Gamma(0,2qr)\right.\\&\left.+4\int_r^\infty dr'\sum_{l=1}^\infty\tilde{C}_{\nu l+\frac{1}{2}}(qr_0)K_{\nu l+\frac{1}{2}}(qr')K_{\nu l-\frac{1}{2}}(qr')\right],\end{aligned}\tag{6.9}$$

and $\tilde{C}_{\nu l+\frac{1}{2}}(v)$ is given by (5.23).

In the case of $\nu>1$ and $0<F<\frac{1}{2}(1-\frac{1}{\nu})$, the induced vacuum magnetic field is given by (6.2) with $B_{\rm I}^{(a)}$ given by the right-hand side of (6.3) and $B_{\rm I}^{(b)}$ given by the right-hand side of (6.6). In the case of $\nu>1$ and $\frac{1}{2}(1+\frac{1}{\nu})<F<1$, the induced vacuum magnetic field is given by (6.2) with $B_{\rm I}^{(a)}$ given by the right-hand side of (6.4) and $B_{\rm I}^{(b)}$ given by the right-hand side of (6.7).

Turning to the total flux of the induced vacuum magnetic field, [see (2.22)], we present it as

$$\Phi_{\rm I}=\Phi_{\rm I}^{(a)}+\Phi_{\rm I}^{(b)},\tag{6.10}$$

where

$$\Phi_{\rm I}^{(a)}=\frac{2\pi}{\nu}\int_{r_0}^\infty drrB_{\rm I}^{(a)}(r),\qquad\Phi_{\rm I}^{(b)}=\frac{2\pi}{\nu}\int_{r_0}^\infty drrB_{\rm I}^{(b)}(r).\tag{6.11}$$

We obtain in the case of $\nu\geq1$ and $\frac{1}{2}(1-\frac{1}{\nu})<F<\frac{1}{2}(1+\frac{1}{\nu})$, or $\frac{1}{2}\leq\nu<1$ and $\frac{1}{2}(\frac{1}{\nu}-1)<F<\frac{1}{2}(3-\frac{1}{\nu})$,

$$\begin{aligned}\Phi_{\rm I}^{(a)}|_{F<1/2,\theta\neq-\pi/2}=\Phi_{\rm I}^{(a)}(r)|_{F>1/2,\theta=\pi/2}=&-\frac{e}{8\pi}\frac{1}{m}\left\{\int_0^\infty\frac{du}{\cosh^3(u/2)}{\rm e}^{-2mr_0\cosh(u/2)}\right.\\&\times\frac{\cos[\nu(F-\frac{1}{2})\pi]\cosh[\nu(F+\frac{1}{2})u]-\cos[\nu(F+\frac{1}{2})\pi)]\cosh[\nu(F-\frac{1}{2})u]}{\cosh(\nu u)-\cos(\nu\pi)}\\&\left.-\frac{2\pi}{\nu}\sum_{p=1}^{[|\nu/2|]}\exp[-2mr_0\sin(p\pi/\nu)]\frac{\sin[(2F-1)p\pi]}{\sin^3(p\pi/\nu)}+\frac{\pi}{2N}(-1)^N\sin(2NF\pi){\rm e}^{-2mr_0}\delta_{\nu,2N}\right\},\end{aligned}\tag{6.12}$$

$$\begin{aligned}\Phi_{\rm I}^{(a)}|_{F>1/2,\theta\neq\pi/2}=\Phi_{\rm I}^{(a)}(r)|_{F<1/2,\theta=-\pi/2}=&\frac{e}{8\pi}\frac{1}{m}\left\{\int_0^\infty\frac{du}{\cosh^3(u/2)}{\rm e}^{-2mr_0\cosh(u/2)}\right.\\&\times\frac{\cos[\nu(F-\frac{1}{2})\pi]\cosh[\nu(F-\frac{3}{2})u]-\cos[\nu(F-\frac{3}{2})\pi)]\cosh[\nu(F-\frac{1}{2})u]}{\cosh(\nu u)-\cos(\nu\pi)}\\&\left.+\frac{2\pi}{\nu}\sum_{p=1}^{[|\nu/2|]}\exp[-2mr_0\sin(p\pi/\nu)]\frac{\sin[(2F-1)p\pi]}{\sin^3(p\pi/\nu)}-\frac{\pi}{2N}(-1)^N\sin(2NF\pi){\rm e}^{-2mr_0}\delta_{\nu,2N}\right\},\end{aligned}\tag{6.13}$$

and

$$\Phi_{\mathrm{I}}^{(a)}|_{F=1/2} = -\frac{e\sin\theta}{8\pi}\int_m^\infty \frac{dq}{\sqrt{q^2-m^2}}\frac{1}{q+m\cos\theta}[\Gamma(2,2qr_0)-4q^2r_0^2\Gamma(0,2qr_0)]. \tag{6.14}$$

In the case of $\nu > 1$ and $0 < F < \frac{1}{2}(1-\frac{1}{\nu})$, $\Phi_{\mathrm{I}}^{(a)}$ is given by the right-hand side of (6.12). In the case of $\nu > 1$ and $\frac{1}{2}(1+\frac{1}{\nu}) < F < 1$, $\Phi_{\mathrm{I}}^{(a)}$ is given by the right-hand side of (6.13).

As follows from (6.12)–(6.14), $\Phi_{\mathrm{I}}^{(a)}$ is damped exponentially at $r_0 \to \infty$. In the case of the opposite limit, i.e., at $r_0 \to 0$, all integrations in $\Phi_{\mathrm{I}}^{(a)}$ can be explicitly performed. It is straightforward to obtain

$$\lim_{r_0\to 0}\Phi_{\mathrm{I}}^{(a)}|_{F=1/2} = -\frac{e}{4\pi m}\arctan\left(\tan\frac{\theta}{2}\right). \tag{6.15}$$

The analysis at $F \neq 1/2$ requires more efforts. Let us consider first the case of $\nu > 1$ and present $j_\varphi^{(a)}$ defined in (5.15) as

$$\begin{aligned} j_\varphi^{(a)}(r)|_{\frac{1}{2}(1-\frac{1}{\nu})<F<\frac{1}{2},\theta\neq-\frac{\pi}{2}} &= j_\varphi^{(a)}(r)|_{\frac{1}{2}<F<\frac{1}{2}(1+\frac{1}{\nu}),\theta=\frac{\pi}{2}} = j_\varphi^{(a)}(r)|_{0<F<\frac{1}{2}(1-\frac{1}{\nu})} \\ &= j_\varphi^{(1,1)}(r)+j_\varphi^{(1,2)}(r)-2j_\varphi^{(1,3)}(r) = \frac{m}{8\pi}\frac{1}{2\pi\mathrm{i}}\int_{C_0}dz\left[1+\frac{1}{2mr\sqrt{-\sinh^2(z/2)}}\right] \\ &\quad\times\exp\left[-2mr\sqrt{-\sinh^2(z/2)}\right]\frac{\sinh(\nu Fz)}{\sinh(z/2)\sinh(\nu z/2)} \end{aligned} \tag{6.16}$$

and

$$\begin{aligned} j_\varphi^{(a)}(r)|_{\frac{1}{2}<F<\frac{1}{2}(1+\frac{1}{\nu}),\theta\neq\frac{\pi}{2}} &= j_\varphi^{(a)}(r)|_{\frac{1}{2}(1-\frac{1}{\nu})<F<\frac{1}{2},\theta=-\frac{\pi}{2}} = j_\varphi^{(a)}(r)|_{\frac{1}{2}(1+\frac{1}{\nu})<F<1} \\ &= j_\varphi^{(1,1)}(r)+j_\varphi^{(1,2)}(r) = -\frac{m}{8\pi}\frac{1}{2\pi\mathrm{i}}\int_{C_0}dz\left[1+\frac{1}{2mr\sqrt{-\sinh^2(z/2)}}\right] \\ &\quad\times\exp\left[-2mr\sqrt{-\sinh^2(z/2)}\right]\frac{\sinh[\nu(1-F)z]}{\sinh(z/2)\sinh(\nu z/2)}, \end{aligned} \tag{6.17}$$

where $j_\varphi^{(1,1)}$, $j_\varphi^{(1,2)}$, and $j_\varphi^{(1,3)}$ are given by (A13), (A15), and (A18) in Appendix A and contour C_0 in the complex z plane is depicted in Fig. 8. Consequently, we get

$$\begin{aligned} B_{\mathrm{I}}^{(a)}(r)|_{\frac{1}{2}(1-\frac{1}{\nu})<F<\frac{1}{2},\theta\neq-\frac{\pi}{2}} &= B_{\mathrm{I}}^{(a)}(r)|_{\frac{1}{2}<F<\frac{1}{2}(1+\frac{1}{\nu}),\theta=\frac{\pi}{2}} = B_{\mathrm{I}}^{(a)}(r)|_{0<F<\frac{1}{2}(1-\frac{1}{\nu})} \\ &= \frac{\nu e}{16\pi r}\frac{1}{2\pi\mathrm{i}}\int_{C_0}dz\frac{\exp\left[-2mr\sqrt{-\sinh^2(z/2)}\right]}{\sqrt{-\sinh^2(z/2)}}\frac{\sinh(\nu Fz)}{\sinh(z/2)\sinh(\nu z/2)}, \end{aligned} \tag{6.18}$$

$$\begin{aligned} B_{\mathrm{I}}^{(a)}(r)|_{\frac{1}{2}<F<\frac{1}{2}(1+\frac{1}{\nu}),\theta\neq\frac{\pi}{2}} &= B_{\mathrm{I}}^{(a)}(r)|_{\frac{1}{2}(1-\frac{1}{\nu})<F<\frac{1}{2},\theta=-\frac{\pi}{2}} = B_{\mathrm{I}}^{(a)}(r)|_{\frac{1}{2}(1+\frac{1}{\nu})<F<1} \\ &= -\frac{\nu e}{16\pi r}\frac{1}{2\pi\mathrm{i}}\int_{C_0}dz\frac{\exp\left[-2mr\sqrt{-\sinh^2(z/2)}\right]}{\sqrt{-\sinh^2(z/2)}}\frac{\sinh[\nu(1-F)z]}{\sinh(z/2)\sinh(\nu z/2)}, \end{aligned} \tag{6.19}$$

$$\begin{aligned} \lim_{r_0\to0}\Phi_{\mathrm{I}}^{(a)}|_{\frac{1}{2}(1-\frac{1}{\nu})<F<\frac{1}{2},\theta\neq-\frac{\pi}{2}} &= \lim_{r_0\to0}\Phi_{\mathrm{I}}^{(a)}\Big|_{\frac{1}{2}<F<\frac{1}{2}(1+\frac{1}{\nu}),\theta=\frac{\pi}{2}} = \lim_{r_0\to0}\Phi_{\mathrm{I}}^{(a)}\Big|_{0<F<\frac{1}{2}(1-\frac{1}{\nu})} \\ &= -\frac{e}{16m}\frac{1}{2\pi\mathrm{i}}\int_{C_0}dz\frac{\sinh(\nu Fz)}{\sinh^3(z/2)\sinh(\nu z/2)}, \end{aligned} \tag{6.20}$$

and

$$\lim_{r_0\to 0}\Phi_{\rm I}^{(a)}\Big|_{\frac{1}{2}<F<\frac{1}{2}(1+\frac{1}{\nu}),\theta\neq\frac{\pi}{2}} = \lim_{r_0\to 0}\Phi_{\rm I}^{(a)}\Big|_{\frac{1}{2}(1-\frac{1}{\nu})<F<\frac{1}{2},\theta=-\frac{\pi}{2}} = \lim_{r_0\to 0}\Phi_{\rm I}^{(a)}\Big|_{\frac{1}{2}(1+\frac{1}{\nu})<F<1} = \frac{e}{16m}\frac{1}{2\pi i}\int_{C_0} dz\frac{\sinh[\nu(1-F)z]}{\sinh^3(z/2)\sinh(\nu z/2)}. \tag{6.21}$$

Only a simple pole at $z=0$ of the integrands contributes to the integrals in (6.20) and (6.21). Calculation of its residue yields

$$\lim_{r_0\to 0}\Phi_{\rm I}^{(a)}\Big|_{\frac{1}{2}(1-\frac{1}{\nu})<F<\frac{1}{2},\theta\neq-\frac{\pi}{2}} = \lim_{r_0\to 0}\Phi_{\rm I}^{(a)}\Big|_{\frac{1}{2}<F<\frac{1}{2}(1+\frac{1}{\nu}),\theta=\frac{\pi}{2}} = \lim_{r_0\to 0}\Phi_{\rm I}^{(a)}\Big|_{0<F<\frac{1}{2}(1-\frac{1}{\nu})} = -\frac{e}{6m}F\left[\frac{1}{4}(\nu^2+3)-\nu^2F^2\right] \tag{6.22}$$

and

$$\lim_{r_0\to 0}\Phi_{\rm I}^{(a)}\Big|_{\frac{1}{2}<F<\frac{1}{2}(1+\frac{1}{\nu}),\theta\neq\frac{\pi}{2}} = \lim_{r_0\to 0}\Phi_{\rm I}^{(a)}\Big|_{\frac{1}{2}(1-\frac{1}{\nu})<F<\frac{1}{2},\theta=-\frac{\pi}{2}} = \lim_{r_0\to 0}\Phi_{\rm I}^{(a)}\Big|_{\frac{1}{2}(1+\frac{1}{\nu})<F<1} = \frac{e}{6m}(1-F)\left[\frac{1}{4}(\nu^2+3)-\nu^2(1-F)^2\right]. \tag{6.23}$$

Considering the case of $\frac{1}{2}<\nu\leq 1$ and $\frac{1}{2}(\frac{1}{\nu}-1)<F<\frac{1}{2}(3-\frac{1}{\nu})$ at $F\neq 1/2$, we obtain that

$$\lim_{r_0\to 0}\Phi_{\rm I}^{(a)}\Big|_{\frac{1}{2}(\frac{1}{\nu}-1)<F<\frac{1}{2},\theta\neq-\frac{\pi}{2}} = \lim_{r_0\to 0}\Phi_{\rm I}^{(a)}\Big|_{\frac{1}{2}<F<\frac{1}{2}(3-\frac{1}{\nu}),\theta=\frac{\pi}{2}}$$

and

$$\lim_{r_0\to 0}\Phi_{\rm I}^{(a)}\Big|_{\frac{1}{2}<F<\frac{1}{2}(3-\frac{1}{\nu}),\theta\neq\frac{\pi}{2}} = \lim_{r_0\to 0}\Phi_{\rm I}^{(a)}\Big|_{\frac{1}{2}(\frac{1}{\nu}-1)<F<\frac{1}{2},\theta=-\frac{\pi}{2}}$$

are given by the right-hand sides of (6.22) and (6.23), respectively. Note that $\lim_{r_0\to 0}\Phi_{\rm I}^{(a)}|_{\theta\neq\pm\pi/2}$ is discontinuous at $F=1/2$ and its limiting values are independent of ν:

$$\lim_{F\to(1/2)_+}\lim_{r_0\to 0}\Phi_{\rm I}^{(a)}\Big|_{\theta\neq\pm\pi/2} = -\lim_{F\to(1/2)_-}\lim_{r_0\to 0}\Phi_{\rm I}^{(a)}\Big|_{\theta\neq\pm\pi/2} = \frac{e}{16m}; \tag{6.24}$$

this is clearly a consequence of (5.26).

As for the remaining part of the total flux, $\Phi_{\rm I}^{(b)}$, it can be presented as

$$\Phi_{\rm I}^{(b)} = e\pi\int_{r_0}^{\infty}\frac{dr}{r}j_\varphi^{(b)}(r)(r^2-r_0^2), \tag{6.25}$$

provided that the following condition holds:

$$\lim_{r\to r_0} j_\varphi^{(b)}(r)(r-r_0)^2 = 0; \tag{6.26}$$

otherwise, the total flux diverges.

By performing a numerical analysis, we find that quantity $\lim_{r\to r_0}\nu r j_\varphi(r)(\frac{r-r_0}{r_0})^2$ depends on θ, actually being independent of other parameters (F, ν, and mr_0); see Fig. 1. As follows from this analysis, relation (6.26) is fulfilled in cases $\theta=0$ and $\theta=\pi$ only. The case of $F=1/2$ needs a special comment, since, due to relation (5.31), the current in this case is an odd function of θ. Whereas the current and, consequently, the induced magnetic field with its flux vanish at $\theta=0$, they can be nonvanishing if discontinuous at $\theta=\pi$. Indeed, periodicity in θ with period 2π,

$$j_\varphi(r)|_{F=1/2,\theta=\pi_\pm} = j_\varphi(r)|_{F=1/2,\theta=-\pi_\mp}, \tag{6.27}$$

together with oddness in θ,

$$j_\varphi(r)|_{F=1/2,\theta=\pi_\pm} = -j_\varphi(r)|_{F=1/2,\theta=-\pi_\pm}, \tag{6.28}$$

results in

$$j_\varphi(r)|_{F=1/2,\theta=\pi_\pm} = -j_\varphi(r)|_{F=1/2,\theta=\pi_\mp}. \tag{6.29}$$

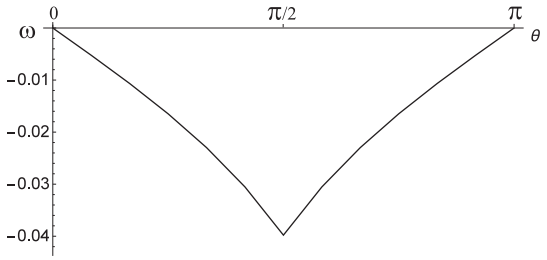

FIG. 1. $\omega(\theta)=\lim_{r\to r_0}\nu r j_\varphi(r)(\frac{r-r_0}{r_0})^2$ is the same at $\nu=3/4,1,2,3,5,10$; $mr_0=10^{-5},10^{-3},10^{-2},10^{-1},1$; and different values of F.

Namely this is obtained from the appropriate formulas at $F = 1/2$ and $\theta = \pi_\pm$:

$$j_\varphi(r)|_{F=1/2,\theta=\pi_\pm} = \pm\frac{m}{2\pi}e^{2m(r_0-r)}. \tag{6.30}$$

As a consequence, we obtain

$$B_{\rm I}(r)|_{F=1/2,\theta=\pi_\pm} = \pm\frac{e\nu m}{2\pi}e^{2mr_0}\Gamma(0,2mr) \tag{6.31}$$

and

$$\Phi_{\rm I}|_{F=1/2,\theta=\pi_\pm} = \pm\frac{e}{8m}e^{2mr_0}[\Gamma(2,2mr_0) - 4m^2r_0^2\Gamma(0,2mr_0)]; \tag{6.32}$$

in particular [cf. (6.15)],

$$\lim_{r_0\to 0}\Phi_{\rm I}|_{F=1/2,\theta=\pi_\pm} = \pm\frac{e}{8m}. \tag{6.33}$$

In the case of $F \neq 1/2$ continuity in θ is maintained, and the induced vacuum current in this case takes the form

$$\begin{aligned}
j_\varphi(r)|_{\theta=\frac{\pi}{2}\mp\frac{\pi}{2}} = {}& \frac{m}{(2\pi)^2}\left\{\mathrm{sgn}\left(F-\frac{1}{2}\right)\int_0^\infty\frac{du}{\cosh(u/2)}\left[1+\frac{1}{2mr\cosh(u/2)}\right]\mathrm{e}^{-2mr\cosh(u/2)}\right.\\
&\times\frac{\cos[\nu(F-\frac{1}{2})\pi)]\cosh[\nu(|F-\frac{1}{2}|-1)u] - \cos[\nu(|F-\frac{1}{2}|-1)\pi]\cosh[\nu(F-\frac{1}{2})u]}{\cosh(\nu u)-\cos(\nu\pi)}\\
&+\frac{2\pi}{\nu}\sum_{p=1}^{[|\nu/2|]}\left[1+\frac{1}{2mr\sin(p\pi/\nu)}\right]\exp[-2mr\sin(p\pi/\nu)]\frac{\sin[(2F-1)p\pi]}{\sin(p\pi/\nu)}\\
&\left.-\frac{\pi}{2N}(-1)^N\sin(2NF\pi)\left(1+\frac{1}{2mr}\right)\mathrm{e}^{-2mr}\delta_{\nu,2N}\right\} + \frac{r}{\pi^2}\int_m^\infty\frac{dqq^2}{\sqrt{q^2-m^2}}\left\{\frac{1}{2}\left[C^{(\pm)}_{\frac{1}{2}+\nu(F-\frac{1}{2})}(qr_0) - C^{(\pm)}_{\frac{1}{2}-\nu(F-\frac{1}{2})}(qr_0)\right.\right.\\
&\left.+\mathrm{sgn}\left(F-\frac{1}{2}\right)(C^{(\pm)}_{\frac{1}{2}+\nu(F-\frac{1}{2})}(qr_0)+C^{(\pm)}_{\frac{1}{2}-\nu(F-\frac{1}{2})}(qr_0))\right]K_{\frac{1}{2}+\nu(F-\frac{1}{2})}(qr)K_{\frac{1}{2}-\nu(F-\frac{1}{2})}(qr)\\
&\left.+\sum_{l=1}^\infty[C^{(\pm)}_{\nu(l+F-\frac{1}{2})+\frac{1}{2}}(qr_0)K_{\nu(l+F-\frac{1}{2})+\frac{1}{2}}(qr)K_{\nu(l+F-\frac{1}{2})-\frac{1}{2}}(qr) - C^{(\pm)}_{\nu(l-F+\frac{1}{2})+\frac{1}{2}}(qr_0)K_{\nu(l-F+\frac{1}{2})+\frac{1}{2}}(qr)K_{\nu(l-F+\frac{1}{2})-\frac{1}{2}}(qr)]\right\},
\end{aligned} \tag{6.34}$$

where

$$\begin{aligned}
C^{(\pm)}_\rho(v) = {}& \{vI_\rho(v)K_\rho(v) \pm mr_0[I_\rho(v)K_{\rho-1}(v) - I_{\rho-1}(v)K_\rho(v)] - vI_{\rho-1}(v)K_{\rho-1}(v)\}\\
&\times[vK^2_\rho(v) \pm 2mr_0K_\rho(v)K_{\rho-1}(v) + vK^2_{\rho-1}(v)]^{-1}.
\end{aligned} \tag{6.35}$$

Consequently, we obtain the following expressions for the induced vacuum magnetic field:

$$\begin{aligned}
B_{\rm I}(r)|_{\theta=\frac{\pi}{2}\mp\frac{\pi}{2}} = {}& \frac{\nu e}{2(2\pi)^2}\frac{1}{r}\left\{\mathrm{sgn}\left(F-\frac{1}{2}\right)\int_0^\infty\frac{du}{\cosh^2(u/2)}\mathrm{e}^{-2mr\cosh(u/2)}\right.\\
&\times\frac{\cos[\nu(F-\frac{1}{2})\pi)]\cosh[\nu(|F-\frac{1}{2}|-1)u] - \cos[\nu(|F-\frac{1}{2}|-1)\pi]\cosh[\nu(F-\frac{1}{2})u]}{\cosh(\nu u)-\cos(\nu\pi)}\\
&\left.+\frac{2\pi}{\nu}\sum_{p=1}^{[|\nu/2|]}\exp[-2mr\sin(p\pi/\nu)]\frac{\sin[(2F-1)p\pi]}{\sin^2(p\pi/\nu)} - \frac{\pi}{2N}(-1)^N\sin(2NF\pi)\mathrm{e}^{-2mr}\delta_{\nu,2N}\right\}\\
&+\frac{\nu e}{\pi^2}\int_r^\infty dr'\int_m^\infty\frac{dqq^2}{\sqrt{q^2-m^2}}\left\{\frac{1}{2}\left[C^{(\pm)}_{\frac{1}{2}+\nu(F-\frac{1}{2})}(qr_0) - C^{(\pm)}_{\frac{1}{2}-\nu(F-\frac{1}{2})}(qr_0) + \mathrm{sgn}\left(F-\frac{1}{2}\right)(C^{(\pm)}_{\frac{1}{2}+\nu(F-\frac{1}{2})}(qr_0)\right.\right.\\
&\left.+C^{(\pm)}_{\frac{1}{2}-\nu(F-\frac{1}{2})}(qr_0))\right]K_{\frac{1}{2}+\nu(F-\frac{1}{2})}(qr')K_{\frac{1}{2}-\nu(F-\frac{1}{2})}(qr') + \sum_{l=1}^\infty[C^{(\pm)}_{\nu(l+F-\frac{1}{2})+\frac{1}{2}}(qr_0)K_{\nu(l+F-\frac{1}{2})+\frac{1}{2}}(qr')K_{\nu(l+F-\frac{1}{2})-\frac{1}{2}}(qr')\\
&\left.-C^{(\pm)}_{\nu(l-F+\frac{1}{2})+\frac{1}{2}}(qr_0)K_{\nu(l-F+\frac{1}{2})+\frac{1}{2}}(qr')K_{\nu(l-F+\frac{1}{2})-\frac{1}{2}}(qr')]\right\}, \qquad F\neq 1/2,
\end{aligned} \tag{6.36}$$

and its flux,

$$\Phi_{\rm I}|_{\theta=\frac{\pi}{2}\mp\frac{\pi}{2}}=\frac{e}{8\pi}\frac{1}{m}\left\{\mathrm{sgn}\left(F-\frac{1}{2}\right)\int_0^\infty\frac{du}{\cosh^3(u/2)}\mathrm{e}^{-2mr_0\cosh(u/2)}\right.$$
$$\times\frac{\cos\left[\nu(F-\frac{1}{2})\pi\right)]\cosh\left[\nu(|F-\frac{1}{2}|-1)u\right]-\cos\left[\nu(|F-\frac{1}{2}|-1)\pi\right]\cosh\left[\nu(F-\frac{1}{2})u\right]}{\cosh(\nu u)-\cos(\nu\pi)}$$
$$\left.+\frac{2\pi}{\nu}\sum_{p=1}^{[|\nu/2|]}\exp[-2mr_0\sin(p\pi/\nu)]\frac{\sin[(2F-1)p\pi]}{\sin^3(p\pi/\nu)}-\frac{\pi}{2N}(-1)^N\sin(2NF\pi)\mathrm{e}^{-2mr_0}\delta_{\nu,2N}\right\}$$
$$+\frac{e}{\pi}\int_{r_0}^\infty dr(r^2-r_0^2)\int_m^\infty\frac{dqq^2}{\sqrt{q^2-m^2}}\left\{\frac{1}{2}\left[C^{(\pm)}_{\frac{1}{2}+\nu(F-\frac{1}{2})}(qr_0)-C^{(\pm)}_{\frac{1}{2}-\nu(F-\frac{1}{2})}(qr_0)\right.\right.$$
$$\left.+\mathrm{sgn}\left(F-\frac{1}{2}\right)(C^{(\pm)}_{\frac{1}{2}+\nu(F-\frac{1}{2})}(qr_0)+C^{(\pm)}_{\frac{1}{2}-\nu(F-\frac{1}{2})}(qr_0))\right]K_{\frac{1}{2}+\nu(F-\frac{1}{2})}(qr)K_{\frac{1}{2}-\nu(F-\frac{1}{2})}(qr)$$
$$\left.+\sum_{l=1}^\infty[C^{(\pm)}_{\nu(l+F-\frac{1}{2})+\frac{1}{2}}(qr_0)K_{\nu(l+F-\frac{1}{2})+\frac{1}{2}}(qr)K_{\nu(l+F-\frac{1}{2})-\frac{1}{2}}(qr)-C^{(\pm)}_{\nu(l-F+\frac{1}{2})+\frac{1}{2}}(qr_0)K_{\nu(l-F+\frac{1}{2})+\frac{1}{2}}(qr)K_{\nu(l-F+\frac{1}{2})-\frac{1}{2}}(qr)]\right\},$$
$$F\neq 1/2. \tag{6.37}$$

With the use of relations (see [42])

$$\int_v^\infty dwwK_\rho^2(w)=\frac{v^2}{2}\left[\frac{d}{dv}K_\rho(v)\right]^2-\frac{v^2+\rho^2}{2}K_\rho^2(v),$$
$$\int_v^\infty\frac{dw}{w}K_\rho(w)K_{\rho'}(w)=\frac{v}{\rho^2-\rho'^2}\left[K_\rho(v)\frac{d}{dv}K_{\rho'}(v)-K_{\rho'}(v)\frac{d}{dv}K_\rho(v)\right],$$

and the Schläfli contour integral representation for the Macdonald function,[2]

$$K_\rho(w)=\frac{1}{4\mathrm{i}\sin(\rho\pi)}\int_{C_0}dz\mathrm{e}^{w\cosh z+\rho z},$$

the integration over r can be performed. As a result, we obtain the following representation for the induced vacuum magnetic flux

$$\Phi_{\rm I}|_{\theta=\frac{\pi}{2}\mp\frac{\pi}{2}}=\frac{e}{8\pi}\frac{1}{m}\left\{\mathrm{sgn}\left(F-\frac{1}{2}\right)\int_0^\infty\frac{du}{\cosh^3(u/2)}\mathrm{e}^{-2mr_0\cosh(u/2)}\right.$$
$$\times\frac{\cos[\nu(F-\frac{1}{2})\pi)]\cosh[\nu(|F-\frac{1}{2}|-1)u]-\cos[\nu(|F-\frac{1}{2}|-1)\pi]\cosh[\nu(F-\frac{1}{2})u]}{\cosh(\nu u)-\cos(\nu\pi)}$$
$$\left.+\frac{2\pi}{\nu}\sum_{p=1}^{[|\nu/2|]}\exp[-2mr_0\sin(p\pi/\nu)]\frac{\sin[(2F-1)p\pi]}{\sin^3(p\pi/\nu)}-\frac{\pi}{2N}(-1)^N\sin(2NF\pi)\mathrm{e}^{-2mr_0}\delta_{\nu,2N}\right\}$$
$$+\frac{e}{2\pi}r_0\int_{mr_0}^\infty\frac{dvv}{\sqrt{v^2-m^2r_0^2}}\left\{\frac{1}{2}\left[C^{(\pm)}_{\frac{1}{2}+\nu(F-\frac{1}{2})}(v)-C^{(\pm)}_{\frac{1}{2}-\nu(F-\frac{1}{2})}(v)\right.\right.$$
$$\left.+\mathrm{sgn}\left(F-\frac{1}{2}\right)\left(C^{(\pm)}_{\frac{1}{2}+\nu(F-\frac{1}{2})}(v)+C^{(\pm)}_{\frac{1}{2}-\nu(F-\frac{1}{2})}(v)\right)\right]D_{\frac{1}{2}+\nu|F-\frac{1}{2}|}(v)$$
$$\left.+\sum_{l=1}^\infty[C^{(\pm)}_{\nu(l+F-\frac{1}{2})+\frac{1}{2}}(v)D_{\nu(l+F-\frac{1}{2})+\frac{1}{2}}(v)-C^{(\pm)}_{\nu(l-F+\frac{1}{2})+\frac{1}{2}}(v)D_{\nu(l-F+\frac{1}{2})+\frac{1}{2}}(v)]\right\},\qquad F\neq 1/2, \tag{6.38}$$

[2]There are no poles in this case, and contour C_0 can be straightened to two horizontal lines at $z=\pm\mathrm{i}\pi$.

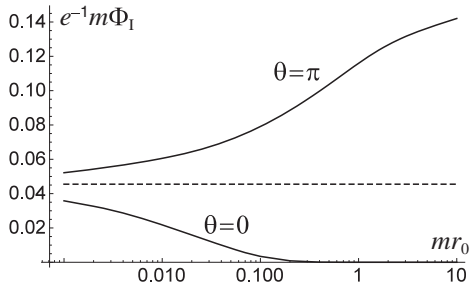

FIG. 2. The dimensionless induced flux, $e^{-1}m\Phi_{\mathrm{I}}|_{\theta=\frac{\pi}{2}\mp\frac{\pi}{2}}$, as a function of mr_0 at $\nu=1$ and $F=0.7$ (solid lines); the dashed line corresponds to the case of $mr_0=0$.

where

$$D_\rho(v)=\rho K_\rho^2(v)-(\rho-1)K_{\rho+1}(v)K_{\rho-1}(v)+v\left[K_\rho(v)\frac{d}{d\rho}K_{\rho-1}(v)-K_{\rho-1}(v)\frac{d}{d\rho}K_\rho(v)\right]; \tag{6.39}$$

in particular,

$$\lim_{r_0\to 0}\Phi_{\mathrm{I}}|_{\theta=\frac{\pi}{2}\mp\frac{\pi}{2}}=-\frac{e}{6m}\left[F-\frac{1}{2}-\frac{1}{2}\mathrm{sgn}\left(F-\frac{1}{2}\right)\right]\times\left\{\frac{3}{4}-\nu^2\left[\frac{1}{4}-\left|F-\frac{1}{2}\right|-F(1-F)\right]\right\},\quad F\neq 1/2. \tag{6.40}$$

As follows from (5.31), $j_\varphi(r)|_{F\neq\frac{1}{2},\theta=\frac{\pi}{2}\mp\frac{\pi}{2}}$ and, consequently, $\Phi_{\mathrm{I}}|_{F\neq\frac{1}{2},\theta=\frac{\pi}{2}\mp\frac{\pi}{2}}$ changes signs under $F\to 1-F$. To be more precise, the dimensionless induced vacuum magnetic flux, $e^{-1}m\Phi_{\mathrm{I}}|_{F\neq\frac{1}{2},\theta=\frac{\pi}{2}\mp\frac{\pi}{2}}$, is positive at $F>1/2$ and negative at $F<1/2$; its absolute value increases with the increase of ν. Whereas $\Phi_{\mathrm{I}}|_{F=\frac{1}{2},\theta=0}$ vanishes, $e^{-1}m\Phi_{\mathrm{I}}|_{F=\frac{1}{2},\theta=\pi_+}$ is positive and $e^{-1}m\Phi_{\mathrm{I}}|_{F=\frac{1}{2},\theta=\pi_-}$ is negative, being of the same absolute value that is independent of ν; see (6.32). Continuity of the results in θ is broken at $\theta=\pi$ and $F=1/2$ only.

A more detailed analysis of the behavior of the induced vacuum magnetic flux can be obtained with the use of numerical computations. Taking $F=0.7$ and $\nu=1$, we calculate the dimensionless flux, $e^{-1}m\Phi_{\mathrm{I}}|_{\theta=\frac{\pi}{2}\mp\frac{\pi}{2}}$, as a function of mr_0; see Fig. 2. In the case of $\theta=0$, this function decreases with the increase of mr_0, becoming vanishingly small ($\lesssim 10^{-7}$) at $mr_0\geq 1$. On the contrary, in the case of $\theta=\pi$, this function increases at no allowance with the increase of mr_0.

The dimensionless flux in the case of $\theta=0$ at several values of ν, as well as of mr_0, is presented as a function of F in Fig. 3. As mr_0 increases, the absolute value of this function decreases as compared to the value at $mr_0=0$, becoming negligible in the vicinity of $F=1/2$. However, the vicinity is shrinked as ν increases (this is also demonstrated by Fig. 4), and the flux at $mr_0\geq 1$ can equal its value at $mr_0=0$ for sufficiently large values of ν, unless $F=1/2$.

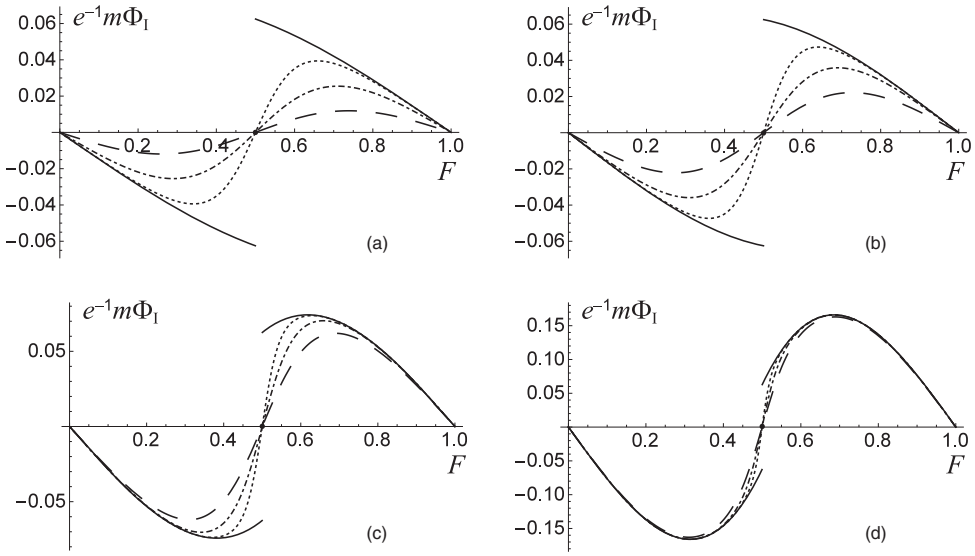

FIG. 3. The dimensionless induced flux at $\theta=0$ as a function of F in the cases of $mr_0=0$ (solid line), $mr_0=10^{-5}$ (dotted line), $mr_0=10^{-3}$ (dash-dotted line), and $mr_0=10^{-2}$ (dashed line): (a) $\nu=3/4$, (b) $\nu=1$, (c) $\nu=2$, and (d) $\nu=4$. The point at $F=1/2$ corresponds to the case of $mr_0=0$.

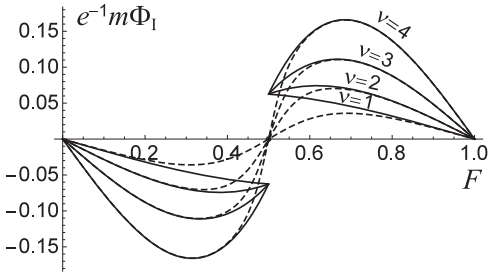

FIG. 4. The dimensionless induced flux at $\theta = 0$ as a function of F in the cases of $mr_0 = 0$ (solid lines) and $mr_0 = 10^{-3}$ (dashed lines).

The dimensionless flux in the case of $\theta = \pi$ at several values of ν, as well as of mr_0, is presented as a function of F on Fig. 5. In the case of $\frac{1}{2} < \nu \leq 2$ the absolute value of this function increases with the increase of mr_0; see Figs. 5(a) and 5(b). However, in the case of $\nu > 2$, the increase takes place in the vicinity of $F = 1/2$ and, otherwise, there is a decrease; see Figs. 5(c) and 5(d) [this is also demonstrated by Fig. 6(a)]. Note that the flux at large values of mr_0 fails to depend on ν (lines corresponding to different values of ν merge together) at least in the case of $\frac{1}{2} < \nu \leq 4$; see Fig. 6(b).

VII. SUMMARY AND DISCUSSION

In the present paper, we have studied the impact of boundary conditions at the edge of the ANO vortex core on the vacuum polarization effects in quantum relativistic spinor matter in two-dimensional space. The most general boundary condition that is compatible with the self-adjointness of the energy operator in first-quantized theory, Dirac Hamiltonian (2.15), is [see (4.2) and (4.7)]

$$(I - \mathrm{i}\beta\alpha^r e^{-\mathrm{i}\theta\alpha^r})\psi|_{r=r_0} = 0, \tag{7.1}$$

where θ is the self-adjoint extension parameter. This condition is also the most general one ensuring the impenetrability of the vortex core edge, i.e., the confinement of the matter field to the region out of the vortex core. We find that a current circulating in the vacuum around the vortex is given by expression (5.11) in the case of $\nu \geq 1$ and $\frac{1}{2}(1-\frac{1}{\nu}) < F < \frac{1}{2}(1+\frac{1}{\nu})$, or $\frac{1}{2} \leq \nu < 1$ and $\frac{1}{2}(\frac{1}{\nu}-1) < F < \frac{1}{2}(3-\frac{1}{\nu})$; it is given by expression (5.13) in the case of $\nu > 1$ and $0 < F < \frac{1}{2}(1-\frac{1}{\nu})$ and by expression (5.14) in the case of $\nu > 1$ and $\frac{1}{2}(1+\frac{1}{\nu}) < F < 1$. At large

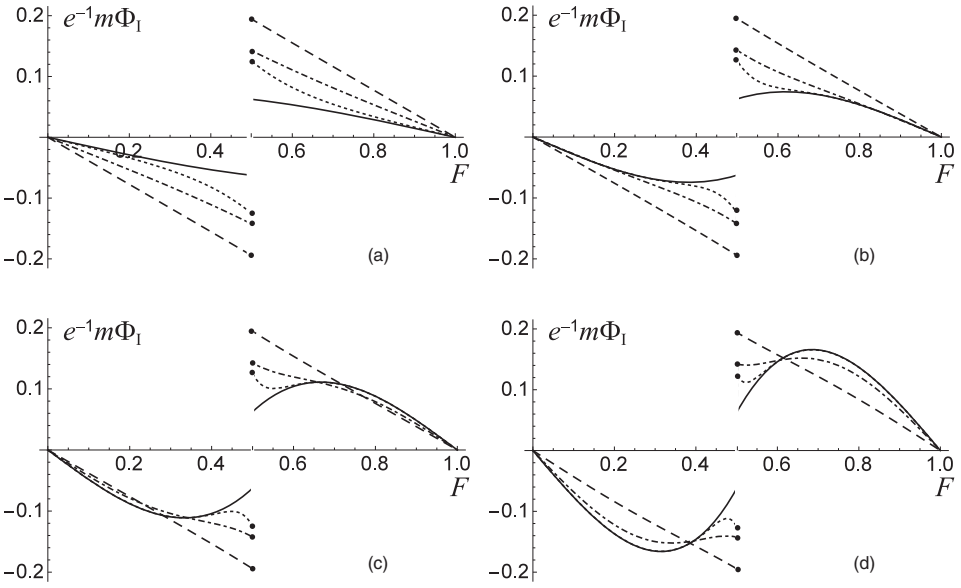

FIG. 5. The dimensionless induced flux at $\theta = \pi$ as a function of F in the cases of $mr_0 = 0$ (solid line), $mr_0 = 10^{-3}$ (dotted line), $mr_0 = 10^{-1}$ (dash-dotted line), and $mr_0 = 1$ (dashed line): (a) $\nu = 1$, (b) $\nu = 2$, (c) $\nu = 3$, and (d) $\nu = 4$. The points at $F = 1/2$ correspond to $\theta = \pi_+$ (positive values) and to $\theta = \pi_-$ (negative values), with the absolute values increasing with the increase of mr_0. The point in the case of $mr_0 = 10^{-3}$ (or less) actually coincides with the point in the case of $mr_0 = 0$; moreover, in cases $mr_0 \gtrsim 10^{-3}$, the points at $F = 1/2$ coincide with the end points of the appropriate curves at $F \neq 1/2$.

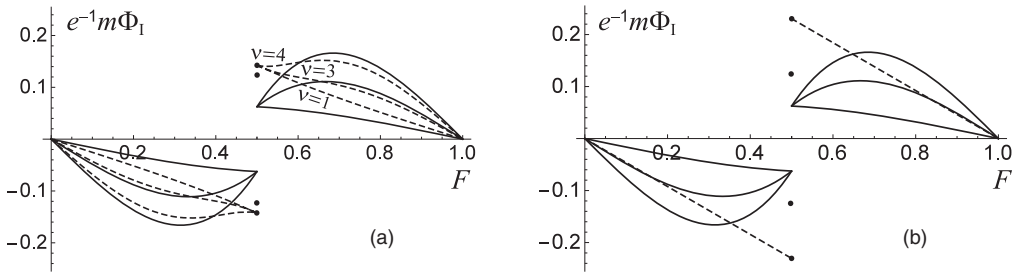

FIG. 6. The dimensionless induced flux at $\theta = \pi$ as a function of F: (a) $mr_0 = 0$ (solid lines) and $mr_0 = 10^{-1}$ (dashed lines), and (b) $mr_0 = 0$ (solid lines) and $mr_0 = 5$ (dashed line).

distances from the vortex, $r \to \infty$, the current decreases exponentially as

$$\left\{ \begin{array}{ll} \sqrt{m/r}\exp(-2mr), & \frac{1}{2} \le \nu < 2, \quad F \ne \frac{1}{2} \\ m\frac{\sin[(2F-1)\pi]}{\sin(\pi/\nu)}\exp[-2mr\sin(\pi/\nu)], & \nu \ge 2, \quad F \ne \frac{1}{2} \\ \sqrt{m/r}\exp(-2mr), & \nu \ge \frac{1}{2}, \quad F = \frac{1}{2} \end{array} \right\},$$

whereas it decreases as $1/r$ in the case of massless spinor matter; see Appendix D.

As a manifestation of the Aharonov-Bohm effect, the current is periodic in the value of the vortex flux, Φ; i.e., it depends on F and not on n_c [see (2.19)]; moreover, it changes sign under simultaneous changes $F \to 1 - F$ and $\theta \to -\theta$ [see (5.31)]. One can introduce the charge conjugation transformation with the vortex flux changing its sign,

$$C\colon \Phi \to -\Phi, \qquad E \to -E, \qquad \Psi \to \sigma^1\Psi^*. \tag{7.2}$$

The boundary condition for a conjugated wave function differs from (7.1):

$$(I - i\beta\alpha^r e^{i\theta\alpha^r})\sigma^1\psi^*|_{r=r_0} = 0. \tag{7.3}$$

By requiring invariance of the boundary condition under such a charge conjugation, one restricts the values of the self-adjoint extension parameter to $\theta = \frac{\pi}{2} \mp \frac{\pi}{2}$. In the latter case the current changes sign under change $F \to 1 - F$; i.e., it is odd, as well as periodic in the value of the vortex flux. Consequently, it vanishes at $\theta = 0$ and $F = 1/2$, while it is discontinuous in θ at $\theta = \pi$ and $F = 1/2$ [see (6.30)].

It is appropriate here to discuss the dependence on the transverse size of the vortex core and the limiting procedure as this size tends to zero, $r_0 \to 0$. For this task it is instructive to decompose the current into r_0-independent, $j_\varphi^{(a)}$, and r_0-dependent, $j_\varphi^{(b)}$, pieces [see (5.15)–(5.22)]; the r_0-dependent piece vanishes at $r_0 \to 0$. It should be noted that, in the case of the infinitely thin $(r_0 = 0)$ vortex, the Dirac Hamiltonian is essentially self-adjoint for $\nu > 1$ and either $0 < F < \frac{1}{2}(1 - \frac{1}{\nu})$ or $\frac{1}{2}(1 + \frac{1}{\nu}) < F < 1$; otherwise, there emerges the self-adjoint extension problem with one, or four, or more parameters. One self-adjoint extension parameter, Θ, appears for $\nu \ge 1$ and $\frac{1}{2}(1 - \frac{1}{\nu}) < F < \frac{1}{2}(1 + \frac{1}{\nu})$, or for $\frac{1}{2} \le \nu < 1$ and $\frac{1}{2}(\frac{1}{\nu} - 1) < F < \frac{1}{2}(3 - \frac{1}{\nu})$. The results for $\nu \ge 1$ and $0 < F < 1$, as well as for $\frac{1}{2} \le \nu < 1$ and $\frac{1}{2}(\frac{1}{\nu} - 1) < F < \frac{1}{2}(3 - \frac{1}{\nu})$, are comprehensively presented in Appendix C. The value of Θ can be fixed by limiting procedure $r_0 \to 0$ starting from the $r_0 > 0$ case. In this way, the condition of minimal irregularity in the $r_0 = 0$ case is obtained in the form of (4.16). If this condition is supplemented with the requirements of invariance under charge conjugation (7.2) and continuity in θ, then it takes the form of (4.16) with $\theta = 0$ at $F = 1/2$; namely in the latter form it was first proposed in [31,32].

As a consequence of the Maxwell equation, the magnetic field strength is also induced in the vacuum, pointing along the vortex axis; the relevant expressions in the case of the most general boundary condition, (7.1), are given by (6.1)–(6.9). This allows us to consider the total magnetic flux which is induced in the vacuum. As follows from our numerical analysis, the latter is finite at $\theta = \frac{\pi}{2} \mp \frac{\pi}{2}$ only, but otherwise, it is divergent. Thus, the physical condition that the induced vacuum magnetic flux be finite corresponds to the requirement of invariance under charge conjugation (7.2). The flux for boundary conditions maintaining the charge conjugation invariance is given at $F \ne 1/2$ by expression (6.38), it vanishes at $\theta = 0$ and $F = 1/2$, and it is nonvanishing and discontinuous in θ at $\theta = \pi$ and $F = 1/2$ [see (6.32)]. The flux in the case of $r_0 = 0$ is discontinuous at $F = 1/2$; moreover, its absolute value at $\theta = \pi$ and $F = 1/2$ [see (6.33)] is twice as large as its absolute value at $\theta = \pi$ in the limit $F \to 1/2$ [see (6.24)]. The case of an infinitely thin vortex is an idealization that is inappropriate to physics reality, since, as has already been noted in the Introduction, the transverse size of the vortex, r_0, is of the order of the correlation length. In the case of $r_0 > 0$, the differences in behavior of the flux at $\theta = 0$ and at $\theta = \pi$ are comprehensively illustrated by Figs. 2–6. Whereas the flux at $\theta = 0$ decreases in its absolute value

with the increase of r_0, the flux at $\theta = \pi$ in general increases at no allowance in its absolute value with the increase of r_0 (although there is a moderate decrease in vicinities of $F = 0$ and $F = 1$ at $\nu > 2$). Such a behavior of the flux, as that at $\theta = \pi$, can hardly be regarded as physical. Quantity r_0^{-1} is identified with the energy scale of spontaneous symmetry breaking, i.e., the mass of the corresponding Higgs particle. It looks rather unlikely that a topological defect influences the surrounding quantum matter with the matter particle mass, m, exceeding the Higgs particle mass, m_{cond}; the more unlikely is the unrestricted growth of this influence with the increase of quotient m/m_{cond}. The influence of a topological defect on the surrounding quantum matter at $m_{\mathrm{cond}} > m$ looks much more physically plausible. Namely this situation is realized in the case of quantum scalar matter obeying the Dirichlet boundary condition at the vortex edge (see [23–26]).

We conclude that, although we have solved the problem analytically with the use of the most general set of boundary conditions ensuring the impenetrability of the vortex core, the analysis of the behavior of the induced vacuum magnetic flux allows us to restrict the variety of admissible boundary conditions. The requirement of the flux to be finite, which is equivalent to the requirement of invariance under charge conjugation (7.2), restricts the values of the self-adjoint extension parameter to $\theta = \frac{\pi}{2} \mp \frac{\pi}{2}$. The further requirement of physical plausibility of the finite flux behavior, which is equivalent to the formal requirement of continuity in the dependence on θ, yields $\theta = 0$. As long as the transverse size of the vortex is taken into account, the induced vacuum effects at $\theta = 0$ are continuous in F and vanishing at $F = 1/2$. At this point we would like to emphasize the crucial distinction between the cases of massive and massless quantum spinor matter. The latter case requires an introduction of the maximal size of the system, $r_{\max}$. We discover that, for $r_{\max} \gg r_0$ (in conformance to the reality), the induced vacuum effects for both $\theta = 0$ and $\theta = \pi$ are physically plausible; moreover, they coincide, being independent of the transverse size of the vortex [see (D15) and (D16) in Appendix D]. Because of this distinction, the results in the massless case are discontinuous at $F = 1/2$ with a jump, which is independent of ν [see (D19)]. Note in this respect that the current and the magnetic field that are induced in the vacuum of quantum scalar matter under the Dirichlet boundary condition are continuous in F and vanishing at $F = 1/2$ even in the $r_0 = 0$ case (see [43–45]). In contrast to this, the emergence of a peculiar mode in the solution to the Dirac equation (see Sec. III) leads to a discontinuity of the results at $F = 1/2$. For massive quantum spinor matter, the discontinuity is present in the $r_0 = 0$ case, but is eliminated by a choice of the physically motivated boundary condition in the $r_0 > 0$ case. The discontinuity nonetheless stays on for massless quantum spinor matter. It would be interesting to perform a similar study for other characteristics of the vacuum, for instance, for the induced vacuum energy-momentum tensor.

ACKNOWLEDGMENTS

The work of Yu. A. S. was supported by the National Academy of Sciences of Ukraine (Project No. 01172U000237), by the Program of Fundamental Research of the Department of Physics and Astronomy of the National Academy of Sciences of Ukraine (Project No. 0117U000240), and by the SEENET-MTP—ICTP (Abdus Salam International Centre for Theoretical Physics) Project No. NT-03 "Cosmology—Classical and Quantum Challenges."

APPENDIX A: CONTRIBUTION OF NONPECULIAR MODES TO THE CURRENT

Using relations (see, e.g., [46])

$$J_\rho(\mathrm{i}z) = \mathrm{e}^{\mathrm{i}\rho\pi/2} I_\rho(z), \qquad Y_\rho(\mathrm{i}z) = \mathrm{i}\mathrm{e}^{\mathrm{i}\rho\pi/2} I_\rho(z) - \frac{2}{\pi}\mathrm{e}^{-\mathrm{i}\rho\pi/2} K_\rho(z), \qquad -\pi < \arg z \le \pi/2,$$
$$I_\rho(-z) = \mathrm{e}^{\mathrm{i}\rho\pi} I_\rho(z), \qquad K_\rho(-z) = \mathrm{e}^{-\mathrm{i}\rho\pi} K_\rho(z) - \mathrm{i}\pi I_\rho(z), \qquad -\pi < \arg z < 0,$$

one can obtain

$$J_\rho(kr)J_{\rho-1}(kr) = \frac{1}{2\pi}[I_\rho(-\mathrm{i}kr)K_{\rho-1}(-\mathrm{i}kr) - I_{\rho-1}(-\mathrm{i}kr)K_\rho(-\mathrm{i}kr) + I_\rho(\mathrm{i}kr)K_{\rho-1}(\mathrm{i}kr) - I_{\rho-1}(\mathrm{i}kr)K_\rho(\mathrm{i}kr)], \tag{A1}$$

$$J_\rho(kr)Y_{\rho-1}(kr) + Y_\rho(kr)J_{\rho-1}(kr) = -\frac{2}{\pi^2}[\mathrm{e}^{-\mathrm{i}\rho\pi}K_\rho(-\mathrm{i}kr)K_{\rho-1}(-\mathrm{i}kr) + \mathrm{e}^{\mathrm{i}\rho\pi}K_\rho(\mathrm{i}kr)K_{\rho-1}(\mathrm{i}kr)], \tag{A2}$$

$$Y_\rho(kr)Y_{\rho-1}(kr) - J_\rho(kr)J_{\rho-1}(kr) = \frac{2\mathrm{i}}{\pi^2}[\mathrm{e}^{-\mathrm{i}\rho\pi}K_\rho(-\mathrm{i}kr)K_{\rho-1}(-\mathrm{i}kr) - \mathrm{e}^{\mathrm{i}\rho\pi}K_\rho(\mathrm{i}kr)K_{\rho-1}(\mathrm{i}kr)]. \tag{A3}$$

With the help of these relations, $j_\varphi^{(1)}$ (5.2) and $j_\varphi^{(2)}$ (5.3) are presented as

$$j_\varphi^{(1)}(r) = -\frac{r}{(2\pi)^2}\int_{-\infty}^{\infty}\frac{dkk^2}{\sqrt{k^2+m^2}}\sum_{l=1}^{\infty}[I_{\nu l+1-G}(-\mathrm{i}kr)K_{\nu l-G}(-\mathrm{i}kr) - I_{\nu l-G}(-\mathrm{i}kr)K_{\nu l+1-G}(-\mathrm{i}kr) - I_{\nu l+G}(-\mathrm{i}kr)K_{\nu l-1+G}(-\mathrm{i}kr) + I_{\nu l-1+G}(-\mathrm{i}kr)K_{\nu l+G}(-\mathrm{i}kr)] \tag{A4}$$

and

$$j_\varphi^{(2)}(r) = \sum_{\mathrm{sgn}(E)}\sum_{l=1}^{\infty}(\lambda_{\nu l+1-G}^{(\wedge)}(r) - \lambda_{\nu l+G}^{(\vee)}(r)), \tag{A5}$$

where

$$\lambda_\rho^{(\wedge/\vee)}(r) = -\frac{r}{2\pi^2}\int_{-\infty}^{\infty}\frac{dkk^2}{\sqrt{k^2+m^2}}\left[\cos^2(\mu_\rho^{(\wedge/\vee)})\frac{(-\mathrm{i}k)^{2\rho-1}}{(\sqrt{k^2})^{2\rho-1}} - \frac{1}{2}\sin(2\mu_\rho^{(\wedge/\vee)})\frac{(-\mathrm{i}k)^{2\rho}}{(\sqrt{k^2})^{2\rho}}\right] K_\rho(-\mathrm{i}kr)K_{\rho-1}(-\mathrm{i}kr) \tag{A6}$$

and it is implied that $\mu_\rho^{(\wedge)}$ and $\mu_\rho^{(\vee)}$, determined by relations (4.9) and (4.10), depend on $\sqrt{k^2}$ instead of k. The integral over real k can be transformed into the integral over a contour circumventing anticlockwise the positive imaginary semiaxis in the complex k plane. It is evident in the case of $j_\varphi^{(1)}$ that the latter contour is reduced to a contour circumventing a part of the positive imaginary semiaxis (see Fig. 7). As a result, we get

$$j_\varphi^{(1)}(r) = \frac{r}{2\pi^2}\int_m^{\infty}\frac{dqq^2}{\sqrt{q^2-m^2}}\sum_{l=1}^{\infty}[I_{\nu l+1-G}(qr)K_{\nu l-G}(qr) - I_{\nu l-G}(qr)K_{\nu l+1-G}(qr) - I_{\nu l+G}(qr)K_{\nu l-1+G}(qr) + I_{\nu l-1+G}(qr)K_{\nu l+G}(qr)], \tag{A7}$$

which can be decomposed as

$$j_\varphi^{(1)}(r) = j_\varphi^{(1,1)}(r) + j_\varphi^{(1,2)}(r) - \frac{r}{\pi^2}\int_m^{\infty}\frac{dqq^2}{\sqrt{q^2-m^2}} \times\left\{\frac{\sin(G\pi)}{\pi}K_G(qr)K_{1-G}(qr) + \frac{1}{2}[I_{1-G}(qr)K_G(qr) - I_G(qr)K_{1-G}(qr)]\right\}, \tag{A8}$$

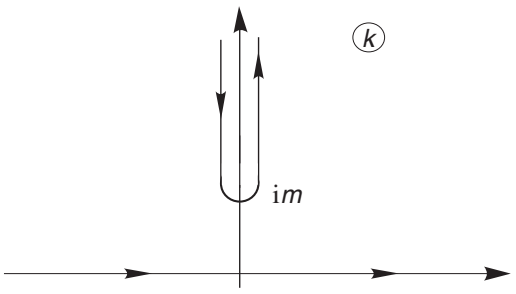

FIG. 7. The integral over real k in (A4) is transformed into the integral over a contour in the complex k plane.

where

$$j_\varphi^{(1,1)}(r) = \frac{1}{2\pi^2}\int_m^{\infty}\frac{dqq^2}{\sqrt{q^2-m^2}}\frac{d}{dq}\sum_{n\in\mathbb{Z}}I_{|\nu n-G|}(qr)K_{\nu n-G}(qr) = \frac{1}{(2\pi)^2}\int_m^{\infty}\frac{dqq^2}{\sqrt{q^2-m^2}} \times\frac{d}{dq}\int_0^{\infty}\frac{dy}{y}\exp\left(-\frac{q^2r^2}{2y}-y\right)\sum_{n\in\mathbb{Z}}I_{|\nu n-G|}(y) \tag{A9}$$

and

$$j_\varphi^{(1,2)}(r) = -\frac{1}{\pi^2}\int_m^{\infty}\frac{dqq}{\sqrt{q^2-m^2}} \times\sum_{n\in\mathbb{Z}}(\nu n-G)I_{|\nu n-G|}(qr)K_{\nu n-G}(qr) = -\frac{1}{2\pi^2}\int_m^{\infty}\frac{dqq}{\sqrt{q^2-m^2}}\int_0^{\infty}\frac{dy}{y}\exp\left(-\frac{q^2r^2}{2y}-y\right) \times\sum_{n\in\mathbb{Z}}(\nu n-G)I_{|\nu n-G|}(y). \tag{A10}$$

Using the Schläfli contour integral representation,

$$I_\rho(y) = \frac{1}{2\pi\mathrm{i}}\int_{C_+}dz\mathrm{e}^{y\cosh z-\rho z} = -\frac{1}{2\pi\mathrm{i}}\int_{C_-}dz\mathrm{e}^{y\cosh z+\rho z},$$

we obtain

$$\sum_{n\in\mathbb{Z}}I_{|\nu n-G|}(y) = \frac{1}{2\pi\mathrm{i}}\left[\int_{C_+}dz\mathrm{e}^{y\cosh z-Gz}\frac{1}{1-\mathrm{e}^{-\nu z}} - \int_{C_-}dz\mathrm{e}^{y\cosh z-Gz}\frac{\mathrm{e}^{\nu z}}{1-\mathrm{e}^{\nu z}}\right] = \frac{1}{4\pi\mathrm{i}}\int_{C_0}dz\mathrm{e}^{y\cosh z}\frac{\cosh[(G-\frac{\nu}{2})z]}{\sinh(\nu z/2)} + \frac{\mathrm{e}^y}{\nu}, \tag{A11}$$

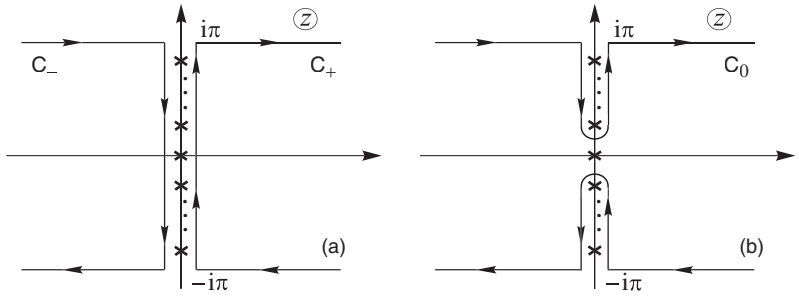

FIG. 8. Complex z plane with simple poles indicated by crosses: (a) contours C_+ and C_-, and (b) contour C_0.

where contours C_+, C_-, and C_0 in the complex z plane are shown in Fig. 8. The vertical segments of contours C_+, C_-, and C_0 are infinitesimally close to the imaginary axis, not coinciding with it in order to avoid simple poles of the integrand at $z=0$ and $z=\pm 2\mathrm{i}p\pi/\nu$ (p is the positive integer, $1\le p\le[|\nu/2|]$). Contour C_0 circumvents poles out of the origin (existing at $\nu\ge 2$), whereas the contribution of the pole at the origin (existing at $\nu\neq 0$) is explicitly separated in (A11). Substituting (A11) into (A9), we change integration variable $y\to v=y(qr)^{-2}$ and take a derivative,

$$j_\varphi^{(1,1)}(r)=\frac{r^2}{2\pi^2}\int_m^\infty\frac{dqq^3}{\sqrt{q^2-m^2}}\int_0^\infty dv\frac{1}{2\pi\mathrm{i}}\int_{C_0}dz\exp\left[-\frac{1}{2v}+2vq^2r^2\sinh^2(z/2)\right]\sinh^2(z/2)\frac{\cosh\left[(G-\frac{\nu}{2})z\right]}{\sinh(\nu z/2)}. \tag{A12}$$

Integrating over q and v, we get

$$\begin{aligned}j_\varphi^{(1,1)}(r)&=-\frac{m}{8\pi}\frac{1}{2\pi\mathrm{i}}\int_{C_0}dz\left[1+\frac{1}{2mr\sqrt{-\sinh^2(z/2)}}\right]\exp\left[-2mr\sqrt{-\sinh^2(z/2)}\right]\frac{\cosh[(G-\frac{\nu}{2})z]}{\sinh(\nu z/2)}\\&=\frac{m}{(2\pi)^2}\left\{\int_0^\infty du\left[1+\frac{1}{2mr\cosh(u/2)}\right]\mathrm{e}^{-2mr\cosh(u/2)}\frac{\sin(G\pi)\cosh[(G-\nu)u]-\sin[(G-\nu)\pi]\cosh(Gu)}{\cosh(\nu u)-\cos(\nu\pi)}\right.\\&\left.-\frac{2\pi}{\nu}\sum_{p=1}^{[|\nu/2|]}\left[1+\frac{1}{2mr\sin(p\pi/\nu)}\right]\mathrm{e}^{-2mr\sin(p\pi/\nu)}\cos(2Gp\pi/\nu)+\frac{\pi}{\nu}\left(1+\frac{1}{2mr}\right)\mathrm{e}^{-2mr}\cos(G\pi)\delta_{\nu,2N}\right\},\end{aligned} \tag{A13}$$

where the finite sum over integer p and the last term with the Kronecker δ symbol (N is the positive integer) are due to a contribution of simple poles on the imaginary axis out of the origin.

In a similar way we calculate the sum in (A10):

$$\begin{aligned}\sum_{n\in\mathbb{Z}}(\nu n-G)I_{|\nu n-G|}(y)&=\frac{y}{2}\left\{\sum_{l=1}^\infty[I_{\nu l-1-G}(y)-I_{\nu l+1-G}(y)]+\sum_{l=0}^\infty[I_{\nu l+1+G}(y)-I_{\nu l-1+G}(y)]\right\}\\&=\frac{y}{4\pi\mathrm{i}}\int_{C_0}dz\mathrm{e}^{y\cosh z}\sinh(z)\frac{\sinh\left[(G-\frac{\nu}{2})z\right]}{\sinh(\nu z/2)}.\end{aligned} \tag{A14}$$

Substituting (A14) into (A10) and integrating over q and y, we get

$$\begin{aligned}j_\varphi^{(1,2)}(r)&=\frac{m}{8\pi}\frac{1}{2\pi\mathrm{i}}\int_{C_0}dz\left[1+\frac{1}{2mr\sqrt{-\sinh^2(z/2)}}\right]\exp\left[-2mr\sqrt{-\sinh^2(z/2)}\right]\frac{\coth(z/2)\sinh\left[(G-\frac{\nu}{2})z\right]}{\sinh(\nu z/2)}\\&=-\frac{m}{(2\pi)^2}\left\{\int_0^\infty du\left[1+\frac{1}{2mr\cosh(u/2)}\right]\mathrm{e}^{-2mr\cosh(u/2)}\tanh(u/2)\frac{\sin(G\pi)\sinh[(G-\nu)u]-\sin[(G-\nu)\pi]\sinh(Gu)}{\cosh(\nu u)-\cos(\nu\pi)}\right.\\&\left.-\frac{2\pi}{\nu}\sum_{p=1}^{[|\nu/2|]}\left[1+\frac{1}{2mr\sin(p\pi/\nu)}\right]\mathrm{e}^{-2mr\sin(p\pi/\nu)}\cot(p\pi/\nu)\sin(2Gp\pi/\nu)\right\}.\end{aligned} \tag{A15}$$

As a result, we obtain the following expression for $j_\varphi^{(1)}$ (A7):

$$j_\varphi^{(1)}(r) = \frac{m}{(2\pi)^2}\left\{\int_0^\infty \frac{du}{\cosh(u/2)}\left[1+\frac{1}{2mr\cosh(u/2)}\right]e^{-2mr\cosh(u/2)}\right.$$
$$\times\frac{\sin(G\pi)\cosh\left[(G-\nu-\frac{1}{2})u\right]-\sin[(G-\nu)\pi]\cosh\left[(G-\frac{1}{2})u\right]}{\cosh(\nu u)-\cos(\nu\pi)}$$
$$+\frac{2\pi}{\nu}\sum_{p=1}^{[|\nu/2|]}\left[1+\frac{1}{2mr\sin(p\pi/\nu)}\right]\exp[-2mr\sin(p\pi/\nu)]\frac{\sin[(2G-1)p\pi/\nu]}{\sin(p\pi/\nu)}+\frac{\pi}{\nu}\left(1+\frac{1}{2mr}\right)e^{-2mr}\cos(G\pi)\delta_{\nu,2N}\Big\}$$
$$\left.-\frac{r}{\pi^2}\int_m^\infty\frac{dqq^2}{\sqrt{q^2-m^2}}\left\{\frac{\sin(G\pi)}{\pi}K_G(qr)K_{1-G}(qr)+\frac{1}{2}[I_{1-G}(qr)K_G(qr)-I_G(qr)K_{1-G}(qr)]\right\}\right. . \tag{A16}$$

Note that $j_\varphi^{(1)}$ [see (5.2) or (A7)] changes sign under substitution $G\to 1-G$. In view of this one gets

$$\int_m^\infty\frac{dqq^2}{\sqrt{q^2-m^2}}K_G(qr)K_{1-G}(qr)=\frac{\pi m}{4r}\int_0^\infty\frac{du}{\cosh(u/2)}\cosh\left[\left(G-\frac{1}{2}\right)u\right]\left[1+\frac{1}{2mr\cosh(u/2)}\right]e^{-2mr\cosh(u/2)}. \tag{A17}$$

Defining

$$j_\varphi^{(1,3)}(r)=-\frac{m}{8\pi}\frac{1}{2\pi i}\int_{C_0}dz\left[1+\frac{1}{2mr\sqrt{-\sinh^2(z/2)}}\right]\exp\left[-2mr\sqrt{-\sinh^2(z/2)}\right]$$
$$\times\frac{\cosh\left[(G-\frac{1}{2})z\right]}{\sinh(z/2)}=\frac{m\sin(G\pi)}{(2\pi)^2}\int_0^\infty\frac{du}{\cosh(u/2)}\cosh\left[\left(G-\frac{1}{2}\right)u\right]\left[1+\frac{1}{2mr\cosh(u/2)}\right]e^{-2mr\cosh(u/2)}, \tag{A18}$$

we can present (A16) as

$$j_\varphi^{(1)}(r)=j_\varphi^{(1,1)}(r)+j_\varphi^{(1,2)}(r)-j_\varphi^{(1,3)}(r)-\frac{r}{2\pi^2}\int_m^\infty\frac{dqq^2}{\sqrt{q^2-m^2}}[I_{1-G}(qr)K_G(qr)-I_G(qr)K_{1-G}(qr)] \tag{A19}$$

with $j_\varphi^{(1,1)}$, $j_\varphi^{(1,2)}$, and $j_\varphi^{(1,3)}$ given by (A13), (A15), and (A18), respectively. Using the latter relation, we finally obtain (5.5).

Turning now to $j_\varphi^{(2)}$ (A5), we obtain by deforming the integration contour to circumvent the positive imaginary semiaxis in the complex k plane

$$\lambda_\rho^{(\wedge/\vee)}(r)=-\frac{r}{2\pi^3}\left\{\int_0^m\frac{dqq^2}{\sqrt{m^2-q^2}}\left[e^{i\rho\pi}\cos^2(\mu_{\rho,+}^{(\wedge/\vee)})+e^{-i\rho\pi}\cos^2(\mu_{\rho,-}^{(\wedge/\vee)})\right.\right.$$
$$\left.-\frac{i}{2}e^{i\rho\pi}\sin(2\mu_{\rho,+}^{(\wedge/\vee)})+\frac{i}{2}e^{-i\rho\pi}\sin(2\mu_{\rho,-}^{(\wedge/\vee)})\right]K_\rho(qr)K_{\rho-1}(qr)+\int_m^\infty\frac{dqq^2}{\sqrt{q^2-m^2}}\left[ie^{i\rho\pi}\cos^2(\mu_{\rho,+}^{(\wedge/\vee)})\right.$$
$$\left.\left.-ie^{-i\rho\pi}\cos^2(\mu_{\rho,-}^{(\wedge/\vee)})+\frac{1}{2}e^{i\rho\pi}\sin(2\mu_{\rho,+}^{(\wedge/\vee)})+\frac{1}{2}e^{-i\rho\pi}\sin(2\mu_{\rho,-}^{(\wedge/\vee)})\right]K_\rho(qr)K_{\rho-1}(qr)\right\}, \tag{A20}$$

where $\mu_{\rho,+}^{(\wedge/\vee)}$ and $\mu_{\rho,-}^{(\wedge/\vee)}$ are determined by relations

$$\tan(\mu_{\rho,\pm}^{(\wedge)})=\left\{\cos\left(\frac{\theta}{2}+\frac{\pi}{4}\right)q\left[\frac{2}{\pi}e^{\pm i\rho\pi}K_{\rho-1}(qr_0)\mp iI_{\rho-1}(qr_0)\right]+\sin\left(\frac{\theta}{2}+\frac{\pi}{4}\right)(m-\Delta)\left[\frac{2}{\pi}e^{\pm i\rho\pi}K_\rho(qr_0)\pm iI_\rho(qr_0)\right]\right\}$$
$$\times\left[-\cos\left(\frac{\theta}{2}+\frac{\pi}{4}\right)qI_{\rho-1}(qr_0)+\sin\left(\frac{\theta}{2}+\frac{\pi}{4}\right)(m-\Delta)I_\rho(qr_0)\right]^{-1}, \tag{A21}$$

$$\tan(\mu_{\rho,\pm}^{(\vee)}) = \left\{\cos\left(\frac{\theta}{2}+\frac{\pi}{4}\right)(m+\Delta)\left[\frac{2}{\pi}e^{\pm i\rho\pi}K_\rho(qr_0)\pm iI_\rho(qr_0)\right]\right.$$
$$\left.+\sin\left(\frac{\theta}{2}+\frac{\pi}{4}\right)q\left[\frac{2}{\pi}e^{\pm i\rho\pi}K_{\rho-1}(qr_0)\mp iI_{\rho-1}(qr_0)\right]\right\}$$
$$\times\left[\cos\left(\frac{\theta}{2}+\frac{\pi}{4}\right)(m+\Delta)I_\rho(qr_0)-\sin\left(\frac{\theta}{2}+\frac{\pi}{4}\right)qI_{\rho-1}(qr_0)\right]^{-1}, \tag{A22}$$

and

$$\Delta=\begin{cases}\mathrm{sgn}(E)\sqrt{m^2-q^2}, & q<m,\\ \mp i\,\mathrm{sgn}(E)\sqrt{q^2-m^2}, & q>m.\end{cases} \tag{A23}$$

In view of relation

$$\sum_{\pm}e^{\pm i\rho\pi}\left[\cos^2(\mu_{\rho,\pm}^{(\wedge/\vee)})\mp\frac{i}{2}\sin(2\mu_{\rho,\pm}^{(\wedge/\vee)})\right]=0, \tag{A24}$$

the first integral in (A20) vanishes, and, as in the case of $j_\varphi^{(1)}$, only the integral over a contour depicted on Fig. 7 contributes; namely the latter is given by the second integral in (A20). In view of relation

$$\sum_{\mathrm{sgn}(E)}\sum_{\pm}e^{\pm i\rho\pi}\left[\pm i\cos^2(\mu_{\rho,\pm}^{(\wedge/\vee)})+\frac{1}{2}\sin(2\mu_{\rho,\pm}^{(\wedge/\vee)})\right]=2\pi C_\rho^{(\wedge/\vee)}(qr_0), \tag{A25}$$

where $C_\rho^{(\wedge)}(v)$ and $C_\rho^{(\vee)}(v)$ are given by (5.7) and (5.8), we get

$$\sum_{\mathrm{sgn}(E)}\lambda_\rho^{(\wedge/\vee)}(r)=-\frac{r}{\pi^2}\int_m^\infty\frac{dqq^2}{\sqrt{q^2-m^2}}C_\rho^{(\wedge/\vee)}(qr_0)K_\rho(qr)K_{\rho-1}(qr). \tag{A26}$$

As a consequence of (A5) and (A26), we obtain (5.6).

APPENDIX B: CONTRIBUTION OF PECULIAR MODES TO THE CURRENT

Similar to that in the beginning of Appendix A, one can obtain

$$J_G(kr)J_{1-G}(kr)-J_{-G}(kr)J_{-1+G}(kr)=-\frac{1}{2\pi}\{[e^{iG\pi}I_G(-ikr)+e^{-iG\pi}I_{-G}(-ikr)]K_{1-G}(-ikr)$$
$$-[e^{-iG\pi}I_{1-G}(-ikr)+e^{iG\pi}I_{-1+G}(-ikr)]K_G(-ikr)$$
$$+[e^{-iG\pi}I_G(ikr)+e^{iG\pi}I_{-G}(ikr)]K_{1-G}(ikr)$$
$$-[e^{iG\pi}I_{1-G}(ikr)+e^{-iG\pi}I_{-1+G}(ikr)]K_G(ikr)\}. \tag{B1}$$

With the help of (A1) and (B1), $j_\varphi^{(3)}$ (5.4) is presented as

$$
\begin{aligned}
j_{\varphi}^{(3)}(r) = &-\frac{r}{2(2\pi)^2}\int_{-\infty}^{\infty}\frac{dkk^2}{\sqrt{k^2+m^2}}\sum_{\mathrm{sgn}(E)}[\tan(\mu_{1-G})+2\cos(G\pi)+\cot(\mu_{1-G})]^{-1}\\
&\times\left\{\tan(\mu_{1-G})[I_{1-G}(-\mathrm{i}kr)K_G(-\mathrm{i}kr)-I_{-G}(-\mathrm{i}kr)K_{1-G}(-\mathrm{i}kr)]\right.\\
&+\left[\frac{(-\mathrm{i}k)^{2G}}{(\sqrt{k^2})^{2G}}I_{1-G}(-\mathrm{i}kr)+\frac{(\sqrt{k^2})^{2G}}{(-\mathrm{i}k)^{2G}}I_{-1+G}(-\mathrm{i}kr)\right]K_G(-\mathrm{i}kr)-\left[\frac{(\sqrt{k^2})^{2G}}{(-\mathrm{i}k)^{2G}}I_G(-\mathrm{i}kr)+\frac{(-\mathrm{i}k)^{2G}}{(\sqrt{k^2})^{2G}}I_{-G}(-\mathrm{i}kr)\right]\\
&\times K_{1-G}(-\mathrm{i}kr)-\cot(\mu_{1-G})[I_G(-\mathrm{i}kr)K_{1-G}(-\mathrm{i}kr)-I_{-1+G}(-\mathrm{i}kr)K_G(-\mathrm{i}kr)]\Big\}\\
&+\frac{\kappa^2}{4\pi r_0}\frac{[1-\mathrm{sgn}(\cos\theta)]\mathrm{sgn}[\tan(\frac{\theta}{2}+\frac{\pi}{4})+\frac{K_G(\kappa r_0)}{K_{1-G}(\kappa r_0)}]}{mK_G(\kappa r_0)K_{1-G}(\kappa r_0)+E_{BS}\{\kappa r_0[K_{1-G}^2(\kappa r_0)-K_G^2(\kappa r_0)]+(2G-1)K_G(\kappa r_0)K_{1-G}(\kappa r_0)\}},
\end{aligned}
\tag{B2}
$$

and it is implied that μ_{1-G}, as determined by (4.11), depends on $\sqrt{k^2}$ instead of k. The integral over real k can be transformed into the integral over a contour circumventing anticlockwise the positive imaginary semiaxis in the complex k plane. The latter contour is reduced to a contour consisting of two parts: one encircling a simple pole emerging at $\cos\theta<0$ and another one circumventing a part of the positive imaginary semiaxis (see Fig. 9). The contribution of the pole cancels out the last term in (B2), and for the remaining part we get

$$
\begin{aligned}
j_{\varphi}^{(3)}(r) &= \frac{r}{(2\pi)^2}\int_m^{\infty}\frac{dqq^2}{\sqrt{q^2-m^2}}\sum_{\mathrm{sgn}(E)}\sum_{\pm}[\tan(\mu_{1-G,\pm})+2\cos(G\pi)+\cot(\mu_{1-G,\pm})]^{-1}\\
&\times\{[\tan(\mu_{1-G},\pm)+\mathrm{e}^{\pm\mathrm{i}G\pi}][I_{1-G}(qr)K_G(qr)-I_{-G}(qr)K_{1-G}(qr)]\\
&-[\cot(\mu_{1-G},\pm)+\mathrm{e}^{\mp\mathrm{i}G\pi}][I_G(qr)K_{1-G}(qr)-I_{-1+G}(qr)K_G(qr)]\}\\
&=\frac{r}{2\pi^2}\int_m^{\infty}\frac{dqq^2}{\sqrt{q^2-m^2}}\left[I_{1-G}(qr)K_G(qr)-I_G(qr)K_{1-G}(qr)\right.\\
&\left.-\frac{\sin(G\pi)}{2\pi}K_G(qr)K_{1-G}(qr)\sum_{\mathrm{sgn}(E)}\sum_{\pm}\frac{\tan(\mu_{1-G,\pm})\pm 2\mathrm{i}\sin(G\pi)-\cot(\mu_{1-G,\pm})}{\tan(\mu_{1-G,\pm})+2\cos(G\pi)+\cot(\mu_{1-G,\pm})}\right],
\end{aligned}
\tag{B3}
$$

where

$$
\tan(\mu_{1-G,\pm})=\mathrm{e}^{\mp\mathrm{i}G\pi}\frac{\cos(\frac{\theta}{2}+\frac{\pi}{4})qI_G(qr_0)-\sin(\frac{\theta}{2}+\frac{\pi}{4})(m\pm\mathrm{i}\,\mathrm{sgn}(E)\sqrt{q^2-m^2})I_{-1+G}(qr_0)}{-\cos(\frac{\theta}{2}+\frac{\pi}{4})qI_{-G}(qr_0)+\sin(\frac{\theta}{2}+\frac{\pi}{4})(m\pm\mathrm{i}\,\mathrm{sgn}(E)\sqrt{q^2-m^2})I_{1-G}(qr_0)}.
\tag{B4}
$$

The sum in (B3) is reduced to the form

$$
\begin{aligned}
&\sum_{\mathrm{sgn}(E)}\sum_{\pm}\frac{\tan(\mu_{1-G,\pm})\pm 2\mathrm{i}\sin(G\pi)-\cot(\mu_{1-G,\pm})}{\tan(\mu_{1-G,\pm})+2\cos(G\pi)+\cot(\mu_{1-G,\pm})}\\
&=\sum_{\pm}\left[\frac{\mathrm{e}^{\mp\mathrm{i}G\pi}(h_{\pm}-1)-\mathrm{e}^{\pm\mathrm{i}G\pi}(h_{\pm}^{-1}-1)}{\mathrm{e}^{\mp\mathrm{i}G\pi}(h_{\pm}+1)+\mathrm{e}^{\pm\mathrm{i}G\pi}(h_{\pm}^{-1}+1)}+\frac{\mathrm{e}^{\mp\mathrm{i}G\pi}(h_{\mp}-1)-\mathrm{e}^{\pm\mathrm{i}G\pi}(h_{\mp}^{-1}-1)}{\mathrm{e}^{\mp\mathrm{i}G\pi}(h_{\mp}+1)+\mathrm{e}^{\pm\mathrm{i}G\pi}(h_{\mp}^{-1}+1)}\right]\\
&=\frac{4(h_+h_--1)}{h_+h_-+h_++h_-+1},
\end{aligned}
\tag{B5}
$$

where

$$
h_{\pm}=\frac{\cos(\frac{\theta}{2}+\frac{\pi}{4})qI_G(qr_0)-\sin(\frac{\theta}{2}+\frac{\pi}{4})(m\pm\mathrm{i}\sqrt{q^2-m^2})I_{-1+G}(qr_0)}{-\cos(\frac{\theta}{2}+\frac{\pi}{4})qI_{-G}(qr_0)+\sin(\frac{\theta}{2}+\frac{\pi}{4})(m\pm\mathrm{i}\sqrt{q^2-m^2})I_{1-G}(qr_0)}.
\tag{B6}
$$

It is straightforward to get

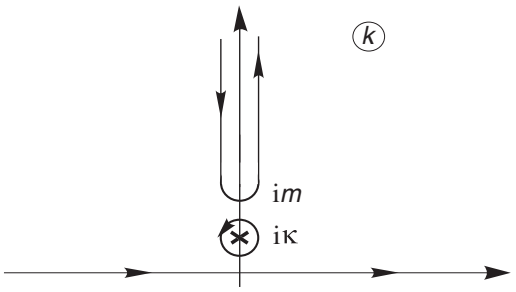

FIG. 9. The integral over real k in (B2) is transformed into the integral over a contour in the complex k plane.

$$\frac{4(h_+h_- - 1)}{h_+h_- + h_+ + h_- + 1} = \frac{4\pi}{\sin(G\pi)} C_{1-G}(qr_0), \tag{B7}$$

where $C_{1-G}(v)$ is given by (5.10). Substituting (B7) into (B3), we obtain (5.9).

APPENDIX C: CASE OF THE INFINITELY THIN VORTEX

We present here the results for the case of the infinitely thin ANO vortex (i.e., $r_0 = 0$).

In the case of $\nu > 1$ and $0 < F < \frac{1}{2}(1 - \frac{1}{\nu})$, partial Hamiltonians with all n are essentially self-adjoint [deficiency indices equal (0,0)], and the modes are given by (3.3) with $\mu_\rho^{(\wedge)} = \mu_\rho^{(\vee)} = \pi/2$. We obtain

$$j_\varphi(r) = -\frac{m}{(2\pi)^2}\left\{\int_0^\infty \frac{du}{\cosh(u/2)}\left[1 + \frac{1}{2mr\cosh(u/2)}\right]e^{-2mr\cosh(u/2)}\right.$$
$$\times \frac{\cos[\nu(F-\frac{1}{2})\pi]\cosh[\nu(F+\frac{1}{2})u] - \cos[\nu(F+\frac{1}{2})\pi]\cosh[\nu(F-\frac{1}{2})u]}{\cosh(\nu u) - \cos(\nu\pi)} - \frac{2\pi}{\nu}\sum_{p=1}^{[|\nu/2|]}\left[1 + \frac{1}{2mr\sin(p\pi/\nu)}\right]$$
$$\left.\times \exp[-2mr\sin(p\pi/\nu)]\frac{\sin[(2F-1)p\pi]}{\sin(p\pi/\nu)} + \frac{\pi}{2N}(-1)^N \sin(2NF\pi)\left(1 + \frac{1}{2mr}\right)e^{-2mr}\delta_{\nu,2N}\right\}, \tag{C1}$$

$$B_1(r) = -\frac{\nu e}{2(2\pi)^2}\frac{1}{r}\left\{\int_0^\infty \frac{du}{\cosh^2(u/2)} e^{-2mr\cosh(u/2)} \frac{\cos[\nu(F-\frac{1}{2})\pi]\cosh[\nu(F+\frac{1}{2})u] - \cos[\nu(F+\frac{1}{2})\pi]\cosh[\nu(F-\frac{1}{2})u]}{\cosh(\nu u) - \cos(\nu\pi)}\right.$$
$$\left. - \frac{2\pi}{\nu}\sum_{p=1}^{[|\nu/2|]} \exp[-2mr\sin(p\pi/\nu)]\frac{\sin[(2F-1)p\pi]}{\sin^2(p\pi/\nu)} + \frac{\pi}{2N}(-1)^N \sin(2NF\pi)e^{-2mr}\delta_{\nu,2N}\right\}, \tag{C2}$$

and

$$\Phi_{\mathrm{I}} = -\frac{e}{6m}F\left[\frac{1}{4}(\nu^2+3) - \nu^2F^2\right]. \tag{C3}$$

In the case of $\nu > 1$ and $\frac{1}{2}(1 + \frac{1}{\nu}) < F < 1$, partial Hamiltonians with all n are essentially self-adjoint as well, and the modes are given by (3.4) with $\mu_\rho^{(\wedge)} = \mu_\rho^{(\vee)} = \pi/2$. We obtain

$$j_\varphi(r) = \frac{m}{(2\pi)^2}\left\{\int_0^\infty \frac{du}{\cosh(u/2)}\left[1 + \frac{1}{2mr\cosh(u/2)}\right]e^{-2mr\cosh(u/2)}\right.$$
$$\times \frac{\cos[\nu(F-\frac{1}{2})\pi]\cosh[\nu(F-\frac{3}{2})u] - \cos[\nu(F-\frac{3}{2})\pi]\cosh[\nu(F-\frac{1}{2})u]}{\cosh(\nu u) - \cos(\nu\pi)} + \frac{2\pi}{\nu}\sum_{p=1}^{[|\nu/2|]}\left[1 + \frac{1}{2mr\sin(p\pi/\nu)}\right]$$
$$\left.\times \exp[-2mr\sin(p\pi/\nu)]\frac{\sin[(2F-1)p\pi]}{\sin(p\pi/\nu)} - \frac{\pi}{2N}(-1)^N \sin(2NF\pi)\left(1 + \frac{1}{2mr}\right)e^{-2mr}\delta_{\nu,2N}\right\}, \tag{C4}$$

$$B_1(r) = \frac{\nu e}{2(2\pi)^2}\frac{1}{r}\left\{\int_0^\infty \frac{du}{\cosh^2(u/2)} e^{-2mr\cosh(u/2)} \frac{\cos[\nu(F-\frac{1}{2})\pi]\cosh[\nu(F-\frac{3}{2})u] - \cos[\nu(F-\frac{3}{2})\pi]\cosh[\nu(F-\frac{1}{2})u]}{\cosh(\nu u) - \cos(\nu\pi)}\right.$$
$$\left. + \frac{2\pi}{\nu}\sum_{p=1}^{[|\nu/2|]} \exp[-2mr\sin(p\pi/\nu)]\frac{\sin[(2F-1)p\pi]}{\sin^2(p\pi/\nu)} - \frac{\pi}{2N}(-1)^N \sin(2NF\pi)e^{-2mr}\delta_{\nu,2N}\right\}, \tag{C5}$$

and

$$\Phi_{\mathrm{I}} = \frac{e}{6m}(1-F)\left[\frac{1}{4}(\nu^2+3)-\nu^2(1-F)^2\right]. \tag{C6}$$

In the case of $\nu \geq 1$ and $\frac{1}{2}(1-\frac{1}{\nu}) < F < \frac{1}{2}(1+\frac{1}{\nu})$ $(0 < G < 1)$, as well as in the case of $\frac{1}{2} \leq \nu < 1$ and $\frac{1}{2}(\frac{1}{\nu}-1) < F < \frac{1}{2}(3-\frac{1}{\nu})$ $(1-\nu < G < \nu)$, the deficiency index for a partial Hamiltonian with $n = n_c$ equals (2.1), and the one-parametric family of self-adjoint extensions is introduced via condition (3.11). The modes corresponding to the continuous spectrum $(|E| > m)$ are given by (3.6) with $\mu_\rho^{(\wedge)} = \mu_\rho^{(\vee)} = \pi/2$ and (3.5) with μ_{1-G} determined from relation

$$\tan(\mu_{1-G}) = \mathrm{sgn}(E)\frac{(1-m/E)^G\Gamma(1-G)}{(1+m/E)^{1-G}\Gamma(G)}2^{1-2G}\tan\left(\frac{\Theta}{2}+\frac{\pi}{4}\right). \tag{C7}$$

In addition, there is a bound state at $\cos\Theta < 0$ with the mode given by (3.15) and the energy $(|E_{BS}| < m)$ determined from relation (3.16). We obtain

$$\begin{aligned} j_\varphi(r) = &-\frac{m}{(2\pi)^2}\left\{\int_0^\infty \frac{du}{\cosh(u/2)}\left[1+\frac{1}{2mr\cosh(u/2)}\right]\mathrm{e}^{-2mr\cosh(u/2)}\right. \\ &\times\frac{\cos[\nu(F-\frac{1}{2})\pi]\sinh(\nu u)\sinh[\nu(F-\frac{1}{2})u]+\sin[\nu(F-\frac{1}{2})\pi]\sin(\nu\pi)\cosh[\nu(F-\frac{1}{2})u]}{\cosh(\nu u)-\cos(\nu\pi)} \\ &-\frac{2\pi}{\nu}\sum_{p=1}^{[|\nu/2|]}\left[1+\frac{1}{2mr\sin(p\pi/\nu)}\right]\exp[-2mr\sin(p\pi/\nu)]\frac{\sin[(2F-1)p\pi]}{\sin(p\pi/\nu)} \\ &\left.+\frac{\pi}{2N}(-1)^N\sin(2NF\pi)\left(1+\frac{1}{2mr}\right)\mathrm{e}^{-2mr}\delta_{\nu,2N}\right\} \\ &-\frac{r}{\pi^2}\int_m^\infty\frac{dqq^2}{\sqrt{q^2-m^2}}C\left(\frac{q}{m}\right)K_{\frac{1}{2}+\nu(F-\frac{1}{2})}(qr)K_{\frac{1}{2}-\nu(F-\frac{1}{2})}(qr), \end{aligned} \tag{C8}$$

$$\begin{aligned} B_{\mathrm{I}}(r) = &-\frac{\nu e}{2(2\pi)^2}\frac{1}{r}\left\{\int_0^\infty\frac{du}{\cosh^2(u/2)}\mathrm{e}^{-2mr\cosh(u/2)}\right. \\ &\times\frac{\cos[\nu(F-\frac{1}{2})\pi]\sinh(\nu u)\sinh[\nu(F-\frac{1}{2})u]+\sin[\nu(F-\frac{1}{2})\pi]\sin(\nu\pi)\cosh[\nu(F-\frac{1}{2})u]}{\cosh(\nu u)-\cos(\nu\pi)} \\ &\left.-\frac{2\pi}{\nu}\sum_{p=1}^{[|\nu/2|]}\exp[-2mr\sin(p\pi/\nu)]\frac{\sin[(2F-1)p\pi]}{\sin^2(p\pi/\nu)}+\frac{\pi}{2N}(-1)^N\sin(2NF\pi)\mathrm{e}^{-2mr}\delta_{\nu,2N}\right\} \\ &-\frac{\nu e}{\pi^2}\int_r^\infty dr'\int_m^\infty\frac{dqq^2}{\sqrt{q^2-m^2}}C\left(\frac{q}{m}\right)K_{\frac{1}{2}+\nu(F-\frac{1}{2})}(qr')K_{\frac{1}{2}-\nu(F-\frac{1}{2})}(qr'), \end{aligned} \tag{C9}$$

and

$$\Phi_{\mathrm{I}} = \frac{e}{2m}\left\{\frac{1}{6}(\nu^2-1)\left(F-\frac{1}{2}\right)-\left[\frac{1}{\pi}\int_1^\infty\frac{dt}{t\sqrt{t^2-1}}C(t)+\frac{1}{3}\left(F-\frac{1}{2}\right)\right]\left[\frac{1}{4}-\nu^2\left(F-\frac{1}{2}\right)^2\right]\right\}, \tag{C10}$$

where

$$C(t) = \frac{1}{\pi}\cos\left[\nu\left(F-\frac{1}{2}\right)\pi\right]\frac{\left(\frac{t}{2}\right)^{\nu(2F-1)}\frac{\Gamma[\frac{1}{2}-\nu(F-\frac{1}{2})]}{\Gamma[\frac{1}{2}+\nu(F-\frac{1}{2})]}\tan\left(\frac{\Theta}{2}+\frac{\pi}{4}\right)-\left(\frac{t}{2}\right)^{-\nu(2F-1)}\frac{\Gamma[\frac{1}{2}+\nu(F-\frac{1}{2})]}{\Gamma[\frac{1}{2}-\nu(F-\frac{1}{2})]}\cot\left(\frac{\Theta}{2}+\frac{\pi}{4}\right)}{\left(\frac{t}{2}\right)^{\nu(2F-1)}\frac{\Gamma[\frac{1}{2}-\nu(F-\frac{1}{2})]}{\Gamma[\frac{1}{2}+\nu(F-\frac{1}{2})]}\tan\left(\frac{\Theta}{2}+\frac{\pi}{4}\right)+\frac{2}{t}+\left(\frac{t}{2}\right)^{-\nu(2F-1)}\frac{\Gamma[\frac{1}{2}+\nu(F-\frac{1}{2})]}{\Gamma[\frac{1}{2}-\nu(F-\frac{1}{2})]}\cot\left(\frac{\Theta}{2}+\frac{\pi}{4}\right)}. \tag{C11}$$

Under the condition of minimal irregularity [see (4.16)], we obtain

$$j_\varphi(r)|_{F\neq\frac{1}{2}}=\frac{m}{(2\pi)^2}\left\{\mathrm{sgn}\left(F-\frac{1}{2}\right)\int_0^\infty\frac{du}{\cosh(u/2)}\left[1+\frac{1}{2mr\cosh(u/2)}\right]\mathrm{e}^{-2mr\cosh(u/2)}\right.$$
$$\times\frac{\cos\left[\nu(F-\frac{1}{2})\pi\right]\cosh\left[\nu(|F-\frac{1}{2}|-1)u\right]-\cos\left[\nu(|F-\frac{1}{2}|-1)\pi\right]\cosh\left[\nu(F-\frac{1}{2})u\right]}{\cosh(\nu u)-\cos(\nu\pi)}$$
$$+\frac{2\pi}{\nu}\sum_{p=1}^{[|\nu/2|]}\left[1+\frac{1}{2mr\sin(p\pi/\nu)}\right]\exp[-2mr\sin(p\pi/\nu)]\frac{\sin[(2F-1)p\pi]}{\sin(p\pi/\nu)}$$
$$\left.-\frac{\pi}{2N}(-1)^N\sin(2NF\pi)\left(1+\frac{1}{2mr}\right)\mathrm{e}^{-2mr}\delta_{\nu,2N}\right\},\tag{C12}$$

$$j_\varphi(r)|_{F=\frac{1}{2}}=-\frac{\sin\theta}{2\pi^2}\int_m^\infty\frac{dqq^2}{\sqrt{q^2-m^2}}\frac{\mathrm{e}^{-2qr}}{q+m\cos\theta},\tag{C13}$$

$$B_1(r)|_{F\neq\frac{1}{2}}=\frac{\nu e}{2(2\pi)^2}\frac{1}{r}\left\{\mathrm{sgn}\left(F-\frac{1}{2}\right)\int_0^\infty\frac{du}{\cosh^2(u/2)}\mathrm{e}^{-2mr\cosh(u/2)}\right.$$
$$\times\frac{\cos\left[\nu(F-\frac{1}{2})\pi\right]\cosh\left[\nu(|F-\frac{1}{2}|-1)u\right]-\cos\left[\nu(|F-\frac{1}{2}|-1)\pi\right]\cosh\left[\nu(F-\frac{1}{2})u\right]}{\cosh(\nu u)-\cos(\nu\pi)}$$
$$\left.+\frac{2\pi}{\nu}\sum_{p=1}^{[|\nu/2|]}\exp[-2mr\sin(p\pi/\nu)]\frac{\sin[(2F-1)p\pi]}{\sin^2(p\pi/\nu)}-\frac{\pi}{2N}(-1)^N\sin(2NF\pi)\mathrm{e}^{-2mr}\delta_{\nu,2N}\right\},\tag{C14}$$

$$B_1(r)|_{F=\frac{1}{2}}=-\frac{\nu e\sin\theta}{2\pi^2}\int_m^\infty\frac{dqq^2}{\sqrt{q^2-m^2}}\frac{\Gamma(0,2qr)}{q+m\cos\theta},\tag{C15}$$

$$\Phi_1|_{F\neq\frac{1}{2}}=-\frac{e}{6m}\left[F-\frac{1}{2}-\frac{1}{2}\mathrm{sgn}\left(F-\frac{1}{2}\right)\right]\left\{\frac{3}{4}-\nu^2\left[\frac{1}{4}-\left|F-\frac{1}{2}\right|-F(1-F)\right]\right\},\tag{C16}$$

and

$$\Phi_1|_{F=\frac{1}{2}}=-\frac{e}{4\pi m}\arctan\left(\tan\frac{\theta}{2}\right).\tag{C17}$$

APPENDIX D: CASE OF MASSLESS QUANTUM SPINOR MATTER

We present here the results for the case of massless quantum spinor matter in the background of the ANO vortex of nonzero transverse size.

In the case of $\nu\geq1$ and $\frac{1}{2}(1-\frac{1}{\nu})<F<\frac{1}{2}(1+\frac{1}{\nu})$ or $\frac{1}{2}\leq\nu<1$ and $\frac{1}{2}(\frac{1}{\nu}-1)<F<\frac{1}{2}(3-\frac{1}{\nu})$, we obtain

$$j_\varphi(r)|_{F<\frac{1}{2},\theta\neq-\frac{\pi}{2}}=\frac{1}{2(2\pi)^2}\frac{1}{r}\left\{\frac{2\pi}{\nu}\sum_{p=1}^{[|\nu/2|]}\frac{\sin[(2F-1)p\pi]}{\sin^2(p\pi/\nu)}-\frac{\pi}{2N}(-1)^N\sin(2NF\pi)\delta_{\nu,2N}-\int_0^\infty\frac{du}{\cosh^2(u/2)}\right.$$
$$\left.\times\frac{\cos\left[\nu(F-\frac{1}{2})\pi\right]\cosh\left[\nu(F+\frac{1}{2})u\right]-\cos[\nu(F+\frac{1}{2})\pi]\cosh\left[\nu(F-\frac{1}{2})u\right]}{\cosh(\nu u)-\cos(\nu\pi)}\right\}$$
$$-\frac{r}{\pi^2}\int_0^\infty dqq\left[\sum_{l=0}^\infty C^{(\wedge)}_{\nu(l-F+\frac{1}{2})+\frac{1}{2}}(qr_0)|_{m=0}K_{\nu(l-F+\frac{1}{2})+\frac{1}{2}}(qr)K_{\nu(l-F+\frac{1}{2})-\frac{1}{2}}(qr)\right.$$
$$\left.-\sum_{l=1}^\infty C^{(\vee)}_{\nu(l+F-\frac{1}{2})+\frac{1}{2}}(qr_0)|_{m=0}K_{\nu(l+F-\frac{1}{2})+\frac{1}{2}}(qr)K_{\nu(l+F-\frac{1}{2})-\frac{1}{2}}(qr)\right],\tag{D1}$$

$$j_\varphi(r)|_{F>\frac{1}{2},\theta\neq\frac{\pi}{2}} = \frac{1}{2(2\pi)^2}\frac{1}{r}\left\{\frac{2\pi}{\nu}\sum_{p=1}^{[|\nu/2|]}\frac{\sin[(2F-1)p\pi]}{\sin^2(p\pi/\nu)} - \frac{\pi}{2N}(-1)^N\sin(2NF\pi)\delta_{\nu,2N} + \int_0^\infty \frac{du}{\cosh^2(u/2)}\right.$$
$$\left.\times\frac{\cos[\nu(F-\frac{1}{2})\pi]\cosh[\nu(F-\frac{3}{2})u] - \cos[\nu(F-\frac{3}{2})\pi]\cosh[\nu(F-\frac{1}{2})u]}{\cosh(\nu u)-\cos(\nu\pi)}\right\}$$
$$-\frac{r}{\pi^2}\int_0^\infty dqq\left[\sum_{l=1}^\infty C^{(\wedge)}_{\nu(l-F+\frac{1}{2})+\frac{1}{2}}(qr_0)|_{m=0}K_{\nu(l-F+\frac{1}{2})+\frac{1}{2}}(qr)K_{\nu(l-F+\frac{1}{2})-\frac{1}{2}}(qr)\right.$$
$$\left.-\sum_{l=0}^\infty C^{(\vee)}_{\nu(l+F-\frac{1}{2})+\frac{1}{2}}(qr_0)|_{m=0}K_{\nu(l+F-\frac{1}{2})+\frac{1}{2}}(qr)K_{\nu(l+F-\frac{1}{2})-\frac{1}{2}}(qr)\right], \tag{D2}$$

$$j_\varphi(r)|_{F\neq\frac{1}{2},\theta=\pm\frac{\pi}{2}} = \frac{1}{2(2\pi)^2}\frac{1}{r}\left\{\frac{2\pi}{\nu}\sum_{p=1}^{[|\nu/2|]}\frac{\sin[(2F-1)p\pi]}{\sin^2(p\pi/\nu)} - \frac{\pi}{2N}(-1)^N\sin(2NF\pi)\delta_{\nu,2N} \mp \int_0^\infty \frac{du}{\cosh^2(u/2)}\right.$$
$$\left.\times\frac{\cos[\nu(F-\frac{1}{2})\pi]\cosh[\nu(F-\frac{1}{2}\pm1)u] - \cos[\nu(F-\frac{1}{2}\pm1)\pi]\cosh[\nu(F-\frac{1}{2})u]}{\cosh(\nu u)-\cos(\nu\pi)}\right\}$$
$$\mp\frac{r}{\pi^2}\int_0^\infty dqq\left\{\frac{I_{\frac{1}{2}\mp\nu(F-\frac{1}{2})}(qr_0)}{K_{\frac{1}{2}\mp\nu(F-\frac{1}{2})}(qr_0)}K_{\frac{1}{2}+\nu(F-\frac{1}{2})}(qr)K_{\frac{1}{2}-\nu(F-\frac{1}{2})}(qr)\right.$$
$$+\sum_{l=1}^\infty\left[\frac{I_{\nu(l-F+\frac{1}{2})\pm\frac{1}{2}}(qr_0)}{K_{\nu(l-F+\frac{1}{2})\pm\frac{1}{2}}(qr_0)}K_{\nu(l-F+\frac{1}{2})+\frac{1}{2}}(qr)K_{\nu(l-F+\frac{1}{2})-\frac{1}{2}}(qr)\right.$$
$$\left.\left.+\frac{I_{\nu(l+F-\frac{1}{2})\mp\frac{1}{2}}(qr_0)}{K_{\nu(l+F-\frac{1}{2})\mp\frac{1}{2}}(qr_0)}K_{\nu(l+F-\frac{1}{2})+\frac{1}{2}}(qr)K_{\nu(l+F-\frac{1}{2})-\frac{1}{2}}(qr)\right]\right\}, \tag{D3}$$

and

$$j_\varphi(r)|_{F=\frac{1}{2}} = -\frac{\sin\theta}{(2\pi)^2}\left[\frac{1}{r-r_0} + 8r\int_0^\infty dqq\sum_{l=1}^\infty \tilde{C}_{\nu l+\frac{1}{2}}(qr_0)|_{m=0}K_{\nu l+\frac{1}{2}}(qr)K_{\nu l-\frac{1}{2}}(qr)\right]. \tag{D4}$$

It should be noted that the current is invariant under transformation $\theta\to\pi-\theta$. Thus the current is continuous in θ, and its values at $\theta=0$ and $\theta=\pi$ coincide, in particular,

$$j_\varphi(r)|_{F=\frac{1}{2},\theta=0} = j_\varphi(r)|_{F=\frac{1}{2},\theta=\pi} = 0. \tag{D5}$$

Since a piece of $j_\varphi(r)$ is proportional to r^{-1}, the corresponding piece of $B_{\rm I}(r)$ is also proportional to r^{-1}. Consequently, flux $\Phi_{\rm I}$ [see (2.22)] is given by an integral that is linearly divergent at $r\to\infty$. Therefore, we have no choice but to introduce cutoff $r_{\max}>r$ and the restricted flux,

$$\Phi_{{\rm I}(r_{\max})} = \frac{2\pi}{\nu}\int_{r_0}^{r_{\max}} drrB_{\rm I}(r), \tag{D6}$$

where, as a consequence of (D1)–(D4),

$$B_{\mathrm{I}}(r)|_{F<\frac{1}{2},\theta\neq-\frac{\pi}{2}}=\frac{\nu e}{2(2\pi)^2}\left(\frac{1}{r}-\frac{1}{r_{\max}}\right)\left\{\frac{2\pi}{\nu}\sum_{p=1}^{[|\nu/2|]}\frac{\sin[(2F-1)p\pi]}{\sin^2(p\pi/\nu)}-\frac{\pi}{2N}(-1)^N\sin(2NF\pi)\delta_{\nu,2N}-\int_0^\infty\frac{du}{\cosh^2(u/2)}\right.$$
$$\left.\times\frac{\cos[\nu(F-\frac{1}{2})\pi]\cosh[\nu(F+\frac{1}{2})u]-\cos[\nu(F+\frac{1}{2})\pi)]\cosh[\nu(F-\frac{1}{2})u]}{\cosh(\nu u)-\cos(\nu\pi)}\right\}$$
$$-\frac{\nu e}{\pi^2}\int_r^{r_{\max}}dr'\int_0^\infty dqq\left[\sum_{l=0}^\infty C^{(\wedge)}_{\nu(l-F+\frac{1}{2})+\frac{1}{2}}(qr_0)|_{m=0}K_{\nu(l-F+\frac{1}{2})+\frac{1}{2}}(qr')K_{\nu(l-F+\frac{1}{2})-\frac{1}{2}}(qr')\right.$$
$$\left.-\sum_{l=1}^\infty C^{(\vee)}_{\nu(l+F-\frac{1}{2})+\frac{1}{2}}(qr_0)|_{m=0}K_{\nu(l+F-\frac{1}{2})+\frac{1}{2}}(qr')K_{\nu(l+F-\frac{1}{2})-\frac{1}{2}}(qr')\right],\tag{D7}$$

$$B_{\mathrm{I}}(r)|_{F>\frac{1}{2},\theta\neq\frac{\pi}{2}}=\frac{\nu e}{2(2\pi)^2}\left(\frac{1}{r}-\frac{1}{r_{\max}}\right)\left\{\frac{2\pi}{\nu}\sum_{p=1}^{[|\nu/2|]}\frac{\sin[(2F-1)p\pi]}{\sin^2(p\pi/\nu)}-\frac{\pi}{2N}(-1)^N\sin(2NF\pi)\delta_{\nu,2N}+\int_0^\infty\frac{du}{\cosh^2(u/2)}\right.$$
$$\left.\times\frac{\cos[\nu(F-\frac{1}{2})\pi]\cosh[\nu(F-\frac{3}{2})u]-\cos[\nu(F-\frac{3}{2})\pi)]\cosh[\nu(F-\frac{1}{2})u]}{\cosh(\nu u)-\cos(\nu\pi)}\right\}$$
$$-\frac{\nu e}{\pi^2}\int_r^{r_{\max}}dr'\int_0^\infty dqq\left[\sum_{l=1}^\infty C^{(\wedge)}_{\nu(l-F+\frac{1}{2})+\frac{1}{2}}(qr_0)|_{m=0}K_{\nu(l-F+\frac{1}{2})+\frac{1}{2}}(qr')K_{\nu(l-F+\frac{1}{2})-\frac{1}{2}}(qr')\right.$$
$$\left.-\sum_{l=0}^\infty C^{(\vee)}_{\nu(l+F-\frac{1}{2})+\frac{1}{2}}(qr_0)|_{m=0}K_{\nu(l+F-\frac{1}{2})+\frac{1}{2}}(qr')K_{\nu(l+F-\frac{1}{2})-\frac{1}{2}}(qr')\right],\tag{D8}$$

$$B_{\mathrm{I}}(r)|_{F\neq\frac{1}{2},\theta=\pm\frac{\pi}{2}}=\frac{\nu e}{2(2\pi)^2}\left(\frac{1}{r}-\frac{1}{r_{\max}}\right)\left\{\frac{2\pi}{\nu}\sum_{p=1}^{[|\nu/2|]}\frac{\sin[(2F-1)p\pi]}{\sin^2(p\pi/\nu)}-\frac{\pi}{2N}(-1)^N\sin(2NF\pi)\delta_{\nu,2N}\mp\int_0^\infty\frac{du}{\cosh^2(u/2)}\right.$$
$$\left.\times\frac{\cos[\nu(F-\frac{1}{2})\pi]\cosh[\nu(F-\frac{1}{2}\pm1)u]-\cos[\nu(F-\frac{1}{2}\pm1)\pi)]\cosh[\nu(F-\frac{1}{2})u]}{\cosh(\nu u)-\cos(\nu\pi)}\right\}$$
$$\mp\frac{\nu e}{\pi^2}\int_r^{r_{\max}}dr'\int_0^\infty dqq\left\{\frac{I_{\frac{1}{2}\mp\nu(F-\frac{1}{2})}(qr_0)}{K_{\frac{1}{2}\mp\nu(F-\frac{1}{2})}(qr_0)}K_{\frac{1}{2}+\nu(F-\frac{1}{2})}(qr')K_{\frac{1}{2}-\nu(F-\frac{1}{2})}(qr')\right.$$
$$+\sum_{l=1}^\infty\left[\frac{I_{\nu(l-F+\frac{1}{2})\pm\frac{1}{2}}(qr_0)}{K_{\nu(l-F+\frac{1}{2})\pm\frac{1}{2}}(qr_0)}K_{\nu(l-F+\frac{1}{2})+\frac{1}{2}}(qr')K_{\nu(l-F+\frac{1}{2})-\frac{1}{2}}(qr')\right.$$
$$\left.\left.+\frac{I_{\nu(l+F-\frac{1}{2})\mp\frac{1}{2}}(qr_0)}{K_{\nu(l+F-\frac{1}{2})\mp\frac{1}{2}}(qr_0)}K_{\nu(l+F-\frac{1}{2})+\frac{1}{2}}(qr')K_{\nu(l+F-\frac{1}{2})-\frac{1}{2}}(qr')\right]\right\},\tag{D9}$$

and

$$B_{\mathrm{I}}(r)|_{F=\frac{1}{2}}=\frac{\nu e\sin\theta}{(2\pi)^2}\left[\frac{1}{r_0}\ln\left(1-\frac{r_0}{r}\right)-\frac{1}{r_0}\ln\left(1-\frac{r_0}{r_{\max}}\right)\right.$$
$$\left.-8\int_r^{r_{\max}}dr'\int_0^\infty dqq\sum_{l=1}^\infty\tilde{C}_{\nu l+\frac{1}{2}}(qr_0)|_{m=0}K_{\nu l+\frac{1}{2}}(qr')K_{\nu l-\frac{1}{2}}(qr')\right].\tag{D10}$$

In the case of $\nu>1$ and $0<F<\frac{1}{2}(1-\nu)$, $j_\varphi(r)$ is given by the right-hand side of (D1) and $B_{\mathrm{I}}(r)$ is given by the right-hand side of (D7). In the case of $\nu>1$ and $\frac{1}{2}(1+\nu)<F<1$, $j_\varphi(r)$ is given by the right-hand side of (D2) and $B_{\mathrm{I}}(r)$ is given by the right-hand side of (D8).

Turning now to flux $\Phi_{\mathrm{I}(r_{\max})}$ (D6), we numerically calculate quantity

$$\omega(\theta)=\lim_{r\to r_0}\nu r j_\varphi(r)\left(\frac{r-r_0}{r_0}\right)^2$$

and compare it in Fig. 10 with the appropriate quantity in the case of the massive spinor field (see Sec. VI). Note that $\omega(\theta)$ in the massless case is strictly symmetric with respect to point $\theta=\pi/2$ (location of the inverted peak in Fig. 10), whereas $\omega(\theta)$ in the massive case is not symmetric, although

this asymmetry is so slight that it is not visible in Figs. 1 and 10. Note also that coefficients $C_\rho^{(\wedge)}(qr_0)|_{\theta=\pm\pi/2}$, $C_\rho^{(\vee)}(qr_0)|_{\theta=\pm\pi/2}$, and $\tilde{C}_\rho(qr_0)|_{\theta=\pm\pi/2}$ in the massive case coincide with those in the massless case, and the differences in the values of $\omega(\theta)$ are due to different measures of integration in the massive and massless cases. As follows from the behavior of $\omega(\theta)$, the induced vacuum magnetic flux, either Φ_{I} (2.22) in the massive case or $\Phi_{\mathrm{I}(r_{\max})}$ (D6) in the massless case, is finite at $\theta = 0$ and $\theta = \pi$ only, with coinciding values at these points in the latter case. Thus we obtain

$$\Phi_{\mathrm{I}(r_{\max})}|_{\theta=\frac{\pi}{2}\mp\frac{\pi}{2}} = 0, \qquad F = 1/2, \tag{D11}$$

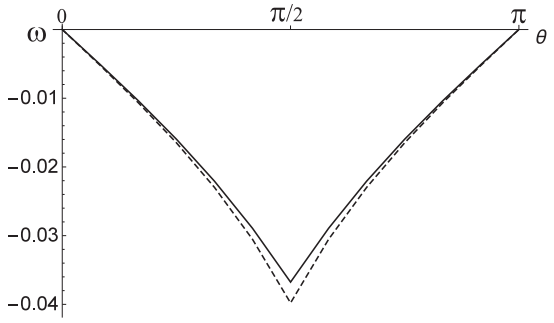

FIG. 10. $\omega(\theta)$ in the case of the massless spinor field (solid line) and in the case of the massive spinor field (dashed line).

and

$$\begin{aligned}\Phi_{\mathrm{I}(r_{\max})}\Big|_{\theta=\frac{\pi}{2}\mp\frac{\pi}{2}} &= e\frac{(r_{\max}-r_0)^2}{r_{\max}}\left\{\frac{1}{4\nu}\sum_{p=1}^{[|\nu/2|]}\frac{\sin[(2F-1)p\pi]}{\sin^2(p\pi/\nu)}-\frac{1}{16N}(-1)^N\sin(2NF\pi)\delta_{\nu,2N}+\mathrm{sgn}\left(F-\frac{1}{2}\right)\frac{1}{8\pi}\int_0^\infty\frac{du}{\cosh^2(u/2)}\right.\\ &\left.\times\frac{\cos[\nu(F-\frac{1}{2})\pi)]\cosh[\nu(|F-\frac{1}{2}|-1)u]-\cos[\nu(|F-\frac{1}{2}|-1)\pi]\cosh[\nu(F-\frac{1}{2})u]}{\cosh(\nu u)-\cos(\nu\pi)}\right\}\\ &+\frac{e}{2\pi}r_0\int_0^\infty dv\left\{\frac{1}{2}\left[C^{(0)}_{\frac{1}{2}+\nu(F-\frac{1}{2})}(v)-C^{(0)}_{\frac{1}{2}-\nu(F-\frac{1}{2})}(v)+\mathrm{sgn}\left(F-\frac{1}{2}\right)\left(C^{(0)}_{\frac{1}{2}+\nu(F-\frac{1}{2})}(v)+C^{(0)}_{\frac{1}{2}-\nu(F-\frac{1}{2})}(v)\right)\right]\right.\\ &\left.\times D^{(0)}_{\frac{1}{2}+\nu|F-\frac{1}{2}|}\left(v;\frac{r_0}{r_{\max}}\right)+\sum_{l=1}^\infty\left[C^{(0)}_{\nu(l+F-\frac{1}{2})+\frac{1}{2}}(v)D^{(0)}_{\nu(l+F-\frac{1}{2})+\frac{1}{2}}\left(v;\frac{r_0}{r_{\max}}\right)-C^{(0)}_{\nu(l-F+\frac{1}{2})+\frac{1}{2}}(v)D^{(0)}_{\nu(l-F+\frac{1}{2})+\frac{1}{2}}\left(v;\frac{r_0}{r_{\max}}\right)\right]\right\},\\ &F\neq 1/2,\end{aligned} \tag{D12}$$

where

$$C_\rho^{(0)}(v) = [I_\rho(v)K_\rho(v) - I_{\rho-1}(v)K_{\rho-1}(v)][K_\rho^2(v) + K_{\rho-1}^2(v)]^{-1} \tag{D13}$$

and

$$\begin{aligned}D_\rho^{(0)}(v;w) &= \rho K_\rho^2(v) - (\rho-1)K_{\rho+1}(v)K_{\rho-1}(v) + v\left[K_\rho(v)\frac{d}{d\rho}K_{\rho-1}(v)\right.\\ &\left.-K_{\rho-1}(v)\frac{d}{d\rho}K_\rho(v)\right] - w^{-2}\left[\rho K_\rho^2\left(\frac{v}{w}\right)-(\rho-1)K_{\rho+1}\left(\frac{v}{w}\right)K_{\rho-1}\left(\frac{v}{w}\right)\right]\\ &-\frac{v}{w}\left[K_\rho\left(\frac{v}{w}\right)\frac{d}{d\rho}K_{\rho-1}\left(\frac{v}{w}\right)-K_{\rho-1}\left(\frac{v}{w}\right)\frac{d}{d\rho}K_\rho\left(\frac{v}{w}\right)\right].\end{aligned} \tag{D14}$$

Retaining only the terms that are maximally divergent in the limit of $r_{\max}\to\infty$, we get

$$\begin{aligned}\Phi_{\mathrm{I}(r_{\max})}|_{\theta=\frac{\pi}{2}\mp\frac{\pi}{2}} &= er_{\max}\left\{\frac{1}{4\nu}\sum_{p=1}^{[|\nu/2|]}\frac{\sin[(2F-1)p\pi]}{\sin^2(p\pi/\nu)}-\frac{1}{16N}(-1)^N\sin(2NF\pi)\delta_{\nu,2N}+\mathrm{sgn}\left(F-\frac{1}{2}\right)\frac{1}{8\pi}\int_0^\infty\frac{du}{\cosh^2(u/2)}\right.\\ &\left.\times\frac{\cos[\nu(F-\frac{1}{2})\pi)]\cosh[\nu(|F-\frac{1}{2}|-1)u]-\cos[\nu(|F-\frac{1}{2}|-1)\pi]\cosh[\nu(F-\frac{1}{2})u]}{\cosh(\nu u)-\cos(\nu\pi)}\right\}\\ &+O(er_0),\quad F\neq 1/2.\end{aligned} \tag{D15}$$

Thus, we obtain the following relation between current $j_\varphi(r)|_{\theta=\frac{\pi}{2}\mp\frac{\pi}{2}}$ and magnetic field strength $B_{\rm I}(r)|_{\theta=\frac{\pi}{2}\mp\frac{\pi}{2}}$ in the physically sensible case of $r_{\max}\gg r_0$:

$$\nu e j_\varphi(r)|_{\theta=\frac{\pi}{2}\mp\frac{\pi}{2}}=\frac{r_{\max}}{r_{\max}-r}B_{\rm I}(r)|_{\theta=\frac{\pi}{2}\mp\frac{\pi}{2}}=\frac{\nu}{\pi r_{\max}r}\Phi_{{\rm I}(r_{\max})}|_{\theta=\frac{\pi}{2}\mp\frac{\pi}{2}},\quad r\gg r_0, \tag{D16}$$

where flux $\Phi_{{\rm I}(r_{\max})}|_{\theta=\frac{\pi}{2}\mp\frac{\pi}{2}}$ is given by (D15).

In particular, we get in the case of $\nu=1$

$$\Phi_{{\rm I}(r_{\max})}|_{\nu=1,\theta=\frac{\pi}{2}\mp\frac{\pi}{2}}=\frac{e}{4}r_{\max}\tan(F\pi)\left|F-\frac{1}{2}\right|\left(\left|F-\frac{1}{2}\right|-1\right)+O(er_0) \tag{D17}$$

and

$$e j_\varphi(r)|_{\nu=1,\theta=\frac{\pi}{2}\mp\frac{\pi}{2}}=\frac{r_{\max}}{r_{\max}-r}B_I(r)|_{\nu=1,\theta=\frac{\pi}{2}\mp\frac{\pi}{2}}=\frac{e}{4\pi r}\tan(F\pi)\left|F-\frac{1}{2}\right|\left(\left|F-\frac{1}{2}\right|-1\right),\quad r\gg r_0. \tag{D18}$$

The last relation for the current was obtained in [47] in the $r_0=0$ case under the condition of minimal irregularity with requirements of the charge conjugation invariance and continuity in θ [see (10.6) in this reference where the definition of the current differs by an extra r^{-1}]. Note a discontinuity at $F=1/2$, which is independent of ν,

$$\lim_{F\to(1/2)_\pm} e j_\varphi(r)|_{\theta\neq\pm\frac{\pi}{2}}=\pm\frac{e}{4\pi^2 r},\quad r\gg r_0. \tag{D19}$$

This is distinct from the case of quantum scalar matter under the Dirichlet boundary condition, when the current that is induced in the vacuum by the infinitely thin vortex is continuous and vanishing at $F=1/2$ [43–45]; see the appropriate expression from these references at $m=0$ and $\nu=1$:

$$e j_\varphi(r)|_{\rm scalar,Dirichlet}=-\frac{e}{4\pi r}\tan(F\pi)\left(F-\frac{1}{2}\right)^2. \tag{D20}$$

[1] A. A. Abrikosov, Sov. Phys. JETP **5**, 1174 (1957).
[2] H. B. Nielsen and P. Olesen, Nucl. Phys. **B61**, 45 (1973).
[3] T. W. B. Kibble, J. Phys. A **9**, 1387 (1976).
[4] T. W. B. Kibble, Phys. Rep. **67**, 183 (1980).
[5] A. Vilenkin, Phys. Rev. D **23**, 852 (1981).
[6] A. Vilenkin, Phys. Rev. D **24**, 2082 (1981).
[7] Ya. B. Zeldovich, Mon. Not. R. Astron. Soc. **192**, 663 (1980).
[8] R. A. Battye, B. Garbrecht, A. Moss, and H. Stoica, J. Cosmol. Astropart. Phys. 01 (2008) 020.
[9] K. S. Novoselov, D. Jiang, F. Schedin, T. J. Booth, V. V. Khotkevich, S. V. Morozov, and A. K. Geim, Proc. Natl. Acad. Sci. U.S.A. **102**, 10451 (2005).
[10] A. K. Geim and K. S. Novoselov, Nat. Mater. **6**, 183 (2007).
[11] M. I. Katsnelson, *Graphene: Carbon in Two Dimensions* (Cambridge University Press, Cambridge, England, 2012).
[12] H. Heiberg-Andersen, Carbon nanonones in *Handbook of Theoretical and Computational Nanotechnology*, edited by M. Rieth and W. Schommers (American Scientific Publishers, Valencia, CA, 2006), pp. 507–517.
[13] S. N. Naess, A. Elgsaeetter, G. Helgesen, and K. D. Knudsen, Sci. Technol. Adv. Mater. **10**, 065002 (2009).
[14] S. Cahangirov, M. Topsakal, E. Akturk, H. Sahin, and S. Ciraci, Phys. Rev. Lett. **102**, 236804 (2009).
[15] H. Liu, A. T. Neal, Z. Zhu, Z. Luo, X. Xu, D. Tomanek, and P. D. Ye, ACS Nano **8**, 4033 (2014).
[16] C. C. Tsuei and J. R. Kirtley, Rev. Mod. Phys. **72**, 969 (2000).
[17] X. L. Qi and S. C. Zhang, Rev. Mod. Phys. **83**, 1057 (2011).
[18] Y. Aharonov and D. Bohm, Phys. Rev. **115**, 485 (1959).
[19] G. V. Dunne, *Topological Aspects of Low Dimensional Systems* (Springer, Berlin, 1999).
[20] E. R. B. de Mello, V. Bezerra, A. A. Saharian, and V. M. Bardeghyan, Phys. Rev. D **82**, 085033 (2010).
[21] S. Bellucci, E. R. B. de Mello, and A. A. Saharian, Phys. Rev. D **83**, 085017 (2011).
[22] E. R. B. de Mello, F. Moraes, and A. A. Saharian, Phys. Rev. D **85**, 045016 (2012).
[23] V. M. Gorkavenko, I. V. Ivanchenko, and Yu. A. Sitenko, Int. J. Mod. Phys. A **31**, 1650017 (2016).
[24] V. M. Gorkavenko, Yu. A. Sitenko, and O. B. Stepanov, J. Phys. A **43**, 175401 (2010).

[25] V. M. Gorkavenko, Yu. A. Sitenko, and O. B. Stepanov, Int. J. Mod. Phys. A **26**, 3889 (2011).
[26] V. M. Gorkavenko, Yu. A. Sitenko, and O. B. Stepanov, Int. J. Mod. Phys. A **28**, 1350161 (2013).
[27] J. von Neumann, *Mathematische Grundlagen der Quantummechanik* (Springer, Berlin, 1932).
[28] M. Reed and B. Simon, *Methods of Modern Mathematical Physics II. Fourier Analysis, Self-Adjointness* (Academic Press, New York, 1975).
[29] P. de Sousa Gerbert and R. Jackiw, Commun. Math. Phys. **124**, 229 (1989).
[30] P. de Sousa Gerbert, Phys. Rev. D **40**, 1346 (1989).
[31] Yu. A. Sitenko, Phys. Lett. B **387**, 334 (1996).
[32] Yu. A. Sitenko, Phys. At. Nucl. **60**, 2102 (1997); **62**, 1084 (E) (1999).
[33] Yu. A. Sitenko and D. G. Rakityansky, Phys. At. Nucl. **60**, 1497 (1997).
[34] Yu. A. Sitenko, Phys. At. Nucl. **62**, 1056 (1999).
[35] Yu. A. Sitenko, Phys. At. Nucl. **62**, 1767 (1999).
[36] Yu. A. Sitenko and N. D. Vlasii, Nucl. Phys. **B787**, 241 (2007).
[37] Yu. A. Sitenko and N. D. Vlasii, J. Phys. Conf. Ser. **129**, 012008 (2008).
[38] Yu. A. Sitenko and N. D. Vlasii, [Fiz. Nizk. Temp. **34**, 1049 (2008)] Low Temp. Phys. **34**, 826 (2008).
[39] Yu. A. Sitenko and V. M. Gorkavenko, [Fiz. Nizk. Temp. **44**, 1618 (2018)] Low Temp. Phys. **44**, 1261 (2018).
[40] K. Johnson, Acta Phys. Pol. B **6**, 865 (1975).
[41] M. G. Alford, J. March-Russel, and F. Wilczek, Nucl. Phys. **B328**, 140 (1989).
[42] A. P. Prudnikov, Yu. A. Brychkov, and O. I. Marychev, *Integrals and Series: Special Functions* (Gordon & Breach, New York, 1986).
[43] Yu. A. Sitenko and A. Yu. Babansky, Mod. Phys. Lett. A **13**, 379 (1998).
[44] Yu. A. Sitenko and A. Yu. Babansky, Phys. At. Nucl. **61**, 1594 (1998).
[45] Yu. A. Sitenko and N. D. Vlasii, Classical Quantum Gravity **26**, 195009 (2009).
[46] *Handbook of Mathematical Functions*, edited by M. Abramowitz and I. A. Stegun (Dover, New York, 1972).
[47] Yu. A. Sitenko, Ann. Phys. (N.Y.) **282**, 167 (2000).

ВИСНОВКИ

В дисертаційній роботі досліджено можливі експериментальні прояви в експериментах на прискорювачах частинок нової фізики, що дуже слабко взаємодіють з частинками Стандартної моделі, та прояви лінійних топологічних дефектів у вигляді космічних струн з "магнітним" полем калібрувальної групи $U_X(1)$, що виникли внаслідок фазових переходів у ранньому Всесвіті. Для опису ефектів, що викликаються космічною "магнітною" струною, використовується модель непроникливої для полів матерії трубки скінченного радіуса з "магнітним" полем. Дана модель дозволила розглянути квантові ефекти у вакуумі полів матерії в самому загальному випадку незалежно від конкретної природи утворення космічної струни припускаючи, що поля матерії заряджені відносно калібрувальної групи $U_X(1)$.

В дисертаційній роботі отримано такі результати.

- Зроблено повний і самоузгоджений опис всіх каналів розпаду масивних скалярів з масою в декілька ГеВ в скалярному розширенні СМ.

- Послідовно розглянуто всі канали народження масивного скаляру з розпадів K та B мезонів, включаючи народження скалярів у розпадах B мезонів у різні збуджені стани каонів. Детально проаналізовано прямі канали народження масивного скаляру в протон-нуклонних зіткненнях в залежності від енергії частинок, що зіштовхуються.

- Знайдено домінуючі канали народження та розпаду масивних скалярів для умов експериментів DUNE (Fermilab), SHiP (SPS CERN) та

експериментів на LHC. Встановлено, що в експерименті DUNE домінуючим каналом народження скалярів є процес глибоконепружнього розсіяння нуклонів, а в експерименті SHiP та експериментах на LHC домінуючим каналом народження скалярів є розпад мезонів.

- Отримано ефективний лагранжіан взаємодії масивного векторного бозону (в розширенні СМ зі взаємодією типу Черна-Саймонса) з кварками різних ароматів. Показано, що ефективна взаємодія векторного бозону з кварками різних ароматів не вимагає застосування процедури перенормування. Показано, що взаємодією векторного бозону з верхніми кварками різних ароматів можна знехтувати.

- Послідовно розглянуто всі канали народження масивного векторного бозону (в розширенні СМ зі взаємодією типу Черна-Саймонса) з розпадів K та B мезонів, включаючи народження векторних бозонів у розпадах B мезонів у різні збуджені стани каонів.

- Отримано оригінальні розв'язки та виражено елементи юкавівської матриці в нейтринному розширенні СМ з параметрами масової матриці активних нейтрино.

- Зроблена оцінка похибки в розрахунках області чутливості експерименту SHiP, пов'язаної з використанням для опису народження правокільних масивних нейтрино в тричастинкових розпадах мезонів спрощених матричних елементів, що використовуються в програмі моделювання процесів зіткнення частинок при високих енергіях PYTHIA, в порівнянні з використанням коректних матричних елементів.

- Запропоновано вибір спрощених матричних елементів в комп'ютерній програмі PYTHIA для опису реакцій народження правокіральних масивних нейтрино в тричастинкових розпадах псевдоскалярного мезона

в інший псевдоскалярний мезон та розпадах псевдоскалярного мезона у векторний мезон, що дають найменше відхилення від коректних розрахунків.

- Отримано аналітичні вирази у вигляді інтегралів з нескінченними межами від рядів з нескінченною кількістю доданків для поляризації вакууму квантованого зарядженого масивного скалярного поля матерії в присутності "магнітної" космічної струни в просторі-часі довільної розмірності для випадків граничної умови на поверхні трубки типу Діріхле та Неймана. За допомогою чисельних методів побудовано графічні залежності індукованої густини енергії у вакуумі скалярного поля матерії за різних значень сталої зв'язку скалярного поля з кривизною простору-часу для випадку граничної умови на поверхні трубки типу Діріхле.

- Отримано чисельні значення повної індукованої енергії у вакуумі квантованого масивного зарядженого скалярного поля в просторі-часі довільної розмірності в присутності "магнітної" космічної струни в просторі-часі довільної розмірності. Показано, що у випадку граничної умови на поверхні трубки типу Діріхле повна індукована енергія не залежить від сталої зв'язку скалярного поля з кривизною простору-часу.

- Показано, що ефект поляризації вакууму квантованого зарядженого скалярного поля матерії в присутності "магнітної" космічної струни у випадку граничної умови на поверхні трубки типу Неймана є суттєво більшим в порівнянні з випадком граничної умови на поверхні трубки типу Діріхле.

- Показано, що ефекти поляризації вакууму визначаються лише дробовою частиною "магнітного" потоку космічної струни, що є проявом

ефекту Ааронова-Бома. Показано, що ефекти поляризації вакууму є незначними при $mcr_0 > \hbar$, вони максимально проявляють себе за умови $mcr_0 \ll \hbar$, де r_0 – товщина трубки, а m – маса кванта поля матерії.

- Показано, що поляризація вакууму буде суттєвою у випадку, коли маса квантованого поля матерії є значно меншою за масу Гіґсівського поля, що призвело до спонтанного порушення симетрії і виникнення топологічного ефекту у вигляді "магнітної" космічної струни. Іншими словами, космічна струна, що була сформована на масштабах теорії Великого об'єднання буде поляризувати вакуум сучасних полів матерії, але не зможе впливати на вакуум полів з масою порядку масштабу теорії Великого об'єднання.

- Отримано аналітичні вирази у вигляді інтегралів з нескінченними межами від рядів з нескінченною кількістю доданків для індукованого магнітного потоку у вакуумі квантованого масивного зарядженого скалярного поля в присутності "магнітної" космічної струни у конічному просторі довільної розмірності в загальному випадку граничної умови типу Робена. Для генерації в системі магнітного поля кванти поля матерії повинні також мати електричні заряди.

- За допомогою чисельних методів досліджено поведінку індукованого магнітного потоку у вакуумі квантованого масивного зарядженого скалярного поля в присутності "магнітної" космічної струни від значень параметра граничної умови типу Робена на всьому проміжку можливих значень цього параметра $-\pi/2 \leq \theta < \pi/2$.

- Показано, що за недодатних значень параметра $-\pi/2 \leq \theta \leq 0$ індукований магнітний потік у вакуумі квантованого масивного зарядженого скалярного поля в присутності "магнітної" космічної струни є

найбільшим для випадку $\theta = -\pi/2$ (гранична умова типу Неймана), а найменшим він є для випадку $\theta = 0$ (гранична умова типу Діріхле).

- Показано, що за додатніх значень параметра $0 < \theta < \pi/2$ існують розв'язки, що відповідають зв'язаним станам. Індукований магнітний потік у вакуумі квантованого масивного зарядженого скалярного поля в присутності "магнітної" космічної струни має складну поведінку з особливими точками яких тим більше, чим ближче значення параметра θ до нуля. Індукований магнітний потік може мати більші значення та не прямувати до нуля при значно більших товщинах космічної струни в порівнянні з потоком, що індукується за граничної умови типу Робена з недодатним значенням параметра θ.

- Отримано загальний вигляд граничної умови на ферміонне поле матерії на поверхні трубки скінченого радіусу виходячи з умови самоспряженого розширення оператора діраковського гамільтоніана в присутності "магнітної" космічної струни у конічному просторі-часі розмірності 2+1. Показано, що гранична умова характеризується одним параметром.

- Отримано аналітичні вирази у вигляді інтегралів з нескінченними межами від рядів з нескінченною кількістю доданків для індукованого магнітного потоку у вакуумі квантованого масивного зарядженого ферміонного поля в присутності "магнітної" космічної струни у конічному просторі-часі розмірності 2+1.

- За допомогою чисельних методів в просторі-часі розмірності 2+1 досліджено поведінку індукованого магнітного потоку у вакуумі квантованого масивного зарядженого ферміонного поля в присутності "магнітної" космічної струни від значень параметра самоспряженого роз-

ширення. Знайдені значення параметра самоспряженого розширення, за яких повний індукований потік є скінченним.

- Показано, що умова скінченності значення індукованого потоку у вакуумі квантованого масивного зарядженого ферміонного поля в присутності "магнітної" космічної струни є недостатньою для визначення фізичних значень параметра самоспряженого розширення. Додатковою умовою є вимога спадання величини квантових ефектів при збільшенні товщини космічної струни.

СПИСОК ВИКОРИСТАНИХ ДЖЕРЕЛ

1. S.L. Glashow, Partial symmetries of weak interactions, *Nucl. Phys.* **22**, 579-588 (1961).

2. S. Weinberg, A Model of Leptons, *Phys. Rev. Lett.* **19**, 1264-1266 (1967).

3. A. Salam, Weak and Electromagnetic Interactions, *Proc. of 8th Nobel Symp.* ed. N Svartholm (Stockholm: Almquist and Wiksells), 367-377 (1968).

4. S.M. Bilenky and S.T. Petcov, Erratum: Massive Neutrinos and Neutrino Oscillations, *Rev. Mod. Phys.* **61**(1), 169 (1989).

5. A. Strumia and F. Vissani, Neutrino masses and mixings and..., *Report number: IFUP-TH/2004-1*, arXiv:hep-ph/0606054 (2006).

6. P.F. de Salas, D.V. Forero, C.A. Ternes, M. Tortola, and J.W.F. Valle, Status of neutrino oscillations 2018: 3σ hint for normal mass ordering and improved CP sensitivity *Phys. Lett. B* **782**, 633-640 (2018).

7. P.J.E. Peebles, Dark Matter, **112**(40), 12246-12248 (2015)

8. V. Lukovic, P. Cabella, and N. Vittorio, Dark matter in cosmology, *Int. J. Mod. Phys. A* **29**, 1443001 (20 pages) (2014).

9. G. Bertone and D. Hooper, History of Dark Matter, *Rev. Mod. Phys.* **90**(4), 045002 (32 pages) (2018).

10. Ph. Brax, What makes the Universe accelerate? A review on what dark energy could be and how to test it, *Rept. Prog. Phys.* **81**(1), 016902 (52 pages) (2018).

11. G. Steigman, Observational tests of antimatter cosmologies, *Ann. Rev. Astron. Astrophys.* **14**, 339-372 (1976).

12. A. Riotto and M. Trodden, Recent progress in baryogenesis, *Ann. Rev. Nucl. Part. Sci.* **49**, 35-75 (1999).

13. L. Canetti, M. Drewes, and M. Shaposhnikov, Matter and Antimatter in the Universe, *New J. Phys.* **14**, 095012 (18 pages) (2012).

14. J. Alwall, P. Schuster, and N. Toro, Simplified models for a first characterization of new physics at the LHC, *Phys. Rev. D* **79**, 075020 (76 pages) (2009).

15. J.D. Lykken, Beyond the Standard Model, *CERN Yellow Report* **CERN-2010-002**, 101-109, arXiv:1005.1676 (2010).

16. G. Cowan, K. Cranmer, E. Gross, and O. Vitells, Erratum: Asymptotic formulae for likelihood-based tests of new physics, *Eur.Phys.J.C* **73**, 2501 (2013).

17. D. Alves et al., Simplified models for LHC new physics searches, *J. Phys. G* **39**, 105005 (40 pages) (2012).

18. V.A. Rubakov and D.S. Gorbunov, *Introduction to the Theory of the Early Universe: Hot big bang theory* (World Scientific, Singapore, 2017).

19. T. Golling et al., Physics at a 100 TeV pp collider: beyond the Standard Model phenomena, *CERN Yellow Rep.* **3**, 441-634 (2017).

20. A. Abada et al., FCC Physics Opportunities: Future Circular Collider Conceptual Design Report Volume 1, *Eur. Phys. J. C* **79**(6), 474 (161 pages) (2019).

21. J. Beacham et al., Physics Beyond Colliders at CERN: Beyond the Standard Model Working Group Report, *J. Phys. G* **47**(1), 010501 (114 pages) (2020).

22. G. Lanfranchi, M. Pospelov, and P. Schuster, The Search for Feebly Interacting Particles, *Ann. Rev. Nucl. Part. Sci.* **71**, 279-313 (2021).

23. D. Curtin et al., Long-Lived Particles at the Energy Frontier: The MATHUSLA Physics Case, *Rept. Prog. Phys.* **82**(11), 116201 (133 pages) (2019).

24. S. Cerci et al., FACET: A new long-lived particle detector in the very forward region of the CMS experiment, *J. High Energ. Phys.* **06**, 110 (15 pages) (2022).

25. A. Ariga et al., Letter of Intent for FASER: ForwArd Search ExpeRiment at the LHC, *Report number: CERN-LHCC-2018-030*, arXiv:1811.10243 (2018).

26. A. Ariga et al., FASER's physics reach for long-lived particles, *Phys. Rev. D* **99**(9), 095011 (30 pages) (2019).

27. M. Anelli et al., A facility to Search for Hidden Particles (SHiP) at the CERN SPS, *Report number: CERN-SPSC-2015-016, SPSC-P-350*, arXiv:1504.04956 (2015).

28. S. Alekhin et al., A facility to Search for Hidden Particles at the CERN SPS: the SHiP physics case, *Rept. Prog. Phys.* **79**(12), 124201 (137 pages) (2016).

29. P. Mermod, Prospects of the SHiP and NA62 experiments at CERN for hidden sector searches, *PoS* **NuFact2017**, 139 (7 pages) (2017).

30. E. Cortina Gil et al., Search for heavy neutral lepton production in K+ decays, *Phys. Lett. B* **778**, 137-145 (2018).

31. M. Drewes, J. Hajer, J. Klaric, and G. Lanfranchi, NA62 sensitivity to heavy neutral leptons in the low scale seesaw model, *J. High Energ. Phys.* **07**, 105 (25 pages) (2018).

32. R. Acciarri et al., Long-Baseline Neutrino Facility (LBNF) and Deep Underground Neutrino Experiment (DUNE): Conceptual Design Report, Volume 2: The Physics Program for DUNE at LBNF, *Report number: FERMILAB-DESIGN-2016-02*, arXiv:1512.06148 (2015).

33. B. Abi et al., Prospects for beyond the Standard Model physics searches at the Deep Underground Neutrino Experiment, *Eur. Phys. J. C* **81**(4), 322 (51 pages) (2021).

34. C. Bird, P. Jackson, R.V. Kowalewski, and M. Pospelov, Search for dark matter in b —> s transitions with missing energy, *Phys. Rev. Lett.* **93**, 201803 (4 pages) (2004).

35. F. Bezrukov and D. Gorbunov, Light inflaton Hunter's Guide, *J. High Energ. Phys.* **05**, 010 (22 pages) (2010).

36. M.W. Winkler, Decay and detection of a light scalar boson mixing with the Higgs boson, *Phys. Rev. D* **99**(1), 015018 (15 pages) (2019).

37. A. Monin, A. Boyarsky, and O. Ruchayskiy, Hadronic decays of a light Higgs-like scalar, *Phys. Rev. D* **99**(1), 015019 (19 pages) (2019).

38. L.B. Okun, LIMITS OF ELECTRODYNAMICS: PARAPHOTONS?, *Sov. Phys. JETP* **56**, 502 (14 pages) (1982).

39. B. Holdom, Two $U(1)$'s and Epsilon Charge Shifts, *Phys. Lett. B* **166**, 196-198 (1986).

40. P. Langacker, The Physics of Heavy Z Gauge Bosons, *Rev. Mod. Phys.* **81**, 1199-1228 (2009).

41. T. Asaka and M. Shaposhnikov, The νMSM, dark matter and baryon asymmetry of the universe, *Phys. Lett. B* **620**, 17-26 (2005).

42. T. Asaka, S. Blanchet, and M. Shaposhnikov, The νMSM, dark matter and neutrino masses, *Phys. Lett. B* **631**, 151-156 (2005).

43. K. Bondarenko, A. Boyarsky, D. Gorbunov, and O. Ruchayskiy, Phenomenology of GeV-scale Heavy Neutral Leptons, *J. High Energ. Phys.* **11**, 032 (54 pages) (2018).

44. A. Boyarsky, M. Drewes, T. Lasserre, S. Mertens, and O. Ruchayskiy, Sterile neutrino Dark Matter, *Prog. Part. Nucl. Phys.* **104**, 1-45 (2019).

45. R.D. Peccei and H.R. Quinn, CP Conservation in the Presence of Instantons, *Phys. Rev. Lett.* **38**, 1440-1443 (1977).

46. S. Weinberg, A New Light Boson?, *Phys. Rev. Lett.* **40**, 223-226 (1978).

47. F. Wilczek, Problem of Strong P and T Invariance in the Presence of Instantons, *Phys. Rev. Lett.* **40**, 279-282 (1978).

48. K. Choi, S.H. Im, and C.S. Shin, Recent Progress in the Physics of Axions and Axion-Like Particles, *Ann. Rev. Nucl. Part. Sci.* **71**, 225-252 (2021).

49. A. Amruth et al., Anomalies in Gravitational-Lensed Images Revealing Einstein Rings Modulated by Wavelike Dark Matter, Nature Astron. **7**, 736-747 (2023).

50. E. D'Hoker and Ed. Farhi, Decoupling a Fermion Whose Mass Is Generated by a Yukawa Coupling: The General Case, *Nucl. Phys. B* **248**, 59-76 (1984).

51. E. D'Hoker and Ed. Farhi, Decoupling a Fermion in the Standard Electroweak Theory, *Nucl. Phys. B* **248**(1), 77-89 (1984).

52. I. Antoniadis, A. Boyarsky, O. Ruchayskiy, Axion alternatives, *Report number: CERN-PH-TH/2006-119*, arXiv:hep-ph/0606306 (2006).

53. I. Antoniadis, A. Boyarsky, S. Espahbodi, O. Ruchayskiy, and J.D. Wells, Anomaly driven signatures of new invisible physics at the Large Hadron Collider, *Nucl. Phys. B* **824**, 296-313 (2010).

54. R. Rajaraman, Solitons and Instantons: *An Introduction to Solitons and Instantons in Quantum Field Theory* (North-Holland Publishing Company, 1982).

55. I. Antoniadis, E. Kiritsis, and T.N. Tomaras, A D-brane alternative to unification, *Phys. Lett. B* **486**, 186-193 (2000).

56. C. Coriano, N. Irges, and E. Kiritsis, On the effective theory of low scale orientifold string vacua, *Nucl. Phys. B* **746**, 77-135 (2006).

57. N. Irges, C. Coriano, and S. Morelli, Stuckelberg Axions and the Effective Action of Anomalous Abelian Models 2. A $SU(3)C \times SU(2)W \times U(1)Y \times U(1)B$ model and its signature at the LHC, Nucl. Phys. B 789 (2008) 133-174.

58. P. Anastasopoulos, M. Bianchi, E. Dudas, and E. Kiritsis, Anomalies, anomalous $U(1)'$s and generalized Chern-Simons terms, *J. High Energ. Phys.* **11**, 057 (52 pages) (2006).

59. P. Anastasopoulos, F. Fucito, A. Lionetto, G. Pradisi, A. Racioppi, and Y.S. Stanev, Minimal Anomalous $U(1)$-prime Extension of the MSSM, *Phys. Rev. D* **78**, 085014 (23 pages) (2008).

60. J.A. Harvey, C.T. Hill, and R. J. Hill, Standard Model Gauging of the Wess-Zumino-Witten Term: Anomalies, Global Currents and pseudo-Chern-Simons Interactions, *Phys. Rev. D* **77**, 085017 (14 pages) (2008).

61. J. Kumar, A. Rajaraman, and J. D. Wells, Probing the Green-Schwarz Mechanism at the Large Hadron Collider, *Phys. Rev. D* **77**, 066011 (7 pages) (2008).

62. D.A. Kirzhnits, Weinberg model in the hot universe, *JETP Lett.* **15**, 529-531 (1972).

63. S. Weinberg, Gauge and Global Symmetries at High Temperature, *Phys. Rev. D* **9**, 3357-3378 (1974).

64. H.B. Nielsen and P. Olesen, Vortex-line models for dual strings, *Nucl. Phys. B.* **61**, 45-61 (1973).

65. T.W.B. Kibble, Topology of Cosmic Domains and Strings, *J. Phys. A* **9**, 1387-1398 (1976).

66. A. Vilenkin, Cosmic Strings and Domain Walls, *Phys. Reports* **121**, 263-315 (1985).

67. A. Vilenkin and E.P.S. Shellard, *Cosmic Strings and Other Topological Defects*, (Cambridge University Press, 2000).

68. M.B. Hindmarsh and T.W.B. Kibble, Cosmic strings, *Rept. Prog. Phys.* **58**, 477-562 (1995).

69. R. Jeannerot, J. Rocher, and M. Sakellariadou, How generic is cosmic string formation in supersymmetric grand unified theories, *Phys. Rev. D* **68**, 103514 (20 pages) (2003).

70. G. Dvali and A. Vilenkin, Formation and evolution of cosmic D strings, *J. Cosmol. Astropart. Phys.* **03**, 010 (18 pages) (2004).

71. E.J. Copeland, R.C. Myers, and J. Polchinski, Cosmic F and D strings, *J. High Energ. Phys.* **06**, 013 (29 pages) (2004).

72. J. Polchinski, Cosmic superstrings revisited, *Int. J. Mod. Phys. A* **20**, 3413-3415 (2005).

73. J. Lizarraga, J. Urrestilla, D. Daverio, M. Hindmarsh, M. Kunz, and A.R. Liddle, Constraining topological defects with temperature and polarization anisotropies, *Phys. Rev. D* **90**(10), 103504 (9 pages) (2014).

74. M. Sazhin, G. Longo, M. Capaccioli, J.M. Alcalá, R. Silvotti, G. Covone, O. Khovanskaya, M. Pavlov, M. Pannella, M. Radovich, and V. Testa, CSL-1: chance projection effect or serendipitous discovery of a gravitational lens induced by a cosmic string?, *Mon. Not. Roy. Astron. Soc.* **343**(2), 353-359 (2003).

75. T. Damour and A. Vilenkin, Gravitational radiation from cosmic (super)strings: Bursts, stochastic background, and observational windows, *Phys. Rev. D* **71**(6), 063510 (13 pages) (2005).

76. Ziwei Wang, Lei Lei, Hao Jiao, Lei Feng, and Yi-Zhong Fan, The nanohertz stochastic gravitational-wave background from cosmic string Loops and the abundant high redshift massive galaxies, arXiv:2306.17150 (2023).

77. J. Antoniadis et. al., The second data release from the European Pulsar Timing Array III. Search for gravitational wave signals, arXiv:2306.16214 (2023).

78. T. Charnock, A. Avgoustidis, E.J. Copeland, and A. Moss, CMB constraints on cosmic strings and superstrings, *Phys. Rev. D* **93**(12), 123503 (19 pages) (2016).

79. A.A. Abrikosov, On the Magnetic properties of superconductors of the second group, *Sov. Phys. JETP* **5**, 1174-1182 (1957).

80. E.M. Serebrianyi, Vacuum polarization by magnetic flux: The Aharonov-Bohm effect, *Theor. Math. Phys.* **64**(2), 846-855 (1986).

81. Yu.A. Sitenko and A.Yu. Babansky, The Casimir-Aharonov-Bohm effect?, *Mod. Phys. Lett. A* **13**, 379-386 (1998).

82. Yu.A. Sitenko and A.Yu. Babansky, Effects of Boson-Vacuum Polarization by a Singular Magnetic Vortex, *Phys. Atom. Nucl.* **61**, 1594-1602 (1998).

83. A.Yu. Babanskii and Yu.A. Sitenko, Vacuum energy induced by a singular magnetic vortex, *Theor. Math. Phys.* **120**, 876–882, (1999).

84. Yu.A. Sitenko and V.M. Gorkavenko, Induced vacuum energy-momentum tensor in the background of a $(d-2)$ – brane in $(d+1)$ – dimensional space-time, *Phys. Rev. D.* **67**, 085015 (19 pages) (2003).

85. Yu.A. Sitenko and N.D. Vlasii, Induced vacuum current and magnetic field in the background of a cosmic string, *Class. Quant. Grav.* **26**, 195009 (12 pages) (2009).

86. H.B.G. Casimir, Introductory remarks on quantum electrodynamics, *Physica* **19**, 846-849 (1953).

87. M. Bordag, U. Mohideen, and V.M. Mostepanenko, New developments in the Casimir effect, *Phys. Reports* **353** 1-205 (2001).

88. Y. Aharonov and D. Bohm, Significance of Electromagnetic Potentials in the Quantum Theory, *Phys. Rev.* **115**, 485-491 (1959).

89. P. de Sousa Gerbert and R. Jackiw, Classical and Quantum Scattering on a Spinning Cone, *Commun. Math. Phys.* **124**, 229-260 (1989).

90. P. de Sousa Gerbert, Fermions in an Aharonov-Bohm Field and Cosmic Strings, *Phys. Rev. D* **40**, 1346-1349 (1989).

91. J. von Neumann, *Mathematische Grundlagen der Quantummechanik* (Springer, Berlin, 1932).

92. M. Reed and B. Simon, *Methods of Modern Mathematical Physics II. Fourier Analysis, Self-Adjointness* (Academic Press, New York, 1975).

93. P. Gornicki, Aharonov-Bohm effect and vacuum polarization *Ann. Phys.* **202**(2), 271-296 (1990).

94. A.Yu. Sitenko, Effects of fermion-vacuum polarization by a singular magnetic vortex: Zeta function and energy, *Phys. Atom. Nucl.* **62**, 1056-1069 (1999).

95. A.Yu. Sitenko, Erratum: Self-adjointness of the Dirac Hamiltonian and induction of vacuum quantum numbers by a singular external field, *Phys. Atom. Nucl.* **62**, 1084 (1999).

96. E.G. Flekkoy and J.M. Leinaas, Vacuum currents around a magnetic flux string, *Int. J. Mod. Phys. A* **06**(29), 5327-5347 (1991).

97. D. Cangemi, E. D'Hoker, and G. Dunne, Effective energy for $2+1$-dimensional QED with semilocalized static magnetic fields: A solvable model *Phys. Rev. D.* **52**(6), 3163-3167 (1995).

98. M.P. Fry, QED in inhomogeneous magnetic fields, *Phys. Rev. D.* **54**(10), 6444-6452 (1996).

99. G. Dunne, T.M. Hall, An exact QED_{3+1} effective action, *Phys. Lett. B.* **419**, 322-325 (1998).

100. M. Bordag and K. Kirsten, Vacuum energy in a spherically symmetric background field, *Phys. Rev. D.* **53**(10), 5753-5760 (1996).

101. M. Bordag and K. Kirsten, Ground state energy of a spinor field in the background of a finite radius flux tube, *Phys. Rev. D.* **60**, 105019 (14 pages) (1999).

102. M. Scandurra, Vacuum energy in the presence of a magnetic string with a delta function profile, *Phys. Rev. D.*, **62**(8), 085024 (10 pages) (2000).

103. P. Pasipoularides, Fermion-induced effective action in the presence of a static inhomogeneous magnetic field, *Phys. Rev. D.* **64**(10), 105011 (14 pages) 2001.

104. P. Pasipoularides, Strong magnetic field asymptotic behaviour for the fermion-induced effective energy in the presence of a magnetic flux tube, *Phys. Rev. D.* **67**(10), 107301 (4 pages) (2003).

105. M. Bordag and I. Drozdov, Fermionic vacuum energy from a Nielsen-Olesen vortex, *Phys. Rev. D.* **68**(6), 065026 (11 pages) (2003).

106. E.R. Bezerra de Mello, V.B. Bezerra, A.A. Saharian, and H.H. Harutyunyan, Vacuum currents induced by a magnetic flux around a cosmic string with finite core, *Phys. Rev. D* **91**(6), 064034 (19 pages) (2015).

107. Yu.A. Sitenko, Electron charge fractionization on surfaces of various geometry in an external magnetic field, *Nucl. Phys. B* **342**(3), 655–679 (1990).

108. Yu.A. Sitenko, Geometry of the base manifold and fermion number fractionization *Phys. Lett. B* **253**, 138–142 (1991).

109. A.V. Mischenko, Yu.A. Sitenko, Spectral boundary conditions and index theorem for two-dimensional compact manifold with boundary, *Ann. Phys.* **218**(2), 199-232 (1992).

ПОДЯКИ

Я хотів би щиро подякувати

- Моєму Вчителю Ситенку Юрію Олексійовичу за те, що починаючи з 1999 року Ви вчили мене теоретичній фізиці, її методам і завданням, показуючи на своєму прикладі як працювати в науці, як знаходити цікаві задачі та як їх розв'язувати. Я також дуже вдячний моєму Вчителю за плідну співпрацю протягом багатьох років, за постійну підтримку, в тому числі і поза межами нашої спільної наукової діяльності.

- Вільчинському Станіславу Йосиповичу, Горбару Едуарду Володимировичу та Бондаренку Кирилу Володимировичу за підтримку, увагу, корисні поради і співпрацю.

- Моїм колегам з кафедри квантової теорії поля та космомікрофізики за доброзичливу атмосферу і підтримку.

ДОДАТОК А

СПИСОК НАУКОВИХ ПРАЦЬ, В ЯКИХ ОПУБЛІКОВАНО ОСНОВНІ НАУКОВІ РЕЗУЛЬТАТИ ДИСЕРТАЦІЇ

1. **V.M. Gorkavenko**, Yu.A. Sitenko, O.B. Stepanov, Polarization of the vacuum of a quantized scalar field by an impenetrable magnetic vortex of finite thickness, *J. Phys. A: Math. Theor.* **43**(17), 175401 (12 pages) (2010).

2. **V.M. Gorkavenko**, S.I. Vilchynskiy, Some constraints on the Yukawa parameters in the neutrino modification of the Standard Model (νMSM) and CP-violation, *Eur. Phys. J. C* **70**(4), 1091-1098 (2010).

3. **V.M. Gorkavenko**, Yu.A Sitenko, O.B. Stepanov, Vacuum energy induced by an impenetrable flux tube of finite radius, *Intern. J. Mod. Phys. A* **26**(22), 3889-3899 (2011).

4. **V.M. Gorkavenko**, Yu.A. Sitenko, O.B. Stepanov, Casimir energy and force induced by an impenetrable flux tube of finite radius, *Intern. J. Mod. Phys. A* **28**(31), 1350161 (17 pages) (2013).

5. **V.M. Gorkavenko**, I.V. Ivanchenko, Yu.A. Sitenko, Induced vacuum current and magnetic field in the background of a vortex, *Intern. J. Mod. Phys. A* **31**(06), 1650017 (11 pages) (2016).

6. Yu.A. Sitenko, **V.M. Gorkavenko**, Induced vacuum magnetic flux in quantum spinor matter in the background of a topological defect in two-dimensional space, *Phys. Rev. D* **100**(8), 085011 (36 pages) (2019).

7. I. Boiarska, K. Bondarenko, A. Boyarsky, **V. Gorkavenko**, M. Ovchynnikov, A. Sokolenko, Phenomenology of GeV-scale scalar portal, *J. High Energ. Phys.* **2019**(11), 1-45 (2019).

8. **V.M. Gorkavenko**, Y.R. Borysenkova, M.S. Tsarenkova, Production of GeV-scale heavy neutral leptons in three-body decays. Comparison with the PYTHIA approach, *J. Phys. G: Nucl. Part. Phys.* **48**(10), 105001 (25 pages) (2021).

9. Yu. Borysenkova, P. Kashko, M. Tsarenkova, K. Bondarenko, **V. Gorkavenko**, Production of Chern-Simons bosons in decays of mesons, *J. Phys. G: Nucl. Part. Phys.* **49**(8), 085003 (29 pages) (2022).

10. Yu.A. Sitenko, **V.M. Gorkavenko**, M.S. Tsarenkova, Magnetic flux in the vacuum of quantum bosonic matter in the cosmic string background, *Phys. Rev. D* **106**(10), 105010 (20 pages) (2022).

11. **V.M. Gorkavenko**, T.V. Gorkavenko, Yu.A. Sitenko, M.S. Tsarenkova, Induced vacuum current and magnetic flux in quantum scalar matter in the background of a vortex defect with the Neumann boundary condition, *Ukr. J. Phys.* **67**(1), 3-10 (2022).

12. **V.M. Gorkavenko**, T.V. Gorkavenko, Yu.A. Sitenko, M.S. Tsarenkova, Induced vacuum energy density of quantum charged scalar matter in the background of an impenetrable magnetic tube with the Neumann boundary condition, *Ukr. J. Phys.* **67**(10), 715-721 (2022).

ТЕЗИ ДОПОВІДЕЙ НА НАУКОВИХ КОНФЕРЕНЦІЯХ

1. **В.М. Горкавенко**, Ю.О. Сітенко, О. Б. Степанов, Густина вакуумної енергії, індукована непроникним магнітним вихором скінченого поперечного розміру. Міжнародна конференція молодих вчених та аспірантів "ІЕФ, 2011". 24-27 травня, 2011, Інститут Електронної Фізики НАН України, Ужгород (Україна). Науковий вісник Ужгородського університету, серія Фізика, випуск **30**, с. 234-239 (2011).

2. S.I. Vilchinskii, **V.M. Gorkavenko**, I.V Rudenok, The influence of the non-zero value of θ_{13} mixing angle on the parameters of the neutrino modification of the Standard Model (νMSM). III Young Scientists Conference Modern Problems of Theoretical Physics. December 21-23, 2011, Bogolyubov Institute for Theoretical Physics of the NAS of Ukraine, Kyiv (Ukraine). Book of abstracts, 13 (2011).

3. **V.M. Gorkavenko**, Yu.A. Sitenko, O.B.Stepanov, Casimir force induced by impenetrable flux tube of finite radius. III Young Scientists Conference Modern Problems of Theoretical Physics. December 21-23, 2011, Bogolyubov Institute for Theoretical Physics of the NAS of Ukraine, Kyiv (Ukraine). Book of abstracts, 55 (2011).

4. I. Ivanchenko, **V.M. Gorkavenko**, Yu. A. Sitenko, Induced vacuum current and magnetic field in the background of a cosmic string modeled by impenetrable magnetic-flux-carrying tube. 20-th Open Young Scientists' Conference on Astronomy and Space Physics. April 22-27, 2013, Kyiv (Ukraine). Abstracts.– K.: ТОВ "Компанія ВАІТЕ", 30 (2013).

5. Yu.A. Sitenko, **V.M. Gorkavenko**, Self-adjointness, confinement and the Casimir effect. International Conference on p-Adic Mathematical Physics and its Applications. September 7-12, 2015, Belgrade (Serbia). Conference proceedings: Facta Universitatis, Series Physics, Chemistry and Technology **14**(3), 319-335 (2016).

6. **V. Gorkavenko**, K. Bondarenko, O. Seleznov, S. Vilchynskiy, Search for light Higgs-like particles in proton collisions with a target at the SHiP experiment. 3-rd Walter THIRRING International School "Fundamentals of Astroparticle and Quantum Physics". September 17-23, 2017, Bogolyubov Institute for Theoretical Physics of the NAS of Ukraine,

Kyiv (Ukraine). List of invited speakers
http://quark.itp.tuwien.ac.at/∼diefaust/2017/

7. **V. Gorkavenko**, Search for light Higgs-like particles in proton collisions with a target at the SHiP experiment. The International Conference "CERN-Ukraine Cooperation: Current State and Prospects". May 15-17, 2018, Institute for Scintillation Materials NAS of Ukraine, Kharkiv (Ukraine). Conference Programme
https://kipt.kharkov.ua/conferences/itp/2018/Programme_CERN-Ukraine.pdf

8. **V.M. Gorkavenko**, Search for Hidden Particles in Intensity Frontier Experiment SHiP. New trends in high-energy physics, 21-th International conference organized by the Bogolyubov Institute for Theoretical Physics, National Academy of Sciences of Ukraine. May 12–18, 2019, Odessa (Ukraine). Proceeding of the conference, 147-152
https://indico.bitp.kiev.ua/event/1/attachments/3/163/Book_conf.pdf

9. **V.M. Gorkavenko** and Yu.A. Sitenko, Polarization of the vacuum of quantized spinor field by a topological defect in two-dimensional space. XI Bolyai-Gauss-Lobachevsky Conference: Non-Euclidean, Non-Commutative Geometry and Quantum Physics. May 19-24, 2019, Bogolyubov Institute for Theoretical Physics, Kyiv (Ukraine). Book of Abstracts, 14 (2019).

10. **V. Gorkavenko**, P. Kashko, K. Bondarenko, Chern-Simons portal. X Young Scientists Conference Modern Problems of Theoretical Physics. December 23-24, 2019, Bogolyubov Institute for Theoretical Physics of the NAS of Ukraine, Kyiv (Ukraine). Book of abstracts, 55 (2019).

11. Y. Borysenkova, K. Bondarenko, **V. Gorkavenko**, A. Svetlichnyi, M. Tsarenkova, Production of HNL in 3-body decays of mesons. Comparison with PYTHIA approach. XI Young Scientists Conference Modern Problems of Theoretical Physics. December 21-23, 2020, Bogolyubov Institute for Theoretical Physics of the NAS of Ukraine, Kyiv (Ukraine). Book of abstracts, 7-9 (2021).

12. M. Tsarenkova, K. Bondarenko, Y. Borysenkova, **V. Gorkavenko**, P. Kashko, Phenomenology of GeV-scale Chern-Simons boson. XI Young Scientists Conference Modern Problems of Theoretical Physics. December 21-23, 2020, Bogolyubov Institute for Theoretical Physics of the NAS of Ukraine, Kyiv (Ukraine). Book of abstracts, 10-13 (2021).